A Benchmarked Dynamic Model of Xenon Behavior in a Molten Salt Reactor

by

Terry J. Price

A thesis submitted to the
School of Graduate and Postdoctoral Studies in partial
fulfillment of the requirements for the degree of

Doctor of Philosophy in Nuclear Engineering

Faculty of Energy Systems and Nuclear Science

Ontario Tech University

Oshawa, Ontario, Canada

December 2019

THESIS EXAMINATION INFORMATION

Submitted by: **Terry J. Price**

Doctorate of Philosophy in **Nuclear Engineering**

Thesis title:	
A Benchmarked Dynamic Model of Xenon Behaviour in a Molten Salt Reactor	

An oral defence of this thesis took place on November 28, 2019 in front of the following examining committee:

Examining Committee:

Chair of Examining Committee	Brian Ikeda
Research Supervisor	Ondrej Chvala
Research Co-supervisor	George Bereznai
Examining Committee Member	Akira Tokuhiro
Examining Committee Member	
Thesis Examiner	
	Kirk Atkinson
University Examiner	
External Examiner	Mohammadreza Baghbanan, Ontario Power Generation

The above committee determined that the thesis is acceptable in form and content and that a satisfactory knowledge of the field covered by the thesis was demonstrated by the candidate during an oral examination. A signed copy of the Certificate of Approval is available from the School of Graduate and Postdoctoral Studies.

Last revision December 13, 2019

This version was compiled on 2019/12/13 at 15:23:00

Acknowledgements

"He was despised and forsaken of men,

A man of sorrows and acquainted with grief;

And like one from whom men hide their face He was despised,

and we did not esteem Him."

Isaiah 53:3

Thank you Dr. Chvala, this wouldn't of got done without the midnight phone calls and 2 am editing sessions. "Above and beyond the call of duty" doesn't even begin to describe what you did.

Dr. Bereznai, you're the toughest old man I've ever met; you made sure everything got done by the book.

Finally, for what it's worth, thanks Dad. You and I both know there's no rest for us, but atleast there's the satisfaction of knowing that the job got done.

To anyone reading this in the future: good luck!

Abstract

Molten salt reactors are a type of nuclear reactor that are being considered for deployment in the fourth generation nuclear power technology. Molten salt reactors use molten a alkali / actinide halide salt melt at temperatures far in excess of temperatures found in a typical pressurized water reactor. This thesis focuses on graphite moderated reactors with fluoride as the halide. The salt melt, called the fuel salt, is circulated between a moderator and a heat exchanger. While within the moderator, the dissolved actinides undergo fission and generate heat. Among products of nuclear fission is gaseous xenon, and in particular the isotope xenon-135 that acts as a neutron absorber. In solid fueled reactors, the xenon is effectively static and trapped within the fuel matrix. In a molten salt reactor, conversely, the fuel matrix is the mobile, circulating fuel salt that transports the xenon along with the rest of the fuel. This thesis focuses on modeling the behavior of xenon in a molten salt reactor. Existing literature in the field is reviewed and compiled. A model of xenon behavior in a molten salt reactor (the Molten Salt Reactor Experiment in particular) has been developed and the model is presented in this thesis. The model is benchmarked against experimental data using best available data, then minimal necessary justifiable adjustment is made to model parameters in order to fit the model to the experimental data. As a result this model is able to fit two transients, something that no xenon model of the molten salt reactor experiment has been able to do previously.

Keywords: Molten Salt Reactor; MSR; Xenon; Xenon 135; Generation IV

AUTHOR'S DECLARATION

I hereby declare that this thesis consists of original work of which I have authored. This is a true copy of the thesis, including any required final revisions, as accepted by my examiners.

I authorize Ontario Tech University (OnTechU) to lend this thesis to other institutions or individuals for the purpose of scholarly research. I further authorize OnTechU to reproduce this thesis by photocopying or by other means, in total or in part, at the request of other institutions or individuals for the purpose of scholarly research. I understand that my thesis will be made electronically available to the public.

The research work in this thesis that was performed in compliance with the regulations of OnTechU's Research Ethics Board.

Terry J. Price

Statement of Contributions

I hereby declare that all work in this thesis is my own except for:

- The Serpent 2 model of the MSRE which was developed by Gavin Ridley of University of Tennessee, Knoxville, as an undergraduate thesis project.

- The idea for doing the second order solution to the reaction diffusion equation graphite stringer model used in the dynamic model was given by Scott Greenwood, staff at the Oak Ridge National Laboratory, after a failed first attempt using a first order method.

- The background and theory, albeit written in my own words, were paraphrased from numerous sources I have read over the years. I am unsure as to how to appropriately cite something that is said in a large number of books.

x

Contents

List of Figures

xix

List of Tables

Introduction

Foreword

Nuclear reactors generate energy through controlled nuclear fission. The key components of a nuclear reactor are the nuclear fuel that undergoes fission, the control rods that regulate the fission process, the primary working fluid that transfers heat to a heat exchanger, and the fuel matrix that contains the results of fission, the fission products. Typically the fuel matrix is a solid uranium dioxide compound. One particular fission product that has a substantial impact on reactor behavior is xenon-135 due to its large neutron poisoning effect. There is a particular type of nuclear reactor called a molten salt reactor where the a molten salt serves as both the working fluid and the fuel matrix. The molten salt is liquid, and the xenon-135 is gas, so the behavior in the liquid fueled reactor is qualitatively different than it would be in a solid fueled reactor.

This thesis focuses on computational modeling of xenon in a molten salt reactor. This is a very important subject since, as shown by our review of the literature (see chapter 2), no scientific consensus has been reached on how to do the modeling. Furthermore, there was an important research opportunity available: the original model of molten salt reactor behavior computed the behavior at only one temperature, however, the behavior of xenon in a molten salt reactor is indeed governed by temperature. Therefore, we decided to build a *dynamic* – meaning temperature dependent – model of molten salt reactor xenon behavior, which is a first of its kind. Chapter 3 presents information how this model was developed.

With the model developed, it needed to be tested to see if it was a reasonable approximation of what actually happened to xenon in a molten salt reactor. To do this, a *sensitivity analysis* was performed that varied one model parameter as the rest were held constant, and compared the output to experimental results. High estimates and low estimates for each model parameter were tested to see how much variations that we thought could be expected would effect the model output. How the sensitivity analysis was done (methodology) is presented in chapter 4. It's important to describe the methodology of the sensitivity analysis since it allows for transparency in our findings – i.e. if someone doubts our results, they can go back and check how they were made. The results of the sensitivity analysis itself were presented in chapter 5, and the overall results are discussed in chapter 6.

After the sensitivity analysis was done, we realized that by performing some slight, justifialbe changes in model parameters that we could recreate experimental results well. The results of this *model fitting* is presented in chapter 7.

Finally, since the model was originally developed to demonstrate feasibility of developing a temperature dependent molten salt reactor xenon model, some sample *dynamic transients* were simulated using the model and the results of these simulations are shown in chapter 8.

Motivation

Since xenon in molten salt reactors (MSRs) is free to migrate, and its migrational behavior is governed by thermophysical properties, it follows the migrational behavior of xenon in a function of the thermal behavior of the reactor. This was noted by Haubenreich and Engel [1], who state, on page 131 of their paper,

> *"The steady-state xenon poisoning in the MSRE* [Molten Salt Reactor Experiment] *varies somewhat with system temperature and pressure..."*

The effects of temperature on xenon related processes can be broken down into two categories:

1. effects on fuel salt and gas volumes;

2. effects on thermophysical properties.

These two effects generate corresponding effects on xenon behavior in an MSR. Although some modeling work related to MSR xenon had been previously conducted, no work was found that attempted to describe the effects of temperature on xenon behavior.

Objective

Although there have been several previous attempts at modeling xenon behavior in a MSR (see Price, Taylor, and Chvala [2] for an overview), we are aware of no prior attempts to model the thermal dynamics of xenon in an MSR. Therefore, in order to create a new contribution to knowledge in the field, the objective of this thesis was to develop a thermal model of MSR xenon behavior.

Novelty and Contribution

In order to understand the novelty and contribution of this thesis, one must first understand the transient / steady state inconsistency detailed in ORNL-TM-3464 [3]. Essentially, the model developed in ORNL-TM-3464 wasn't able to fit both transient and steady state results,

> *"The calculations using previously accepted transport mechanisms and parameter values showed again that the steady-state results with argon cover gas could be readily duplicated. However, such calculations required the use of stripping efficiencies that were much lower than the bubble removal rates that were observed in the reactor when excess bubbles were present. It is, of course, conceivable that bubble stripping efficiency for xenon might be much lower than the rate at which a new void distribution is approached. This would be the case if, for example, stripped bubbles were replaced by bubbles containing an abnormally high xenon*

concentration because of the existence of a 'foam' blanket on the salt surface in the pump There is evidence from observations in the pump bowl that some kind of foam layer was indeed present; however, its characteristics are not well defined and any conclusions about its effect on the xenon behavior would be highly speculative. When the low stripping rates required for these steady-state results were applied to transient calculations with high argon void fractions, they produced decreases in the xenon poisoning that were much slower than those observed in the reactor after power operations..." — ORNL-TM-3464 p. 93 [3]

This hypothesized foam allowed them to postulate very low stripping rates that allowed them to fit their model to steady state results. When, however, these low stripping rates were applied to transient calculations, the model produced indefensible results.

With this understanding established, the contributions of the thesis may be stated: this thesis provides three major contributions to the field:

- The largest and most complete list of literature related to MSR xenon behavior to date has been compiled. This list is shown in the annex of this thesis.

- A first of a kind MSR xenon dynamics model has been developed and bench marked.

- A solution to the transient / steady state inconsistency described.

Approach

This section describes the approach taken to research involved in this thesis. This description is highly technical, and readers unfamiliar with molten salt reactors are encouraged to review Section 1.3 in order to gain some level of technical familiarity with MSRs.

This thesis presents a model of MSR xenon behavior which accounts for the effects of temperature on xenon dynamics. The model was built with reference data was taken from

Oak Ridge National Laboratory (ORNL) Technical Memorandum (TM) and other ORNL reports.

The model was bench-marked against startup and shutdown transients from the MSRE. The transient data was obtained from data published in ORNL-TM-3464 [3]. Sensitivity analysis was performed on these transients with upper and lower bounds for the parameters. Model parameters were then adjusted to demonstrate that the model can be fit to experimental data.

Outline of Thesis

This thesis has four major parts.

First, a brief primer and background is provided in which reactor theory, MSRs, xenon, and xenon behavior in MSRs is briefly described.

Second, there is the literature review in which a state of the art is provided in which the techniques and methods used in previous MSR xenon behavior analyses are reviewed. A description of how the model presented in this thesis fits in to the existing corpus of work related to MSR xenon analysis.

Next, the a model description is given at the component level. Each subsystem of the model is described along with the interaction. Major parameter values are also listed along with references from where these parameter values were derived.

Finally, the bench marking results are presented in the form of a sensitivity analysis. The major model parameter were perturbed and the resultant variation on model performance investigated. The primary cause of these variations is described. Error due to variation in parameters is also provided and the model is fit to experimental results. Finally the model's dynamic transient capabilities are show cased.

The thesis concludes by summarizing the work done, and describing some future work that may be performed.

CHAPTER 1

Background and Theory

1.1 Introduction

Nuclear reactors are devices that produce energy from the fission of actinide nuclear fuel. Nuclear reactors can be used in numerous applications where large quantities of energy are required; examples include, but are not limited to, electric power production, thermochemical process heat production, nuclear propulsion of naval vessels, or energy production for deep space missions.

Nuclear reactors are typified by a number of components. Table 1.1 lists and describes typical components in a nuclear reactor and gives examples of components that could be used in a reactor.

Molten salt reactors are unique in that their primary working fluid and their fuel matrix are the same thing and circulate within the reactor core. This is beneficial in that it allows for numerous unique applications and advantages such as the ability to control the migration of gaseous fission products through stripping processes, online fuel reprocessing, or reduced fuel cycle costs.

The objective of this chapter is to present information necessary to understand the rest of the thesis. This chapter does this by introducing the reader to many of the fundamen-

Component	Functional Description	Examples
Nuclear fuel	undergoes nuclear fission to generate heat	uranium 235
Moderator	Slows fast neutrons generated in fission in order to increase the reaction probability of a free neutron in a reactor	graphite, heavy water
Fuel matrix	Contains the nuclear fuel	Sintered uranium dioxide
Primary working fluid	transfer heat from the fuel to the heat exchanger	light water, liquid sodium metal
Reactivity control mechanism	Increase or decrease the effective neutron absorption cross section of the reactor core and there by control the ratio of neutrons born per neutrons absorbed	Cadmium coated steel rods, thermal reactivty effects (Doppler shift)
Heat Exchanger	Removes heat from the primary working fluid and transfers it to a secondary side	tube in shell, radiator

Table 1.1: Typical components of a nuclear reactor

tal concepts involved in describing the research as well as providing a unique primer on molten salt reactor xenon physics — a subject upon which there is very little introductory material. Effectively, this chapter provides some preliminary background material related to understanding the proceeding contents of this thesis.

A brief primer on reactor physics is given, including a discussion on nuclear fission, radioactive decay, and how neutrons interact with matter. Next, molten salt reactors, in particular, are discussed along with a qualitative description of fluid fuel reactors, a discussion of previously developed reactors, and the involvement of molten salt reactors in the upcoming Generation IV fleet of nuclear reactors set for deployment in the 2020s. Next, xenon 135, the isotope which this thesis is principally concerned with, is discussed with a brief history of its discovery, a description of the nuclear evolution (decay chain) of xenon 135, the physical properties of xenon 135 are examined with a discussion on how it affects nuclear reactors. Finally, the behavior of xenon 135 in molten salt reactors is discussed. The discussion begins with an overview of how xenon behaves in molten salt reactors, then delves into

the underlying assumption involved with molten salt reactor xenon theory – the in solution assumption and the ideal dilute solution assumption. Finally, the migration of xenon into the graphite, bubbles, and egress from the system through the xenon stripper is discussed.

We'd also like to note that this primer is, to the best of our knowledge, the first primer written on molten salt reactor xenon theory since the work done at Oak Ridge National Laboratory (ORNL) in the 1950s to 1970s and is novel in that it is the first primer written with the benefit of a retrospective view of the development of the molten salt reactor xenon theory.

1.2 Reactor Physics

1.2.1 Nuclear Fission

The atomic theory of matter states that all matter is made of sub nanometer particles called atoms. Within the atom is a dense region of *matter* (albeit the word *matter* begins to break down at this point) called the *nucleus*. The nucleus is comprised of positively charged *protons* and neutral *neutrons* and is about a femtometer (1×10^{-15} m) in scale.

A nucleus may split in two or more pieces in a process called *fission*. The most common way to induce fission in engineering applications is through a free neutron. Since neutrons are neutral, they do not interact with the target nucleus through electric forces and therefore retain their velocity until impact into a nucleus. The impact and subsequent absorption of a neutron can impart sufficient energy into the target nucleus that it splits apart in fission.

Nuclear fission produces a number of *fission products*, which includes:

- bound clusters of protons and neutrons known as fission fragments;

- high energy photons which are gamma radiation;

- free neutrons

The fission products, free neutrons, and mass equivalence of the gamma radiation of a nucleus that has undergone fission have a net mass less than the original nucleus. This is because a portion of the matter from the original nucleus has been transformed into energy through Einstein's mass / energy equivalence principle,

$$E = mc^2. \tag{1.1}$$

This energy is distributed to the fission products and is extracted from nuclear fuel through the working fluid of a nuclear reactor.

Since free neutrons are also released in nuclear fission this can induce a *chain reaction* in nuclear fuel and it is the exploitation of this chain reaction mechanism that has given rise to the nuclear reactor.

1.2.2 Radioactive Decay

An atom's particular nuclear configuration gives it a certain level of tendency to remain in its current configuration — stability. An atom may reconfigure itself through the process of *radioactive decay.* The three predominate modes of decay are:

- Alpha decay – emission of a helium nucleus

- Beta (minus) decay – transmutation of a proton in a neutron and the subsequent emission of an electron

- Gamma decay – deexcitation of the nucleus through the emission of a high energy photon

Each of these decay modes reconfigure the transmuting nucleus into a more stable configuration.

Each decay mode has associated with it a *Decay Constant*, which is defined as the negative

of the rate of change of a radioactive isotope per atom,

$$-\lambda \stackrel{defined}{=} \frac{1}{N}\frac{dN}{dt}. \tag{1.2}$$

A closely related concept is the radioactive half life which is defined as the amount of time it takes a population of atoms to reduce by a factor of two,

$$t_{1/2} \stackrel{defined}{=} t \quad : \quad 2N(t = t_{1/2}) = N(t = t_0). \tag{1.3}$$

Finally, we note that a particular atom may undergo consecutive radioactive decays and the series of isotopes the atom transmutes through is called its *decay chain.*

1.2.3 Neutron Interaction With Matter

Since neutrons are neutrally charged, they do not interact with an atom's electron cloud and only interact with the nucleus of an atom. Because of this, neutrons can pass through large amounts of matter without interacting and the interaction of neutrons with matter is described through probability theory.

Neutrons may interact with matter in numerous different ways. Examples include scattering, alpha production, absorption, and fission. The two modes of interaction we are concerned with in this thesis are fission and absorption. Fission has already been described. Neutron absorption is where a neutron is absorbed by a target nucleus.

The probability a neutron undergoes interaction of type i in matter per unit distance traveled in matter is called its *macroscopic cross section*, Σ_i and is defined,

$$\Sigma_i \stackrel{def.}{=} \frac{dR_i}{dx}, \tag{1.4}$$

where R_i is the probability of a reaction of type R_i will occur. The macroscopic neutron absorption cross section is written Σ_a, and the macroscopic neutron fission cross section is

written Σ_f.

The interaction of a neutron with a nucleus can be conceptualized as firing a *dart* at a target with a cross sectional area σ. If the dart lands within the target with area σ_i, the target nucleus undergoes a reaction of type i. This quantity is known as the microscopic cross section and through proofs shown in numerous text books is related to the macroscopic cross section by the product of the microscopic cross section and the number density of atoms in a substance,

$$\Sigma_i = N\sigma_i. \tag{1.5}$$

In order for the parameterization of neutronic interaction with matter to be complete, we need to also define a quantity which describes the rate at which neutrons pass through matter. For this, consider a sphere of unit surface area. The rate at which neutrons pass through the surface of this sphere, in either direction, is called the neutron flux, ϕ, and it is the product of neutron flux and the macroscopic cross section for a reaction of type i, Σ_i, that gives the reaction rate per unit volume for neutrons in a substance,

$$R_i = \Sigma_i \phi. \tag{1.6}$$

Finally, we note that a fission only produces a finite number of fission fragments. As a result, each isotope, i, has a certain probability of being produced, γ_i, which is called the *fission yield* of isotope i. Therefore, if we want to determine the volumetric rate of production of a particular isotope, we multiply the fission yield by the yield of that isotope,

$$\dot{N}_i = \gamma_i \Sigma_f \phi. \tag{1.7}$$

1.3 Molten Salt Reactors

1.3.1 The Working Principle of Molten Salt Reactors

Molten salt reactors (MSRs) are a type of nuclear reactor that contains, controls, and collects energy from a chain reaction and through continuous cooling of the nuclear fuel. Unlike a solid fuel reactor, where the nuclear fuel remains relatively stationary under nominal operating conditions, the nuclear fuel in a molten salt reactor circulates in a fuel salt that acts as both the primary working fluid and the fuel matrix.

An illustration of a molten salt reactor in shown in Figure 1.1. The corresponding flow path for the diagram is shown in Figure 1.2. The fuel salt circulates in the *primary loop* between the reactor core and the heat exchanger (9), with inertia imparted to it via a fuel pump (10). In this way, the reactor may be partitioned into in-core and out-of-core regions. Furthermore, the total system of both the in-core and out-of-core regions is referred to, in general, as the *reactor*. This distinction is shown in Figure 1.2. In reference to Figure 1.1, the fuel salt enters the in-core region through an inlet (13) and proceeds down a downcomer (12) into the lower plenum (11) whereupon it moves up a set of fuel channels (1) cut into blocks of graphite, referred to as graphite stringers (2). Note, the graphite stringers are formed of a porous matrix of graphite which have both a gaseous pore-space and a solid matrix component. Once past the graphite stringers, the fuel salt enters into the upper plenum (7), which has an interface to a cover gas region (5), before heading out the reactor outlet (14), and entering the out-of-core region. The totality of the graphite stringers is referred to as the graphite moderator or moderating region. It is when the fuel salt is within this moderating region that free neutrons become sufficiently thermalized to induced nuclear fission and thereby generate heat. Once the fuel salt has left the outlet, it enters the out-of-core region, whereupon the heat generated in fission is transferred to a secondary working fluid through a heat exchanger. Optionally, the fuel salt may pass through a *xenon stripper*

(not depicted) as it transitions between the in-core and out-of-core regions.[1] No work has been found which standardizes any MSR terminology. One additional aspect that is highly important to the analysis of xenon in MSRs is the existence of circulating bubbles (not depicted), also called circulating voids, within the fuel salt.

---

[1]Eades, Chaleff, Venneri, and Blue called these region in-core and ex-core in their 2016 paper. [4]
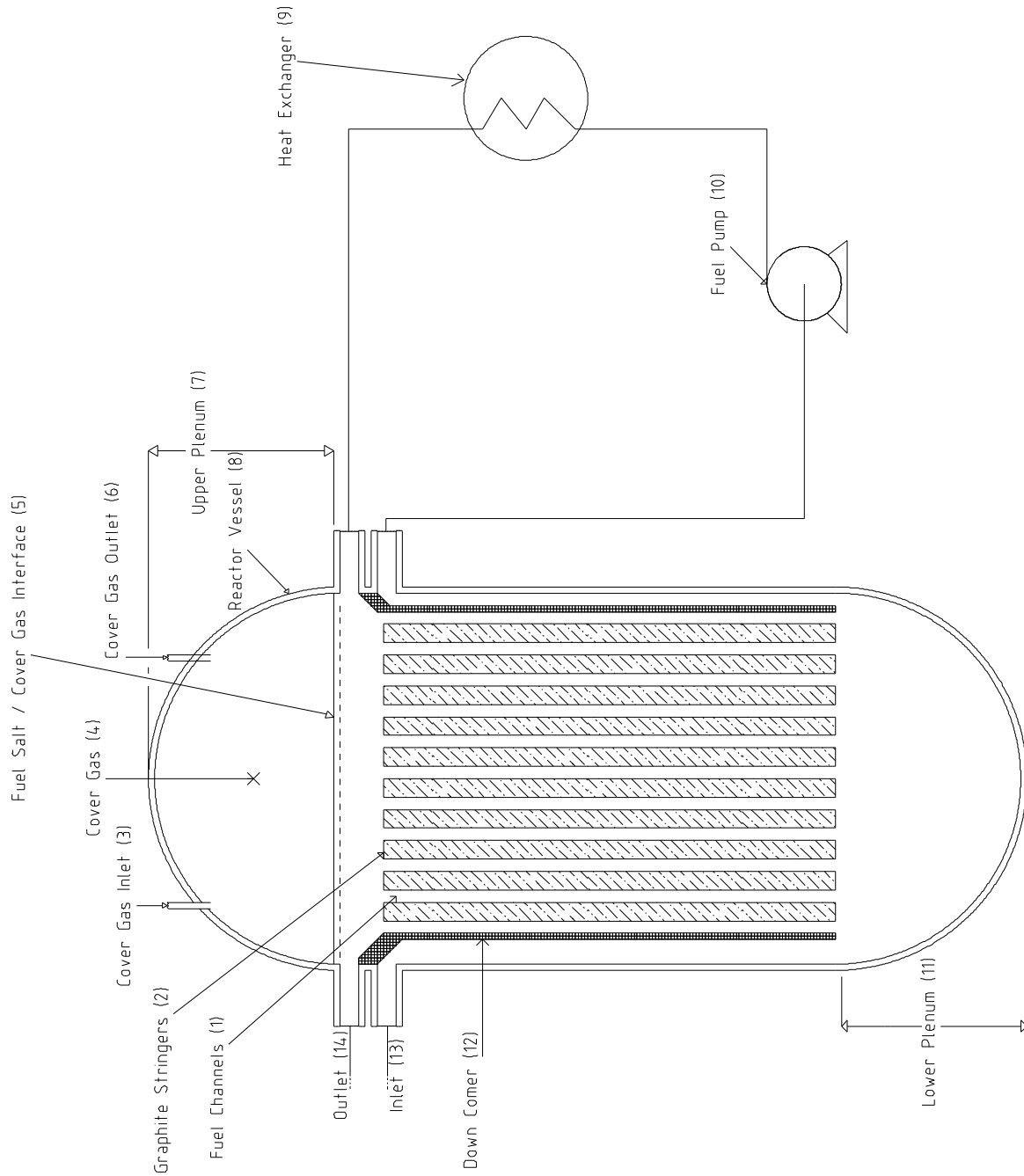
Figure 1.1: A diagram of a molten salt reactor that illustrates its major components
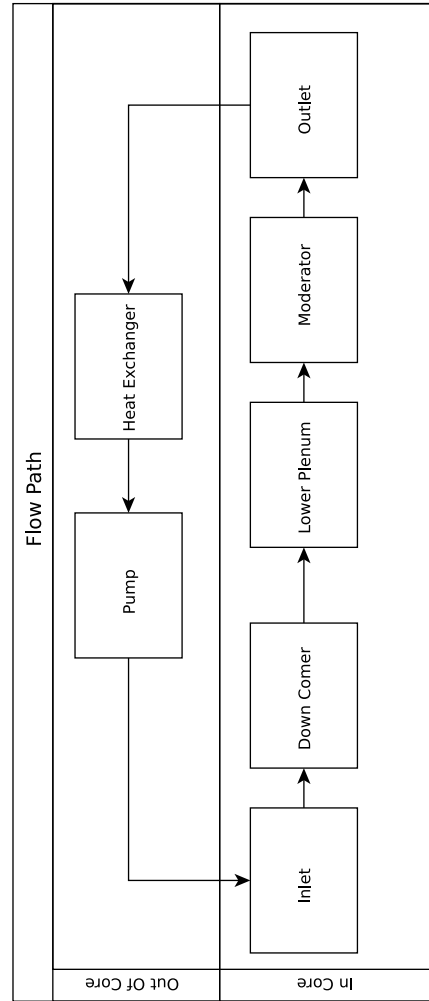
Figure 1.2: A diagram of a molten salt reactor flow path that illustrates the path the fuel salt takes and subdivides the core into in core and out of core regions.

1.3.2   Previous Reactors

There have been three molten salt reactors built to date:

- the Aircraft Reactor Experiment (ARE)[2], a $2.5\,\mathrm{MW}_{th}$ experimental propulsion unit for use in a nuclear powered bomber aircraft – operated in 1954,

- the Pratt & Whitney Aircraft Reactor 1 (PWAR1), a zero-power experimental pile – operated in 1957,

- the Molten Salt Reactor Experiment (MSRE) A $7.4\,\mathrm{MW}_{th}$ experimental reactor – operated 1964-1969.

All of these reactors were operated at ORNL in Oak Ridge, Tennessee and are experimental (not production designs).

In addition to these three reactors there were additional research efforts, which never reached the construction phase. These *paper reactors* include:

- the Molten Salt Fast Reactor (MSFR), fast-spectrum MSRs, reported in 1956,

- the Molten Salt Breeder Reactorss (MSBRs), a series of breeding Molten Salt Reactors (MSRs), including a single and dual fluid variety, reported in 1966,

- the Molten Salt Demonstration Reactor (MSDR), a $350\,\mathrm{MW}_e$ power producing reactor, reported in 1971,

- the Denatured Molten Salt Reactor (DMSR), a $1000\ \mathrm{MW}_e$ proliferation resistant molten reactor reported in 1980.

Roughly speaking, there have been three distinct phases of MSR development. The first phase, which lasted roughly from 1953-1959 was primarily focused on the development of MSRs for military aircraft propulsion. Key projects in this first phase included the ARE

---

[2]Note: some literature was found which appear to refer to the ARE as the *Fused Salt Reactor Experiment*

and PWAR-1 reactors. Many development activities were military in origin or under the auspices of the aec. The second era of MSR development activities was focused on civilian applications of MSRs and lasted roughly from 1960-1980. During this time, the MSRE was developed, and conceptual work was done on the MSBRs; this era concluded with work on the DMSR. In the period between 1980 to 2000, comparatively little work was done in the field of MSRs. On the subject of the discontinuation of the MSR at Oak Ridge National Laboratory, Alvin Weinberg, the director of the lab during much of its involvement with the MSRs, wrote in his 1994 autobiography,

> "Why didn't the molten-salt system, so elegant and so well thought-out prevail? I've already given the political reason: that the fast breeder arrived first and was therefore able to consolidate its political position within the AEC. But there was another, more technical reason. The molten-salt technology is entirely different from the technology of any other reactor. To the inexperienced, molten-salt technology is daunting. This certainly seemed to be Milton Shaw's attitude towards molten salts – and he after all was the director of reactor development at the AEC during the molten-salt development. Perhaps the moral to be drawn is that a technology that differs too much from an existing technology has not one hurdle to overcome – to demonstrate its feasibility – but another, even greater one – to convince influential individuals and organizations who are intellectually and emotionally attached to a different technology that they should adopt the new path. This, the molten-salt system could not do. It was a successful technology that was dropped because it was too different from the main lines of reactor development. But if weakness in other systems are eventually revealed, I hope that in a second nuclear era, the molten-salt technology will be resurrected." [5, p.130]

Bruce Hoglund has also posted commentary on why the MSR program was abandoned on his website in a 2010 essay titled "Why the Molten Salt Reactor (MSR) Was Not Developed

by the USA". [6]

1.3.3   Involvement in Generation IV

A resurgence in interest in MSRs is seen, starting in the early 2000s. One paper written in this third period of development was David LeBlanc's 2010 paper *Molten salt reactors: A new beginning for an old idea* [7] which concluded the prior work on MSRs had reduced research and development needs to *"far less than many may imagine"*.

Since then, the molten salt reactor technology has been under active development, and it is being actively considered for deployment within the Generation-IV nuclear power program. [8]

1.4   Xenon 135

1.4.1   History and Significance of Xenon

The following history is summarized from the account by Richard Rhodes [9].

The importance of Xe-135 in the operation of nuclear reactors was discovered early in the history of the field. Although the earliest, low power, reactors did not encounter any operating experience with xenon poisoning, the problem revealed itself when the 250 MW_{th} Hanford B reactor began operation in 1945. The reactor achieved initial criticality in the Morning of September 26, 1945 and operated normally throughout the work day. In the evening, after the project scientists had gone home, the reactor power level began dropping. Operators began removing control rods to attempt to raise reactor power, however, by early morning on the 27th, the reactor had effectively shut down.

The next day, the reactor began to mysteriously regain power, however by the evening of that day the reactor shut down again. Scientists, at the time, were aware of the possibility of fission product poisoning, but were unsure as to how exactly it would occur. Project

physicist John A. Wheeler searched the table of isotopes and after numerous calculations, finally concluded that it was the chain of I-135 and Xe-135 explained the observed *breathing* behavior of the reactor.

General Groves, the military command of the Manhattan project was informed of the issue by Arthur Compton, and reportedly took the news *acidly.* Compton was reported to have apologized to Groves for a *"fundamentally new discovery regarding the neutron properties of matter"*[3].

Regardless of what particular type of reactor is operating, so long as nuclear fission takes place, xenon 135 will be produced. This makes its study, description, and production highly important to the successful operation of nuclear reactor. Fluid fuel reactors, such as a molten salt reactor, are unique in that the xenon generated through nuclear fission can migrate about the reactor on account of the fluid nature of both the fuel salt (liquid) and the xenon (gas).

1.4.2 Evolution of Xe-135

The production and decay of Xe-135 is typically modeled with the production and decay of Te-135 and I-135, shown in Figure 1.3. Xe-135 (8) enters the system either direction through fission production (7) or from the decay of I-135 (6). Xe-135 exists the system either when it beta decays (12) to Cs-135 with a characteristic 9.1 h half life or it absorbs a neutron (9) and transmutes into Xe-136. I-135 (5) is a progenitor of Xe-135 and beta decays into it with a characteristic half life of 6.57 h. I-135 can either be produced directly from fission (4), or from the decay of Te-135 (2). Te-135 is produced by fission (1) and has a characteristic half life (3) of 19 s. During the early modeling efforts of xenon in the MSRE, Te-135 hadn't been separated from I-135 yet, and many reports either omit its existence or have the wrong half life for Te-135. The majority of Xe-135 in the system comes from the decay of I-135 rather than direct fission production since the fission yields for Te-135 and I-135 are about an order

---

[3]See 'The Making of the Atomic Bomb' by R. Rhodes for more information
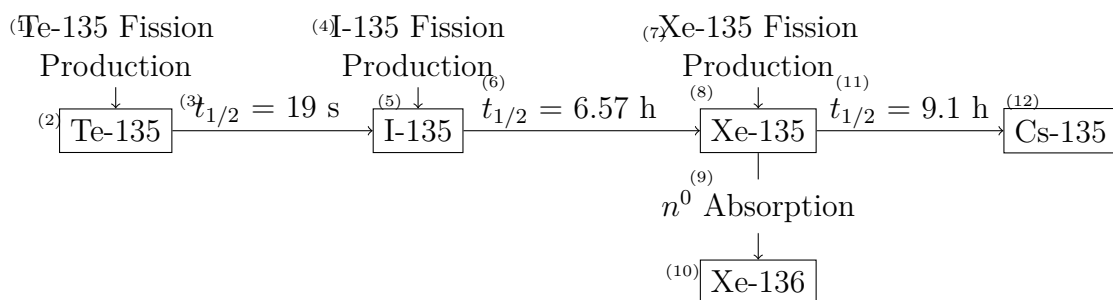
Figure 1.3: Illustration of xenon decay chain

of magnitude greater than that for Xe-135.

1.4.3 Properties of Xe-135

Xe-135 is unusual in that it has an extremely large thermal neutron absorption cross section — usually cited as around 2.6 Mb (see [10]). This is because neutron capture in a Xe-135 nucleus will give the nucleus 82 (a so called *magic number*) neutrons which will complete its neutron shell.

Due to the quantum mechanical and electronic properties of atomic xenon, the question *"What is the size of a xenon atom?"* is a question in of itself. That is to say, since a xenon atom is not a solid physical object, what is it that we mean when we say *"the size of a xenon atom"*? This sentiment is reflected in Pau, Berg, and McMillan's 1990 paper on the application of Stoke's law to ions in aqueous solution,

> "One of the most difficult questions involved in the transition from a continuum medium to the case of real solvent molecules of size comparable to the atomic dimensions of the mobile ion is unit is the meaning to be attached to the particle 'radius'." [11]

Table 1.4.3 lists some radii of xenon from various sources. Blander, Grimes, Smith and Watson report the radii of rare gas atoms in a solid would be a lower limit of a hole created

Type	Radius [Å]	Reference
Covalent Radius	1.36	[13, p. 9-58]
van der Waal's Radius	2.16	[ibid.]
Lennard-Jones Collision Radius	2.02	[14, p.24]
Grimes, Blander, Watson	2.18	[12]
Kinetic Theory	1.75	[15, p. 249]

Table 1.2: Atomic Radii of Xenon

by a gas atom in a molten salt. [12]

1.4.4   Poisoning Effects in Nuclear Reactors

When Xe-135 accumulates in a nuclear reactor, it is said to *poison* the reactor. When a nuclear reactor undergoes a power maneuver in which power is lowered, the quantity of xenon in a reactor follows a characteristic curve in which the quantity of Xe-135 in the reactor temporarily increases beyond its steady state value for a period of several hours before decaying away. The period in time in which the xenon is above its steady state value is known as the *iodine pit* [4]. If the height of this iodine pit is large enough, the reactor will *poison out.* since the reactivity control mechanisms cannot compensate for the negative reactivity introduced by the xenon.

1.5   Xenon in Molten Salt Reactors

This section provides a brief overview of the behavior of Xenon in MSRs. For a full review, see [2].

1.5.1   The Overall Theory of Xenon in Molten Salt Reactors

Figure 1.4 illustrates the overall behavior of xenon in an MSR. As described in Subsection 1.4.2, xenon enters the system in the fuel salt through the Te-I-Xe (135) decay chain

---

[4]A pit rather than a hill since the xenon introduces negative reactivity. When the reactivity contribution from Xe-135 is plotted with respect to time, it produces a characteristic *pit* shape.
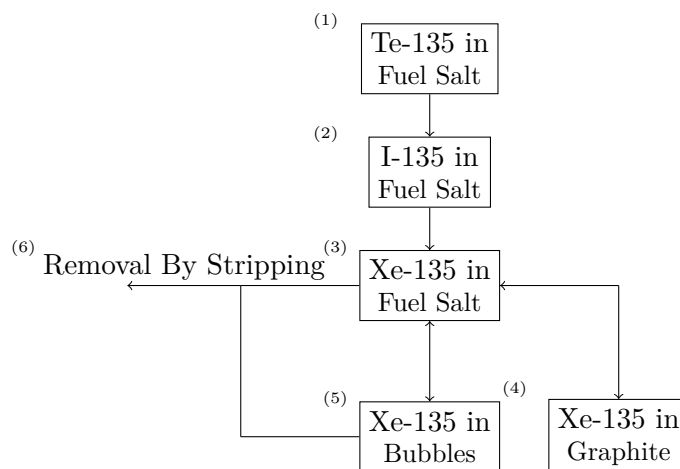
Figure 1.4: Overview of xenon migration in an MSR

— (1), (2), and (3). Xenon enters the system in the fuel salt (3) and is then free to migrate between the fuel salt and the bubbles[5], (5), or the fuel salt and the graphite, (4). Some early work, ORNL-TM-3464 [3], hypothesized bubbles may be able to ingress indirectly into the graphite, but we think this unlikely considering during normal operation, the graphite is hotter than the fuel salt (and therefore, presumably, the bubbles as well). Xenon in either the bubbles or the fuel salt is then removed by the xenon stripper, (6), which in the design of the Molten Salt Reactor Experiment, was located outside of the reactor core inside of the pump bowl.

According to Henry's law, there is a preference for dissolved gas species to favour the gas phase over the liquid phase, and therefore, a minority of xenon will be found dissolved in the fuel salt itself. Furthermore, the mass transfer coefficient on the bubbles is significantly larger than that of the graphite and therefore, most of the xenon will be found in the circulating voids.

---

[5]The bubbles are also called the *circulating voids* elsewhere in the literature.

1.5.2   The In Solution Assumption

One of the more interesting aspects of the Xe-135 decay chain (shown in Figure 1.3) is that Xe-135 is a noble gas at MSR operational temperatures whereas Te-135 and I-135 are either solids or liquids. We therefore use the *in solution assumption* in our analysis of MSR xenon behavior. The in solution assumption states that Te-135 and I-135 remain dissolved in the fuel salt whereas the Xe-135 is free to migrate. Experimental evidence in the MSRE indicates this assumption is valid and is discussed in further detail in ORNL-TM-3464 [3].

1.5.3   The Ideal Dilute Solution Assumption and Henry's Law

The mass transfer equations used in MSR xenon theory make ample use of Henry's law to relate the liquid and gas phase xenon concentrations. Formally, Henry's law is defined as,

$$\lim_{C_i \to 0} H_i = \frac{C_i}{p_i}, \tag{1.8}$$

where C_i is the concentration of species i in the liquid phase and p_i is the partial pressure of species i in the gas phase. Note, Henry's law is defined for when the concentration of the dissolved species in the liquid phase approaches zero, which is the definition of an *ideal dilute solution*. Therefore, the fuel salt in MSR xenon analysis is assumed to act as an ideal dilute solution so as to allow for the application of Henry's law.

1.5.4   Transfer Coefficients and Dimensionless Numbers

All mass transfer processes used in this model are governed by so called *mass transfer coefficients* or mass velocities (due to their usual units, m/s), typically denoted k_m. Specifically, these transfer coefficients are the *overall mass transfer coefficients* in that they account for both side of a liquid / gas interface. An overall mass transfer coefficient, in the case of a liquid gas interface, is approximately the same as the liquid side mass transfer coefficient

since diffusive processes on the gas side occur at time scales much faster than that which is found on the liquid side — essentially, diffusion on the gaseous side is instantaneous.

Mass transfer coefficients are predicted through experimentally determined *mass transfer correlations*, which typically provide the Sherwood number Sh, as a function of the Reynolds number, Re, and the Schmidt number, Sc,

$$Sh = f(Re, Sc). \tag{1.9}$$

The Sherwood, Reynolds and Schmidt numbers are all known as *dimensionless numbers* since they have no units associated with them, i.e., they are dimensionless. The Reynolds number is a property of both fluid properties (thermophysical properties) as well as flow velocity (i.e. flow conditions), whereas the Schmidt number is a property of material properties alone. The Sherwood number, Sh, is the ratio of convective to diffusive mass transfer and is expressed as,

$$Sh = \frac{k_m}{D/L}, \tag{1.10}$$

where k_m is the mass transfer coefficient, D is the mass diffusion coefficient, and L is the characteristic length of the system. Multiplication of the Sherwood number by the mass diffusion coefficient, D, and division by the characteristic length of the system, L, yields the mass transfer coeffeicnt, k_m.

The Reynolds number is the ratio of inertial to viscous forces in a fluid flow. It's calculated by,

$$Re = \frac{\rho u L}{\mu}, \tag{1.11}$$

where ρ is the density of the fluid in which the flow is taking place, u is the flow velocity of the fluid, L is the characteristic length of the system, and μ is the viscosity of the fluid of the flow.

Finally, the Scmidt number, Sc, is the ratio of viscous diffusion to mass diffusion, and is

determined through,

$$Sc = \frac{\mu}{\rho D}. \tag{1.12}$$

More information on dimensionless numbers and mass transfer coefficients can be found in numerous chemical engineering text books such as Sherwood's book, [16], on the subject.

1.5.5 Migration Into Graphite

The graphite moderator in many MSR designs, including the MSRE, is not a solid block of graphite, but, rather, is a porous matrix of compressed and bound graphite particles. The space between these particles is called the *pore space* or *void space* and occupied about 10% of the volume of the MSRE graphite. The pores of the MSRE graphite were sufficiently small (1 μm to 3 μm, see ORNL-4148 [17]) that fuel salt could not penetrate into the pore space. Since xenon is a gas, it is assumed to be able to come out of solution and migrate into the graphite pore space.

Since fuel salt does not penetrate into the graphite, there is no xenon nor xenon progenitor production within the graphite, and all xenon within the graphite originated from the fuel salt. The xenon, however, is still subject to decay and burnout processes.

The migration of xenon into the graphite stringer is modeled by the expression,

$$J = k_m \left(C_L - \frac{HRT}{\epsilon} C_{Gr} \right), \tag{1.13}$$

which is derived from Fick's law for Porous media.

Although some work, such as ORNL-TM-3464 [3], has used a lumped volume approach to modeling mass transfer to graphite stringers, this model uses a transient reaction diffusion equation in cylindrical coordinates,

$$\frac{\partial C_{Xe}}{\partial t} = \frac{D_g}{\epsilon} \left(\frac{\partial^2 C_{Xe}}{\partial r^2} + \frac{1}{r} \frac{\partial C_{Xe}}{\partial r} \right) - \left(\sigma_a^{Xe} \phi + \lambda_{Xe} \right) C_{Xe}, \tag{1.14}$$

where ϕ is the neutron flux within the graphite stringer itself (note, the graphite neutron flux is different than the fuel salt neutron flux).

1.5.6   Migration into Bubbles

Migration of xenon into the bubbles is modeled by,

$$J = k_m(C_L - HRTC_B). \tag{1.15}$$

The bubbles are assumed to be sufficiently small and diffusive and advective processes within the bubbles sufficiently fast that they can be modeled with a lumped volume approach.

The bubble surface area is calculated through a *reference diameter* in which the total gas volume in the reactor is divided into a number of spherical bubbles with diameters equal to the reference diameter and the mass transfer area found by determining the total surface area for all of those bubbles.

1.5.7   Xenon Stripping

The xenon stripper removes xenon by spraying fuel salt through numerous small holes on the xenon stripper into a pool of fuel salt. The increased surface area of the xenon stripper allows the fuel salt to contact the cover gas and subsequently expel the xenon through mass transfer.

The xenon stripper operation is characterized by three variables, the volumetric flow rate, $\dot{Q}$, of the stripper, the bubble stripping efficiency, η_B, and the fuel salt stripping efficiency, η_{FS}.

The rate of removal of xenon from the fuel salt is calculated through,

$$\dot{N}_{Xe}^{FS. \ Strpr.} = \eta_{FS} C_{Xe}^{FS} \dot{Q}^{Strpr.}, \tag{1.16}$$

and the rate of removal of xenon from the bubble phase is calculated through,

$$\dot{N}_{Xe}^{B.Strpr.} = \eta_B C_B V_B^1 \dot{Q}^{Strpr.} C_{Xe}^B.$$

(1.17)

1.6 Summary and Chapter Conclusion

This chapter has aimed to present the reader with information necessary to understand the rest of the thesis and has done so by laying out a minimal primer on the background theory required to understand the work. A brief primer on reactor theory is provided for the sake of completeness and to ensure the reader and the author have a common frame of reference for the forthcoming discussion[6] Molten salt reactors are described at a conceptual level and previous reactors, both experimental and constructed, have been reviewed. The history, evolution, and properties of Xe-135 have been discussed along with a brief explanation on how it effects nuclear reactors.

Finally, the behavior of xenon in MSRs has been described. This is, to the best of our knowledge, the first primer on MSR xenon behavior written since ORNL-4541 [18] in 1971 and includes several aspects not discussed in ORNL-4541. The in solution assumption for tellurium and iodine is described along with the ideal dilute solution assumption. Migration of xenon into graphite and the circulating voids is also discussed. The action of the xenon stripper is described.

---

[6]It also seems *right* to start a nuclear engineering thesis at the level of atoms.

CHAPTER 2

Literature Collection and Review

2.1 Introduction

With necessary background information now presented to understand the rest of the thesis, this chapter presents work related to the literature review that was performed. The bulk of the literature review for this thesis is documented in several papers at various stages of publication:

- *"Molten Salt Reaction Xenon Analysis"*, accepted for publication in 2020 in the Journal of Nuclear Engineering and Radiation Science by the American Society of Mechanical Engineers (ASME), coauthored with O. Chvala and R. Taylor

- *"A Review of Molten Salt Reactor Xenon Analysis Literature"*, accepted for publication in 2020 in the Journal of Nuclear Engineering and Radiation Science by theASME, coauthored with O. Chvala.

- *A Review of Circulating Voids and Gaseous Fission Product Behavior In Molten Salt Reactors*, under review with the Journal of Nuclear Engineering and Radiation Science by the ASME, coauthored with O. Chvala and R. Taylor

- *Xenon in Molten Salt Reactors: The Effects of Solubility, Circulating Particulate, Ionization, and the Sensitivity of the Circulating Void Fraction*, under review with the Journal of Nuclear Engineering and Technology , coauthored with O. Chvala and R. Taylor

We would like to note that since this point in molten salt reactor research and development efforts, more work has been done prior to 1970 than after 2004, it seems reasonable that a large portion of any thesis written on molten salt reactors ought to be a literature review.

Regardless, we present, herein, our collection of literature related to molten salt reactor xenon analysis as well as a concise literature review related to modeling efforts. The chapter concludes by describing how the work presented in this thesis fits in and relates to the existing corpus of work.

The objective of this chapter is to demonstrate that a substantial effort has been undertaken to understand prior work done in the field and therefore substantiate the claim that the work presented later is fundamentally new work.

2.2 Collection of Literature

Throughout this project a large database of literature related to MSR xenon behavior had been collected. This database, as far as we can tell, is the first time in the entire history of the field that all the literature related to xenon in molten salt reactors had been assembled in one place.

It would be a loss to science if a record of this database wasn't kept somewhere, so we've included it here as an annex to this thesis. The table in the Appendix provides a listing of literature found related to MSR xenon behavior. It is primarily comprised of ORNL reports, but also contains some papers from academia. Our review indicates, this table is the largest and most complete listing of MSR xenon analysis literature available.

2.3 State of The Art of MSR Xenon Behavior Modeling

Modeling of Xenon in molten salt reactors began in 1956 with the work of Robertson [19]. The xenon models developed by Robertson performed both transient and steady state calculations and postulated that xenon behavior in the ARE could be modeled with a single gas compartment and a single liquid compartment. Xenon was transferred between these two compartments through *phase transfer constants* rather than the near ubiquitous application of Henry's law and mass transfer coefficients present in later models. Functionality was also implemented xenon stripping along with the traditional burnup and decay mechanisms were also implemented. Note at this point, Te-135 hadn't been isolated from I-135, and therefore only I-135 was implemented as a progenitor to Xe-135.

The next major work was in 1961 by Miller [20] who developed the first MSR xenon model to consider graphite behavior and use Henry's law to relate the gas phase and liquid phase xenon concentrations. The graphite behavior was modeled with a reaction diffusion equation in slab geometry and mass transfer between the graphite and fuel salt was governed by a Dittus Bottler (introduced by Churchill) like heat transfer correlation which had been transformed into a mass transfer correlation using a heat / mass transfer analogy. This model only calculated steady state solutions and was incapable of generating transient solutions.

In 1964, Haubenreich, Engel, and Prince [21] reported on the development of a *"set of simultaneous differential equations"* to describe MSRE xenon behavior. The report states the equations account for radial and axial variation in fuel flow as well as a distribution of neutron flux. The actual equations themselves were not reported, but it was reported that an *"approximate analysis"* was made in which the full set of equations were reduced to include only the major mechanisms and the core was discretized into four radial regions. A steady state solution was generated for this approximate analysis. In our review of the literature,the full version of this model is potentially the most detailed MSR xenon model that had been generated up to that point and it is a tragedy that it has likely been lost to

history.

A brief treatment of steady state xenon behavior in a molten salt chloride reactor (MSCR) was presented by Alexander in 1965 [22] (section by Alexander, report authored by Alexander, Carter, Craven, Janney, Kerlin, and Van Winkle). The model included considerations for graphite diffusion, iodine decay, sparging, and used Henry's law to relate the gas phase and liquid phase xenon concentrations.

in 1966 Ball [23] reported on the development of a real time analog simulator for the MSRE which included a three compartment xenon model. The model tracked iodine content, fuel salt xenon content, and xenon in the graphite. Xenon was produced through iodine decay and was removed from the system through decay, burnup, or stripping or transferred into graphite through diffusion where it under went either burnup or decay.

A reactivity dynamics model of the MSRE was developed in also in 1966 by Ball and Kerlin [24]. The model was formulated as a set of four simultaneous ordinary differential equations and included considerations for iodine, decay, burnup, and absorption into graphite. The model generated transient solutions and was integrated into an overall dynamics model of MSRE nuclear behavior.

One of the most significant MSR xenon modeling efforts was reported in 1967 by Kedl and Houtzel [25]. Their model was a steady state model which calculated xenon poisoning in the MSRE using a 72 node discretization of the core. This model was the first to include the production of Te-135 separately from iodine, however, the half life used in their calculations was about 10 seconds longer than the currently accepted half life of $19\,\text{s}$. The graphite stringers were modeled using a reaction diffusion equation in cylindrical coordinates and considerations for a flux profile, burn up, decay, and xenon stripping were included. This model was also the first to consider the effects of mass transfer into bubbles and was the first to demonstrate the major effect bubbles would have on xenon behavior.

The next major modeling effort was reported by Engel and Steffy in 1971 [3]. The model was a lumped parameter model that was capable of generating both transient and steady

state solutions. Graphite was modeled using a lumped volume model and lumped volumes were used for in core, pump bowl and out of core behavior of xenon. The out of core region was further discretized into a regions going to, and coming from, the fuel pump. Each lumped volume was subdivided into a lumped volume for liquid fuel salt and a circulating gas phase. The model included a xenon stripper as well. Attempts were made to fit the model to experimental data, however, no one parameter set could be used to reasonably explain all observed transient and steady state conditions. This inconsistency is important in this thesis since the model developed herein appears to resolve this inconsistency.

The next modeling effort was done by Shimazu [26] in 1977 and was the first piece of work done on MSR xenon behavior done outside of ORNL. The model included considerations for bubble behavior, graphite behavior and xenon stripping, and generated transient solutions for a molten salt breeder reactor. The model was the first to couple a solution to a annular reaction diffusion equation into a set of simultaneous ordinary differential equations describing xenon behavior in the rest of the reactor.

At this point, the field effectively fell silent for the next 27 years.

Then in 2004, Suzuki and Shimazu [27] published a paper which coupled Shimazu's 1977 xenon model into a nuclear kinetics model to study potential control systems for a MSR. There was fundamentally nothing new in this model, however, it did serve to signal that there was renewed interest in the field.

In 2016, Eades, Chaleff, Venneri, and Blue [4] studied the effects of Xe-135m on xenon poisoning in an MSR. When the original MSR xenon models were produced, there was no available data describing the Xe-135m neutron absorption cross section, or how it would affect xenon poisoning in an MSR. 1D and 0D models of MSR xenon behavior were developed and transient scenarios were run with both of them. The paper concluded that there was good agreement between 0D and 1D models of MSR xenon behavior and Xe-135m did have a significant impact on steady state xenon behavior.

Although the work of Chen, Ruimin, Jongh, and Guimin [28] in 2017 is presented in

Chinese, it appears to have modified the ORNL-TM-3464 xenon model and applied it to the Chinese Thorium Molten Salt Reactor Liquid Fuel (TMSR-LF). An English translation of this paper would be beneficial.

The work of Wu, Guo, Cai, Yu Zou, Han, and Chen [29] presents a one dimensional model of MSR xenon behavior and investigates the effects of perturbation in flow rate on transient xenon behavior. This model is unique and a similar model does not appear anywhere in the ORNL literature. This work was extended in 2018 [30] to include the effects of helium bubbling on the xenon behavior.

Finally, in 2018, Taylor, Salko, and Colins [31] implemented general species transport in the CASL VERA reactor physics code which allowed the code to implement xenon transport.

2.4   How This Work Fits In

ORNL-TM-3464 [3] was the first multi-region lumped volume xenon model. The work by Shimazu [26] was the first transient xenon model to model xenon behavior in the graphite with a reaction diffusion equation. This model builds off of both of these models — it is a lumped volume model which models graphite behavior through a reaction diffusion equation.

Additionally, this model implements something never before attempted, all of the model subsystems account for the effects of temperature on the xenon within the subsystems. This allows for the calculation of all system properties as functions of temperature and hence allows the investigation into the thermal behavior of the system. Furthermore, by implementing the code in the modern system dynamics software, Simulink, the possibility is opened for numerous types of non linear analyses which would have been previously impractical to compute.

2.5   The Lack of Validation

This review of literature has not been able to find anything that would indicate a model that could be reasonably be said to be *'validated'* has been generated. Indeed, the model that has come closest to validation appears to be the ORNL-TM-3464 [3] xenon model, which had difficulty fitting the model to experimental results (see the comentary in the introduction for more information).

2.6   Summary and Conclusion

Ultimately, the literature review has shown that, although numerous efforts have been made in developing kinetic MSR xenon models, no prior efforts have been made in developing a thermal dynamical model. Furthermore, no modeling efforts have been found that could reasonably be said to be validated.

A substantial effort has been undertaken to understand prior work done in the field and has done by presenting a review of literature related to MSR xenon modeling efforts. A database of literature collected during the course of the work has been presented. The first state of the art of MSR xenon modeling efforts has been written and presented in this chapter. Finally, the way in which the dynamic model fits into the corpus of existing work has been described. The next chapter will describe how the model works.

CHAPTER 3

Model Description

3.1 Introduction

The prior chapter has established the environment in which the current model is presented in. This chapter presents a description of the dynamical model that is the main output of this research. Since descriptions of software programs are invariably lacking[1], the reader may also examine the model at the corresponding Github repository [32].

The objective of this chapter is to provide a technical description of the model from which the results of the model were generated and thereby bolster claims of transparency in research and assist in efforts to reproduce the model.

The model calculates the rates of Xe-135, I-135, and Te-135 production using a macroscopic fission cross sections. This cross section was generated using a Serpent 2 [33] model of the MSRE. A description of this model is provided in Section 3.2.

Xe-135 is generated both directly from fission as well as from the decay of I-135 and Te-135. The behavior of Te-135 and I-135 behavior were accounted for in the progenitor subsystem, discussed in Section 3.3.

The fuel salt subsystem, discussed in Section 3.4, handles the xenon behavior within

---

[1]Describing how software is made is a lot like describing architecture, the language of architecture is architecture itself and the language of software is software itself.

the fuel salt itself, including migration to and from the fuel salt from the bubbles and graphite. The fuel salt is divided into a number of regions (lumped volumes), each with its own set of temperature dependent thermophysical properties and dimensionless numbers. The lumped volume subsystem is discussed in Section 3.6 and the dimensionless numbers are discussed in Section 3.5. The xenon behavior within the graphite is computed with the graphite subsystem, discussed in Section 3.10. The bubble subsystem, discussed in Section 3.8, computes the behavior of xenon within the circulating voids. Finally, the xenon stripper subsystem, discussed in Section 3.9, accounts for removal of xenon through the xenon stripper. The total xenon content in the fuel salt, bubbles, and graphite are weighted and summed by reactivity coefficients that transform xenon concentrations in the system into a xenon reactivity defect which can then be benchmarked.

3.2   Serpent Model

The macroscopic fission cross section of the MSRE was a parameter that was not found elsewhere in literature. Therefore, it was generated using a model of the MSRE, built from reference data, using the Serpent 2 reactor physics code.

Serpent 2 is a three dimensional, continuous energy, monte carlo reactor physics code capable of numerous calculations including the effective neutron multiplication factor, k_{eff}, as well as from homogenized group constants such as the one group macroscopic fission cross section, Σ_f, used in this model [33].

Information about the validation of the Serpent code is provided in [34]. Of interest to our efforts, §4.3 ¶1 of [Ibid.] states, the Seprent code was found to be in good agreement with the Benchmark for Evaluation And Validation of Reactor Simulations (BEAVRS) benchmark, a pressurized water reactor benchmark case set up by the Massachusetts Institute of Technology (MIT) Computational Reactor Physics Group (CRPG) [35].

A cross sectional visualization of the the Serpent 2 model is shown in Figure 3.1. The

figure shows a top view as well as a side view cut at the mid plane. The model was developed by a University of Tennessee student, Gavin Ridley, using available reference data from ORNL-TM-0728 [36]. The code for the model is available online at Gavin's MSRE Github Repository [37].
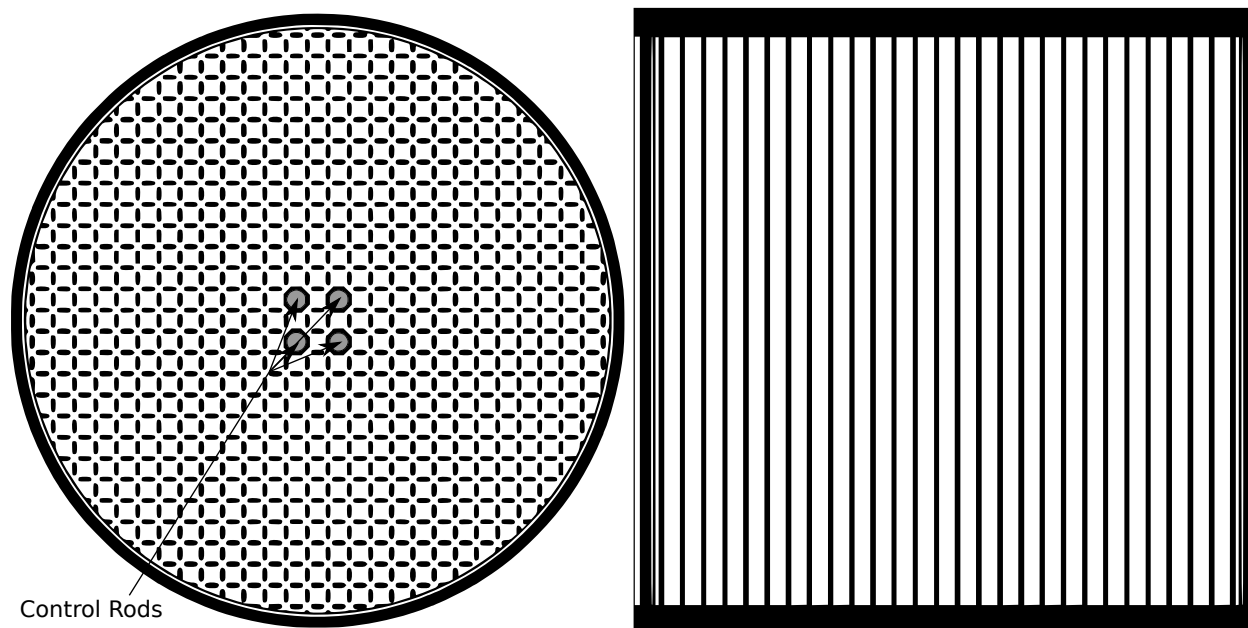
Figure 3.1: Visualization of Serpent MSRE model; top and side view, cut through the center plane. The control rods are shown by the four gray circles in the center of the top view.

Benchmarking of the Serpent model was done by modeling control rods in the reactor and comparing the calculated rod worths to measurements reported in ORNL-TM-0728 [36], page 101. Table 3.2 shows the results of this benchmarking. Although the calculated rod worths are, apparently, near the reported rod worths, the two figures are not within the error bounds of the calculated worths. This could be caused by numerous factors such as omissions made during modeling — the MSRE data we have available is not benchmark reference data; rather, it's data from technical reports that are, in themselves, imperfect.

The macroscopic fission cross section generated using this model was evaluated to be $0.15\,(\mathrm{m}^{-1})$, and it was this value that was used in the Xenon model implemented in Simulink.

No. Rods Inserted	k_{eff}	Error [±pcm]	Calculated Worth [pcm]	Reported Worth [pcm]
0	1.04735	34		
1	1.0169	31	3.045×10^3	2.8×10^3
2	0.99323	35	5.412×10^3	5.0×10^3
3	0.97324	39	7.411×10^3	6.7×10^3

Table 3.1: Results of Serpent 2 control rod worth simulations with data from ORNL-TM-0728 with 35% ^{235}U fuel.

3.3 Progenitor Subsystem
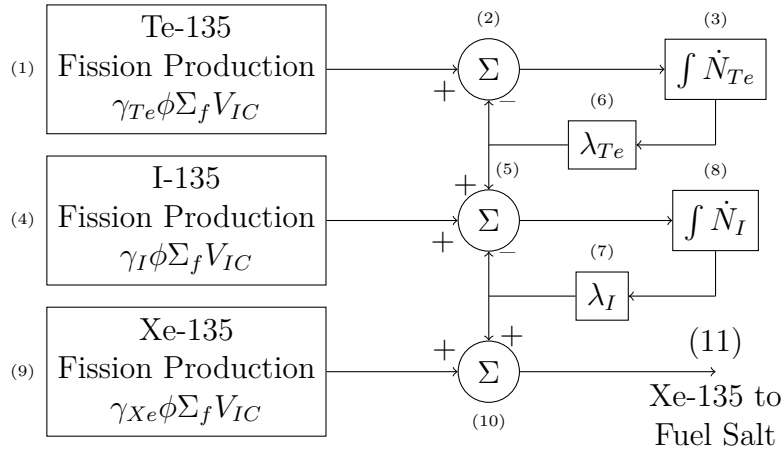
Figure 3.2: Illustration of progenitor subsystem

An illustration of the xenon progenitor subsystem is shown in Figure 3.2. The progenitors system implements the *in solution assumption* in which Te-135 and I-135 are both assumed to remain in solution as a homogeneous mixture. The subsystem tracks the total quantity of Te-135 and I-135 in the fuel salt rather than its concentration.

The isotopes, Te-135, I-135, and Xe-135 are all produced by fission in blocks (1), (4), and (8) respectively. Production of an isotope, i, is governed by an equation of the form,

$$\dot{N}_i = \gamma_i \phi \Sigma_f V_{IC}, \tag{3.1}$$

where γ_i is the fission yield for isotope i, ϕ is the neutron flux, Σ_f is the macroscopic fission

Isotope	Fission Yield
Te-135	3.22×10^{-2}
I-135	2.94×10^{-2}
Xe-135	2.57×10^{-3}

All yields from [38].

Table 3.2: Fission product yields for U-235 used in the dynamic model

cross section, and V_{IC} is the in-core volume. The fission yields used assume the fissioning isotope was pure U-235 with no U-238 — i.e. the fission yields were taken from U-235 data.. The fission yields for the poison isotopes are shown in Table 3.3. The neutron flux, ϕ, at full power, was taken to be the average thermal neutron flux of $1.5 \times 10^{17}\,\mathrm{m^{-1}\,s^{-2}}$ described in ORNL-TM-0728 [36, p. 101]. The macroscopic fission cross section, Σ_f, was a one group cross section generated using the Serpent model described in Section 3.2. The in-core volume, V_{IC} was $1.29\,\mathrm{m^3}$, and was calculated by summing the *"core"*, *"lower head"*, and *"upper head"* volumes described in ORNL-TM-0728 [36], page 102. (More details on the volumes used in the model are provided in Section 3.6) The rationale behind including the upper and lower head volumes in the model's in-core volume is that the *"core"* volume described in ORNL-TM-0728 is taken to be the fuel salt volume between the upper and lower planes of the graphite stringers (i.e. that which is inside the fuel channels only) whereas it is assumed the neutron flux in the upper and lower heads (plenum) is non-negligible and should be factored into any production calculations.

The quantity of Te-135 and I-135 in the system is tracked by the integrators shown in blocks (3) and (8) respectively. The decay of isotope, i, is accounted for by using the radioactive decay law,

$$\dot{N}_i = -\lambda_i N_i, \tag{3.2}$$

where N_i is the quantity of isotope i and the λ_i is its decay constant which can be found from the half life using $\lambda_i = ln(2)/t^i_{1/2}$. This is implemented in blocks (6) and (7) respectively. The half life data used in the model is shown in Table 3.3.

The rate of accumulation of a poison isotope is the difference between the fission pro-

Isotope	Half Life	Decay Constant (s^{-1})
Te-135	19 s	3.65×10^{-2}
I-135	6.57 h	2.9306×10^{-5}
Xe-135	9.2 h	2.0924×10^{-5}

Data can be found in numerous sources such as [39].

Table 3.3: Half life data used in the dynamic model

duction rate and its decay rate. This is implemented in blocks (2) and (5) for Te-135 and I-135 respectively. Decay of Xe-135 is accounted for by the fuel salt, graphite, and bubble models respectively, and therefore is not implemented in the progenitor subsystem. The transmutation of Te-135 into I-135 is accounted for by adding the rate from block (6) into block (5). Likewise, the transmutation of I-135 into Xe-135 is accounted for by feeding the output of block (7) into block (10). Finally, the output of the system, (11), is used as an input into the fuel salt subsystem, indicted by block (1) in Figure 3.3.

3.4 Fuel Salt Subsystem

The fuel salt subsystem is illustrated in Figure 3.3. The subsystem assumes the fuel salt circulates sufficiently fast for the entire fuel salt to be treated as a well mixed solution.

Nuclear processes that affect the evolution of Xe-135 are implemented in blocks (1), (2), and (3). The nuclear production of Xe-135 from the progenitor subsystem, which was shown in Figure 3.2, is accounted for in block (1). Decay of Xe-135 in the fuel salt is accounted for by block (2) which implements Equation 3.1. The magnitude of the decay constant can be found in Table 3.3. Nuclear transmutation of Xe-135 into Xe-136 (burnout) is accounted with block (3) which implements,

$$\frac{N_{Xe}}{V_L^{FS}} \phi \sigma_a^{Xe} V_L^{IC}, \tag{3.3}$$

The volume normalization constant is taken to be the entire liquid contents of the fuel salt, V_L^{FS}, whereas the production volume is taken to be the in core liquid volume, V_L^{IC}

For the burnout block, (3), the neutron flux, ϕ, at full power, was taken to be the average

$$\text{(1) Nuclear Production Into Fuel Salt}$$
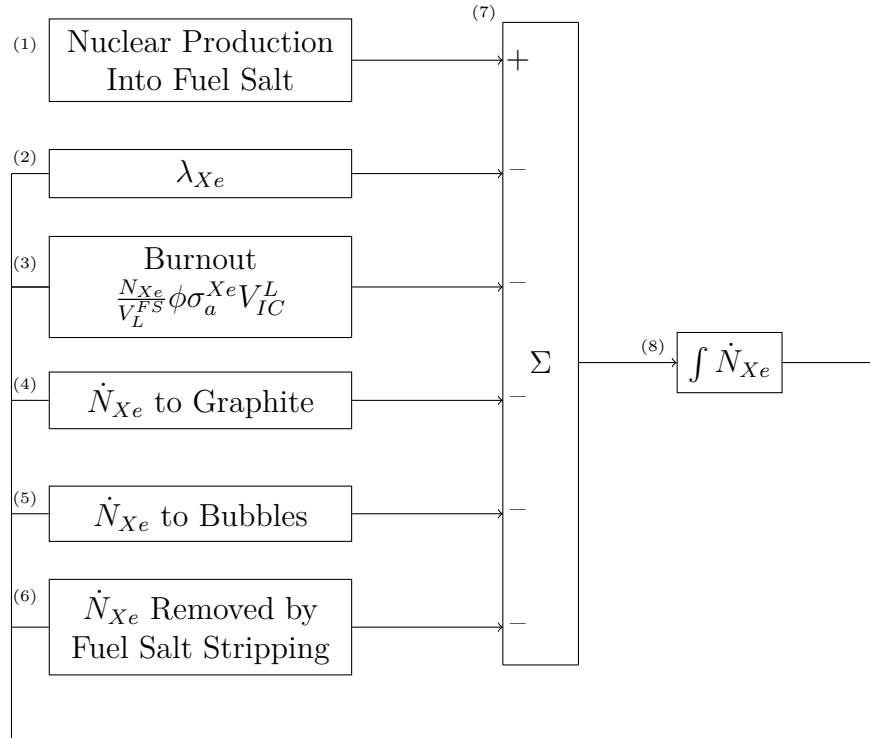
Figure 3.3: Illustration of fuel salt subsystem

thermal neutron flux of $1.5 \times 10^{17}\,\mathrm{m^{-1}\,s^{-2}}$ described in ORNL-TM-0728 [36, p. 101]. The microscopic neutron absorption cross section used, σ_a^{Xe}, was $1.18\,\mathrm{Mb}$, taken from ORNL-4069 [25, p. 42].

The next three blocks, (4), (5), and (6), describe mass transfer processes in the reactor. Block (4) accounts for migration into the graphite subsystem, described in Section 3.7. Block (5) accounts for migration into the circulating voids (bubbles) and is described in Section 3.8. Finally, block (6) accounts for removal of xenon from the fuel salt (but not the bubbles — described later) and is described in Section 3.9.

All of these source and sink terms (blocks (1) through (6)) are summed by block (7) which is fed into an integrator at block (8) which tracks the quantity of Xe-135 dissolved in the liquid phase of the fuel salt.

3.5 Thermophysical Properties and Dimensionless Numbers

3.5.1 Material Properties

Each of the graphite and bubble nodes used in the model calculates their thermophysical properties and dimensionless numbers locally. This subsystem is diagrammed in Figure 3.4. The magnitude of the thermophysical properties and the Schmidt number is plotted in Figure 3.5. For the proceeding discussion, numbers enclosed by parentheses are referring to Figure 3.4 and statements about plots are referring to Figure 3.5.
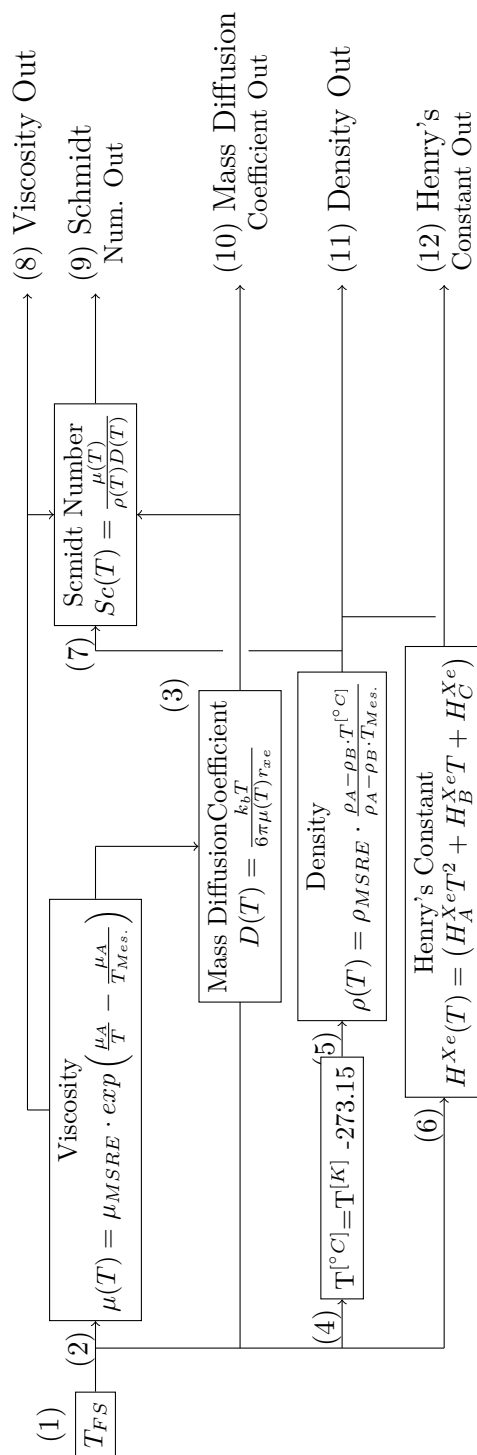
Figure 3.4: Diagram of subsystem that calculates thermophysical properties and dimensionless numbers

The thermophysical property subsystem has three inputs:

- T_{FS}, the local fuel salt temperature (1);

- U, the local fuel salt velocity (14);

- L, the local characteristic hydraulic length for a given node.

The outputs for the subsystem are:

- μ, fuel salt viscosity (8);

- Sc, the Schmidt number[2] (9);

- D, the mass diffusion coefficient (10);

- ρ, the density of the fuel salt (11);

- $H_i^{CP} = \frac{C_i}{p_i}$. the Henry's constant, defined in terms of dissolved concentration and partial pressure (12);

- The local Reynolds number.

Each node in the lumped volume subsystem (Section 3.6) has has its own instance of the thermophysical property subsystem.

The variation of MSRE fuel salt density and viscosity with temperature was not found in the literature. ORNL-TM-2316 [40], however, does provide several temperature dependent correlations for density, on page 8, and viscosity, on page 28, for several potential MSRE fuel salts that were under consideration. Furthermore, ORNL-TM-0728 [36], page 8, also provides the density and viscosity for fuel salt used in the MSRE at 1200°F (649 °C). Therefore, in order to provide some sort of temperature dependence of the fuel salt used in the model, a *temperature scaling factor* was generated. The final density/viscosity was derived at by multiplying the reported density/viscosity at 1200°F by the scaling factor. The scaling

---

[2]The ratio of momentum to mass diffusivity

Variation of Thermophysical Properties With Temperature
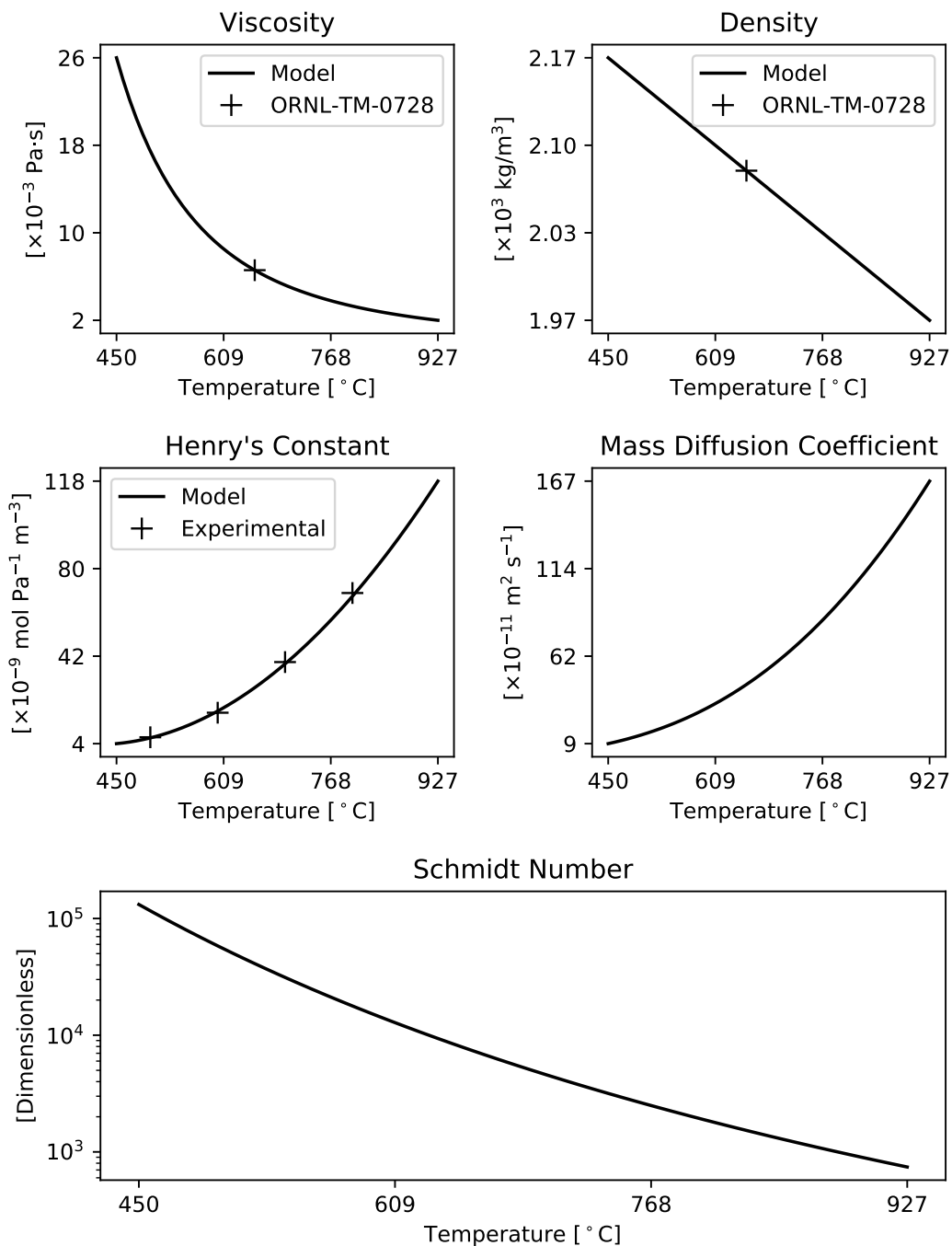
Figure 3.5: Plots thermophysical properties used in the dynamic model

factor was derived by evaluating the density/viscosity of fuel salt F1 in ORNL-TM-2316 at the model's fuel salt temperature and dividing that quantity by the density/viscosity of fuel salt F1 in ORNL-2316 at 1200°F:

$$\rho \text{ Scaling Factor} = \frac{\rho(T)}{\rho(T_{Mes.})}, \tag{3.4}$$

$$\mu \text{ Scaling Factor} = \frac{\mu(T)}{\mu(T_{Mes.})}, \tag{3.5}$$

where $T_{Mes.}$ is the temperature at which the MSRE fuel salt had its density and viscosity measured (1200°F). Therefore, the final output density/viscosity is given by an expression of the form

$$\rho(T) = \rho_{MSRE} \cdot (\rho \text{ Scaling Factor}), \tag{3.6}$$

or,

$$\mu(T) = \mu_{MSRE} \cdot (\mu \text{ Scaling Factor}), \tag{3.7}$$

respectively.

Fuel salt F1 was used from ORNL-TM-2316 because it as judged to have the closest chemical composition to the fuel salt used in the MSRE. The *"highly enriched"* fuel salt variant was used as a source for the base density/viscosity data.

The viscosity correlation was presented in ORNL-TM-2316 in the form,

$$\mu(T) = \mu_K \cdot exp\left(\frac{\mu_A}{T}\right), \tag{3.8}$$

and the density correlation was presented in the form,

$$\rho(T) = \rho_A - \rho_B T. \tag{3.9}$$

The constants used in equations 3.8 and 3.9 are presented in Table 3.4.

Constant	Value
ρ_A	$3.62 \times 10^0 \, \mathrm{g \, cm^{-3}}$
ρ_B	$6.6 \times 10^{-4} \, \mathrm{g \, cm^{-3} \, °C^{-1}}$
μ_K	$8.4 \times 10^{-2} \, \mathrm{cP}$
μ_A	$6.6 \times 10^{-4} \, \mathrm{K}$

Table 3.4: Magnitude of parameters used in viscosity and density correlations

Note, the temperature in Equation 3.8 is expected to be in Kelvin whereas the temperature in Equation 3.9 is expected to be in degrees Celsius. The dynamic model natively stores the temperature in Kelvin, so unit conversion for the density calculation in block (5) is handled by block (4).

The viscosity is calculated by block (2) which implements the equation,

$$\mu(T) = \mu_{MSRE} \cdot exp\left(\frac{\mu_A}{T} - \frac{\mu_A}{T_{Mes.}}\right). \tag{3.10}$$

The multiplicative constant, μ_K, shown in Equation 3.8 is removed by simplification, and the entire equation is transformed from the evaluation of two exponentials to a single exponential by the well known rule that states the quotient of two exponential functions is equal to the exponential of the difference of the arguments to those original exponentials. Note, since the correlation implemented by Equation 3.8 returns a value in centipoise, this must be converted to a pascal second, which is congruent with the model's native SI units, through a multiplication operation that is not depicted.

The density calculation, implemented in block (5), takes as its input parameter the temperature in degrees Celsius and outputs the local fuel salt density in kilograms per cubic meter, and this is depicted by block (4).

The top row of Figure 3.5 shows the dependence of both the viscosity and density on temperature. The measured value of the MSRE fuel salt, reported on page 8 of ORNL-TM-0728 [36], is denoted by a "+" sign on these plots. The data is plotted from $450\,°\mathrm{C}$ (MSRE fuel salt liquidus temperature is $448\,°\mathrm{C}$) to $927\,°\mathrm{C}$ ($1200\,\mathrm{K}$). Over this temperature range, comparing the low temperature value to the high temperature value, the viscosity decreases

by a factor of 13 whereas the density decreases by about 1%. It is therefore foreseeable that establishing an accurate temperature dependence for viscosity is far more important than establishing an accurate temperature dependence for density.

Next is block (6), the block that calculates the magnitude of Henry's constant. Again, the particular variant of Henry's constant that is calculated is the pressure-concentration (H^{CP}) variation rather than the dimensionless (H^{CC}) variation. This block implements a quadratic fitting function of the form,

$$H^{Xe} = H_A^{Xe}T^2 + H_B^{Xe}T + H_C^{Xe}, \tag{3.11}$$

to obtain the temperature dependence of Henry's constant on temperature. The constants H_a^{Xe}, H_b^{Xe}, and H_c^{Xe} are fitting parameters. The data that was fitted was obtained from experiments with FLiBe salt presented in a 1962 paper by Watson, Evans, Grimes, and Smith [41]. The raw data was presented as a dimensionless Henry's constant, so they needed to be normalized by their measurement temperature and the ideal gas constant to derive the appropriate dimensional form of the constant. The magnitudes of the fitting parameters are shown in Table 3.5.1. A plot of this fitting function along with the experimental data points from which the fitting function is derived is shown in the first column of the second row of Figure 3.5. Although a linear function could have been used to fit the data, our experience indicates a quadratic function provides a superior fit (R-Squared value of 0.9635 for linear vs. 0.9994 for quadratic). A better fitting function would require more experimental data points at higher temperatures.

Constant	Magnitude	Unit
H_a^{Xe}	4.426×10^{-13}	$\mathrm{mol\,m^{-3}\,Pa^{-1}\,K^{-2}}$
H_b^{Xe}	-6.124×10^{-10}	$\mathrm{mol\,m^{-3}\,Pa^{-1}\,K^{-1}}$
H_c^{Xe}	2.153×10^{-7}	$\mathrm{mol\,m^{-3}\,Pa^{-1}}$

Table 3.5: Magnitudes of parameters used in the generation of Henry's constant

The mass diffusion coefficient is calculated using block (3). The block implements the

Einstein-Stokes equation to calculate the mass diffusion coefficient for a diffusing spherical particle in a continuous medium,

$$D(T) = \frac{k_b T}{6\pi\mu(T)r_{Xe}}, \tag{3.12}$$

where T is the temperature of the fuel salt, in Kelvin, k_b is Boltzmann constant ($1.38 \times 10^{-23}\,\mathrm{N\,m\,K^{-1}}$), $\mu(T)$ is the viscosity of the fuel salt at temperature T, and r_{Xe} is the radius of the xenon atom diffusing in fuel salt. The radius of the diffusing atom was set to 216 pm. The temperature evaluated viscosity is input into this block (3) from block (2), the viscosity calculation block. A plot of the mass diffusion coefficient with respect to temperature is shown in the second column of the second row of Figure 3.5. Note the clearly non-linear temperature dependence of the function; this is caused by the non-linearity of the viscosity with respect to temperature.

Finally, the non-dimensional number, the Schmidt number is calculated using blocks (7). The Schmidt number is purely a function of material parameters, and has for its inputs, viscosity, density, and the mass diffusion coefficient. A logarithmic plot of the Schmidt number with respect to temperature is shown in the last row of Figure 3.5. This plot shows that the Schmidt number decreases by more than two orders of magnitude between the high and low temperatures plotted.

3.5.2   The Reynolds Number

The method by which the Reynolds number is calculated is dependent on the type of node the Reynolds number is being calculated in. There are two types of nodes used in calculating the Reynolds number:

- Cylindrical piping sections

- No correlation available

The cylindrical piping sections have their Reynolds number calculated through the typical,

$$Re = \frac{\rho U L}{\mu}, \tag{3.13}$$

whereas nodes with no correlation available calculate the Reynolds number by a *scaling method.* The subsystems to calculate each of these Reynolds numbers is shown on Figure 3.6.
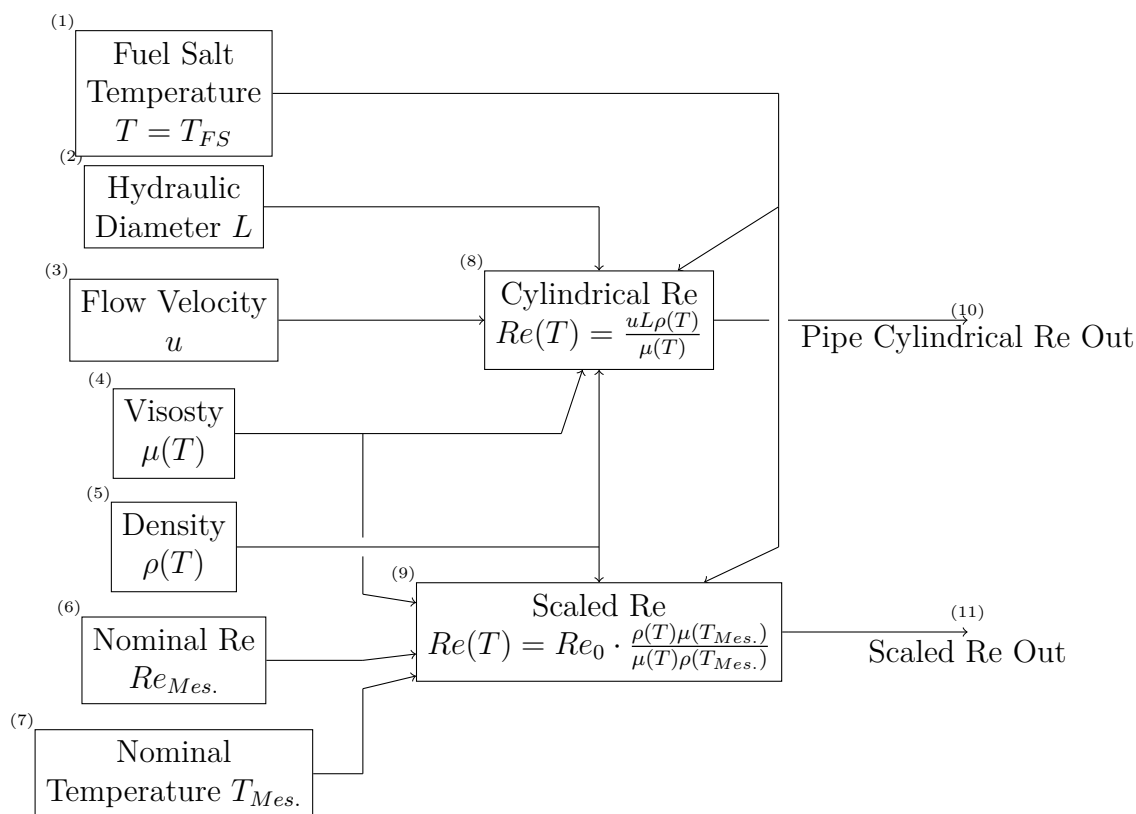
Figure 3.6: Subsystem to calculate the Reynolds number for a node

The Reynolds numbers are calculated with blocks (8) and (9). All blocks take in that node's fuel salt temperature, block (1), as a temperature argument. The outputs to the subsystem are the pipe Reynolds number (10) and the scaled Reynolds number (11). Note, that for a given node, only one of these Reynolds numbers is calculated and therefore signals need not necessarily be present in all lines. Additionally, all methods of calculation also take in the viscosity, μ, and the density, ρ, through blocks (4) and (5) respectively and these

values are provided by the thermophysical property system described previously..

The block that calculates the pipe Reynolds number takes in the fuel salt flow velocity, u, through block (3) and the hydraulic diameter of the cylindrical diameter, L, through block (2).

The scaled Reynolds number block, block (11), scales a predetermined Reynolds number, Re_0, by the ratio of the Reynolds number evaluated at temperature T, and the Reynolds number evaluated at some nominal temperature, $T_{Mes.}$. The predetermined Reynolds number is supplied by block (6) and the nominal temperature is supplied by block (7). The geometry and the flow velocity are assumed to be the same in both the nominal and perturbed temperature cases, and therefore the flow velocity, u, and hydraulic diameter, L, terms cancel out, and the calculation is able to be performed without them.

Finally, the fuel pump Reynolds number is not calculated since it is not directly used in any calculations.[3]

3.6   The Lumped Volume Subsystem

The bubble model used in the dynamic model is illustrated with Figure 3.7. The parameters used in the bubble model are shown on Table 3.8. The fourth column in this table describes the method, pipe or scaling, by which the Reynolds number is calculated in that node, and these methods are described in Section 3.5.2. The fuel salt flow path for the bubble model is illustrated with Figure 3.8.

Regions G_1, G_2, G_3, and G_4 are graphite fuel channel regions inside the core. the region numbering corresponds to the region numbers on page 14 of ORNL-TM-0378 [43]. Note, the graphite regions are somewhat specialized in that they also posses a property which describes the number of fuel channels within that region. The distribution of these fuel channels is described in Table 3.6. Additionally, each fuel channel is 1.6 m high (see ORNL-4069 [25]page 6) and has an equivalent cylindrical radius of 0.79 cm (see ORNL-4069 [25]page 65) and it

---

[3]However, it could be through a *stirred* Reynolds number — see [42].

Region #	Number of Channels
1	12
2	940
3	108
4	78

Data from ORNL-TM-0378 [43, p. 14]

Table 3.6: Number of fuel channels for each graphite region

is from these measurements and the number of fuel channels in a given region that mass transfer area from the to fuel salt to the graphite is calculated.

LH and *UH* are the lower and upper heads described on pages 96 and 103 of ORNL-TM-0728 [36]. P_{100}, P_{101}, and P_{102} correspond to lines 100, 101, and 102, described on page 173 of ORNL-TM-0728 [ibid.]. *FP* is the fuel pump and pump bowl described on page 12 of the same report. Finally, *HX* is the heat exchanger described on page 14 of the same report.

Volume and residency time data for all regions except the graphite regions, G_i, were taken from page 101 of ORNL-TM-0728 [36]. Volumes for the graphite regions were calculated by multiplying the total core volume, from page 101 of ORNL-TM-0728 [36], by the fraction of the total fuel channels occupying that region, from page 14 of ORNL-TM-0378 [43], formally this is written $N_i/N_{Tot.}$. Fuel salt velocities for the graphite regions were also taken from page 14 of ORNL-TM-0378. The hydraulic diameter for the graphite regions was taken from page 65 of ORNL-4069 [25]. The residence time for each graphite region was found by dividing the fuel salt velocity in that region by the length of the fuel channel (1.6 m according to page 80 of ORNL-TM-0728 [36]).

Reynolds numbers for each node were calculated according to the *pipe* or *scaling* method described in Section 3.5.2.

Precise magnitudes of the Reynolds numbers for the upper and lower heads was not found. Furthermore, the presence of *"swirl vanes"* or other equipment complicates the calculation of the Reynolds number due to uncertainty on how the characteristic length should be calculated in the lower head and the presence of a complex flow field due to the swirling

action.

Page 26 of ORNL-TM-3229 [44] sates *"...the Reynolds number in the upper head is high for both and fuel salt and the flow is turbulent."*. The only reference to the Reynolds number of the lower head found was on page 15 of ORNL-TM-3229 [44] which stated Reynolds number of the lower head is *"high"*; it is unclear as to how large precisely *"high"* is, however, on page 10 of the report, a *high* Reynolds number is described as over 10^4. Therefore, the base Reynolds number used for both the upper and lower heads section was 10^4.

The subsystem that manages the gas and liquid volumes for each lumped volume is illustrated in Figure 3.9. The system inputs are:

- (1) – The nominal node volume, V_0, the total *filled* volume of the node

- (2) – The nominal circulating void fraction, f_{CV}^0, which is the circulating void fraction ($\frac{V^G}{V^L+V^G}$) at the reference temperature

- (3) The reference temperature, T_{ref}, which is the nominal temperature of the node

- (4) The node temperature, T, which is the current temperature of the node.

The reference temperatures were set such that the upper head to the heat exchanger were equal to the reactor outlet temperature, the heat exchanger temperature is the mean between inlet and outlet temperatures, and the nodes after the heat exchanger to the lower head was equal to the reactor inlet temperature. The outlet and inlet temperatures, 907.5 K (1225 °F) and 935.4 K (1175 °F) respectively, were taken from ORNL-TM-0728 [36], page 78. The heat exchanger reference temperature was set to the mean between the inlet and outlet temperatures.

Each graphite region, G_1–G_4, has associated it with an *effective radius* which describes the radial position of the annulus (or cylinder for the central region, G_1) of the graphite region. These radii were taken from ORNL-TM-0378 [43], p.14, and are shown in Table 3.6.

The graphite and fuel salt temperatures were digitized from the radius-dependent measurements of graphite and fuel salt temperature at steady state presented on page 42 of

Region	Effective Radius
1	3.78" / 9.6 cm
2	24.76" / 62.89 cm
3	26.10" / 66.29 cm
4	27.58" / 70.05 cm

Table 3.7: Graphite stringer radius effective radius

ORNL-TM-378 [43]. The G_1–G_4 nodes were set such that the node temperature was equal to the mean of the these digitized temperatures from the inner effective radius to the outter effective radius.

The nominal gas volume is the volume of gas at the reference temperature in the node and is calculated by node (5). The nominal gas volume has for its inputs V_0, the nominal node volume, (1), and f_{CV}^0, the nominal circulating void fraction, (2). The nominal gas volume is then simply the product of the nominal circulating void fraction, f_{CV}^0, and the nominal node volume, V_0,

$$V_0^G = f_{CV}^0 V_0. \tag{3.14}$$

The model assumes that the gas volume displaces the liquid. The nominal liquid volume, V_0^L, is calculated through block (6), and has as its inputs, (1), the nominal node volumes, V_0, and (5), the nominal gas volume. The nominal liquid volume, V_0^L is the difference between the nominal node volume and the amount of gas nominally in the node,

$$V_0^L = V_0 - V_0^G. \tag{3.15}$$

The reference density, $\rho(T_{ref})$, is the density of liquid fuel salt evaluated at the reference temperature, T_{ref}, and is implemented in block (7). The density is provided by the thermophysical properties subsystem, described in Section 3.4. The current density, $\rho(T)$, is the density of the liquid fuel salt evaluated at the current node temperature, T, and is implemented in block (8). The inputs for these blocks are blocks (3) and (4), the reference and node temperatures respectively, T_{ref} and T.

The nominal fuel salt mass, M^0_{FS}, is the mass of the liquid fuel salt at the reference temperature, and is implemented through block (10). The nominal fuel salt mass is the product of the nominal liquid volume, V^L_0, and the density of the fuel salt at the reference temperature, $\rho(T_{ref})$.

Block (13) takes the nominal fuel salt mass, M^0_{FS}, and multiplies it by the current liquid fuel salt density, $\rho(T)$, to get the current volume of liquid that would be in the node if it were to be totally expanded by the temperature variation,

$$V_L = \rho(T)M^0_{FS}. \tag{3.16}$$

Block (9) calculates the volume of gas from the node at the current node temperature, T. It does so by applying Charle's law ($\frac{V_1}{V_2} = \frac{T_1}{T_2}$) to the nominal gas volume, V^G_0, supplied by block (5). The state from which the gas is being expanded from is the reference temperature; therefore,

$$V_G = V^G_0 \frac{T}{T_{ref}}. \tag{3.17}$$

The amount of gas in the node is the current gas volume, and is output through line (19).

The amount of liquid fuel salt in the node is calculated by block (14) and is output by line (17). Block (14) subtracts the amount of gas in the node, V_G at the current node temperature, T, from the nominal node volume, V_0.

Finally, the amount of liquid displaced by the gas in the node is determined by blocks (15) and (16). Block (15) sums the current liquid, V_L, and gas volumes,V_G, expanded to the current node temperature, T, to get the total volume if both the gas and liquid were expanded. Block (16) then subtracts the value calculated by block (15) to determine the excess liquid volume out (liquid only since gas displaces liquid), and this is output through line (18).
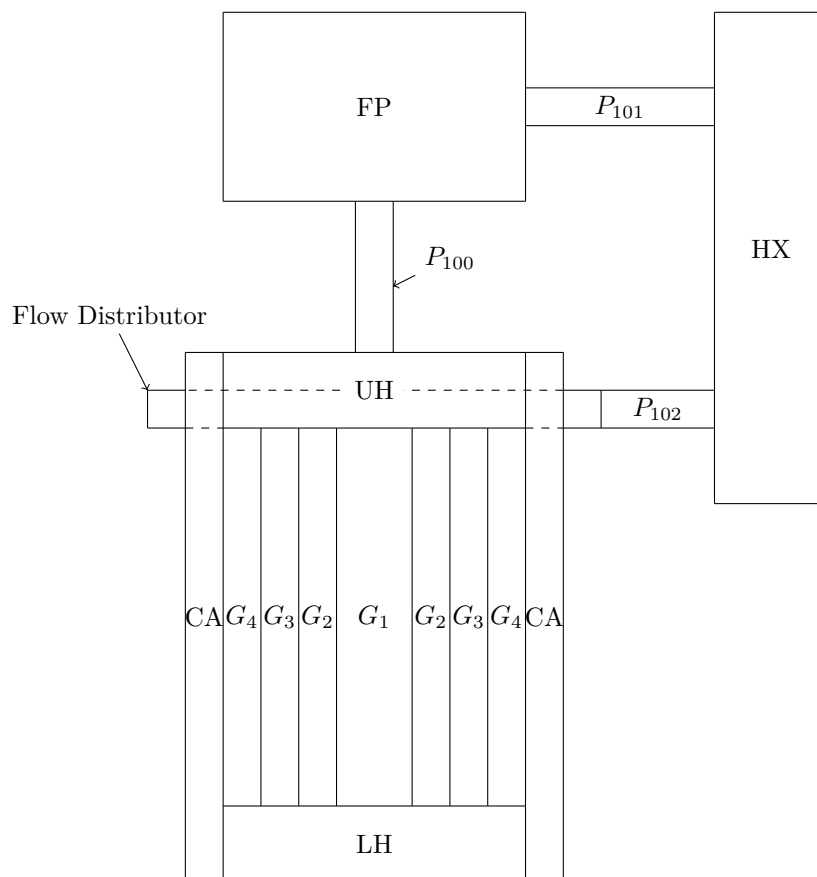
Region Code	Definition
$G_1/G_2/G_3/G_4$	Graphite Region
LH	Lower Head
UH	Upper Head
$P_{100}/P_{101}/P_{102}$	Piping Region
FP	Fuel Pump
HX	Heat Exchanger

Figure 3.7: Cross sectional illustration of bubble behavior subsystem

Region Code	Definition
$G_1/G_2/G_3/G_4$	Graphite Region
LH	Lower Head
UH	Upper Head
$P_{100}/P_{101}/P_{102}$	Piping Region
FP	Fuel Pump
HX	Heat Exchanger
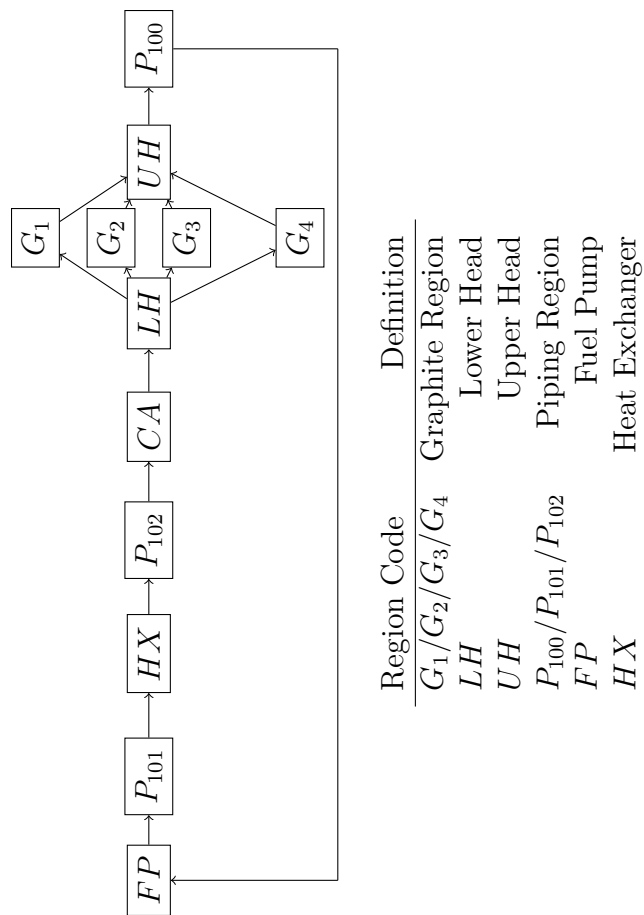
Figure 3.8: Flow path of bubble behavior subsystem

Region	Volume (m^3)	Residence Time(s)	Reynolds Number Method	Hydraulic Diameter (cm)	Salt Velocity at 1200 GPM ($m\,s^{-1}$)	Nominal Re
G_1	7.5×10^{-3}	2.6	Pipe	1.6	0.61	
G_2	0.59	8.9	Pipe	1.6	0.18	
G_3	6.8×10^{-2}	3.6	Pipe	1.6	0.45	
G_4	4.9×10^{-2}	6.4	Pipe	1.6	0.25	
UH	0.30	3.9	Scaling			1×10^4
LH	0.28	3.8	Scaling			1×10^4
CA	0.28	3.6	Scaling			2.58×10^4
P_{100}	0.60×10^{-2}	0.8	Pipe	12.8	5.97	
P_{101}	2.3×10^{-2}	0.3	Pipe	12.8	5.97	
P_{102}	6.2×10^{-2}	0.8	Pipe	12.8	5.97	
FP	0.12	4.1	None			
HX	0.17	2.3	Pipe	1.2	4.2×10^{-2}	

Note: Re calculated from methodology described in Section 3.8.

Table 3.8: Data used in Bubble Model
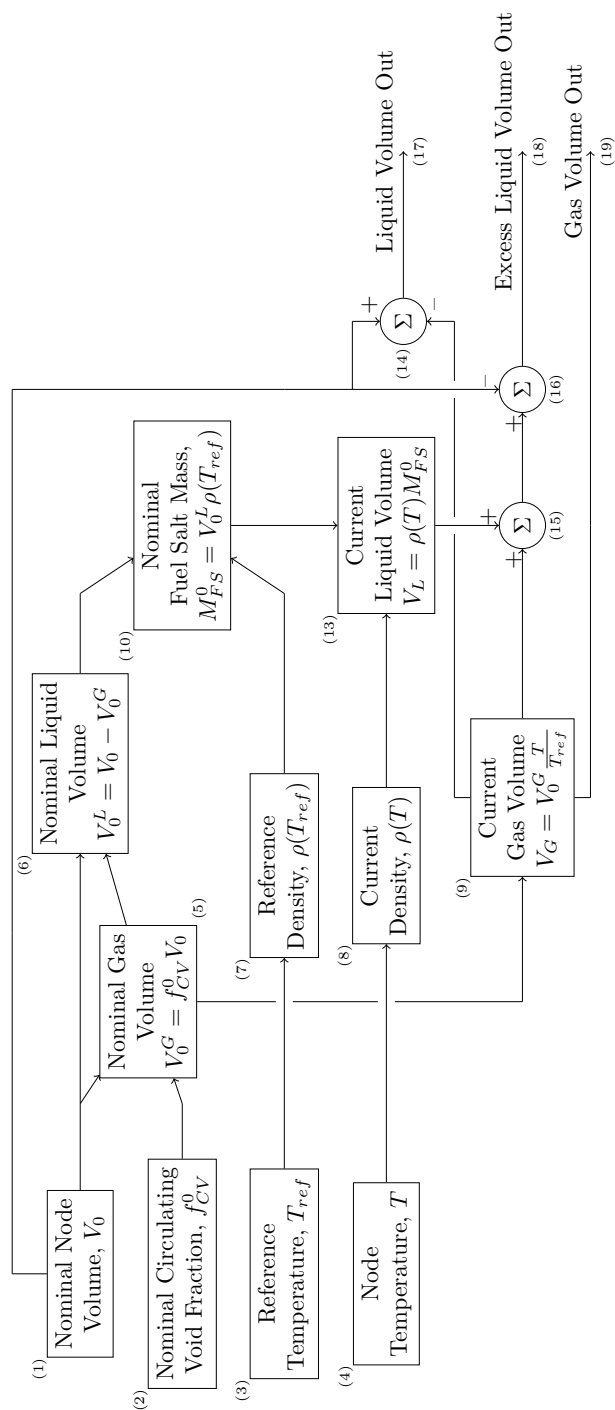
Figure 3.9: Illustration of lumped volume subsystem

3.7 The Graphite Subsystem

The subsystem which computes the behavior of a graphite region is shown in Figure 3.10. The inputs of the system are:

- (1), The neutron flux in the graphite, ϕ_G,

- (2), the graphite neutron flux, T_G,

- (3), the fuel salt velocity in that graphite region, U_{FS},

- (4), the quantity of Xe-135 in the fuel salt, N_{Xe}^{FS}.

As previously mentioned, each graphite region has an effective radius, which is taken from ORNL-TM-0378 [43], page 14 — the fuel salt velocity, U_{FS}, is derived from the same source.. The neutron flux, ϕ_G, for each region was determined as follows:

- ORNL-TM-0378 [43], page 23, presents neutron flux measurements as a function of radial position.

- The data presented was digitized.

- The average neutron flux across the annular radius was taken to be the neutron flux for that region.

A similar process was used to set the graphite region temperature, T_G, using the data presented on page 42 of ORNL-TM-0378 [43]. The fuel salt Xe-135 quantity, N_{Xe}^{FS}, is input from the fuel salt subsystem described in Section 3.4.

Block (4) calculates the graphite mass transfer coefficient, k_m, through a Dittus-Boelter like correlation (which was introduced by McAdams) which has been transformed into a mass transfer correlation through a heat/mass transfer analogy,

$$k_m = \frac{D}{2r_{fc}} 0.023 Re^{0.8} Sc^{0.4}. \tag{3.18}$$

The Reynolds number, Re, Schmidt Number, Sc, and the mass diff fusion coefficient, D, are all provided through the thermophysical property system described in Section 3.5.

The neutron flux, ϕ_G, graphite temperature, T_{Gr}, graphite mass transfer coefficient, k_m, and the fuel salt Xe-135 content, N_{Xe}^{FS}, are all fed into block (5), the graphite stringer model (described later), which outputs, (7), the mean Xe-135 concentration, C_{Xe}^{Gr}, and, (8), the single stringer mass flux, J. The mean Xe-135 concentration, C_{Xe}^{Gr}, is output from the subsystem directly through line (11). The single stringer mass flux, J, is multiplied by (9), the surface area of a single fuel channel, A_{FC}^{1}, and, (10), the number of fuel channels in the region to derive the total mass flux out, which is output through line (12).
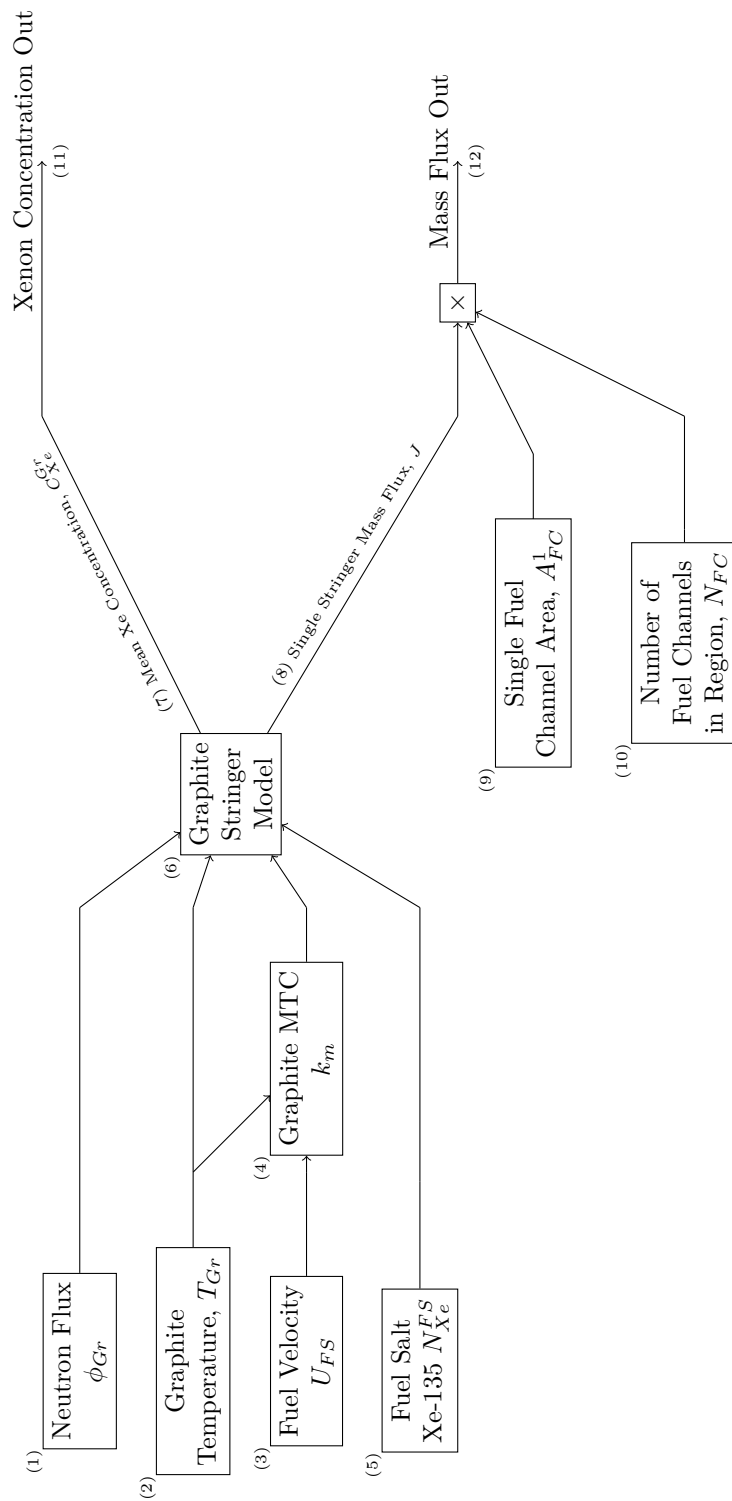
Figure 3.10: Subsystem for a graphite region

The working of the graphite stringer model, block (6) in Figure 3.10, is shown in Figure 3.11.

The first three inputs to the stringer model are,

- (1), the graphite porosity, ϵ,

- (2), the graphite mass diffusion coefficient, D_{Gr},

- (3) the fuel channel radius, r_{fc}.

These are all fed into block (10), which generates the *base graphite stringer matrix*. The base graphite stringer matrix is the first three matrices that are generated to solve radial coordinates, partial differential equation,

$$\frac{\partial C_{Xe}}{\partial t} = \frac{D_{Gr}}{\epsilon} \left(\frac{\partial^2 C_{Xe}}{\partial r^2} + \frac{1}{r} \frac{\partial C_{Xe}}{\partial r} \right) - (\phi \sigma_a^{Xe} + \lambda_{Xe}) C_{Xe}, \tag{3.19}$$

where the shorthand $C_{Xe} = C_{Xe}^{Gr}(r,t)$ has been adopted. The left hand boundary condition is a zero flux condition,

$$\left(\frac{\partial C_{Xe}}{\partial r} \right)_{r=0} = 0, \tag{3.20}$$

and the right hand boundary condition is a robin condition prescribing the mass transfer into the stringer,

$$\left(\frac{\partial C_{Xe}}{\partial r} \right)_{r=r_{fc}} = k_m \left(C_{FS} - \frac{HRT}{\epsilon} C_G \right). \tag{3.21}$$

The solution uses a 20 node, right hand side ghost node, second order finite difference (FDM) decomposition with the method of lines to convert the partial differential equation into a series of 21 ordinary differential equations that can be solved by Simulink. The spatial decomposition of the graphite stringer is radial with each node at a uniform distance of,

$$\Delta r = \frac{r_{fc}}{20}. \tag{3.22}$$

Furthermore, the node positions are indexed by,

$$r_i = i\Delta r, \tag{3.23}$$

such that $i \in [0, 21]$. The extra index (21) is to allow for the inclusion of the RHS ghost node. N is denoted to be the index of the final node, 21.

In order to decouple the temperature dependent behavior of the right hand side boundary condition from the rest of the equation, it is partially implemented in a separate additive matrix H, represented by block (14) — described later. The reaction term, of Equation 3.19 is implemented through the B matrix (where B $= (\phi\sigma_a^{Xe} + \lambda_{Xe})$, in contrast to constant A on the base matrix), shown in block (18) – also described later. These three matrices, the base matrix (10), additive matrix H (14), and additive matrix B, are all added together through summation block (15) before being fed to the rest of the system.

With regards to block (10), the base matrix, let us, for convenience, define,

$$A \stackrel{defined}{=} \frac{D_{Gr}}{\epsilon}, \tag{3.24}$$

The first three entries of row 1 in the base matrix matrix are,

$$M_1 = \begin{bmatrix} -\frac{5A}{4\Delta r^2} \\ \frac{A}{\Delta r^2} \\ \frac{A}{4\Delta r^2} \end{bmatrix}^T \tag{3.25}$$

.

The first five entries of the second row of the base matrix are,

$$
M_2 = \begin{bmatrix} \frac{A}{\Delta r^2} - \frac{A}{3\Delta r r_2} \\[8pt] \frac{-2A}{\Delta r^2} - \frac{A}{2\Delta r r_2} \\[8pt] \frac{-A}{\Delta r^2} + \frac{A}{2\Delta r r_2} \\[8pt] \frac{-A}{\Delta r^2} + \frac{A}{2\Delta r r_2} \\[8pt] \frac{A}{6\Delta r r_1} \end{bmatrix}^T
\tag{3.26}
$$

Rows [3,18] are generated with,

$$
M_i = \begin{bmatrix} \frac{-A}{12\Delta r^2} + \frac{A}{12\Delta r r_i} \\[8pt] \frac{4A}{3\Delta r^2} - \frac{2A}{3\Delta r r_i} \\[8pt] \frac{-5A}{2\Delta r^2} \\[8pt] \frac{4A}{3\Delta r^2} + \frac{2A}{3\Delta r r_i} \\[8pt] \frac{-A}{12\Delta r^2} - \frac{A}{12\Delta r r_i} \end{bmatrix}^T ,
\tag{3.27}
$$

where i is the row number, and the insertion is performed beginning at column i.

The second last row, row 19 is generated with

$$
M_{N-1} = \begin{bmatrix} \frac{-A}{12\Delta r^2} - \frac{A}{12\Delta r r_{N-1}} \\[8pt] \frac{A}{3\Delta r^2} + \frac{A}{2\Delta r r_{N-1}} \\[8pt] \frac{A}{2\Delta r^2} - \frac{3A}{2\Delta r r_{N-1}} \\[8pt] \frac{-5A}{3\Delta r^2} + \frac{5A}{6\Delta r r_{N-1}} \\[8pt] \frac{11A}{12\Delta r^2} + \frac{A}{4\Delta r r_{N-1}} \end{bmatrix}^T ,
\tag{3.28}
$$

and is inserted starting at column 16 (N-5).

The final row is inserted starting at column 16 (N-5), and is,

$$M_N \begin{bmatrix} \frac{-A}{12\Delta r^2} \\ \frac{A}{3\Delta r^2} \\ \frac{A}{2\Delta r^2} \\ \frac{-5A}{3\Delta r^2} \\ \frac{11A}{12\Delta r^2} \end{bmatrix}^T . \tag{3.29}$$

The final composition of these matrices is shown in Equation 3.7.

$$M = \begin{bmatrix} M_{11} & M_{12} & M_{13} & M_{14} & M_{15} & 0 & \cdots & \cdots & \cdots & 0 \\ 0 & M_{21} & M_{22} & M_{23} & M_{24} & M_{25} & 0 & \cdots & \cdots & 0 \\ 0 & \cdots & M_{i1} & M_{i2} & M_{i3} & M_{i4} & M_{i5} & 0 & \cdots & 0 \\ \vdots & \vdots & \vdots & \vdots & \vdots & \vdots & \vdots & \vdots & \vdots & \vdots \\ 0 & \cdots & \cdots & \cdots & 0 & M_{(N-1)1} & M_{(N-1)2} & M_{(N-1)3} & M_{(N-1)4} & M_{(N-1)5} \\ 0 & \cdots & \cdots & \cdots & 0 & M_{N1} & M_{N2} & M_{N3} & M_{N4} & M_{N5} \end{bmatrix} \qquad (3.30)$$

Region	Flux ($\mathrm{m^{-2}\,s^{-1}}$)
1	7.49×10^{17}
2	6.35×10^{17}
3	2.03×10^{17}
4	1.30×10^{17}

Table 3.9: Graphite Region Neutron Fluxes

Block (14) generates additive matrix H which is a 21 ×21 zero matrix with element (N, N-1) set to 1. The H matrix is multiplied by (4), T, the graphite temperature, (5), Henry's constant, H_{Xe}, and (11), R, the ideal gas constant (HRT). The H matrix is also divided by (1), the graphite porosity, which is inverted through block (12).

The B matrix, supplied by block (18), is a 21 × 21 identity matrix with element (1,1) set to zero and element (N, N-1) set to 1. The B matrix (B for burnout) is multiplied by the reaction rate, which is the product, (18), of the neutron flux, ϕ, (7), and the neutron absorption cross section, σ_a^{Xe}, (8). The Xe-135 decay constant, λ_{Xe}, is added to the reaction rate, and this total is multiplied by the B-matrix before being added to the H matrix and the base matrix through block (15). Each graphite region has its own neutron flux which were set to values taken from ORNL-TM-0378 [43], page 23, and these values are shown in Table 3.9.

The output of the matrix summation, block (15), is fed into a matrix multiplication block, (22), which multiplies the resultant matrix of block (15) with a vector representing the concentration of xenon in each node of the FDM decomposition, (26).

In order to complete the solution to the FDM decomposition, the non-homogeneous term needs to be injected (added) to the result of the matrix multiplication, and this is done through summation block (26). Block (23) compiles a vector,

$$
\begin{bmatrix} 0 \\ \vdots \\ \frac{r_{ghost}}{k_m} \end{bmatrix},
\tag{3.31}
$$

to the solution, where k_m is the mass transfer coefficient supplied by block (6), which was supplied by block (4) in Figure 3.10. The other term, r_{ghost}, is the ghost node radius, which is placed Δr beyond the radius of the graphite stringer, $r_{ghost} = r_0 + \Delta r$.

Block (24) compiles the vector,

$$
\begin{bmatrix}
0 \\
\vdots \\
\dfrac{N_{Xe}^{FS}}{V_L^{FS}}
\end{bmatrix},
\tag{3.32}
$$

where N_{Xe}^{FS} is the fuel salt xenon content, provided by block (20) through tothe fuel salt sub system described in Section 3.4, and V_L^{FS} is the fuel salt liquid content, provided through block (21) which is fed by the sum of all the liquid volumes generated in the thermophysical property subsystem, described in Section 3.5.

These terms are multiplied together by block (25.A) before being added to summation block (25).

Finally, the output for this subsystem are, (36), the graphite stringer mean Xe-135 concentration, C_{Gr}^{Xe}, and, (7), the graphite stringer Xe-135 mass flux out, J. The mean graphite stringer concentration is calculated through the a volume weighted average of the xenon concentration in each FDM node,

$$
\frac{\sum_i V_G^i C_{Xe}^i}{\sum_i V_G^i},
\tag{3.33}
$$

where $\vec{C}_{Xe} = [C_{Xe}^0 ... C_{Xe}^N]$ (these are graphite concentrations, the Gr superscript is dropped for convenience) is supplied through block (26) and $\vec{V}_G = [V_G^0 ... V_G^N]$ are the volumes of each FDM node, generated through block (32). The mathematical operations for the averaging operation are provided through blocks (31), (32), (33), (34), and (35) respectively.

Mass transfer out of the graphite stringer, J, is handled through line (37). It is calculated through,

$$
J = k_m \left(C_{FS}^{Xe} - \frac{HRT}{\epsilon} C_G^{Xe} \right).
\tag{3.34}
$$

The mass transfer coefficient, k_m, is supplied through block (6). The coefficient to the

graphite xenon concentration stringer, $\frac{HRT}{\epsilon}$, is supplied by the output of block (13). The fuel salt xenon concentration is supplied by block (24) which calculates $C_{FS}^{Xe} = \frac{N_{Xe}^{FS}}{V_L^{FS}}$, where the fuel salt xenon content, N_{Xe}^{FS}, is supplied through block (26) and the fuel salt liquid volume, V_L^{FS}, is supplied through block (21). The graphite xenon concentration, C_G^{Xe} used in this mass transfer equation is taken to be the right most node xenon concentration, selected by block (27). Blocks (26), (29), and (30) supply the mathematical machinery to calculate the mass transfer flux, J.

Figure 3.11: Graphite stringer model

3.8 The Bubble Subsystem

The top layer of the bubble model subsystem is illustrated in Figure 3.12. The four processes that affect the mass balance in the bubble subsystem are (1) mass transfer between the fuel salt and the bubbles, (2) burnout, (3) radioactive decay, and (6) removal of Xe-135 from the bubbles via the xenon stripper. These source/sink terms are summed through block (4), before being passed into scalar integrator (7). The coalescence and breakup rates are assumed sufficiently frequent to allow for the Xe-135 content in all bubbles to be represented by a single integrator.

The operation of the burnout block, (2), is similar to the operation of the burnout block in the fuel salt subsystem (Section 3.4), except the normalization volume in the total volume of circulating voids in the system, V_{CV}^{Tot}, which is found by summing the circulating void volumes in each lumped volume node, and the volume of reaction in the volume of circulating voids in the core, V_{CV}^{IC}, which is found by summing all of the circulating void volumes of the in core lumped volumes. The operation of the decay block, (3), is also identical to the operation of the decay block in the fuel salt subsystem (Section 3.4). The operation of the xenon stripper bubble removal block, (6), is provided by the xenon stripper subsystem and is described in detail in Section 3.9.
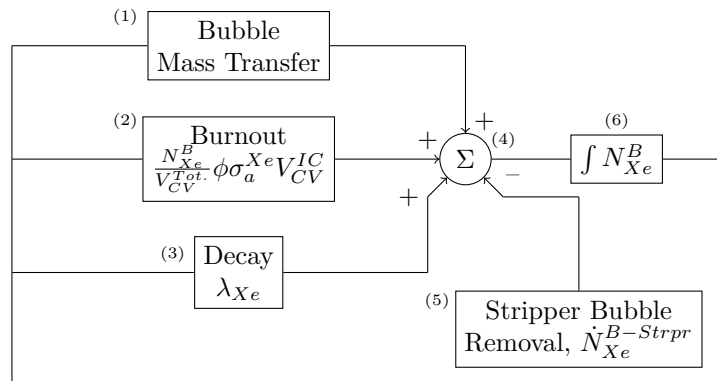
Figure 3.12: Bubble model subsystem

The operation of the mass transfer block, (1) in Figure 3.12, is shown in detail in Fig-

ure 3.13, which is now discussed. The purpose of the bubble mass transfer subsystem is to calculate the rate of change of Xe-135 content in the bubbles due to mass transfer processes, $\dot{N}^B_{Xe}$, and output this through line (14).

Essentially, the system solves an equation of the form,

$$\dot{N}^B_{Xe} = k_m A(C^{Xe}_{FS} - HRTC^{Xe}_B). \tag{3.35}$$

The term $k_m A$ is the product of the mass transfer coefficient and total area and it is calculated for every node before being summed to get the total $k_m A$ term. This system is described in detail later.

Blocks (1), (2), and (8) calculate the C^{Xe}_{FS} term. Block (2) is the total liquid volume which is found by summing the liquids volumes of the individual nodes. Blocks (3), (4), and (9) calculate the C^{Xe}_B term. The fuel salt Xe-135 content, N^{FS}_{Xe}, block (1), is passed in from the fuel salt subsystem (see Section 3.4). The bubble Xe-135 content, N^B_{Xe}, block (3), is passed in from the bubble model subsystem (see Figure 3.12).

The coefficients to the C^{Xe}_B term, HRT, are taken from the thermophysical property subsystem (see Section 3.5). Henry's constant, H_{Xe}, is provided through block (7) which takes its temperature from the node temperature block, T, block (5). Finally, block (6), provides the ideal gas constant, R, and these constants are combined with the C^{Xe}_B term from block (9) through block (10).

Summation block (11) calculates the difference between the two previously described terms before being multiplied by the bubble mass transfer coefficient and area, $k_m A$, from block (13) through block (12), and the result is output through line (14).
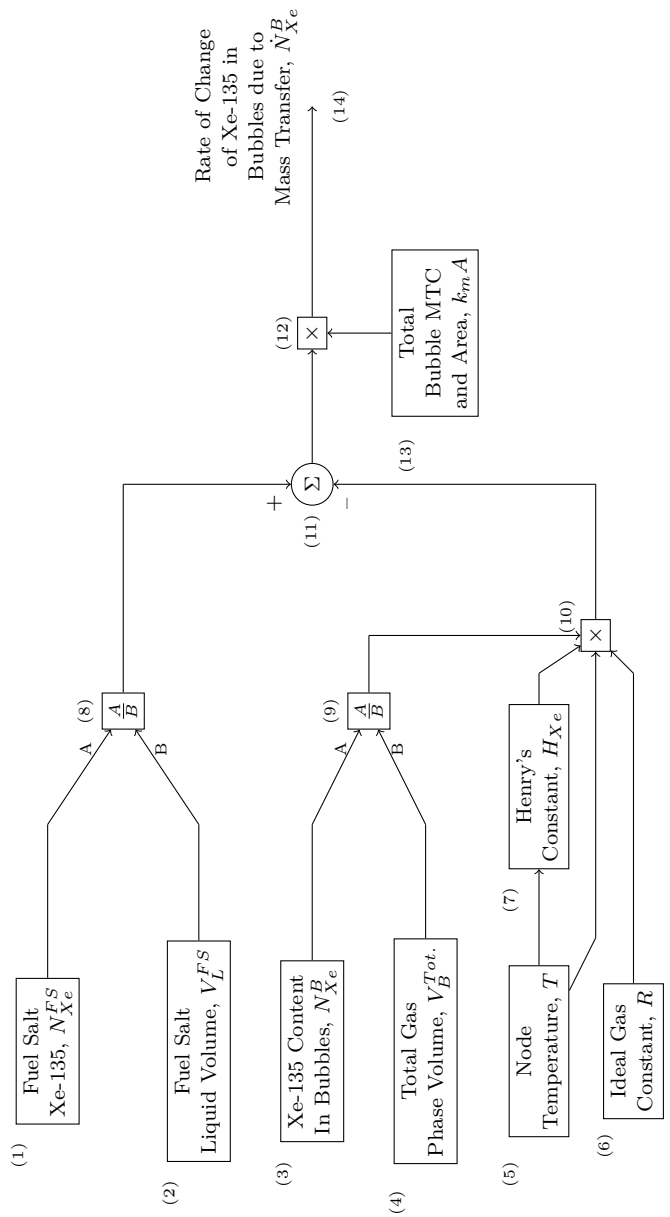
Figure 3.13: Bubble mass transfer subsystem

The subsystem that determines the bubble mass transfer coefficient and area, $k_m A$, is shown in Figure 3.14. For all of the proceeding calculations, bubbles are assumed sufficiently spherical to be represented by a spherical bubble model and this spherical bubble model is parameterized by a bubble radius, r_b, which is nominally set to $0.254\,\mathrm{mm}$.

The surface area of a single bubble, A_B^1, is calculated through block (1) and the single bubble volume, V_B^1, is calculated through node (3). Both of these calculations use the nominal bubble radius, r_b. Node (2) is the node gas volume, V_G, and this is divided by the single bubble volume, block (3). The division is performed by block (5) and determines the number of bubbles in the node. The number of bubbles is then multiplied by the surface area of a single bubble, from block (1), the get the total bubble surface area in the node.

The method to calculate the mass transfer coefficient is dependent on the node in which the mass transfer coefficient is being calculated. The mass transfer correlations used to calculate the mass transfer coefficient are shown in Table 3.10. The mass transfer correlation is implemented in block (7) which derives its dimensionless numbers and thermophysical properties from the thermophysical property subsystem (Section 3.5).
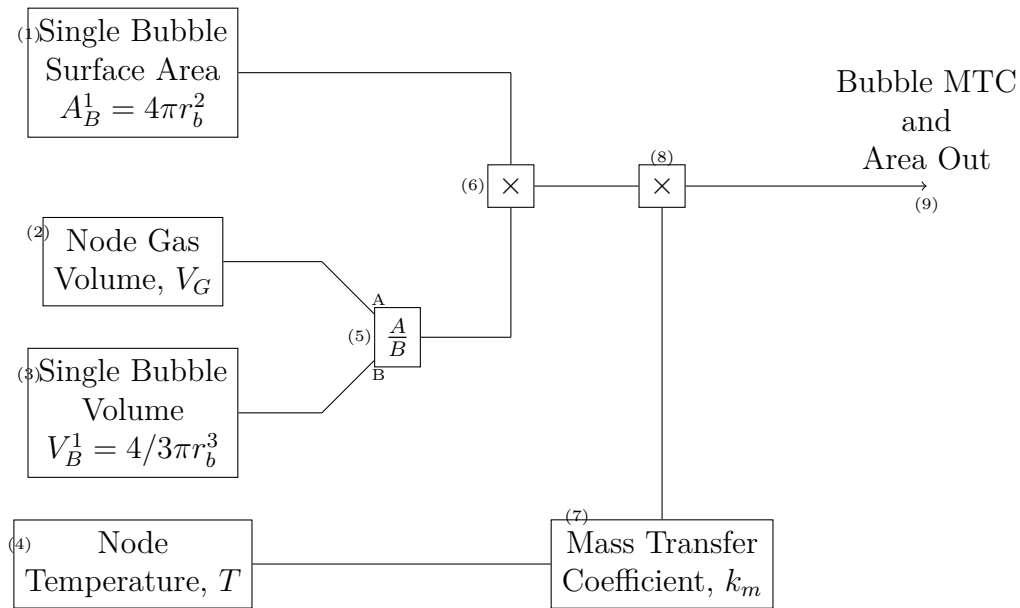
Figure 3.14: Subsystem to determine a node's bubble mass transfer area and mass transfer coefficient

Description	Correlation	Nodes Applied To	Notes	Source
Single bubbles of gas in liquid, continuous phase coefficient, very small bubbles	$\frac{k_m 2 r_b}{D} = 1.0(ReSc)^{1/3}$	CA, UH, LH	r_B: bubble radius.	Perry's Handbook [45] page 5-69
Small rigid particles in turbulent pipeline flow	$\frac{k_m 2 r_p}{D} = 0.0096 Re^{0.931} Sc^{0.346}$	G_1–G_4, P_{100}–P_{102}, HX	r_p: pipe radius	ORNL-TM-2245 page 23 [46]
Highly agitated systems; solid particles, drops, and bubbles; continuous phase coefficient	$k_m = \frac{0.13}{Sc^{2/3}}\left(\frac{(P/V)\mu g}{\rho}\right)^{1/4}$	FP	V: Tank volume, the volume of the pump bowel. P: Pump power	Perry's Handbook [45] page 5-70

Note: The pump power, P, is nominally 47.5 horse power (35.4 kW) and is taken from ORNL-TM-0728 [36] page 151. The tank volume, V, is the sum of the fuel pump gas and liquid volumes as well as the sum of the excess volumes from all other lumped volume nodes.

Table 3.10: Bubble mass transfer correlations used in dynamic model

3.9 The Xenon Stripper Subsystem

The operation of the xenon stripper is shown in Figure 3.15. The system has two outputs, the rate of removal of Xe-135 from the fuel salt, $\dot{N}_{Xe}^{FS\ Strpr.}$, provided through line (18), and the rate of removal of xenon from the bubbles, $\dot{N}_{Xe}^{B\ Strpr.}$, line (16). Both of these mechanisms are dependent on *stripping efficiency*, η_B, and η_{FS} for the bubble and fuel salt respectively and the efficiency used in this model are derived from the data presented on page 50 of ORNL-4069 [25].

The rate of removal of xenon from the fuel salt is calculated through,

$$\dot{N}_{Xe}^{FS.\ Strpr.} = \eta_{FS} C_{Xe}^{FS} \dot{Q}^{Strpr.}, \tag{3.36}$$

where η_{FS}, the fuel salt stripping efficiency, is provided by block (15), $\dot{Q}^{Strpr.}$ is the volumetric flow rate of fuel salt through the xenon stripper, provided by block (3), and C_{Xe}^{FS} is the fuel salt xenon concentration, which is provided by the computation of block (11). Block (5), the fuel salt Xe-135 content, N_{Xe}^{FS}, is provided by the fuel salt subsystem (Section 3.4). Block (6), the the total fuel salt liquid volume, is found by summing all the liquid volumes in all the nodes in the lumped volume sub system (Section 3.6). The fuel salt stripping efficiency, η_{FS}, is nominally set to 10%. This fuel salt stripping efficiency was obtained from ORNL-4069, [25].

The bubble Xe-135 stripping action is output through line (17) and is calculated through,

$$\dot{N}_{Xe}^{B.Strpr.} = \eta_B C_B V_B^1 \dot{Q}^{Strpr.} C_{Xe}^B. \tag{3.37}$$

The bubble stripping efficiency, η_B, is provided by block (14), and is nominally set to 12%. This bubble stripping efficiency was obtained from ORNL-4069, [25]. The bubble concentration, C_B, is provided by the operation of block (9) and is the number of bubbles in the fuel salt per unit volume. Block (8) provides the total number of bubbles in the fuel salt by

dividing the total gas volume in the fuel salt, V_G^{FS}, provided by block (2), by the volume of a single bubble, V_B^1, provided by block (3). Summation block (10) provides the total fuel salt volume (both liquid and gas phases). Block (12) does the computation and line (16) provides the output.

The output of the bubble action, (16), is fed into the bubble subsystem whereas the output of the fuel salt action, (17), is fed into the fuel salt subsystem.
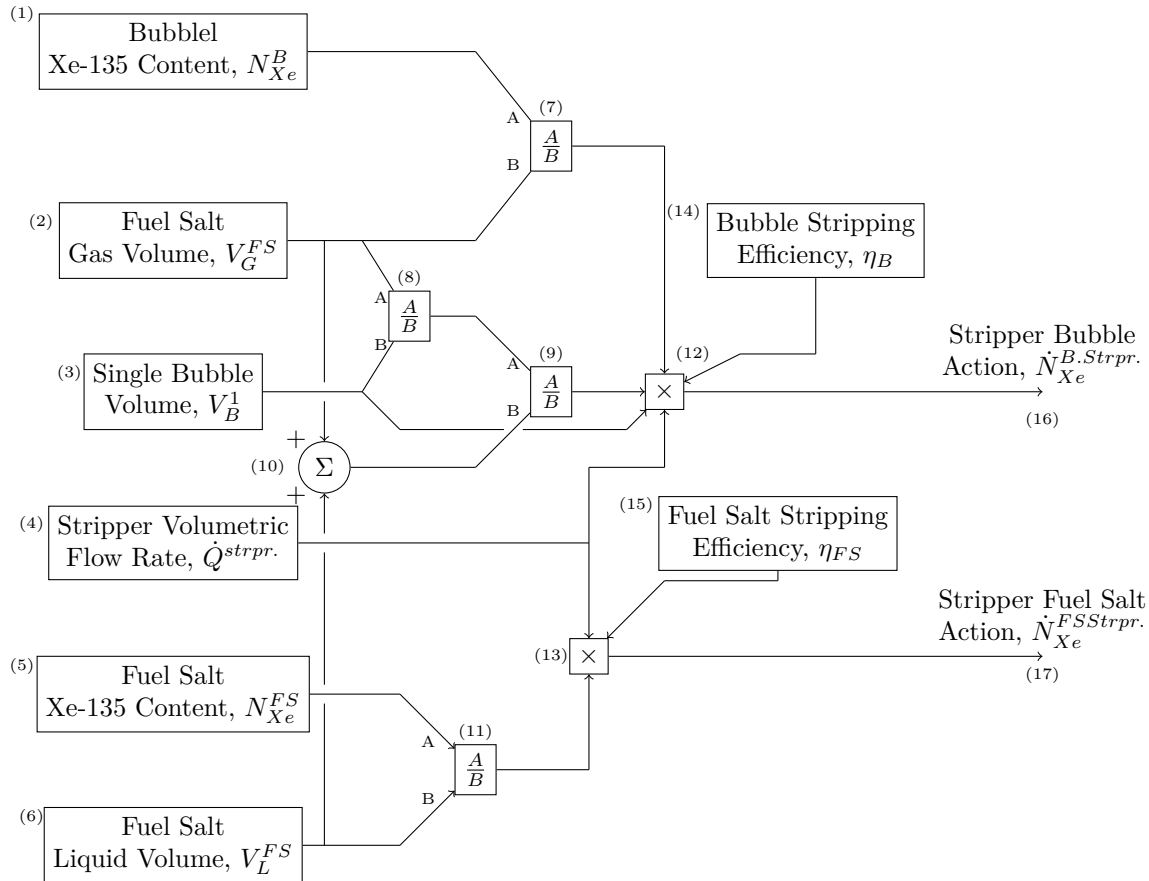
Figure 3.15: Xenon stripper system

3.10 Nuclear Properties and Reactivity Coefficients

Xenon concentration in both the fuel salt and graphite are converted to reactivity defects through reactivity coefficients. The reactivity coefficients, taken from page 54 of ORNL-

TM-3464 [3], are shown in Table 3.11. These reactivity coefficients are used to transform the xenon concentrations in the various reactor models into xenon poison fractions (effective reactivity lost due to xenon). The xenon concentration in a compartment is multiplied by the reactivity coefficient for that compartment. The total reactivity lost is calculated by summing the reactivity losses from each compartment.

The fuel salt reactivity coefficient was applied to both the fuel salt and bubble Xe-135 content. The combined fuel salt and bubble xenon concentration was calculated through,

$$\frac{N_{Xe}^B + N_{Xe}^{FS}}{V_L^{FS} + V_G^{FS}}. \tag{3.38}$$

Region	Reactivity Coefficient ($\frac{\delta k}{k} \frac{atoms}{cm^3}$)
Combined Fuel Salt + Bubble	5.17×10^{-18}
Graphite Region 1	3.34×10^{-18}
Graphite Region 2	6.99×10^{-18}
Graphite Region 3	6.69×10^{-18}
Graphite Region 4	7.91×10^{-19}

Table 3.11: Dynamic model reactivity coefficients

3.11   Summary and Chapter Conclusion

This chapter has aimed to present a technical description of the model used in this thesis and has done so by providing a system by system description of the model and its components. The approach taken in this model is new in several aspects. Foremost, the model analyzes all thermophysical properties, lumped volumes, and mass transfer constants as functions of temperature which allows for dynamic analyses to be performed. Second, the bubble model of the MSRE is the most complete developed to date — the ORNL-TM-3464 [3] bubble model only included 5 regions whereas this model more than doubles that. Furthermore, this is the first time a graphite stringer has been modeled as a second order solution to a reaction diffusion equation and done so using multiple flow regions. Finally, the nuclear

data used includes the proper half life for Te-135, which was not done in prior MSRE xenon models, since the half life was not known at the time.

CHAPTER 4

Methodology of Sensitivity Analysis

4.1 Introduction

The prior chapter described the inner workings on the model. This chapter provides a description of the methodology used in the sensitivity analysis. First, the goal of the sensitivity analysis is described. Next, the benchmarking methodology is detailed — i.e. specifically how the benchmarking was done. The parameters studied are described and rationale is given for the study of each parameter. The scoring methodology for the quantification of the effect of the perturbation is explained. A brief discussion is given related to the precision of the model. The goal of the chapter is to provide a transparent description as to how the sensitivity analysis was done and thereby improving the repeatability of the work.

4.2 Goal of Sensitivity Analysis

The sensitivity analysis will allow us to orientate ourselves in the model's parameter space. We will gain an understanding of how perturbation of parameters affects the model's performance with respect to the benchmarks. Once this has been established, we can then perform minimum necessary variation of model parameters in order to attempt to fit the model to experimental data and then hypothesize why variation of these parameters leads

to the model fitting the data.

In order to accomplish this, for each perturbed parameter the following sensitivity analyses were performed:

- Start up / Build up transient,

- Shut down transient,

- Steady state distribution of xenon.

4.3   Benchmarking

Benchmarking of the model was done by comparing the prediction produced by the model from start up (build up) and shut down transients to those published in ORNL-TM-3464 [3]. Although the shut down transient data is reported in terms of reactivity worth, the build up transient data is reported in terms of *fraction of steady-state*. Therefore, each analysis for the build up transient was normalized to its steady state value.

The start up transient was simulated by setting all system integrators to a zero initial condition and allowing the model to evolve from this initial state to its state after $t = 40\,\text{h}$. Steady state was established by allowing the model to evolve from its zero initial state to its state at $t = 5.8\,\text{d}\,/\,5 \times 10^5\,\text{s}$. The shut down transient was simulated by setting setting all of the neutron flux signals to zero after it had reached steady state and allowing the model to evolve for another $40\,\text{h}$.

4.4   Sensitivity Analysis and Error Bounds

The model's nominal case was determined by selecting model parameter values that correspond to the best available data in the literature. These parameter values may or may not be correct. Therefore, the 11 parameters that were judged to be most crucial in determining the models confidence were selected for sensitivity analysis. This also provides some sense

of an *error bar.* Although the benchmark data from the ORNL literature had no error bars associated with it, by perturbing the parameters to within some upper and lower bounds, some maximal and minimal bounds can be established on the model output itself.

Each result from the sensitivity analysis bounds the parameter under study by some factor that was judged to be a reasonable estimate of potential variation, and transient simulations were run with both the high and low variation cases. Additionally, the nominal case was also run and the results plotted.

4.5 Parameters Studied and Significance of Parameters

4.5.1 Overview of Parameters Studied

The following parameters were studied as part of the sensitivity analysis:

- Volume

- Temperature

- Density and Viscosity

- Mass Transfer Coefficients

- Fission Yields

- Cross Sections

- Neutron Fluxes

- Bubble and Xenon Radii

- The Circulating Void Fraction

- Reactivity Coefficients

- Xenon Stripper Parameters

Note, in many studies, such as the volume sensitivity analysis, several parameters were grouped together in order to simplify the analysis. In the case of the volume, core volumes were lumped into either in core or out of core volumes and the analysis was performed on these lumps.

4.5.2   Rationale For Study of Volume

In order to simplify the analysis, the perturbations are either applied to the *overall volume* — all the nodes simultaneously — the *in core volume* — the graphite regions, upper head and lower heads — or the *out of core volume* — the complement of the in core volume.

System volumes are important to perform sensitivity analysis on since the in core and out of core volumes are not rigidly defined terms. There are areas such as the upper head or lower head which could be reasonably be argued to be either in core or out of core since neutron flux does not immediately drop to zero outside of the region occupied by the graphite stringers. If the model shows substantial sensitivity to volume perturbation, it indicates more refined measurements and notions of in core or out of core volumes need to be constructed in order to increase model confidence.

4.5.3   Rationale For Study of Temperature

In order to simplify the analysis, the perturbations are either applied to the *overall temperature* — all the nodes simultaneously — the in *core temperature* — the graphite regions, upper head and lower heads — or the *out of core temperature* — the complement of the in core temperature. Note, for the in core temperatures, both the fuel salt and graphite temperatures were perturbed.

The temperature is an important factor to perform sensitivity analysis on since, (1) measurements of out of core temperatures were not found in the literature, and (2) the thermal model of the system is approximated with only the measured in core temperatures for fuel salt and graphite, the fuel inlet temperature, and fuel outlet temperatures. If the

model demonstrates a significant response to thermal perturbation, it inductees a more sophisticated thermal model should be used in its formulation.

4.5.4   Rationale for Study of Density and Viscosity

Sensitivity analysis is performed on both the nominal density and the nominal viscosity; that is, the density and viscosity before any thermal scaling is applied to them. The density and viscosity are important factors to perform sensitivity analysis on since the density and viscosity values used in the model were derived from in lab measurements rather than in situ measurements. In lab measurements need not, and often do not, match up with in situ measurements. If the model shows substantial sensitivity to density and viscosity it indicates that more sophisticated models or measurements of density or viscosity would be beneficial for improving model confidence.

Note, the density is perturbed without any corresponding perturbation to fuel salt volume.

4.5.5   Rationale for Study of Fission Yields

Fission yields are important factors to perform sensitivity analysis on since the actinide composition of the fuel salt changes with burn up and operation of the reactor and each actinide has its own fission yield. If the fission yield is a significant factor the xenon behavior of the system, it indicates that detailed measurements of fuel salt composition would be beneficial in increasing model confidence. All of the instances of the normalized build up transient sensitivity analysis indicate good agreement with the MSRE build up data.

4.5.6   Rationale for Study of Cross Sections

Sensitivity analysis was performed with perturbation of the macroscopic fission cross section and microscopic Xe-135 absorption cross section.

The macroscopic fission cross section is an important parameter to perform sensitivity analysis on since the model from which it was derived was not benchmarked on any sort of standardized benchmark data — which does not exist for the MSRE. The microscopic absorption cross section for Xe-135 also benefits from sensitivity analysis since the value used in the model was taken from ORNL-4069 [25] and is cited as a *personal communication* with no supporting documentation.

Relatively large bounds were used to study the effect of perturbation of these cross section. This was done so that it could be determined if inaccuracies in them were the result of the mismatch between the experimental and model predicted xenon poisoning.

4.5.7 Rationale for Study of Neutron Fluxes

Sensitivity analysis was performed with perturbation of the neutron fluxes. Both the fuel salt and graphite neutron fluxes were perturbed. When the graphite neutron flux was perturbed all fluxes in all of the graphite regions were scaled by the same factor and this was done in order to simplify the analysis.

The fluxes are important factors to perform sensitivity analyses on since they were all taken from a single source that lacked substantial documentation on experimental methodology. Furthermore, there is uncertainty about the precise magnitude of the power the MSRE was running at when the experimental measurements were made.

4.5.8 Rationale for Study of Bubble and Xenon Radii

Sensitivity analysis was performed with perturbation of the xenon radius and bubble radius. These are important factors to perform sensitivity analyses on since the bubble radius was determined from a single estimate in MSRE operating experience and the xenon radius used in the Einstein Stokes equation approximates atoms as hard spheres and there is no *hard sphere radius* — atoms aren't hard spheres.

4.5.9 Rationale for Study of Circulating Void Fraction

Sensitivity analysis was performed with perturbation of the circulating void fraction. Void fractions of 0.1%, 0.4% (nominal) were run along with a high bound of 3% to account for early measurements of the void fraction.

The circulating void fraction is an important parameter to perform sensitivity analysis on since, despite numerous efforts, the methodology to measure the circulating void fraction in the MSRE never reached consensus nor maturity and because of this any record of the circulating void fraction ought to be interpreted and applied with caution.

4.5.10 Rationale for Study of Reactivity Coefficients

Sensitivity analysis was performed with perturbation of the reactivity coefficients. This is important since the reactivity coefficients were taken from reference documentation and minimal explanation on how these coefficients were derived was found. Furthermore, it is unknown if the coefficients precisely map one to one from the source's geometry to the dynamic models geometry.

4.5.11 Rationale for Study of Xenon Stripper Parameters

Sensitivity analysis was performed with perturbation of the xenon stripper parameters: the fuel salt stripping efficiency, the bubble stripping efficiency, and the xenon stripper volumetric flow rate.

There is substantial uncertainty in the magnitude of the stripping efficiencies since the fuel salt stripping efficiency was measured on a CO_2, water system and bubble stripping efficiency was never measured. Furthermore, no information was found on how the xenon stripper flow rate was measured, although, since this was likely a common activity in the lab, it was likely done to a decent degree of accuracy. Regardless it is because of these uncertainties that the xenon stripper parameters are important to perform sensitivity analysis on.

4.5.12 Rationale for Mass Transfer Coefficients

In order to simplify the analysis, the mass transfer coefficients for the graphite was varied in all regions simultaneously and the mass transfer coefficients for the bubbles were varied in all volumes simultaneously.

The mass transfer coefficients are important factors to perform sensitivity analysis on since they have a number of substantial uncertainties associated with them including the accuracy and validity of heat / mass transfer coefficients, the applicability of mass transfer coefficients measured in laboratory apparatus to piece wise application in a reactor, and the compounded uncertainty of dimensionless numbers and thermophysical properties associated with the derivation of the mass transfer coefficients. If the mass transfer coefficients prove to be significant factors in determining the xenon behavior of the model, it indicates that more work should be done in determining the mass transfer coefficients and verifying their application to situations in the reactor.

4.6   Quantification of The Effect of Perturbation

In order to quantify the relative importance of each parameter that was perturbed under sensitivity analysis we define the *integral difference between bounds per percent change score* (or, just the score) as the quantity,

$$\text{score} = \frac{\int P_{high}(t)dt - \int P_{low}(t)dt}{\Delta PC}, \tag{4.1}$$

where $P_{high}(t)$ is the xenon poisoning at time t for the high bound perturbation, $P_{low}(t)$, is the xenon poisoning at time t for the low bound perturbation, and ΔPC is the percentage points the parameter under investigation was changed in the sensitivity analysis. The time domain of integration is a 6.44×10^5 s (6.44×10^5 s + 40 h) run in which the reactor is brought up from zero power then shut down after 5×10^5 s and allowed to evolved for another 40 h.

4.7 On The Accuracy of The Model

This chapter has aimed to provide a transparent description as to how the sensitivity analysis was done and has done so by describing the goal of the sensitivity analysis, describing how the benchmarking was done, describing the notion of error bounds, describing the parameters studied and their significance and the rationale for study.

This model uses data from various sources and correlations. Many of these sources do not have error bounds. For example, the Xe-135 neutron absorption cross section from ORNL-4069 [25] was reported from a *personal communication* without error bounds, methodology, nor error analysis. This is common practice in MSR literature. Although the numbers generated by this model are reported to two or three significant figures, this does not imply that the model can confidently predict results to within two or three significant figures. At this stage in MSR xenon theory we're still trying to figure *if* a model can predict the behavior rather than *how accurately* a model can predict behavior. As previously mentioned, an estimate of the model's error (if the model actually describes the phenomenology of the model) can be derived through variation of parameters in the sensitivity analysis. As such, we do not precisely know the volume of the upper head, but we believe the results are accurate to within ± 20%, and we can run the model within the values and observe the results. Therefore, the following numbers are presented as is with the understanding that they are estimates of what the actual behavior would be.

CHAPTER 5

Results of Benchmarking and Sensitivity Analysis

5.1   Introduction

The prior chapter described the how the sensitivity analysis would be performed. This chapter presents the results of the benchmarking and sensitivity analysis. Since the sensitivity analysis varies one parameter as all other parameters are held constant, the descriptions of the plots are necessarily repetitious. A description of how the plots are laid out is given, followed by a presentation of each of the plots generated through the sensitivity analysis. The objective of this chapter is to present the results of the sensitivity analysis.

5.2   Layout of Plots

Each of the forthcoming sections, except for the section on the perturbation of reactivity coefficients contains:

- A figure showing the results of the build up transient benchmark

- A figure showing the results of the shut down transient benchmark

- Figures showing the distribution of xenon at steady state.

For the figure that shows the results of the build up transient, available benchmark data was presented in terms of values normalized against the steady state xenon poisoning. Therefore, the left hand column of each build up transient benchmark presents the benchmark against normalized results, whereas the right hand column presents non normalized results.

The shut down transient and build up transient sensitivity analyses have high, low, and nominal plots made for each analysis. The shaded area in each plot represents the range of outcomes that are bounded by the high and low cases.

For the steady state studies, the distribution was studied at the level of the reactivity coefficient. Therefore, each plot displays the homogenized fuel salt and bubble xenon concentration, the average xenon concentration, and, to study xenon egress from the system, the xenon stripping rate.

5.3 Volume

Figure 5.1 shows the results for the start up transient sensitivity analysis as the volumes are perturbed. The left column shows the normalized results, which are directly comparable to the reported MSRE build up data whereas the right column shows the non normalized results. All of the instances of the normalized build up transient sensitivity analysis indicate good agreement with the MSRE build up data. It is clearly visible that perturbation any of the volumes has effectively no influence on the normalized shape of the build up transient. The right column shows the non normalized results of the analysis.

Figure 5.2 shows the results for the shut down transient sensitivity analysis as the volumes are perturbed. For both Figures 5.1 and 5.2, the plot in the first row shows the results of the sensitivity analysis as the overall volume is perturbed, the second row shows the results for

the perturbation of the in core volume, and the last row shows the results as the out of core volume is perturbed. All of the plots underestimate the magnitude and time characteristics of the shut down transient response. There is a slightly positive correlation between the xenon poisoning and overall volume; a positive correlation between the in core volume and the xenon poisoning; and, a negative correlation between the out of core volume and the xenon poisoning. Furthermore, these correlations are observed in both the shut down and build up transient cases.

The results of the sensitivity analysis for the steady state distribution of xenon are shown in Figures 5.3, 5.4, and 5.5 for the overall volume, in core volume and out of core volume cases respectively. For each of these figures, the results for the homogenized fuel salt and bubble xenon concentration are shown in the first row, the average graphite xenon concentration is shown in the second row, and the total xenon stripping rate is shown in the final row.

There is a slightly positive correlation between homogenized fuel salt and bubble xenon concentration as well as average graphite xenon concentration and the overall volume. The fuel salt and bubble homogenized xenon concentration increases from $6.502 \times 10^{12}\,\mathrm{cm^{-3}}$ to $6.753 \times 10^{12}\,\mathrm{cm^{-3}}$. The average graphite xenon concentration increases and from $2.351 \times 10^{12}\,\mathrm{cm^{-3}}$ to $2.44 \times 10^{12}\,\mathrm{cm^{-3}}$. The correlation for xenon stripping and overall volume is positive and increases from $3.210 \times 10^{15}\,\mathrm{s^{-1}}$ to $4.880 \times 10^{15}\,\mathrm{s^{-1}}$.

With regards to the in core volume perturbation, the correlation for the homogenized fuel salt and bubble xenon concentration as well as the average graphite xenon concentration is positive, and the correlation for the stripping rate is also positive and considerably more so than the overall volume. The fuel salt and bubble xenon concentration increases from $6.502 \times 10^{12}\,\mathrm{cm^{-3}}$ to $6.753 \times 10^{12}\,\mathrm{cm^{-3}}$; the graphite xenon increases from $2.351 \times 10^{12}\,\mathrm{cm^{-3}}$ to $2.44 \times 10^{12}\,\mathrm{cm^{-3}}$; and, the xenon stripping rate increases from $3.21 \times 10^{15}\,\mathrm{cm^{-3}}$ to $4.88 \times 10^{15}\,\mathrm{cm^{-3}}$.

Finally, when the out of core volume is perturbed, the homogenized fuel salt and bubble xenon concentration as well as the average graphite concentration correlations are negative

and the xenon stripping rate correlation is positive. The fuel salt and bubble homogenized concentration decreases from $7.063\,\mathrm{cm^{-3}}$ to $6.284 \times 10^{12}\,\mathrm{cm^{-3}}$. The average graphite xenon concentration decreases from $2.575 \times 10^{12}\,\mathrm{cm^{-3}}$ to 2.258×10^{12} Finally, the xenon stripping rate increases from $4.008 \times 10^{15}\,\mathrm{s^{-1}}$ to $4.077 \times 10^{115}\,\mathrm{s^{-1}}$.

Figure 5.1: Results of build up sensitivity analysis with respect to volume
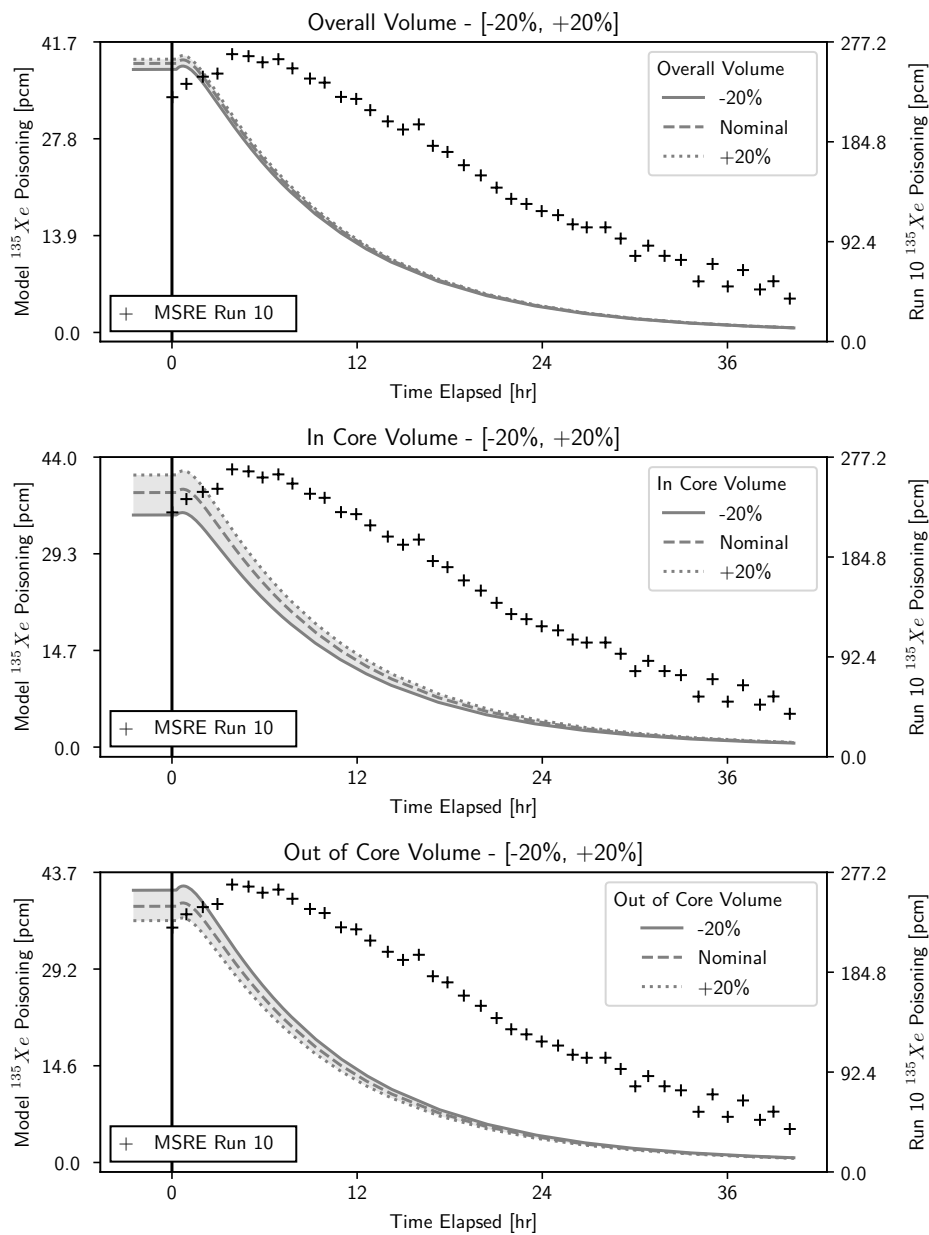
Figure 5.2: Results of shutdown sensitivity analysis with respect to volume

Figure 5.3: Steady state (SS) distribution of Xe-135 in the dynamic model as a result of perturbation of overall system volume

Figure 5.4: Steady state concentration of Xe-135 in the dynamic model as a result of perturbation of in core volume

Figure 5.5: Steady state concentration of Xe-135 in the dynamic model as a result of perturbation of out of core volume

5.4 Temperature

Figure 5.6 shows the results for the start up transient sensitivity analysis as the temperatures are perturbed. The left column shows the normalized results, which is directly comparable to the reported MSRE build up data whereas the right column shows the non normalized results. It is clearly visible that perturbation any of the temperatures has effectively no influence on the normalized shape of the build up transient. The right column shows the non normalized results of the analysis. All of the instances of the normalized build up transient sensitivity analysis indicate good agreement with the MSRE build up data.

Figure 5.7 shows the results for the shut down transient sensitivity analysis as the temperatures are perturbed. All of the plots underestimate the magnitude and time characteristics of the shut down transient response.

For both Figures 5.6 and 5.7, the plot in the first row shows the results of the sensitivity analysis as the overall temperature is perturbed, the second row shows the results for the perturbation of the in core temperature (including graphite), and the last row shows the results as the out of core temperature is perturbed. There is a positive correlation between the xenon poisoning and overall temperature; a positive correlation between the in core temperature and the xenon poisoning; and, a slightly positive correlation between the out of core temperature and the xenon poisoning. Furthermore, these correlations are observed in both the shut down and build up transient cases.

The results of the sensitivity analysis for the steady state distribution of xenon are shown in Figures 5.8, 5.9, and 5.10 for the overall temperature, in core temperature and out of core temperature cases respectively. For each of these figures, the results for the homogenized fuel salt and bubble xenon concentration are shown in the first row, the average graphite xenon concentration is shown in the second row, and the total xenon stripping rate is shown in the final row.

With regards to the overall system temperature perturbation, the correlation for the

homogenized fuel salt and bubble xenon concentration and overall temperature is negative; for average graphite xenon concentration, it is positive; and, for the stripping rate, it is negative. The fuel salt and bubble xenon concentration decreases from $6.924 \times 10^{12}\,\mathrm{cm}^{-3}$ to $6.001 \times 10^{12}\,\mathrm{cm}^{-3}$; the graphite xenon increases from $9.422 \times 10^{11}\,\mathrm{cm}^{-3}$ to $8.536 \times 10^{12}\,\mathrm{cm}^{-3}$; and, the xenon stripping rate decreases from $4.152 \times 10^{15}\,\mathrm{cm}^{-3}$ to $3.534 \times 10^{15}\,\mathrm{cm}^{-3}$.

With regards to the in core temperature perturbation, the correlation for the homogenized fuel salt and bubble xenon concentration and overall temperature is negative; for average graphite xenon concentration, it is positive; and, for the stripping rate, it is negative. The fuel salt and bubble xenon concentration decreases from $6.926 \times 10^{12}\,\mathrm{cm}^{-3}$ to $6.005 \times 10^{12}\,\mathrm{cm}^{-3}$; the graphite xenon increases from $8.043 \times 10^{11}\,\mathrm{cm}^{-3}$ to $8.322 \times 10^{12}\,\mathrm{cm}^{-3}$; and, the xenon stripping rate decreases from $4.193 \times 10^{15}\,\mathrm{cm}^{-3}$ to $3.536 \times 10^{15}\,\mathrm{cm}^{-3}$.

Finally, with regards to the out of core temperature perturbation, the correlations for the homogenized fuel salt and bubble xenon concentration, average graphite xenon concentration, and total stripping rate are all non-monotonic. The nominal fuel salt and bubble homogenized xenon concentration is $6.651 \times 10^{12}\,\mathrm{cm}^{-3}$. With a 20% decrease in out of core temperature, the homogenized bubble and fuel salt xenon concentration is $6.619 \times 10^{12}\,\mathrm{cm}^{-3}$. With a 20% increase in out of core temperature, the homogenized fuel salt and bubble xenon concentration is $6.625 \times 10^{12}\,\mathrm{cm}^{-3}$. The average graphite xenon concentration at the nominal out of core temperature is $2.406 \times 10^{12}\,\mathrm{cm}^{-3}$. With a 20% decrease in out of core temperature, the average graphite xenon concentration is $2.659 \times 10^{12}\,\mathrm{cm}^{-3}$. With a 20% increase in out of core temperature, the average graphite xenon concentration is $3.763\,\mathrm{cm}^{-3}$. The xenon stripping rate is nominal $4.045 \times 10^{15}\,\mathrm{s}^{-1}$. With a 20% decrease in temperature, the xenon stripping rate is $3.99 \times 10^{15}\,\mathrm{s}^{-1}$. With a 20% increase in temperature, the xenon stripping rate is $3.948 \times 10^{15}\,\mathrm{s}^{-1}$.
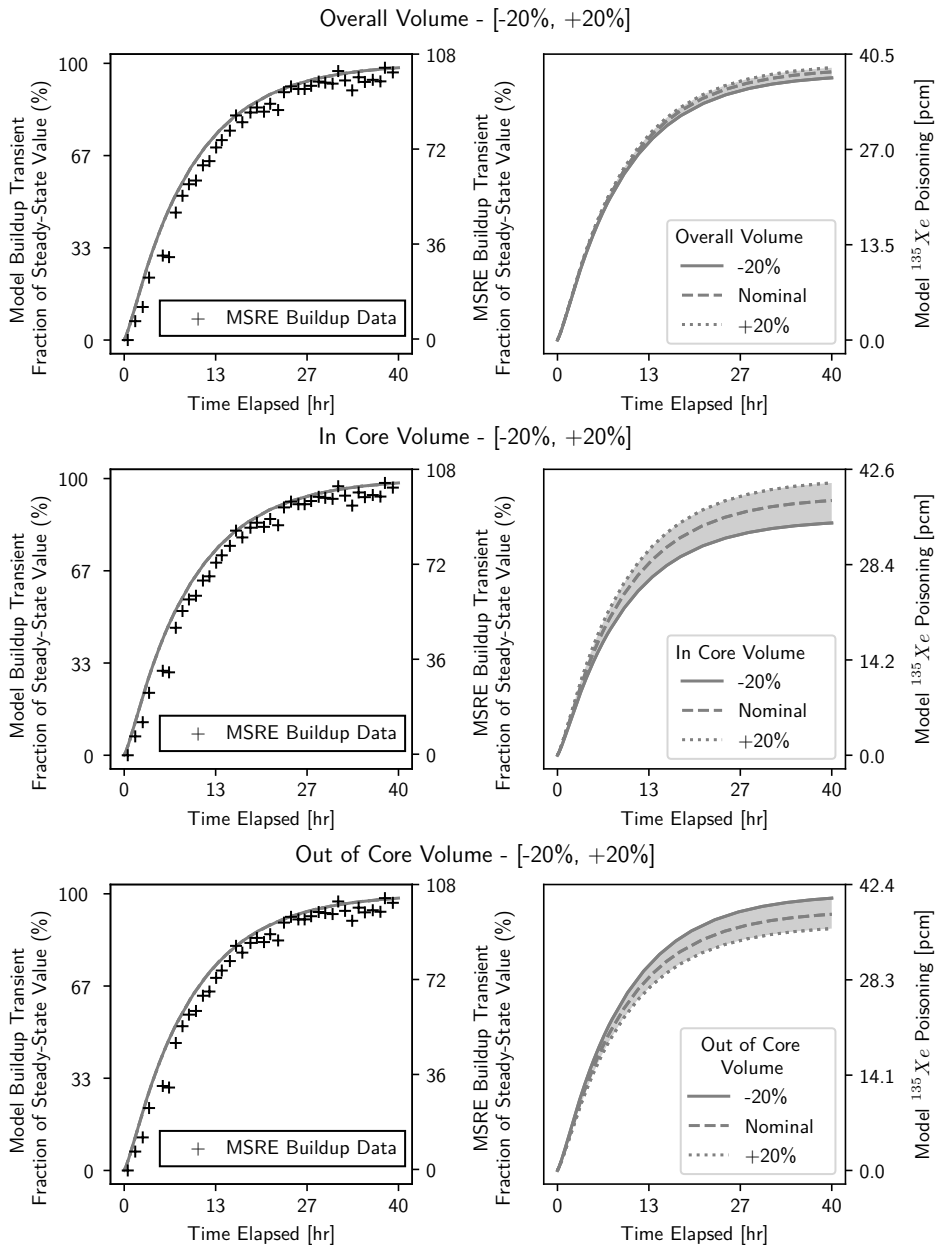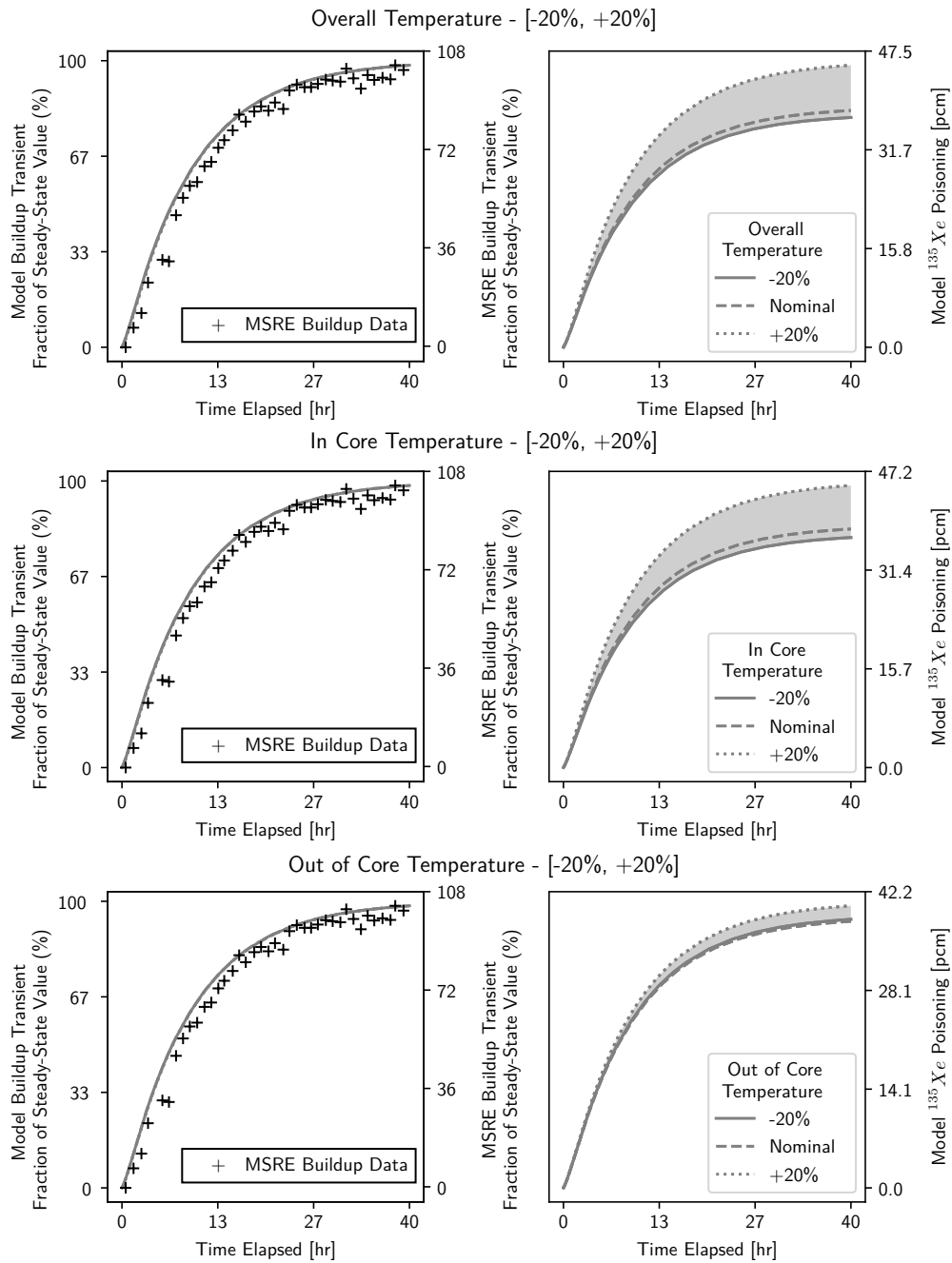
Figure 5.6: Results of build up transient sensitivity analysis with respect to temperature
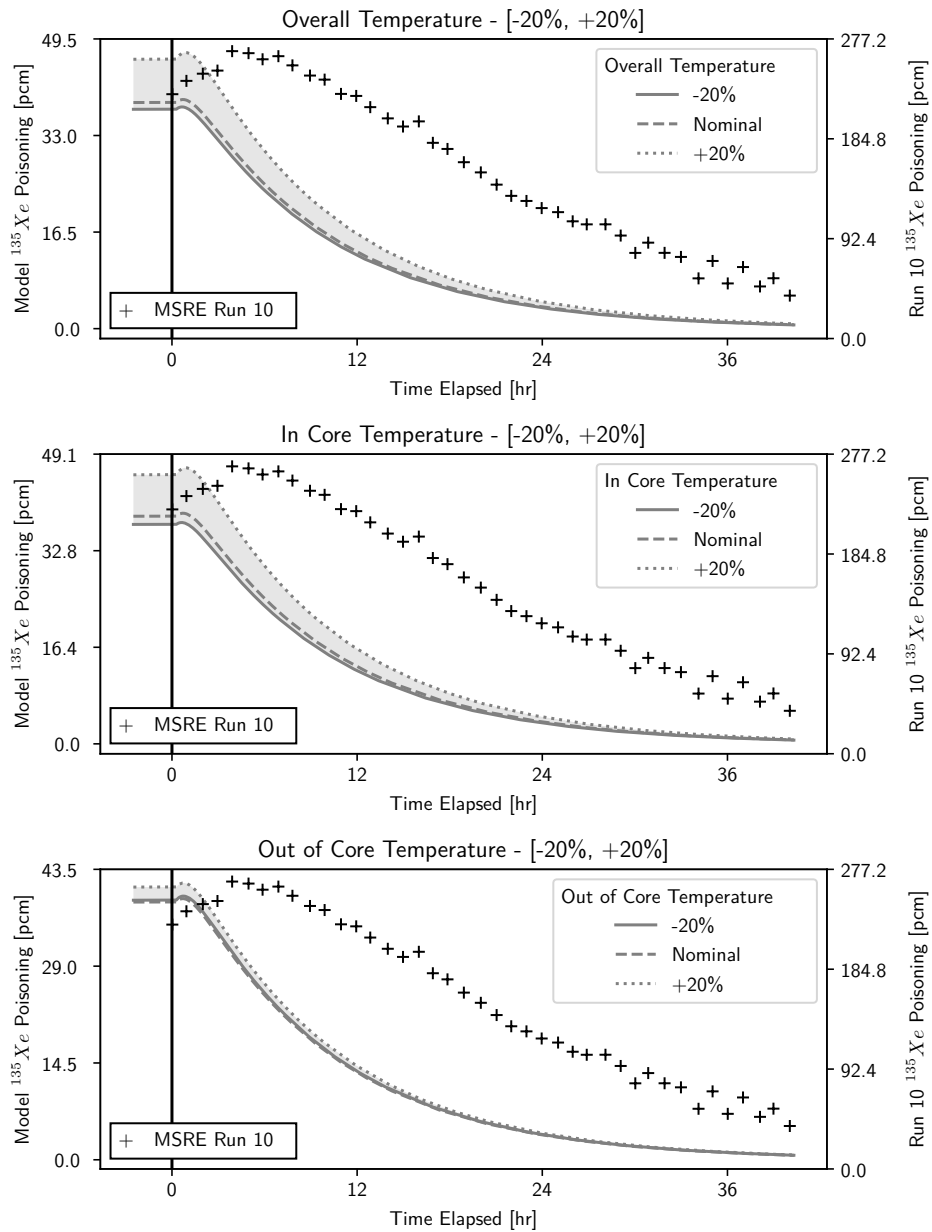
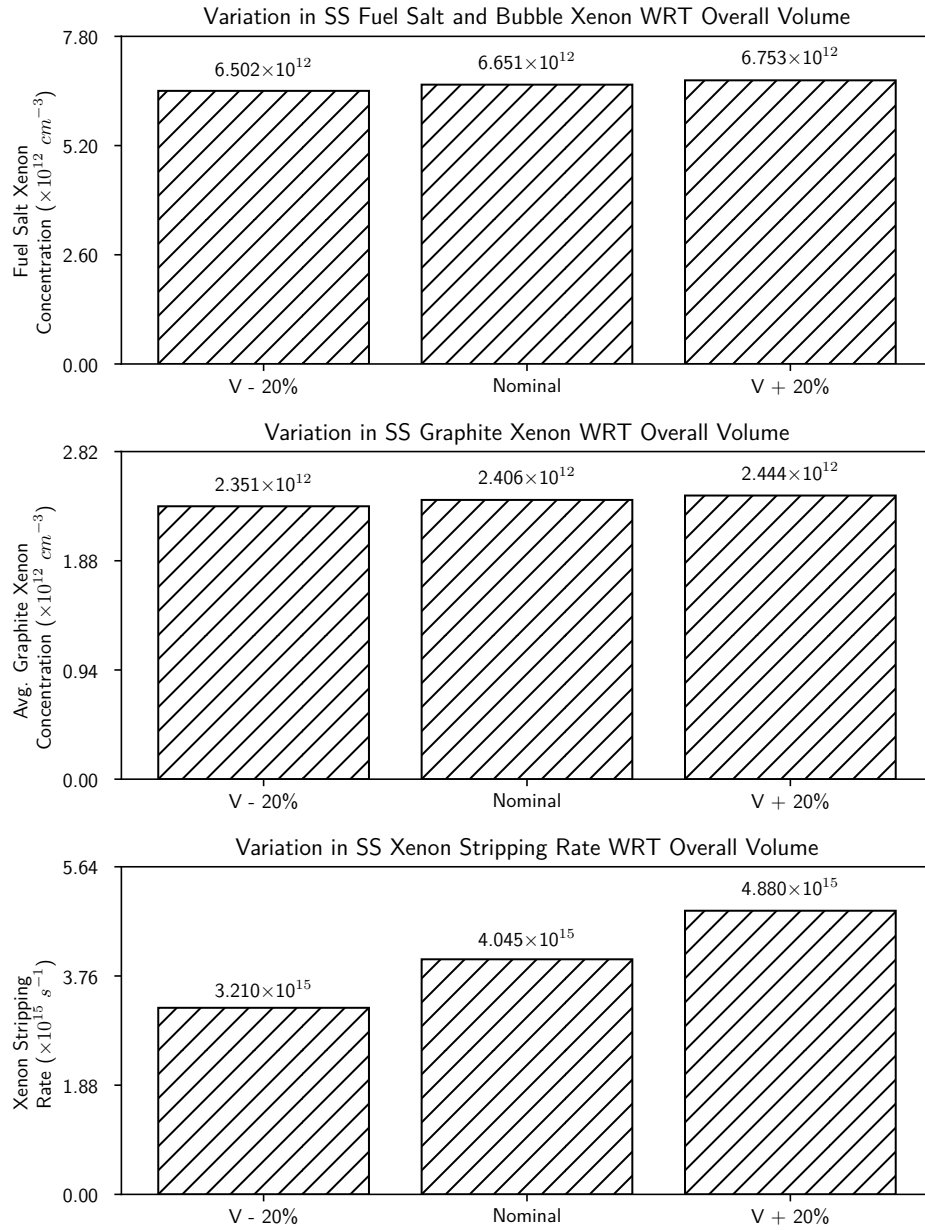Figure 5.7: Results of sensitivity analysis with respect to temperature

Figure 5.8: Steady state concentration of Xe-135 in the dynamic model as a result of perturbation of overall system temperature
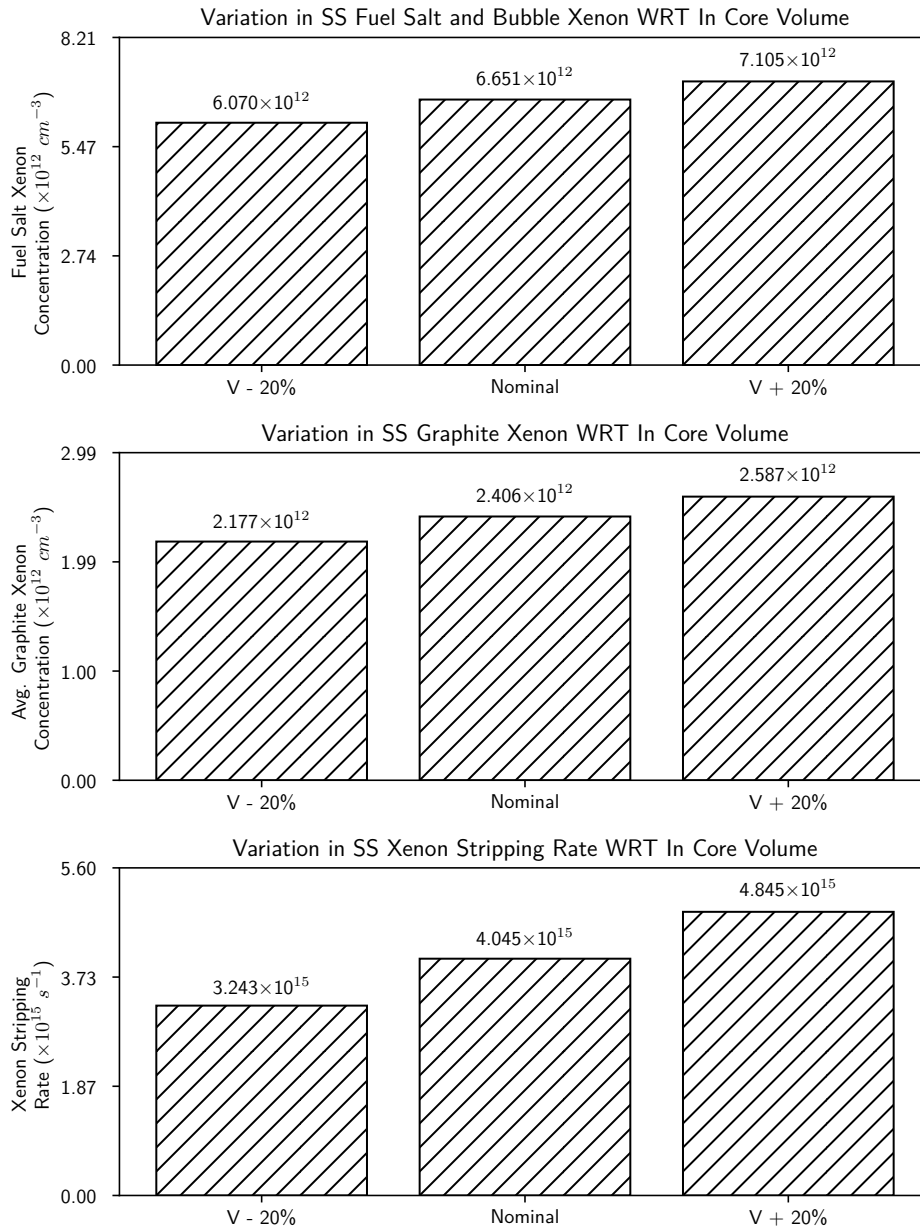
Figure 5.9: Steady state concentration of Xe-135 in the dynamic model as a result of perturbation of in core temperature
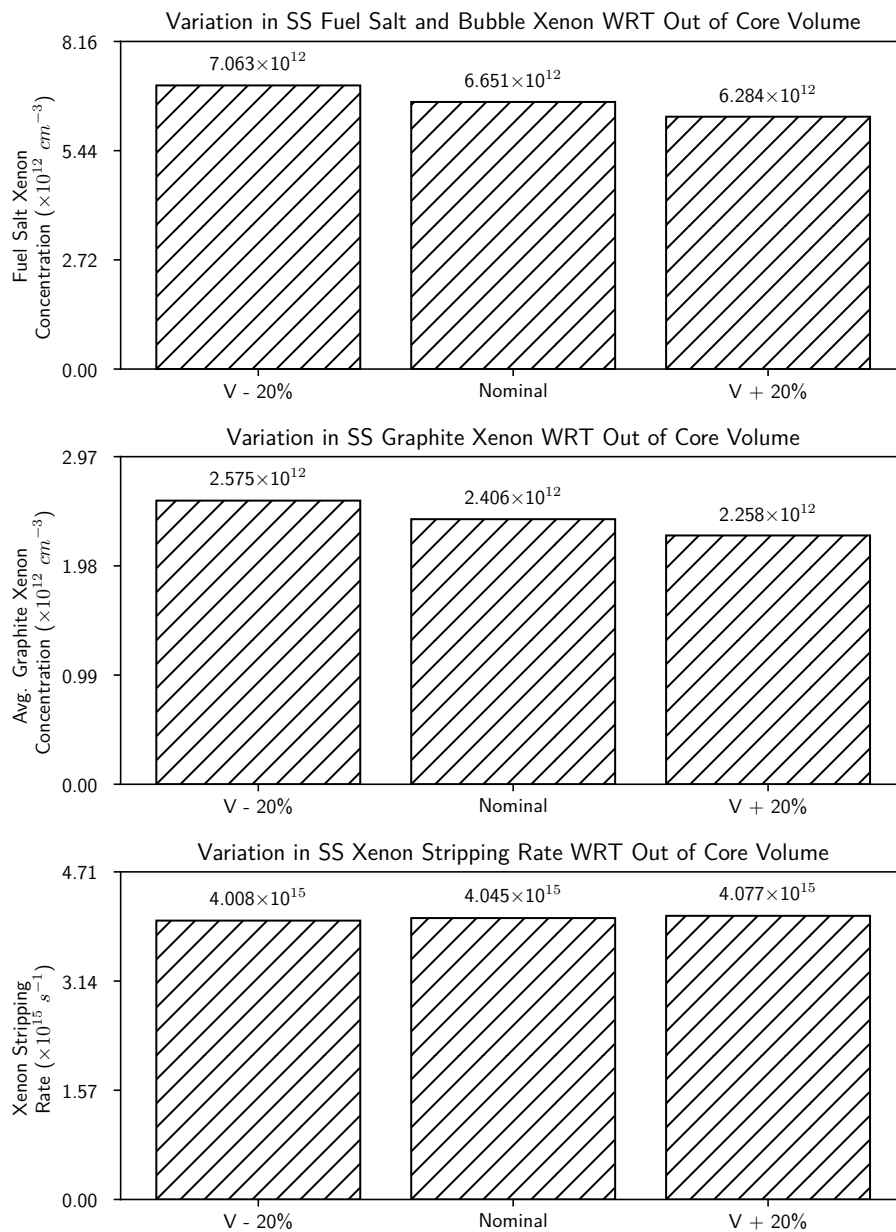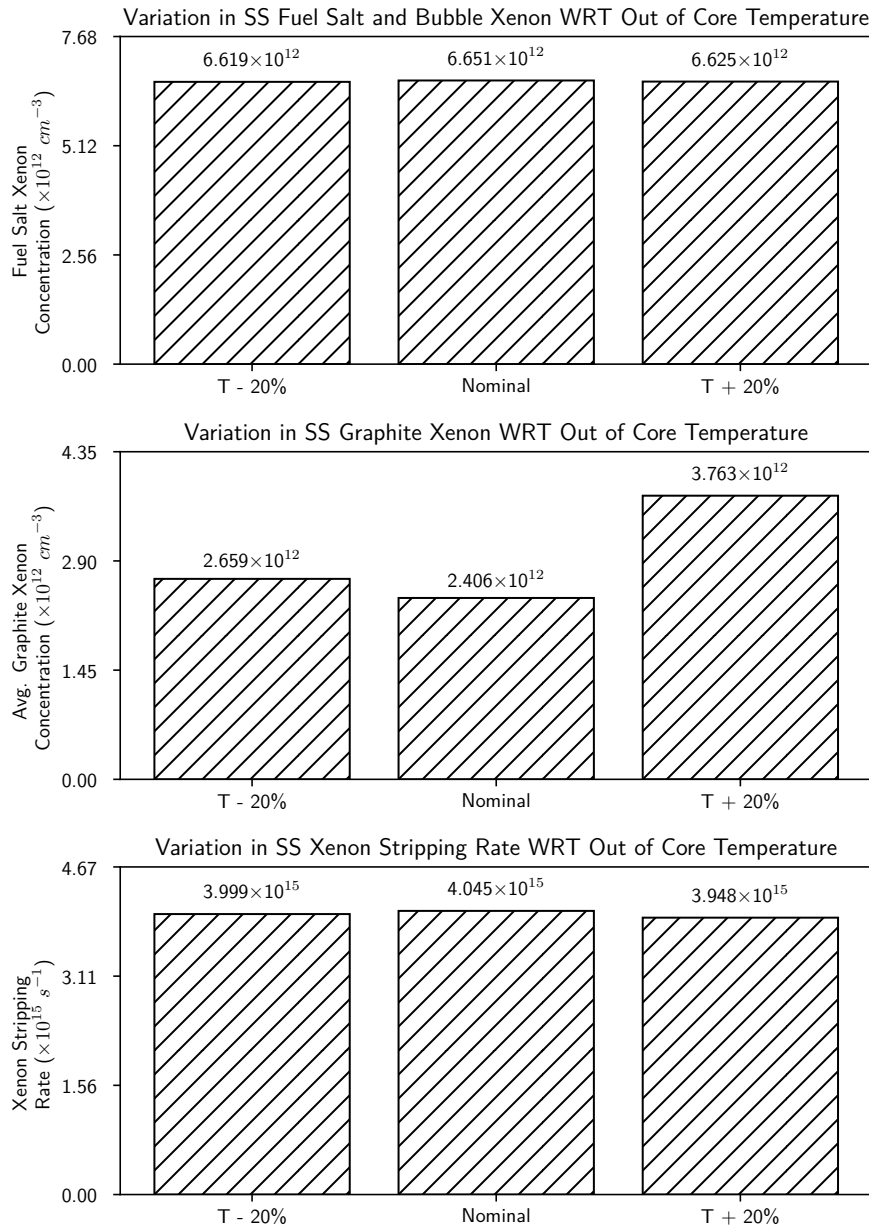
Figure 5.10: Steady state concentration of Xe-135 in the dynamic model as a result of perturbation of out of core temperature

5.5   Density and Viscosity

Figure 5.11 shows the results for the start up transient sensitivity analysis as the fuel salt density and viscosity is perturbed. The left column shows the normalized results, which is directly comparable to the reported MSRE build up data whereas the right column shows the non normalized results. It is clearly visible that perturbation any of the density or viscosity have effectively no influence on the normalized shape of the build up transient. The right column shows the non normalized results of the analysis. All of the instances of the normalized build up transient sensitivity analysis indicate good agreement with the MSRE build up data.

Figure 5.12 shows the results for the shut down transient sensitivity analysis as the fuel salt density or viscosity is perturbed. All of the plots underestimate the magnitude and time characteristics of the shut down transient response.

For both Figures 5.11 and 5.12, the plot in the first row shows the results of the sensitivity analysis as the density is perturbed and the second row shows the results for the perturbation as the viscosity is perturbed. It is observed in these plots that there is a positive correlation between the xenon poisoning and density; a negative correlation between the viscosity and the xenon poisoning. Furthermore, these correlations are observed in both the shut down and build up transient cases.

The results of the sensitivity analysis for the steady state distribution of xenon are shown in Figures 5.13 and 5.14 for density and viscosity respectively. For each of these figures, the results for the homogenized fuel salt and bubble xenon concentration are shown in the first row, the average graphite xenon concentration is shown in the second row, and the total xenon stripping rate is shown in the final row.

With regards to the density perturbation, the correlation for the homogenized fuel salt and bubble xenon concentration and density is negative; for average graphite xenon concentration, it is positive; and, for the stripping rate, it is negative. The fuel salt and bubble

xenon concentration decreases from $6.676 \times 10^{12}\,\mathrm{cm}^{-3}$ to $6.628 \times 10^{12}\,\mathrm{cm}^{-3}$; the graphite xenon increases from $2.175 \times 10^{12}\,\mathrm{cm}^{-3}$ to $2.610 \times 10^{12}\,\mathrm{cm}^{-3}$; and, the xenon stripping rate increases from $4.063 \times 10^{15}\,\mathrm{cm}^{-3}$ to $4.029 \times 10^{15}\,\mathrm{cm}^{-3}$.

With regards to the in viscosity perturbation, the correlation for the homogenized fuel salt and bubble xenon concentration is positive; for average graphite xenon concentration, it is negative; and, for the stripping rate, it is positive. The fuel salt and bubble xenon concentration increases from $6.585 \times 10^{12}\,\mathrm{cm}^{-3}$ to $6.698 \times 10^{12}\,\mathrm{cm}^{-3}$; the graphite xenon increases from $2.874 \times 10^{12}\,\mathrm{cm}^{-3}$ to $2.079 \times 10^{12}\,\mathrm{cm}^{-3}$; and, the xenon stripping rate increases from $4.009 \times 10^{15}\,\mathrm{cm}^{-3}$ to $4.069 \times 10^{15}\,\mathrm{cm}^{-3}$.
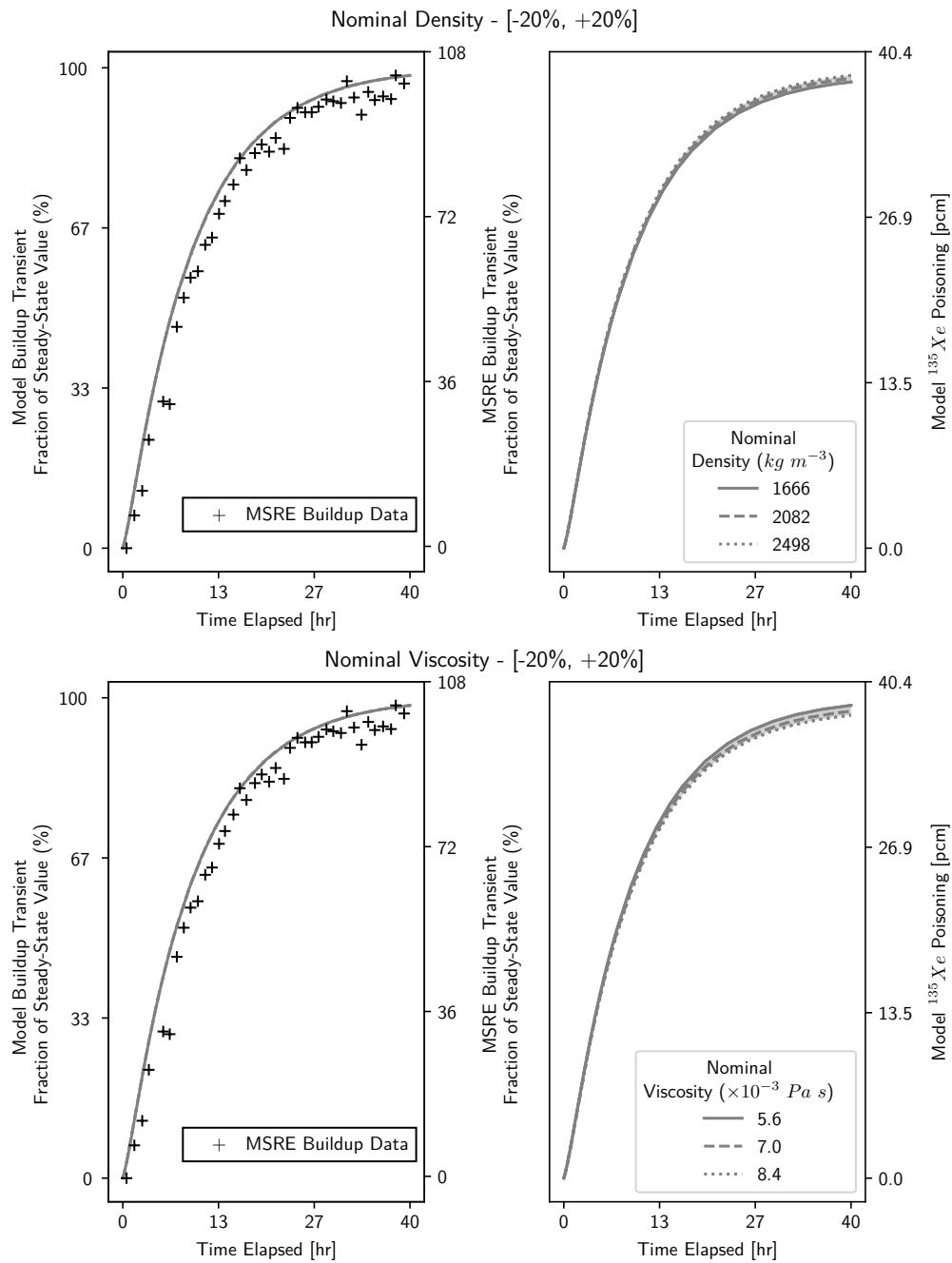
Figure 5.11: Results of build up transient sensitivity analysis with respect to nominal density and viscosity
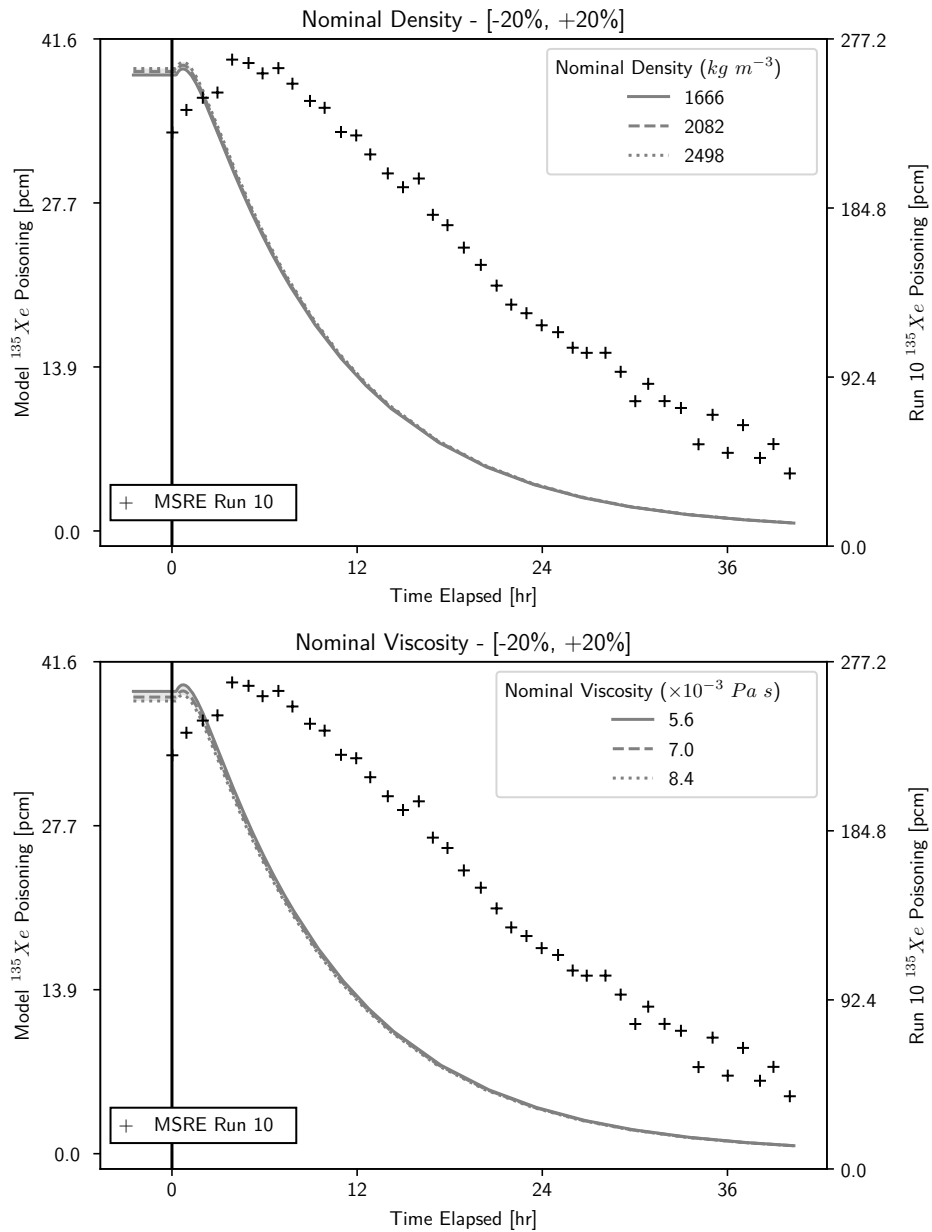
Figure 5.12: Results of sensitivity analysis with respect to nominal density and viscosity
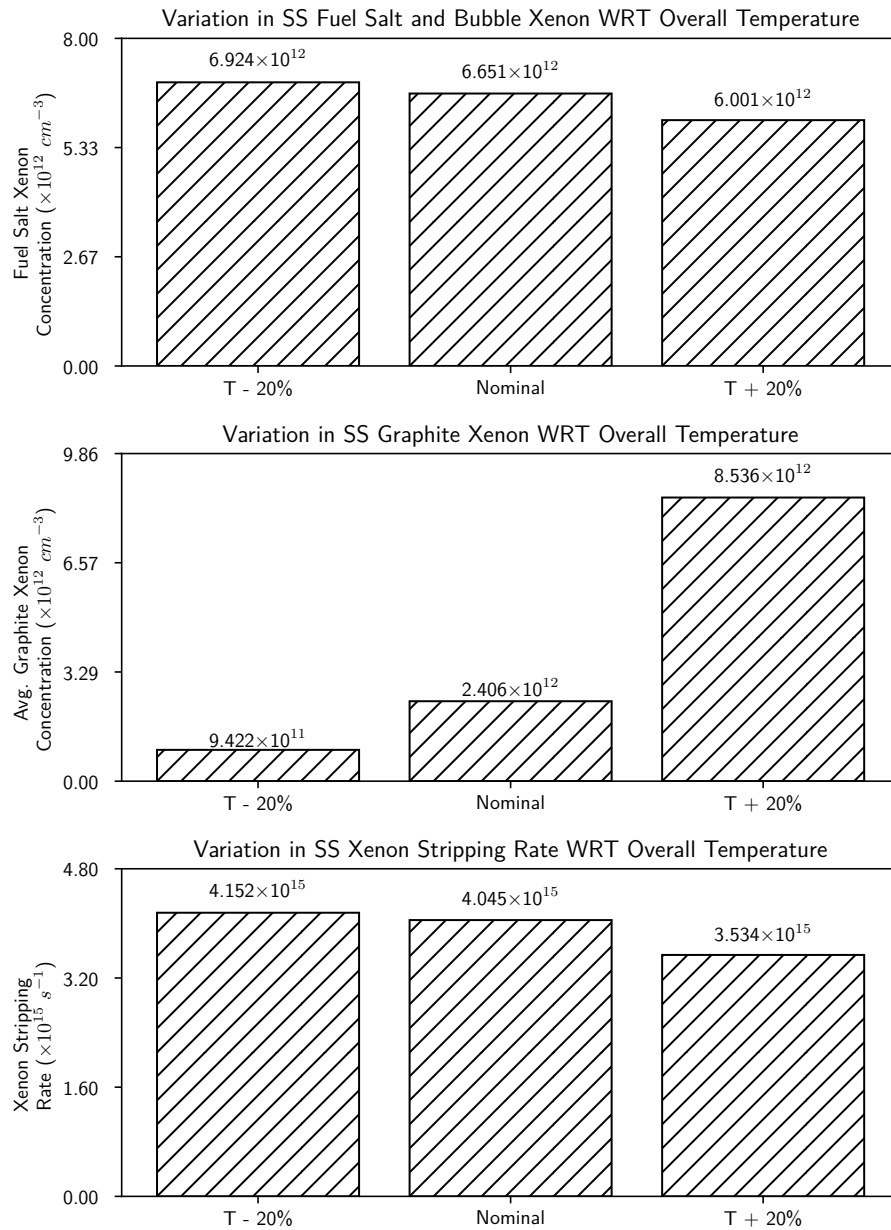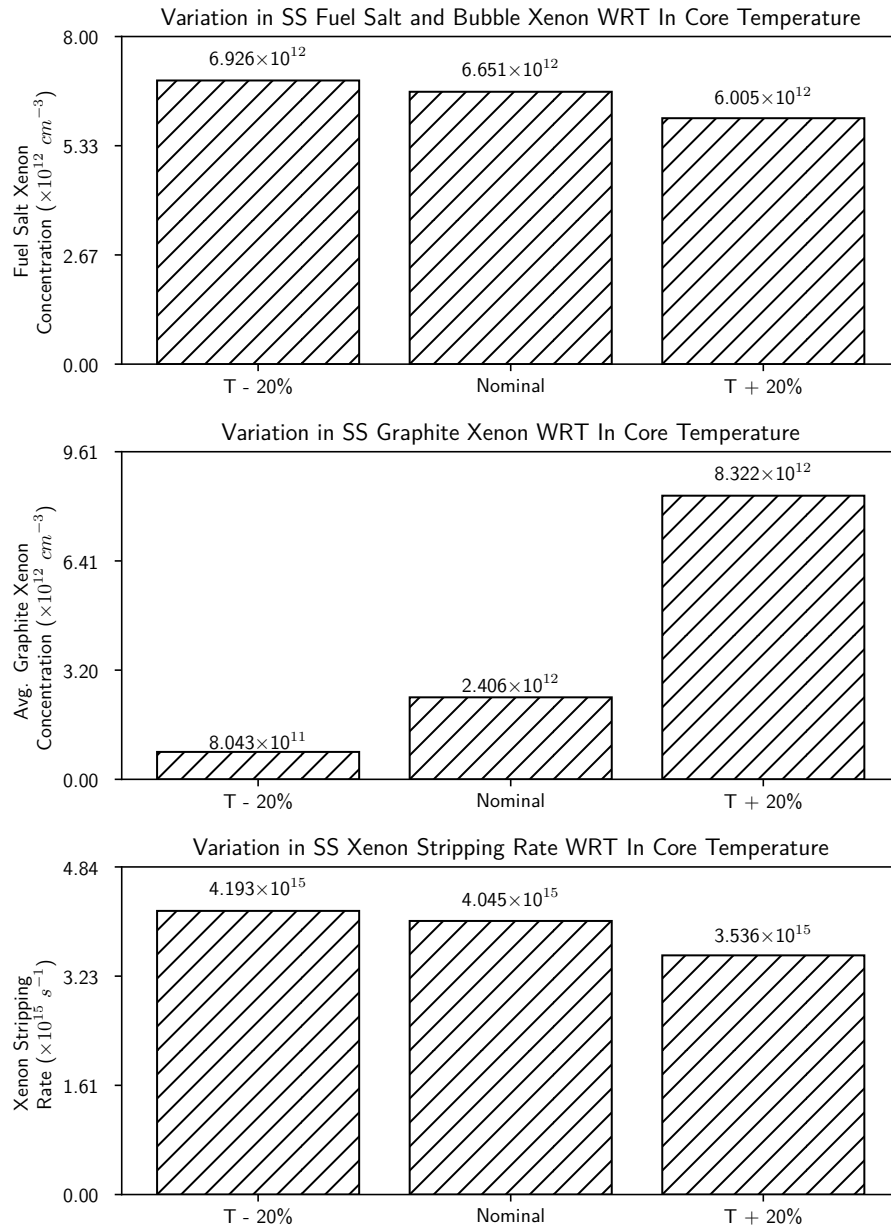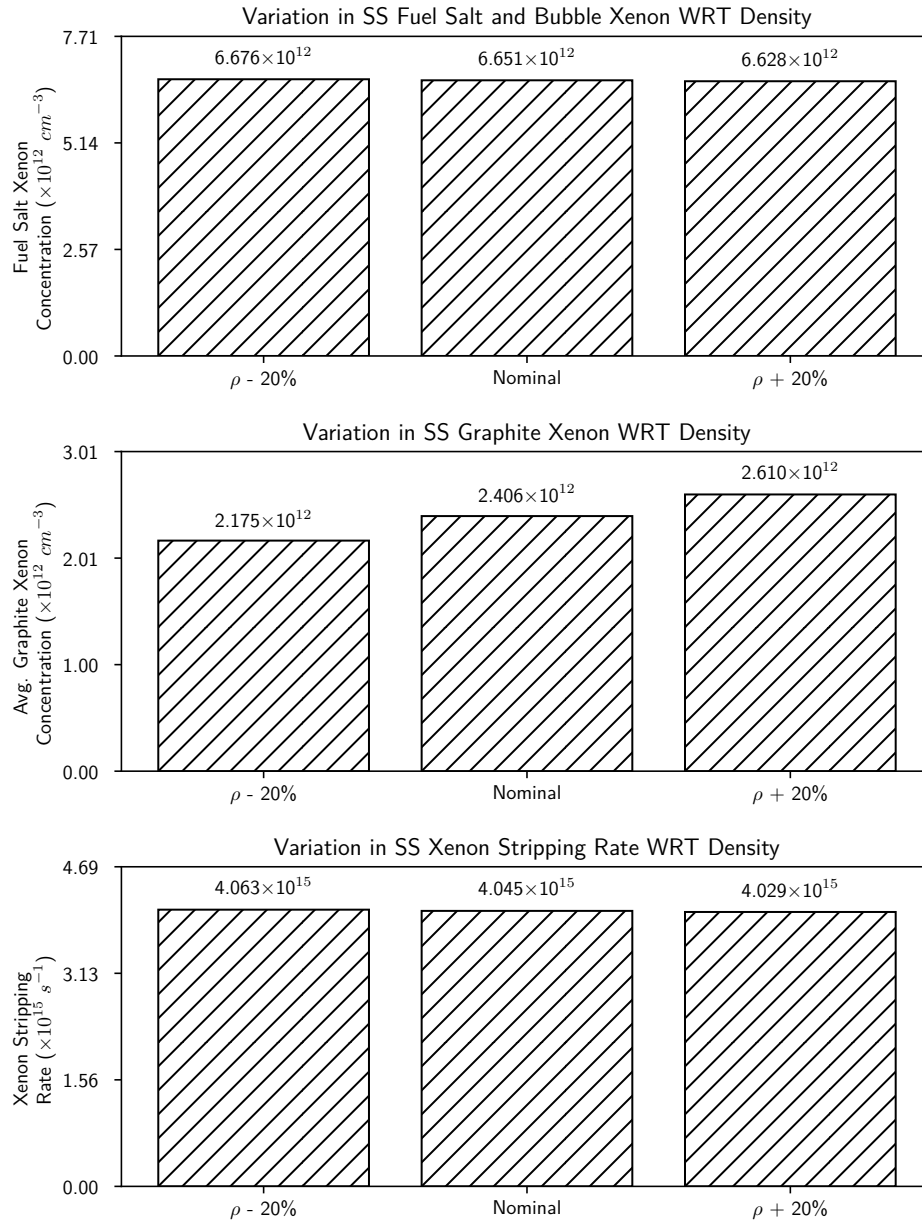
Figure 5.13: Steady state concentration of Xe-135 in the dynamic model as a result of perturbation of density
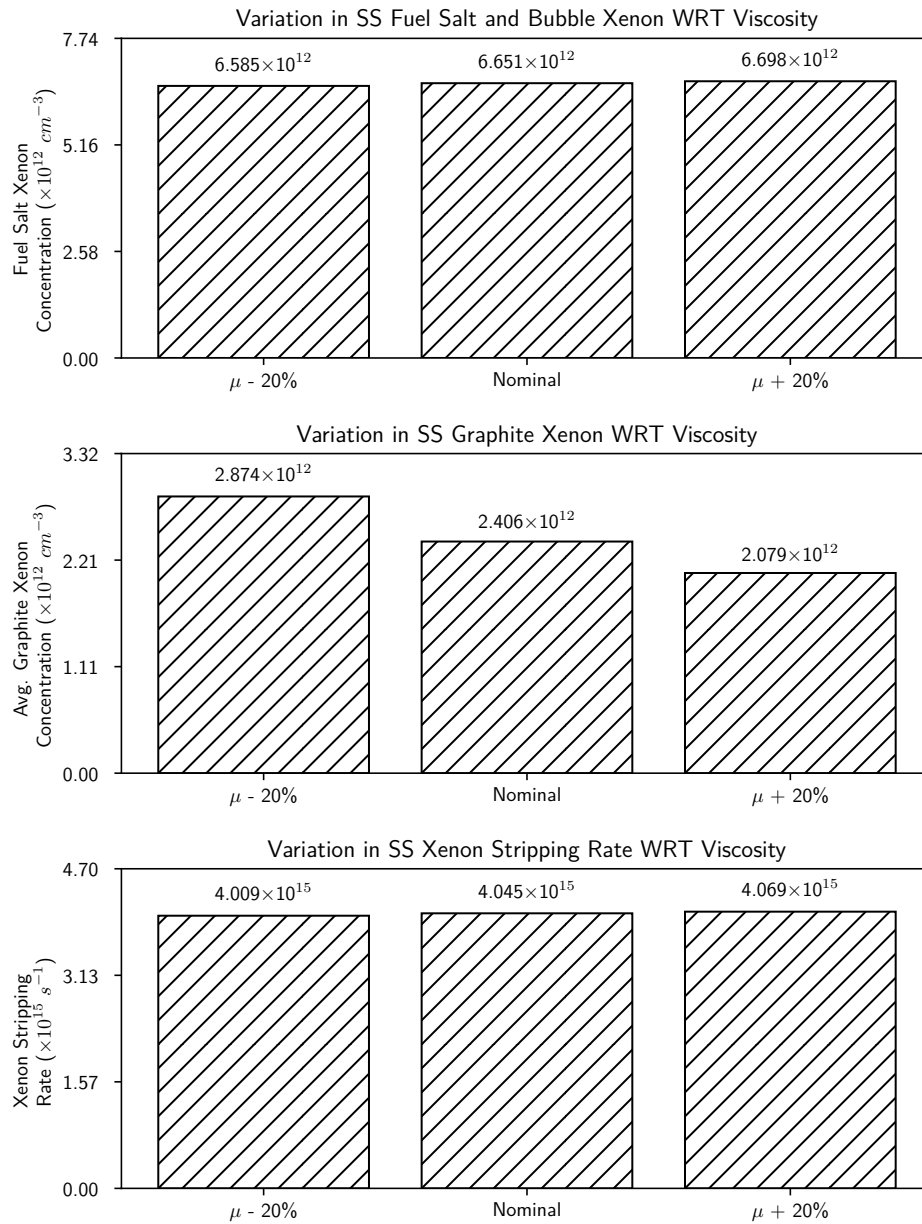
Figure 5.14: Steady state concentration of Xe-135 in the dynamic model as a result of perturbation of viscosity

5.6   Mass Transfer Coefficients

Figure 5.15 shows the results for the start up transient sensitivity analysis as the graphite and bubble mass transfer coefficients are perturbed. The left column shows the normalized results, which is directly comparable to the reported MSRE build up data whereas the right column shows the non normalized results. It is clearly visible that perturbation any of the mass transfer coefficients have effectively no influence on the normalized shape of the build up transient. The right column shows the non normalized results of the analysis. All of the instances of the normalized build up transient sensitivity analysis indicate good agreement with the MSRE build up data.

Figure 5.16 shows the results for the shut down transient sensitivity analysis as the fuel salt mass transfer coefficients are perturbed. All of the plots underestimate the magnitude and time characteristics of the shut down transient response.

For both Figures 5.15 and 5.16, the plot in the first row shows the results of the sensitivity analysis as the graphite mass transfer coefficient is perturbed and the second row shows the results for the perturbation as the bubble mass transfer coefficient is perturbed. It is observed in these plots that there is a positive correlation between the xenon poisoning and graphite mass transfer coefficient; a negative correlation between the bubble mass transfer coefficient and the xenon poisoning. Furthermore, these correlations are observed in both the shut down and build up transient cases.

The results of the sensitivity analysis for the steady state distribution of xenon are shown in Figures 5.17 and 5.18 for graphite and bubble mass transfer coefficients respectively. For each of these figures, the results for the homogenized fuel salt and bubble xenon concentration are shown in the first row, the average graphite xenon concentration is shown in the second row, and the total xenon stripping rate is shown in the final row.

With regards to the graphite mass transfer coefficient perturbation, the correlation for the homogenized fuel salt and bubble xenon concentration and density is negative; for average

graphite xenon concentration, it is positive; and, for the stripping rate, it is negative. The fuel salt and bubble xenon concentration decreases from $6.737 \times 10^{12}\,\text{cm}^{-3}$ to $6.567 \times 10^{12}\,\text{cm}^{-3}$; the graphite xenon increases from $1.715 \times 10^{12}\,\text{cm}^{-3}$ to $3.073 \times 10^{12}\,\text{cm}^{-3}$; and, the xenon stripping rate decreases from $4.097 \times 10^{15}\,\text{cm}^{-3}$ to $3.994 \times 10^{15}\,\text{cm}^{-3}$.

With regards to the in bubble mass transfer coefficient, the correlation for the homogenized fuel salt and bubble xenon concentration is non-monotonic; for average graphite xenon concentration, it is negative; and, for the stripping rate, it is positive. The fuel salt and bubble xenon concentration decreases from $6.641 \times 10^{12}\,\text{cm}^{-3}$ to $6.656 \times 10^{12}\,\text{cm}^{-3}$; the graphite xenon decreases from $2.731 \times 10^{12}\,\text{cm}^{-3}$ to $2.227 \times 10^{12}\,\text{cm}^{-3}$; and, the xenon stripping rate decreases from $4.017 \times 10^{15}\,\text{cm}^{-3}$ to $4.060 \times 10^{15}\,\text{cm}^{-3}$.
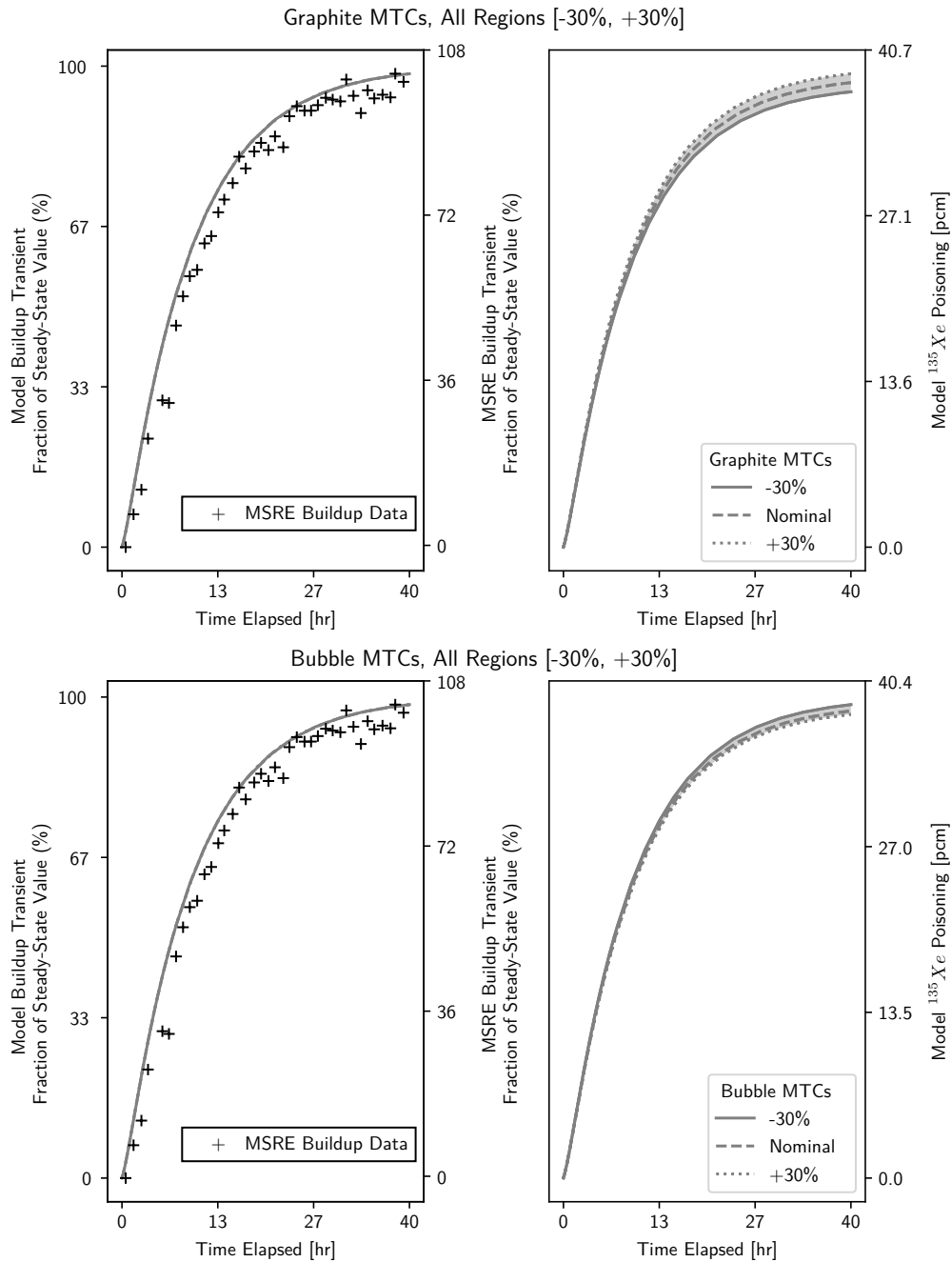
Figure 5.15: Results of build up transient sensitivity analysis with respect to graphite and bubble mass transfer coefficients
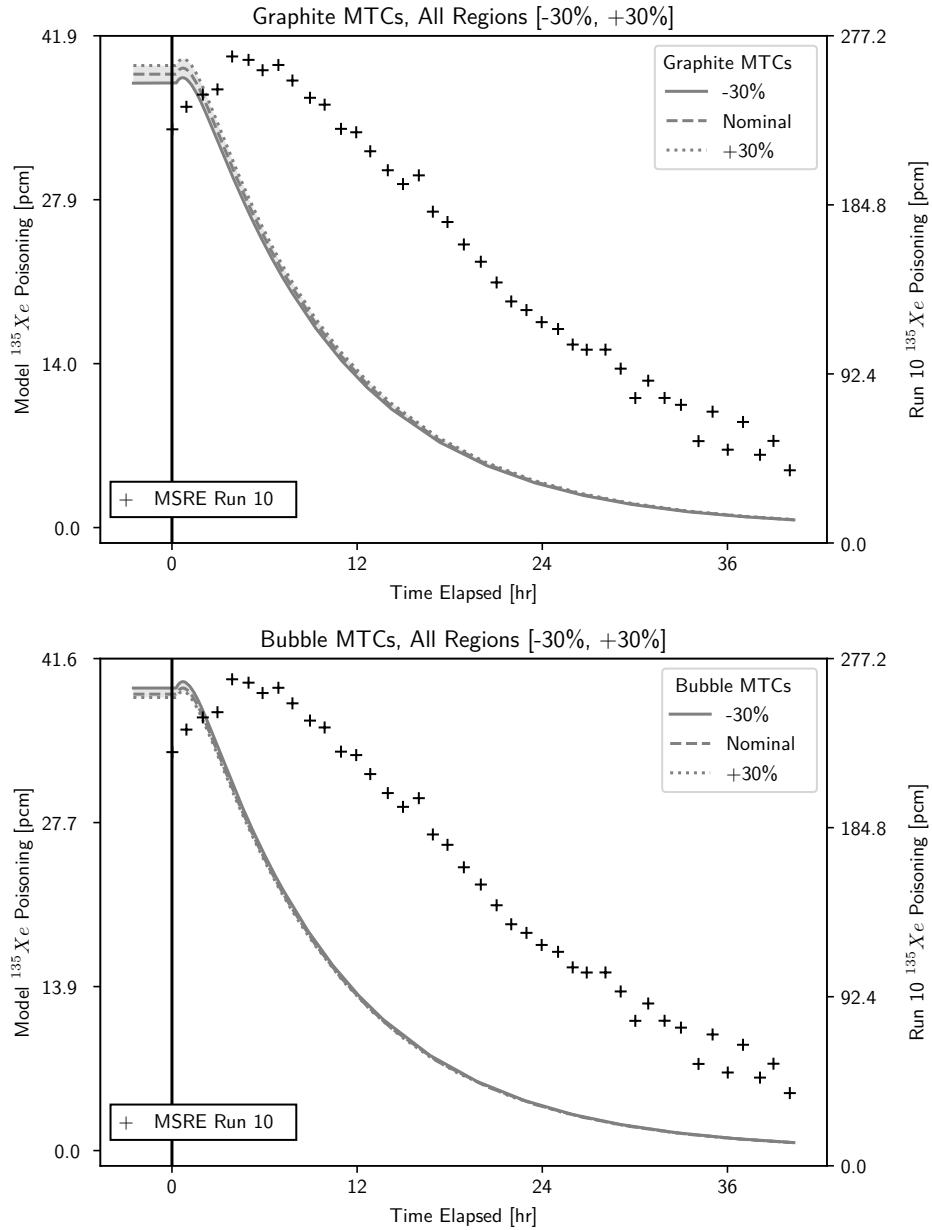
Figure 5.16: Results of sensitivity analysis with respect to graphite and bubble mass transfer coefficients
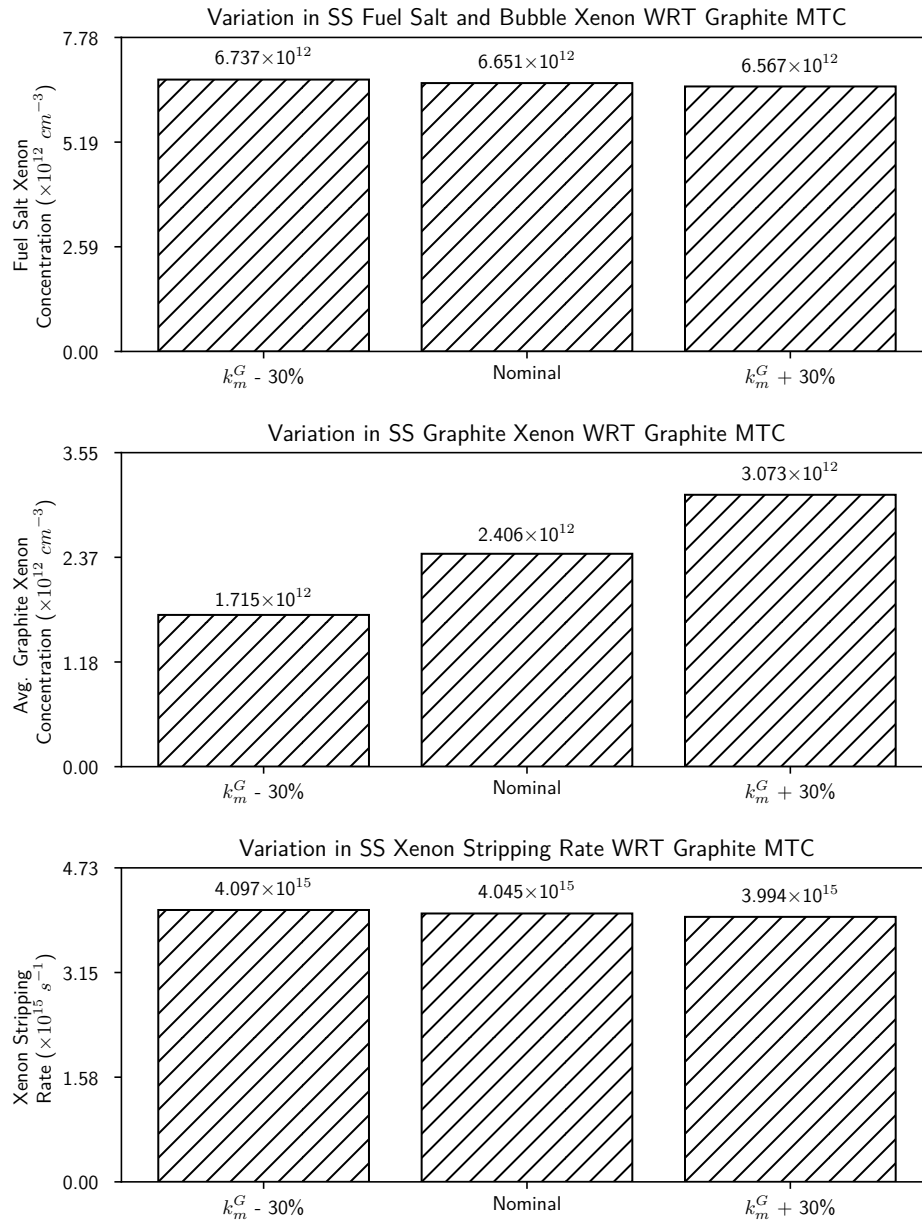
Figure 5.17: Steady state concentration of Xe-135 in the dynamic model as a result of perturbation of graphite mass transfer coefficient
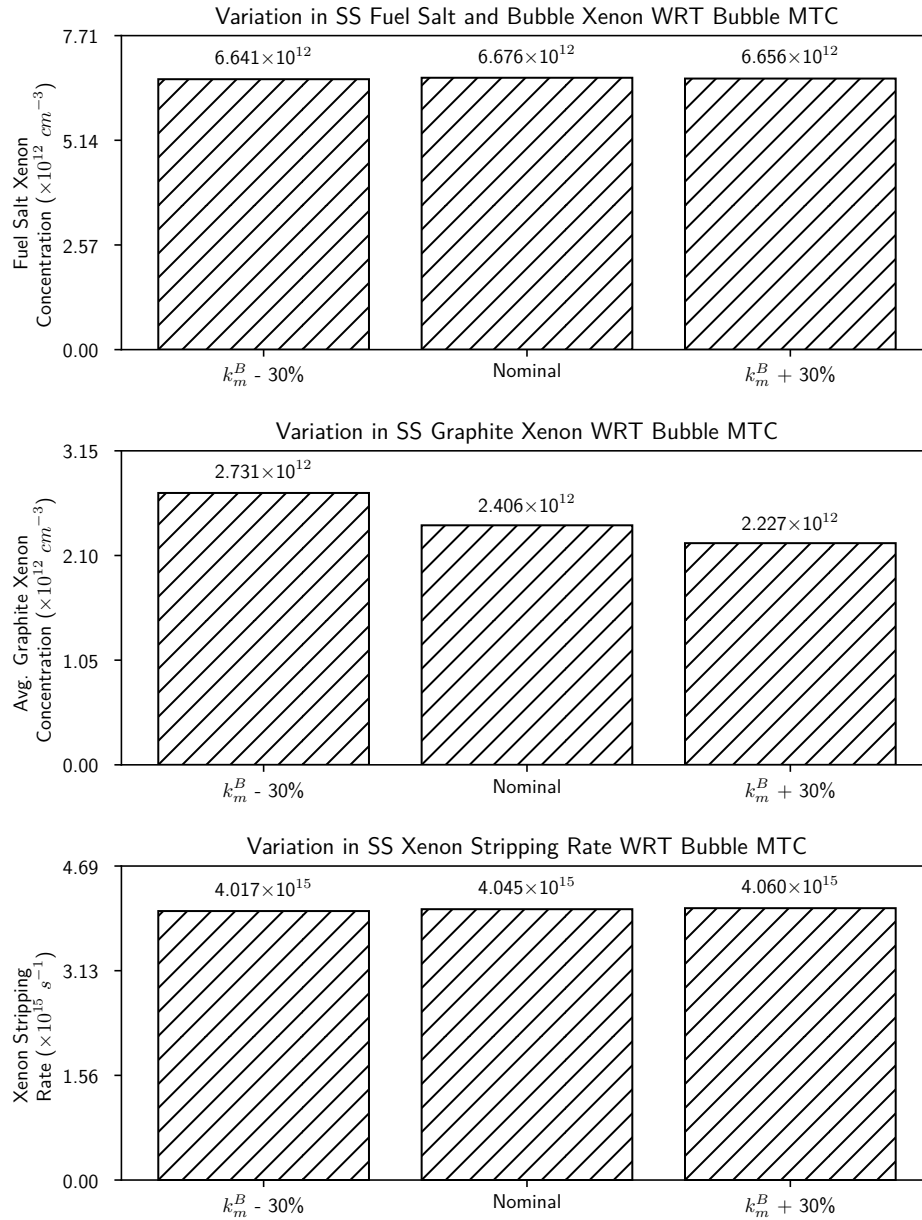
Figure 5.18: Steady state concentration of Xe-135 in the dynamic model as a result of perturbation of bubble mass transfer coefficient

5.7 Fission Yield

Figure 5.19 shows the results for the start up transient sensitivity analysis as the fission yields are perturbed. All of the plots underestimate the magnitude and time characteristics of the shut down transient response.

The left column shows the normalized results, which is directly comparable to the reported MSRE build up data whereas the right column shows the non normalized results. It is clearly visible that perturbation any of fission yields have effectively no influence on the normalized shape of the build up transient. The right column shows the non normalized results of the analysis.

Figure 5.20 shows the results for the shut down transient sensitivity analysis as the fission yields are perturbed. For both Figures 5.19 and 5.20, the plot in the first row shows the results of the sensitivity analysis as the Te-135 fission yield is perturbed, the second row shows the results as the I-135 fission yield is perturbed, and the final row shows the results as the Xe-135 fission yield is perturbed. It is observed in these plots that there is a positive correlation between the xenon poisoning and any of the fission yields.

The results of the sensitivity analysis for the steady state distribution of xenon are shown in Figures 5.21, 5.22, and 5.23 for the Te-135, I-135, and Xe-135 fission yields respectively. For each of these figures, the results for the homogenized fuel salt and bubble xenon concentration are shown in the first row, the average graphite xenon concentration is shown in the second row, and the total xenon stripping rate is shown in the final row.

With regards to any of the fission yields, the correlation between fission yield and the steady state xenon concentration of any of the model compartments or stripping rates is positive.

With regards to Te-135, the fuel salt and bubble xenon concentration increases from $6.149 \times 10^{12} \, \mathrm{cm^{-3}}$ to $7.152 \times 10^{12} \, \mathrm{cm^{-3}}$; the graphite xenon increases from $2.225 \times 10^{12} \, \mathrm{cm^{-3}}$ to $2.587 \times 10^{12} \, \mathrm{cm^{-3}}$; and, the xenon stripping rate increases from $3.740 \times 10^{15} \, \mathrm{cm^{-3}}$ to

$4.349 \times 10^{15}\,\mathrm{cm}^{-3}$.

With regards to I-135, the fuel salt and bubble xenon concentration increases from $6.194 \times 10^{12}\,\mathrm{cm}^{-3}$ to $7.107 \times 10^{12}\,\mathrm{cm}^{-3}$; the graphite xenon increases from $2.241 \times 10^{12}\,\mathrm{cm}^{-3}$ to $2.571 \times 10^{12}\,\mathrm{cm}^{-3}$; and, the xenon stripping rate increases from $3.767 \times 10^{15}\,\mathrm{cm}^{-3}$ to $4.322 \times 10^{15}\,\mathrm{cm}^{-3}$.

With regards to Xe-135, the fuel salt and bubble xenon concentration increases from $6.611 \times 10^{12}\,\mathrm{cm}^{-3}$ to $6.691 \times 10^{12}\,\mathrm{cm}^{-3}$; the graphite xenon increases from $2.392 \times 10^{12}\,\mathrm{cm}^{-3}$ to $2.421 \times 10^{12}\,\mathrm{cm}^{-3}$; and, the xenon stripping rate increases from $4.020 \times 10^{15}\,\mathrm{cm}^{-3}$ to $4.069 \times 10^{15}\,\mathrm{cm}^{-3}$.
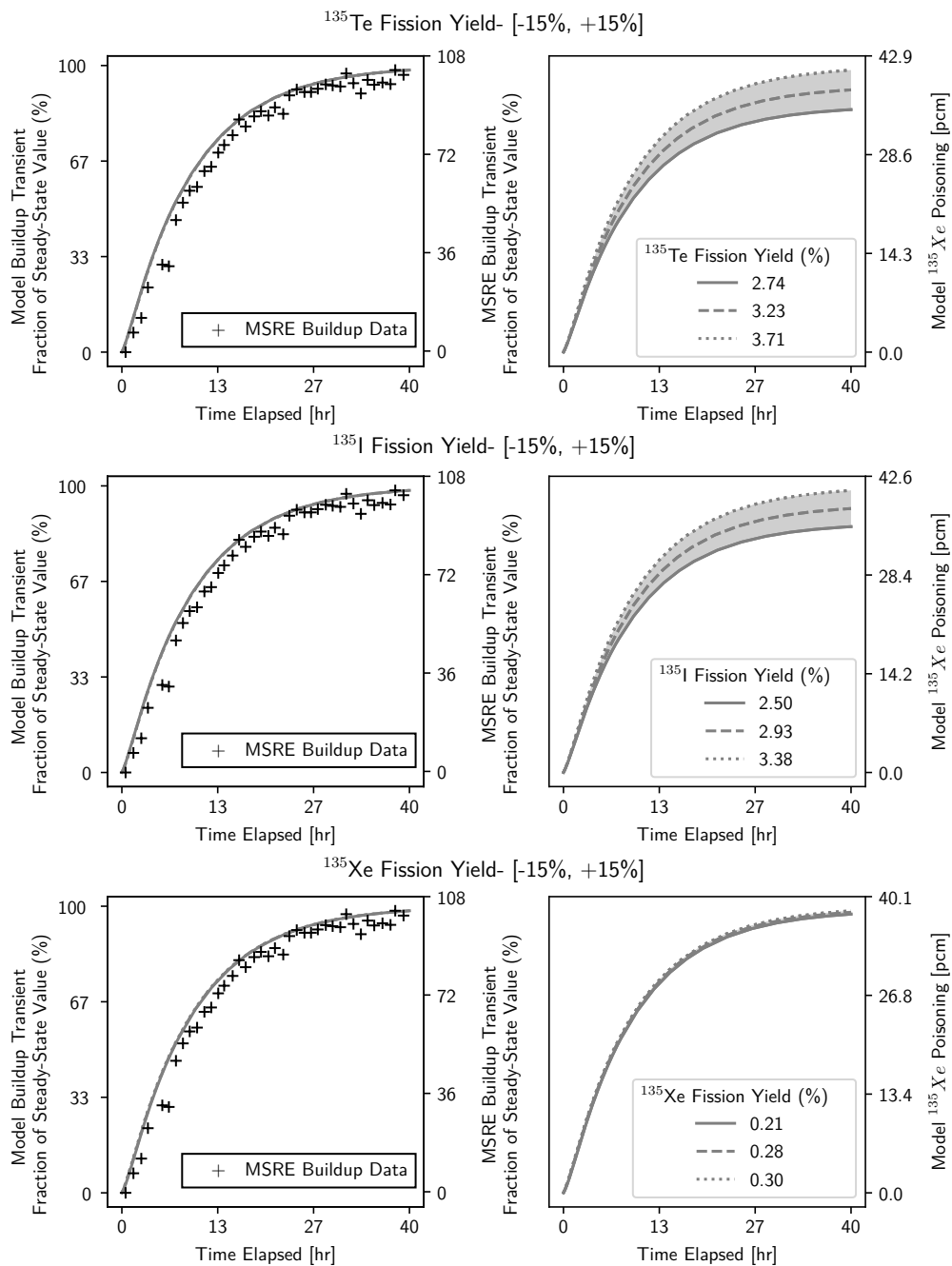
Figure 5.19: Results of build up transient sensitivity analysis with respect to fission yield
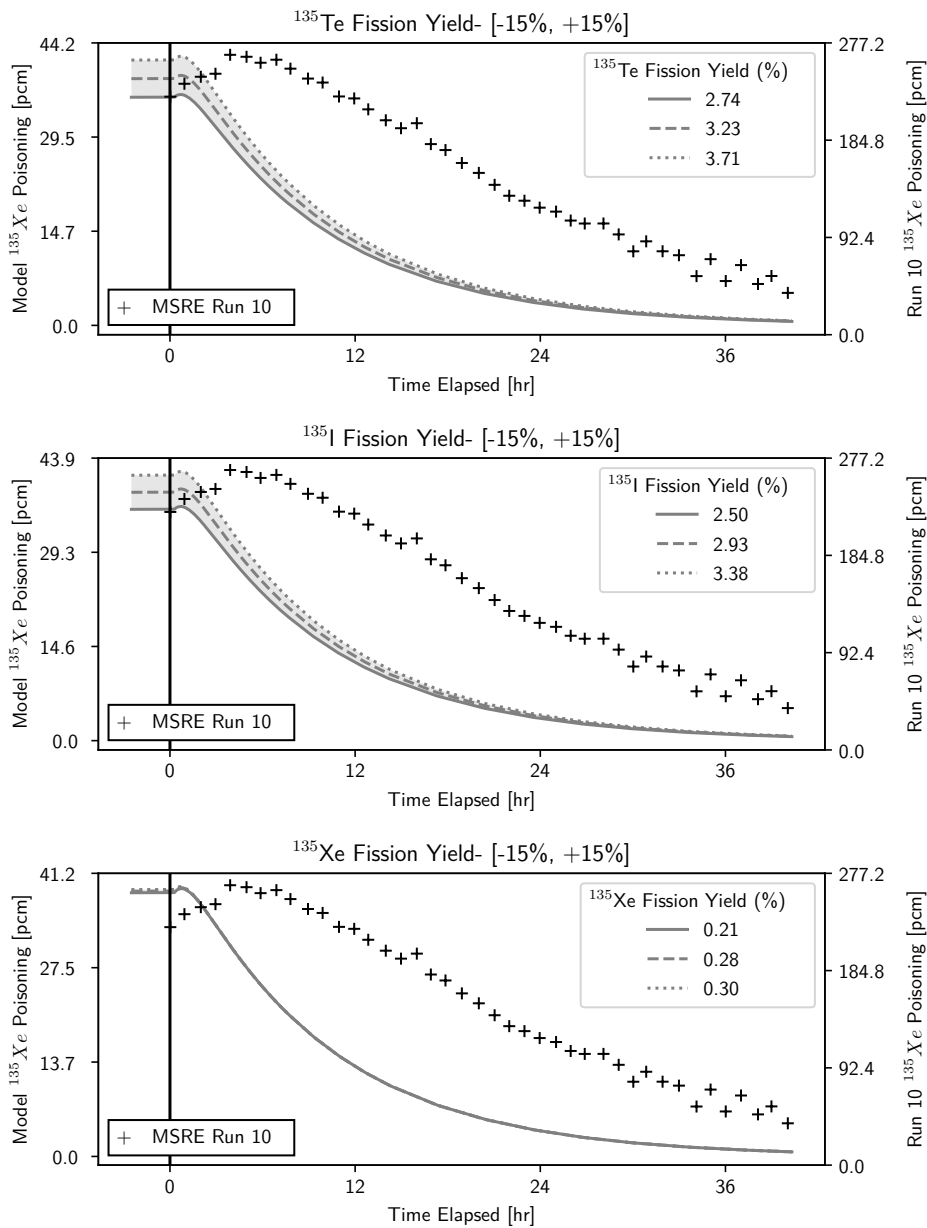
Figure 5.20: Results of sensitivity analysis with respect to fission yield
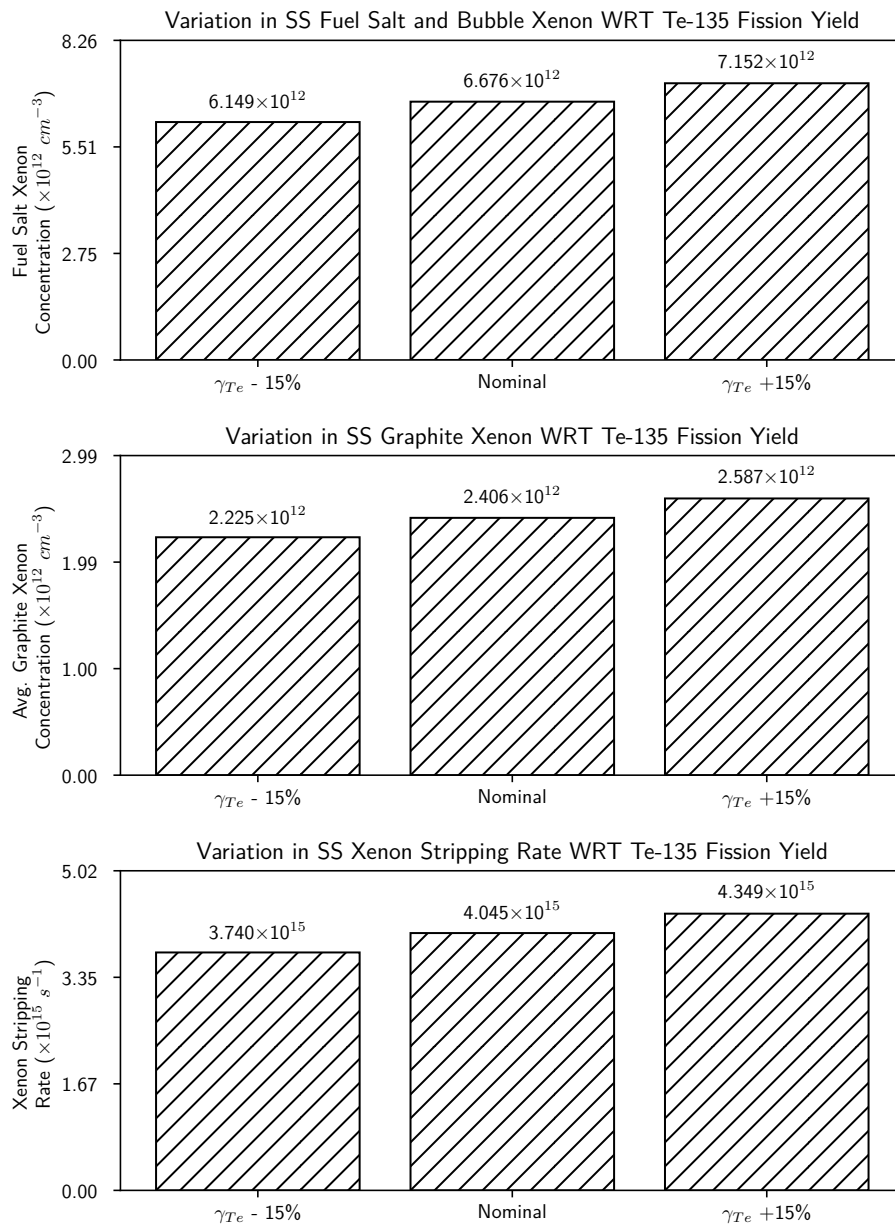
Figure 5.21: Steady state concentration of Xe-135 in the dynamic model as a result of perturbation of Te-135 fission yield
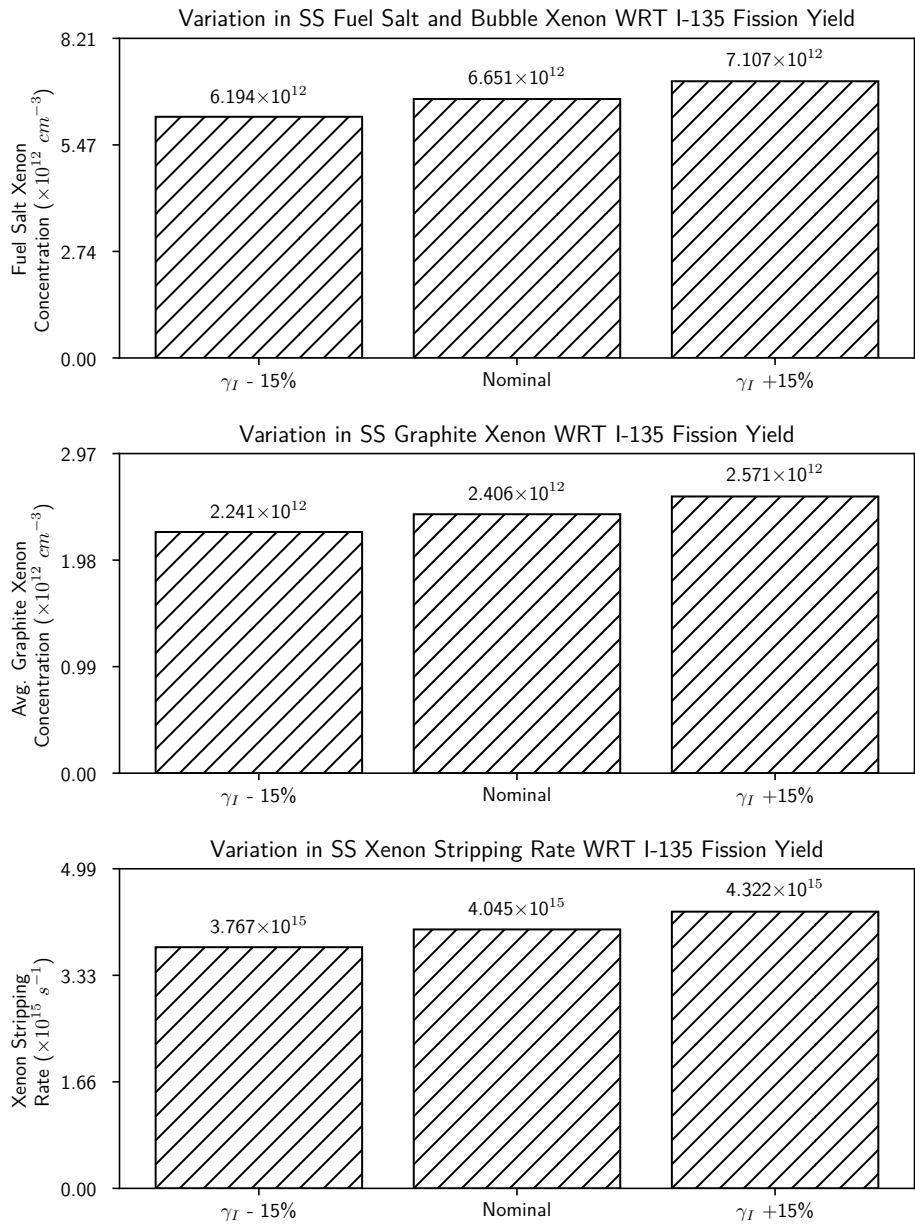
Figure 5.22: Steady state concentration of Xe-135 in the dynamic model as a result of perturbation of I-135 fission yield
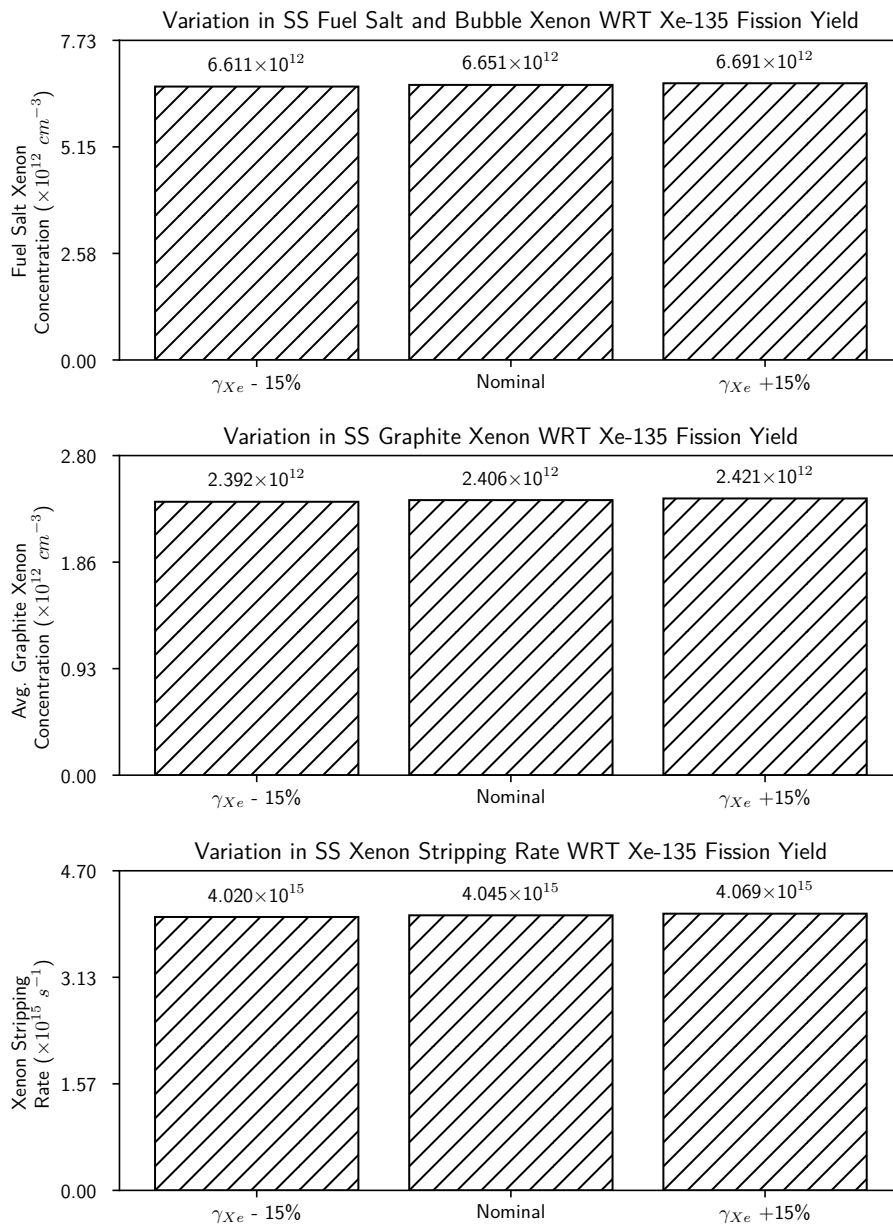
Figure 5.23: Steady state concentration of Xe-135 in the dynamic model as a result of perturbation of Xe-135 fission yield

5.8 Cross Sections

Figure 5.24 shows the results for the start up transient sensitivity analysis as the cross sections are perturbed. The left column shows the normalized results, which is directly comparable to the reported MSRE build up data whereas the right column shows the non normalized results. It is clearly visible that perturbation any of fission yields have effectively no influence on the normalized shape of the build up transient. The right column shows the non normalized results of the analysis. All of the instances of the normalized build up transient sensitivity analysis indicate good agreement with the MSRE build up data.

Figure 5.25 shows the results for the shut down transient sensitivity analysis as the cross sections. All of the plots underestimate the magnitude and time characteristics of the shut down transient response.

For both Figures 5.24 and 5.25, the plot in the first row of plots shows the results of the sensitivity analysis as the macroscopic fission cross section is perturbed whereas the second row shows the results of the sensitivity analysis as the microscopic absorption cross is perturbed.

It is observed in these plots that there is a positive correlation between the xenon poisoning and the fission cross section and a negative correlation between the xenon poisoning and the Xe-135 absorption cross section.

The results of the sensitivity analysis for the steady state distribution of xenon are shown in Figures 5.26 and 5.27 for the macroscopic fission and microscopic Xe-135 absorption cross sections respectively. For each of these figures, the results for the homogenized fuel salt and bubble xenon concentration are shown in the first row, the average graphite xenon concentration is shown in the second row, and the total xenon stripping rate is shown in the final row.

The homogenized fuel salt and bubble xenon concentration, average graphite xenon concentration, and stripping rates all correlate positively with the macroscopic fission cross

section whereas the absorption cross section correlates negatively with these measurements.

With regards to the macroscopic fission cross section, the fuel salt and bubble xenon concentration increases from $5.653 \times 10^{12}\,\mathrm{cm^{-3}}$ to $7.648 \times 10^{12}\,\mathrm{cm^{-3}}$; the graphite xenon increases from $2.045 \times 10^{12}\,\mathrm{cm^{-3}}$ to $2.767 \times 10^{12}\,\mathrm{cm^{-3}}$; and, the xenon stripping rate increases from $3.438 \times 10^{15}\,\mathrm{cm^{-3}}$ to $4.651 \times 10^{15}\,\mathrm{cm^{-3}}$.

With regards to the microscopic Xe-135 absorption cross section, the fuel salt and bubble xenon concentration increases from $6.734 \times 10^{12}\,\mathrm{cm^{-3}}$ to $6.570 \times 10^{12}\,\mathrm{cm^{-3}}$; the graphite xenon increases from $2.471 \times 10^{12}\,\mathrm{cm^{-3}}$ to $2.344 \times 10^{12}\,\mathrm{cm^{-3}}$; and, the xenon stripping rate increases from $4.096 \times 10^{15}\,\mathrm{cm^{-3}}$ to $3.995 \times 10^{15}\,\mathrm{cm^{-3}}$.
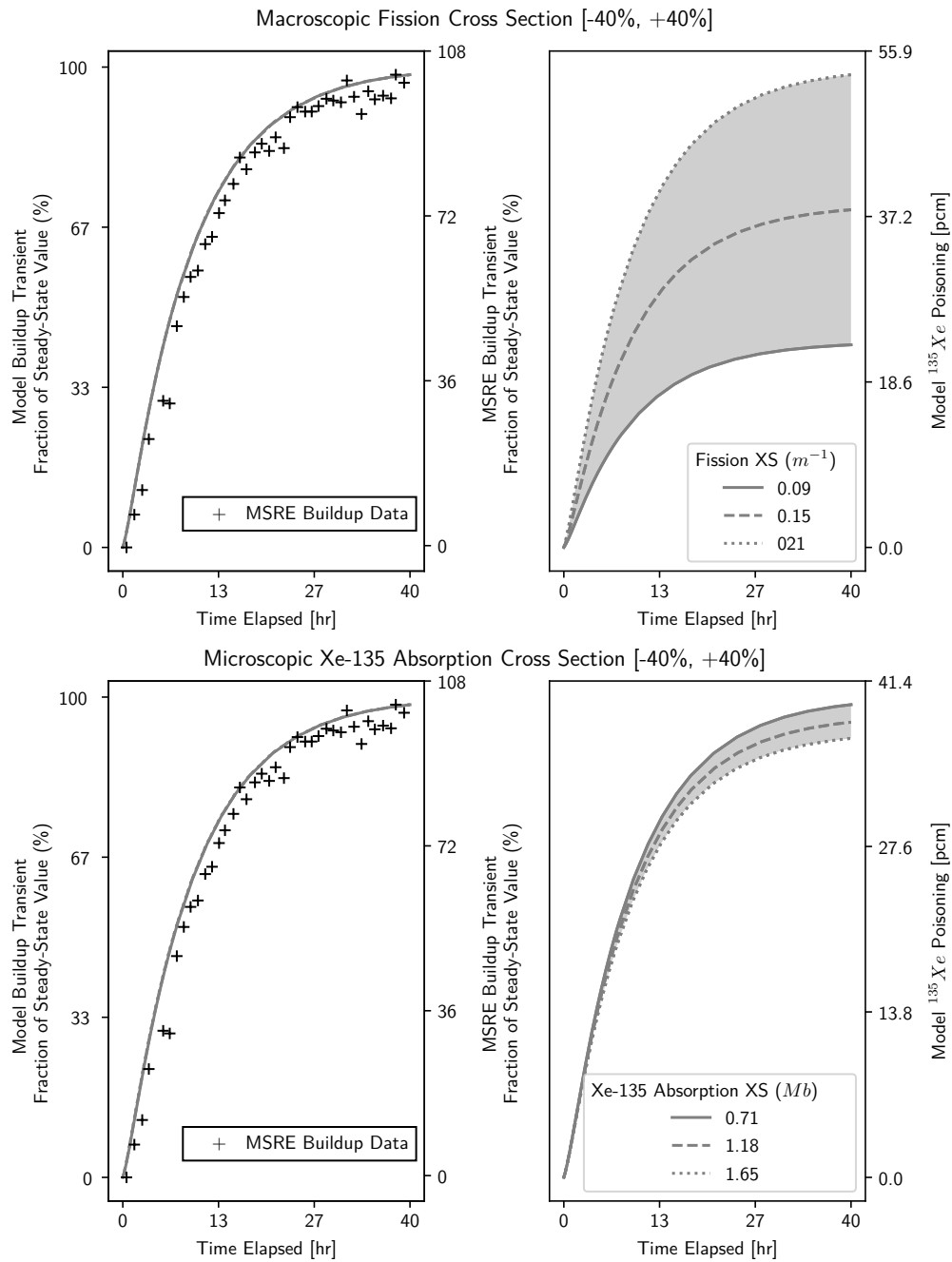
Figure 5.24: Results of build up transient sensitivity analysis with respect to cross section
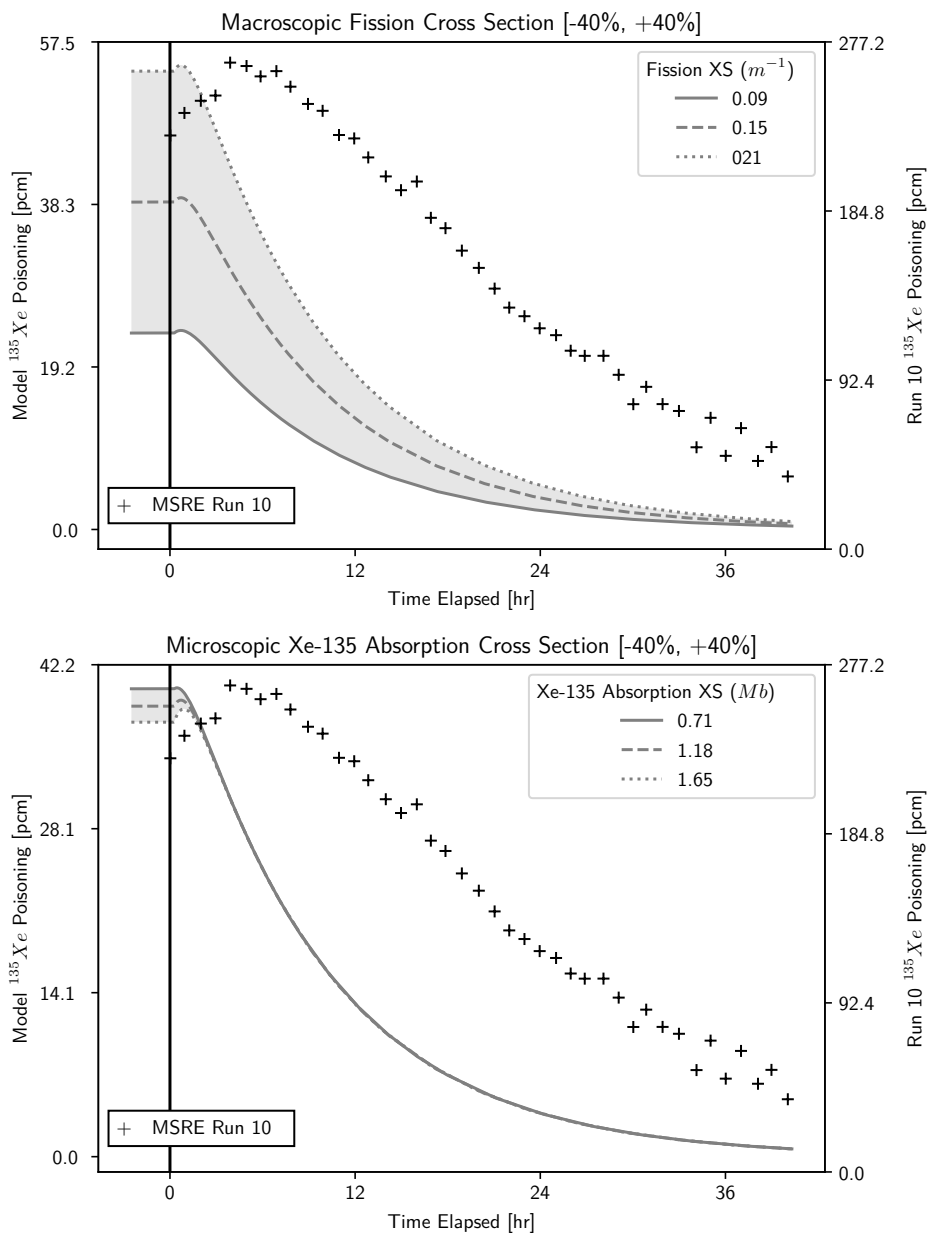
Figure 5.25: Results of sensitivity analysis with respect to cross section
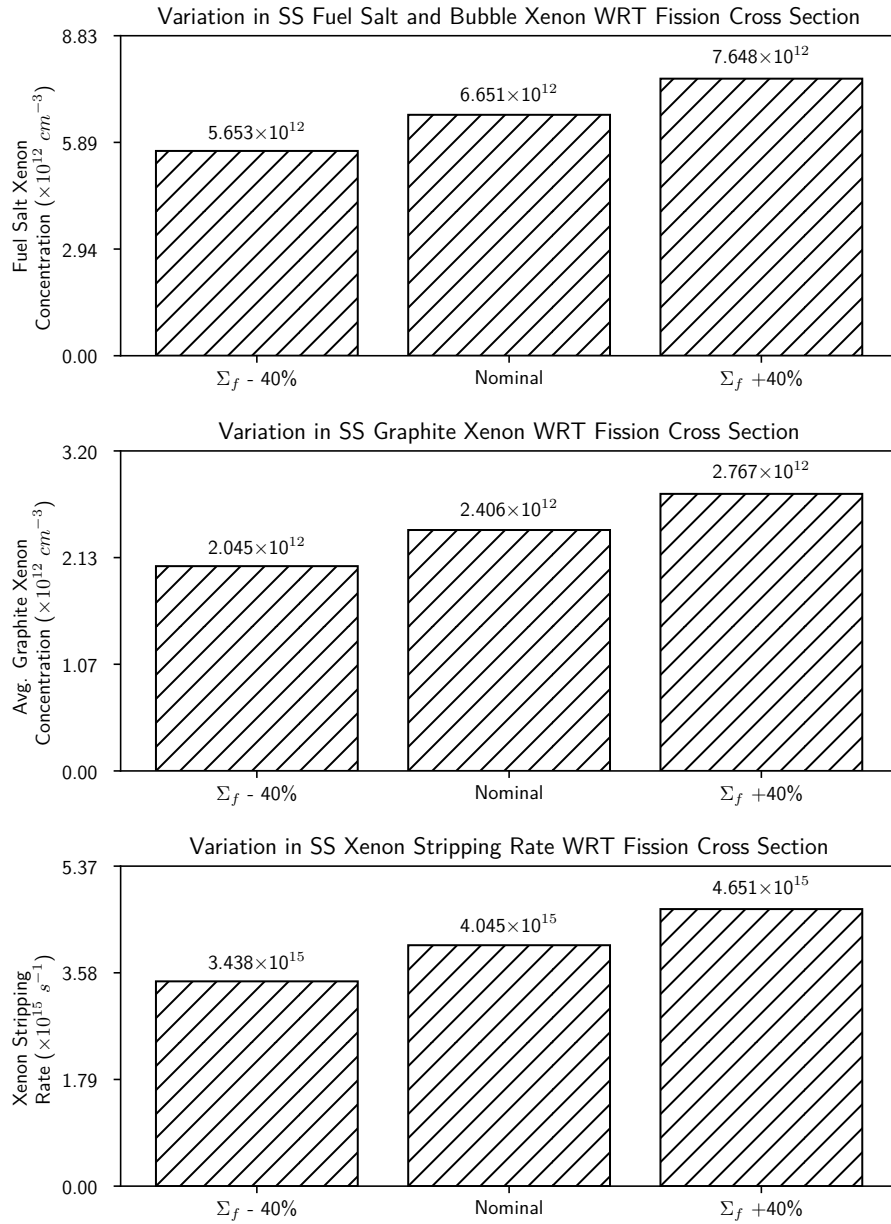
Figure 5.26: Steady state concentration of Xe-135 in the dynamic model as a result of perturbation of macroscopic fission cross section
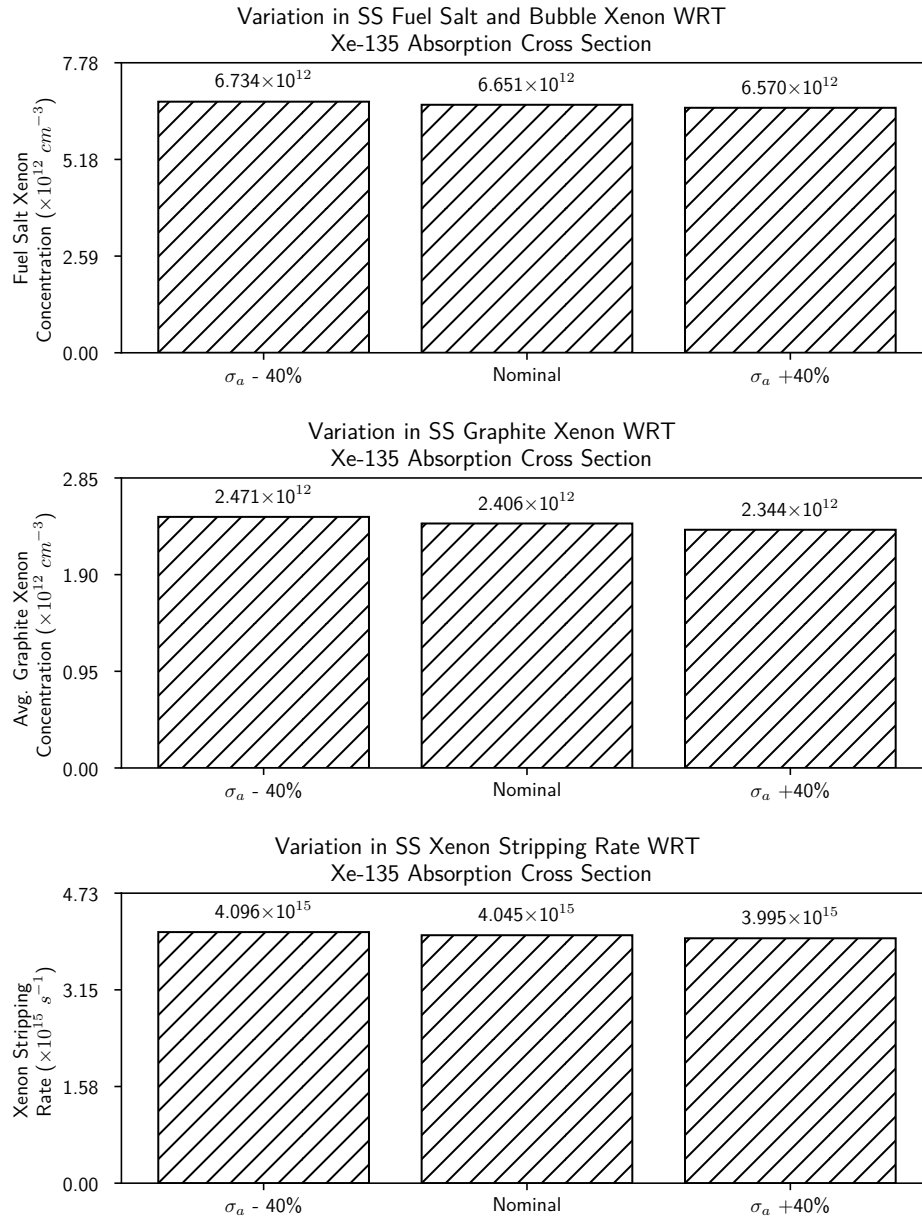
Figure 5.27: Steady state concentration of Xe-135 in the dynamic model as a result of perturbation of microscopic absorption cross section for Xe-135

5.9   Neutron Flux

Figure 5.28 shows the results for the start up transient sensitivity analysis as the neutron fluxes are perturbed. The left column shows the normalized results, which is directly comparable to the reported MSRE build up data whereas the right column shows the non normalized results. It is clearly visible that perturbation any of the fission yields have effectively no influence on the normalized shape of the build up transient. The right column shows the non normalized results of the analysis. All of the instances of the normalized build up transient sensitivity analysis indicate good agreement with the MSRE build up data.

Figure 5.29 shows the results for the shut down transient sensitivity analysis as the neutron fluxes are perturbed. All of the plots underestimate the magnitude and time characteristics of the shut down transient response.

For both figures 5.28 and 5.29, the plot in the first row of plots shows the results of the sensitivity analysis as the fuel salt neutron flux is perturbed, the plot in the second row shows the results of the sensitivity analysis as the graphite neutron flux is perturbed and the plot in the final row shows the results of the sensitivity analysis as both are perturbed simultaneously.

It is observed in these plots that there is a positive correlation between the xenon poisoning and the fuel salt neutron flux and a negative correlation between the xenon poisoning and the graphite neutron flux.

When both the graphite and fuel salt neutron fluxes are perturbed simultaneously, the net result is a positive correlation that approximates the fuel salt only perturbation.

The results of the sensitivity analysis for the steady state distribution of xenon are shown in figures 5.30, 5.31 and 5.32 for the fuel salt, graphite, and simultaneous perturbation respectively. For each of these figures, the results for the homogenized fuel salt and bubble xenon concentration are shown in the first row, the average graphite xenon concentration is shown in the second row, and the total xenon stripping rate is shown in the final row.

The homogenized fuel salt and bubble xenon concentration, average graphite xenon concentration, and stripping rates all correlate positively with the fuel salt neutron flux. In regards to fuel salt flux,$4.773 \times 10^{12}\,\text{cm}^{-3}$ to $8.438 \times 10^{12}\,\text{cm}^{-3}$; the graphite xenon increases from $1.713 \times 10^{12}\,\text{cm}^{-3}$ to $3.077 \times 10^{12}\,\text{cm}^{-3}$; and, the xenon stripping rate increases from $2.904 \times 10^{15}\,\text{cm}^{-3}$ to $5.130 \times 10^{15}\,\text{cm}^{-3}$.

When the graphite neutron flux is perturbed, there is effectively no change in the fuel salt and bubble xenon concentration or xenon stripping rate, but there is a negative correlation with the graphite xenon concentration. The fuel salt and bubble xenon concentration is unchanged at $6.51 \times 10^{12}\,\text{cm}^{-3}$; the graphite xenon decreases from $10^{12}\,\text{cm}^{-3}$ to $10^{12}\,\text{cm}^{-3}$; and, the xenon stripping rate decreases from $10^{15}\,\text{cm}^{-3}$ to $10^{15}\,\text{cm}^{-3}$.

When the all the neutron fluxes are perturbed simultaneously, the change in xenon distribution is effectively the same as that which was produced by the fuel salt only change. The fuel salt and bubble xenon concentration increases from $4.773 \times 10^{12}\,\text{cm}^{-3}$ to $8.438 \times 10^{12}\,\text{cm}^{-3}$; the graphite xenon increases from $1.778 \times 10^{12}\,\text{cm}^{-3}$ to $2.971 \times 10^{12}\,\text{cm}^{-3}$; and, the xenon stripping rate increases from $2.094 \times 10^{15}\,\text{cm}^{-3}$ to $5.130 \times 10^{15}\,\text{cm}^{-3}$.

Figure 5.28: Results of build up transient sensitivity analysis with respect to neutron flux

Figure 5.29: Results of sensitivity analysis with respect to neutron flux

Variation in SS Fuel Salt and Bubble Xenon WRT Fuel Salt Neutron Flux

Variation in SS Graphite Xenon WRT Fuel Salt Neutron Flux

Variation in SS Xenon Stripping Rate WRT Fuel Salt Neutron Flux
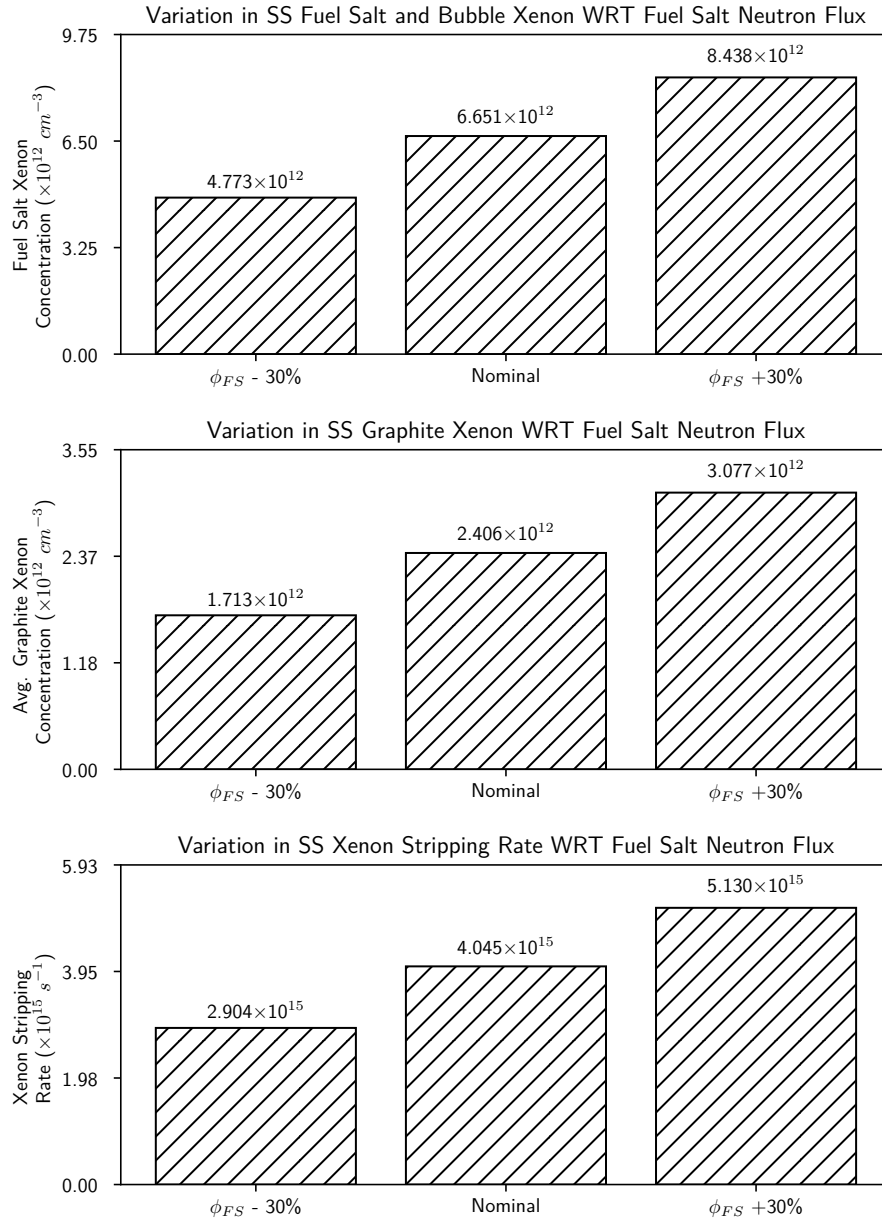
Figure 5.30: Steady state concentration of Xe-135 in the dynamic model as a result of perturbation of fuel salt neutron fluxes
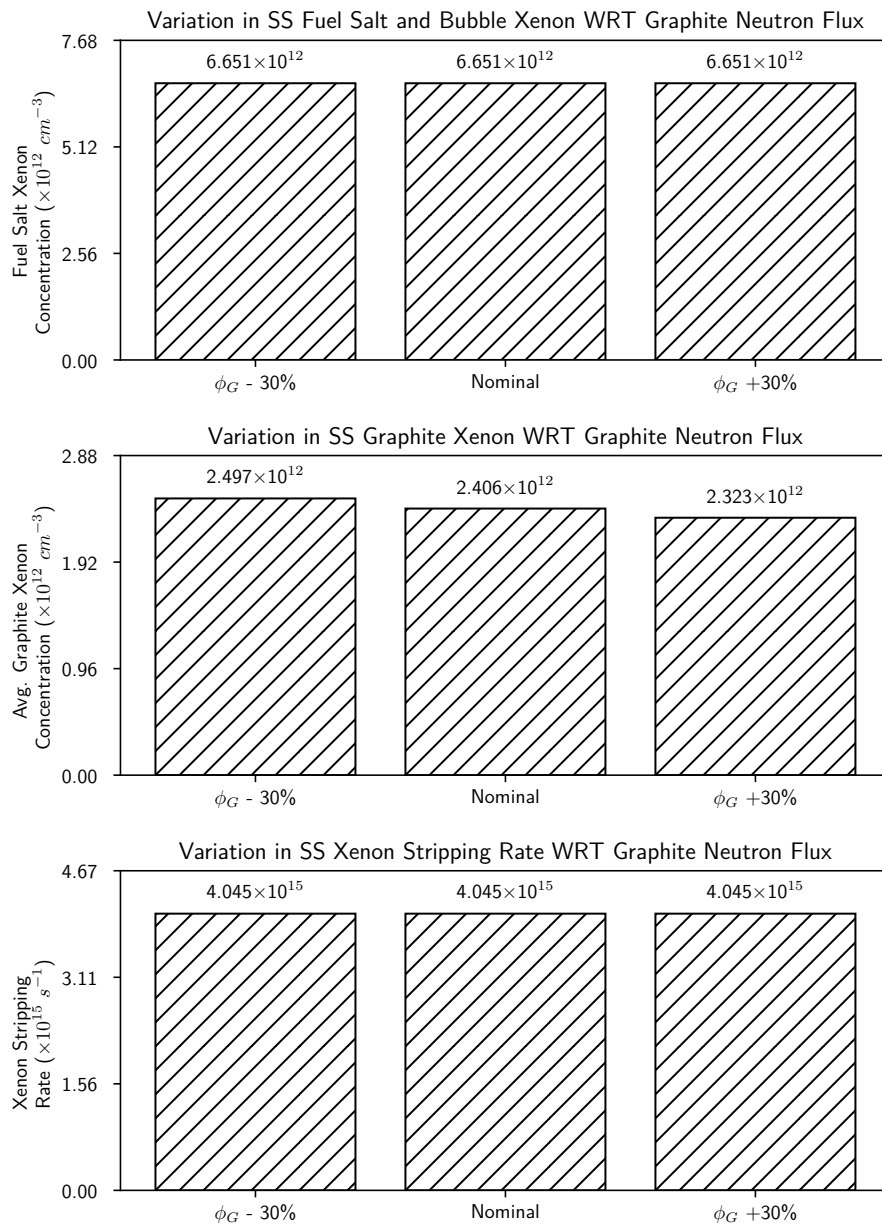
Figure 5.31: Steady state concentration of Xe-135 in the dynamic model as a result of perturbation of graphite neutron fluxes
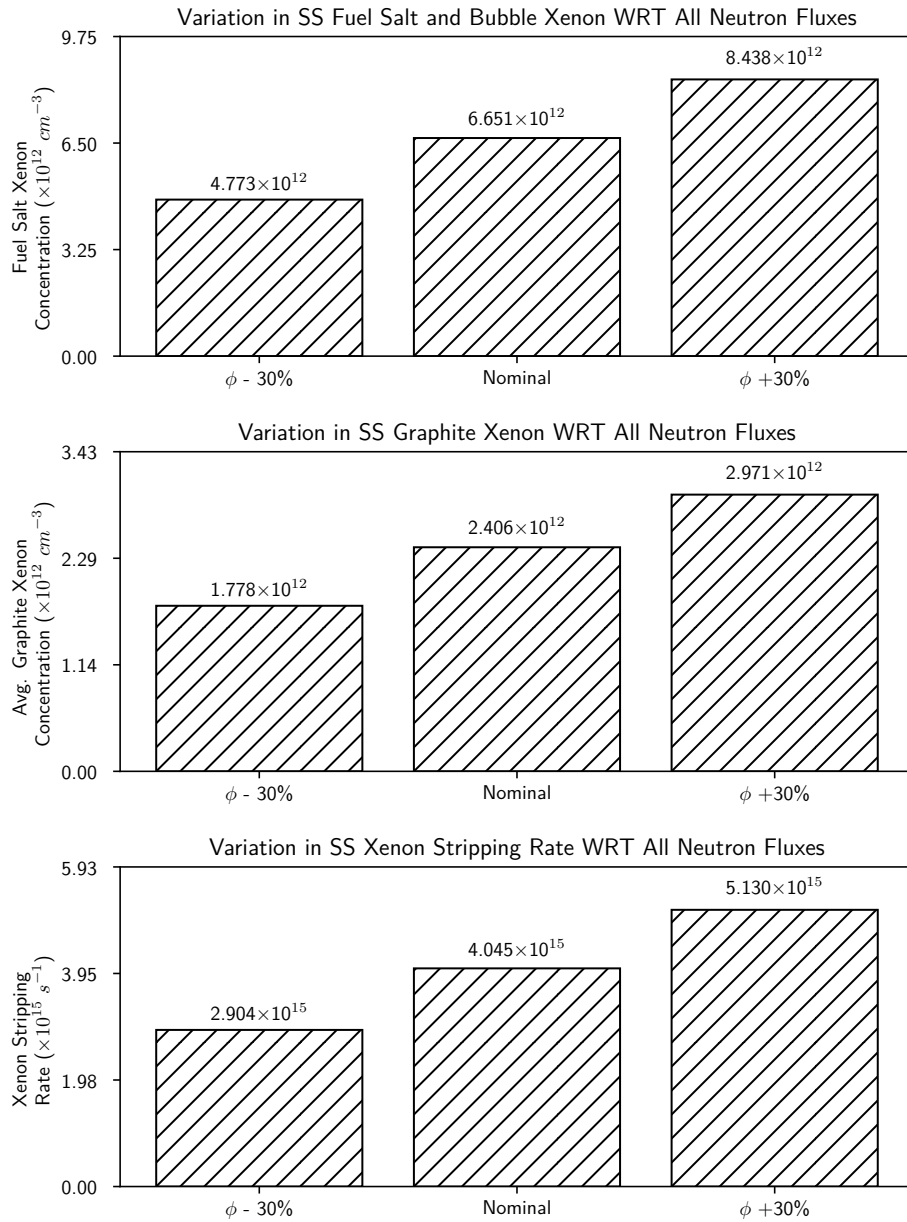
Figure 5.32: Steady state concentration of Xe-135 in the dynamic model as a result of perturbation of all neutron fluxes

5.10 Bubble and Xenon Radii

Figure 5.33 shows the results for the start up transient sensitivity analysis as the neutron fluxes are perturbed. The left column shows the normalized results, which is directly comparable to the reported MSRE build up data whereas the right column shows the non normalized results. It is clearly visible that perturbation any of bubble or xenon radii has effectively no influence on the normalized shape of the build up transient. The right column shows the non normalized results of the analysis. All of the instances of the normalized build up transient sensitivity analysis indicate good agreement with the MSRE build up data.

Figure 5.34 shows the results for the shut down transient sensitivity analysis as the xenon radius and the bubble radius is perturbed. All of the plots underestimate the magnitude and time characteristics of the shut down transient response.

For both Figures 5.33 and 5.34, the plot in the first row of plots shows the results of the sensitivity analysis as the bubble radius is perturbed and the plot in the second row shows the sensitivity analysis as the xenon radius is perturbed.

It is observed in both of these plots that there is a positive correlation between the transient xenon poisoning and the bubble radius, and a negative correlation between the transient xenon poisoning and the xenon radius.

The results of the sensitivity analysis for the steady state distribution of xenon are shown in figures 5.35 and 5.36 for the bubble and xenon radius perturbations respectively. For each of these figures, the results for the homogenized fuel salt and bubble xenon concentration are shown in the first row, the average graphite xenon concentration is shown in the second row, and the total xenon stripping rate is shown in the final row.

The homogenized fuel salt a bubble xenon content correlates negatively the bubble radius whereas the graphite xenon content as well as the stripping rate correlates positively. The fuel salt and bubble xenon concentration decreases from $6.661 \times 10^{12} \, \mathrm{cm}^{-3}$ to $6.636 \times 10^{12} \, \mathrm{cm}^{-3}$; the graphite xenon increases from $2.070 \times 10^{12} \, \mathrm{cm}^{-3}$ to $2.870 \times 10^{12} \, \mathrm{cm}^{-3}$; and, the xenon

stripping rate decreases from $4.073 \times 10^{15}\,\mathrm{cm^{-3}}$ to $4.005 \times 10^{15}\,\mathrm{cm^{-3}}$.

As for the xenon radius, the fuel salt and bubble xenon concentration correlates and the total xenon stripping rate correlates positively whereas the graphite xenon content correlates negatively. The fuel salt and bubble xenon concentration increases from $6.636 \times 10^{12}\,\mathrm{cm^{-3}}$ to $6.729 \times 10^{12}\,\mathrm{cm^{-3}}$; the graphite xenon increases from $2.486 \times 10^{12}\,\mathrm{cm^{-3}}$ to $2.023 \times 10^{12}\,\mathrm{cm^{-3}}$; and, the xenon stripping rate increases from $4.039 \times 10^{15}\,\mathrm{cm^{-3}}$ to $4.071 \times 10^{15}\,\mathrm{cm^{-3}}$.
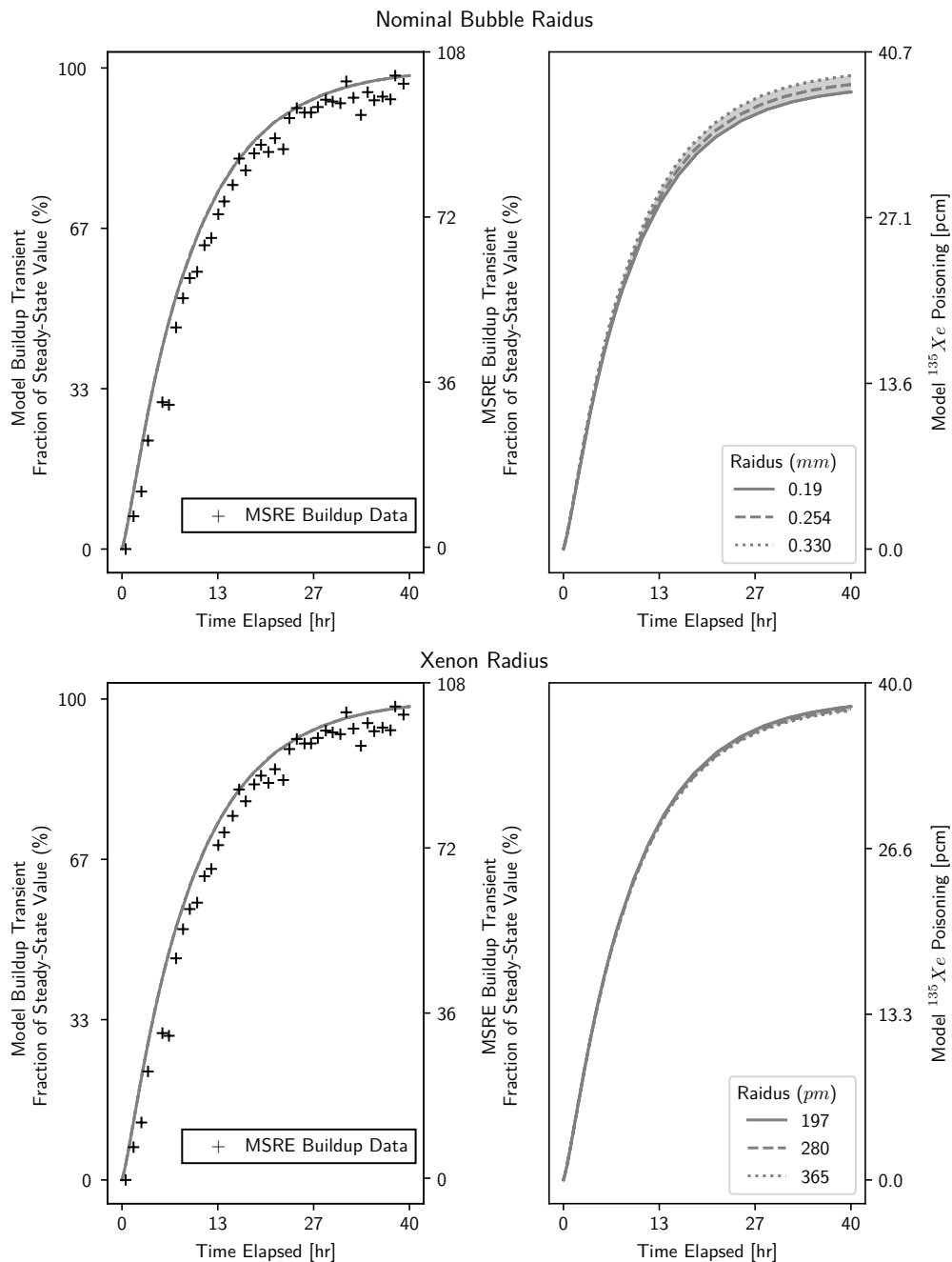
Figure 5.33: Results of build up transient sensitivity analysis with respect to the xenon and bubble radius

Figure 5.34: Results of sensitivity analysis with respect to the xenon and bubble radius
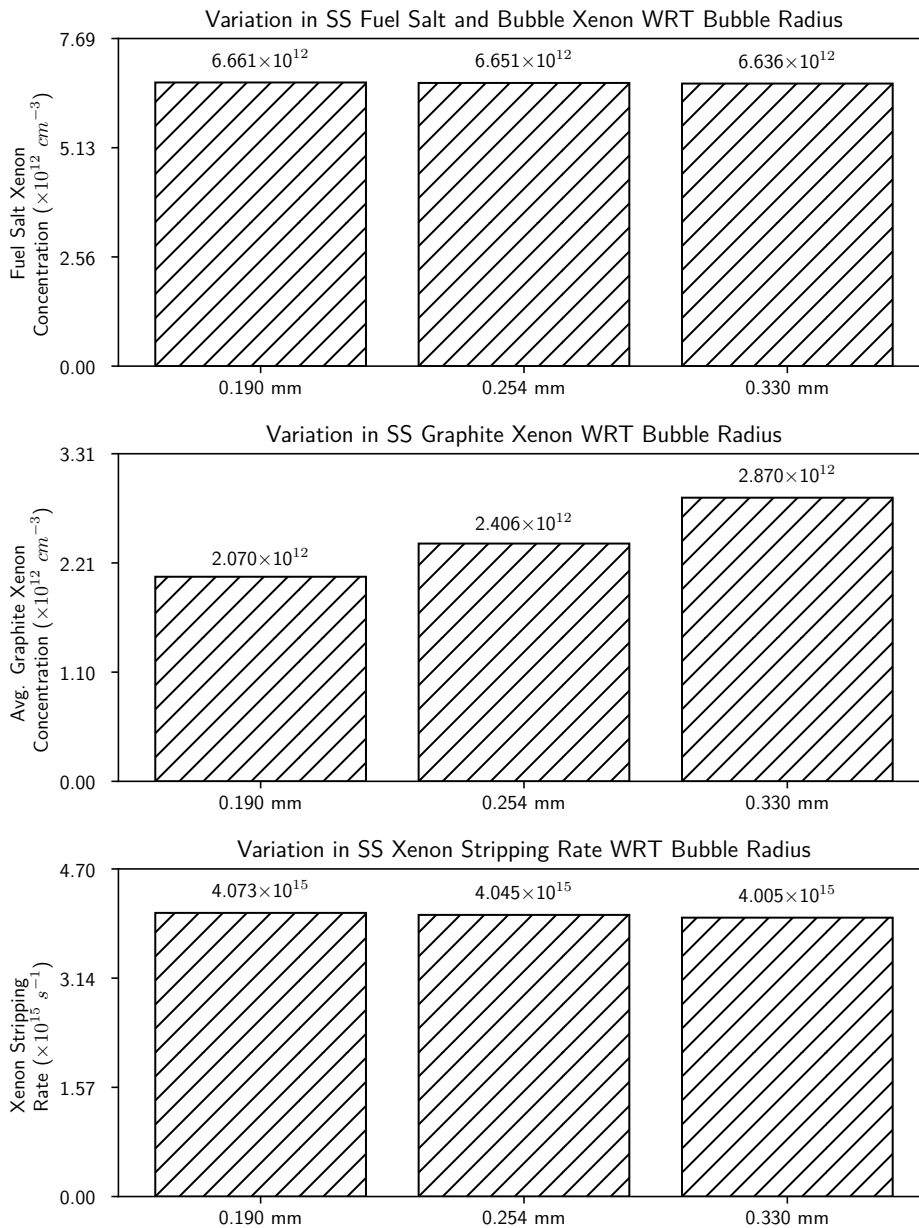
Figure 5.35: Steady state concentration of Xe-135 in the dynamic model as a result of perturbation of nominal bubble radius
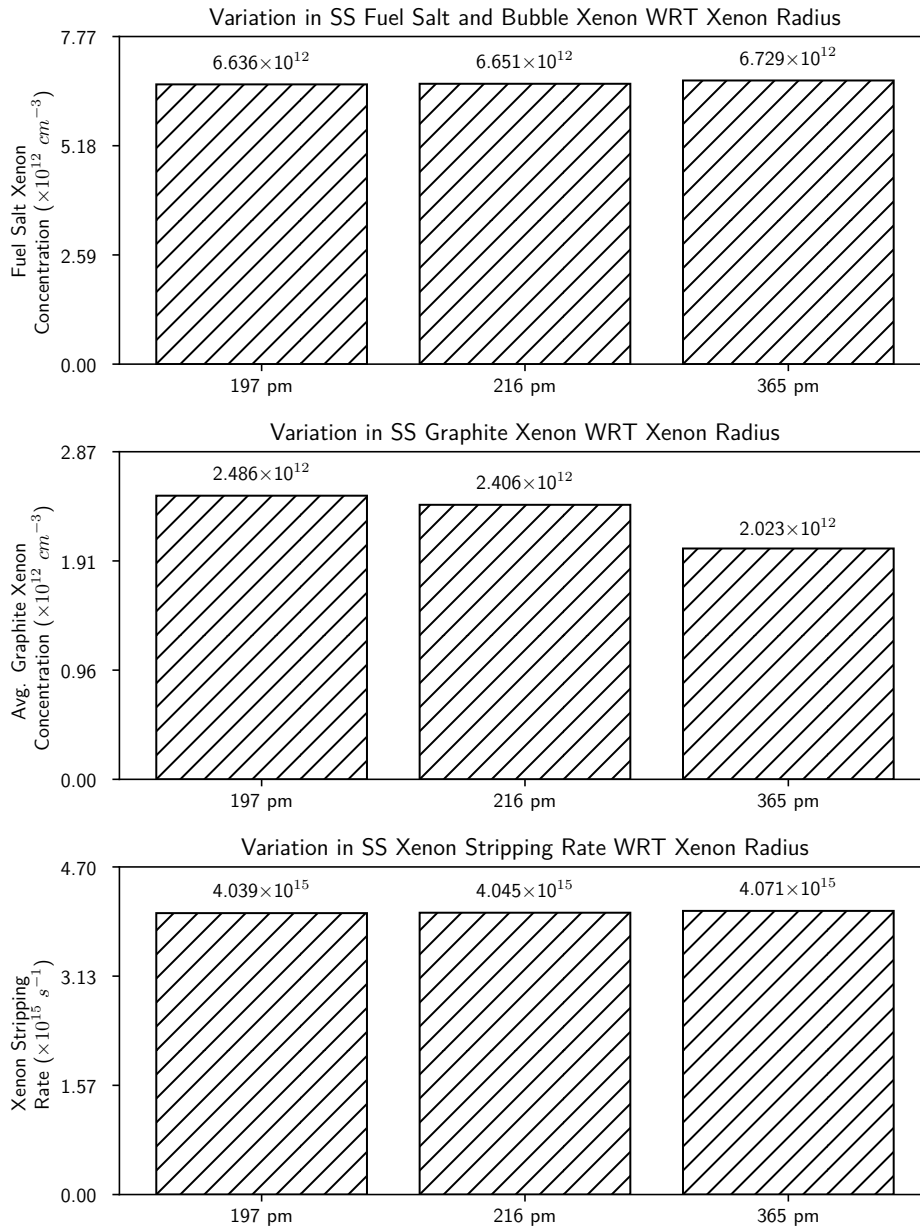
Figure 5.36: Steady state concentration of Xe-135 in the dynamic model as a result of perturbation of xenon radius

5.11 Circulating Void Fraction

Figure 5.37 shows the results for the start up transient sensitivity analysis as the circulating void fraction is perturbed. The left column shows the normalized results, which is directly comparable to the reported MSRE build up data whereas the right column shows the non normalized results. It is clearly visible that perturbation any of void fraction has effectively no influence on the normalized shape of the build up transient. The right column shows the non normalized results of the analysis. All of the instances of the normalized build up transient sensitivity analysis indicate good agreement with the MSRE build up data.

Figure 5.38 shows the results for the shut down transient sensitivity analysis as the xenon radius and the bubble radius is perturbed. All of the plots underestimate the magnitude and time characteristics of the shut down transient response.

For both Figures 5.37 and 5.38, the plot in the first row of plots shows the results of the sensitivity analysis as the bubble radius is perturbed and the plot in the second row shows the sensitivity analysis as the xenon radius is perturbed.

It is observed in both of these plots that there is a negative correlation between the transient xenon poisoning and the circulating void fraction.

The homogenized fuel salt a bubble xenon content correlates non monotonically with the void fraction. The graphite xenon concentration correlates negatively with circulating void fraction. The xenon stripping rate correlates positively with circulating void fraction. At the nominal 0.4% circulating void fraction, the homogenized fuel salt and bubble xenon content was $6.651 \times 10^{12}\,\text{cm}^{-3}$; at 0.1% void fraction it was $6.520 \times 10^{12}\,\text{cm}^{-3}$; whereas, at 3% void fraction it was 6.539×10^{12} The average graphite xenon concentration decreased from $7.351 \times 10^{12}\,\text{cm}^{-3}$ to $3.435 \times 10^{11}\,\text{cm}^{-3}$. The xenon stripping rate increases from $3.634 \times 10^{15}\,\text{cm}^{-3}$ to $4.110 \times 10^{15}\,\text{cm}^{-3}$.
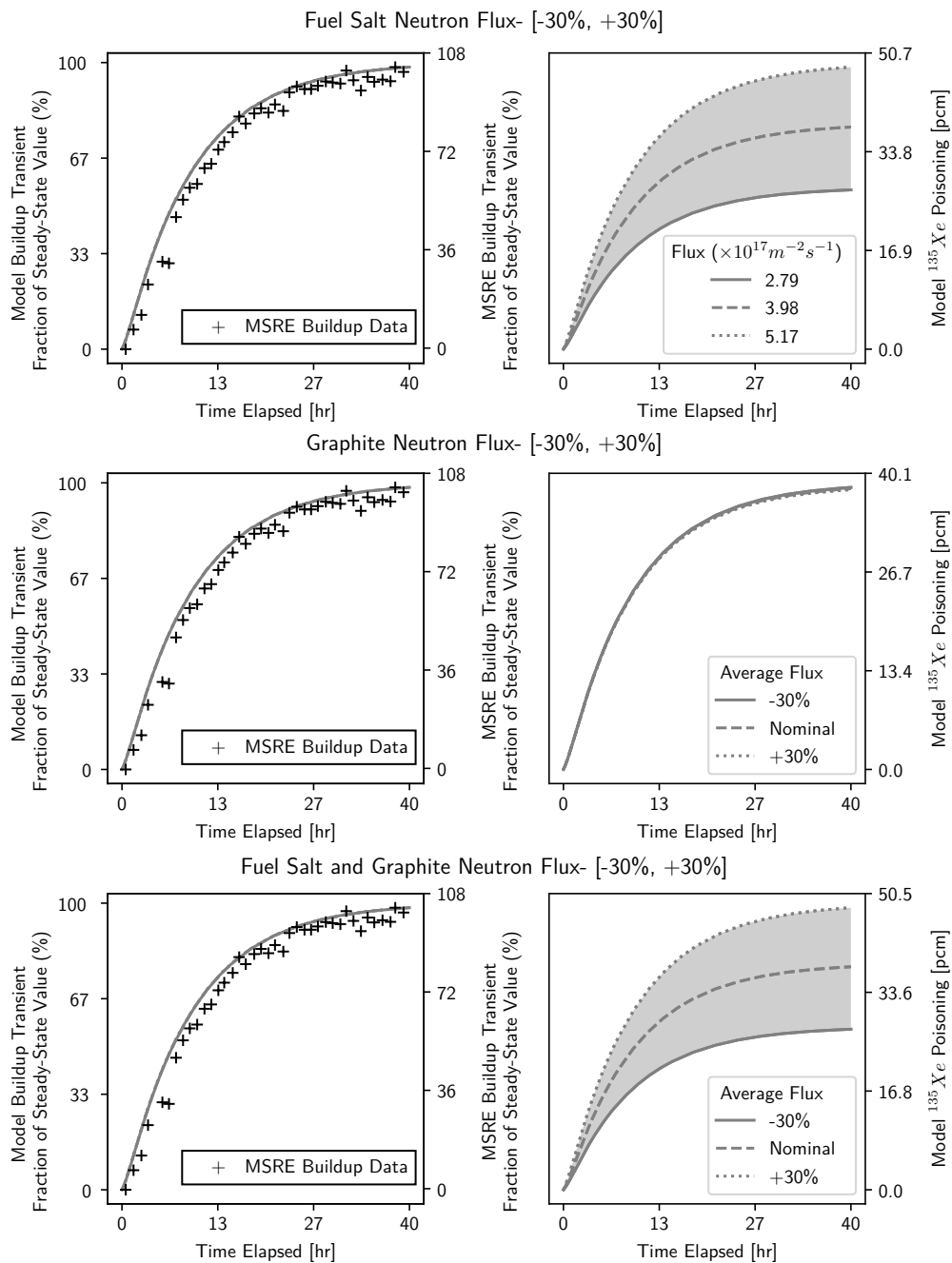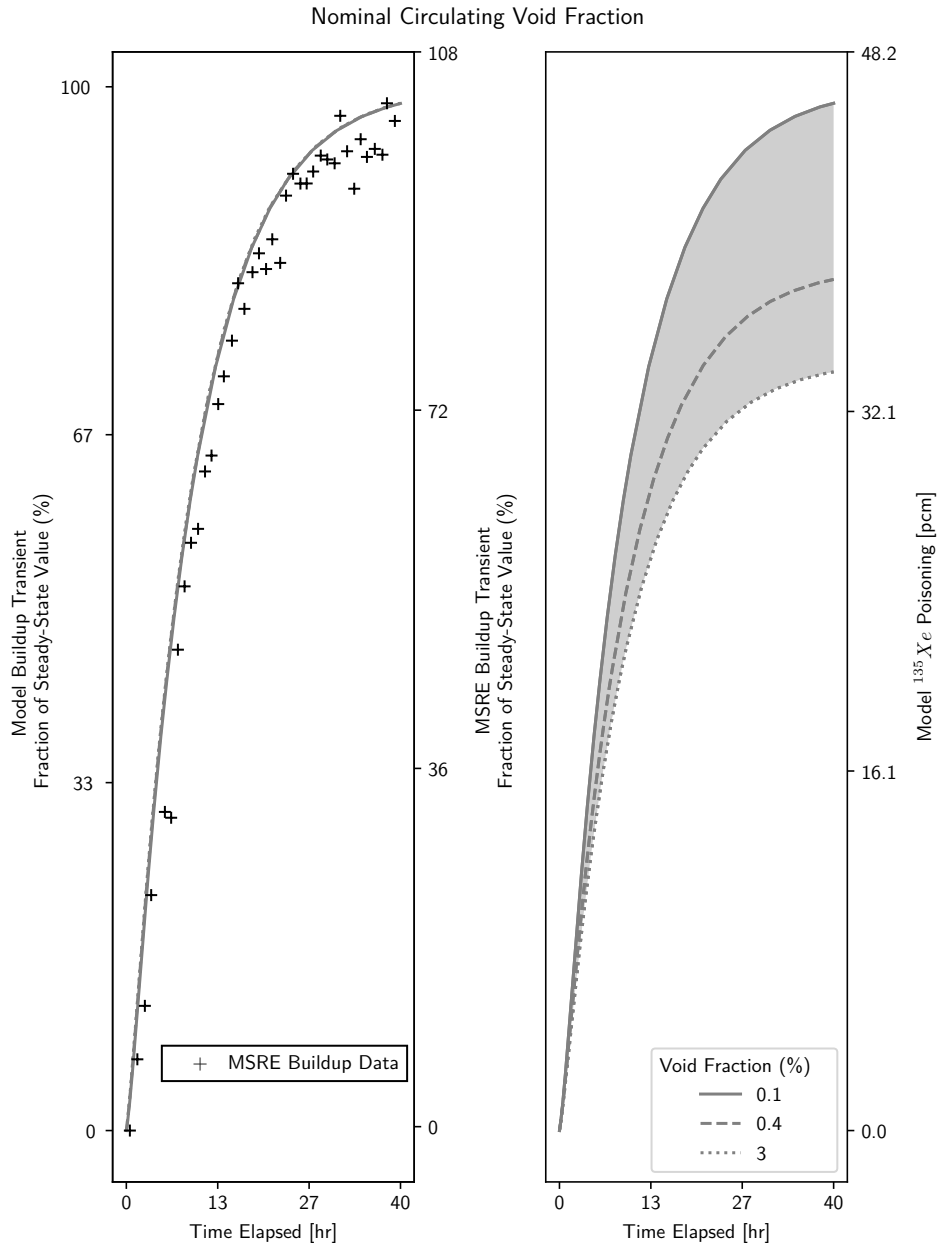
Figure 5.37: Results of build up transient sensitivity analysis with respect to the circulating void fraction
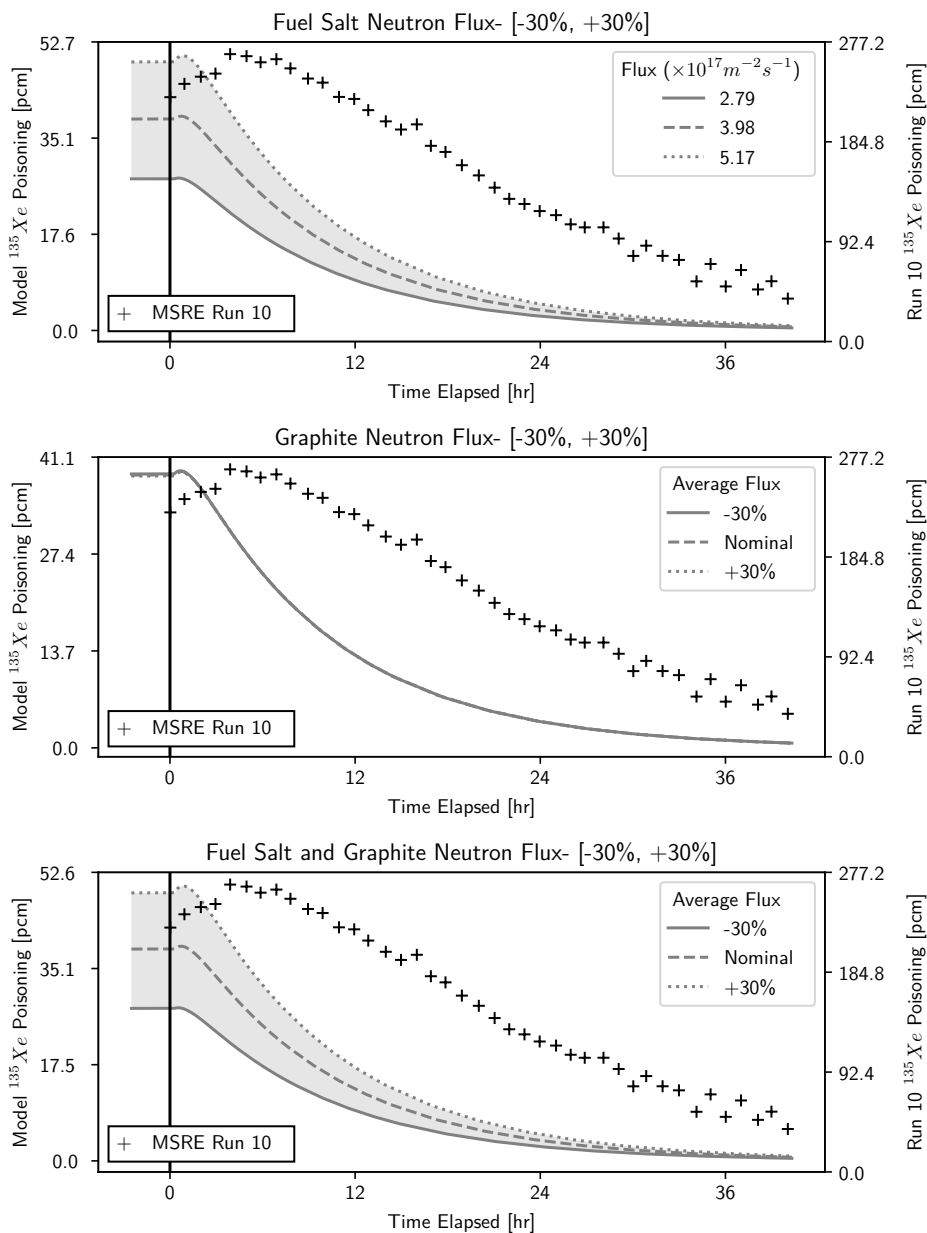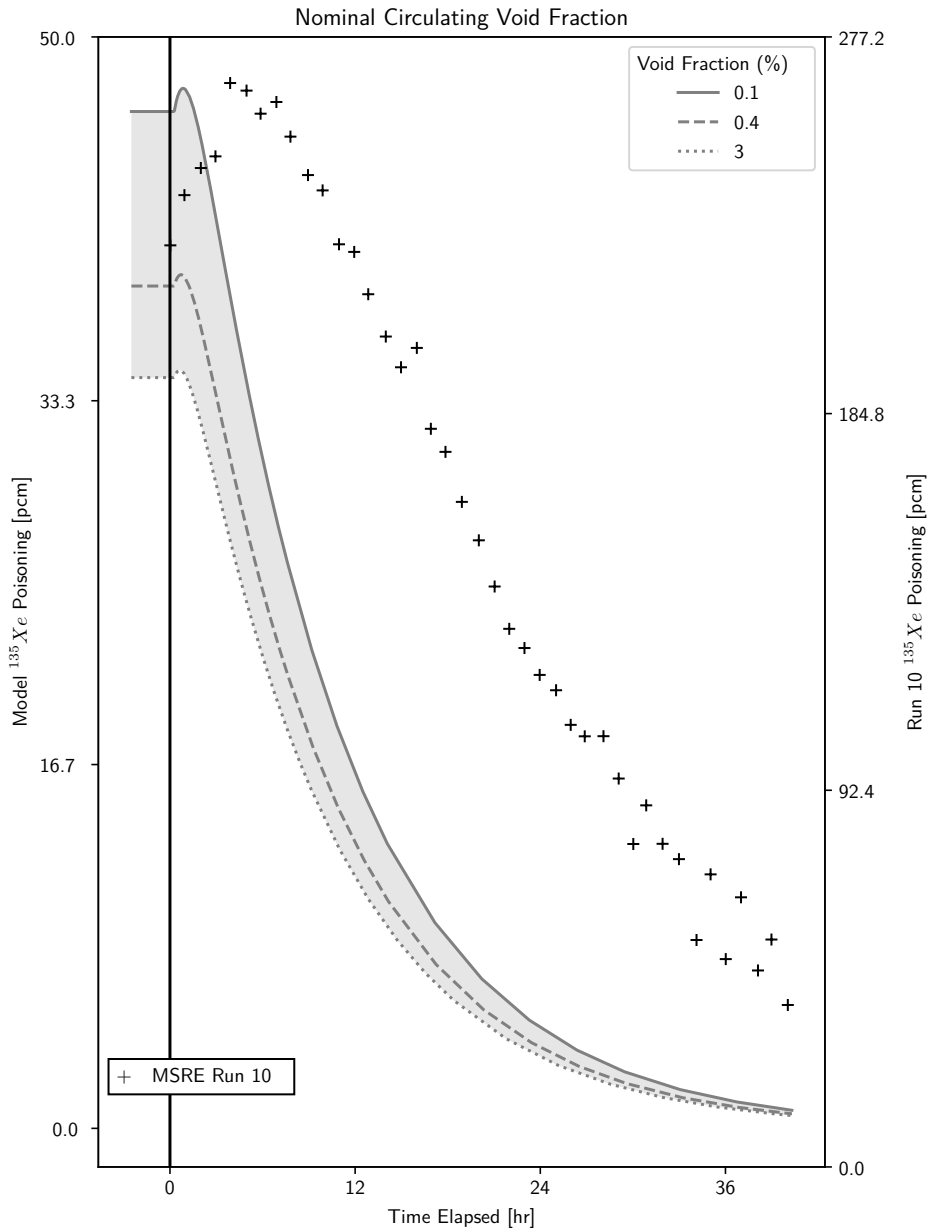
Figure 5.38: Results of sensitivity analysis with respect to the circulating void fraction
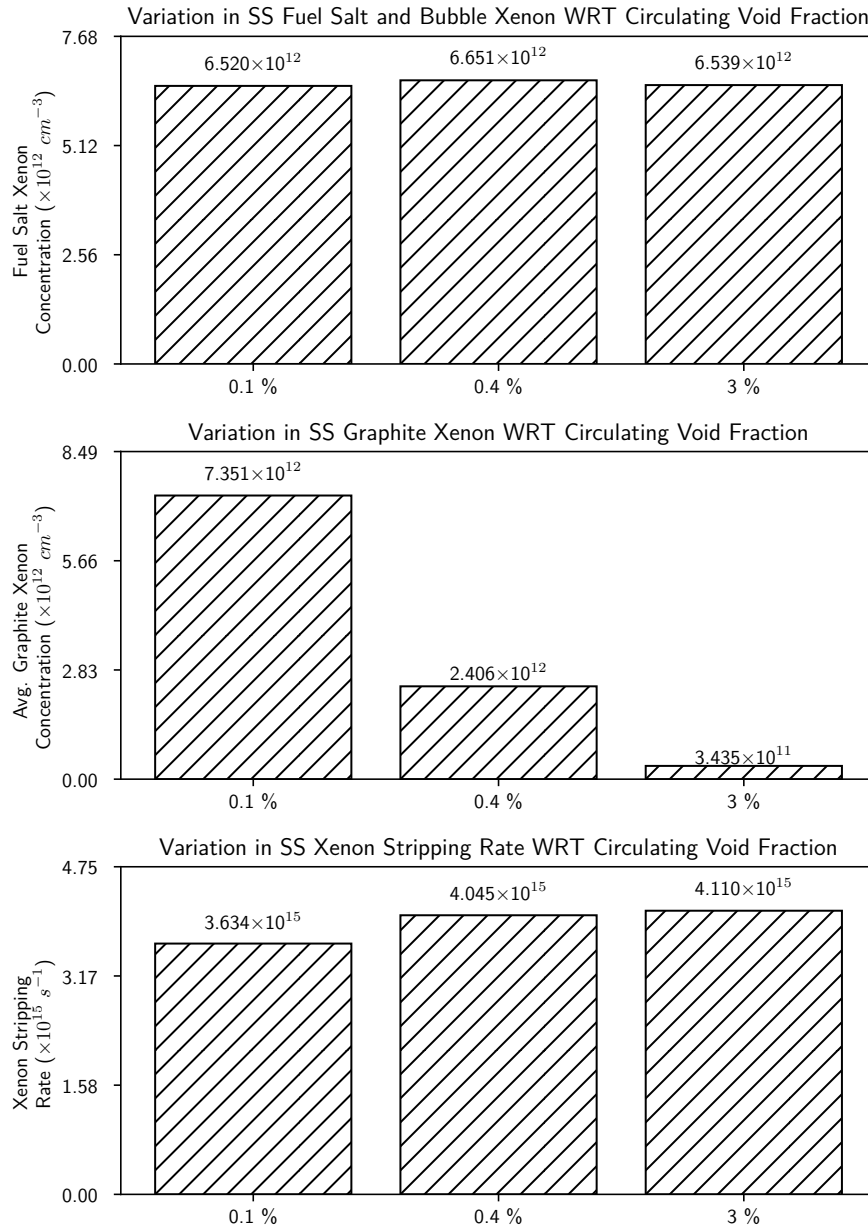
Figure 5.39: Steady state concentration of Xe-135 in the dynamic model as a result of perturbation of circulating void fraction

5.12 Reactivity Coefficients

Figure 5.41 shows the results of the sensitivity analysis with respect to the reactivity coefficients of xenon in both the fuel salt and bubbles as well as graphite. Figure 5.40 shows the same analysis but for the build up transient. There is a positive correlation between the reactivity coefficients and the xenon poisoning, this is, of course, because increasing the relative xenon poisoning per atom of xenon in the reactor increases the xenon poisoning of the reactor. Additionally, we observe that the sensitivity of the system to variation in the fuel salt reactivity coefficient is substantially greater than what is observed in the variation of the graphite reactivity coefficient. This is because there is substantially more xenon in the bubble phase, which is homogenized into the fuel salt for reactivity calculations, than there is in the graphite. Steady state analysis was not performed as the reactivity coefficients does not change the distribution of xenon in the system.
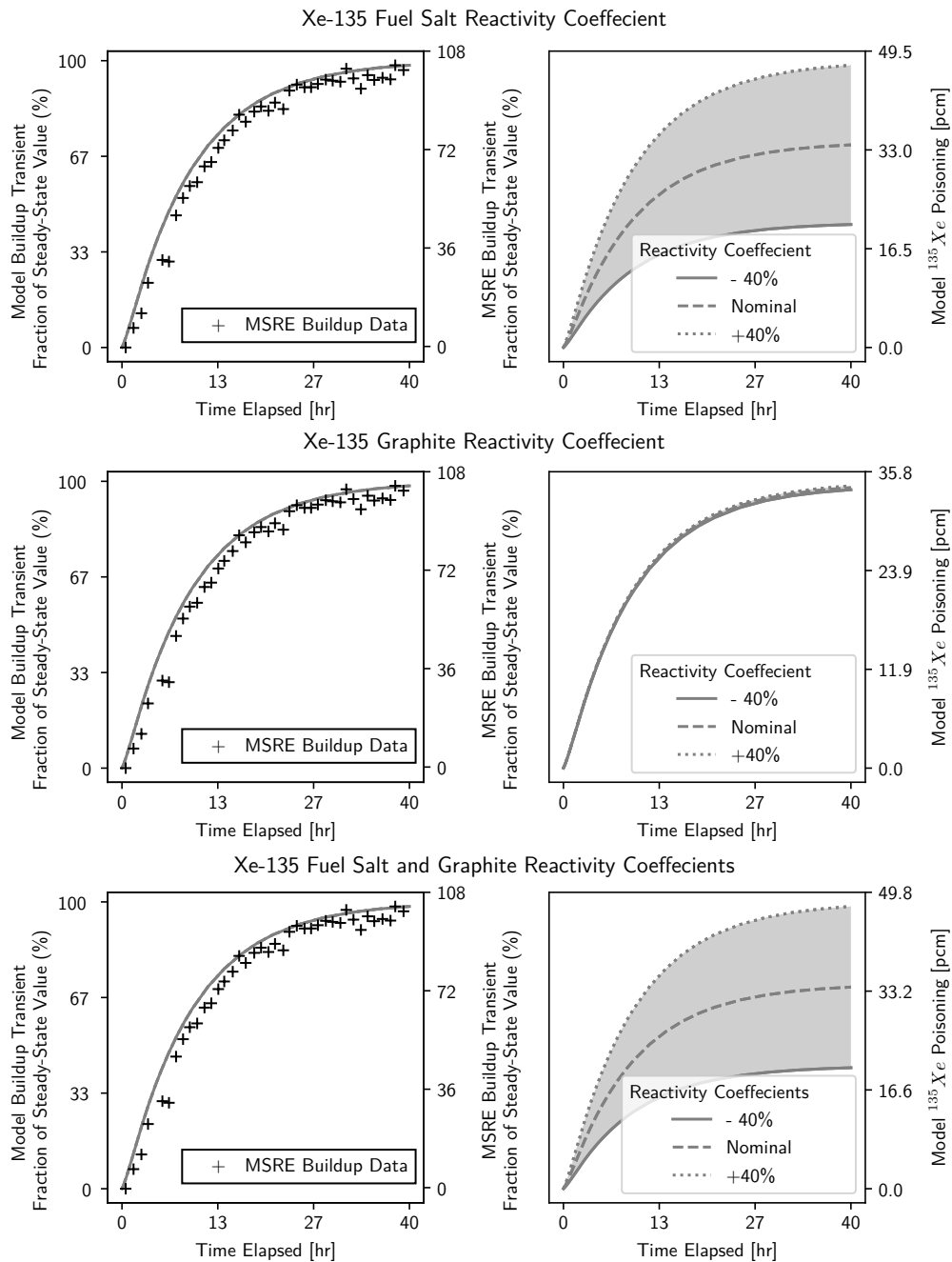
Figure 5.40: Results of sensitivity analysis with respect to the stripper parameters
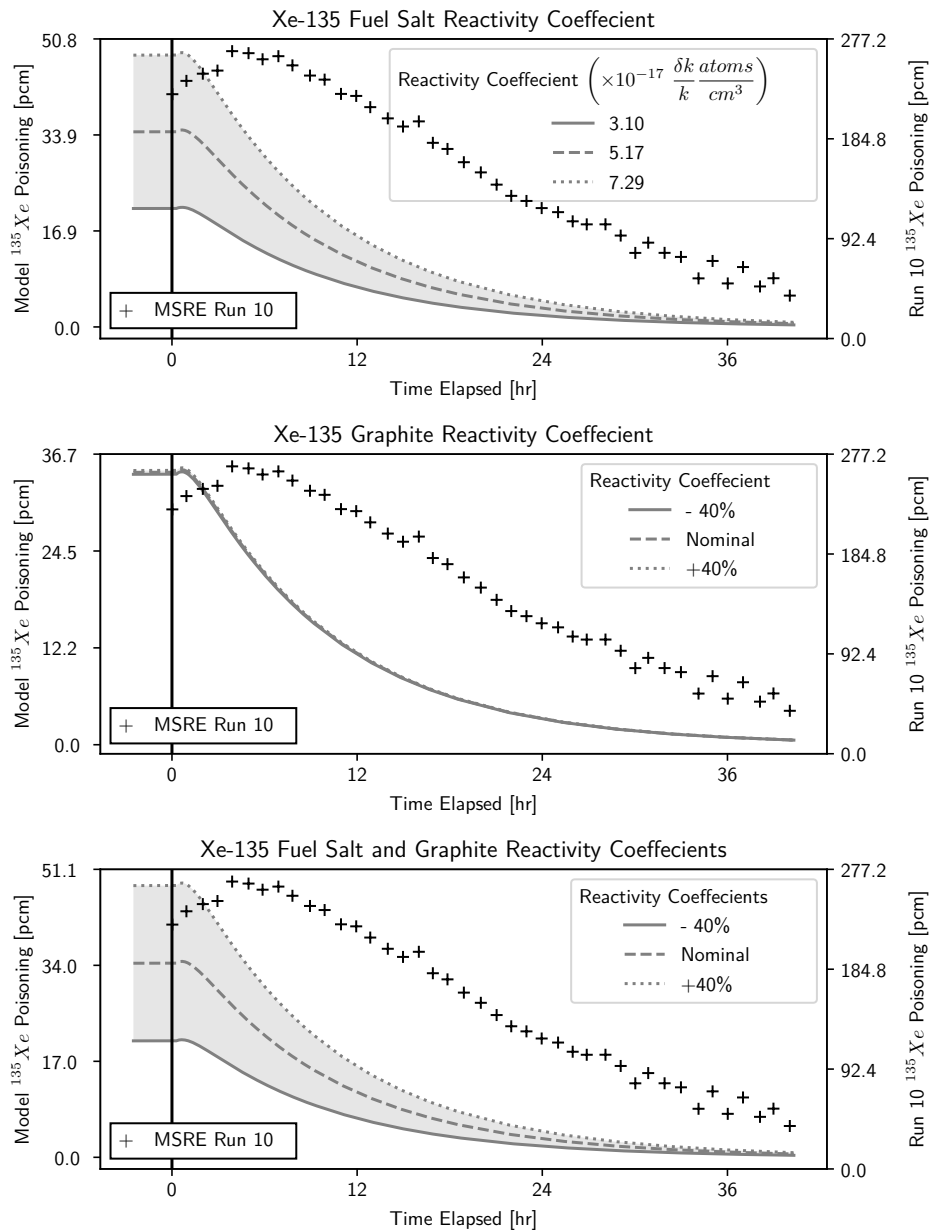
Figure 5.41: Results of sensitivity analysis with respect to the reactivity coefficients

5.13   Xenon Stripper Parameters

Figure 5.42 shows the results for the start up transient sensitivity analysis as the circulating void fraction is perturbed. The left column shows the normalized results, which is directly comparable to the reported MSRE build up data whereas the right column shows the non normalized results. Unlike all the other results, there is some variation in the build up transient time characteristics as the bubble stripping rate is varied, however, this variation is not substantial enough to produce significant deviance from the benchmark data. Regardless, it is reasonable to state, all of the instances of the normalized build up transient sensitivity analysis indicate good agreement with the MSRE build up data.

Figure 5.43 shows the results for the shut down transient sensitivity analysis as the stripper parameters are perturbed. All of the plots underestimate the magnitude and time characteristics of the shut down transient response, however, the perturbation of the bubble stripping efficiency does show a low bubble stripping efficiency will substantially increase the magnitude and time characteristics of the xenon in the system.

For both Figures 5.42 and 5.43, the plot in the first row of plots shows the results of the sensitivity analysis as the bubble radius is perturbed and the plot in the second row shows the sensitivity analysis as the xenon radius is perturbed.

It is observed in both of these plots that there is a negative correlation between the transient xenon poisoning and fuel salt stripping efficiency, bubble stripping efficiency and xenon stripper flow rate.

The results of the sensitivity analysis for the steady state distribution of xenon are shown in Figures 5.44, 5.46, and 5.45 for the fuel salt stripping efficiency, xenon stripper flow rate and bubble stripping efficiency respectively. For each of these figures, the results for the homogenized fuel salt and bubble xenon concentration are shown in the first row, the average graphite xenon concentration is shown in the second row, and the total xenon stripping rate is shown in the final row.

In the case of the fuel salt stripping efficiency, the fuel salt and bubble xenon concentration decreases from $6.5952 \times 10^{12} \, \text{cm}^{-3}$ to $5.577 \times 10^{12} \, \text{cm}^{-3}$; the graphite xenon increases from $2.515 \times 10^{12} \, \text{cm}^{-3}$ to $2.017 \times 10^{12} \, \text{cm}^{-3}$; and, the xenon stripping rate increases from $4.004 \times 10^{15} \, \text{cm}^{-3}$ to $4.189 \times 10^{15} \, \text{cm}^{-3}$.

In the case of the bubble stripping efficiency, the fuel salt and bubble xenon concentration decreases from $6.268 \times 10^{12} \, \text{cm}^{-3}$ to $2.017 \times 10^{12} \, \text{cm}^{-3}$; the graphite xenon decreases from $6.268 \times 10^{12} \, \text{cm}^{-3}$ to $2.017 \times 10^{12} \, \text{cm}^{-3}$; and, the xenon stripping rate increases from $1.991 \times 10^{15} \, \text{cm}^{-3}$ to $4.189 \times 10^{15} \, \text{cm}^{-3}$.

In the case of the stripper flow rate, the fuel salt and bubble xenon concentration decreases from $8.023 \times 10^{12} \, \text{cm}^{-3}$ to $5.696 \times 10^{12} \, \text{cm}^{-3}$; the graphite xenon decreases from $2.733 \times 10^{12} \, \text{cm}^{-3}$ to $2.177 \times 10^{12} \, \text{cm}^{-3}$; and, the xenon stripping rate increases from $3.875 \times 10^{15} \, \text{cm}^{-3}$ to $4.163 \times 10^{15} \, \text{cm}^{-3}$

5.14 Quantification of The Effect of Perturbation

The integral difference between bounds per percent change score (see §4.6) for each perturbed parameter is shown in Table 5.1.

5.15 Summary and Chapter Conclusion

This chapter has aimed to present the results of the sensitivity analysis and has done so by presenting plots for each of the sensitivity analyses performed.
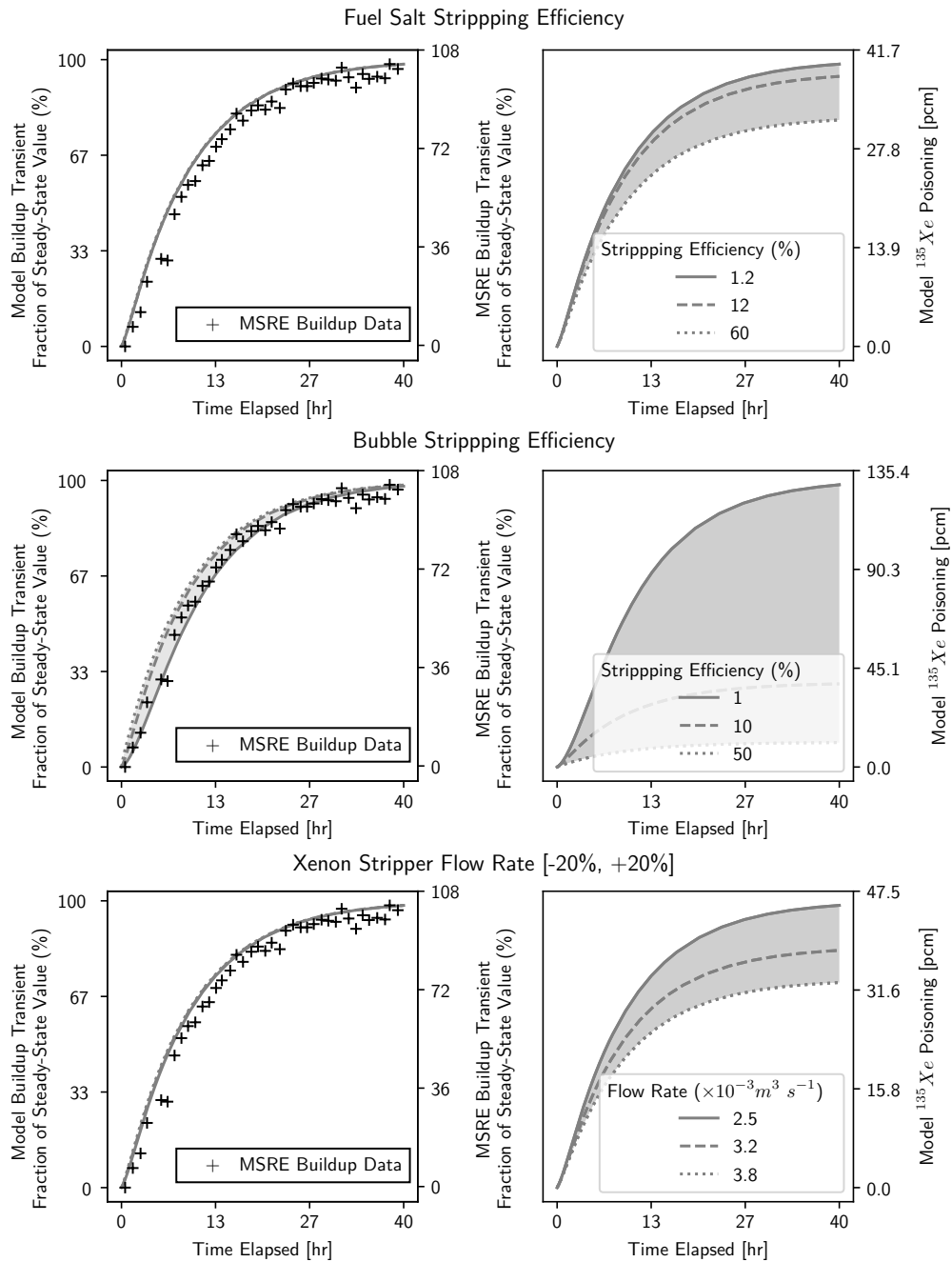
Figure 5.42: Results of build up transient sensitivity analysis with respect to the reactivity coefficients
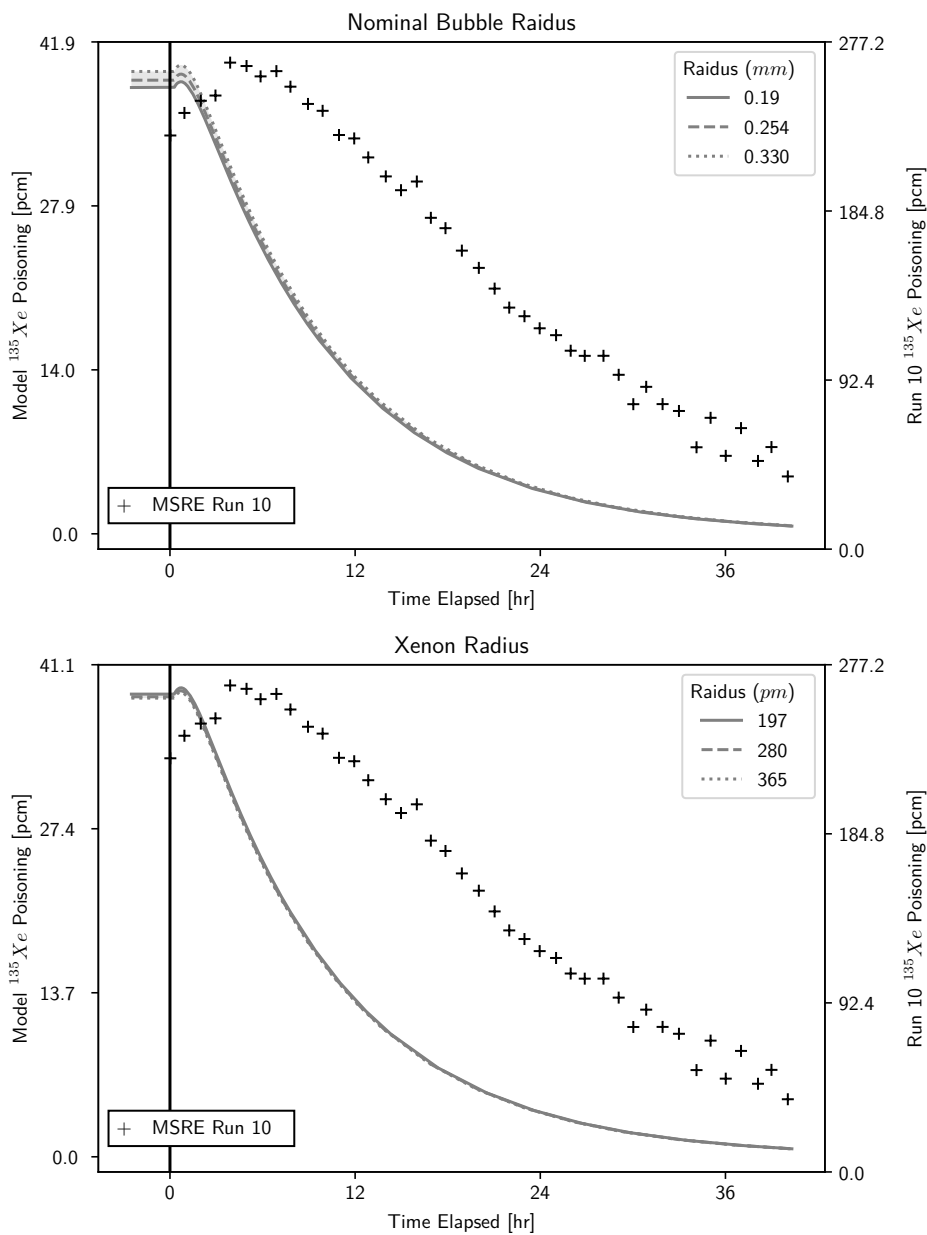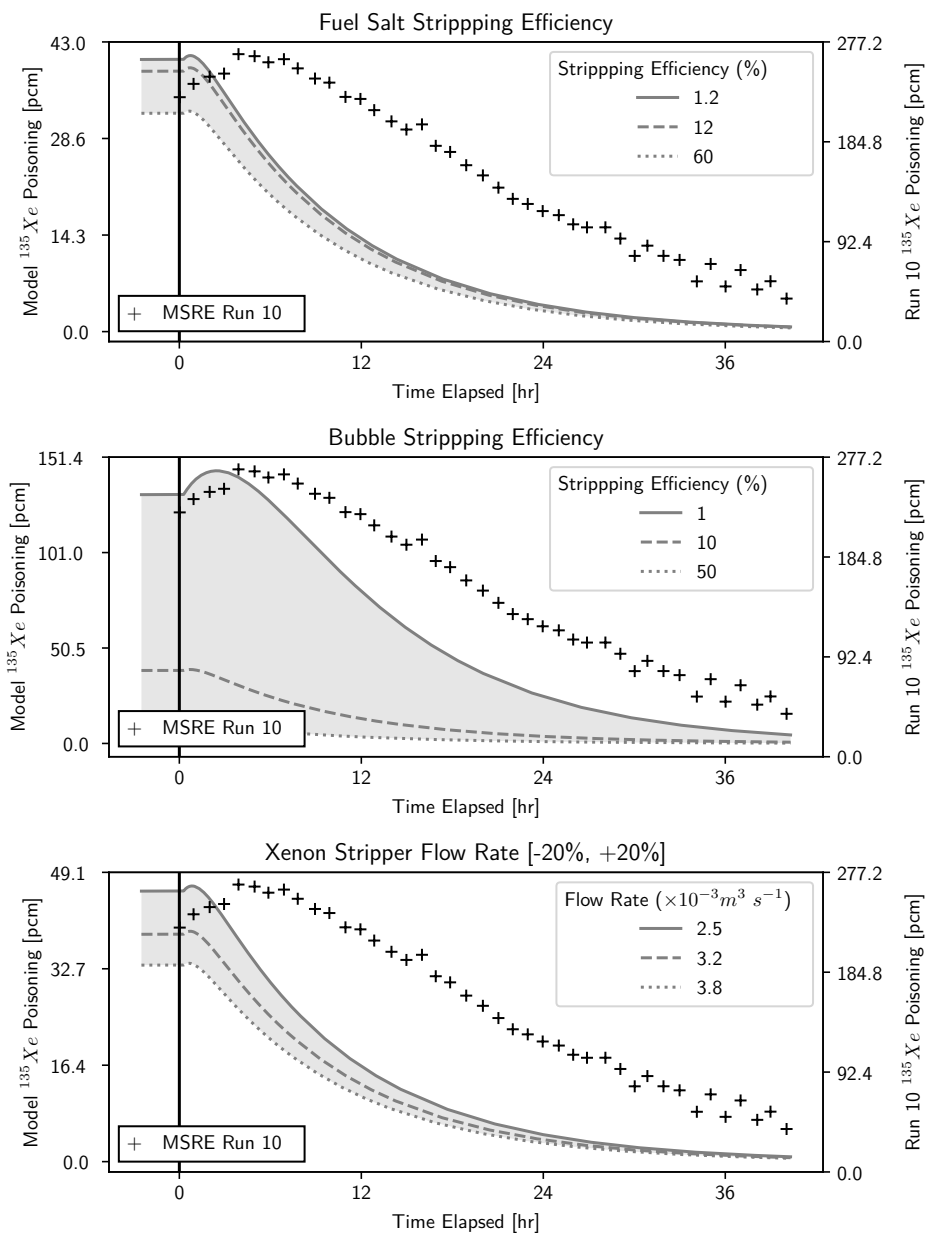
Figure 5.43: Results of sensitivity analysis with respect to the reactivity coefficients
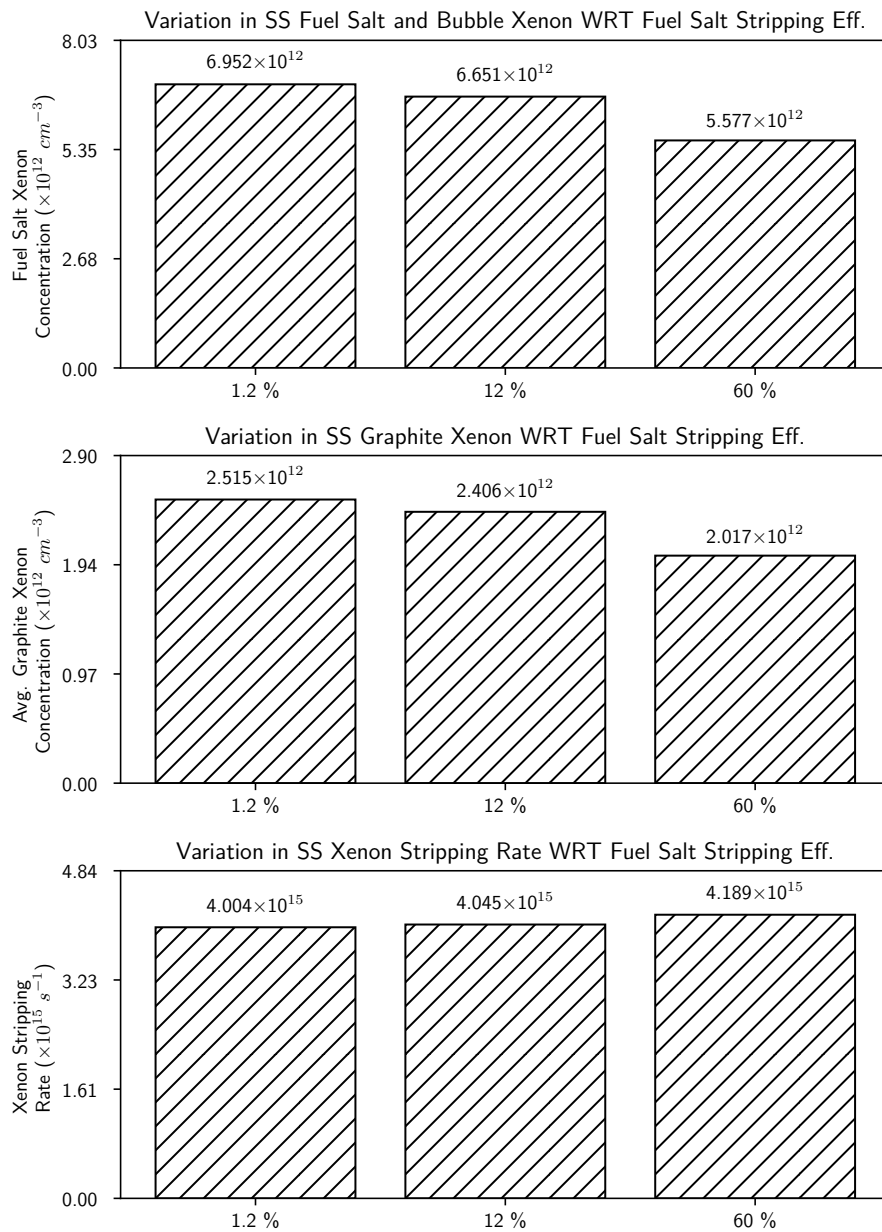
Figure 5.44: Steady state concentration of Xe-135 in the dynamic model as a result of perturbation of fuel salt stripping efficiency
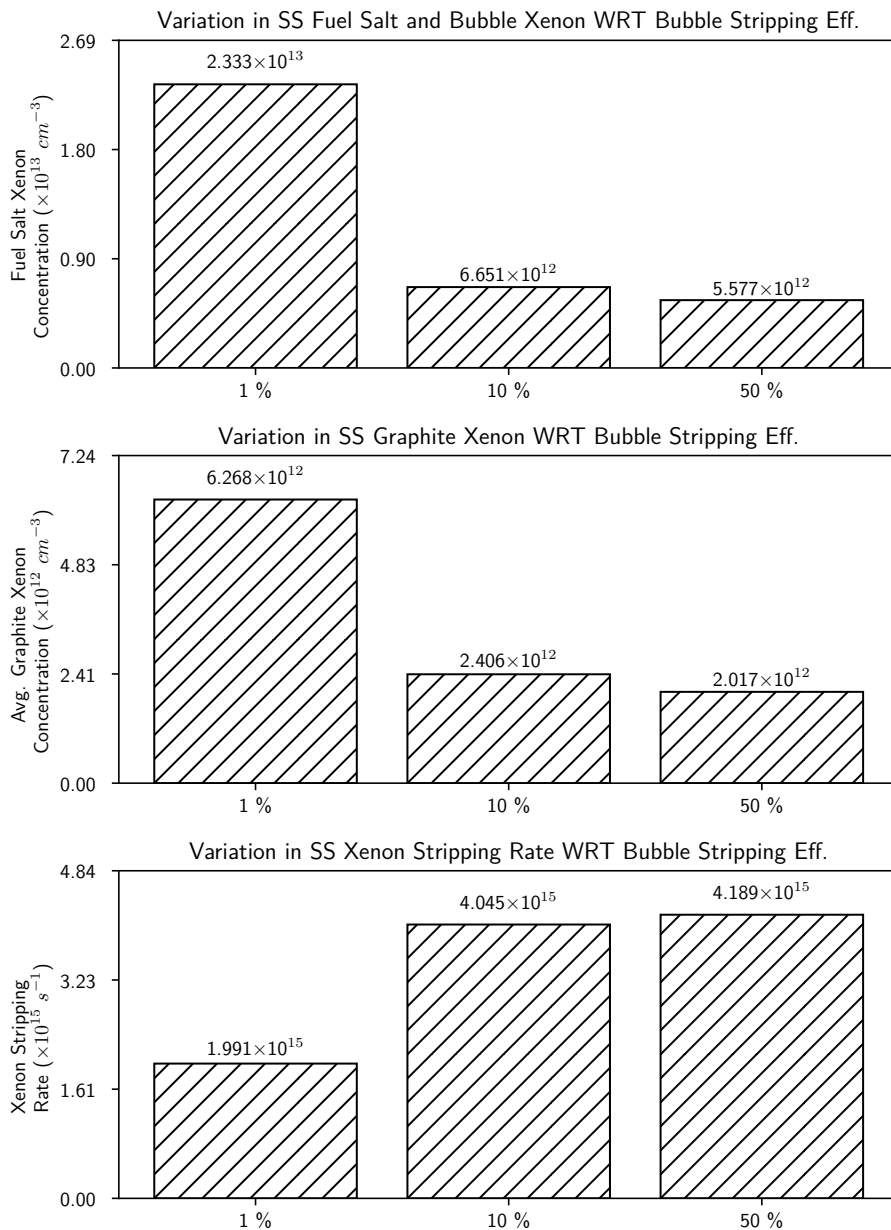
Figure 5.45: Steady state concentration of Xe-135 in the dynamic model as a result of perturbation of bubble stripping efficiency
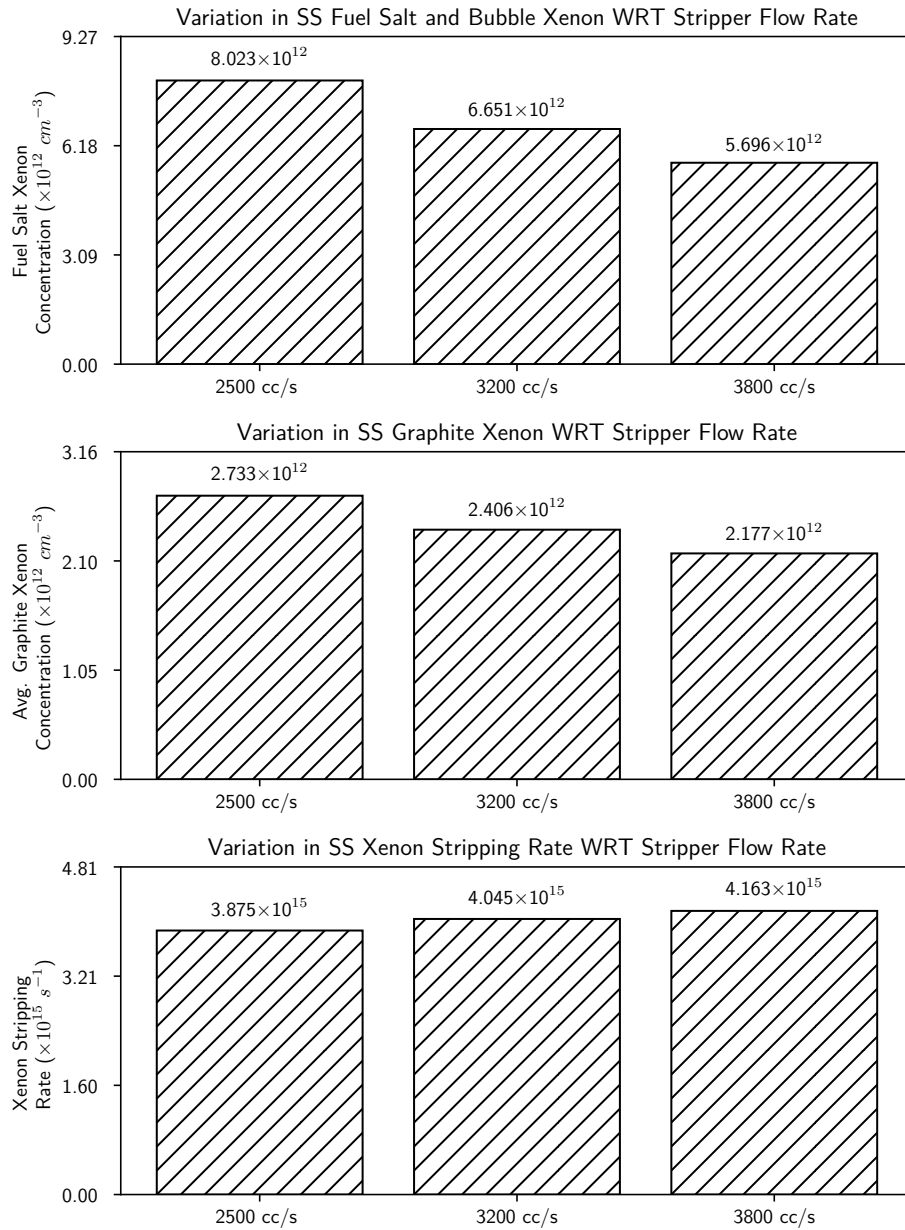
Figure 5.46: Steady state concentration of Xe-135 in the dynamic model as a result of perturbation of xenon stripper volumetric flow rate

Parameter	Score (Δ pcm diff per % change) %
Total Volume	3.88×10^0
Macroscopic Fission Cross Section	1.94×10^0
Both Fuel Salt and Graphite Reactivity Coefficients	1.94×10^0
Fuel Salt Reactivity Coefficients	1.91×10^0
Fuel Salt Neutron Flux	1.80×10^0
Fuel Salt and Graphite Neutron Flux	1.78×10^0
Stripper Flow Rate	-1.59×10^0
Bubble Stripping Efficiency	-1.27×10^0
Overall Temperature	1.09×10^0
In Core Temperature	1.08×10^0
Te-135 Fission Yield	9.76×10^{-1}
I-135 Fission Yield	8.89×10^{-1}
In Core Volume	7.68×10^{-1}
Out of Core Volume	-5.80×10^{-1}
Out of Core Temperature	2.48×10^{-1}
Absorption Cross Section	-1.66×10^{-1}
Graphite MTC	1.27×10^{-1}
Bubble Radius	1.15×10^{-1}
Viscosity	-1.03×10^{-1}
Circulating Void Fraction	-9.16×10^{-2}
Fuel Salt Stripping Efficiency	-8.23×10^{-2}
Xe-135 Fission Yield	7.76×10^{-2}
Density	6.87×10^{-2}
Bubble MTC	-6.73×10^{-2}
Graphite Reactivity Coefficient	3.43×10^{-2}
Xenon Radius	-2.88×10^{-2}
Graphite Neutron Flux	-2.40×10^{-2}

Table 5.1: Perturbation effect quantification scores

CHAPTER 6

Discussion of Benchmark Results

6.1 Introduction

The prior chapter presented the results of the benchmarking and sensitivity analysis. The objective of this chapter is to provide some element of high level insight and critical analysis into the results that the model has produced and does so by discussing the results from the previous chapter. Descriptive mechanisms of variation are proposed for each of the parameters studied. The orientation in parameter space is stated — i.e. what is the relationship between xenon poisoning in the various compartments of the model and the perturbation of a parameter. The quantification of the effect of each perturbation is also discussed for each parameter. Finally, the significance of each studied parameter is discussed as well as any potential error associated it.

6.2 Mechanisms of Variation

6.2.1 Overview

This section describes the hypothesized primary mechanism of variation for each perturbation in the sensitivity analysis. In reality, each variation is caused by the interplay of

hundreds of interwoven variables, however, much can be useful in gaining some level of intuitive explanation as to what is happening in the model.

6.2.2 Mechanism of Variation for Volume

Increasing the in core volume increases the magnitude of the production terms. This is likely caused by an increasing in the relative volume of fuel salt for production of xenon and its precursors Increasing the out of core volumes increases the relative fraction of decay to production. This results in an increase of fuel salt, bubble, and graphite xenon content as well as stripping rate.

Increasing the out of core volume increases the relative fraction of xenon subject to only decay processes without any production. This results in a decreased amount of xenon in the fuel salt, bubbles, and graphite. There is an increased rate of xenon stripping likely due to an increased quantity of gas phase which the xenon can migrate into and be subsequently stripped from the reactor.

The positive correlation between the xenon stripping rate and variation in the volumes is caused by an increased quantity of gas in the reactor. The more gas in the reactor, the more xenon can migrate to the gas phase and subsequently be stripped from the system.

Variation in these parameters has a near negligible effect on transient shape, which is reasonable since increasing the volume of fuel salt only has secondary effects on the migration of xenon in the reactor. The reason why increasing the volume of the fuel salt only has secondary effects on the migration of xenon in the reactor is because increasing the volumes does not affect any of the transfer coeffecients.

6.2.3 Mechanism of Variation for Temperature

Increasing the in core temperature shifts the balance of xenon into the gas phase and has a major influence on the content of xenon within the graphite stringers. The decrease in fuel salt and bubble xenon with in core temperatures is likely due to fuel salt being pushed out of

the core by the expanding gas phase. The negative relationship between in core temperature and xenon stripping which is likely due to increased xenon hold up in the graphite stringers with respect to temperature (mass balance again shifts to gas phase)

There is a non monotonic relationship between out of core temperature and xenon content graphite stringer xenon content. This is likely due to competing processes of variation in mass transfer, change in gas phase volume, and changes to the relative fraction of xenon in the out of core region to xenon in the in core region. This same non monotonic behavior is also observed in the xenon hold in the graphite and the xenon stripping rates and is likely due to the same competing processes. It cannot be due to gas push out of fuel salt since any fuel salt pushed out by gas expansion will expand into the pump bowl which is in the out of core region.

When combined, the effects of the in core region dominate and the resultant is approximately the same as the in core variation alone.

6.2.4   Mechanism of Variation for Density and Viscosity

The effects on fuel salt and bubble xenon content with variation in both viscosity and density are effectively negligible. There is, however, some substantial change in graphite xenon content, but, since the graphite is of only secondary nuclear importance, this does not manifest in any substantial change in the transient analyses. Regardless, any variation due to perturbation in viscosity or density is a secondary consequence since viscosity and density (without change to volume) only affects mass transfer processes, and variation in mass transfer coefficients has only a minor effect on xenon behavior in the model.

6.2.5   Mechanism of Variation for Mass Transfer Coefficients

Increasing the graphite mass transfer coefficients increases the amount of xenon in the graphite. This is due to an increased rate of xenon migration into the graphite.

An increase in the bubble mass transfer coefficients has a non monotonic relationship

with the fuel salt and bubble xenon content. This is likely due to competing processes of xenon migration into the bubble phase and increased removal from bubble stripping due to increased xenon migration into the bubble phase. This dynamic is shown in the positive and monotonic relationship between bubble mass transfer coefficient and xenon stripping rate.

The mass transfer coefficients have an effectively a negligible impact on both the magnitude and time characteristics of xenon in both the start up and shut down transient benchmarks. Although mass transfer coefficient changes the migration of xenon in the system, any effects it has on xenon removal from the system are secondary.

6.2.6   Mechanism of Variation for Fission Yields

With respect to any of the fission yields, a larger fission yields leads to a larger production term. The Xe-135 correlation, however, is substantially less than that of I-135 or Te-135; this is because the Xe-135 fission yield is substantially less than that of I-135 and Te-135. More xenon production leads to more xenon in the fuel salt, graphite, and bubbles, and also, more xenon being stripped.

Variation in fission yield has a negligible impact on variation in transient time characteristics. This is because the per atom migration terms remain unaffected by variation in xenon production.

6.2.7   Mechanism of Variation for Cross Sections

An increased fission cross section increases the fission production rate whereas an increased absorption cross section increases the burnout rate. The increases caused by these cross sectional changes manifest in increased xenon content in the system as well as increased xenon stripping. A corresponding mutatis mutandis applies to the negative correlation between Xe-135 absorption cross section and xenon content in the system as well as stripping rate.

There is some variation in the shut down transient time characteristics caused by variation in the fission and absorption cross sections. The behavior of the system after the iodine pit

appears to be unperturbed by variation in the microscopic absorption cross section. This is due to the burnout process stopping after the shut down. Changes in these parameters seem to point the system in a direction in which it better corresponds to the experimental results.

6.2.8 Mechanism of Variation for Neutron Fluxes

There is a positive relationship between fuel salt (and bubble) neutron flux and xenon poisoning. This is because the magnitude of the source terms is greater than the magnitude of the burnout when normalized by neutron flux. There is some effect on the height of the iodine pit and the magnitude of the fuel salt neutron flux. Increasing the neutron flux leads to a larger burnout term which in turn leads to a larger iodine peak once the flux is set to zero.

Variation on graphite neutron flux has effectively no change on fuel salt and bubble xenon content. This is because graphite neutron flux only effects burnout within the graphite. Furthermore, because of the minor reactivity coefficient of the graphite stringers, variation in neutron flux within the graphite stringers has a negligible overall effect on transient response.

6.2.9 Mechanism of Variation for Bubble and Xenon Radii

In regards to the bubble correlation, an increased bubble radius causes fewer bubbles to enclose the same volume of gas. This leads to a decreased density of bubbles in the fuel salt which leads to decreased removal of xenon by the xenon stripper. Variation in the bubble radius does have some effect on the graphite xenon content. This seemed counter intuitive to us at first, so the graphite sub model was checked for reference to bubble radius. No reference to bubble radius were found in the graphite model. The lumped volume model was also checked to ensure the circulating void fraction was unchanged with respect to bubble radius. One explanation for this phenomenon is as follows: Increasing the bubble radius decreases net surface area to which mass can be transferred to the gas phase (fewer bubbles

same volume). This decreases the rate at which gas is transferred to the bubble phase, which increases the amount of xenon in the fuel salt, which increases the magnitude of the concentration differential which drives xenon into the graphite.

6.2.10   Mechanism of Variation for The Circulating Void Fraction

Increasing the void fraction decreases the quantity of fuel salt in core. As the gas quantity increases, the production terms decreases. Furthermore, as gas quantity increases, the amount of gas space for xenon migration increases. There is, however, a competing process in that as fuel salt is pushed out of the core, the burn up term also decrease. The dynamics of these competing processes likely causes the non monotonic behavior in the fuel salt and bubbles.

Additionally, we observe that decreasing the void fraction also increases the height of the iodine pit (peak). This is because a decreased void fraction will decrease the proportion of xenon in the gas phase and therefore, the xenon will need to first migrate to the gas phase before being removed by the stripper which will increase the overall removal time of xenon from the system.

The steady state behavior indicates increasing the circulating void fraction substantially lowers the graphite xenon content. This is likely due to a scrubbing effect of the fuel salt caused by the increased quantity of gas in the reactor. The fuel salt and gas phase xenon content is relatively unaffected. Considering this along with the observations from the stripping rate, there appears to be a saturating effect with further increased void fraction. Increasing the amount of gas in the fuel salt does not lead to further increases in stripping rate since the xenon stripper is already scrubbing the xenon out of the gas phase.

6.2.11   Mechanism of Variation for Reactivity Coefficients

There is a direct correlation between the reactivity coefficients and the xenon poisoning, this is, of course, because increasing the relative xenon poisoning per atom of xenon in the

reactor increases the xenon poisoning of the reactor.

6.2.12   Mechanism of Variation for Xenon Stripper Parameters

The explanations for the observed behavior is as follows: an increased stripping efficiency (fuel salt or bubble) will lead more xenon being stripped which will lead to decreased xenon poisoning and an increased flow rate through the stripper will also lead to increased stripping and decreased xenon poisoning.

6.3   Orientation In Parameter Space Perturbation

In order to establish a rough orientation in the design space, table 6.1 displays the directionality, with respect to xenon poisoning, of each parameter space perturbation at the nominal operating point.

Parameter	Overall Correlation	Fuel Salt & Bubble Correlation	Graphite Correlation	Stripping Rate Correlation
Overall Volume	Positive	Positive	Positive	Positive
In Core Volume	Positive	Positive	Positive	Positive
Out of Core Volume	Negative	Negative	Negative	Positive
Overall Temperature	Positive	Negative	Positive	Negative
In Core Temperature	Positive	Negative	Positive	Negative
Out of Core Temperature	Positive	Non Monotonic	Non Monotonic	Non Monotonic
Density	Positive	Negative	Positive	Negative
Viscosity	Negative	Positive	Negative	Positive
Graphite MTC	Positive	Negative	Positive	Negative
Bubble MTC	Negative	Non Monotonic	Negative	Positive
Any Fission Yield	Positive	Positive	Positive	Positive
Fission Cross Section	Positive	Positive	Positive	Positive
Absorption Cross Section	Negative	Negative	Negative	Negative
Fuel Salt Neutron Flux	Positive	Positive	Positive	Positive
Graphite Neutron Flux	Negative	No Change	Negative	No Change
Overall Neutron Flux	Positive	Positive	Positive	Positive
Bubble Radius	Positive	Negative	Positive	Positive
Xenon Radius	Negative	Positive	Negative	Positive
Circulating Void Fraction	Negative	Non Monotonic	Negative	Positive
Fuel Salt Stripping Efficiency	Negative	Negative	Negative	Positive
Bubble Stripping Efficiency	Negative	Negative	Negative	Positive
Stripper Flow Rate	Negative	Negative	Negative	Positive

Table 6.1: Orientation in parameter space

6.4 Quantification of The Effect of Perturbation

Below is a commentary on Table 5.1, the quantification on each of the parameters involved in the sensitivity analysis:

- **Total Volume:** The model was most sensitive to relative change in this volume. Since, by balance of probabilities, the volumes reported in the ORNL literature were accurate, the high sensitivity of the model to variation in this parameter is not a reason for significant loss in model confidence. Model volumes were well reported in the supporting ORNL documentation, and estimation of volumes is a centuries old science, so there is little reason to believe that there is significant error in the reported quantities. Furthermore, the total system volume evaluates, at operational temperature, to be about $2\,\mathrm{m}^3$, which is roughly the same quantity reported elsewhere in the literature.

- **Macroscopic fission cross section:** The model's relatively high sensitivity to the macroscopic fission cross section is an area of concern. Although the neutronics code Serpent has undergone numerous benchmark exercises, and the Serpent model of the MSRE, that was developed, has been benchmarked through the reactivity worth's of its control rods, there is still reason to interpret the results from the Serpent model with an element of caution. There is no standardized benchmark nor reference data for the MSRE and this ultimately means that there is no consensus on how the MSRE neutronics should be modeled.

- **Both the fuel salt and graphite reactivity coefficients:** The reactivity coefficients used in the model were used as is. Although there was some supporting documentation in ORNL-TM-3464 [3] detailing how they were calculated, the importance factors used in their deviation were not found and detailed documentation describing their calculation was also not found. There is some concern that the mapping of the

graphite reactivity coefficients to the graphite used in the model is incorrect, however, when simulations were run with reversed reactivity coefficients, no significant change was noticed in the model output.

- **Fuel salt reactivity coefficient:** Since the the bubble xenon content is homogenized with the fuel salt xenon content for the purposes of the calculation of the xenon reactivity effect, and as there is a tendency for xenon to accumulate in the gas phase, the fuel salt reactivity coefficient is considerably more important than the graphite reactivity coefficient.

- **Fuel salt neutron flux:** The fuel salt neutron flux is one of the more significant factors that challenge confidence in the model. The product of the core volume, macroscopic fission cross section, and fuel salt neutron flux gives a power generation rate that is lower than the expected power output of the reactor. This lower power level could be from numerous sources such as incorrect cross section or volume measurements, or in correct readings of heat production, or unaccounted for sources of heat such as pump heat. Furthermore, minimal documentation was provided detailing how the fuel salt neutron flux profiles were measured.

- **Fuel Salt and Graphite Neutron Flux:** When the fuel salt and graphite neutron fluxes are varied in unison, the net effect is slightly less than when only the fuel salt neutron flux is varied. This is likely due to the effect that varying the fuel salt neutron flux primarily effects the production terms whereas varying the graphite neutron flux only effects the burnout terms — simultaneous perturbation, to some effect, cancels out the competing effects. Regardless, assuming that the effect of circulating voids on the neutron flux is negligible, there should be a straightforward analytic relationship between the fuel salt neutron flux and the graphite neutron flux that would allow for an added means of cross checking.

- **Stripper Flow Rate:** The measurement of flow rates, seems to be, a fairly standard procedure at a national lab, and, as such, we see little reason to doubt the reported xenon stripper flow rate of 15 gpm was correct. There is, however, no associated information detailing how this number was measured or known. It is possible, however, considering that the xenon stripper was the highest point in the system, that gas may of accumulated in the stripper kidneys and altered the in situ flow rate.

- **Bubble Stripping Efficiency :** This is likely the single most important parameter. It is because of this parameter that we are able to hypothesize the existence of foam that allows the model to fit both the start up and shutdown transient. This parameter is discussed in detail in the next section.

- **Overall Temperature:** The thermal model used in the xenon model was simplified and based on only the core inlet and outlet temperature measurements. No information was found that detailed fuel salt temperature around the fuel salt circulation loop.

- **Te-135 and I-135 Fission Yields:** The uncertainty associated with these quantities is the fuel salt actinide composition, which affects the effective fission yields of the the fuel salt. The fuel salt was modeled as pure U-235, which is likely a good approximation given the limited run time, high fissile material content, and low power output of the MSRE. Further refinement would required detailed knowledge of the fuel salt actinide composition. The slightly higher score of the Te-135 is due to the fact that the fission yield of Te-135 is slightly hire than that of I-135.

- **In Core Volume:** The in core volume affects both the production and burnout terms, and the volume which constitutes the in core volume is not stringently defined. There may be some fuel salt out of what would be reasonable considered *in core* where the neutron flux is non negligible, and the production and burn out terms are correspondingly non negligible. There is considerable uncertainty, in particular, with the cooling annulus — is the neutron flux in the cooling annulus sufficiently low for it

to be considered part of the out of core volume? In retrospect, considering that power production term is under predicted, it seems likely that the cooling annulus should indeed be considered part of the in core volume. Another way to calculate the in core volume would be to divide the power generation rate by the energy per fission, neutron flux and the macroscopic fission cross sections, parameters that we are more confident in.

- **Out of Core Volume:**   One of the major uncertainties in the out of core volume is the influence of dead space due to the freeze flange. Furthermore, it is unknown if the runs from which benchmark data were derived took place before or after the heat exchanger tube retrofit.

- **Out of Core Temperature:** Again, the the thermal model use in this xenon model was simplified. One particular area of concern is the thermal effects due to the fuel pump — does the fuel pump heat up the fuel salt sufficiently enough to cause a major perturbation in the fuel salt temperature?

- **Absorption Cross Section:** The Xe-135 neutron absorption cross section given in ORNL-4069 [25] and used in the model was totally undocumented and cited as a personal communication. That being said, it is fortunate that its influence is relatively small compared to some of the more major factors considering that it is being used as is. We do note, however, that the Xe-135 neutron absorption cross section, at thermal velocities, is 2.6 Mb, and it is known that the MSRE neutron spectrum was faster than a typical thermal reactor, and therefore its reported 1.18 Mb cross section seems justifiable.

- **Graphite MTC:** The perturbation of the graphite Mass Transfer Coeffecient (MTC) was done such that all regions were perturbed in unison. More detailed analysis would decompose this into a per region analysis, and then, if more detailed flow field information was known / inferred, a per channel decomposition. The total influence of a given

region's MTC needs to be weighted by the number of fuel channels in that region; so, although the central region has the highest MTC, the fact that it also has the fewest fuel channels decreases its overall influence. Furthermore, the MTC correlations used for determining the graphite MTCs were derived from non-molten salt systems, and this is significant since the atoms that comprise molten salts and xenon atoms have similar atomic radii.

- **Bubble Radius** it is fortunate that that bubble radius is of secondary importance to model behavior considering that the bubble radius used in the model was derived from a single estimate found in a water analogue of the MSRE. No information was found that detailed the bubble radius in the MSRE. The bubble radius is a function of flow conditions and therefore will vary with the reaction. An improved bubble model could be implemented through some sort of multigroup method using different bubble radii.

- **Viscosity:** Assuming that the laboratory measurements of fuel salt viscosity are reliable, the major uncertainty related to fuel salt viscosity is how the in situ evolution of fuel salt effects the viscosity of the fuel salt. Furthermore, in addition to changes in the fuel salt itself is the addition of particulate and other contaminants that may affect fuel salt viscosity. Fortunately, variation in this parameter produces a minor effect on overall xenon behavior.

- **Circulating Void Fraction:** Ultimately, the science of circulating void fraction measurement in the MSRE never reached anything like maturity, and it was still an active research area when the MSRE was shut down. The relatively high mass transfer coefficients of the circulating voids ensures that whatever xenon content is within the bubbles quickly reaches equilibrium and thereby diminishes the effect of circulating void fraction perturbation on the overall xenon behavior. The low relative score of the circulating void fraction provides confidence in the model's results. If the score was higher, then this would be indicative that the model could not confidently produce

predictions considering that there is little confidence in the measurements of the circulating void fraction in the first place. Furthermore, there is a sensitive dependence on the circulating void fraction with respect to pump speed, and if the model were sensitive to operational perturbation in pump speed it would require detailed modeling of the time evolution of the circulating void fraction.

- **Fuel Salt Stripping Efficiency :**   The low score of the fuel salt stripping efficiency , is due, in part, to the fact that xenon tends to accumulate in the gas phase rather than the liquid phase, as predicted by Henry's constant. The bubble stripping efficiency is much higher than the liquid fuel salt stripping efficiency. The fuel salt stripping efficiency was measured in a CO2 / water analogue, and no evidence nor rationale was found that indicated the validity of using a water analogue for molten salts.

- **Xe-135 Fission Yield** The system is significantly less sensitive to the Xe-135 fission yield than the I-135 and Te-135 fission yields since the Xe-135 fission yield is roughly an order of magnitude less than the Te-135 or I-135 fission yields. Again, the major uncertainty with regards to the Xe-135 fission yield is the fuel salt composition and how it is affected by burn up.

- **Density** The system is not very sensitive to the fuel salt density. This is likely due to the fact that the fuel salt density does not affect the amount of fuel salt in core — fuel salt expands into the pump bowel. Therefore, variation in fuel salt density affects only the proportion of fuel salt the undergoes a decay only processes.

- **Bubble Mass Transfer Coeffecient:** The low sensitivity to the bubble MTC is fortunate since there was little indication if a mobile or immobile interface mass transfer correlation should be used with predicting the bubble MTC. Furthermore, mass transfer correlations measured in chemical systems applied in a piece wise manner to a nuclear reactor has questionable validity.

- **Graphite Reactivity Coefficient:** A minority of the xenon is found in the graphite compared to the bubble phase, and this, in turn, leads to a low sensitivity of the system to perturbation in the graphite reactivity coefficient. This situation would change if the system operated at high bubble stripping efficiencies or very low void fractions.

- **Xenon Radius:** The xenon radius has the second lowest sensitivity score out of all the parameters investigated. This is fortunate since the intelligibility and meaning of the *radius* of xenon gas within fuel salt is questionable in the first place. Clearly, there are numerous other factors that warrant investigation before the xenon radius is refined.

- **Graphite Neutron Flux** The system has the lowest sensitivity to the graphite neutron flux. This is contrary to its high sensitivity with the fuel salt neutron flux. This is because significantly less xenon is found in the graphite than the bubbles. This suggests that it may be possible to remove the graphite modeling all together from an operable MSR xenon model for the sake of simplicity.

6.5 Parameter Significance and Error

Clearly, the bubble stripping efficiency is the most important parameter in determining xenon behavior with the model; although there are some parameters, such as the total volume or the fission cross section that have a relatively higher per percentage point sensitivity. The bubble stripping efficiency parameter, to the best of our knowledge, was never measured. Beyond the bubble stripping efficiency, the fuel salt stripping efficiency and flow rate of the xenon stripper are also significant parameters. It seems reasonable to conclude that the reported xenon stripper flow rate was accurate since measurement of flow rates is a well established and typical procedure at a national laboratory. The fuel salt stripping efficiency, conversely, was measured as part of a Master's thesis at the University of Tennessee, Knoxville, and as such may be a source of error. Effectively, without a confident measurement of bubble

stripping efficiency, a model cannot be reasonably argued to be valid — it can, however, be shown to be capable of fitting available data.

Beyond measurement of stripper parameters, reactivity coefficients, the circulating void fraction, and the macroscopic fission cross section have secondary importance in determining system xenon behavior. The neutron absorption cross section, on the other hand, appears to be a substantially more minor parameter than the fission cross section, which is fortunate since the source for the reported Xe-135 absorption cross section is a personal communication reported in ORNL-4069 [25]. The circulating void fraction, in particular, may be a particularly troublesome parameter due to the extensive and inconclusive work that went into measuring the MSRE circulating void fraction. The benchmarking of the Serpent model substantiates the claim that the fission cross section is accurate, however, no such similar homogenized parameter was found in the MSRE literature. Reported xenon reactivity coefficients and their functional form is inconsistent across the literature, however given that, as will be shown in the next section, fitting was essentially successful without variation in them, it seems reasonable to suggest that they are essentially correct. Although the apparent variation in xenon poisoning due to change in fission cross section is significant over the range studied, the apparent variation does not seem to be able of explaining the difference in model prediction and experimental results. For this reason, and given that the range of cross sections studied is large, both the fission and absorption cross sections appear to be minor influences on system xenon behavior.

Overall, due to the minor impact on poisoning magnitude, and transient characteristics, as well as the established nature of fission yield data, we believe variation in the fission yield to have a minor impact on predicted xenon behavior by the model. Precise measurements of MSRE fuel salt composition at the time of the benchmark measurements would improve the confidence of this parameter setting. This adds credulity to the model since the exact power history and therefore fuel composition of the MSRE is not known.

The power level of the reactor, when determined by $E_f \Sigma_f \phi V_{IC}$, is about a factor of 2

below what the expected power output of the reactor is, so differences in the neutron flux, or a different parameter in the equation, may also partially explain some of the difference in xenon poisoning. The graphite neutron flux is, however, a negligible parameter in determining xenon behavior in the reactor. Overall, since variation in neutron flux can help explain some of the variation in shut down transient time characteristic, the importance of the neutron flux on xenon behavior is judged to be significant. That being said, variation in neutron flux alone cannot fully explain the difference in observed and model predicted xenon poisoning with respect to the shut down transient.

The system temperature and volume does have a minor effect on the xenon poisoning of the system, however, these parameters are easily bounded with certainty by the measurements made in the MSRE.

Variation in parameters related to mass transfer — the nominal bubble radius, the xenon radius, the mass transfer coefficients, and the viscosity — appears to be negligible. Given the uncertainty regarding which mass transfer correlations should be used, and the appropriateness of applying mass transfer coefficients measured in water/gas systems to molten salt systems, and the uncertainty related to the bubble size, this is a bolstering outcome.

The relationship between xenon poisoning and the radius of xenon is near negligible. This is likely because the xenon radius is only one variable in the calculation of the mass diffusion coefficient, which is only one variable in the calculation of mass transfer coefficients, which have already been shown to have a minor impact on xenon poisoning.

The oscillatory behavior at the right tail of the experimental shutdown transient data may be an evidence of some sort of hitherto unknown phenomenology affecting the apparent xenon reactivity load which may explain some of the difference between the model and experimental results. It can also be just an artifact since the measurement does not show any errors. The lack of error analysis is, unfortunately, a common problem with the MSRE data.

In reviewing all of the data, the only perturbation that appears to have an impact on

the shape of the normalized start up transient benchmark is the bubble stripping efficiency. Even with large variation in the parameter, there appears to only be a minor change in the shape of the curve, which, in our opinion, is a good fit. The same commentary can be made for the shut down transient curve. The only parameter which seems to have a major impact on the shape of the shut down transient curve is the bubble stripping efficiency.

6.6 Chapter Summary and Conclusion

This chapter has aimed at providing some element of high level insight and critical analysis into the results that the model has produced and has done so by discussing the results presented in the sensitivity analyses. This contributes to the overall goal of the research by demonstrating that model results have intuitive and physically meaningful results. Mechanisms of variation are proposed. The xenon poisoning has been ascribed an orientation in parameter space for the various parameters investigated. The quantified effect of the perturbation has also been discussed for each parameter, the significance and error related to the parameters has been discussed.

In reality, any linguistic description a of model is an approximation of the model itself, and a model is an approximation of reality itself, so any discussion of the results of the model are necessarily more simplistic than what happens in actuality. The fact is, as will be shown in the next chapter, by changing two parameters, the model can be made to fit the experimental data, and this is significant — no other model has been able to do this in multiple cases[1]. This means that it is at least *possible* for the model to be an appropriate representative of reality. Said another way, the experimental results are within the model's parameter space. Certainly, we can be more confident in a model that can predict experimental results than a model that cannot.

---

[1]The ORNL-TM-3464 [3] was able to fit the model to experimental data in one of case, but this model, to the best of our knowledge, is the first time that the model has been able to recreate multiple experimental results with intelligible estimates of model parameters.

CHAPTER 7

Model Fitting

7.1 Introduction

As shown in the prior two chapters, the model categorically under predicted the xenon poisoning magnitude and characteristic with the shut down transient benchmark. After some experimentation, we found that we could substantially lower the fuel salt and stripping efficiencies and effectively recreate the benchmark data. This is significant in that only two parameter changes were required to recreate the experimental data. Furthermore, some evidence was found that justified these changes. This chapter presents the results of this *model fitting* exercise and provides evidence to justify the change of these parameters. Finally, based on our experience, some insight is offered on potentially why the model presented in ORNL-TM-3464 was not able to generate similar results. The objective of this chapter is to demonstrate the model can be fitted to experimental results with minor deviation.

7.2 Fitting Results

Figures 7.1 and 7.2 show the results of reducing fuel salt and bubble stripping efficiencies by a factor of 1000 (0.1% and 0.12% efficiency for bubbles and fuel salt respectively) on the start up and shut down transient benchmarks. In our opinion, the fit matches the data

sufficiently, given the uncertainty in the error of the data. Since this result was achieved by reducing a single set of parameters, we hypothesize that the primary cause of the discrepancy between expected and fit data is the existence of a foam that covers the xenon stripper and effectively prevents it from removing xenon from the fuel salt.

ORNL-TM-3464 [3] (page 93) also hypothesized the existence of a foam cover the fuel salt, but their claim was that the foam would cover the surface of the fuel salt and prevent the exchange of gas phase xenon with the cover gas. Furthermore, the ORNL-TM-3464 xenon model was unable to fit both steady state and transient results using stripping parameters that were low — only the steady state solution was able to fit the experimental data using low stripping parameters whereas these same caused an unacceptably slow transient response.

7.3 Evidence for Fitted Parameter Estimates

There is some experimental evidence, beyond the apparent match with fitted parameters, that substantiates this hypothesis. ORNL-3872 [47], page 23, estimated the MSRE void fraction to be between 1.2% and 3%. ORNL-3027 [48], page 27, states the void fraction between the bubbler lines of the pump bowl was 20%. ORNL-TM-3027 [48], page 20, states the bubbler lines were 3.510" / 8.915 cm and 1.636" / 4.155 cm from the volute center line respectively. Based on measurements of of the pump bowel drawing on page 13 of ORNL-TM-0728 [36], the volute center line sits 9.952"/ 22.644 cm above the bottom of the pump bowel. This means the line which is equidistant from either bubbler would be 7.369" / 18.717 cm above the base of the pump bowel. Additionally, the xenon spray ring was measured to be 11.048" / 28.062 cm above the base of the pump bowel. Given that the xenon spray ring is only an additional 3.679" / 9.345 cm above the mid line to the bubblers, we think it reasonable to conclude that the xenon spray ring is submerged in bubble rich, foam like fuel salt / cover gas mixture, and it is because it is covered with this foam, that the spray ring cannot remove xenon from the system.

7.4 Retrospective on the ORNL-TM-3464 Xenon Model

Perhaps the reason why the ORNL-TM-3464 xenon model was unable to reproduce experimental results with low xenon stripping efficiencies is that they used a lumped volume approach to modeling the graphite stringers, whereas our dynamic model used a second order FDM solution to a porous medium reaction diffusion equation. To test this hypothesis, a lumped volume model of graphite stringer behavior was built using they nuclear and mass transfer parameters as were used on the FDM model. The MSRE run 10 transient was simulated by both these models and the results are shown in Figure 7.3. Clearly, the lumped volume approach is much slower and larger in magnitude than the reaction diffusion equation approach. This is due to ignoring the internal transport of xenon within the graphite stringer, which keeps the majority of xenon near the surface of the stringer.

7.5 Chapter Summary and Conclusion

The objective of this chapter is to demonstrate that the model can be fit to experimental results with minor deviation, and has done so by presenting the results of the model fitting exercise, providing justification and evidence as to why the associated parameter changes are appropriate, and suggested a rationale as to why the ORNL-TM-3464 xenon model was unable to recreate both transient and steady state results.

It may be argued that the model is invalid due to its sensitivity and dependence on the bubble stripping efficiency, but we're not trying to claim the model is valid. Our claim here is simply that the model CAN recreate experimental results, and do so in not just one but two benchmark cases, which is an improvement over prior modeling attempts.
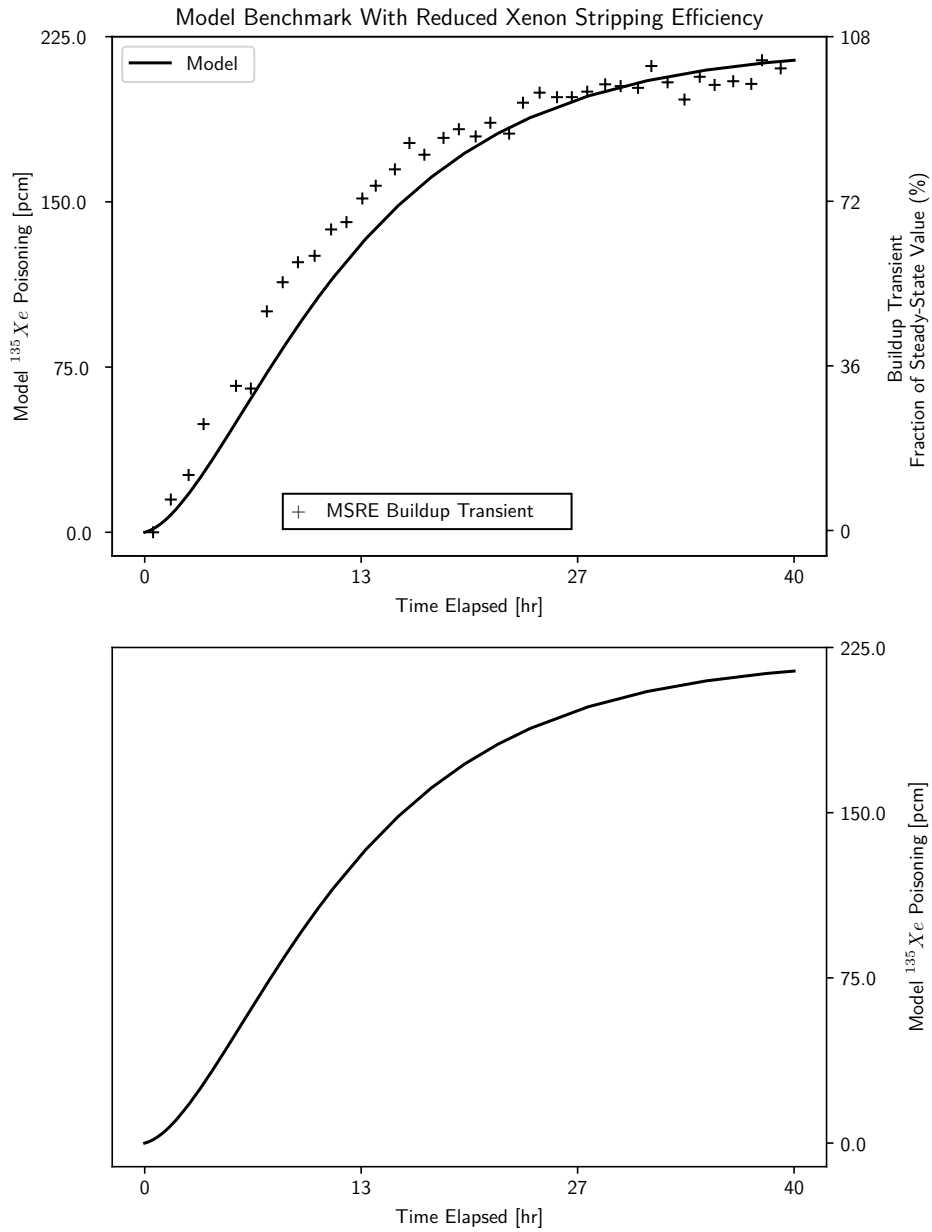
Figure 7.1: Comparison of build up transient model prediction with reduced bubble and fuel salt stripping efficiencies with model data
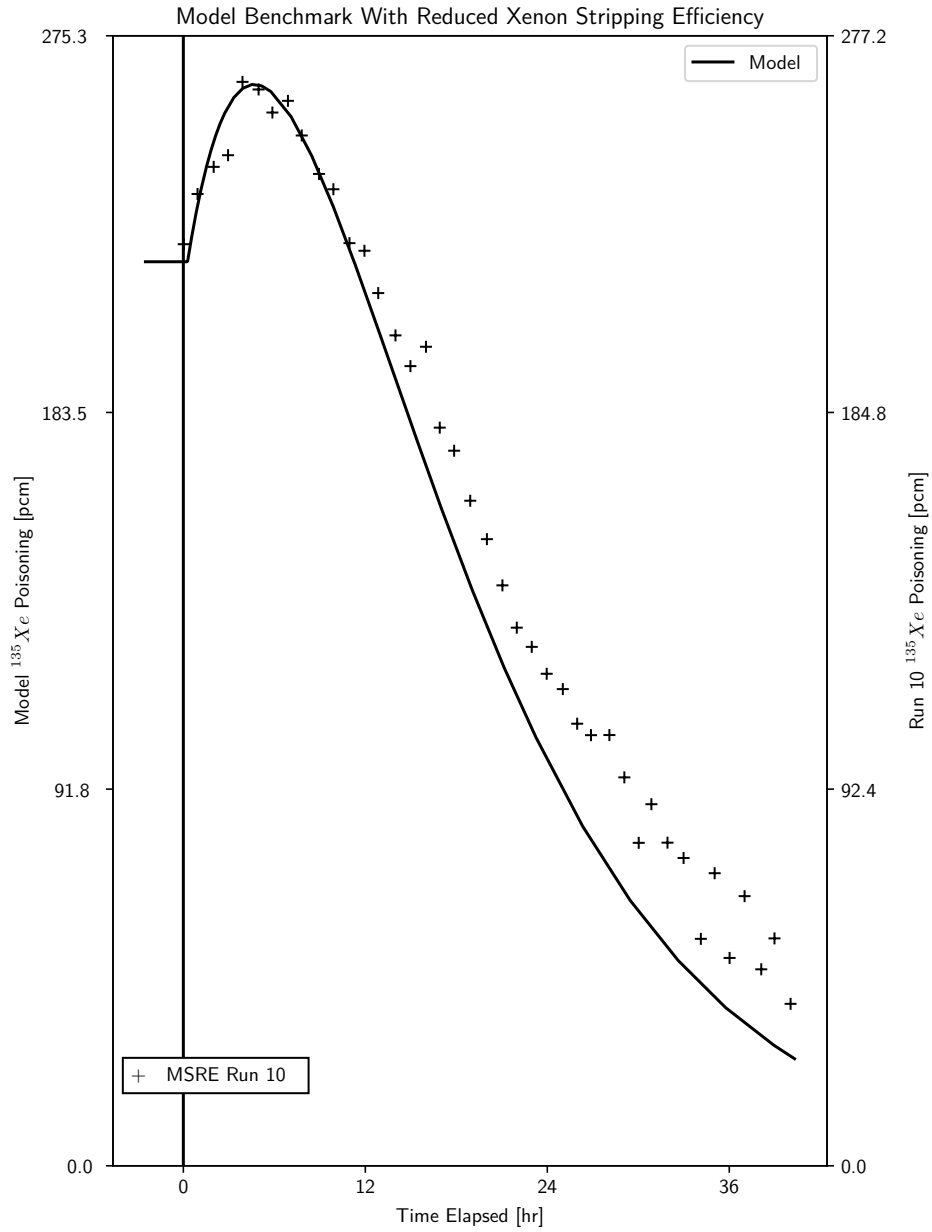
Figure 7.2: Comparison of model prediction with reduced bubble and fuel salt stripping efficiencies with model data
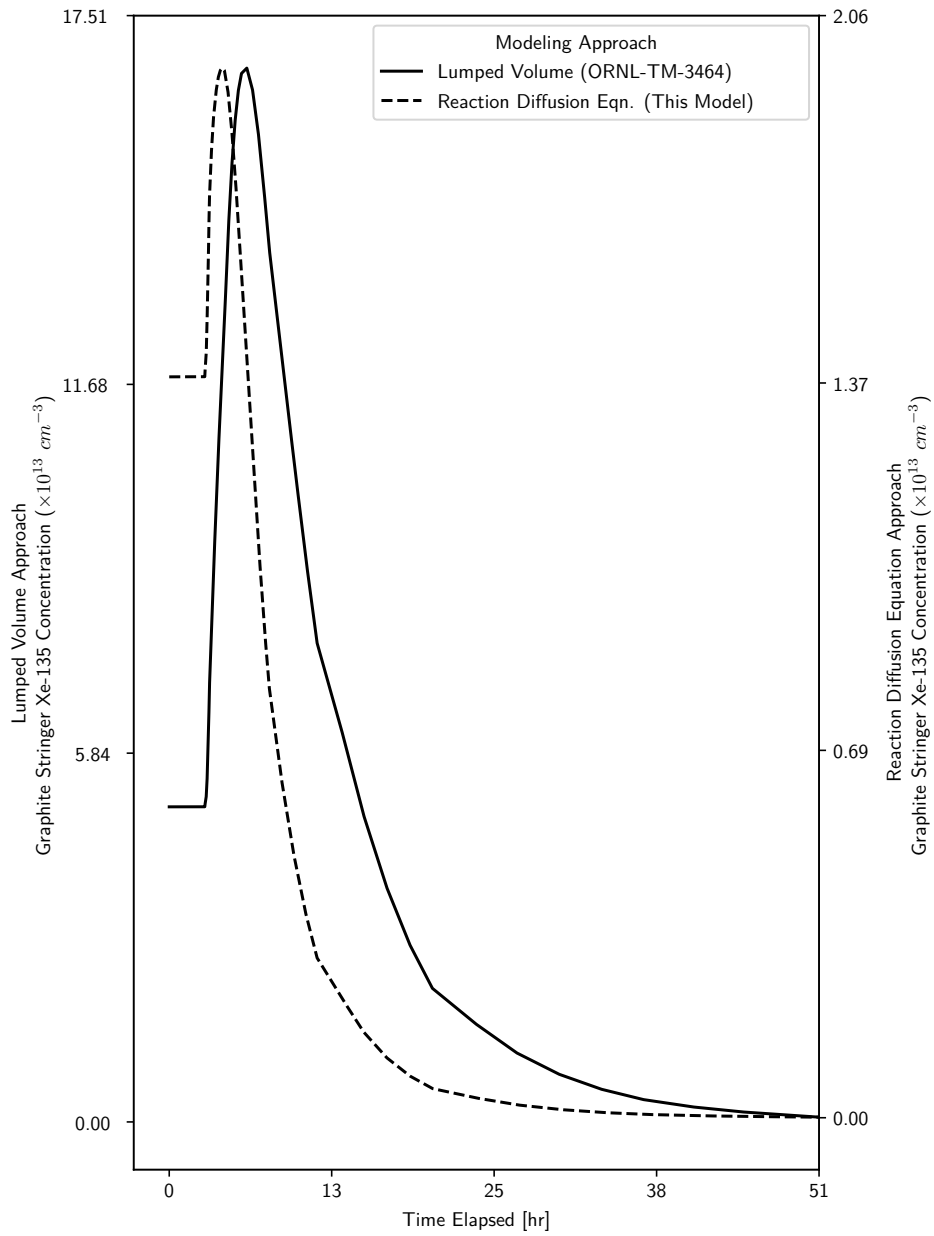
Figure 7.3: Comparison of approaches in graphite stringer modeling methodology

CHAPTER 8

Demonstration of Dynamic Transients

8.1 Introduction

The initial goal of the dynamic model was to demonstrate the feasibility of creating an MSR xenon model that described the temperature dependent behavior of xenon in an MSR. Looking at the literature on the surface, one would never know that modeling efforts, to date, had been met with limited success. We intended to take the current state of the art and build off it to include dynamical features. Our success in fitting the model to benchmark data was completely unexpected.

Nevertheless, in congruence with the original aims of the project, this chapter presents the results of three potential dynamic transients that may affect MSR xenon behavior. Numerous other xenon transients are possible, but this chapter simply aims to demonstrate the capabilities of the model — capabilities that haven't been demonstrated in any other model to date[1]. The objective of this chapter is to showcase the capabilities of the dynamic model.

8.2 Dynamic Transients

In order to showcase the capabilities of the model, three transient scenarios were run:

---

[1]C.F. Table A.1 if there is any question as to the validity of this claim

- A global thermal transient

- A localized heating transient

- A gas ingress transient.

To the best of our knowledge, this is the first model capable of simulating these types of transients.

Figure 8.1 demonstrates a thermal transient in which the overall system temperature undergoes a step increase of 10% at $t = 0$. This is, as far as we are aware, the first time the effects of a thermal transient on MSR xenon behavior has been studied. We observe a hitherto unknown peaking behavior that is instigated by the onset of the thermal transient. This is essentially caused by the instantaneous expansion of the fuel salt which increases its carrying capacity of xenon, which is subsequently expelled from the system and the system is left with reduced xenon content.

Figure 8.2 demonstrates a thermal transient in which the fuel salt and graphite within region 1 of the graphite stringer develops a localized hot spot. The temperature in both the fuel salt and the graphite is increased by a factor of 150% over a period of 30 seconds. This causes a localized increase in the graphite xenon concentration primarily due to changes in temperature and mass transfer coefficient.

Figure 8.3 demonstrates the effect of a rapid increase in the circulating void volume on xenon behavior. In this transient the nominal circulating void phase is increased by a factor of four over five minutes. Essentially, the gas pushes fuel salt out of the core and into the external loop and this causes a drop in the graphite xenon content.

8.3 Summary and Conclusion

The aim of this chapter was to showcase the capabilities of the dynamic model. This was done by simulating transients for thermal and gas ingress transients. Numerous other types
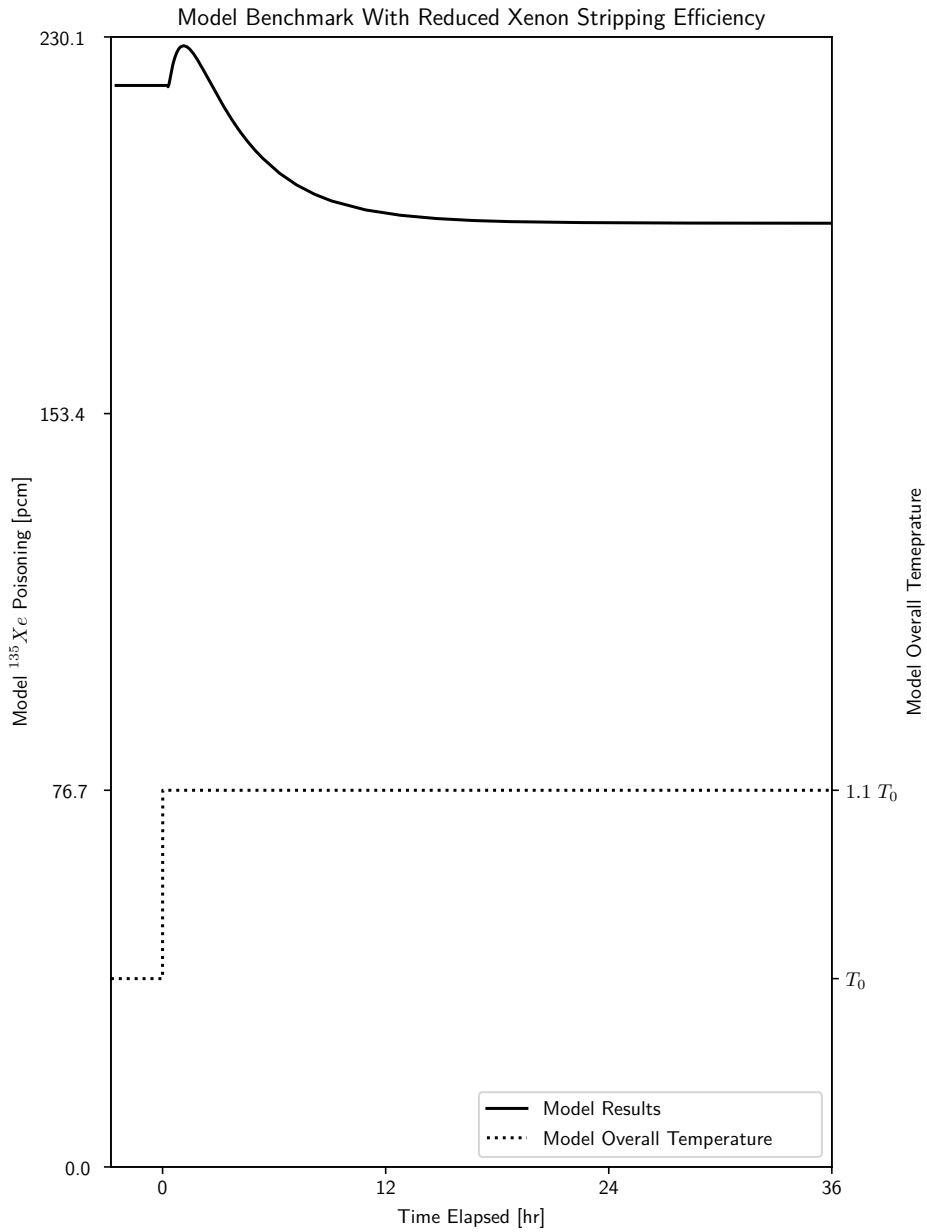
Figure 8.1: Demonstration of the effect of overall heating on xenon behavior
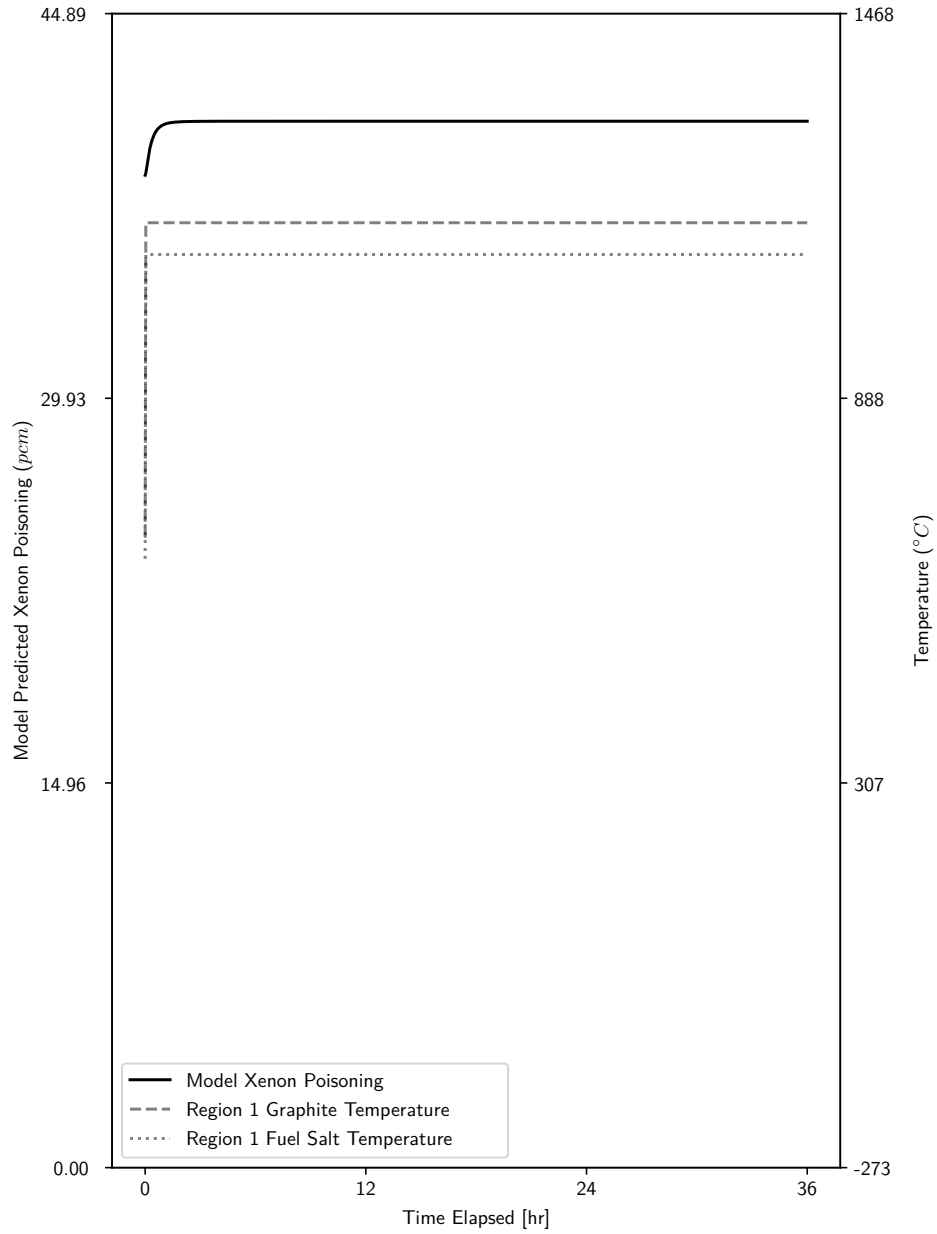
Figure 8.2: Demonstration of the effect of local heating in graphite region 1 on xenon behavior
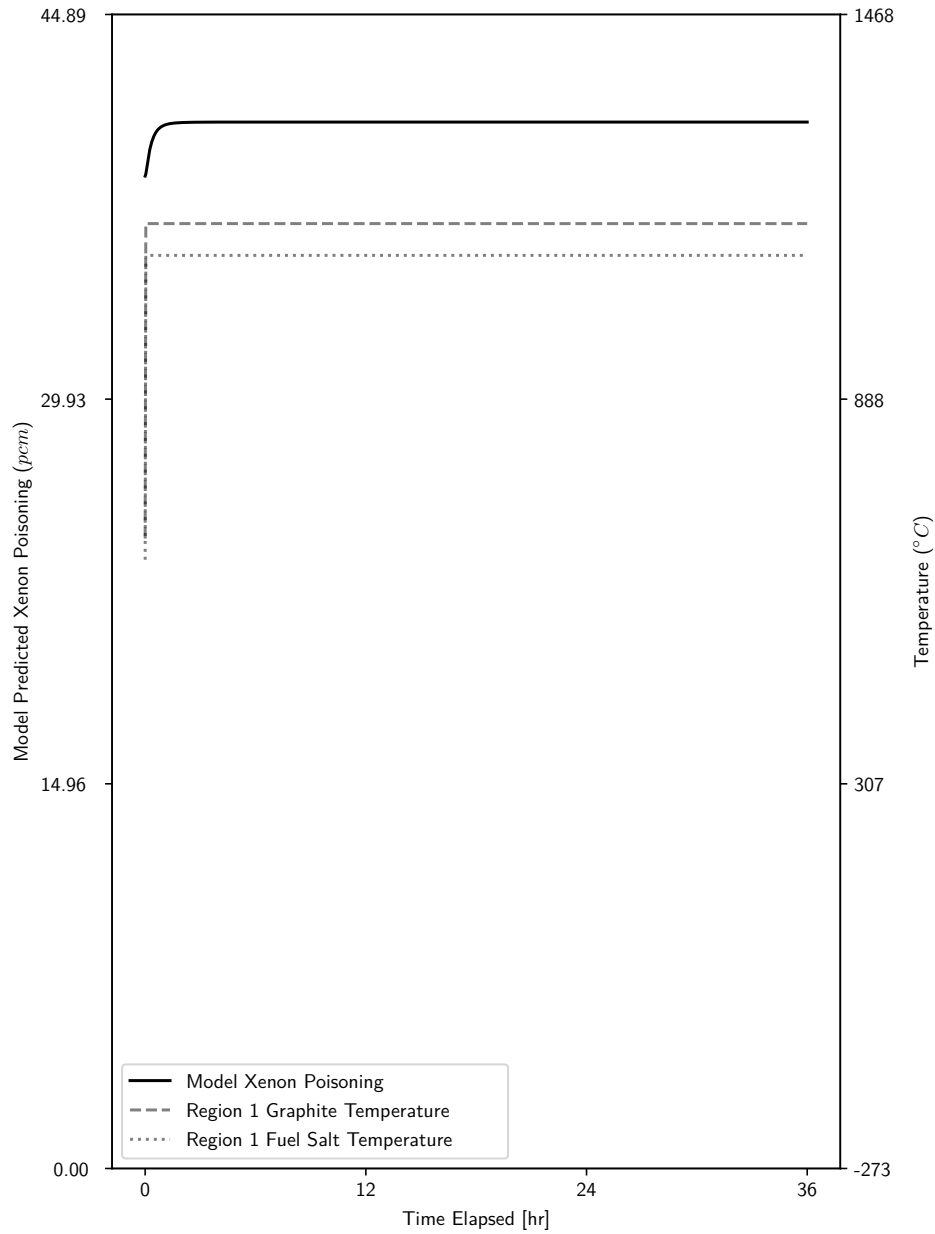
Figure 8.3: Demonstration of the effect the rapid ingress of gas into the fuel salt on xenon behavior

of thermally induced xenon transients are possible to simulate using the model. Indeed, using the capabilities of Simulink, any of the model parameters can be perturbed and a corresponding transient solution generated.

Conclusions

Conclusion

A dynamic model of MSRE xenon behavior has been developed and the original objective of developing a MSR xenon dynamics model has been achieved. Although the model parameters derived from reference data considerably produced model results that considerably under-predicted the xenon behavior of the reactor, lowering the model stripping efficiencies substantially improved the model correspondence to experimental work. This lead to the the hypothesis that foam covers the xenon stripper in the MSRE during operation and prevents the xenon stripper from functioning in a manner analogous to its laboratory behavior. Measurements of the MSRE circulating void fraction in the pump bowel has been substantiated by evidence.

A similar foam hypothesis was described in ORNL-TM-3464 [3] to explain the apparent need for low stripping parameters in the steady state calculations. These low stripping parameters, when applied to transient calculations in the ORNL model produced transient predictions that were far too long. Our model appears to resolve this inconsistency by modeling the graphite stringers through a reaction diffusion equation rather than using a lumped parameter model. This, in the opinion of the author, is one of the most significant advances to the field in the past 50 years.

Finally, the model has also demonstrated, for the first time, the feasibility of developing a xenon model that can describe the effects of thermal transients on reactor xenon behavior.

Future Work

Ultimately, future work on MSR xenon behavior is limited by the availability of the benchmark data. Although there is some significant work that can be done in organizing and summarizing information available in the ORNL reports, the field appears essentially stuck until a suitable experimental apparatus can be developed.

The operation of the model fundamentally depends on the application of the ideal dilute solution assumption and the in solution assumption, and it would be pertinent for experimental apparatus to be designed to establish clear, quantitative, criteria under which these assumptions are valid.

The effect the reactor's time evolution has on xenon behavior is also a major unknown. Experimental apparatus ought to be constructed to determine the effect corrosion and circulating particulate has on xenon behavior.

Finally, there may be some additional work that can be done on the modeling front. Given the apparent lack of impact graphite has on xenon behavior, it may be possible to construct a xenon model without modeling graphite. This would substantially simplify model development thereby reduce development time. That being said, measurements of the xenon distribution within the graphite stringers would be beneficial to the development and validation of such a model.

Appendices

APPENDIX A

Listing of Literature Related to MSR Xenon Behavior

Table A.1: MSR Xenon Literature

Year	Title	Pages	Model?	Authors	Citation
1954	ORNL-CF-54-5-1: The Xenon Problem in the ART [1]		?	Meem	[49]
1956	ORNL-1924: A Theoretical Study of Xe-135 Poisoning Kinetics in Fluid-Fueled, Gas Sparged Nuclear Reactors			Robertson	[19]
1957	ORNL-2376: ART Fuel Pump and Xenon Removal System Development, Test Evaluation and Aircraft Application			Samuels, Lackey	[50]

[1] A copy of this report was not found. It is referenced in ORNL-1294. [19, p. 5]

Table A.1: MSR Xenon Literature

Year	Title	Pages	Model?	Authors	Citation
1960	ORNL-CF-60-2-2: Xenon Control in Fluid Fuel Reactors			Burch, Watson, Weeren	[51]
1961	ORNL-CF-61-5-62: Xenon Poisoning in Molten Salt Reactors		✓	Miller	[20]
1962	ORNL-CF-62-11-69: Preliminary Equations to Describe Iodine and Xenon Behavior in the MSRE			Engel	[52]
1962	ORNL-TM-262: Xenon Diffusion in Graphite: Effects of Xenon Absorption in Molten Salt Reactors Containing Graphite			Watson, Evans	[53]

Table A.1: MSR Xenon Literature

Year	Title	Pages	Model?	Authors	Citation
1963	ORNL–3529: Molten Salt Reactor Program Semi-Annual Progress Report for Period Ending July 31, 1963 - Subsection Titled 'Xenon Transport in MSRE System'	44-45	d		[54]
1964[2]	ORNL–TM-496: Methods of Computing the Reactivity Effects of Distributed Xenon, Graphite Shrinkage, and Fuel Soakup in the MSRE		?	Prince	[55]

[2]Under preparation in 1964. Used as reference in [21]. A copy of this document was not found.

Table A.1: MSR Xenon Literature

Year	Title	Pages	Model?	Authors	Citation
1964	ORNL-TM-730: MSRE Design and Operations Report. Part III. Nuclear Analysis	81-85		Haubenreich, Engel, Prince, Claiborne	[21]
1965	ORNL-TM-1060: Molten Salt Converter Reactor. Design Study and Power Cost Estimates for a 1000 MWe Station	230-234	✓	Alexander	[22]
1965	ORNL-TM-1070: Stability Analysis of the Molten-Salt Reactor Experiment	65	✓	Ball, Kerlin	[24]

Table A.1: MSR Xenon Literature

Year	Title	Pages	Model?	Authors	Citation
1966	ORNL–TM-1145: Simulators for Training Molten-Salt Reactor Experiment Operators	10	✓	Ball	[23]
1966	ORNL–4037: Molten-Salt Reactor Program Semiannual Progress Report for Period Ending August 31, 1966. Subsection Titled Xenon Diffusion and Possible Formation of Cesium Carbide in a MSBR	158-165	✓	Briggs	[56]

Table A.1: MSR Xenon Literature

Year	Title	Pages	Model?	Authors	Citation
1967	ORNL-TM-1810: A Model for Computing the Migration of Very Short-Lived Nobel Gases into MSRE Graphite		✓	Kedl	[57]
1967	ORNL-4148: Gas Transport in MSRE Moderator Graphite. Review of Theory and Counterdiffusion Experiments			Malinauskas, Rutherford, Evans	[17]
1967	ORNL-4069: Development of a Model For Computing Xe-135 Migration in the MSRE		✓	Kedl, Houtzeel	[25]

Table A.1: MSR Xenon Literature

Year	Title	Pages	Model?	Authors	Citation
1968	ORNL-TM-2245: Removal of Xenon-135 From Circulating Fuel Salt of the MSBR by Mass Transfer to Helium Bubbles			Peebles	[46]
1969	ORNL-4389:Gas Transport in MSRE Moderator Graphite	36		Evans, Rutherford, Malinaukas	[58]
1969	Graphite and Xenon Behavior and Their Influence on Molten-Salt Reactor Design			Scott, Eatherly	[59]

Table A.1: MSR Xenon Literature

Year	Title	Pages	Model?	Authors	Citation
1971	ORNL-4541:Conceptual Design Study of a Single-Fluid Molten-Salt Breeder Reactor: Annex A	170		Robertson	[18]
1971	ORNL-TM-3464: Xenon Behavior in the Molten Salt Reactor Experiment		✓	Engel, Steffy	[3]
1972	ORNL-CF-72-6-12: Sidestream Processing for Continuous Iodine and Xenon Removal from the MSBR Fuel			Wichner, Baes	[60]

Table A.1: MSR Xenon Literature

Year	Title	Pages	Model?	Authors	Citation
1972	ORNL-TM-4122: Development of a Venturi Type Bubble Generator for use in the Molten Salt Reactor Xenon Removal System			Gabbard	[61]
1977	Transient Xenon Analysis in a Molten Salt Breeder Reacctor		✓	Shimazu	[26]
2004	Transient Xenon Effect on Plant Control in MSRs		✓	Suzuki, Shimazu	[27]
2016	The Influence of Xe-135m on Steady State Xenon Worth in Thermal Molten Salt Reactors		✓	Eades, Chaleff, Venneri, Blue	[4]

Table A.1: MSR Xenon Literature

Year	Title	Pages	Model?	Authors	Citation
2017	Xenon Analysis of Thorium Molten Salt Experiment Reactor-Liquid Fuel [sic.]		✓	Chen, Ruimin, Jingen Guimin	[28]
2017	Flow Effect on I-135 and Xe-135 Evolution Behavior in a Molten Salt Reactor		✓	Wu, Guo, Cai, Yu, Zou, Han, Chen	[29]
2018	Implementation of General Species Transport Capability into VERA-CS for Molten Salt Reactor Analysis		✓	Taylor, Salko, Collins	[31]

Table A.1: MSR Xenon Literature

Year	Title	Pages	Model?	Authors	Citation
2018	Influence of Xe-135 Dynamic Behavior on Core Operation Safety for a Molten Salt Reactor		✓	Wu, Li, Hu, Chen, Yu, Zou, and Cai	[30]

Nomenclature

Alphabetic and Greek Symbols

$\dot{N}$	Rate of change of isotope i quantity
γ	Fission yield of isotope i
ϕ	Neutron flux
Σ	Macroscopic Neutron Absorption Cross Section
V	In core volume
λ	Decay Constant
t	Time
T	Temperature
Sc	Schmidt Number
k	Constant / Coefficient
r	Radius
f	Fraction
U	Velocity
Re	Reynolds Number
J	Mass Flux
ϵ	Porosity
A	Constant, $A = D_{Gr}/\epsilon$
M	Matrix
R	Ideal gas constant
η	Efficiency

Subscripts and Superscripts

i	Isotope or Node Index
f	Fission
Te	Te-135
Xe	Xe-135
IC	In Core
$1/2$	Half-Life
L	Liquid
G	Gas/
$[°C]$	degrees Celsius
$[K]$	Kelvin
FS	Fuel Salt
μ	Viscosity
D	Mass diffusion coefficient
b	bubble
ρ	Mass Density
$MSRE$	Molten Salt Reactor Experiment Reference Value
A	Fitting Constant A
B	Bubble/ Fitting Constant B
C	Fitting Constant C
$Mes.$	Reference Measurement
CP	Concentration-Pressure Varient
CC	Concentration-Concentration Varient
0	Nominal Value
$Tot.$	Total
CV	Circulating Void
ref	Reference
1	State 1/ Single
2	State 2
m	Mass
fc	Fuel Channel
Gr	Graphite
a	Absorption
N	Ultimate index
$ghost$	Ghost node
$Strpr.$	Stripper

Bibliography

[1] P. Haubenreich and J. Engel. Experience with the Molten-Salt Reactor Experiment. *Nuclear Applications and Technology*, 8(2):118–136, 1969.

[2] Terry Price, Ondrej Chvala, and Robert Z Taylor. Molten salt reactor xenon analysis: Review and decomposition. *Journal of Nuclear Engineering and Radiation Science*, 2019.

[3] J. Engel and R. Steffy. ORNL-TM-3464: Xenon Behavior in the Molten Salt Reactor Experiment. Technical report, Oak Ridge National Laboratory, Oak Ridge, TN, USA, 1971.

[4] M. Eades, E. Chaleff, P. Venneri, and T. Blue. The Influence of Xe-135m on Steady-State Xenon Worth in Thermal Molten Salt Reactors. *Progress in Nuclear Energy*, 93: 397–405, 2016.

[5] A. Weinberg. *The First Nuclear Era: The Life and Times of a Technological Fixer*. American Institute of Physics, 1994. ISBN 9781563963582.

[6] B. Hoglund. MoltenSalt.org, 2012. URL `http://moltensalt.org/`. Last Accessed 9/5/2018.

[7] D. LeBlanc. Molten salt reactors: A new beginning for an old idea. *Nuclear Engineering and Design*, 240(6):1644–1656, 2010. ISSN 00295493. doi: 10.1016/j.nucengdes.2009.12.033.

[8] J. Serp, M. Allibert, O. Beneš, S. Delpech, O. Feynberg, V. Ghetta, D. Heuer, D. Holcomb, V. Ignatiev, J. Kloosterman, L. Luzzi, E. Merle-Lucotte, J. Uhlíř, R. Yoshioka, and D. Zhimin. The Molten Salt Reactor (MSR) in Generation IV: Overview and Perspectives. *Progress in Nuclear Energy*, 77:308–319, 2014.

[9] R. Rhodes. *The Making of the Atomic Bomb.* The Making of the Nuclear Age. Simon & Schuster, 1986.

[10] J.R. Lamarsh and A.J. Baratta. *Introduction to Nuclear Engineering: Pearson New International Edition.* Pearson Education Limited, 2013. ISBN 9781292038230.

[11] P. Pau, J. Berg, and W. McMillan. Application of stokes' law to ions in aqueous solution. *Journal of Physical Chemistry*, 94(6):2671–2679, 1990.

[12] M. Blander, W. Grimes, N. Smith, and G. Watson. Solubility of Noble Gases in Molten Fluorides. II. In the Lif-NaF-LF Eutectic Mixtures. *The Journal of Physical Chemistry*, 63(7):1164–1167, 1959.

[13] W. Haynes, editor. *CRC Handbook of Chemistry and Physics, 97th Edition.* CRC Press, 2016.

[14] R. Svehla. R-132: Estimated viscosities and thermal conductivities of gases at high temperatures. Technical report, NASA, 1962.

[15] M. Born. *Atomic Physics: 8th Edition.* Dover Publications, 2013.

[16] T. Sherwood, R. Pigford, and C. Wilke. *Mass Transfer.* McGraw-Hill, 1975.

[17] A. Malinauskas, J. Rutherford, and R. Evans. ORNL-4148: Gas Transport in MSRE Moderator Graphite. Part 1: Review of Theory and Counterdiffusion Experiments. Technical report, Oak Ridge National Laboratory, 1967.

[18] R. Robertson. ORNL-TM-4541: Conceptual Design Study of a Single-Fluid Molten-Salt Breeder Reactor. Technical report, Oak Ridge National Laboratory, 1971.

[19] M. Robinson. ORNL-1924: A Theoretical Study of Xe-135 Poisoning Kinetics in Fluid-Fueled, Gas-Sparged Nuclear Reactors. Technical report, Oakridge National Laboratory, 1956.

[20] ORNL-CF-61-5-62: Xenon Poisoning in Molten Salt Reactors. Technical report, 1961.

[21] P. Haubenreich, J. Engel, B. Prince, and H. Claiborne. ORNL-TM-730: MSRE Design and Operations Report. Part III. Nuclear Analysis. Technical report, Oak Ridge National Laboratory, 1964.

[22] L. Alexander, W. Carter, C. Craven, D. Janney, T. Kerlin, and R. Van Winkle. ORNL-TM-1060: Molten Salt Converter Reactor. Design Study and Power Cost Estimates for a 1000 MWe Station. Technical report, Oak Ridge National Laboratory, 1965.

[23] S. Ball. ORNL-TM-1445: Simulators for Training Molten-Salt Reactor Experiment Operators. Technical report, Oak Ridge National Laboratory, 1966.

[24] S. Ball and T. Kerlin. ORNL-TM-1070: Stability Analysis of the Molten-Salt Reactor Experiment. Technical report, Oak Ridge National Laboratory, 1965.

[25] R. Kedl and A. Houtzeel. ORNL-4069: Development of a Model for Computing Xe-135 Migration in the MSRE. Technical report, Oak Ridge National Laboratory, Oak Ridge, TN, USA, 1967.

[26] Y. Shimazu. Transient Xenon Analysis in a Molten Salt Breeder Reactor. *Journal of Nuclear Science and Technology*, 14(11):805–810, 1977.

[27] K. Suzuki and Y. Shimazu. Transient Xenon Effect on Plant Control in MSRs-Validation of Simulation Model. In *Proceedings of ICAPP '04*, Pittsburgh, PA, USA, 2004.

[28] G. Chen, J. Ruimin, C. Jingen, and L. Guimin. Xenon Analysis of Thorium Molten Salt Experiment Reactor-Liquid Fuel. *Nuclear Techniques*, 40(4):40602, 2017.

[29] J. Wu, C. Guo, X. Cai, C. Yu, C. Zou, J. Han, and J. Chen. Flow effect on I-135 and Xe-135 Evolution Behavior in a Molten Salt Reactor. *Nuclear Engineering and Design*, 314:318–325, 2017.

[30] J. Wu, X. Li, J. Hu, J. Chen, C. Yu, C. Zou, and X. Cai. ICONE26-82352: Influence of Xe-135 Dynamic Behavior on Core Operation Safety for a Molten Salt Reactor. In *Proceedings of the 2018 26th International Conference on Nuclear Engineering, ICONE26*, 2018.

[31] Z. Taylor, R. Salko, and B. Collins. Implementation of General Species Transport Capability into VERA-CS for Molten Salt Reactor Analysis. In *Transactions of the American Nuclear Society*, volume 118, Philadelphia, Pennsylvania, 2018.

[32] Terry price msre xenon model repository, jun .

[33] Jaakko Leppänen, Maria Pusa, Tuomas Viitanen, Ville Valtavirta, and Toni Kaltiaisenaho. The Serpent Monte Carlo code: Status, development and applications in 2013. *Annals of Nuclear Energy*, 82:142–150, 2015. ISSN 18732100. doi: 10.1016/j.anucene.2014.08.024.

[34] Jaakko Leppänen, Maria Pusa, Tuomas Viitanen, Ville Valtavirta, and Toni Kaltiaisenaho. The Serpent Monte Carlo code: Status, development and applications in 2013. In *SNA+ MC 2013-Joint International Conference on Supercomputing in Nuclear Applications+ Monte Carlo*, page 6021. EDP Sciences, 2014. ISBN 2759812693.

[35] crpg. URL `https://crpg.mit.edu/`.

[36] R. Robertson. ORNL-TM-0728: MSRE Design and Operations Report. Technical report, Oak Ridge, TN, USA, 1965.

[37] Gavin Ridley MSRE Repository, jun 2018. URL `https://github.com/arfc/msr-neutronics`.

[38] Japan Atomic Energy Agency - Nuclear Data Center - Fission Product Yields, 2018. URL `https://wwwndc.jaea.go.jp/cgi-bin/FPYfig`. Last Visited 21/6/2019.

[39] E. Baum, H. Knox, and T. Miller. *Nuclides and Isotopes: Chart of the Nuclides.* Lockheed Martin, Bethesda, Maryland, United States, 16 edition, 2010.

[40] S. Cantor, W. Cooke, S. Dworkin, D. Robbins, E. Thoma, and M. Watson. ORNL-TM-2316: Physical Properties of Molten-Salt Reactor Fuel, Coolant and Flush Salts. Technical report, Oak Ridge National Laboratory, Oak Ridge, TN, USA, 1968.

[41] G. Watson, R. Evans III, W. Grimes, and N. Smith. Solubility of Noble Gases in Molten Fluorides. In LiF-BeF2. *Journal of Chemical and Engineering Data*, 7(2):285–287, 1962.

[42] E B Nauman. *Chemical Reactor Design, Optimization, and Scaleup.* Wiley, Hoboken, NJ, USA, 2008. ISBN 9780470282069.

[43] P. Engel, J., Haubenreich. ORNL-TM-0378: Temperature in the MSRE Core During Steady-State Power Operation. Technical report, Oak Ridge National Laboratory, Oak Ridge, TN, USA, 1962.

[44] R. J. Kedl. ORNL-TM-3229: Fluid Dynamic Studies of the Molten-Salt Reactor Experiment (MSRE) Core. Technical report, Oak Ridge National Laboratory, Oak Ridge, TN, USA, 1970.

[45] R. Perry and D. Green. *Perry's Chemical Engineers' Handbook, Seventh Edition.* McGraw-Hill, New York, NY, USA, 7th edition, 2008.

[46] F. Peebles. ORNL-TM-2245: Removal of Xenon-135 from Circulating Fuel Salt of the MSBR by Mass Transfer to Helium Bubbles. Technical report, Oak Ridge National Laboratory, Oak Ridge, TN, USA, 1968.

[47] R. Briggs. ORNL-3872: Molten-Salt Reactor Program Semiannual Progress Report for Period Ending August 31, 1965, 1965.

[48] J. Engel, P. Haubenreich, and A. Houtzeel. ORNL-TM-3027: Spray, Mist, Bubbles, and Foam in the Molten Salt Reactor Experiment. Technical report, Oak Ridge National Laboratory, 1970.

[49] J. Meem. ORNL-CF-54-5-1: The Xenon Problem in the ART. Technical report, Oak Ridge National Laboratory, 1954.

[50] G Samuels and Lackey. ORNL-2376: ART Fuel Pump and Xenon Removal System Development, Test Evaluation and Aircraft Application. Technical report, Oak Ridge National Laboratory, Oak Ridge, TN, USA, 1957.

[51] W. Burch, M. Watson, and H. Weeren. ORNL-CF-60-2-2-: Xenon Control in Fluid Fuel Reactors. Technical report, Oak Ridge National Laboratory, 1960.

[52] J. Engel. ORNL-CF-62-11-69: Preliminary Equations to Describe Iodine and Xenon Behavior in the MSRE. Technical report, Oak Ridge National Laboratory, 1962.

[53] G. Watson and R. Evans. ORNL-TM-262: Xenon Diffusion in Graphite Effects of Xenon Absorption in Molten Salt Reactors Containing Graphite. Technical report, Oak Ridge National Laboratory, 1962.

[54] R. Briggs. ORNL-3529: Molten Salt Reactor Program Semi-Annual Progress Report For Period Ending July 31, 1963. Technical report, Oak Ridge National Laboratory, Oak Ridge, TN, USA, 1963.

[55] B. Prince. ORNL-TM-496: Methods of Computing the Reactivity Effects of Distributed Xenon, Graphtie Shrinkage, and Fuel Soakup in the MSRE. Technical report, Oak Ridge National Laboratory. No date. Under preparation in 1964.

[56] R. Briggs. ORNL-4037: Molten-Salt Reactor Program Semiannual Progress Report for Period Ending August 31, 1966. Technical report, Oak Ridge National Laboratory, 1967.

[57] R. Kedl. ORNL-TM-1810: A Model for Computing the Migration of Very Short Lived Nobel Gases into MSRE Graphite. Technical report, Oak Ridge National Laboratory, 1967.

[58] Evans, R., Rutherford, J., and A. Malinauskas. ORNL-4389: Gas Transport in the MSRE Moderator Graphite: II. Effects of Impregnation; III. Variation of Flow Properties. Technical report, Oak Ridge National Labs, 1969.

[59] D. Scott and W. Eatherly. Graphite and Xenon behavior and their influence on molten-salt reactor design. *Nuclear Applications and Technology*, 8(2):179–189, 1970.

[60] R. Wichner and C. Baes. ORNL-CF-72-6-12: Sidestream Processing for Continuous Iodine and Xenon Removal from the MSBR Fuel. Technical report, Oak Ridge National Laboratory, 1972.

[61] C. Gabbard. ORNL-TM-4122: Development of a Venturi Type Bubble Generator for use in the Molten Salt Reactor Xenon Removal System. Technical report, Oak Ridge National Laboratory, 1972.

Acronyms

ARE Aircraft Reactor Experiment.

ASME American Society of Mechanical Engineers.

DMSR Denatured Molten Salt Reactor.

MSBR Molten Salt Breeder Reactors.

MSDR Molten Salt Demonstration Reactor.

MSFR Molten Salt Fast Reactor.

MSR Molten Salt Reactor.

MSRE Molten Salt Reactor Experiment.

MTC Mass Transfer Coeffecient.

ORNL Oak Ridge National Laboratory.

PWAR1 Pratt & Whitney Aircraft Reactor 1.

Attachments

Attachment 1

Initial Xenon Modeling Paper

A Dynamic Model for Molten Salt Reactor Xenon Behavior

Written November 2018 – March 2019

Unpublished

A Dynamic Model for Molten Salt Reactor Xenon Behavior

Terry J. Price[1]
Terry.Price@UOIT.net

Ondrej Chvala[2]
OChvala@UTK.edu

Zack Taylor[2]
RTaylo45@Vols.UTK.edu

January 2019

Abstract

This article details the development and performance of a non-linear model that describes molten salt reactor xenon behavior. A review of modeling efforts to date is given. The model developed includes multi-region bubble and graphite models. Thermal effects are included on the bubble interfacial area, thermal physical properties, and mass-transfer coefficients. An attempt is made to model the Molten Salt Reactor Experiment, and validation is performed against the krypton experiment. Power maneuver transients were performed as well as thermal transients.

1 Introduction

Molten Salt Reactors (MSRs) are type of nuclear reactor, which have been proposed for deployment as part of the Generation IV reactor program, which use a molten alkali fluoride fuel salt as both a fuel matrix and a working fluid. MSRs, as documented by Serp et al. [1], were developed at Oak Ridge National Laboratory (ORNL), starting in the 1950s and ending in the 1980s.

The significance of the ^{135}Xe fission product, with its 2.6 Mb [2] neutron absorption cross section, was discovered* on September 27, 1944, at the 250 MW [4, p. 109] Hanford B reactor, when poisoning from ^{135}Xe unexpectedly caused the reactor to shut down several hours after its initial criticality. Subsequently, a theory of ^{135}Xe poisoning has been developed and is documented in numerous sources such as the introductory nuclear engineering book by Lamarsh and Baratta [5].

Structurally, there are three aspects of an MSR that have, in past analyses, be considered important to the analysis of ^{135}Xe behavior in an MSR. The first is the `graphite pore space`; In an MSR, the fuel salt circulates between a graphite moderator and a heat exchanger. The graphite moderator is a porous medium which has both a solid graphite matrix as well as a voided pore-space. The pore size of the graphite moderator is assumed to be sufficiently small such that the fuel salt will not wet the surface; given the surface is non-wetted it follows that fuel salt will not penetrate into the pore space of the graphite moderator and the contents of the pore space are therefore assumed to be gaseous. Second there are `circulating bubbles` (called circulating voids elsewhere in MSR xenon anal-

ysis literature) in the fuel-salt. Finally, some MSR designs may implement a `xenon stripper` in the design that mechanically removes ^{135}Xe and other dissolved gasses from the fuel salt.

In brief, the theory of ^{135}Xe behavior states ^{135}Xe is either generated directly from nuclear fission or as a decay product from ^{135}I , and ^{135}Xe can be removed from the system either through burn-out, which is neutron absorption and subsequent transmutation into ^{136}Xe, or through β^- decay into ^{135}Cs. ^{135}I , in turn, is also either generated from fission or as a result of the β^- decay of ^{135}Te . The decay chain starts with ^{135}Te , which transmutes, through β^- decay, into ^{135}I . The neutron absorption cross-sections of ^{135}Te and ^{135}I are assumed to be negligible, and, as such, ^{135}Te and ^{135}I are not affected by a burn-out process. The half-lives of ^{135}Xe , ^{135}I , and ^{135}Te are 9.1 h, 6.6 h, and 19 s respectively. [2] † For the sake of clarity, ^{135}Xe , ^{135}I and ^{135}Te are collectively called `poison isotopes`.

Although, in a solid fueled reactor, there may be some migration of the poison isotopes, through diffusion, for the intents and purposes of modeling efforts, all of the solid fueled reactor xenon theories we are aware of assumes the ^{135}Xe is immobilized in the fuel matrix. Conversely, the fluid nature of the fuel salt in a MSR allows the ^{135}Xe to migrate about the reactor. As described in the Annex of ORNL-TM-4541 [7], MSR xenon theory describes not only the generation, loss, and evolution of ^{135}Te , ^{135}I and ^{135}Xe , but also includes considerations into the migration of

---

*For a full account, see [3]

†The half-life of ^{135}Te didn't arrive at its currently accepted value of 19 s until 1969 [6], and, we propose this as an explanatory factor in the observation that some earlier MSR xenon analyses are either missing ^{135}Te as an ^{135}Xe progenitor or have ^{135}Te half-lives that are different than the currently accepted value of 19 s.

1

^{135}Xe in circulating bubbles in the fuel salt, as well as migration in to the graphite pore-space. The ^{135}I and ^{135}Te are assumed to stay in solution whereas the ^{135}Xe is free is to migrate because of its gaseous and noble properties.

Although references to earlier reports were found, the earliest analysis of MSR ^{135}Xe behavior we could obtain a copy of is the 1956 report ORNL-1924 [8]; the report details a model of ^{135}Xe behavior for the Aircraft Reactor Experiment (ARE) and the Aircraft Reactor Test (ART)‡ that includes considerations of not only ^{135}I , and ^{135}Xe behavior and evolution, but also migration between a liquid and a gas phase as well as removal of ^{135}Xe from the gas phase via a gas flow.

The next major modeling effort was in 1961 by Miller [9], who developed an MSR xenon model which included efforts to model the graphite migration of ^{135}Xe as well as a model of a xenon stripper.

The Molten Salt Reactor Experiment (MSRE) was a 7.4 MW$_{Th}$ experimental molten salt reactor which ran from 1964-1969 at Oak Ridge National Laboratory. We are aware of two major reports which describe ^{135}Xe models for the MSRE, the 1967 report, ORNL-4069 [10] and the 1971 report, ORNL-TM-3464 [11]. The ORNL-4069 model included all the previous phenomena but also was the first to investigate the effects of circulating bubbles on MSR xenon poisoning. The ORNL-TM-3464 model was the first nodal model of MSR xenon behavior and included nodes for circulating bubbles, liquid fuel-salt, the graphite moderator, and a xenon stripper. These models, in ONRL-TM-3464, were formulated as first-order linear ordinary differential equations. Finally, we note the ORNL-TM-3464 model was also the first to be used in transient analysis.

In 1977, Shimazu [12] developed a simplified approach to MSR xenon modeling and was the first to perform transient analysis using this simplified approach. This model was used in the 2004 work of Suzuki and Shimazu which integrated a MSR ^{135}Xe model into a balance-of-plant model and investigated required reactivity worth's for MSR control.

---

‡Two MSRs developed for the Aircraft Nuclear Propulsion Program

In 2016, Eades, Chaleff, Venneri, and Blue [13] investigated the effects of ^{135m}Xe on MSR ^{135}Xe poisoning with a 0D and 1D model. Additionally in 2017, Chen, Ruimin, Jingen, and Guimin [14] applied a MSR xenon analysis based on ORNL xenon modeling efforts to the *"Thorium Molten Salt Reactor-Liquid Fuel (TMSR-LF)"*. Finally, the last modeling effort we are aware of, in 2017, was the work of Wu et Al. [15] whomst investigated the effects of fuel salt flow on ^{135}Xe behavior.

In 2018, Wu et Al. [16] extended their work to investigate the start-up ^{135}Xe behavior of an MSR and the effects of a helium bubbler failure on ^{135}Xe behavior. Furthermore, Taylor, Salko, and Collins [17] announced they are working towards implementing xenon behavior modeling in the VERA-CS [17] reactor physics code suite.

Haubenenreich and Engel report [18] steady state xenon poisoning varies with temperature. To the best of our knowledge, no MSR xenon modeling effort to date has attempted to account for the the effects of temperature on ^{135}Xe behavior.

Our work models ^{135}Xe behavior in an MSR using non-linear equations for graphite mass transfer in a nodal model. In addition, the the usual burn-out, decay, production, and progenitor production behaviors, the bubble behavior and graphite behavior are multi-region. Thermophysical properties, such as density, viscosity, the mass diffusion coefficient are modeled as functions of temperature, and as such, ^{135}Xe behavior can be described as a function of temperature.

2 Methodology

A molten salt reactor lattice was modeled in the reactor physics code Serpent 2 [19]. The fuel channel was circular and had a radius of 1.454 cm (such that the surface area of the fuel channel was equivalent to the surface are of an MSRE fuel channel). The fuel salt was a replica of the MSRE fuel salt as per the constituents listed in ORNL-TM-0728 [20]. The fuel salt concentration composition was taken to be identical to the MSRE fuel salt with *"highly enriched"* ^{235}U fuel [7, p. 8]. The square graphite stringer width and breadth was 4.919 cm. The model was set to

generate one-group constants and a simulation was performed 20,000 particle histories at 120 cycles - the first 20 of which inactive. The JEFF 3.1.1 [21] cross section data were used. The simulation was run on a quad-core Intel i7-7700HQ CPU running at 2.8 GHz; there was 16 Gb of installed system memory. The value for Σ_f, later used in the model, was taken from this Serpent 2 calculations.

Other nuclear data included the full-power flux, the fission yields, the decay constants, and the microscopic neutron absorption cross-section. The full-power flux was taken the averaged MSRE flux with U-235 fuel [7]. The fission yields were taken from the Japanese Atomic Energy Agency (JAEA) fission product database [22]. Decay constants were taken from the chart of nuclides compiled by Baum, Knox and Miller [2]. The microscopic neutron absorption cross-section for ^{135}Xe was taken from ORNL-4069 [10].

The ^{135}Te , ^{135}I are generated in the fuel salt, from fission, and are assumed to remain in solution there. This in-solution assumption is congruent with the assumptions made in prior modeling efforts such as that done in the ORNL-TM-3464 ^{135}Xe model [11, p. 3]. The ^{135}Xe , conversely, is able to migrate from the fuel-salt and into the graphite and bubbles.

The graphite mass transfer coefficient was calculated, for each flow region, with the Dittus-Botler equation in its mass transfer formulation,

$$Sh = Re^{0.8}Sc^{0.4}. \tag{1}$$

More information about mass transfer analogies can be found in numerous sources such as the 1975 book on mass transfer written by Sherwood, Pigford and Wilke [23, p. 159].

In order to calculate the Sherwood number (Sh) for each region, the Reynold's (Re) and Schmidt (Sc) numbers needed to be calculated for each region. The temperature dependence of fuel salt properties for MSRE fuel salt were not found, so fuel salt F1 in the 1968 database, ORNL-TM-2316 [24], was used as an analogue due toits compositional similarity to MSRE fuel salt. The viscosity of the fuel salt was determined by the correlation,

$$\mu(T) = 0.084 \ e^{4340/T}, \tag{2}$$

where the viscosity, μ, is in [cP] and the temperature, T, is the fuel salt temperature in [°C]. The density of the fuel salt was determined by the correlation,

$$\rho(T) = 3.627 - 6.6 \times 10^{-4}(T), \tag{3}$$

where the density, ρ is in [g/cm^3] and temperature, T, is in [°C].

The fuel-salt mass diffusion coefficient, D, was determined by the Einstein-Stokes equation [25, p. 126], with the radius of ^{135}Xe is taken to be equal to that of the Van der Waals radius of 216 pm [26].

The graphite stringers were modeled by a porous media reaction diffusion equation,

$$\frac{\partial C_{Xe}^G}{\partial t} = \frac{D_g}{\epsilon}\left(\frac{\partial (C_{Xe}^G)^2}{\partial r^2} + \frac{1}{r}\frac{\partial C_{Xe}^G}{\partial r}\right) - (\sigma_a^{Xe}\phi + \lambda_{Xe})C_{Xe}^G, \tag{4}$$

subject to a zero-flux condition at the left side,

$$\frac{D_g}{\epsilon}\left(\frac{\partial C_{Xe}^G}{\partial r}\right)_{r=L} = 0, \tag{5}$$

and a convective mass flux boundary condition on the right side,

$$\frac{D_g}{\epsilon}\left(\frac{\partial C_{Xe}^G}{\partial r}\right)_{r=R} = K_m^G\left(C_{Xe}^{FS} - \frac{HRT}{\epsilon}C_{Xe}^G\right), \tag{6}$$

which also determines the rate of mass transfer between the graphite and the fuel salt when multiplied by the wetted area of each fuel channel. The temperature dependence of Henry's constant, H, was modeled by fitting a second degree polynomial to the experimental data for Xenon in LiF-BeF$_2$ presented by Watson, Evans, and Grimes. [27] The partial differential equation, Equation 4, was transformed into a differential algebraic equation using a second-order finite difference method with a single ghost node on the right side. To improve performance, it was desired to generate only matrices of constant values and keep control quantities as separate scalar quantities. Therefore, the finite difference matrix was separated into sub-matrices of constant values. Where appropriate, each sub-matrix be multiplied by an appropriate scalar control signal, and the resulting control-signal-modified sub-matrices are added together to recover

the original finite difference matrix with the control signals intact.

In order to reduce computational time, the graphite model was implemented such that the graphite behavior in four distinct `flow regions` was represented by a single `representative stringer`. The flow regions were based on the flow regions listed in ORNL-TM-0378 [28], each with a corresponding temperature and flow velocity set. The mass flux for the single representative stringer was then multiplied by the number of stringers in that region to get the total mass flux for a particular region.

Circulating void modeling was performed with a lumped volume approach. Lumped volumes were generated for each of the flow regions, the upper and lower plena, the down-comers, the piping, the pump-bowl, and the heat-exchanger. Fuel-salt expansion and contraction was accounted for in the pump-bowl volume. The bubble breakage and coalescence rate was assumed to be sufficient such that all bubbles transferred mass into a single effective lumped volume. The rate of mass transfer is governed by mass-transfer coefficient calculated for each node, with the node's flow conditions and temperature.

The mass balance equation written on bubble mass transfer is therefore governed by,

$$\frac{\partial N_{Xe}^{B}}{\partial t} = \sum K_m^{B.i} A_B^{i.} \left(C_{FS} - HRT \frac{N_{Xe}^{B}}{V_B^{Tot.}} \right) \quad (7)$$
$$- (\sigma_a^{Xe}\phi - \lambda_{Xe})N_{Xe}^{B} - \dot{N}_{Xe}^{Strpr.Bbl.}.$$

For the pipes, heat-exchanger tubes, and fuel-channel regions, the mass transfer coefficient for ^{135}Xe transfer between the fuel salt and the bubbles is given by a correlation, presented in ORNL-TM-2245 [29] for *"small rigid particles carried along by turbulent liquid in a pipe"*,

$$Sh = 0.0096 Re^{0.913} Sc^{0.346}. \quad (8)$$

For the plena, a mass transfer correlation was taken for *"single bubbles of gas in liquid..."* from Perry's *"Chemical Engineers' Handbook"* [30]; for the pump-bowl, for lack of a better correlation, a correlation for bubbles in a *"highly agitated system..."* was used, from the same source. Regardless, in all of these

correlations, the gas-side mass transfer coefficient was assumed to be negligible compared to the liquid-side mass transfer coefficient.

The effective bubble area available in each node for mass transfer into bubbles was calculated by dividing the volume in each node by the volume per bubble, based on a reference diameter (0.254 mm as per the observations in ORNL-TM-3464 [11]), to determine the number of bubbles in that node, then multiplying the number of bubbles in a node by the area per bubble, assuming spherical bubbles, to determine the total bubble area in a node available for mass transfer. Note, the volume in each node was varied as a function of temperature by modeling the bubble volume as an ideal gas, taking the total derivative and varying the temperature from T_1 to T_2 to derive,

$$\left(\frac{\partial V}{\partial T} \right)_{P,n} = \frac{nR}{P}. \quad (9)$$

The xenon stripper was modeled with two sub-models, one for the fuel salt stripping and another for the bubble stripping. The liquid stripping efficiency was set to 0.1 whereas the bubble stripping efficiency was set to 0.12; these efficiencies are congruent with those found in ORNL-4069 [10]. The volumetric flow rate through the xenon stripper was set to 7.5×10^{-2} m^3 s^{-1}. The removal rate of ^{135}Xe from the fuel salt is determined by

$$\dot{N}_{Xe}^{Strpr.\ FS} = \eta_{FS} C_{Xe}^{FS} \dot{Q}_V^{Strpr.} \quad (10)$$

The bubble stripping was determined by,

$$\dot{N}_{Xe}^{Strpr.\ Bbl.} = \frac{N_B^{PB}}{V_{FS}^{PB}} \dot{Q}_V^{Strpr.} \eta_b V_B^1 C_{Xe}^{B}. \quad (11)$$

In total, the system can be described by a number of sink and source terms, shown in Table 1; note, the in-solution assumption prevents the migration of ^{135}I and ^{135}Te .

The model was developed and implemented in Mathworks Simulink [31]. Simulink's automatic solver selection was used with all integrator initial conditions set to zero; a solution was generated for t=1×10^6 s using a variable time step in order to reach steady-state. Two research questions were investigated using

4

Compartment	Pathway	Type
Fuel Salt ^{135}Xe	Fission Production	Source
	^{135}I Decay	Source
	Radioactive Decay	Sink
	Burnout	Sink
	Graphite Transfer	Migration
	Bubble Transfer	Migration
	Xenon Stripper	Sink
Fuel Salt ^{135}I	Fission Production	Source
	^{135}Te Decay	Production
	Radioactive Decay	Sink
Fuel Salt ^{135}Te	Fission Production	Source
	Radioactive Decay	Sink
Bubbles ^{135}Xe	Fuel Salt Transfer	Migration
	Radioactive Decay	Sink
	Burn Out	Sink
	Stripping	Sink
Graphite ^{135}Xe	Fuel Salt Transfer	Migration
	Radioactive Decay	Sink
	Burn Out	Sink

Table 1: Source and Sink Terms for Xenon Model

the model: is there any significant advantage to using a multi-region graphite model, such as that used in ORNL-TM-3464 [11], or, is the use of a single graphite region, such as that used by Shimazu [12], sufficient? What effects do temperature perturbations have on MSR ^{135}Xe behavior? In order to investigate the first question, two variants of the model were built, one with a multi-region graphite model, and the other with a single graphite region with using parameters averaged all regions.

Validation was attempted by simulating the run 4, the run which had the fewest operational changes, of the krypton experiment [10] with the model. The model was altered to mimic the krypton experiment by removing the progenitor and burn out models, changing the half-life, and injecting gas directly into the fuel-salt. The off gassing rate was assumed to be equal to the stripping rate of krypton via the xenon stripper. In the krypton experiment simulation, gas was injected until the model reached steady-state,

then shut off; the comparison was commenced at the point where the gas was shut-off in both the experimental data and the model produced data.

The model's capabilities are demonstrated in two ways: First, power reduction maneuvers were performed, for reductions of 20%, 40%, 60%, 80%, and 100% reductions in power and the resultant variation in graphite and fuel salt were examined. Second, the effect of a thermal transient on xenon behavior is demonstrated by analyzing the result of a 10 % increase in fuel salt and graphite temperature on transient behavior.

3   Results and Discussion

Figure 1 shows the results of the krypton experiment validation. We note that after about 4×10^3 s the model under-predicts the egress rate of Krypton by a factor of ≈ 7, Our investigations indicate although there is evidence that the mass-transfer formulation of Dittus-Bottler correlation has some experimental validation (C.F. [32]), the validation was performed in *wetted-wall* columns, whereas the situation in fuel channels are *dry-wall* columns with a liquid interior. We therefore believe the difference between between predicted and actual mass transfer coefficients has a large factor to play in the differences between experimental and model results.

In regards to the difference between multi-region and averaged graphite models, the most pronounced differences were observed at steady-state during which the homogenized graphite and fuel-salt xenon concentrations in the multi-region model exceeded the same xenon concentrations in the averaged model by a factor of about 0.1 %; Additionally, the average graphite xenon concentrations, in the multi-region model, exceeded the averaged model by 2.67 %.

The power reduction maneuvers, shown in figure 3 demonstrate a characteristic *humped* behavior in both the fuel salt and graphite xenon concentrations. Note, the *peaking* behavior of the graphite is less pronounced then the peaking behavior of the fuel-salt and bubbles. This is likely do to the fact that there are no xenon progenitors in the graphite, and, therefore, the progenitors must first transmute into

5
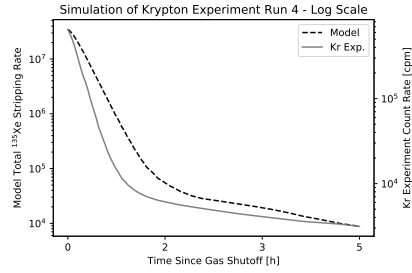
Figure 1: Validation results; model: normalized combined bubble and fuel salt Kr stripping rate; Kr Exp.: normalized count rate in off gas line
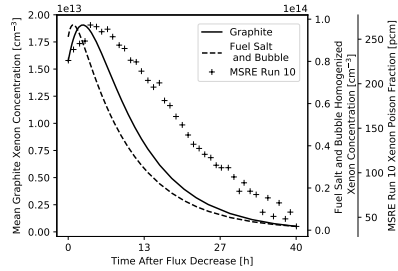
Figure 2: Benchmark Against MSRE Run 10

xenon, then migrate into the graphite.

Finally, the effects of the thermal transient are shown in Figure 4. It is seen that increasing temperature leads to an decreasing concentration of xenon in the fuel salt and bubbles and a increased concentration in the graphite. Note, the transient effects on ^{135}Xe behavior last beyond the period of time at which the thermal transient is applied.

4 Conclusion

This paper has examined a model for xenon behavior in molten salt reactors. The model attempted to recreate the Molten Salt Reactor Experiment. The model included multi-region graphite and bubble submodels as was as thermal models for thermophysical properties used in the model. At the very least, this model demonstrates the feasibility of including thermal behaviors in molten salt reactor xenon analysis modeling.

Future work may include modeling graphite mass diffusion coefficients directly from pore-size measurements, more detailed modeling of cover-gas behavior, and integration with the model developed by Singh et Al. [33].

Figure 3: Variation in xenon concentration after a power reduction

Figure 4: Thermal transient, graphite and fuel-salt temperature increased by 10% at t = 0 h.

Nomenclature

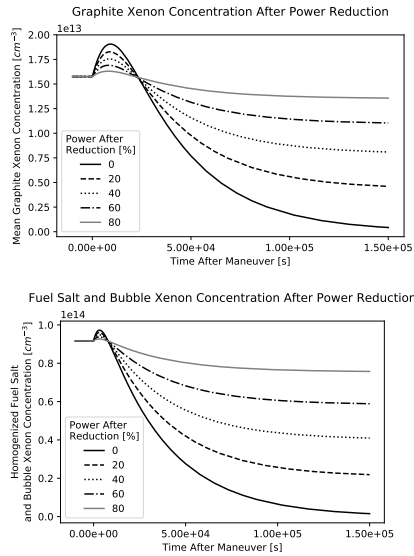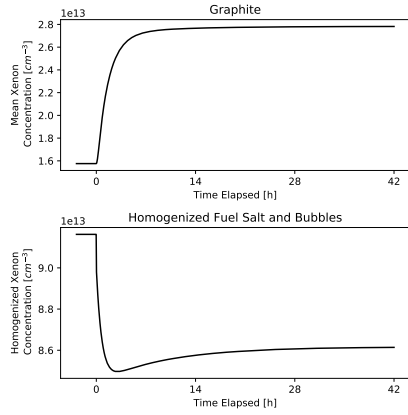|	
$\dot{N}_{Xe}^{Strpr.Bbl.}$	Rate of ^{135}Xe removal from bubble removal with the xenon stripper
ϵ	Graphite porosity
λ_{Xe}	Xenon radioactive decay constant
μ	Dynamic viscosity
ϕ	Neutron flux
ρ	Density
σ_a^{Xe}	Microscopic neutron absorption cross section for ^{135}Xe
A_B^i	Total bubble surface area for compartment i
C_{FS}	Fuel salt ^{135}Xe concentration
C_{Xe}^G	Graphite ^{135}Xe concentration
D	Fuel-salt mass diffusion coeffecient
D_g	Graphite mass diffusion coefficient
H	Henry's constant
J	Mass flux
k_b	Boltzman's constant
K_m^G	Overall mass transfer coefficient between graphite and fuel-salt
$K_m^{B.i}$	Overall bubble mass transfer coefficient for compartment i
L	Left-end coordinate
n	Number of moles of gas
N_{Xe}^B	Bubble ^{135}Xe quantity
P	Pressure
R	Ideal gas constant
R	Right-end coordinate
r	Radial Coordinate
Re	Reynold's number
Sc	Scmidt number
Sh	Sherwood number
T	Temperature
t	Time coordinate

References

[1] J. Serp, M. Allibert, O. Beneš, S. Delpech, O. Feynberg, V. Ghetta, D. Heuer, D. Holcomb, V. Ignatiev, J. Kloosterman, L. Luzzi, E. Merle-Lucotte, J. Uhlíř, R. Yoshioka, and D. Zhimin. The Molten Salt Reactor (MSR) in Generation IV: Overview and Perspectives. *Progress in Nuclear Energy*, 77:308–319, 2014.

[2] E. Baum, H. Knox, and T. Miller. *Nuclides and Isotopes: Chart of the Nuclides*. Lockheed Martin, 16 edition, 2010.

[3] R. Rhodes. *The Making of the Atomic Bomb*. The Making of the Nuclear Age. Simon & Schuster, 1986. ISBN 9780684813783.

[4] T. Filburn and S. Bullard. *Three Mile Island, Chernobyl and Fukushima: Curse of the Nuclear Genie*. Springer International Publishing, 2016.

[5] J. Lamarsh and A. Baratta. *Introduction to Nuclear Engineering*. Pearson Education, 2017. ISBN 9780134570051.

[6] J. Kathawa, C. Fry, and M. Thoennessen. Discovery of Palladium, Antimony, Tellurium, Iodine, and Xenon Isotopes. *Atomic Data and Nuclear Data Tables*, 99(1):22–52, 2013.

[7] R. Robertson. ORNL-TM-4541: Conceptual Design Study of a Single-Fluid Molten-Salt Breeder Reactor. Technical report, Oak Ridge National Laboratory, 1971.

[8] M. Robinson. ORNL-1924: A Theoretical Study of Xe-135 Poisoning Kinetics in Fluid-Fueled, Gas-Sparged Nuclear Reactors. Technical report, Oakridge National Laboratory, 1956.

[9] J. Miller. ORNL-CF-61-5-62: Xenon Poisoning in Molten Salt Reactors. Technical report, Oak Ridge National Laboratory, 1961.

[10] R. Kedl and A. Houtzeel. ORNL-4069: Development of a Model for Computing Xe-135 Migration in the MSRE. Technical report, Oak Ridge National Laboratory, 1967.

[11] J. Engel and R. Steffy. ORNL-TM-3464: Xenon Behavior in the Molten Salt Reactor Experiment. Technical report, Oak Ridge National Laboratory, 1971.

[12] Y. Shimazu. Transient Xenon Analysis in a Molten Salt Breeder Reactor. *Journal of Nuclear Science and Technology*, 14(11):805–810, 1977.

[13] M. Eades, E. Chaleff, P. Venneri, and T. Blue. The Influence of Xe-135m on Steady-State Xenon Worth in Thermal Molten Salt Reactors. *Progress in Nuclear Energy*, 93:397–405, 2016.

[14] G. Chen, J. Ruimin, C. Jingen, and L. Guimin. Xenon Analysis of Thorium Molten Salt Experiment Reactor-Liquid Fuel. *Nuclear Techniques*, 40(4):40602, 2017.

[15] J. Wu, C. Guo, X. Cai, C. Yu, C. Zou, J. Han, and J. Chen. Flow effect on I-135 and Xe-135 Evolution Behavior in a Molten Salt Reactor. *Nuclear Engineering and Design*, 314:318–325, 2017.

[16] J. Wu, X. Li, J. Hu, J. Chen, C. Yu, C. Zou, and X. Cai. ICONE26-82352: Influence of Xe-135 Dynamic Behavior on Core Operation Safety for a Molten Salt Reactor. In *Proceedings of the 2018 26th International Conference on Nuclear Engineering, ICONE26*, 2018.

[17] Z. Taylor, R. Salko, and B. Collins. Implementation of General Species Transport Capability into VERA-CS for Molten Salt Reactor Analysis. In *Transactions of the American Nuclear Society*, volume 118, Philadelphia, Pennsylvania, 2018.

[18] P. Haubenreich and J. Engel. Experience with the Molten-Salt Reactor Experiment. *Nuclear Applications and Technology*, 8(2):118–136, 1970.

[19] Jaakko Leppanen. *Serpent – a Continuous-energy Monte Carlo Reactor Physics Burnup Calculation Code*. 2012. URL http://montecarlo.vtt.fi/.

[20] R. Robertson. ORNL-TM-0728: MSRE Design and Operations Report. Technical report, 1965.

[21] A. Santamarina, D. Bernard, P. Blaise, M. Coste, A. Courcelle, T. Huynh, C. Jouanne, P. Leconte, O. Litaize, S. Mengelle, et al. The jeff-3.1. 1 nuclear data library. *JEFF report*, 22(10.2):2, 2009.

[22] Japan Atomic Energy Agency - Nuclear Data Center - Fission Product Yields, 2018. URL https://wwwndc.jaea.go.jp/cgi-bin/FPYfig.

[23] T. Sherwood, R. Pigford, and C. Wilke. *Mass Transfer*. McGraw-Hill, 1975.

[24] S. Cantor, W. Cooke, S. Dworkin, D. Robbins, E. Thoma, and M. Watson. ORNL-TM-2316: Physical Properties of Molten-Salt Reactor Fuel, Coolant and Flush Salts. Technical report, Oak Ridge National Laboratory, 1968.

[25] E. Cussler. *Diffusion: Mass Transfer in Fluid Systems*. Cambridge University Press, third edition, 2007.

[26] W. Haynes, editor. *CRC Handbook of Chemistry and Physics, 97th Edition*. CRC Press, 2016.

[27] G. Watson, R. Evans III, W. Grimes, and N. Smith. Solubility of Noble Gases in Molten Fluorides. In LiF-BeF2. *Journal of Chemical and Engineering Data*, 7 (2):285–287, 1962.

[28] P. Engel, J., Haubenreich. ORNL-TM-0378: Temperature in the MSRE Core During Steady-State Power Operation. Technical report, Oak Ridge National Laboratory, 1962.

[29] F. Peebles. ORNL-TM-2245: Removal of Xenon-135 from Circulating Fuel Salt of the MSBR by Mass Transfer to Helium Bubbles. Technical report, Oak Ridge National Laboratory, 1968.

[30] R. Perry and D. Green. *Perry's Chemical Engineers' Handbook, Seventh Edition*. McGraw-Hill Education, 2008.

[31] Mathworks Simulink. URL https://www.mathworks.com/products/simulink.html.

[32] T. Sherwood. Mass transfer and friction in turbulent flow. *Transactions of the American Institute Chemical. Engineers*, 36:817, 1940.

[33] V. Singh, A. Wheeler, M. Lish, O. Chvála, and B. Upadhyaya. Nonlinear dynamic model of Molten-Salt Reactor Experiment – Validation and Operational Analysis. *Annals of Nuclear Energy*, 113:177–193, 2018.

Attachment 2

Experience Performing Molten Salt Reactor Multiphysics Transient Analysis With Serpent 2

Unpublished

Experience Performing Molten Salt Reactor Multiphysics Transient Analysis With Serpent 2

Terry Price

January 2019

1   Introduction

This document records my efforts attempting to perform coupled multiphysics analysis of an MSR using the Serpent 2 code. This article documents our experience doing so and the challenges we encountered. It's written for a future graduate student in mind with a technical background in Python and Serpent 2.

The nuclear fission process produces free neutrons either promptly or through delayed neutron precursors (DNP). When the DNP undergo radioactive decay, they release a free neutron which may then go on to induce further fission reactions. In a solid fueled reactor, these DNP are effectively motionless and their migration does not to be considered in a transient analysis. Converse to this, DNPs in a MSR will advect with the motion of the fuel-salt. Due to this, there is a coupling between the motion of the fuel salt and the neutronic behavior of the reactor. In addition to the migration of DNPs, the thermal behavior of the reactor, due to the the Doppler broadening of neutron reaction cross-sections, has an effect on reactor neutronics behavior. The reactor thermal behavior is additionally influenced by the motion of the fuel salt and transport of heat from the fuel salt to to the graphite. Therefore, due to the advective and thermal effects of the fuel-salt, coupled multi-physics analysis is an important aspect in the analysis of MSR transient behavior.

Serpent 2 [3] is a Monte Carlo reactor physics code developed at the VTT technical research centre of Finland. In 2013, development efforts on Serpent 2 began to focus on multi-physics coupling. [4]

In 2015, Leppänen et al. [5] reported work on coupling Seprent 2 to a CFD code, PORFLO, along with a system scale thermal-hydraulics code, COSY, and a fuel behavior module, FINIX as part of the Numerical Multi-Physics (NUMPS) project. Aufiero, Fiorina, and Laureau [1] coupled Serpent 2 and OpenFOAM to perform a transient analysis on a Godiva assembly. Additionally, Touminen [7] coupled the CFD solver, OpenFOAM [2], with Serpent 2 to perform steady-state coupled multi-physics analysis on a solid fueled reactor assembly.

2 Information on Serpent 2 Cards and Lessons Learned

This section documents the specialized Serpent 2 cards used and relevent experience with them.

2.1 the savesrc and dynsrc cards

Writting the neutron precurssors to disk is facilitated by the `set savesrc` card. The serpent wiki has documetnation avalabile for the `set savesrc` card. Our coupling did not use any of the optional parameters (PN, PP, NX, NY, or NZ). One path of investigation is to see if memory usage can be improved if a larger mesh size is used.

When this card is used, four files will be created under the serpent path directory. These files and their usage in coupling is as follows:

- **.main** - ASCII format. The precursor decay constants are obtained from this file. Group 1 corresponds to lambda 1, group 2 corresponds to lambda 2, etc.

- **.prec** - ASCII format. Not used.

- **.live** - Binary format. Not used

- **.precpoints** - A binary file which stores the neutron precuror data. This is described in detail in Section 2.2. Note, these files are hidden on account of their dot (.) prefix.

In order for a transient simulation to work, an initial run must be done with the `set savesrc` card. Once this is done, subsequent simulations and simulate the next timestep by loading the four files generated by the `set savesrc` card with the `set dynsrc` card. The serpent wiki has documentation for the syntax of these cards. **NB:** Our simulation used the point-wise (option 1) precursor tracking mode.

2.2 The .precpoints file

The `.precpoints` file stored the precuror locations in a binary format. The `.precpoints` file needed to be decoded by reading in 72 byte chunks. Each 72 byte chunk was comprised of 9, 8 byte floats. The file structure is illustrated in Figure 1. The first three bytes are the X, Y, and Z coordinates of the precursors respectively. The next three set of bytes are always set* to 1, 0, 0 and are unused. The next set of bytes, the `T` bytes, are either 1 or 0 depending on the type of simulation performed. The `W` bytes are the normalized statistical weight of the precursors. Finally, the `G` bytes indicate the precursor group that the

---

*These are decimal values. In binary, the values are 0b0000-0001, 0b0000-0000, and 0b-0000-0000 respectively.
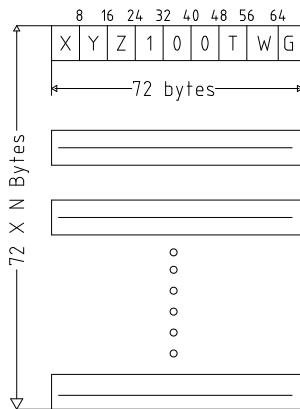
Figure 1: Structure of the `.precpoints` file

precursors belongs to - the decay constants of the group are, again, stored in the `.main` file. The file itself contain `N` precursors, each 72 bytes long. Routines were written to decode this file into 8 byte `floats` and then re-encode a data set into the appropriate binary format. Reading and writing of the .precpoints file was facilitated with the *struct* python package.

2.3   The tme card

The time behavior of Serpent 2 is set with the `tme` card. There are two ways in which this card can be used:

- as a detector instruction;

- as a simulation instruction.

There is documentation availble for the tme card on the Serpent wiki.

In order to run a transient simulation, put the name of the tme card on the end of the `set nps` card. e.g.

```
tme simutime 2 10 0 1
set nps 100 5 simutime
```

In order for a detector to record its results in a transient attach the name of the tme card as an argument to a `di` parameter `det` card.

```
tme dettime 2 30 0 30
det 1 dc 1 di dettime
```

Lessons Learned

- Problem stability can be increased by reducing the timestep size

- Timesteps on the order of 1 second are too large

- A criteria used for determining how much time would be necessary to simulate was 10 times the circulation time.

- Another criteria could be a multiple of the longest half life of a precursor (not used)

- Our initial experiments showed that the computer time necessary to run a full transient was feasible with a single fuel channel.

2.4   The ifc Card

The ifc card allows for interface with external files that describe the temperature and density of a material. A complete description of the ifc card is available on the serpent wiki. Feasibility testing with the ifc card was performed. A type 1 ifc card was used.

Lessons Learned

- The unit for the ifc file tmperature is kelvin

- The following error:

```
fatal error in function ReadIFCPAvg:

fscanf error
```

  is caused by having only temperature entries in the ifc input file. The ifc file needs both temperature and density values even if the density values are constant.

- There is a maximum number of points that can be used in a single ifc card. Documentation for this maximum was not found. We recall it being about 10,000.

- Note, since the number of ifc points are limited, this means that the spatial resolution of the temperature distribution is limited. Therefore, it would be wise to have points set such that there is high fidelity near regions of temperature discontinuity (graphite/fuel slat boundary).

2.5   PBUF and NBUF

During our experience developing the coupled analysis, numerous problems were encountered with the buffers (spaces in memory)`PBUF` and `NBUF`. These buffers can be defined as follows:

- **NBUF** The buffer for neutron activity;

- **PBUF** The buffer for precursor activity.

The Serpent wiki has an entry for the `set nbuf` entry which describes its syntax. There is anoter card, `set pbuf` which is undocumented. Presumably, the `set nbuf` and `set pbuf` cards have the same argument format.

Ville Valovirta stated on the Serpent 2 Forums,

> "It is best to think of the nbuf, pbuf and gbuf as being the relative size of the buffers compared to the number of neutrons (or photons) to be simulated per batch: I.e. setting nbuf to 1 and population to "set pop 10000 100 100" would allocate memory for just 10000 neutrons. In reality, with OpenMP parallelization slightly larger buffers are allocated.
>
> As for population control of neutrons, if you are asking about transient simulations, the neutron population is automatically controlled to the requested batch size at time-interval boundaries so if you keep running out of nbuf (and/or pbuf) you can also try to run the simulation using shorter time-intervals."

NB: Our experience indicates a nbuf size on the order of 20 necessary for transient simulations to begin working.

3   Multiphysics Coupling Methodology

A test case was built to test the coupling environment. The test case had a $\varnothing 20$ cm cylinder of UO_2 at 10 w/o % enrichment. The cylinder was surrounded by graphite block with a side-length of 180 cm. Periodic boundary conditions were used on the sides of the lattice to simulate an infinite lattice. Vertically, the reactor geometry was broken into three parts, delineated by the letters `A`, `B`, and `C`. Point `A` is the inlet to the reactor. Point `B` is the reactor outlet. Segment `A-B` is the in-core (IC) region. Segment `B-C` is the out-of-core (OOC) region. Point `C` is the point in the external loop where the fuel-salt enters the in-core region - the periodic flow boundary. Point `B` is st at 90 cm. Point `C` is st at 180 cm. The test case is illustrated in Figure 2.

Units in cm

Ø20

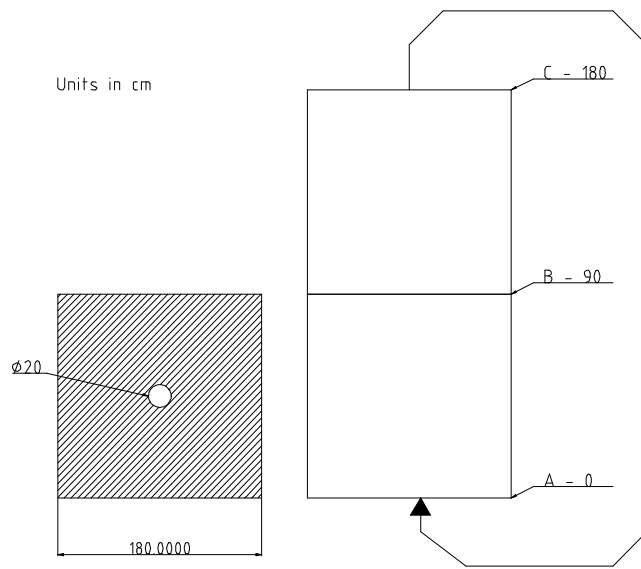180.0000

C - 180

B - 90

A - 0

Figure 2: Core geometry of test case

The coupling software performed an initial run of the case file and then took following steps

```
1          # Initialization
2          Create and initialize A as float
3          Create and initialize B as float
4          Create and initialize C as float
5          Create and initialize OOC as dataframe
6          Create and initialize IC as dataframe
7          Create and initialize velocity as float
8          Create and initialize time_per_step
9          Create and initialize number_of_steps
10         Create and initialize buf as dataframe
11
12         Run Serpent
13
14         # Execution loop
15         while idx < number_of_steps:
16             read .precpoints into IC
17             Move precursors in IC by velocity*
                   time_per_step
18             Move precursors in OOC by velocity*
                   time_per_step
19             Cut precursors in IC past B into buf
20             Paste buf into OOC
21             Cut precursors in OOC past C into buf
22             Subtract C from each precursor's position in
                   buf
23             Paste buf into IC
24             Decay all precursors in OOC
25             Decay all precursors in IC
26             Generate output_file in .precpoints format
27             Overwrite output_file as .precpoints
28             Run Serpent
29             idx++
```

the *decay* action occurs by the following algorithm

```
1  Given a set of precursors with field precursor group
       corresponding to their energy group
2  Create decayConstants[6] and initialize to the value of
       the decay constants
3  Create dt and initialize to the length of the time step
       set in the tme card
4
5  Foreach precursor group g:
6      Foreach precursor p in g:
```

```
7         R = a  random  real  number  between  0  and  1
8         p_decay = decayConstant[g]*dt
9         If  R < p_decay:
10              Remove  p  from  the  set  of  precursors
```

The implementation of this method is listed in Annex B.

4 Testing

System information for the testing is provided in Table 1.

CPU Speed	2,8 GHz
Number of Cores	4
Memory	16 Gb
Serpent Version	2.1.29

Table 1: Implementation System Information

Initial testing of the system used a very high flow velocity and the k_{eff} in the initial run to the next time-step. A substantial drop in k_{eff} was found in the second time step, which indicated the system was correctly moving the precursors.

A full test of the system was set up using the parameters on Table 2.

Time step length	0.3 s
Number of histories	5×100
Number of time steps	50
nbuf size	80
pbuf size	20

Table 2: Testing problem setup

4.1 Results

The simulation crashed after 45 iterations (13.5 s) of simulation time. The message *"Insufficient neutron buffer size, increase value of parameter 'nbuf'"* was displayed. The results are shown on Figure 3.

Given a nbuf size of 80 was used with a very low number of particle histories, and the simulation saturated the available system memory, it was felt that further simulations on the system would be untenable.

5 Future Work

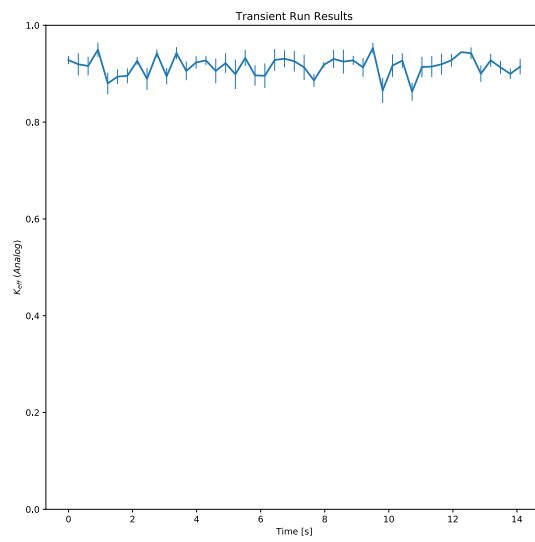Two potential solutions were generated to continue the work:

Figure 3: Results of test run

1. Implementation of the multiphysics coupling method on a cluster with a large amount of memory

2. Modeling the full loop and forgoing any sort of precursor removal and storage operations.

Annex A: Source Code to Decode, Modify, and Rewrite .precpoints

The Python 3 code listed below opens a .precpoints file, and modifies its z-position.

```python
import struct
import shutil
import pandas as pd

fileHead = "source" #put in the same arguement here as I had for
    savesrc

fileList = [fileHead + "." + x for x in ["main","prec","live"]]

for f in fileList:
    shutil.copyfile("./" + f,"./ModdedFiles/" + f)

with open('./source.precpoints','rb') as f:
    rawData = f.read()

#each chunk is 72 bytes long
chunks = [rawData[x:x+72] for x in range(0,len(rawData),72)]

#each chunk is comprised of 9 doubles
## DD -> decoded data.
DD = [struct.unpack('d'*9,c) for c in chunks]

#ll is for list of lists.
DDll = [[i for i in c] for c in DD]

#########create the pandas database#######
df = pd.DataFrame(DDll)
df = df.rename(index=str, columns={0:"X", 1:"Y", 2:"Z", 3:"NA1",
    4:"NA2", 5:"NA3", 6:"NA4", 7:"wgt", 8:"grp"})
df.head()


#write the precursors file
```

```
32    #do the position modificaiton here
33        for i in range(len(DD11)):
34        DD11[i][2] = DD11[i][2] +200 #200 cm for testing

35
36    flatData = [item for sublist in DD11 for item in sublist ]
37    #p for pack.
38    DDp = struct.pack('d'*len(flatData),*flatData)

39
40    with open("./ModdedFiles/" + fileHead + ".precpoints" ,'wb') as
   ↪    bf:
41        bf.write(DDp)
```

Annex B: Execution Manager Source Code

The code listed in the sections below below opens a manages the execution of
Serpent 2 and performs precursor movement. Note, this program is run natively
in Windows, but Serpent is run through Linux (the Cygwin [6] shell which allows
Linux software to run in Windows).

Exec˙Manager.py

```
1    import struct
2    import shutil
3    import pandas as pd
4    import os
5    import subprocess
6    from subprocess import Popen, PIPE, STDOUT
7    import random
8    import numpy as np

9

10
11   def runSS():
12       inCmd = r'"/home/terry/SSSCoup/SSSTrans/SS/runSS.sh"'
13       cmd = r'C:\cygwin64\bin\bash.exe --login ' + inCmd
14       p = Popen(cmd, shell=True, stdin=PIPE, stdout=PIPE,
          ↪    stderr=STDOUT)
15       output = p.stdout.read()
16       return output

17
18   def runTrans():
19       inCmd = r'"/home/terry/SSSCoup/SSSTrans/Trans/runTrans.sh"'
20       cmd = r'C:\cygwin64\bin\bash.exe --login ' + inCmd
21       p = Popen(cmd, shell=True, stdin=PIPE, stdout=PIPE,
          ↪    stderr=STDOUT)
```

```python
22      output = p.stdout.read()
23      return output

24
25  def readPP(fileName):
26      #read the file name source file and return a pandas
        ↪ dataframe object.
27      with open('./' + fileName + '.precpoints','rb') as f:
28          rawData = f.read()
29      chunks = [rawData[x:x+72] for x in range(0,len(rawData),72)]
30      decodedData = [struct.unpack('d'*9,c) for c in chunks]
31      decodedDataList = [[i for i in c] for c in decodedData]
32      df = pd.DataFrame(decodedDataList)
33      df = df.rename(index=str,columns={0:"X", 1:"Y", 2:"Z",
        ↪ 3:"NA1", 4:"NA2", 5:"NA3", 6:"NA4", 7:"wgt", 8:"grp"})
34      return df

35
36  def gen_OOC_DF():
37      df = pd.DataFrame(columns=['X', 'Y', 'Z', 'NA1', 'NA2',
        ↪ 'NA3', 'NA4', 'wgt', 'grp'])
38      return df

39
40  def gen_IC_DF():
41      df = pd.DataFrame(columns=['X', 'Y', 'Z', 'NA1', 'NA2',
        ↪ 'NA3', 'NA4', 'wgt', 'grp'])
42      return df

43
44  def doMove(df,v,dt):
45      wc = df.copy() #wc means working copy
46      wc['Z'] = wc['Z'] +  v*dt
47      return wc

48
49  def precsPastBoundary(df,z):
50      return df[df['Z'] > z]

51
52  def cullPrecsPastBoundary(df,z):
53      return df[df['Z'] < z]

54

55
56  def doDecay(df,dt):
57      #dn/dt = -lN  so the probability of decay per atom is 'l*dt'
58      #from .main file...
59      decayConst =  {0 : 1.246670E-02, 1: 2.829170E-02, 2:
        ↪ 4.252440E-02, 3 : 1.330420E-01, 4 : 2.924672E-01, 5 :
        ↪ 6.664877E-01, 6 : 1.634781E+00, 7 : 3.554600E+00}
60      #need the group constants.
61      remaining = []
```

```python
      for idx,v in df.iterrows():
          rr = random.random() #random roll
          dc = decayConst[int(v['grp'])]
          p_remove = dc * dt #roll a normalized dice and remove if
          ↪    the roll is less than this value.
          if rr > p_remove:
              remaining.append([idx,v])

      retVal = pd.DataFrame([x[1] for x  in remaining])
      return retVal


def Update_OOC_DB(pp,OOC):
    dt = 1 #seconds CONSTANT. DON'T FORGET TO SET THIS.
    v = 0.5 #cm/s CONSTNAT, DON'T FORGET TO SET THIS.
    postMove = doMove(pp,2,3)
    appendedOOC = OOC.append(pastBoundary)
    return appendedOOC


def write_source_file(fileName,df):
    fileName = "tst.precpoints"
    df = IC
    toWrite = [item for idx,row in df.iterrows() for item in
    ↪    row]
    outData = struct.pack('d'*len(toWrite),*toWrite)
    with open(fileName,'wb') as f:
        f.write(outData)
    return

def writeRunOut(toWrite,N):
    with open(f'Output/runOuts/run{N}.txt','w+') as f:
        f.writelines(out.decode('ascii'))
#3 points, ABC,
##-> A - start of IC region -90
## ->B - end of IC region +90
## ->C - end of OOC region +180 ##assuming OOC height == IC
↪    height.
## The boundary cube rages from +90 to -90.
A = -90
B = 90
C = 180
OOC = gen_OOC_DF()
IC = gen_IC_DF() #blank
```

```
105   #for loop
106   v = 30
107   steps = 50
108   tMax = 100
109   dt = tMax/steps
110   ############### Actual execution loop #########
111   out = runSS()
112   writeRunOut(out,'SS')
113
114   out = runTrans() #initial run
115   writeRunOut(out,'0')
116
117   pp = readPP('Output/src')
118
119   for idx, t in enumerate(np.linspace(0,tMax,steps)):
120       pp = readPP('Output/src')
121
122       IC = doMove(pp,v,dt) #PM is for postMoveOOC
123       OOC = doMove(OOC,v,dt)
124
125       #do In-core cut
126       cutIC = precsPastBoundary(IC,B)
127       IC = IC.drop(cutIC.index)
128       OOC = OOC.append(cutIC)
129
130       #do out-of-core cut.
131       cutOOC = precsPastBoundary(OOC,C)
132       IC = IC.append(cutOOC)
133       OOC = OOC.drop(cutOOC.index)
134
135       #do decay
136       OOC = doDecay(OOC,dt);
137       IC = doDecay(IC,dt)
138
139       write_source_file('Output/src.precpoints',IC)
140       out = runTrans()
141       writeRunOut(out,idx)
```

runTrans.sh

```
1   #!/bin/sh
2   pwd=`pwd`
3   pName="/SSSCoup/SSSTrans/Trans/Trans.SSSIN"
4   cd /home/terry/S2bin/
```

```
5  ./sss2.exe -omp 4 $pwd$pName | tee
   ↪  ~/SSSCoup/SSSTrans/Trans/Trans.out
6  cd $pwd
```

runSS.sh

```
1  #!/bin/sh
2  pwd=`pwd`
3  pName="/SSSCoup/SSSTrans/SS/SS.SSSIN"
4  cd /home/terry/S2bin/
5  ./sss2.exe -omp 20 $pwd$pName | tee ~/SSSCoup/SSSTrans/SS/SS.out
6  cd $pwd
```

SS.SSSIN

```
1  set title "Creating source for a time dependent
      simulation"
2  set acelib "./xs/sss_jeff311u.xsdata"
3  %     Geometry is just a cube
4
5  surf 1   cylz 0.0 0.0 10.0
6  surf 2   cube 0.0 0.0 0.0 90.0
7
8  %     Cell definitions:
9
10 cell 1 0  fuel   1       % Pin lattice
11 cell 2 0 mod  2 1
12 cell 99 0 outside 2
13
14 %     Fuel material is a homogenized LWR material:
15
16 mat fuel      12.4375010
17  8016.03c      1.18473E+1
18  92235.03c      95.27118E 1
19  92238.03c      9.75256E+1
20
21 mat mod   2.226
22  6000.03c     1
23
24 set power 1.0
25
26 set pop 1000 10 2
27
```

```
28  %       Save neutron and precursor source to "./source"
        files
29  set savesrc "./source"
```

Trans.SSSIN

```
 1  set acelib "./xs/sss_jeff311u.xsdata"
 2
 3  set title "Running the dynamic simulation"
 4  set acelib "./xs/sss_jeff311u.xsdata"
 5
 6  surf 1  cylz 0.0 0.0 10.0
 7  surf 2  cube 0.0 0.0 0.0 90.0
 8
 9  %       Cell definitions:
10
11  cell 1 0  fuel   1        % Pin lattice
12  cell 2 0 mod  2 1
13  cell 99 0 outside 2
14
15  %       Fuel material is a homogenized LWR material:
16
17  mat fuel      12.4375010
18   8016.03c      1.18473E+1
19   92235.03c      95.27118E 1
20   92238.03c      9.75256E+1
21
22  mat mod   2.226
23   6000.03c      1
24
25  %       Set up time structures for simulation and detectors
        :
26  %       30 time bins for detector
27  tme dettime 2 30 0 3e1
28
29  %       1 time interval for simulation (no population
        control)
30  tme simutime 2 10 0 1
31
32  %       Increase the size of neutron buffer since there is
        no pop. control
33  set nbuf 50
34
35  %       Neutron population:
36  set nps 100 5 simutime
```

16

```
37
38 %       Link source (use point wise precursor tracking)
39 set dynsrc "./source" 1
40
41 %       Tally neutron population as a function of time
42 det 1 dc 1 di dettime
43
44 set savesrc "/home/terry/SSSCoup/SSSTrans/Output/src"
45
46 set pbuf 20
47 set nbuf 80
```
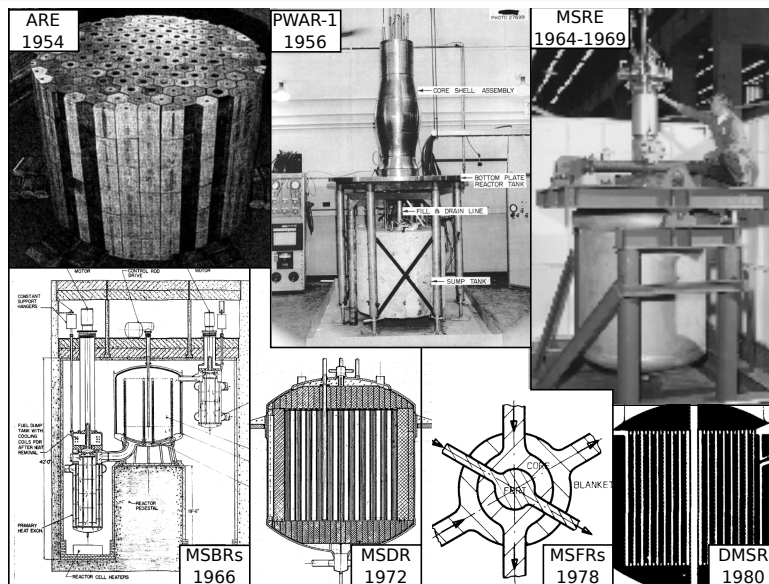
References

[1] Manuele Aufiero, Carlo Fiorina, Axel Laureau, Pablo Rubiolo, and Ville Valtavirta. Serpent–OpenFOAM coupling in transient mode: simulation of a Godiva prompt critical burst. *Proceedings of M&C+ SNA+ MC*, pages 19–23, 2015.

[2] Hrvoje Jasak, Aleksandar Jemcov, and Zeljko Tukovic. OpenFOAM: A C++ library for complex physics simulations. In *International workshop on coupled methods in numerical dynamics*, volume 1000, pages 1–20. IUC Dubrovnik, Croatia, 2007.

[3] J. Leppanen. VTT-640: Development of a New Monte Carlo Reactor Physics Code. Technical report, VTT, Helsinki, 2017. Website: http://montecarlo.vtt.fi/.

[4] Jaakko Leppänen. Development of a dynamic simulation mode in Serpent 2 Monte Carlo code. *Proceedings of M&C*, pages 5–9, 2013.

[5] Jaakko Leppänen, Ville Hovi, Timo Ikonen, Joona Kurki, Maria Pusa, Ville Valtavirta, and Tuomas Viitanen. The numerical multi-physics project (NUMPS) at VTT technical research centre of Finland. *Annals of nuclear energy*, 84:55–62, 2015. ISSN 0306-4549.

[6] Jeffrey Racine. The cygwin tools: a gnu toolkit for windows. *Journal of Applied Econometrics*, 15(3):331–341, 2000.

[7] Riku Tuominen. Coupling Serpent and OpenFOAM for neutronics-CFD multi-physics calculations. 2015.

Attachment 3

MSR Xenon Analysis: Review and Current Status

Presentation at the 2018 Generation 4 Small Reaction Conference (G4SR) in Ottawa,

Canada

MSR Xenon Analysis: Review and Current Status

Terry J. Price[1]   Ondrej Chvala[2]

[1]Faculty of Energy Systems and Nuclear Science
University of Ontario Institute of Technology

[2]Department of Nuclear Engineering
University of Tennessee Knoxville

G4SR-1, 2018
Ottawa

1. MSRs in 30 seconds
2. History
3. Timeline
4. Primer

5. Problems and Unanswered Research Questions
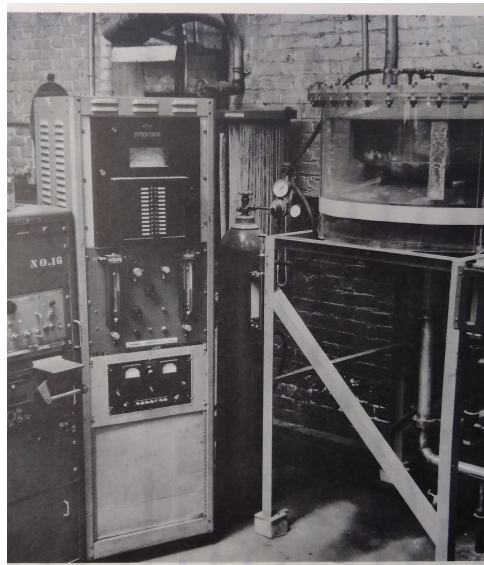6. Graphite Mass Transfer
7. Take Home Message

MSRs in 30 seconds

Nuclear fuel dissolved in a liquid alkali-fluoride fuel-salt which circulates between a heat exchanger and a moderator
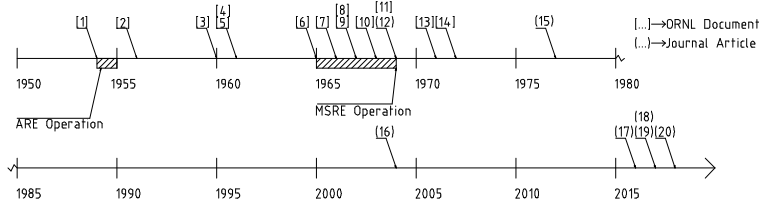
A Brief History of MSR Xenon

- Impetus for ARE was xenon concerns
- Continuous investigations throughout the MSR program
- Two major models of MSRE xenon made
- Predictive modeling has been, to date, unsuccessful
- Some limited success with fitting a model to experimental data
- Documented largely in ORNL reports of varying availability
- Renewed interest since $\approx$ 2004

Experimental setup to test MSRE xenon stripper efficiency

Timeline of MSR Xenon Research

1	1954	ORNL-CF-54-5-1: The Xenon Problem in the ART	Meem	11	1969	ORNL-4389:Gas Transport in MSRE Moderator Graphite	Evans, Rutherford, Malinaukas
2	1956	ORNL-1924: A Theoretical Study of Xe-135 Poisoning Kinetics in Fluid-Fueled, Gas Sparged Nuclear Reactors	Robertson	12	1969	Graphite and Xenon Behavior and Their Influence of Molten-Salt Reactor Design	Scott, Eatherly
3	1960	ORNL-CF-61-5-62: Xenon Poisoning in Molten Salt Reactors	Miller	13	1971	ORNL-TM-3464	Engel, Steffy
4	1962	ORNL-CF-62-11-69: Preliminary Equations to Describe Iodine and Xenon Behavior in the MSRE	Engel	14	1972	ORNL-CF-72-6-12: Sidestream Processing for Continuous Iodine and Xenon Removal From MSBR Fuel	Wichner, Baes
5	1962	ORNL-TM-262: Xenon Diffusion in Graphite: Effects of Xenon Absorption in Molten Salt Reactors Containing Graphite	Watson, Evans	15	1977	Transient Xenon Analysis in a Molten Salt Breeder Reactor	Shimazu
6	1965	ORNL-TM-1070	Ball Kerlin	16	2004	Transient Xenon Effect on Plant Control in MSRs	Suzuki, Shimazu
7	1966	ORNL-4037: Xenon Diffusion and Possible Formation of Cesium Carbinde in a MSBR	Briggs	17	2016	The Influence of Xe-135m on Steady-State Xenon Worth in Thermal Molten Salt Reactors	Eades, Chalef, Venneri, Blue
8	1967	ORNL-TM-1810	Kedl	18	2017	Xenon Analysis of Thorium Molten Salt Experiment Reactor-Liquid Fuel	Chen, Ruimin, Jingen, Guimin
9	1967	ORNL-4069: Development of a Model for Computing Xe-135 Migration in the MSRE	Kedl, Houtzeel	19	2017	Flow Effect on I-135 and Xe-135 Evolultion Behavior in a Molten Salt Reactor	Wu, Guo, Cai, Yu, Zou, Han, Chen
10	1968	ORNL-TM-2245: Removal of Xenon-135 From Circulating Fuel Saltt of the MSBR by Mass Transfer to Helium Bubbles	Peeblees	20	2018	Implementation of General Species Transport Capability into VERA-CS-for Molten Salt Reactor Analysis	Taylor, Salko, Collins

A Brief Primer on MSR Xenon Theory

FISS.

PROG.   O.G.

FS

G   ST   CG

B

Decay / Burnup
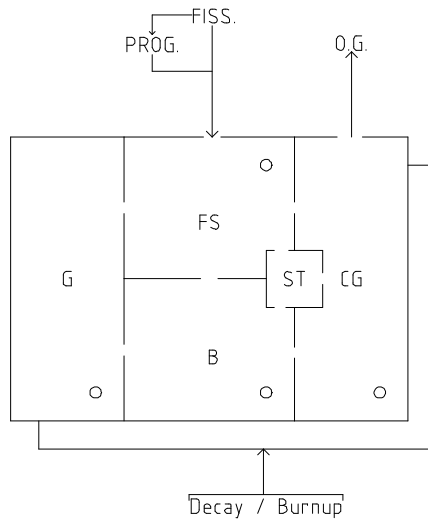
G:	Graphite	B:	Bubbles	CG:	Cover Gas
ST:	Xenon Stripper	OG:	Off Gassing	FISS:	Fission Production
PROG:	Xenon Proginators ^{135}I and ^{135}Te			FS:	Fuel Salt

Comparison of Some MSR Xenon Models

Miller 1961	Kedl Houtzeel 1968	Engel Steffy 1971	Shimazu 1977 / 2004
Modeled: Graphite Xenon Stripper **Investigated**: Effects of graphite diffusion coeffecient and stripper efficency	**Modeled**: Graphite Xenon Stripper Bubbles Discretized Core **Investigated**: 1) Predicted MSRE Xenon Poison Fraction (Steady State) 2) Effects of Bubbles Later used for on-line calculations	**Modeled**: Graphite Xenon Stripper Bubbles Lumped Parameter **Investigated**: 1) Fitting to Experimental Data 2) Transient Analysis	**Modeled**: Graphite Xenon Stripper Bubbles Set of ODEs / PDEs **Investigated**: 1) Transient Analysis 2) Required Reactivty Control

Problems and Unanswered Research Questions

Many research questions and problems:

1. To date, there has been no MSR xenon model developed that has successfully predicted the poison fraction a priori.

2. Are any of the previously developed phenomenologically correct? What minor phenomena (e.g. adsorption) have we omitted under what circumstances do these minor terms become non-trivial?

3. Even if have a model that is phenomenologically correct, how can we be sure the various parameters (e.g. rate constants, etc.) are correct?

4. Are there transient conditions which would bring a model out of its operable regime?

5. Are there solubility related effects we should be concerned about? How does the accumulation of gaseous fission products relate to the solubility limit is measured in-lab?

6. Can the time evolution of the reactor alter the phenomenology relevant to MSR xenon behavior? E.G. ^{135}I and corrosion products or ^{135}Te and a mobile solid phase? Pore clogging of graphite?
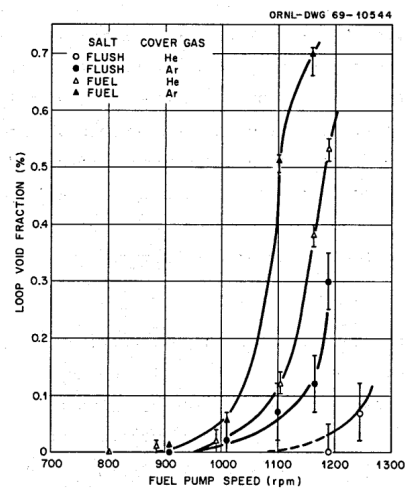
and so many more....

VARIATION OF CIRCULATING VOID FRACTION WITH PUMP SPEED. HOW CAN THIS BE PREDICTED?

A Look at One Problem: Graphite Mass Transfer
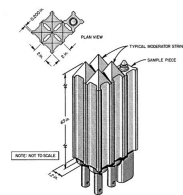
Graphite Stringers

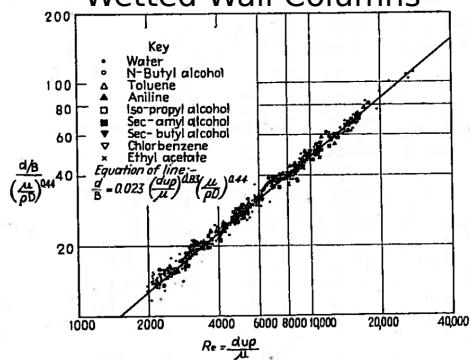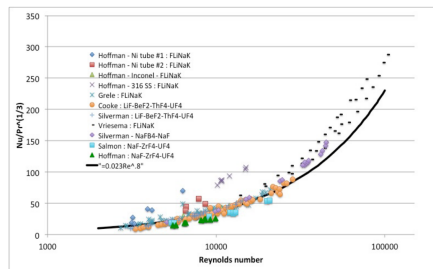Instalation in MSRE

Microscopy
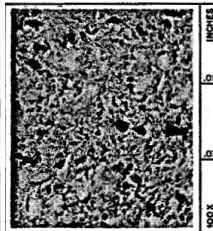
Technical Drawing

Evidence for The Validity of Dittus-Boelter

$$J = \kappa_M (C_L - HRT\ C_G)$$
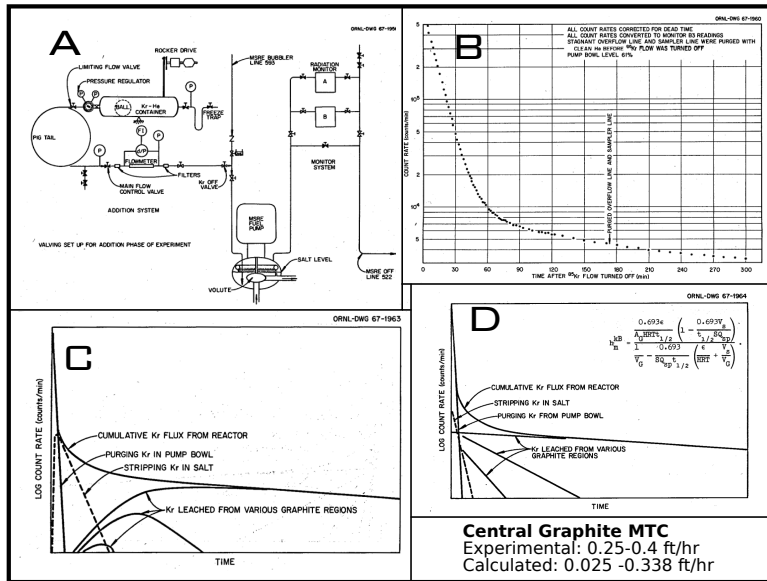
Sherwood 1954
Mass Transfer In
Wetted Wall Columns

Yoder 2014
Heat Transfer In Molten Salts

WHAT ABOUT MASS TRANSFER IN MOLTEN SALTS?

9/12

MSRE Experimental Work

Central Graphite MTC
Experimental: 0.25-0.4 ft/hr
Calculated: 0.025 -0.338 ft/hr

Is It Valid?

Arguments For:

- DB relationship valid for heat transfer in molten salts.
- DB relationship valid for mass transfer of various non molten-salt substances in wetted wall column.
- Kr experiment was able to find experimental evidence that aligned with predicted results.

Arguments Against:

- MSR fuel channels are mechanically different than wetted wall columns.
- The *exponential peeling* process used to get the MTC in the Kr experiment was done by hand and at the judgment of the investigator, who probably knew the expected result before hand and may have been influenced by an *outcome bias*.
- ORNL-4069 model over-predicted measured Xe poison fraction by more than a factor of three.

Take Home Message

What you can take away from this presentation:

- There was continuous development of MSR xenon models throughout the MSR program.
- Renewed interest starting in about 2004. There have been more publications on the subject in the last three years than the previous 40.
- Many unanswered questions. Are the models phenomenologically correct?
- No evidence was found that indicate predictive modeling has ever been successfully performed.
- Lots of potential for experimental work!

Attachment 4

MSR Molten Salt Reactor Xenon Analysis Primer, History, State of the Art, and Modeling

Efforts

Unpublished Presentation

SUMMARY
Molten Salt Reactor Xenon Analysis
Primer, History, State of the Art, and Modeling Efforts

Terry J. Price[1]**, Ondrej Chvala**[2]

[1]University of Ontario Institute of Technology
2000 Simcoe Street North, Oshawa, Ontario, Canada

[2]University of Tennessee Knoxville
427 Nuclear Engineering Building, Knoxville, Tennessee, USA

Terry.Price@UOIT.net, OChvala@UTK.edu

ABSTRACT

The proposed paper will summarize our work in molten salt reactor (MSR) xenon analysis.
A brief primer on MSR xenon theory will be given, along with a historical overview and a
description of the state-of-the-art. Finally, our modeling efforts will be described, and our
results to date presented.

KEYWORDS: MSR, Xenon, Reactor Physics, Neutron Poisoning, Molten Salt Reactor

1. INTRODUCTION

Molten salt reactors (MSRs) are a type of generation IV nuclear reactor which use an alkali-fluoride
salt, called a fuel salt, as both a fuel-matrix and primary working fluid. Heat is generated in the fuel
salt from neutron mediated nuclear fission. A fission-product generated from the fission process
is ^{135}Xe , which is a strong neutron poison on account of its high thermal neutron absorption
cross-section. The analysis of the behavior of ^{135}Xe in solid-fueled reactors, such as a pressurized
water reactor, can be simplified due the the trivial amount of migration of ^{135}Xe in the fuel-matrix.
^{135}Xe behavior in MSRs, however, is more complex given the migratory and non-soluble nature of
xenon in alkali-fluoride salts.

MSRs were primarily developed at Oak Ridge National Laboratory (ORNL) in the 1950s-1970s.
Three operating MSRs were developed, the Aircraft Reactor Experiment (ARE), in 1954; the Pratt
and Whitney Aircraft Reactor (PWAR-1), in 1956; and the Molten Salt Reactor Experiment (MSRE),
which operated between 1965 and 1969.

For the purposes of further discussion, let us undergo a brief familiarization with a typical MSR [*].
In an MSR, as illustrated in Figure 1, the fuel salt circulates in the *primary loop* between the reactor

---

[*]The MSR described hereon is derived from the authors experience with MSRs, which is primarily the MSRE. Individual reactor
designs will vary from this description. The purpose is to provide an illustration for further explanation

core and the heat exchanger(9), with inertia imparted to it via a fuel pump (10). In this way, the reactor may be partitioned into in-core and out-of-core regions. Furthermore, the total system of both the in-core and out-of-core regions is referred to as the reactor-system. The fuel salt enters the in-core region through an inlet (13) and proceeds down a down comer (12) into the lower plenum (11) whereupon it moves up a set a fuel channels (1) cut into graphite blocks of graphite, referred to as graphite stringers (2). Once past the graphite stringers, the fuel salt enters into the upper plenum (7), which has an interface to a cover gas region (5), before heading out the reactor outlet (14), and entering the out-of-core region. The totality of the graphite stringers is referred to as the graphite moderator or moderating region. It is when the fuel salt is within this moderating region that free neutrons become sufficiently thermalized to induced nuclear fission and thereby generate heat. Once the fuel salt has left the outlet it enters the out-of-core region, whereupon the heat generated in fission is transferred to a secondary working fluid through a heat exchanger. Optionally, the fuel salt may pass through a *xenon stripper* (not depicted) as it transitions between the in-core and out-of-core regions. One additional aspect that is highly important to the analysis of xenon in MSRs is the existence of circulating bubbles (not depicted), also called circulating voids within the fuel salt. In the MSRE, the bubbles were estimated to have a mean diameter of 2.54 mm. [1]

From the prior description of MSR structure, we abstract out three *compartments* that are are crucial to the analysis of xenon in an MSR. These compartments are,

- Fuel Salt: The circulating working fluid and fuel matrix where the ^{135}Xe , ^{135}Te , and ^{135}I are generated.

- Graphite: Namely the void-space of the graphite matrix. In prior analyses only ^{135}Xe was assumed to be able to migrate to the graphite.

- Bubbles: Circulating in the fuel-salt. No information was found on their overall composition. In prior analyses, only ^{135}Xe was assumed to be able to migrate to the bubbles.

and the concentration, evolution, and migration of xenon in each of these compartments determine the totality of xenon behavior in the MSR system.

Many authors [†] state the system of three coupled ordinary differential equations,

$$\dot{N}_{Xe} = \gamma_{Xe}\Sigma_f\phi V_{RC} + \lambda_I N_I - \lambda_{Xe} N_{Xe} - \Sigma_a^{Xe}\phi V_{RC}, \tag{1a}$$

$$\dot{N}_I = \gamma_I \Sigma_f \phi V_{RC} - \lambda_I N_I + \lambda_{Te} N_{Te}, \tag{1b}$$

$$\dot{N}_{Te} = \gamma_{Te}\Sigma_f\phi V_{RC} - \lambda_{Te} N_{Te}. \tag{1c}$$

as descriptive of xenon behavior in a solid fueled reactor. In Equation 1, the evolution of xenon is mediated by the evolution of ^{135}I and ^{135}Te in the reactor system, and the entire reactor is homogenized as a single point.

In a MSR, however, the xenon can migrate throughout the reactor, and may be in a differential concentrations in different locations in the reactor system. As stated in the annex of ORNL-4541
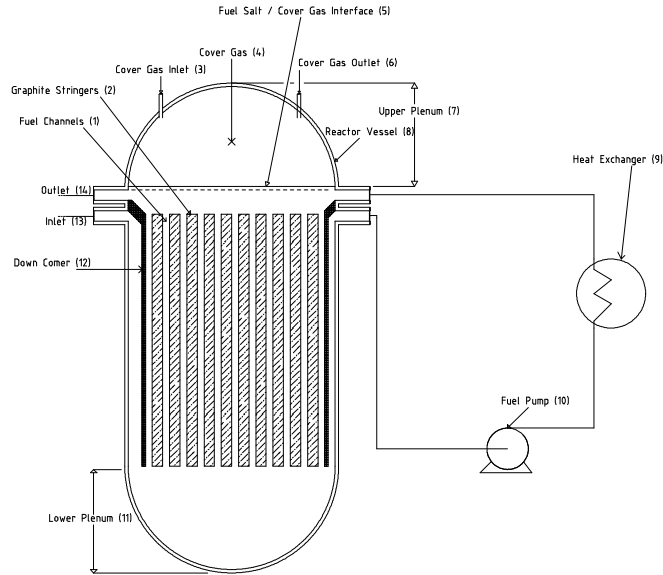

[†]C.F. [2] for example

Figure 1: MSR component diagram

[3] the rate balance equations,

$$
\begin{aligned}
\{Generation\ rate\} &= \{burnup\ rate\ in\ salt\} \\
&+ \{migration\ rate\ to\ graphite\} \qquad \text{(2a)} \\
&+ \{migration\ rate\ to\ bubbles\}, \\
\{Migration\ rate\ to\ graphite\} &= \{decay\ rate\ in\ graphite\} \\
&+ \{burnup\ in\ graphite\}, \qquad \text{(2b)} \\
\{Migration\ rate\ to\ bubbles\} &= \{decay\ rate\ in\ bubbles\} \\
&+ \{burnup\ in\ bubbles\} \qquad \text{(2c)} \\
&+ \{stripping\ rate\ in\ bubbles\},
\end{aligned}
$$

describe noble gas migration in an MSR. [3, p. 170] Furthermore, prior analyses have assumed the the ^{135}Xe progenitors ^{135}I and ^{135}Te remain in solution whereas the ^{135}Xe is free to migrate. The totality of these consideration significantly increases the requisite complexity of a model of MSR xenon behavior.

2. Topics to Be Discussed

As part of our ongoing efforts to model dynamic MSR behavior[‡], we have invested a substantial effort into understanding and modeling MSR xenon behavior. Our efforts include,

- Historical review of MSR xenon analysis work;

- Summarization and elucidation of MSR xenon theory;

- Monte Carlo modeling MSRE xenon poisoning in the MSRE;

- Dynamics modeling of MSR xenon behavior;

- Benchmarking of a model of MSRE xenon behavior against experimental data;

- Investigation into mass transfer coefficients and processes in an MSR.

The intended paper and presentation will detail our work and summarize our findings. Time permitting, a brief primer on MSR xenon theory will be made along with a historical overview of work to date. Figure 2 shows some of the results we intend to exposit.
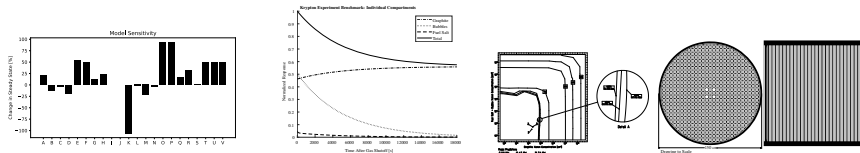
Figure 2: Some of the results to be shown.

REFERENCES

[1] R. Kedl and A. Houtzeel. *ORNL-4069: Development of a Model for Computing Xe-135 Migration in the MSRE* (1967).

[2] J. Lamarsh. *Introduction to Nuclear Reactor Theory*. Addison-Wesley (1966).

[3] R. C. Robertson. *ORNL-TM-4541: Conceptual Design Study of a Single-Fluid Molten-Salt Breeder Reactor* (1971).

[4] V. Singh, A. Wheeler, M. Lish, O. Chvála, and B. Upadhyaya. "Nonlinear dynamic model of Molten-Salt Reactor Experiment Validation and operational analysis." *Annals of Nuclear Energy*, **volume 113**, pp. 177–193 (2018).

[‡]C.F. [4]

Attachment 5

Molten Salt Reactor Xenon Analysis: Review and Decomposition

Published in the ASME Journal of Nuclear Engineering

Molten Salt Reactor Xenon Analysis: Review and Decomposition

Terry J. Price[*1], Ondrej Chvala[†2], and Zack Taylor [‡2]

[1]University of Ontario Institute of Technology
[2]University of Tennessee Knoxville

July 2018

Abstract

This document analyzes molten salt reactor (MSR) xenon theory and decomposes it with respect to the existing corpus of literature. A history of xenon behavior in MSRs is presented. Relevant literature is tabulated. Assumptions in MSR xenon theories are made explicit. A lexicography of graphite stringers is proposed. The behavior of bubbles is investigated along with interfacial area perturbation in response to thermodynamic state perturbation. This document serves as an underpinning to further investigation into the MSR xenon theory.

1 Introduction

1.1 Overview

The behavior of xenon, in particular ^{135}Xe , is of principal importance in the prediction and description of nuclear reactor behavior. This document decomposes and discusses the relevant features, governing equations, and constitutive formula involved in the analysis of xenon in a Molten Salt Reactor (MSR). This document is designed to be used in conjunction with the Oak Ridge reports ORNL-4069, ORNL-TM-3464 and the appendix of ORNL-TM-4541. [1] [2] [3, p. 170] Many of the ORNL reports cited in this paper can be retrieved from MoltenSalt.org [4] or Energy From Thorium PDF Archive [5].

An MSR uses a circulating alkali halide fuel salt melt as both a fuel matrix and a working fluid. The words *fused salt* and *ionic liquid* also appear in the literature in reference to molten salts. MSR development started in the 1950s at

---

the Oak Ridge National Laboratory (ORNL) in the United States. This effort reached apogee with the design, development, and subsequent operation of the Molten Salt Reactor Experiment (MSRE) in the 1960s. The MSR program at ORNL resulted in several conceptual designs of large MSR power systems, the final one being the Denatured Molten Salt Reactor (DMSR) published in the 1980s. Details about the history of the MSR program at ORNL are documented by MacPherson and Dolan. [6] [7, p. 2] Renewed interest of MSRs is coincident with their inclusion among the Generation IV (GenIV) concepts, see Serp. [8]. Without the loss of generality, and due to the overview focus of this work, the discussion herein assumes that the fuel salt uses a fluorine halogen, and the core is graphite moderated.

For our purposes, let us undergo a brief familiarization with the structural and process components of a simple single-fluid MSR. The description hereafter is not specific to any particular MSR concept, but is a technological level description using the terminology of Lorenz; that is, it is a description of the system at the level of components, which are given as *black-boxes*. [9] The components of an MSR are shown in Figure 1 and the flow path is shown in Figure 2. The xenon mass transfer process is also illustrated in Figure 3; xenon enters the system from the top *Prog/Fiss* arrow, then can circulate to any of the *rooms* through the *doors*, or exit the system by either burnout or decay, which is represented by holes in the floor, or by a cover gas removal, represent by the upward facing arrow labeled O.G. (off gassing).

In reference to Figure 3, fuel enters the reactor vessel through the inlet and moves down to the lower plenum via the down comer. Once in the lower plenum, the fuel salt intramixes and travels up the fuel channels which have been cut into graphite stringers. The graphite stringers constitute the moderator. When within the moderating region, the fuel undergoes fission and heat is generated. Once the fuel salt has passed through the fuel channels, it leaves the reactor through the outlet and enters the heat exchanger where it deposits its heat content. The fuel salt then leaves the heat exchanger and enters the fuel pump where momentum is imparted into it by the impeller. The fuel salt then leaves the pump and enters the inlet and the cycle is repeated. Pressure is maintained in reactor vessel via the cover gas in the upper plenum. Cover gas is injected into the upper plenum via the cover gas inlet and removed via the cover gas outlet. The entire primary circuit can be divided into in-core and out-of-core volumes. The primary circuit will likely also contain additional components, particular to the specific reactor design, which have not been depicted, including a dedicated gas stripper, equipment to sample salt, adjust chemistry, refuel the reactor, etc.; nevertheless, we believe Figures 1 and 2 are typical of MSR designs and contain the elements common to all MSRs.

The migratory behavior of xenon in molten salt is qualitatively different than that in a solid fuel. When the fuel is solid, the migration of xenon is of secondary importance to the analysis of the xenon behavior. In an MSR, the xenon circulates with the fuel salt, and undergoes a number of mass transfer processes in the various regions of the reactor. This permits the possibility of xenon or other fission gas removal from the nuclear fuel, which is a unique
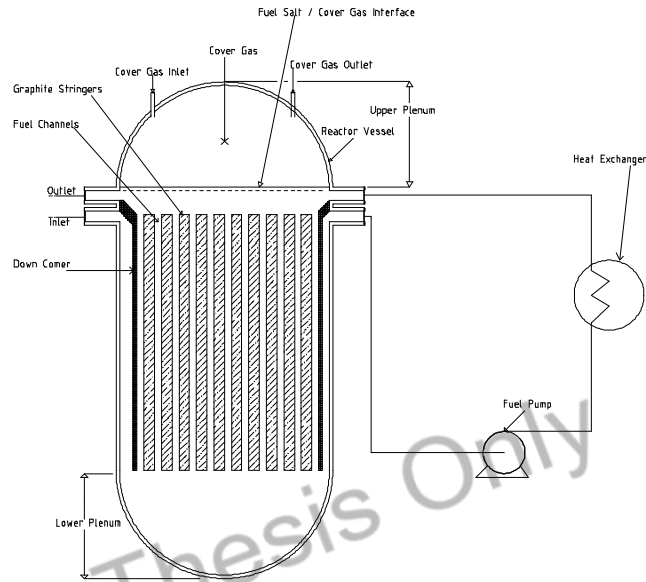
2

Figure 1: MSR component diagram

capability of the molten fuel. After its production from nuclear fission or iodine decay, the xenon moves throughout the reactor, dissolved in the circulating salt; in the circulating gaseous voids (bubbles); diffusing into the moderating graphite; or leaving the core to the cover gas or through a sparging equipment. The source, sink, and migration processes in MSR xenon theory are summarized in Table 1.

Figure 4 shows a qualitative description of processes in MSR xenon theory. ^{135}Xe originates from either fission or the ^{135}Xe progenitors, ^{135}I and ^{135}Te are fission products and are produced in nuclear fission. The aforementioned isotopes shall be referred to as the *poison species*. ^{135}Te transmutes into ^{135}I which transmutes into ^{135}Xe . ^{135}Xe transmutes into ^{135}Cs. All the previously mentioned decay processes are facilitated through beta-minus decay. The poison species are all generated inside of the fuel salt. The ^{135}Te and ^{135}I remain in the fuel salt solution, whereas the ^{135}Xe is able to migrate from the fuel salt to the cover-gas, circulating voids (bubbles) and cover-gas due to its noble and gaseous nature. There may also be a mass transfer directly from bubbles to the

3
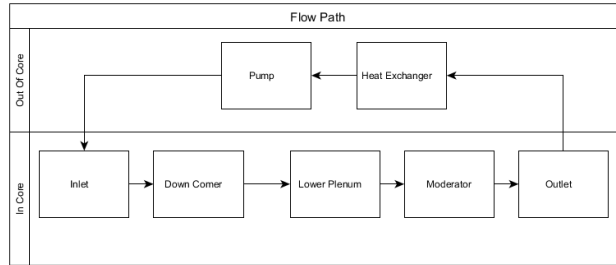
Figure 2: MSR flow path

Table 1: Definitions of terms in MSR xenon analysis.

Source Terms	Sink Terms	Migration Terms
Fission Production	Radioactive Decay	Mass Transfer to Circulating Voids
Production From Progenitors	Burn Out	Removal via Cover Gas Outlet Line
	Removal via Cover Gas Outlet Line	Mass Transfer to Cover Gas

graphite. The neutron absorption cross sections of ^{135}Te and ^{135}I are assumed to be negligible. In addition to burn-out and radioactive decay, ^{135}Xe may be removed from the system through the removal of the cover-gas.

There is a distinction in terminology between diffusive off-gassing and mechanical sparging. In off-gassing, diffusion drives dissolved gas past an interface, whereas sparging refers to a mechanical gas removal process. An example of sparging is the xenon spray-ring in the Molten Salt Reactor Experiment (discussed in the next section). The ORNL literature uses the term stripping occasionally in place of sparging.

1.2   Literature Chronology

Table 2 lists all literature related to MSR xenon analysis found. [1] The timeline of MSR xenon analysis is illustrated in Figure 5. The first consideration of MSR xenon behavior was found to be published in 1954. No literature was found for a 26 year period between 1978 and 2004. The most prolific period of publication was the region of time cotemporal with the MSRE operational period.

---

[1]Some additional literature was found related to the engineering of xenon removal systems, which was not included.
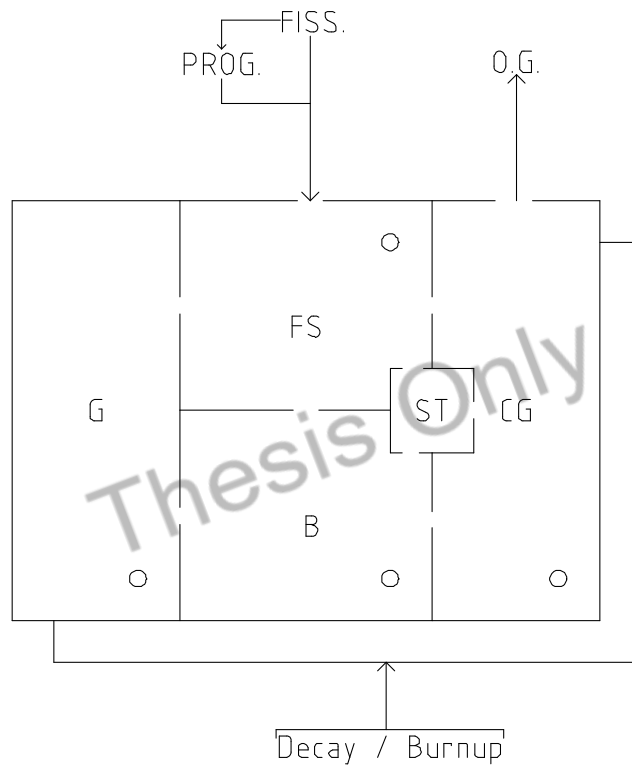
Figure 3: Compartmental illustration of xenon mass transfer.
G: Graphite, FS: Fuel Salt, B: Bubbles, ST: Xenon Stripper, CG: Cover Gas,
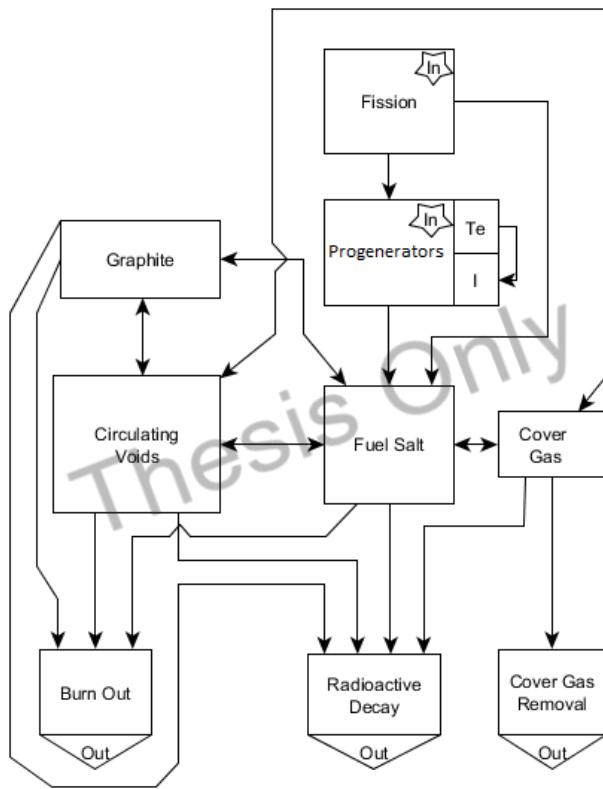OG: Offgassing, Fiss: Fission production, Prog: Xenon Progenitors ^{135}I and
^{135}Te

Figure 4: Xenon mass transfer pathways

7

Table 2: MSR Xenon Literature

Year	Title	Pages	Model?	Authors	Citation
1954	ORNL-CF-54-5-1: The Xenon Problem in the ART [2]		?	Meem	[11]
1956	ORNL-1924: A Theoretical Study of Xe-135 Poisoning Kinetics in Fluid-Fueled, Gas Sparged Nuclear Reactors			Robertson	[10]
1960	ORNL-CF-60-2-2: Xenon Control in Fluid Fuel Reactors			Burch, Watson, Weeren	[12]
1961	ORNL-CF-61-5-62: Xenon Poisoning in Molten Salt Reactors			Miller	[13]
1962	ORNL-CF-62-11-69: Preliminary Equations to Describe Iodine and Xenon Behavior in the MSRE			Engel	[14]
1962	ORNL-TM-262: Xenon Diffusion in Graphite: Effects of Xenon Absorption in Molten Salt Reactors Containing Graphite			Watson, Evans	[15]

[2] A copy of this report was not found. It is referenced in ORNL-1294. [10, p. 5]

Table 2: MSR Xenon Literature

Year	Title	Pages	Model?	Authors	Citation
1965	ORNL-TM-1070: Stability Analysis of the Molten-Salt Reactor Experiment	65		Ball, Kerlin	[16]
1966	ORNL-4037: Molten-Salt Reactor Program Semi-annual Progress Report for Period Ending August 31, 1966. Subsection Titled Xenon Diffusion and Possible Formation of Cesium Carbide in a MSBR	158-165		Briggs	[17]
1967	ORNL-TM-1810: A Model for Computing the Migration of Very Short-Lived Nobel Gases into MSRE Graphite			Kedl	[18]
1967	ORNL-4148: Gas Transport in MSRE Moderator Graphite. Review of Theory and Counter diffusion Experiments			Malinauskas, Rutherford, Evans	[19]
1967	ORNL-4069: Development of a Model For Computing Xe-135 Migration in the MSRE			Kedl, Houtzeel	[1]
1968	ORNL-TM-2245: Removal of Xenon-135 From Circulating Fuel Salt of the MSBR by Mass Transfer to Helium Bubbles			Peebles	[20]

Table 2: MSR Xenon Literature

Year	Title	Pages	Model?	Authors	Citation
1969	ORNL-4389: Gas Transport in MSRE Moderator Graphite	36		Evans, Rutherford, Malinaukas	[21]
1969	Graphite and Xenon Behavior and Their Influence on Molten-Salt Reactor Design			Scott, Eatherly	[22]
1971	ORNL-4541: Conceptual Design Study of a Single-Fluid Molten-Salt Breeder Reactor: Annex A	170		Robertson	[3]
1971	ORNL-TM-3464: Xenon Behavior in the Molten Salt Reactor Experiment			Engel, Steffy	[2]
1972	ORNL-CF-72-6-12: Sidestream Processing for Continuous Iodine and Xenon Removal from the MSBR Fuel			Wichner, Baes	[23]
1977	Transient Xenon Analysis in a Molten Salt Breeder Reactor			Shimazu	[24]
2004	Transient Xenon Effect on Plant Control in MSRs			Suzuki, Shimazu	[25]

9

Table 2: MSR Xenon Literature

Year	Title	Pages	Model?	Authors	Citation
2016	The Influence of Xe-135m on Steady State Xenon Worth in Thermal Molten Salt Reactors			Eades, Chaleff, Venneri, Blue	[26]
2017	Xenon Analysis of Thorium Molten Salt Experiment Reactor-Liquid Fuel [sic]			Chen, Ruimin, Jingen Guimin	[27]
2017	Flow Effect on I-135 and Xe-135 Evolution Behavior in a Molten Salt Reactor			Wu, Guo, Cai, Yu, Zou, Han, Chen	[28]
2018	Implementation of General Species Transport Capability into VERA-CS for Molten Salt Reactor Analysis			Taylor, Salko, Collins	[29]

10

Figure 5: MSR xenon research timeline
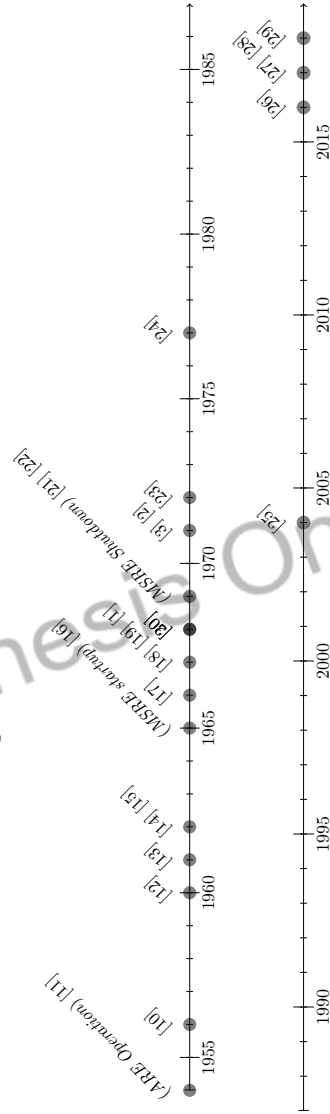
1.3 Xenon in Historical MSRs

There were three experimental MSRs built and operated: the Aircraft Reactor Experiment; the Pratt and Whitney Aircraft Reactor-1; and, the Molten Salt Reactor Experiment.

The Aircraft Reactor Experiment (ARE) was designed to demonstrate a basic MSR feasibility in an effort to develop a nuclear propulsion source on an aircraft. [3] ARE used a NaF-ZrF$_4$-UF$_4$ fuel salt, a beryllium oxide moderator, and outlet temperature of 1133 K. [32, p. 62] The ARE operated for 100 MW-hours over the course of nine days in 1954. [ibid] Bettis et al. report a positive temperature coefficient of reactivity, related to xenon poisoning in solid fuel reactors, was considered to be significant enough to warrant abandoning them in design considerations for the ARE project. [33] The ARE used a xenon removal system built into the fuel pumps. The xenon removal system was comprised of a mixing chamber in which the fuel salt was sprayed through a helium atmosphere onto the wall of a mixing chamber. The result was a foam/salt mixture with a high gas interface surface area. The large surface area facilitated the transfer of gaseous fission products from the salt to the gas. The foam/salt mixture was then pumped into an expansion volume, where the helium and gaseous products therein were removed via an off-gas system. [34, p. 31-32] An experiment performed on the ARE, named Experiment H-11, showed that no more than 5% of the xenon produced by the reactor remained in the fuel salt. [35, p. 67] This poison fraction was determined by finding the predicted reactivity lost from xenon poisoning without any xenon removal, and comparing it to the measured amount of xenon poisoning (measured by control rod position).

The Pratt and Whitney Aircraft Reactor (PWAR-1) was zero-power test bed with a beryllium moderator and reflector. [7, p. 286] Critical, zero-power experiments with external heating were performed on the reactor in 1957. [36, p. 2] No evidence was found which indicated xenon behavior in the PWAR-1 was not studied. Furthermore, due to its zero power nature, its likely that studies of xenon in the PWAR-1 were not feasible.

The Molten Salt Reactor Experiment (MSRE) was an 8 MWth graphite moderated MSR built and operated in the 1960s. [6, p. 376] The MSRE underwent two distinct operational phases, one with a ^{235}U based fuel salt, starting in 1965, and another with a ^{233}U based fuel salt, starting in 1968. [37, p. 6] The two major reports that detail xenon behavior in the MSRE were ORNL-4069 and ORNL-TM-3464. [1, 2]

Two xenon models were described in ORNL-4069, one with and another without bubbles included. The experience leading to the decision to include bubbles in the model is described in ORNL-TM-1796. [38, p. 14] Both of these models included considerations for the xenon stripper, absorption into graphite, and xenon progenitors. The reactor was subdivided into 72 annular regions and

---

[3]A reactor referred to as the *Fused Salt Reactor Experiment* (FSRE) is described in the report by Ergen. [31] The description of this reactor is similar to the ARE. We posit that the FSRE is the same reactor as the ARE; however, nothing was found in the literature that explicitly stated this.

the xenon poisoning was formulated for each region. The per-region poisoning was weighted by the adjoint flux, and the poisoning for the entire reactor was found by summing the poison fraction across all the regions. Sensitivity analyses were performed with both models. ORNL-4069 (published in 1967) indicated that at higher void fractions, the majority of the xenon would be found in the circulating bubbles rather than the graphite or fuel salt. [1, p. 56] This finding is preceded by a report, ORNL-4037, wherein Prince et al. state:

> "This plot [showing xenon distribution in graphite, fuel-salt, and bubbles as a function of circulating void fraction] shows circulating bubbles work to decrease the loss of reactivity to ^{135}Xe . As the void fraction is increased, most of the dissolved xenon migrates to the bubbles, dropping the dissolved xenon concentration greatly. The concentration potential [driving force] necessary for ^{135}Xe to migrate to the graphite is reduced accordingly." [17, p. 15]

This was a new development, for in 1961 the analysis by Miller that ignored the circulating bubbles showed that given his assumptions, the majority of xenon was found in the graphite. [13, p. 7] The claim in ORNL-4069, that bubbles may contain significantly more xenon than the fuel salt, was corroborated in ORNL-TM-3027 (published 1970) which states few bubbles dispersed in the fuel salt can contain far more xenon than all of the fuel salt. [30, p. 47] ORNL-4069 concludes with the following xenon-related conclusions [1, p. 58]:

1. The presence or lack of bubbles has a significant impact on the outcome of the model. When bubbles were included in the model, the xenon poison fraction could be made to agree with preliminary observed xenon poison fractions.

2. Many assumptions including the volatization of iodine were made in the model, and the model ought not be considered final.

3. ^{135}Xe poisoning shows an insensitivity to the void fraction and diffusion coefficient of the graphite.

Note that the insensitivity to void fraction and diffusion coefficient need not imply anything about the magnitude of the xenon poisoning.

The other major report detailing xenon in the MSRE was ORNL-TM-3464, written in 1971. [2] The report provides a description of processes affecting ^{135}Xe behavior in the MSRE; predictions about MSRE xenon behavior; observations of xenon behavior during the MSRE operation; an analysis of xenon within the MSRE cover-gas; details the generation of a model that describes the MSRE xenon behavior; and discusses the results of this model.

Two separate xenon models were developed in ORNL-TM-3464, one for a soluble, and another for an insoluble cover-gas. The model that assumed a soluble cover-gas used a separate coupled cover-gas model, whereas the model that assumed an insoluble cover-gas used an integrated cover-gas model.

The structure of the xenon model was as follows: regions contained sub-regions, which contained nodes. One isotopic species concentration was associated with each node. The fuel-loop was treated in four regions, each treated as a well-stirred tank. The regions were the pump-bowl piping and heat exchanger, reactor core, and piping to the pump bowl. The piping and heat exchanger was further divided into liquid and gas-bubble sub-regions. The reactor core was subdivided into a liquid region, a gas-bubble region,, and six graphite sub-regions. The piping to the pump bowl was identical to the piping and heat exchanger sub-region in that it contained both liquid and gas-bubble sub-regions. Finally, the pump bowl had sub-regions for the gas-space, old (previously circulated) bubbles, and liquid. Each sub-region had nodes for ^{135}I, ^{135}Xe, and ^{135m}Xe, where appropriate. The graphite within the core was subdivided into four radial regions with mass-transfer between the regions accounted for by diffusion. Subdivision was in the radial direction. However, unlike the xenon model in ORNL-4069, subdivision in the axial direction was not considered. Each radial region had an appropriate regional flux and nuclear importance incorporated within. Each of the nodes had a material balance equation written on it in the form of a system of first-order linear differential equations. This system was then solved for both the steady-state solution vector as well as for the transient behavior.

ORNL-TM-3464 concludes the following: [2, p. 96]

1. The totality of xenon behavior for MSRs had not been accurately predicted by prior analyses.

2. Subsequent analyses have been partially successful in describing xenon behavior, but there continues to be areas of uncertainty.

3. There was a considerable difference in xenon behavior depending on if Helium or Argon cover gas was used.

4. Attempts at reactor behavior description required liquid/gas mass transfer coefficients, and stripping efficiencies substantially different than the predicted values.

5. A description of xenon behavior required considerations for mass transfer from the circulating voids to the graphite.

6. The circulating void to graphite behavior was a function of both circulating void size and fraction.

Finally, ORNL-TM-3464 posses a set of five research questions. The authors of ORNL-TM-3464 believe the answer to these research question will lead to increased accuracy in the modeling of MSR xenon behavior. No detailed attempts at answering these questions have been found.

1.4 Properties of Relevant Isotopes and Fuel Salt

There are three isotopes we are chiefly concerned with, ^{135}Te, ^{135}I, and ^{135}Xe. Some analyses, such as that in ORNL-TM-1070 [16] ignore tellurium. The effects of ^{135m}Xe have also been investigated in ORNL-TM-3464 [2] and by Eades. [26]

The poison isotopes progress down the decay chain through nuclear decay. The ^{135}Te $\rightarrow^{135}$I $\rightarrow^{135}$Xe chain with a ^{135m}Xe branch is depicted in Figure 6. ^{135}Te decays into ^{135}I through a beta minus decay with a 19 s half-life. [39,
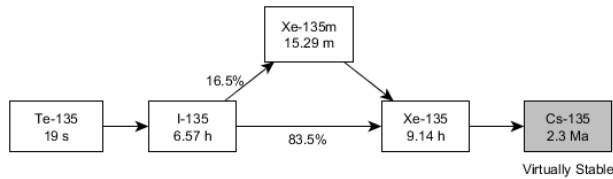
Figure 6: Xenon decay chain

p. 56] Iodine then undergoes a beta minus decay and transmutes into either ^{135}Xe or its meta-stable form, ^{135m}Xe with a 6.57 h half-life. [ibid.] Any ^{135m}Xe formed de-excites into ^{135}Xe through a gamma emission with a 15.3 min half-life. [26, p. 298] ^{135}Xe finally transmutes into ^{135}Cs with a half-life of 9.14 h. [39, p. 56] The ^{135}Cs is virtually stable with its 2.3 Ma half-life. [ibid] All of these isotopes are also produced directly from fission, as products of other nuclear reactions, and from radioactive decay.

The thermal neutron absorption cross section for ^{135}Xe is 2.6 Mb. [40, p. 54-9] The neutron absorption cross section for ^{135}Xe averaged over the MSRE neutron spectrum is 1.18 Mb[4]. [1, p. 42] The xenon model in ORNL-4069 did not include any considerations of ^{135m}Xe; however, the xenon model in ORNL-TM-3464 did. The ORNL-TM-3464 xenon model did not include any consideration for neutron absorption in ^{135m}Xe since the cross-section was was unknown at the time. [2, p. 3] Since then, Eades, who reported the ^{135m}Xe thermal neutron absorption cross-section is 10 Mb, has investigated its effect on MSRs. [26]

The thermophysical properties of molten salt influences the behavior of xenon in a MSR. Yoder warns that the accuracy of heat transfer correlations in molten salt systems are limited by the accuracy of the thermophysical properties. [41] By extension, the accuracy of mass-transfer correlations, through heat/mass transfer analogies, are limited by the accuracy of thermophysical properties. Some sources of thermophysical data for use in modeling efforts are given by Cantor, Sohal, Lopez and Janz. [42, 43, 44]

---

[4]This claim is based on a personal communication between the authors of ORNL-4069 and B.E. Prince. No details as to how this value was arrived at are given.

In the work by Cantor, fuel salt F4 is closest in composition to the MSRE fuel salt as given in ORNL-TM-0728. The uranium enrichment of fuel salt F4 was not found. Nevertheless, given the 1.3% difference in mass between ^{235}U and ^{238}U, the difference in thermophysical properties between enriched an unenriched fuel salt can be assumed to be negligible. In addition to these data, Grimes, Blander, and Watson give information on solubility limits and Henry's constants for xenon and other noble gasses. [45, 46, 47] We observe there is a temperature and pressure dependence for Henry's constants and the xenon solubility limits. An equation for Henry's constant for noble gasses in molten salts, is given by Petrucci, [48, p. 239]

$$H = \text{Exp}\left(\frac{-18.08r^2\sigma}{RT^{[K]}}\right), \tag{1}$$

This equation may be used if Henry's law data cannot be found for a particular salt.

1.5 Xenon Production and Evolution

Xenon and its progenitors are produced as fission products. It is assumed that neutron induced fission is the only significant source of fission in an MSR, and fission pathways such as photofission or muon induced fission from extraterrestrial radiation are insubstantial.

The fission production rate is given by:

$$\dot{N}_i = \int\int_{RC} \gamma_i \Sigma_f(E, \vec{x})\phi(E, \vec{x})dVdE, \tag{2}$$

where the volume of integration is the reactor core (in-core) volume (i.e., not the external loop - ex-core). The fission yield γ_i is a probability of producing a particular fission nuclide and depends on the actinide in which the fission occurs, and the incident neutron energy. The Japanese Atomic Energy Agency maintains a user friendly database of fission product yields (JENDL). [49] The fission product yields of xenon and its progenitors for some actinides commonly used as nuclear fuel are shown in Table 3.

Table 3: Fission product yields (in % of fissions resulting in a given product) of xenon and its progenitors for three different actinides. [49]

	Xe-135	I-135	Te-135
U-235	0.257	2.935	3.225
Pu-239	1.066	4.286	2.192
Pu-241	0.227	3.001	3.729

Two observations can be made from this table. First, ^{135}Xe has the smallest fission yield compared to ^{135}I and ^{135}Te . First xenon poisoning predominately arises from the progenitor inventory rather than directly from fission. Second,

since the nuclear fuel changes actinide composition with burn-up, and the fission yield is a function of actinide it occurs in, it follows that the xenon poisoning will also change as the fuel undergoes burn up.

The time evolution of xenon in the system, without any mass transfer, can be described by set of three coupled ordinary differential equations:

$$\dot{N}_{Xe} = \gamma_{Xe}\Sigma_f\phi V_{RC} + \lambda_I N_I - \lambda_{Xe}N_{Xe} - \Sigma_a^{Xe}\phi V_{RC}, \tag{3a}$$

$$\dot{N}_I = \gamma_I\Sigma_f\phi V_{RC} - \lambda_I N_I + \lambda_{Te}N_{Te}, \tag{3b}$$

$$\dot{N}_{Te} = \gamma_{Te}\Sigma_f\phi V_{RC} - \lambda_{Te}N_{Te}. \tag{3c}$$

The terms in equation 3 are of two types, a fission production term:

$$\dot{N}_i = \gamma_i\Sigma_f\phi V_{RC}, \tag{4}$$

which is similar to equation 2, except with the integration across energy carried out and the space integration replace by multiplication by volume; and, a decay term:

$$\dot{N}_i = \lambda_i N_i, \tag{5}$$

which can either be a source or sink depending on its sign.

The nomenclature for the symbols used in these equations is found on 42.

Appendix A of ORNL-TM-4541 provides the rate balance equations:

$$\{\text{Generation rate}\} = \{\text{burnup rate in salt}\}$$
$$+ \{\text{migration rate to graphite}\} \tag{6a}$$
$$+ \{\text{migration rate to bubbles}\},$$

$$\{\text{Migration rate to graphite}\} = \{\text{decay rate in graphite}\}$$
$$+ \{\text{burnup in graphite}\}, \tag{6b}$$

$$\{\text{Migration rate to bubbles}\} = \{\text{decay rate in bubbles}\}$$
$$+ \{\text{burnup in bubbles}\} \tag{6c}$$
$$+ \{\text{stripping rate in bubbles}\}$$

for noble gas migration in an MSR. [3, p. 170]

A typical migration term can be expressed in the form: [ibid.]

$$\{\text{Migration rate}\} = k_m A(C - C_{int}). \tag{7}$$

The derivation of expressions for migration rates will be discussed later. It is then seen that the quantity of xenon in the system is a function of time:

$$N_{Xe} = N_{Xe}(t). \tag{8}$$

The macroscopic absorption cross-section is the probability Σ_a that a neutron, traveling through a medium, will become absorbed in the medium, per unit length. The macroscopic absorption cross-section can be conceptualized

17

as having two components, the absorption cross-section of the reactor material itself Σ_a^r, and the absorption cross-section of the xenon in the system Σ_a^{Xe}. Thus, we can express the absorption cross-section of the reactor as:

$$\Sigma_a = \Sigma_a^r + \Sigma_a^{Xe}. \tag{9}$$

Seeing that the xenon quantity in the reactor is a function of time, it follows that the macroscopic absorption cross section is likewise a function of time:

$$\Sigma_a = \Sigma_a(t) = \Sigma_a^r + \sigma_a^{Xe} N_{Xe}(t). \tag{10}$$

The neutron diffusion equation can then be written as:

$$\frac{1}{v}\dot{\phi} = \nu\Sigma_f\phi - (\Sigma_a^r + \sigma_a^{Xe} N_{Xe}(t))\phi - \nabla^2\phi. \tag{11}$$

It is thus seen that the presence of xenon in the system affects the time-evolution of neutron flux in the reactor and we frame the proceeding discussion with this knowledge in context.

1.6 Philosophical Considerations of MSR Xenon Theory

We see that MSR xenon analysis exists at a certain *level of analysis* that includes some phenomena and neglects others. Deeper levels of analysis include more phenomena than shallow levels of analysis. We note that there is not a singular MSR xenon theory, in the sense there is a singular Newton's law of universal gravitation; rather, each attempt at the construction of a MSR xenon model can be seen as an attempt at the furthered development of a theory. This is congruent with the notion that action precedes understanding in the sensemaking process. [50, p. 642]

Nevertheless, we can state whatever MSR xenon theory has been developed is *intelligible*[50, p. 31] in that it is amenable to a pragmatic application of the theory to generate models, as evidenced by the prior models developed for MSR xenon analysis. That said, MSR xenon theory is not *coherent* as there is no singular framework for predicting xenon behavior, rather, it is a patchwork of theories that has been combined together to generate a model; for example, the difference between the measurement and application environment of Henry's constant.

2 Assumptions and Considerations

2.1 Iodine and Tellerium Behavior

The behavior of ^{135}I and ^{135}Te is governed through an *in-solution assumption*, in which they are both assumed to remain in solution in the fuel-salt and not migrate to the bubbles, circulating voids, or cover-gas.

The iodine in-solution assumption may not be entirely accurate. ORNL-4865 reported salt samples from the MSRE had a portion[5] of their expected ^{131}I missing. [51, p. 28] Contrary to this, ORNL-4069 claims very little iodine was found in the MSRE off-gas system. [1, p. 42] Additionally, ORNL-4069 states an unpublished internal report that discussed the volatilization of free iodine in the MSRE supports the iodine in-solution assumption vis-á-vis its thermodynamic properties. [ibid.] Furthermore, when the iodine in-solution assumption was stated in ORNL-TM-3464, a reference to ORNL-3913 was given, presumably as a justification for the assumption. [52, p. 38-40] ORNL-3913 describes an experiment in which the iodine was removed from a FLiBe (Fluorine Lithium Beryllium) melt by reaction with HF gas; however, no explanation was found as to how the findings of the experiment relate to the validity of the in-solution assumption.

The tellurium in-solution assumption is justified by considering the 19 s half-life of ^{135}Te . [1, p. 42] ORNL-4865 claims tellurium would act as a dissolved gas in a manner similar to xenon given its vaporization temperature. [51, p. 29] We posit a mass transfer processes affecting tellurium would need to do so on a time-scale comparable to the ^{135}Te half-life in order for the tellurium in-solution assumption to be invalid.

Finally, the burn-out of ^{135}I and ^{135}Te is assumed to be negligible. This is justified on the grounds that the neutron absorption cross-section of both ^{135}Te and ^{135}I is on the order of 1 b. [53]

2.2 Xenon Behavior

Xenon is a noble gas and does not normally form chemical species. Past work has assumed xenon is in a free atomic gaseous state in the fuel-salt, and free to migrate about the primary circuit. This may not be entirely true. Xenon was found to form a compound with fluorine, XeF_2 when subject to radiation, heat, or light. [54] A discussion of noble gas compounds is given by Asimov. [55, p. 228] Mackenzie and Wiswall irradiated a sample of xenon and fluorine with gamma radiation from a ^{60}Co source and observed the synthesis of xenon compounds. [56]

That being said, it is foreseeable that the formation of xenon compounds would depend on the availability of free fluorine to bond with. Details about the amount of free fluorine in MSRE fuel salt were not found. The following considerations may be useful in a discussion about the existence of free fluorine. Sridharan and Allen [57, p. 252] state that the higher valence states of $UF_{(n)}$ compounds added to the fuel salt can undergo multiple reductions, which would liberate free fluorine into the salt. Ignatiev [58, p. 266] states polyvalent salts, such as $UF_{(n)}$, are *acidic* and tend to form complexes with F^-. Delpech [59, p. 39] reports the BeF_2 in FLiBe tends to form compounds with fluorides; the amount of free fluorine in FLiBe depends on the LiF/BeF_2 ratio; and, in the case of 66-34 mol% LiF-BeF_2, the activity of free fluoride atoms is very low.

---

[5]Most samples had between 30-60% of their ^{135}I missing

Further, ORNL research in the 1970s indicated that intergranular attack on primary circuit's structural alloy (Hastelloy-N) can be much reduced by controlling fuel salt's oxidation potential, expressed as a ratio of U_{4+} over U_{3+}, at below 60. [60] Such control may be necessary in any future MSR, and would keep the amount of free fluorine very low.

If the activity of fluorine in a salt melt is high, then it is foreseeable that there may be some binding of xenon. Nevertheless, for the purposes of MSR xenon theory, we assume that xenon does not form any compounds. No investigations nor mass transfer theories were found that accounted for the potential of xenon compound formation.

2.3   Ideal Dilute Solution and Ideal Gasses

The mass transfer equations in MSR xenon analysis, discussed in Section 4.1, use the ideal gas law, $p = CRT$, and Henry's law, $C = Hp$, in their formulation. The application of Henry's law assumes an *ideal dilute solution* of xenon in the molten salt in which the concentration of xenon approaches zero. As the xenon/salt solution deviates from an ideal dilute solution, so does its adherence to Henry's law. Furthermore, the application of the ideal gas law assumes the gas pressure is sufficiently low that collisions of gas molecules are negligible.

A number of other equations of state exist such as the van der Waals or Peng-Robinson equations. A measure of the ideality of a gas can be found using the compressibility factor, $Z = pV/nRT$, which for ideal gasses is defined as 1. NIST REFPROP [61] contains compressibility factor data for many substances. No analyses were found that accounted for non-ideal gas behavior.

In consideration of the ideal dilute solution assumption, we observe the following: Fletcher reports a macroscopic discrete phase inclusion will form if the radius of an embryo of dispersed phase atoms exceeds the critical radius: [62]

$$r_c = \frac{2\sigma}{\Delta G_V}. \tag{12}$$

Westh and Haynes investigated the bounds of the domain of dissolved gas concentrations where Henry's Law is applicable, the Henry region, in water and hexane using a number of solutes. [63] Westh and Haynes were unable to determine the Henry region due to the limits of the calorimeter used; however, they were able to give a lower limit for non-Henry behavior on the order of 10^{-4} for hexane solvents and solutes, and 10^{-5} for a water solute and a number of solvents. As previously mentioned, Grimes, Blander, and Watson established solubility limits for xenon in molten salts, above which no further xenon could dissolve in their experimental apparatus. [45, 46, 47]

Given these observations, consider Figure 7 which represents all potential concentrations of xenon and other-gases within the molten salt system. There is then, three regions: H, N, and B. The Henry region, H, is where Henry's law is applicable; the Non-Henry region, N is where Henry's law is not applicable, but the salt melt has yet to reach gas saturation; finally, B, the *bubble-out region*, is
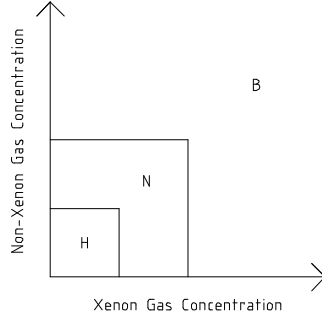
Figure 7: MSR gas concentration map

where the salt-melt has reached saturation and additional gas evolution forms dispersed gas-phase inclusions rather than dissolving into the salt melt. No evidence has been found that indicates the H/N boundary exhibits any sort of sharp discontinuous behavior, and we suspect the transition from Henry-like to non-Henry-like behavior exhibits a *smooth* character. One potential criterion for the H/N boundary is a xenon concentration such that the ratio of the xenon to partial pressure is greater than multiple, K, of the Henry constant for xenon in the salt melt,

$$C_i^L \text{ S.T. } \frac{C_i^L}{P_i^G} > KH_i. \tag{13}$$

Since the Henry constant is a function of temperature, pressure and composition, it likewise follows the location of the H/N boundary is a function of temperature, pressure, and composition.

Consider a volume of salt melt with xenon and other gasses dissolved in it. This salt melt also contains actinides that are undergoing fission. As the actinides undergo fission a fraction of their fission products are gaseous. If we track the behavior of these gaseous fission products, including xenon, then there is a certain probability per unit time that the gaseous products will join a gas embryo of radius greater than the critical radius, as given by Equation 12. This probability is a function of the quantity of the gas within the salt melt. We therefore posit the N/B boundary is a concentration of all gasses in the salt melt such that a gas atom is more likely than not to join a gas embryo of radius greater than the critical radius.

The critical radius is a function of the surface tension and Gibbs free energy, which are in turn are functions of temperature and composition. Furthermore the Gibbs free energy is a function of pressure. Since the location N/B boundary is a function of critical radius, it follows that the N/B boundary location is

likewise a function of temperature, pressure, and composition.

Our review indicates all MSR xenon models to date have assumed the reactor operated in the H region.

2.4   Well Mixed Fuel Salt

Both Eades et al. and Wu et al. have developed one-dimensional models of MSR xenon poisoning. [26, 28] Eades et al., split their 1D MSR model into in-core and out-of-core equations, and found the zero-dimensional model agrees with the 1D model. Wu et al. found that at low power, the circulation of the fuel salt decreases ^{135}I and ^{135}Xe concentration up to 50%. In ORNL-4069 the fuel salt was assumed to act as a well stirred tank for xenon. [1, p. 21] The same assumptions was made for ORNL-TM-3464. [2, p. 6] These assumptions are justified on the condition,

$$t_{1/2}^{Xe} >> t_{Circ}. \tag{14}$$

This condition may not also be true for ^{135}Te with its 19 s half-life; however, ^{135}Te itself has no substantial impact on reactor neutronics, and the condition certainly holds for its successor, ^{135}I .

2.5   Nobel Gas Decay and Graphite Non-Homogeneity

Prior investigations of MSR xenon behavior have assumed both the mass diffusion coefficient of the graphite, D_g, and the graphite void fraction, ϵ, were invariant with respect to position and time; that is, the graphite stringers were assumed to be homogeneous right cylinders. Furthermore, the rate of diffusion of xenon into the graphite is assumed to be uniform with respect to the radial and axial position. Converse to this, we have identified three phenomena that may lead to stringer non-homogeneity: fission product decay, pressure differential induced xenon cross-flow, and non-homogeneity from manufacturing. Fission product decay and cross flow are operational causes of non-homogeneity whereas manufacturing non-homogeneity is pre-operational.

When ^{135}Xe, a noble gas, undergoes a beta minus decay, it transmutes into the alkali metal ^{135}Cs. If Cs-C or another compound accumulates within the pore space the void fraction and mass diffusion coefficient will be affected. The formation of Cs-C from ^{135}Xe was investigated by Baes. [17, p. 15] Baes used some assumed values to calculate partial pressure of ^{135}Cs in the graphite due to migration from the partial pressure of ^{135}Xe in the salt-graphite surface. Baes concluded:

1. The amount of ^{135}Cs accumulation in the graphite is "very small".

2. If it is assumed that all the ^{135}Cs born in the graphite were to remain in the graphite, the rate of accumulation would be low.

No investigations on the accumulation of other species due to the transmutation of other fission products were found.

22

Additionally, since the graphite is porous, two fuel channels opposite of each other will induce a pressure differential across the channel if the flow conditions are dissimilar. Diffusion across the porous graphite was the subject of the *counter diffusion experiments* reported in ORNL-4148. [19, p. 23] We propose extended flow across a graphite stringer, through its pore space, will result in non-uniform changes to the pore structure of the stringer.

The manufacturing process of the graphite stringers may result in a non-homgeous pore structure. ORNL-4148 reports the MSRE graphite stringers being installed in the MSRE were non-homogeneous. [19, p.25] Furthermore, it was stated impregnation treatments, which reduce the graphite pore size, non-uniformly change the graphite pore structure.

2.6 Isothermal Henry's Constant

Henry's constants are tabulated as a function of a single temperature. In Robbin's *static head-space method* [64], which determines Henry's constant, a constant temperature bath was used to keep both the liquid and gas being measured in isothermality with each other. MSR graphite is subject to both the heat transfer with the salt as well as the heating from gamma and neutron collisions. ORNL-TM-0378 reports a steady state difference in graphite and fuel salt temperature in the MSRE on the order of $30\,°C$. [65, P. 42] Information on applicability of Henry's law to a situation in which the liquid and gas phases are at different temperatures was not found. Prior analyses have used a single, temperature invariant, Henry's constant.

Furthermore, Henry's law is defined for a system at equilibrium. An MSR is not at equilibrium. No information was found on the application of Henry's constant to non-equilibrium systems.

2.7 Considerations in Nuclear Pathway

Prior xenon analysis assume the $^{135}Te \rightarrow ^{135}I \rightarrow ^{135}Xe$ decay pathway is the only means through which xenon may enter the system. Firestone et al. [66] state the A=135 decay pathway begins with ^{135}Sb, with its $1.71\,s$ half-life and 0.145% thermal fission yield from ^{235}U. Firestone et al. [ibid.] also report ^{135}Xe production has been observed in (p,d) and (d,t) reactions.

Activation of ^{135}Xe into ^{135m}Xe has also been been frequently ignored in prior analyses. Chu [67] reports ^{135}Xe activation may occur both with thermal and fast neutrons. ORNL-TM-3464 [2] accounts for mass transfer of ^{135m}Xe but assumes the neutron absorption cross-section to be negligable. The neutronic effects of ^{135m}Xe on MSR xenon poisoning was investigated by Eades et al. [26] All other analyses we are of aware of have ignored the effects of ^{135m}Xe.

2.8 Dynamics of Constants

In prior analyses, the mass transfer coefficients, diffusion coefficients, and Henry's constants used in MSR xenon analyses are assumed to be invariant with respect

to dynamic behavior. That is, they are expressible in terms which includes no time derivatives. For example, ORNL-4069 derived mass transfer coefficients from a heat/mass analogue of the Dittus Bottler equation. [1, p. 71]

Liu and Fukuda measured the Nusselt number of a horizontal heated cylinder in a helium gas flow. [68] The experiment was performed with both transient and steady-state heat production in the cylinder. In the transient case, the heat applied followed an exponential function in time. Liu and Fukuda found the ratio of transient and steady-state Nusselt number exceeded 1 only when the period of the heat transient was shorter than 1 s. Mass transfer analogies provide a conversion between heat transfer coefficients and mass transfer coefficients. [69, p. 159] Since there exists a particular case wherein the transient Nusselt number was different than the steady-state Nusselt number, it follows the transient mass transfer coefficients in an MSR may be different than a steady-state mass transfer coefficients. No work using transient mass transfer coefficients was found.

2.9   Graphite Volume Changes

There are two relevant mechanisms by which MSR graphite can change its size, irradiation induced creep (shrinkage followed by expansion), and thermal expansion. The graphite volume changes induces a corresponding volume change in the pore-space that may induce changes in xenon behavior.

Burchell et al. have reviewed of models for radiation induced creep of nuclear graphite. [70] Scott and Eatherly investigated the creep behavior of MSR graphite. [22] They reported on the radial distortion of the graphite as a function of irradiation time, but a total estimate of graphite volume change was not found in their work.

Thermal expansion also contributes to volume change of graphite. At the microscopic level, the graphite crystal lattice can expand in two directions, parallel to the hexagonal axis, and parallel to the basal plane of the lattice. Burchell, in the book edited by Delhaes, gives a discussion on microscopic thermal expansion effects in graphite. [71, p. 89]

The time-scale of irradiation induced changes in graphite volume is on the order of years, as evidenced by the conclusions of Scott and Eatherly. [22] The characteristic time for thermal changes in the MSR graphite is derived from the heat equation:

$$\rho c T_t = k T_{xx} \rightarrow \Delta t = \frac{\rho c (\Delta x)^2}{k}. \tag{15}$$

We assume the variation in the thermophysical properties with respect to temperature is negligible. Thus, as Table 2.9 shows, the time scale of thermal expansion is on the order of minutes. It therefore follows the transient irradiation creep behavior can be assumed to be static with respect to xenon transient behavior, and the thermal expansion behavior is additive to the static volume of the irradiated graphite.

Table 4: Characteristic thermal time for MSRE graphite.

Parameter	Value	Unit	Source
k	193.8 / 58.8 [1,2]	$W\,m^{-1}\,°C^{-1}\,s^{-1}$	[72, p. 11]
C	1760 [2]	$J\,kg^{-1}\,°C^{-1}$	[ibid.]
ρ	1860 [2]	$kg\,m^{-3}$	[ibid.]
L	0.051^{3}	m	[73, p. 80]
t_{Therm}	43.94 / 144.8 [1]	s	

1) Parallel and normal to the grain respectively. 2) At 650 °C. 3) Width on a side.

Table 5: Boiling point of poison species at MSRE operating pressure. Data from Wolfram Alpha. [75]

	ΔH_f $[J\,kg^{-1}]$ $\times 10^4$	T_{boil} $[°C]$ $P=101kPa$	T_{boil} $[°C]$ $P=344kPa$
Te	38.0	987	1013
I	16.5	185	198
Xe	9.6	-108	-87

2.10   The State of Mater

The MSRE had a design pressure of 344 kPa. [73, p. 78] The variation in phase transition temperature with respect to pressure can be found through the Clausius-Clapeyron equation. [74, p. 126] The boiling temperature variation can be found with:

$$T_2^{[K]} = \left(\frac{1}{T_1^{[K]}} - \frac{R}{\Delta H_v} \ln \left(\frac{P_2}{P_1} \right) \right)^{-1} , \qquad (16)$$

where T_2 and T_1 are the temperatures in Kelvin. The boiling temperatures of the poison species, at the MSRE design pressure, are shown in Table 5.

The phase transition temperature of a particular isotope differs from the phase transition temperature of the parent species of that isotope. Case in point is deuterium, which has a boiling point about three degrees higher than protium (normal hydrogen). [76, p. 23] The phase transition temperature shown in Table 5 is for the chemical species, which is mixture of isotopes of the particular species. The difference between a particular poison isotope's phase transition temperature and that of its parent chemical species can be assumed to be negligible. This is justified considering the difference in atomic mass between the poison isotope and that of its corresponding element is less than one percent.

No information was found that indicated either way that there is a change in MSR xenon behavior as the temperature of an MSR passed across a particular phase transition temperature. We believe it is unlikely that the phase of the poison species has any meaningful significance considering the poison species were mixed or dissolved in the fuel salt (I.E. can a single atom or cluster of atoms even be called a liquid or gas?). In prior work, iodine and tellurium were

25

assumed to dissolve in the fuel salt, whereas the xenon was assumed to come out of solution and effectively form a heterogeneous mixture. No information was found related to the effect inclusion of a substance in a mixture has on that substance's phase transition temperature. We propose the missing iodine, as reported in ORNL-4865 [51, p. 28], may be evidence for some distillation behavior of the iodine.

2.11 Graphite Stringer Considerations

The work of ORNL-4069 and Shimazu both modeled graphite stringers as a cylindrical transient diffusion initial boundary value problem:

$$C = C(r, t) \tag{17a}$$

$$C_t = \frac{D_g}{\epsilon} \left(C_{rr} + \frac{1}{r} C_r \right) - (\sigma\phi + \lambda_{Xe})C \tag{17b}$$

$$C_r(r = 0) = 0 \tag{17c}$$

$$C_r(r = R) = k_m \left(C_{FS} - \frac{HRT^{[K]}}{\epsilon} C \right) \tag{17d}$$

$$C(t = 0) = 0, \tag{17e}$$

Abstracting the cylindrical Laplacian into a differential operator, we can write the Equation 17b as a reaction-diffusion equation:

$$C_t = \frac{D_g}{\epsilon} \nabla^2 C - (\sigma\phi + \lambda_{Xe})C. \tag{18}$$

As shown in ORNL-TM-0728, the graphite stringers are square-cylinders with rounded square fuel channels cut into their sides. [73, p. 80] Therefore, application of Equation 17 thereby transforms the concave geometry of the graphite stringer into an *equivalent cylinder* as illustrated in Figure 8.
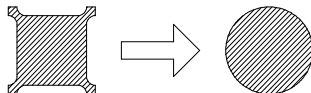
Figure 8: Transformation of graphite stringer geometry

Glicksman and Lienhard state the approximation of geometry by cylinders is a tactic used in solving heat transfer problems. [77] Beyond this no justification nor validation was found for this transformation.

Equation 17 further assumes the porous-media advection term is negligible. As mentioned in Section 2.5, diffusion experiments on a graphite specimen from the MSRE show that gas flow across the specimen was induced when a pressure differential was applied across it. [19, p. 26] Each fuel channel operates at a particular pressure which is a function of the fuel salt flow velocity and the

position of the fuel channel in the reactor. [65, p. 14] Two fuel channels operating at different pressures and contacting the same graphite stringer will induce a pressure gradient across the stringer. No investigations of xenon advection across graphite stringers was found.

Equation 17b assumes the graphite pore space to be entirely interconnected, and xenon at any point in the graphite is assumed to be able to migrate to any other point in the graphite. As expounded by Bear et al., it is possible for a porous medium to be comprised of multiple disjoint domains. [78, p. 7] Furthermore, as described in Section 2.5, there is the potential for structural non-homogeneity to exist within the MSRE graphite. This would cause D_g or ϵ to vary as a function of position.

2.12 Negligible Adsorption

In prior xenon models, adsorption onto reactor surfaces has been assumed to be negligible. Xenon can either be adsorbed directly or a xenon progenitor can be adsorbed. The review of literature has revealed four potential adsorption sinks in MSRs: the graphite pore-space, corrosion products, circulating particulate, and the reactor structural material.

ORNL-4069 states that xenon is not significantly adsorbed on graphite at MSRE operational temperatures ($\approx$657 °C). [1, p. 42] Justification for this claim is given by references to two journal articles, one by Salzano and Eshaya, and another by Cannon et al. The report by Salzano and Eshaya concerns the sorption[6] of xenon on graphite at high temperature, and concludes:

> "Above 500°C the quantity of xenon held by surface adsorption is probably less than 1% [of] that held in the voids." [79]

No information on the negligible adsorption assumption was found in the paper by Cannon et al. [80]

ORNL-TM-3464 reported corrosion scales can contain a significant holdup of iodine. [2, p. 5] Reference is made to ORNL-TM-228, presumably as a justification. [81] The evidence for iodine adsorption in ORNL-TM-228 is given with the statement:

> "A model which postulated that a pseudo-equilibrium existed between iodine in solution and that adsorbed on the walls fit most of the data obtained when it assumed that only 10% of the iodine in the high pressure system was circulating, [and] the other 90% [was] being adsorbed on the walls." [ibid. p.10]

No explicit mention of corrosion scale was found in ORNL-TM-228.

For metal adsorption, ORNL-4069 states, *"...it is unlikely xenon will be adsorbed on metal surfaces"*. [1, p. 42] No justification nor reference is given for this claim. No information was found detailing adsorption of iodine or tellurium

---

[6]Sorption refers to the superordinate process which encapsulates both adsorption and absorption.

on Hastelloy-N. No information was found on the use of another metal as an adsorption analog for Hastelloy-N.

As for poison species sorption on circulating particulate, the only information found on this was in ORNL-TM-346 [2, p. 5], in which it is stated the effect is assumed negligible. We identified one research question related to this phenomena: *what is the composition and adsorption characteristics of the circulating particulate MSRs?* The potential risk posed by this unknown adsorption term can be engineered against by limiting the amount of circulating particulate in the system (though, for example, filtration).

2.13 Valid Theory

The validity of existing work may be framed along a spectrum from totally invalid to totally valid. A totally invalid theory would be characterized by major phenomena missing and an inability to match experimental data, whereas a totally valid theory would encapsulate all the phenomena and provide predictive capabilities. It is assumed that the theory of xenon migration in molten salt reactors, as described in the ORNL reports, and articulated by Shimazu is essentially correct in its formulation and application.

That being said, the theory in itself has yet to be fully validated. The a priori xenon model developed in ORNL-4069 was felt to be essentially correct and used in online xenon calculations in the MSRE. [2, p. 16] ORNL-TM-3464 reports,

> "Although we achieved reasonable success in describing the steady-state xenon poisoning with both helium and argon cover gas, we could not adequately describe the transient behavior". [2, p. 91]

The authors believe that there is mixed evidence to support the assumption of a valid theory.

3 The Structure of The Graphite Stringers and Its Relation to Xenon Migration

An MSR core, as viewed from the top, cut along the mid-plane, has two major components, the peripheral region, and the lattice block; illustrated in Figure 9. The lattice region is comprised of a number of graphite stringers assembled in a lattice. Each lattice position is occupied by a unit cell, which consists of a graphite stringer and one or more fuel channels that have been cut into the graphite stringer. There is upward salt flow within the fuel channels of the lattice region and the peripheral region. Thus, MSRs are characterized by a number of fuel channels and graphite stringers. The number of fuel channels is prescribed by the number, geometry, and arrangement of the graphite stringers. The lattice region may be further subdivided into a number of radial flow regions based on the Reynolds number of the flow in the fuel channels in that region. The hydraulic model in ORNL-TM-0378 uses five regions to describe the MSRE core. [65, p. 13]
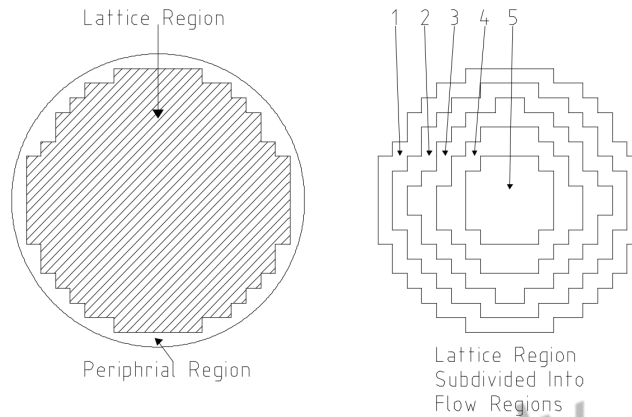
Figure 9: MSR core regions

The unit cell consists of a graphite stringer body and a number of fuel channels slots (C.F. in Figure 11). The perimeter of the stringer body is subdivided into a wetted perimeter and a dry perimeter. When two or more unit cells are arranged in a lattice, their meshed configuration creates a number of fuel channels. The perimeter of the stringer body is subdivided into a wetted perimeter and a dry perimeter. The wetted perimeter is the interior of a fuel-channel wheras the dry perimeter is the interior of an inter-stringer space (discussed later). Some potential configurations of graphite stringers are shown in Figure 10. As we can observe, the number of fuel channels may or may not be equal to the number of graphite stringers. Therefore, depending on the particular reactor being modeled, it may or may not be appropriate to simplify a graphite stringer into a single object (such as a cylinder) surrounded by fuel-salt flow.

The inter-stringer space is the space between neighbouring graphite stringers arranged in a lattice, shown in Figure 12. Either the graphite stringer are in direct contact with each other, or there is a substance between them. There may also be regions along the length of the stringer that are in direct contact, and other regions with substance between the stringers. The characteristics of the inter-stringer space may evolve as the reactor ages (creep expansion, irradiation, fission product evolution and migration, thermal expansion, etc). No information nor modeling efforts were found related to the inter-stringer space or xenon migration in it. Homogenization of graphite stringers, which has been preformed in prior analyses, assumes the inter-stringer space presents a negligible impediment to mass transfer between stringers.

29
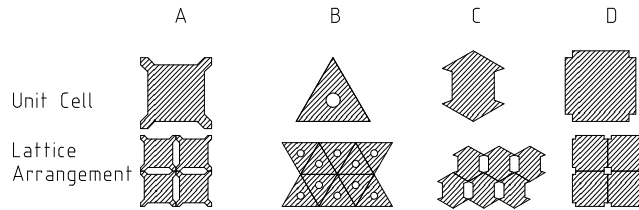
Figure 10: Types of MSR stringers
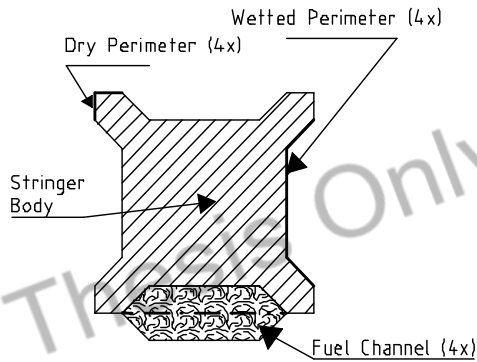
Figure 11: A unit cell

Graphite stringers can be classified as either interior, exterior, or equipment contacting. This is shown in Figure 13, which depicts an MSR core comprised of square graphite stringers with rectangular fuel channels located on the sides of each stringer. There are five lattice locations, indicated by black circles, where equipment such as sample baskets or control rods are inserted into the core. The graphite stringers which are next to these equipment locations may be called equipment contacting stringers, indicated by the letter A. The letter B indicates interior graphite stringers which are completely surrounded by other stringers. Finally, the graphite stringers which are at the periphery of the core lattice are called exterior stringers (letter C). The exterior stringers are typified by contact of a peripheral fuel-salt flow on one or more face of the stringer.

4 Mass Transfer

4.1 Mass Transfer Across Phases

Equation 7 can be derived as follows, the term C_{int} in the equation is, in some sense, not well defined. The liquid interface can be defined as the monolayer of atoms that are in contact with the gaseous phase, whereas concentration is a volumetric term. To overcome this difficulty, we employ the *two-film model* to model the rate of mass transfer across a gas/liquid phase interface. Figure 14 shows a phase interface as conceptualized by the two-film theory.

The two-film model is detailed by Albright. [82, p. 604] In brief, the model partitions space into bulk liquid, liquid film, gas film, and bulk gas layers. Between the liquid and gas film layers is a liquid/gas interface. Each film layer is modeled by Whitman's stagnant film model wherein each film layer is of thickness x_0 and is assumed quiescent. [ibid. 602] The mass transfer process is then governed by diffusion and the mass flux across the film layer is governed by Fick's first law,

$$J = -DC_x, \tag{19}$$

where the diffusion coefficient is the mass diffusion coefficient for a particular solute.

The mass transfer coefficient for a given film layer is defined as:

$$k_m = \frac{1}{R_m} = \frac{D}{x_0}. \tag{20}$$

In this way the mass transfer problem can be reduced to a series resistance problem, illustrated in Figure 15

According to Perry, the mass diffusion coefficients of gasses are much greater than that of liquids. [83, sec. 5 p. 48]

Therefore, since:

$$D_g >> D_L, \tag{21}$$

and, considering Equation 20, it follows:

$$R_m^G + R_m^L \approx R_m^L, \tag{22}$$

and the overall mass transfer coefficient, $K_m \approx 1/R_m^L$.

We can thus approximate the mass transfer across the phase interface as:

$$J = K_m(C_B^L - C_{int}^L). \tag{23}$$

We next invoke Henry's law for an ideal gas which states:

$$\lim_{C^L \to 0} \frac{C^L}{P^G} = H. \tag{24}$$

More information on Henry's law is given by Albright. [82, p. 13] Applying Henry's law, Equation 23 can be rewritten as:

$$J = K_m(C^B - HP_i^{F,G}). \tag{25}$$

31

Since the relative magnitude of the mass diffusion coefficient of xenon in a gas is much greater than the relative magnitude of the mass diffusion coefficient of xenon in a liquid, it follows that the diffusion of xenon on the gas side of a gas/liquid interface will be much faster than the diffusion process of xenon in the liquid side. Therefore, from the perspective of the liquid diffusion process time scales, the equilibration process on the gas side is effectively instantaneous and therefore we assume, the partial pressure of the dissolved gas in the gas film layer is approximately equal to the partial pressure of the gas in the bulk:

$$P_i^{F,G} \approx P_i^{B,G}. \tag{26}$$

Thus:

$$J = K_m(C^B - HP_i^{B,G}). \tag{27}$$

Invoking the ideal gas law, $P = CRT^{[K]}$, we write

$$J = K_m(C^{B,L} - HRT^{[K]}C^{B,G}). \tag{28}$$

Forms of this equation are ubiquitous in MSR xenon analysis literature.

In the transfer of mass from the fuel salt to graphite, the concentration term for the graphite is divided by an effective void fraction term:

$$J = K_m \left(C^{B,L} - \frac{HRT^{[K]}}{\epsilon} C^{B,G} \right), \tag{29}$$

so the porosity of the material is accounted for.

4.2 Fuel Channel Mass Transfer Coefficients and Analogies

No information was found that detailed experimental work done to determine the fuel-salt to fuel-channel xenon mass transfer coefficient. The fuel channel mass transfer coefficient in ORNL-4069 was calculated via heat transfer correlations (including the Dittus Bottler correlation) that had their Nusselt numbers replaced with Sherwood numbers and the Prandtl numbers replaced with the Schmidt numbers. [1, p. 71]

The justification for this technique is based on the analogy (isomorphism principle) of heat and mass transport; the Sherwood number is the mass transfer analog of the Nusselt number and mutatis mutandis the Prandtl and Schmidt numbers. [84, p. 21, 504] We are concerned with the applicability of the Dittus Bottler correlation, given the flow in the MSRE fuel channels was found to be laminar whereas the Dittus Bottler equation is for a turbulent flow. [85, p. 37] [86, p. 5.26]

Yoder [41] examined the correspondence of a Dittus Bottler like heat transfer correlation (as well as several other heat transfer correlation) in molten salts down to a Reynolds number of ∼5,000. Yoder concludes the standard deviation of the heat transfer predictions is relatively large for Reynolds number <40,000.

There are many other ways to determine the mass transfer coefficient through analogy, and these methods are reviewed, in the case condensation of an air/steam mixture on a flat plate, by Ambrosini, Forgione, and Oriolo, who conclude there is *"limited discrepancy"* among the different types of mass transfer analogies. [87] It should be noted the fuel channels of the MSRE were not completely circular cylinders, they were rounded rectangles. [73, p. 80] No information was found pertaining to forced convection mass transfer correlations in rounded rectangular ducts.

Finally, we posit since (A) the mass transfer correlation are given in terms of Reynolds and Schmidt numbers, and (B) Reynolds and Schmidt numbers are functions of temperature and flow conditions, (C) it follows that the mass transfer coefficients, and thus the xenon behavior in an MSR, is likewise a function of the fuel salt flow velocity and temperature $(A \wedge B \implies C)$:

$$k_m = k_m(v, T^{[°C]}). \tag{30}$$

4.3 Diffusion

There are two diffusion coefficients used in the formulation of MSR xenon theory, one for diffusion within the graphite, and another for diffusion within the fuel salt.

The diffusion coefficient in the graphite is a function of the atomic mass of the diffusing species. ORNL-4069 [1, p. 65] reports two different graphite mass diffusion coefficients were used in their calculations, one for Xenon and one for Krypton. The porous media mass diffusion coefficient encapsulates a number of mechanistically different diffusion phenomena such as viscous diffusion, Knudsen diffusion, surface diffusion, and molecular sieving. [88, p. 190]

The Knudsen mechanism was the dominate mechanism of diffusion in MSRE graphite. [19, p. 37] The Knudsen diffusion coefficient can be predicted from the expression: [88, p. 194]

$$D_{Kn} = \frac{L_{Pore}}{3} \left(\frac{2K_B T^{[K]}}{m} \right)^{1/2}, \tag{31}$$

ORNL-4389 [21, p. 12] states after impregnation, the primary peak of the MSRE graphite porosity distribution occurred at $80\,\text{nm}$. The MSRE graphite temperature was between 679 and 704 °C. [3, p. 56] Given these parameters, Equation 31 evaluates to $8.7 \times 10^{-7} \text{cm}^2/\text{s}$, which is within the range of mass diffusion coefficients, 3.0×10^{-8} to $8.7 \times 10^{-5} \text{cm}^2/\text{s}$ considered feasible in the MSRE. [2, p. 54]

The mass diffusion coefficient for xenon in the fuel salt is used in the calculation of mass-transfer coefficients through the Sherwood number:

$$\mathbf{Sh} = \frac{k_m L}{D}, \tag{32}$$

which is given from mass transfer correlations of the form: [88, p. 257]

$$\mathbf{Sh} = f(\mathbf{Re}, \mathbf{Sc}). \tag{33}$$

ORNL-4069 [1, p p.62] states the mass diffusion coefficient can be found through analogy to a heavy metal, water system; however, the way in which this is done was cited as a personal communication to C. Chester. No documentation of this personal communication were found. Details about the use of a water analog in a molten metal system were found in a paper by Kang et al. [89, p. 107]

In addition to the heavy-metal, water analog, ORNL-4069 state the mass diffusion coefficient may be found through the Wilk-Chang equation and Einstein-Stokes equation. [1, p. 62] Zhang offers discussion on means by which the mass diffusion coefficient may be calculated for ionic liquids. [90, p. 11] Wilkes states there is no fundamental difference between molten salts and ionic liquids beyond the arbitrary choice of melting temperature, therefore, the discussion of ionic liquid mass diffusion coefficients may be applicable to molten salts. [91]

The Einstein-Stokes equation:

$$D = \frac{K_B T^{[K]}}{6\pi\mu r_{Xe}},$$
(34)

requires three parameters, the temperature, the viscosity, and the atomic radii. [88, p. 127]

Brockis and Reddy discuss the applicable of the Einstein-Stokes equation to molten salts and state:

> "The essential applicability of this phenomenological equation is clearly shown by using the numerical comparison of $D\mu/T = K_B/6\pi r$. The right-hand side is 0.7×10^9 for $r = 300 \, \text{pm}$, and the mean of the experimental values is 0.6×10^9, which is not bad!" [92, p. 654]

Viscosity data can be found in the sources by Cantor, Sohal and Janz as described in Section 1.4. [42, 43, 44] A discussion of sources for molten salt viscosity data is given in the chapter by Lizin in Dolan's book. [7, p. 388] If no experimental data are available, viscosity may be estimated from either theoretical means or from methods based on the principal of experimental additivity, as discussed by Bretsznajder and Dankwerts. [93, p. 205]

We are unsure about what atomic radii data would be best suited for calculations. The Einstein-Stoke equation is derived assuming (1) the diffusing particle is a hard sphere, and (2) the diffusing particle is much larger than the particles in which it is diffusing. Pau, Berg, and McMillan state, in the context of the Stokes law:

> "One of the most difficult questions involved in the transition from a continuum medium to the case of real solvent molecules of size comparable to the atomic dimensions of the mobile ion is unit is the meaning to be attached to the particle 'radius' ". [94]

Several potential atomic radii are listed in Table 6.

Table 6: Atomic radii of xenon.

Type	Radius [Å]	Reference
Covalent Radius	1.36	[95, p. 9-58]
van der Waal's Radius	2.16	[ibid.]
Lennard-Jones Collision Radius	2.02	[96, p.24]
Kinetic Theory	1.75	[97, p. 249]

Given the radiation field present in an MSR, an additional complexity arises in considering the effect xenon ionization has on the atomic radius. Born states,

> "We see [in an attached tabulation of ionic radii] that the negative ions, which have an inert gas configuration with a smaller nuclear charge then the corresponding inert gas, are larger than the latter, the reason being of course that the electrons in these ions are more loosely bound so that their orbits have greater radii. A corresponding, mutatis mutandis, hold for positive ions also."

Thus, the ionic radius is a function of the degree of ionization of the xenon atom.

According to James, the average kinetic energy of fission fragments is in excess of $160\,\mathrm{MeV}$. [98] Oberstedt, Bilnert, and Gatera state the prompt gamma ray energy from $^{235}\mathrm{U}$ fission is in excess of $6\,\mathrm{MeV}$. [99, p. 86] In addition to these sources of ionization, we assert there exists radiation, in the form of alpha, beta, and gamma emanation, from the fission fragments. The sum of all the ionization energies in xenon is $0.2\,\mathrm{MeV}$. [100] It therefore follows the radiation field in an MSR is capable of completely ionizing any xenon in the reactor.

Since the ionic radius is a function of the degree of ionization, and the xenon in a MSR may be ionized, it follows that any consideration into atomic radius ought to consider the effect of ionization on the atomic radius. A corollary to this is the atomic radii in Table 6 may be greater than the effective atomic radius of xenon in an MSR.

Furthermore, since

$$\mathbf{Sh} \propto \frac{1}{D} \wedge D \propto \frac{1}{r_{Xe}} \implies \mathbf{Sh} \propto r_{Xe} \implies k_m \propto r_{Xe}, \tag{35}$$

Therefore we propose the mass transfer coefficients, k_m, in a nuclear system will be lower than those in a non-nuclear mock-up.

5   Circulating Void Behavior

5.1   Bubbles

Bubbles, also called circulating voids in the ORNL literature, are another factor in MSR xenon behavior. The effects of circulating voids were first investigated in ORNL-4069 [1], published in 1967, a full six years after the initial MSR xenon

35

analysis by Miller [13] (published in 1961). The report ORNL-TM-3027 [30, p. 20] details bubble behavior in the MSRE pump bowl. A thesis written for the ORNL MSR program, ORNL-TM-3718 [101], deals with a bubble mass transfer in a turbulent pipeline flow. The entertainment of bubbles in molten salts is documented in ORNL-TM-2373. [102] MSR xenon sparging using circulating helium bubbles is described in ORNL-TM-2245. [20]

Given a particular void fraction, the number of bubbles can be calculated by the expression:

$$N_B = \frac{fV_{FS}}{v_B},$$ (36)

where,

$$V_B = N_B v_B.$$ (37)

The volume of the bubble is assumed to be spherical and is calculated using an assumed reference diameter:

$$v_B = \frac{4\pi}{3} r_B^3.$$ (38)

The validity of the spherical shape assumption in bubble columns has been investigated by Quigley et al. [103] who concluded that their data support the use of spherical bubbles for area calculations in bubble columns. It can be argued that the behavior of bubbles in MSRs and bubble columns is sufficiently analogous to warrant the application of conclusions made about bubble behavior in bubble columns to be applied to bubble behavior in MSRs.

The ORNL xenon models assumed a bubble size based on observations in the water mock-up of the MSRE, which is detailed in ORNL-3419. [104, p. 38] The xenon models in ORNL-4069 and ORNL-TM-3464 considered a range of bubbles $1.27\,\text{mm} – 5.08\,\text{mm}$ in diameter. Subsequently, Hesketh correlated maximum bubble size in turbulent flow with the expression:

$$d_{max} = \left(\frac{\mathbf{We}_{crit}}{2}\right)^{0.6} \frac{\sigma^{0.6}}{(\rho_c^2 \rho_d)^{0.2}} \epsilon^{-0.4}.[105]$$ (39)

The Weber number, $\mathbf{We}$, describes the ratio of inertial to surface tension forces in a drop.[7] The critical Weber number, $\mathbf{We}_{crit}$, in Equation 39, is the Weber number associated with the critical diameter: the diameter, below which, drops will not break up. A more comprehensive review of Weber numbers and critical Weber numbers is given by Khavkin. [106, p. 258]

The maximum bubble size given by Equation 39 is not the same as the effective bubble diameter. A system's distribution of bubble size can be described by a probability density function. The average of this density function can be used as an effective bubble diameter which can be used as a reference diameter, r_b, in interfacial area calculations. Ogawa [107], and numerous other authors not cited, report bubble size distributions in bubble columns can be represented

---

[7]A drop is the super-ordinate category of gaseous bubbles and liquid droplets. Essentially, a drop is a discrete fluid phase inclusion.

by a log-normal distribution. No information was found that indicated a similar bubble distribution had been generated for an MSR, or if such a generalized distribution was feasible. It is foreseeable that each specific reactor would have its own unique distribution of bubble sizes.

Although the bubbles are assumed to be spherical in shape, this may not necessarily be the case. The Eötvös number:

$$\mathbf{Eo} = \frac{(\rho_c - \rho_d)L^2}{\sigma}, \tag{40}$$

in conjunction with the Motron number:

$$\mathbf{Mo} = \frac{g\mu_c^4(\rho_c - \rho_d)}{\rho_c^2\sigma^3}, \tag{41}$$

and Reynolds number can be used to determine the category of a freely rising bubble's shape. [108] The bubble shape has an effect on the surface area to volume ratio.

A determining factor in the mass transfer coefficient is the mobility of the bubble interface. Pebbles states:

> "At least for bubbles having diameters greater than few millimeters, the surface condition is more reasonable expressed as being...a mobile interface" [20, p. 14]

No further information was found concerning the mobility of bubble interfaces in MSRs.

5.2 Change in Interfacial Area With System Perturbation

In the course of our investigations, we required information on how the interfacial area changed in a perturbation to the system state. In consideration of the ideal gas law:

$$PV = nRT^{[K]}, \tag{42}$$

, it follows,

$$V = V(T^{[K]}, P_b, n). \tag{43}$$

Thus,

$$dV = \left(\frac{\partial V}{\partial T^{[K]}}\right)_{P_b,n} dT^{[K]} + \left(\frac{\partial V}{\partial P}\right)_{T^{[K]},n} dP_b + \left(\frac{\partial V}{\partial n}\right)_{P_b,T^{[K]}} dn. \tag{44}$$

Bubble pressure is equal to the sum of the liquid pressure and a contribution from surface tension forces,

$$P_b = P_l + \frac{2\sigma_l}{r_b}, \tag{45}$$

Assuming we are interested in bubbles of a size on the order a few millimeters, therefore, $\frac{2\sigma_l}{r_b} << P_l$, and Equation 45 becomes $P_b = P_l$. We henceforth drop the pressure subscript.

With Equation 42,

$$\left(\frac{\partial V}{\partial T^{[K]}}\right)_{P,n} = \frac{nR}{P}, \tag{46a}$$

$$\left(\frac{\partial V}{\partial P}\right)_{T^{[K]},n} = -\frac{nRT^{[K]}}{P^2}, \tag{46b}$$

$$\left(\frac{\partial V}{\partial n}\right)_{P,T^{[K]}} = \frac{RT^{[K]}}{P}. \tag{46c}$$

Therefore:

$$dV = \frac{nR}{P}dT^{[K]} - \frac{nRT^{[K]}}{P^2}dP + \frac{RT^{[K]}}{P}dn. \tag{47}$$

We seek to find the change in surface area with respect to change in volume as the system transitions from state $(P_1, T_1^{[K]}, n_1)$ to $(P_2, T_2^{[K]}, n_2)$. As summarized by DeVoe, the integral of the total derivative of a state function can be calculated by summing the derivatives of its constituent terms along a given path. [109, p. 477] We use the path $(P_1 \to P_2)_{T^{[K]},n}, (T_1^{[K]} \to T_2^{[K]})_{P,n}, (n_1 \to n_2)_{T^{[K]},P}$

$$\int_{V_1}^{V_2} dV = \int_{T_1^{[K]}}^{T_2^{[K]}} \frac{nR}{P}dT^{[K]} - \int_{P_1}^{P_2} \frac{nRT^{[K]}}{P^2}dP + \int_{n_1}^{n_2} \frac{RT^{[K]}}{P}dn, \tag{48}$$

$$\to V_2 - V_1 = \frac{n_1 R}{P_2}\left(T_2^{[K]} - T_1^{[K]}\right) + n_1 RT_1^{[K]}\left(\frac{1}{P_2} - \frac{1}{P_1}\right) + \frac{RT_2^{[K]}}{P_2}(n_2 - n_1). \tag{49}$$

Assuming spherical bubbles:

$$V = \frac{4}{3}\pi r_B^3, \tag{50}$$

and,

$$A = 4\pi r_B^2. \tag{51}$$

Therefore:

$$\frac{dA}{dV} = 2^{5/3}\left(\frac{\pi}{3}\right)^{1/3}V^{-1/3}. \tag{52}$$

$$\int_{A_1}^{A_2} dA = 2^{5/3}\left(\frac{\pi}{3}\right)^{1/3}\int_{V_1}^{V_2}V^{-1/3}\ dV \tag{53}$$

$$\to A_2 = 2^{2/3}(3\pi)^{1/3}\left(V_2^{2/3} - V_1^{2/3}\right) + A_1. \tag{54}$$

Substitute Equation 49 into 54 (step not written for brevity). In the resultant equation, state $(P_1, T_1^{[K]}, n_1)$ and A_1 and V_1 can be calculated from a reference bubble diameter and void fraction using the ideal gas law. This in turn allows for the calculation of the deviation of the surface area as the system transitions between state $(P_1, T_1^{[K]}, n_1)$ to $(P_2, T_2^{[K]}, n_2)$.

38

6 Conclusions

This paper has reviewed literature related to MSR Xenon analysis. The primary documents used in this review have been compiled into a chronology. This chronology has revealed two distinct periods of MSR xenon research, the first period lasted from about 1954 to 1977 and was primarily conducted at Oak Ridge National Laboratory (ORNL). The second period began in 2004 and is ongoing to the present day. The second period is not centralized around ORNL. No models of MSR xenon behavior were found which could be reasonably argued to be *validated*, and as such, it is reasonable to conclude that there may be issues with the phenomenological formulation of MSR xenon models. Furthermore, we observe that there is a dearth of available benchmark data for validation of MSR xenon models. The two sources which we forsee having utility in benchmark exercsies are the results of the krypton experiment, presented in ORNL-4069 [1], and a the steady-state and transient xenon poison fraction measurements given in ORNL-TM-3464 [2].

There are two pertinent points related to nuclear properties involved in MSR xenon behavior. First, the half-life of ^{135}Te was not known until 1969 [110] and therefore earlier work on MSR ^{135}Xe analysis was not aware of the ^{135}Te half-life. Second, the neutron absorption cross-section of ^{135m}Xe was unknown when the ORNL analyses were performed. The 2016 work by Eades, Chaleff, Venneri, and Blue [26] has subsequently explored ^{135m}Xe behavior in MSRs.

In regards to the properties of the fuel salt related to xenon behavior, Yoder [41] warns that the accuracy of heat transfer correlations are limited by the accuracy of fuel salt thermophysical data available. Through heat/mass transfer analogies, it follows mass transfer correlations, which are used in MSR xenon analysis are also limited in accuracy by the accuracy of available fuel salt thermophysical data. There are several compilations of fuel salt thermophysical data; however, no information was found which described how these thermophysical properties evolve with depletion or reactor life.

MSRs xenon analyses have been formulated at multiple *levels of analysis*. For example, the 1977 analysis of Shimazu [24] assumed all the graphite could be adequately represented by a single graphite equation. Contrary to this, the 1971 analysis in ORNL-TM-3464 [2] discretized the graphite into five distinct regions, each with its mass transfer coefficient and ^{135}Xe concentration. This same observation can be seen in the analysis of flow in MSR Xenon analysis: the analysis of ORNL-4069 [1] assumed that the entire reactor could be modeled as a single well-stirred pot, whereas the model presented by Wu et al. [28] explicitly investigated the effects of flow on MSR ^{135}Xe behavior. Work was not found which determined what level of analysis was necessary for an accurate representation of ^{135}Xe behavior in MSRs.

The *in-solution assumption*, which has been used in prior MSR xenon analyses, states the ^{135}Xe is free to migrate into the graphite and bubbles whereas the ^{135}I and ^{135}Te will remain in the fuel-salt solution. Evidence was found to justify this claim for the MSRE, however, given the in-solution assumption is predicated on the chemical properties of the fuel salt, it is not clear if this

assumption would be valid for other reactors, especially those which do not use a FLiBe fuel salt.

Prior MSR xenon analyses have assumed the fuel salt acts as an ideal dilute solution and the ^{135}Xe acts as an ideal gas. Under these assumptions, Henry's law can be used to related the liquid-side ^{135}Xe concentration to the gas-side ^{135}Xe concentration. Contrary to this, it seems reasonable to claim there is a concentration of ^{135}Xe , or (potentially) other dissolved gasses, beyond which these assumptions are inappropriate. No information which indicated the necessary conditions for a molten salt to behave Henry-like. Furthermore, no information was found which detailed the concentration of ^{135}Xe in the fuel salt during operation.

Measurements of Henry's constant found are tabulated in terms of a single temperature. Due to neutron and gamma heating, the graphite temperature of an MSR may substantially differ from the fuel-salt temperature, and no information was found in regards to applying Henry's law to a bi-thermal situation.

The assumption that the fuel-salt acts as a well-mixed fluid, and the concentrations of ^{135}Xe , ^{135}I , and ^{135}Te are constant throughout the solution, is a common feature of many MSR xenon analyses. The work of Wu et al. [28] does investigate the effects of fuel salt flow on ^{135}Xe behavior. Given that the re-circulation time of many MSRs is on the order of seconds or dozens of seconds, this, in our estimate, is likely a reasonable assumption for ^{135}Xe and ^{135}I , given their multi-hour half-lives. However, its application to ^{135}Te is questionable given its 19 s half-life. In support of this claim is the claim of ORNL-4865 [51] that only 1-20% of the Tellurium is distributed to the fuel-salt. Conversely, given the short half-life of ^{135}Te , it is foreseeable the ^{135}Te decays into ^{135}I before any substantial mass transfer occurs.

In prior analyses, the structure of the graphite stringers was assumed to be sufficiently homogeneous that both the mass diffusion coefficient and the porosity of the graphite could be represented by constants independent of position. Baes's analysis [17] indicates that the rate of formation of Cs-C in graphite will be negligibl. Analyses for the formation rates of other solid substances and the potential for *pore clogging* were not found. Furthermore, according to ORNL-4148 [19], the graphite stringers in the MSRE were observed to have non-homogeneous mass diffusion coefficients and porosities that varied with position.

We note that in prior analyses, mass transfer coefficients have assumed to be constants. In transient conditions, temperature and flow velocity may change, which would induce a corresponding change in the mass transfer coefficient. Furthermore, as demonstrated by Liu and Fukuda, [68], the Nusselt number may be different in transient conditions compared to steady state; presumably, by the heat/mass transfer analogy the Sherwood number may also change in transient conditions. Despite this, constant mass transfer coefficients have been used in both prior steady-state and transient analyses.

Since xenon migrates to the pore-space of the graphite stringers, changes in volume to the graphite pore-space may be an essential factor in MSR xenon behavior. These changes to the volume are induced by two mechanisms, ther-

mally induced volume changes and radiation-induced volume changes (creep). The radiation-induced expansion of graphite occurs at a much longer time scale than the thermally induced expansion of graphite, thus may be considered constant during xenon transients. This effect should be explored over the core lifetime.

There is also the question as to what state of matter the xenon and its precursors are in – liquid or gas. This question is predicated on the question, does the *state of matter* have any intelligible meaning for the clusters of atoms that form in consideration of MSR Xenon behavior. Of particular interest is the fact that some high-temperature MSRs may exceed the liquid/gas phase transition temperature of ^{135}Te . No information was found related to any potential effects due to phase transition.

In prior analyses, the graphite stringers were simplified into either right circular cylinders or slabs and the pore space was assumed to be entirely interconnected. Presumably, there are some graphite stringer shapes which cannot be reduced into these geometries. No information was found related to the error introduced by this simplification. Additionally, in regards to graphite stringers, there is a large internal surface area to the pores-space upon which an adsorption mechanism may influence the behavior of ^{135}Xe or its progenitors. Given MSRs operate at a high temperature, it is reasonable to assume adsorption will be negligible.

Although mass transfer equations of the form,

$$ J = K_m \left(C^{B,L} - HRT^{[K]}C^{B,G} \right), \tag{55} $$

where T is the temperature in Kelvin, are used in numerous MSR Xenon analyses, these equations are predicated on the fuel salt acting (as previously mentioned) as an ideal dilute solution. No validation work was found related to these rate equations. Presumably, given the prevalence of the above equation in the literature, such validation would have been performed early in the MSR program; however, documentation produced in this period is sparse.

Finally, we observe prior analyses have assumed a constant circulating void fraction. As shown in this paper, there is a variation in circulating void fraction (and thus as the interfacial area for mass transfer) with respect to thermodynamic perturbation of the system. This may be of substantial importance given the potential for a large fraction of ^{135}Xe to be found in the circulating voids, as reported by ORNL-4069 [1]. Furthermore, there is an unanswered question as to what the relationship is between maximum bubble size and the total bubble area available for mass transfer.

Overall this represents the first step on our path towards modeling of xenon in MSR systems. More research and study needs to be done. In future work, we intend to develop a MSR xenon model that can be used in dynamics analysis. This model will be incorporated into an ongoing project to model MSR dynamic behavior (C.F. Singh et al. [111]).

7 Research Questions

During our review numerous research questions were generated.

- Is a *ground-up* approach to MSR xenon modeling, such as was done in ORNL-4069 [1] feasible or is it necessary to *calibrate* a model, such as was done in ORNL-TM-3464 [2], to existing data?

- Are there any reports on MSR xenon behavior which have been lost? What internal memos were circulated early on about xenon behavior in the ARE program?

- Are mass transfer correlation which are developed in wetted-wall columns valid for the *dry-wall* situations in MSR fuel channels?

- What is the maximum temperature difference between the fuel-salt and the graphite for which Henry's law is reasonably valid?

- Are radiation induced changes in graphite structure relevant to xenon behavior?

- What is the concentration of dissolved ga past which fuel-salt stops behaving as an ideal dilute solution?

- Has all the phenomenology relevant to MSR xenon behavior been discovered?

- Can bubbles attach to the graphite stringers or other surfaces? If so, does this attachment significantly affect xenon behavior?

- Are there any changes in xenon behavior when an MSR passes the phase transition temperature of ^{135}Te?

- Are mass transfer correlations, which are measured at steady-state, valid for transient analyses?

Nomenclature

Unscripted Latin Characters

Eo	Eötvös Number (Bond Number)	[−]
Mo	Motron Number	[−]
Re	Reynolds Number	[−]
Sc	Schmidt Number	[−]
Sh	Sherwood Number	[−]

A	Area	[m]
C	Concentration	[m^{-3}]
c	Specific Heat	[J kg^{-1} K^{-1}]
D	Mass Diffusion Coefficient	[m s^{-2}]
E	Energy	[J]
f	Generic Function, Circulating Void Fraction	[−]
H	Henry's Constant	[mol m^{-3} Pa^{-1}]
J	Mass Flux	[m^{-1} s^{-2}]
K	Arbitrary Constant	[−]
k	Thermal Conductivity	[W m^{-1} K^{-1}]
L	Characteristic Length	[m]
m	Mass of Diffusing Species	[kg]
n	Number of moles	[−]
R	Universal Gas Constant	[J K^{-1} mol]
r	Radial Position	[m]
t	Time	[s]
V	Volume	[m^3]

Nomenclature with Scripts or Greek Characters

$\dot{N}$	Rate of change of of the quantity of a particular isotope	[s^{-1}]
$\dot{N}_I$	Rate of Change of Iodine	[s^{-1}]
$\dot{N}_{Te}$	Rate of Change of Tellurium	[s^{-1}]
$\dot{N}_{Xe}$	Rate of Change of Xenon	[s^{-1}]
ϵ	Graphite Void Fraction, Specific Power of Fluid Flow	[−]/[J kg^{-1}]
γ_i	Fission Yield of Isotope 'i'	[−]
γ_I	Iodine Fission Yield	[−]
γ_{Te}	Tellurium Fission Yield	[−]
γ_{Xe}	Xenon Fission Yield	[−]
λ_I	Iodine Decay Constant	[s^{-1}]

λ_{Te}	Tellurium Decay Constant	$[s^{-1}]$
λ_{Xe}	Xenon Decay Constant	$[s^{-1}]$
μ	Viscosity	$[Pa\,s]$
μ_c	Continuous (fuel-salt) viscosity	$[Pa\,s]$
ν	Average Number of Neutrons Released per Fission	$[-]$
ϕ	Neutron flux	$[m^{-1}\,s^{-2}]$
ρ	Density	$[kg\,m^{-3}]$
ρ_c	Density of Continuous Phase (Fuel Salt)	$[kg\,m^{-3}]$
ρ_d	Density of Dispersed Phase (Circulating Voids)	$[kg\,m^{-3}]$
σ	Surface Tension, Microscopic Neutron Absorption Cross Section	$[N\,m^{-1}]/[m^2]$
Σ_a^r	Reactor Macroscopic Neutron Absorption Cross Section excluding ^{135}Xe	$[m^{-1}]$
Σ_a^{Xe}	Xenon Macroscopic Absorption Cross Section	$[m^{-1}]$
σ_a^{Xe}	Xenon Microscopic Neutron Absorption Cross section	$[m]$
Σ_f	Macroscopic Neutron Absorption Cross Section	$[m^{-1}]$
$T^{[°C]}$	Temperature, Celsius	$[°C]$
$T^{[K]}$	Temperature, Kelvin	$[K]$
$\vec{x}$	Position vector	$[m]$
C_B^L	Bulk Concentration, Liquid Phase	$[m^{-3}]$
C_i^L	Concentration of Species 'i' in Liquid	$[m^{-3}]$
C_x	First Spatial Derivative of Concentration	$[m^{-3}]$
C_{int}	Interfacial Concentration	$[m^{-3}]$
C_{int}^L	Interfacial Liquid Concentration	$[m^{-3}]$
D_g	Mass Diffusion Coefficient for Gas	$[m\,s^{-2}]$
D_L	Mass Diffusion Coefficient for Liquid	$[m\,s^{-2}]$
D_{Kn}	Knudsen Mass Diffusion Coefficient	$[m\,s^{-2}]$
d_{max}	Maximum Diameter	$[m]$
G_V	Volumetric Gibb's Energy	$[J\,m^{-3}]$

44

H_i	Henry's Constant for Species 'i'	$[\mathrm{mol\,m^{-3}\,Pa^{-1}}]$
K_B	Boltzman's Constant	$[\mathrm{m\,kg^2\,s^{-1}\,K^{-2}}]$
K_m	Overall Mass Transfer Coefficient	$[\mathrm{m\,s^{-1}}]$
k_m	Mass Transfer Coefficient	$[\mathrm{m\,s^{-1}}]$
N_B	Number of Bubbles	$[-]$
N_I	Quantity of Iodine	$[-]$
N_{Te}	Quantity of Tellurium	$[-]$
N_{Xe}	Quantity of Xenon	$[-]$
P_i	Partial Pressure of Species 'i'	$[\mathrm{Pa}]$
$P_i^{B,G}$	Partial Pressure of Species 'i' in the Gas Bulk	$[\mathrm{Pa}]$
$P_i^{F,G}$	Partial Pressure of Species 'i' At the Gas Film Layer	$[\mathrm{Pa}]$
R_m^G	Mass Transfer Resistance, Gas Phase	$[\mathrm{s\,m^{-1}}]$
R_m^L	Mass Transfer Resistance, Liquid Phase	$[\mathrm{s\,m^{-1}}]$
r_B	Radius of a Bubble	$[\mathrm{m}]$
R_m	Mass Resistance	$[\mathrm{s\,m^{-1}}]$
r_{Xe}	Xenon Radius	$[\mathrm{m}]$
T_t	First Time Derivative of Temperature	$[\mathrm{^{\circ}C\,s^{-1}}]$
$t_{1/2}^{Xe}$	$^{135}\mathrm{Xe}$ Half Life	$[\mathrm{s}]$
t_{Circ}	Fuel-Salt Circulation Time	$[\mathrm{s}]$
T_{xx}	Second Space Derivative of Temperature	$[\mathrm{^{\circ}C\,m^{-1}}]$
v	Velocity	$[\mathrm{m\,s^{-1}}]$
V_B	Total Bubble Volume	$[\mathrm{m^3}]$
v_B	Volume of a Single Bubble	$[\mathrm{m^3}]$
V_{RC}	Reactor Core, the In Core Volume	$[\mathrm{m^3}]$
V_{RC}	Volume of Reactor Core	$[\mathrm{m^3}]$
x_0	Film Thickness	$[\mathrm{m}]$
$\mathbf{We}_{Crit}$	Critical Weber Number	$[-]$

References

[1] R. Kedl and A. Houtzeel. *ORNL-4069: Development of a Model for Computing 135Xe Migration in the MSRE.* Tech. rep. Oak Ridge National Laboratory, 1967 (cit. on pp. 1, 8, 11–13, 15, 19, 22, 24, 27, 32–35, 39, 41, 42).

[2] J. Engel and R. Steffy. *ORNL-TM-3464: Xenon Behavior in the Molten Salt Reactor Experiment.* Tech. rep. Oak Ridge National Laboratory, 1971 (cit. on pp. 1, 9, 11–15, 22, 23, 27, 28, 33, 39, 42).

[3] R. Robertson. *ORNL-TM-4541: Conceptual Design Study of a Single-Fluid Molten-Salt Breeder Reactor.* Tech. rep. Oak Ridge National Laboratory, 1971 (cit. on pp. 1, 9, 11, 17, 33).

[4] B. Hoglund. *MoltenSalt.org.* 2010. URL: http://moltensalt.org/ (cit. on p. 1).

[5] *Energy From Thorium.* URL: https://energyfromthorium.com/pdf/ (cit. on p. 1).

[6] H. MacPherson. "The Molten Salt Reactor Adventure". In: *Nuclear Science and Engineering* 90.4 (1985), pp. 374–380 (cit. on pp. 2, 12).

[7] T. Dolan. *Molten Salt Reactors and Thorium Energy.* Woodhead Publishing, 2017 (cit. on pp. 2, 12, 34).

[8] J. Serp et al. "The Molten Salt Reactor (MSR) in Generation IV: Overview and Perspectives". In: *Progress in Nuclear Energy* 77 (2014), pp. 308–319 (cit. on p. 2).

[9] F. Lorenz. "Modeling Level: A Question of Semantics". In: *IMACS ESIEE CESA '96 Multiconference.* Lille, France, 1996, pp. 1198–1202 (cit. on p. 2).

[10] M. Robinson. *ORNL-1924: A Theoretical Study of Xe-135 Poisoning Kinetics in Fluid-Fueled, Gas-Sparged Nuclear Reactors.* Tech. rep. Oakridge National Laboratory, 1956 (cit. on pp. 7, 11).

[11] J. Meem. *ORNL-CF-54-5-1: The Xenon Problem in the ART.* Tech. rep. Oak Ridge National Laboratory, 1954 (cit. on pp. 7, 11).

[12] W. Burch, M. Watson, and H. Weeren. *ORNL-CF-60-2-2-: Xenon Control in Fluid Fuel Reactors.* Tech. rep. Oak Ridge National Laboratory, 1960 (cit. on pp. 7, 11).

[13] J. Miller. *ORNL-CF-61-5-62: Xenon Poisoning in Molten Salt Reactors.* Tech. rep. Oak Ridge National Laboratory, 1961 (cit. on pp. 7, 11, 13, 36).

[14] J. Engel. *ORNL-CF-62-11-69: Preliminary Equations to Describe Iodine and Xenon Behavior in the MSRE.* Tech. rep. Oak Ridge National Laboratory, 1962 (cit. on pp. 7, 11).

[15] G. Watson and R. Evans. *ORNL-TM-262: Xenon Diffusion in Graphite: Effects of Xenon Absorption in Molten Salt Reactors Containing Graphite.* Tech. rep. Oak Ridge National Laboratory, 1962 (cit. on pp. 7, 11).

[16] S. Ball and T. Kerlin. *ORNL-TM-1070: Stability Analysis of the Molten-Salt Reactor Experiment.* Tech. rep. Oak Ridge National Laboratory, 1965 (cit. on pp. 8, 11, 15).

[17] R. Briggs. *ORNL-4037: Molten-Salt Reactor Program Semiannual Progress Report for Period Ending August 31, 1966.* Tech. rep. Oak Ridge National Laboratory, 1967 (cit. on pp. 8, 11, 13, 22, 40).

[18] R. Kedl. *ORNL-TM-1810: A Model for Computing the Migration of Very Short Lived Nobel Gases into MSRE Graphite.* Tech. rep. Oak Ridge National Laboratory, 1967 (cit. on pp. 8, 11).

[19] A. Malinauskas, J. Rutherford, and R. Evans. *ORNL-4148: Gas Transport in MSRE Moderator Graphite. Part 1: Review of Theory and Counterdiffusion Experiments.* Tech. rep. Oak Ridge National Laboratory, 1967 (cit. on pp. 8, 11, 23, 26, 33, 40).

[20] F. Peebles. *ORNL-TM-2245: Removal of Xenon-135 from Circulating Fuel Salt of the MSBR by Mass Transfer to Helium Bubbles.* Tech. rep. Oak Ridge National Laboratory, 1968 (cit. on pp. 8, 11, 36, 37).

[21] Evans, R., Rutherford, J., and A. Malinauskas. *ORNL-4389: Gas Transport in the MSRE Moderator Graphite: II. Effects of Impregnation; III. Variation of Flow Properties.* Tech. rep. Oak Ridge National Labs, 1969 (cit. on pp. 9, 11, 33).

[22] D. Scott and W. Eatherly. "Graphite and Xenon Behavior and Their Influence on Molten-Salt Reactor Design". In: *Nuclear Applications and Technology* 8.2 (1970), pp. 179–189 (cit. on pp. 9, 11, 24).

[23] R. Wichner and C. Baes. *ORNL-CF-72-6-12: Sidestream Processing for Continuous Iodine and Xenon Removal from the MSBR Fuel.* Tech. rep. Oak Ridge National Laboratory, 1972 (cit. on pp. 9, 11).

[24] Y. Shimazu. "Transient Xenon Analysis in a Molten Salt Breeder Reactor". In: *Journal of Nuclear Science and Technology* 14.11 (1977), pp. 805–810 (cit. on pp. 9, 11, 39).

[25] K. Suzuki and Y. Shimazu. "Transient Xenon Effect on Plant Control in MSRs - Validation of Simulation Model". In: *Proceedings of ICAPP '04.* Pittsburgh, PA, USA, 2004 (cit. on pp. 9, 11).

[26] M. Eades et al. "The Influence of Xe-135m on Steady-State Xenon Worth in Thermal Molten Salt Reactors". In: *Progress in Nuclear Energy* 93 (2016), pp. 397–405 (cit. on pp. 10, 11, 15, 22, 23, 39).

[27] G. Chen et al. "Xenon Analysis of Thorium Molten Salt Experiment Reactor-Liquid Fuel". In: *Nuclear Techniques* 40.4 (2017). Note: The identifier 40602 is written in the paper header. (cit. on pp. 10, 11).

[28]   J. Wu et al. "Flow Effect on I-135 and Xe-135 Evolution Behavior in a Molten Salt Reactor". In: *Nuclear Engineering and Design* 314 (2017), pp. 318–325 (cit. on pp. 10, 11, 22, 39, 40).

[29]   Z. Taylor, R. Salko, and B. Collins. "Implementation of General Species Transport Capability into VERA-CS for Molten Salt Reactor Analysis". In: *Transactions of the American Nuclear Society*. Vol. 118. Philadelphia, Pennsylvania, 2018 (cit. on pp. 10, 11).

[30]   J. Engel, P. Haubenreich, and A. Houtzeel. *ORNL-TM-3027: Spray, Mist, Bubbles, and Foam in the Molten Salt Reactor Experiment*. Tech. rep. Oak Ridge National Laboratory, 1970 (cit. on pp. 11, 13, 36).

[31]   W. Egen. *CF-57-2-130: The Physics of the Fused-Salt Reactor Experiment*. Tech. rep. Oak Ridge National Laboratory, 1957 (cit. on p. 12).

[32]   R. O'Sullivan, J. Tomlinson, and T. Griffiths. *Feasibility Study of a Pilot Scale Molten Salt Reactor Demonstration*. 2015 (cit. on p. 12).

[33]   E. Bettis et al. "The Aircraft Reactor Experiment—Design and Construction". In: *Nuclear Science and Engineering* 2.6 (1957), pp. 804–825 (cit. on p. 12).

[34]   A. Fraas and A. Savolainen. *ORNL-2095: Design Report on the Aircraft Reactor Test*. Tech. rep. 1956 (cit. on p. 12).

[35]   W. Cottrell et al. *ORNL-1845: Operation of the Aircraft Reactor Experiment*. Tech. rep. Oak Ridge National Laboratory, 1955 (cit. on p. 12).

[36]   D. Scott et al. *ORNL-2536: A Zero Power Reflector-Moderated Reactor Experiment at Elevated Temperature*. English. Tech. rep. Oak Ridge National Laboratory, 1958 (cit. on p. 12).

[37]   C. Forsberg. "Molten Salt Reactor Experience Applicable to LS-VHTR Refueling". In: *LS-VHTR Meeting*. Oak Ridge National Laboratory, 2006 (cit. on p. 12).

[38]   J. Engel and B. Prince. *ORNL-TM-1796: The Reactivity Balance in the MSRE*. Tech. rep. Oak Ridge National Laboratory, 1967 (cit. on p. 12).

[39]   E. Baum. *Nuclides and Isotopes: Chart of the Nuclides*. 16th ed. Knolls Atomic Power Laboratory, 2010 (cit. on p. 15).

[40]   S. Mughabghab. *Neutron Cross Sections: Neutron Resonance Parameters and Thermal Cross Sections, Part A: Z 1-60*. Elsevier Science, 2012 (cit. on p. 15).

[41]   G. Yoder. "Examination of Liquid Fluoride Salt Heat Transfer". In: *Proceedings of ICAPP 2014*. Charlotte, 2014 (cit. on pp. 15, 32, 39).

[42]   S. Cantor et al. *ORNL-TM-2316: Physical Properties of Molten-Salt Reactor Fuel, Coolant and Flush Salts*. Tech. rep. Oak Ridge National Laboratory, 1968 (cit. on pp. 15, 34).

[43]   M. Sohal et al. *Engineering Database of Liquid Salt Thermophysical and Thermochemical Properties*. Tech. rep. Idaho National Laboratory, 2010 (cit. on pp. 15, 34).

[44] G. Janz. *Molten Salts Handbook*. Elsevier Science, 2013 (cit. on pp. 15, 34).

[45] W. Grimes, N. Smith, and G. Watson. "Solubility of Noble Gases in Molten Fluorides. I. In Mixtures of NaF–ZrF4 (53-47 Mole %) and NaF–ZrF4–UF4 (50–46–4 Mole %)". In: *The Journal of Physical Chemistry* 62.7 (1958), pp. 862–866 (cit. on pp. 16, 20).

[46] M. Blander et al. "Solubility of Noble Gases in Molten Fluorides. II. In the Lif–NaF–LF Eutectic Mixtures". In: *The Journal of Physical Chemistry* 63.7 (1959), pp. 1164–1167 (cit. on pp. 16, 20).

[47] G. Watson et al. "Solubility of Noble Gases in Molten Fluorides. In LiF-BeF2." In: *Journal of Chemical and Engineering Data* 7.2 (1962), pp. 285–287 (cit. on pp. 16, 20).

[48] S. Petrucci. *Ionic Interactions: From Dilute Solution to Fused Salts*. Elsevier Science, 2012 (cit. on p. 16).

[49] *Japan Atomic Energy Agency - Nuclear Data Center - Fission Product Yields*. 2018. URL: https://wwwndc.jaea.go.jp/cgi-bin/FPYfig (cit. on p. 16).

[50] H. de Regt, S. Leonelli, and K. Eigner. *Scientific Understanding: Philosophical Perspectives*. University of Pittsburgh Press, 2009 (cit. on p. 18).

[51] E. Compere et al. *ORNL-4865: Fission Product Behavior in the Molten Salt Reactor Experiment*. Tech. rep. Oak Ridge National Laboratory, 1975 (cit. on pp. 19, 26, 40).

[52] R. Briggs. *ORNL-3913: Molten-Salt Reactor Program Semiannual Progress Report For Period Ending February 28,1966*. Tech. rep. 1966 (cit. on p. 19).

[53] A. J. Koning et al. *TENDL-2015: TALYS-Based Evaluated Nuclear Data Library*. Note: the absorption cross section plots by clicking on the *PREPRO* link for a chosen isotope. 2015. URL: https://tendl.web.psi.ch/tendl_2015/tendl2015.html (cit. on p. 19).

[54] M. Tramšek and B. Žemva. "Synthesis, Properties and Chemistry of Xenon (II) Fluoride". In: *Acta Chim. Slov* 53 (2006), pp. 105–116 (cit. on p. 19).

[55] I. Asimov. *A Short History of Chemistry*. Greenwood Press, 1979 (cit. on p. 19).

[56] D. MacKenzie and R. Wiswall Jr. "Compound Formation by γ-Irradiation of Xenon-Fluorine Mixtures". In: *Inorganic Chemistry* 2.5 (1963), p. 1064 (cit. on p. 19).

[57] F. Lantelme and H. Groult. *Molten Salts Chemistry: From Lab to Applications*. Elsevier Science, 2013 (cit. on p. 19).

[58] M. Gaune-Escard. *Molten Salts: From Fundamentals to Applications*. Springer Netherlands, 2012 (cit. on p. 19).

[59] S. Delpech et al. "Molten Fluorides for Nuclear Applications". In: *Materials Today* 13.12 (2010), pp. 34–41 (cit. on p. 19).

[60] J. Keiser. *ORNL/TM-6002: Status of Tellurium–Hastelloy N Studies in Molten Fluoride Salts*. Tech. rep. Oak Ridge National Laboratory, 1977 (cit. on p. 20).

[61] E. Lemmon, M. Huber, and M. McLinden. *NIST Reference Fluid Thermodynamic and Transport Properties—REFPROP*. 2002. URL: https://www.nist.gov/srd/refprop (cit. on p. 20).

[62] N. Fletcher. "Size Effect in Heterogeneous Nucleation". In: *The Journal of chemical physics* 29.3 (1958), pp. 572–576 (cit. on p. 20).

[63] P. Westh, C. Haynes, and Y. Koga. "How Dilute Is the Henry's Law Region? II". In: *The Journal of Physical Chemistry B* 102.25 (1998), pp. 4982–4987 (cit. on p. 20).

[64] G. Robbins, S. Wang, and J. Stuart. "Using The Static Headspace Method to Determine Henry's Law Constants". In: *Analytical Chemistry* 65.21 (1993), pp. 3113–3118 (cit. on p. 23).

[65] J. Engel and P. Haubenreich. *ORNL-TM-378: Temperature in the MSRE Core During Steady-State Power Operation*. Tech. rep. Oak Ridge National Laboratory, 1962 (cit. on pp. 23, 27, 28).

[66] R. Firestone and V. Shirley. *Table of Isotopes, 8th Edition*. Wiley, 1996 (cit. on p. 23).

[67] S. Chu, L. Ekström, and R. Firestone. *The LUND/LBNL nuclear data search, version 2.0, Entry for Xe-135m*. June 1999. URL: http://nucleardata.nuclear.lu.se/toi/nuclide.asp?iZA=540435 (cit. on p. 23).

[68] Q. Liu and K. Fukuda. "Transient Heat Transfer for Forced Convection Flow of Helium Gas". In: *JSME International Journal Series B Fluids and Thermal Engineering* 45.3 (2002), pp. 559–564 (cit. on pp. 24, 40).

[69] T. Sherwood, R. Pigford, and C. Wilke. *Mass transfer*. McGraw-Hill, 1975 (cit. on p. 24).

[70] T. Burchell, K. Murty, and J. Eapen. "Irradiation Induced Creep of Graphite". In: *JOM: The Journal of the Minerals, Metals & Materials Society* 62 (2010), pp. 93–99 (cit. on p. 24).

[71] P. Delhaes. *Graphite and Precursors*. CRC Press, 2014 (cit. on p. 24).

[72] S. Beall et al. *ORNL-TM-732: MSRE Design and Operations Report, Part V*. English. Tech. rep. United States: Oakridge National Laboratory, 1964 (cit. on p. 25).

[73] R. Robertson. *ORNL-TM-0728: MSRE Design and Operations Report*. Tech. rep. 1965 (cit. on pp. 25, 26, 33).

[74] P. Atkins, J. De Paula, and J. Keeler. *Atkins' Physical Chemistry*. Oxford University Press, 2018 (cit. on p. 25).

[75] S. Wolfram. *Wolfram Alpha*. URL: www.wolframalpha.com (cit. on p. 25).

[76]   A. Goodwin, K. Marsh, and W. Wakeham. *Measurement of the Thermodynamic Properties of Single Phases*. Experimental Thermodynamics. Elsevier Science, 2003 (cit. on p. 25).

[77]   L. Glicksman and J. Lienhard. *Modeling and Approximation in Heat Transfer*. Cambridge University Press, 2016 (cit. on p. 26).

[78]   J. Bear and Y. Bachmat. *Introduction to Modeling of Transport Phenomena in Porous Media*. Springer Netherlands, 2012 (cit. on p. 27).

[79]   F. Salzano and A. Eshaya. "Sorption of Xenon in High Density Graphite at High Temperatures". In: *Nuclear Science and Engineering* 12.1 (1962), pp. 1–3 (cit. on p. 27).

[80]   M. Cannon et al. "Adsorption of Xenon and Argon on Graphite". In: *Nuclear Science and Engineering* 12.1 (1962), pp. 4–9 (cit. on p. 27).

[81]   W. Burch. *ORNL-TM-228: Measurement of Xenon Poisoning in the HRT*. Tech. rep. Oak Ridge National Laboratory, 1962, ' (cit. on p. 27).

[82]   L. Albright. *Albright's Chemical Engineering Handbook*. Taylor & Francis, 2008 (cit. on p. 31).

[83]   R. Perry and D. Green. *Perry's Chemical Engineers' Handbook, Seventh Edition*. McGraw-Hill Education, 2008 (cit. on p. 31).

[84]   T. Dobre and J. Marcano. *Chemical Engineering: Modeling, Simulation and Similitude*. Wiley, 2007 (cit. on p. 32).

[85]   J. Engel and Haubenreich P. *ORNL-TM-378: Temperature in the MSRE Core During Steady-State Power Operation*. Tech. rep. (cit. on p. 32).

[86]   W. Rohsenow, J. Hartnett, and Y. Cho. *Handbook of Heat Transfer*. McGraw-Hill, 1998 (cit. on p. 32).

[87]   W. Ambrosini et al. "On Various Forms of the Heat and Mass Transfer Analogy: Discussion and Application to Condensation Experiments". In: *Nuclear Engineering and Design* 236.9 (2006), pp. 1013–1027 (cit. on p. 33).

[88]   E. L. Cussler. *Diffusion: Mass Transfer in Fluid Systems*. Third. Cambridge University Press, 2007 (cit. on pp. 33, 34).

[89]   M. Muruganant, A. Chirazi, and B. Raj. *Frontiers in Materials Processing, Applications, Research and Technology: Select Proceedings of FiMPART 2015*. Springer Singapore, 2017 (cit. on p. 34).

[90]   S. Zhang et al. *Physicochemical Properties of Ionic Liquid Mixtures*. en. New York, NY: Springer, 2016 (cit. on p. 34).

[91]   John S Wilkes. "Molten Salts and Ionic Liquids - Are They Not the Same Thing?" In: *ECS Transactions* 3.35 (2007), pp. 3–7. ISSN: 1938-6737 (cit. on p. 34).

[92]   J. Bockris and A. Reddy. *Modern Electrochemistry, Volume 1, Ionics*. Kluwer Academic Publishers, 1998 (cit. on p. 34).

[93] S. Bretsznajder and P. Danckwerts. *Prediction of Transport and Other Physical Properties of Fluids*. Pergamon Press, 2013 (cit. on p. 34).

[94] P. Pau, J. Berg, and W. McMillan. "Application of Stokes' Law to Ions in Aqueous Solution". In: *Journal of Physical Chemistry* 94.6 (1990), pp. 2671–2679 (cit. on p. 34).

[95] W. Haynes. *CRC Handbook of Chemistry and Physics, 97th Edition*. CRC Press, 2016 (cit. on p. 35).

[96] R. Svehla. *R-132: Estimated Viscosities and thermal Conductivities of Gases at High Temperatures*. Tech. rep. NASA, 1962 (cit. on p. 35).

[97] M. Born. *Atomic Physics: 8th Edition*. Dover Publications, 2013 (cit. on p. 35).

[98] M. James. "Energy Released in Fission". In: *Journal of Nuclear Energy* 23 (1969), pp. 517–536 (cit. on p. 35).

[99] S. Oberstedt et al. "Prompt fission γ -Ray Spectra Characteristics - a First Summary". In: *Physics Procedia* 64 (2015), pp. 83–90 (cit. on p. 35).

[100] A. Kramida, Y. Ralchenko, and J. Reader. *NIST Atomic Spectra Database Ionization Energies Data for Xenon*. 2018. URL: http://bit.ly/2mXDzxn (cit. on p. 35).

[101] T. Kress. *ORNL-TM-3718: Mass Transfer Between Small Bubbles and Liquids in Cocurrent Turbulent Pipeline Flow*. Tech. rep. Oak Ridge National Laboratory, 1972 (cit. on p. 36).

[102] H. Kohn. *ORNL-TM-2373: Bubbles, Drops, and Entrainment in Molten Salts*. Tech. rep. Oak Ridge National Laboratory, 1968 (cit. on p. 36).

[103] C. Quigley, A. Johnson, and B. Harris. "Size and Mass Transfer Studies of Gas Bubbles". In: *Chemical Engineering Progress Symposium Series, American Institute of Chemical Engineers*. Vol. 1. New York, 1955, p. 31 (cit. on p. 36).

[104] P. Briggs. *ORNL-3419: Molten Salt Reactor Program Semiannual Progress Report for Period Ending January 31, 1963*. Tech. rep. Oak Ridge National Laboratory, 1963 (cit. on p. 36).

[105] R. Hesketh, A. Etchells, and T. Russell. "Experimental Observations of Bubble Breakage in Turbulent Flow". In: *Industrial & Engineering Chemistry Research* 30.5 (1991), pp. 835–841 (cit. on p. 36).

[106] Y. Khavkin. *Theory and Practice of Swirl Atomizers*. Combustion: An International Series. Taylor & Francis, 2003 (cit. on p. 36).

[107] K. Ogawa. *Chemical Engineering: A New Perspective*. Elsevier Science, 2007 (cit. on p. 36).

[108] J. Grace, T. Wairegi, and T. Nguyen. "Shapes and Velocities of Single Drops and Bubbles Moving Freely Through Immiscible Liquids". In: *Transactions of the Institute for Chemical Engineering* 54 (1976), pp. 167–173 (cit. on p. 37).

52

[109] H. DeVoe. *Thermodynamics and Chemistry*. Prentice Hall, 2001 (cit. on p. 38).

[110] J. Kathawa, C. Fry, and M. Thoennessen. "Discovery of Palladium, Antimony, Tellurium, Iodine, and Xenon Isotopes". In: *Atomic Data and Nuclear Data Tables* 99.1 (2013), pp. 22–52 (cit. on p. 39).

[111] V. Singh et al. "Nonlinear dynamic model of Molten-Salt Reactor Experiment – Validation and Operational Analysis". In: *Annals of Nuclear Energy* 113 (2018), pp. 177–193 (cit. on p. 41).

Inter-Stringer
Space
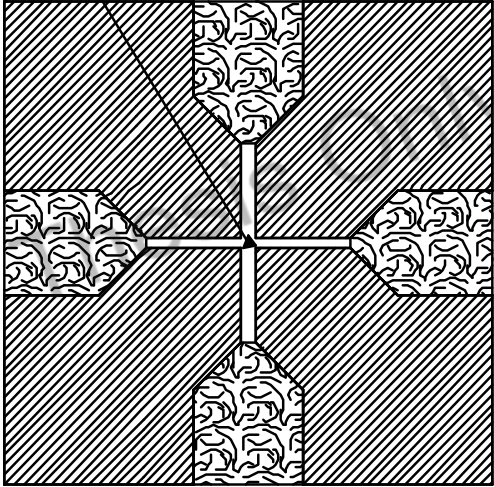
Figure 12: Detail of interstringer space

54
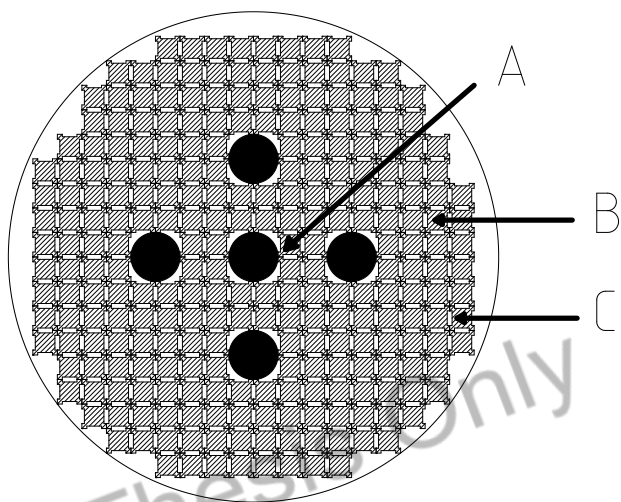
Figure 13: Classification of graphite stringers
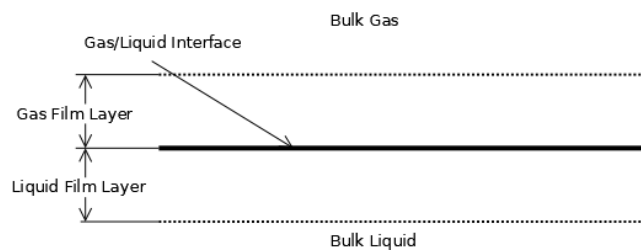
Figure 14: Illustration of the two-film theory
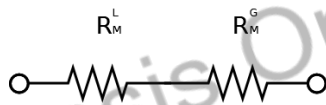
Figure 15: Mass transfer modeled as a two resistance problem

Attachment 6

A Review of Circulating Voids and Gaseous Fission Product Behavior In Molten Salt

Reactors

Published in the ASME Journal of Nuclear Engineering

A Review of Circulating Voids and Gaseous Fission Product Behavior In Molten Salt Reactors

Terry Price
Ontario Technical University
`terry.price@uoit.net`

Zack Taylor
University of Tennessee, Knoxville
`rtaylo45@vols.utk.edu`

Ondrej Chvala
University of Tennessee, Knoxville
`ochvala@utk.edu`

March 2019

Abstract

Molten salt reactors are a family of advanced, Generation-IV, nuclear reactors that use a circulating molten alkali fluoride fuel salt as both a primary working fluid and fuel matrix. Since the fuel salt is liquid, gases become entrained in the fuel salt flow, and these entrained gases are called circulating voids. This paper reviews some aspects of circulating voids on reactor behavior. A formal definition of the circulating void fraction is given. A time-line of Oak Ridge reports on circulating void behavior is presented. Methods to measure the circulating void fraction are described. Foam induced by gas entrained in the fuel salt is discussed. The discovery of circulating voids in the MSRE is detailed. Aspects related to bubble size and interfacial area are reviewed. The Laplace pressure is examined. The void and pressure coefficients of reactivity are examined. Some requirements for a bubble model for xenon behavior analysis are proposed. The effects of bubble surface mobility are examined. Finally, sources of gas production in the fuel salt are investigated.

1   Introduction

Molten Salt Reactors (MSRs) are a class of Generation IV nuclear reactors that use a circulating molten alkali-halide fuel salt as both the primary working fluid as well the fuel matrix. This paper focuses on MSRs with fluoride as the halide and a graphite moderator. There have been three molten salt reactors built and operated to date:

- 1954: The Aircraft Reactor Experiment (ARE)

- 1957: The Pratt and Whitney Aircraft Reactor 1 (PWAR-1)

- 1965-1969: Molten Salt Reactor Experiment (MSRE)

All of these reactors were run at Oak Ridge National Laboratory (ORNL). In addition to these experimental reactors, numerous conceptual design studies have been performed on MSRs. The publication history of reports for the MSR program at ORNL is shown in Figure 1.

Gas becomes entrained in the fuel salt flow. This circulating gas is commonly referred to in the literature as *circulating voids*.

2   Circulating Void Fraction

Bubbles and circulating voids have been used synonymously in literature. A distinction may be drawn in that bubbles in an MSR can be subdivided into

1
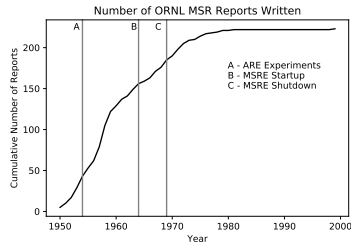
Figure 1: Number of ORNL Reports Written on MSRs. Data taken from Energy From Thorium [1].

those which circulate with the fuel salt around the primary loop — the circulating voids, and those which are introduced only for a brief period of time before exiting — the non-circulating voids. An example of non-circulating voids under the preceding terminology are the bubbles introduced into the pump bowel by the gas sparging apparatus.

Circulating voids are known to have two impacts on MSR behavior. First they are a means by which fission products, especially gaseous fission products (such as ^{135}Xe), can migrate about the reactor. Second by changing the distribution of fuel salt in the reactor core, the voids alters the nuclear configuration of the core and effectively withdraw (or potentially inserts) reactivity into the reactor.

The circulating void fraction is often reported in the literature as a single scalar quantity, usually a percentage. This, however, has the connotation that the circulating void fraction is a constant at all points in the reactor. This is not necessarily true. ORNL-TM-2373 [2, p. 27] provides evidence that there is considerable variation in the apparent density of the fuel salt in the pump bowl, and this variation is caused by entrained voids. Furthermore, temperature and pressure variation in the flow path of the fuel salt will likewise cause variation in the volume of gas that comprises the circulating void fraction through expansion or compression of the gas phase.

The circulating void fraction is a dimensionless quantity and, in a loose sense, represents the relative quantity of gas entrained in MSR fuel salt compared to the relative quantity of liquid fuel salt. Potentially, the circulating void fraction could be either defined in terms of mass, volume, or ratios of moles of substance. To the best of our knowledge, no formal definition of the circulating void fraction has been given in the literature.

Considering the mass of the fuel salt is much greater than the mass of entrained gas, it is unlikely that the circulating void fractions that have been reported in the literature would be defined in terms of mass. To this point, there are two excerpts from ORNL-4233 [3] which are indicative of this claim: first,

> *"At steady state, the volume fraction of gas in the circulating stream varies around the loop proportionally to the inverse of the local pressure..."* [ibid.],

and second,

> *"...densitometer measurements indicated that 2% to 3% of voids by volume were in circulation..."* [ibid.]

Furthermore, we are unaware of any in situ measurements of circulating void composition, therefore, it seems untenable to define the circulating void fraction in terms of the molar composition of the gas.

It therefore seems appropriate to assume the circulating void fraction reported elsewhere in the literature as a volumetric fractions.

In terms of volume, there are two potential ways to define the circulating void fraction, represented by Equation 1 or Equation 2. Equation 1 defines the circulating void fraction as the ratio of the volume of gas in the reactor to the volume liquid fuel salt in the reactor. Equation 2 defines the circulating void fraction as the ratio of the gas in the reactor to the total volume of the fuel salt and gas in the reactor.

$$f_{CV}^{I} = \frac{V_{gas}}{V_{FS}}, \quad (1)$$

or as,

$$f_{CV}^{II} = \frac{V_{gas}}{V_{FS} + V_{gas}}. \quad (2)$$

2

We propose the second way, shown in Equation 2, is the correct one since doing so would sum the gas and fuel salt void fractions to 1, This however, to the best of our knowledge, has not been formally defined.

Precision in this definition is important since the circulating void fraction in the MSRE ranged, depending on the measurement made, between less than 0.1 % [4] to 3% [3]. The deviation between these two definitions increases monotonically with the amount of gas in the reactor. Equation 3 states the simplified expression for the ratio of the f_{CV}^I to the f_{CV}^{II} definition of the circulating void fraction.

$$\frac{f_{CV}^I}{f_{CV}^{II}} = 1 + \frac{V_{gas}}{V_{FS}};\qquad(3)$$

therefore, at higher quantities of entrained gas, precision in definition becomes increasingly important.

3 Timeline of ORNL Reports

Figure 2 shows a time-line of all available ORNL reports focused on MSR bubble behavior. In addition to these reports, the progress report ORNL-4832 (1973) [5, p. 29] reports on the development of gaseous fission product removal equipment, and includes a subsection that details bubble formation and coalescence tests, which were not found reported elsewhere.

4 Methods to Measure the Circulating Void Fraction

The earliest attempt to measure the circulating void fraction in-situ was reported in ORNL-3529 (1963) [11]. The report states a 10 Ci *"cesium source"* (isotopic composition unspecified) [ibid., p. 50] was installed diametrically opposed to a radiation detector on the pump inlet pipe in the MSRE prototype pump loop to create a densitometer. By measuring variation in the apparent fuel salt density (as a fraction of radiation attenuated), a measure of the circulating void fraction was obtained.

The first known method to measure the circulating void fraction in the MSRE was the pressure release tests reported in ORNL-4037 (1967) [12, p. 22]. In these tests, the reactor over-pressure was increased by a factor of about three then suddenly released. When the pressure was released, the fuel salt expanded and the salt level in the pump bowel was perturbed. This change in the level was associated with the expansion of gas entrained within the salt flow. The report also mentions the operation of a *"salt densometer"* to measure the circulating void fraction in-situ, but details of these measurements were not found.

Another attempt to measure the circulating void fraction was reported in ORNL-TM-2315 (1968) [4]. The report describes a project that attempted to correlate the circulating void fraction with measurements of neutron noise in the MSRE.

The report concludes, *"Theoretical studies show the absolute void fraction could be measured* [in the MSRE] *by crosscorrelating* [sic.] *the neutron noise signal with a pressure noise signal obtained from a transducer placed in the primary loop of the MSRE"* [ibid., p. 28].

Another project to measure the circulating void fraction in the MSRE was reported in ORNL-TM-2318 (1968) [7]. The technique attempted to correlate pressure perturbations with the circulating void fraction. The report concludes *"...the analytical prediction of the reactivity-to-pressure frequency response function was only nominally correct."*.

Finally, ORNL-TM-2997 (1970) [13, p. 17] reports on the creation of a densitometer for the MSRE. The project used a similar approach as that which was used on the MSRE fuel pump test loop [11, p. 50]: a 40 Ci ^{137}Cs source was placed such that it was diametrically opposite a radiation detector on the pump inlet fuel salt piping of the MSRE, and variation in salt density was measured.

On a tertiary note, no measurements of the composition of the circulating voids were found. ORNL-TM-2315 [4, p. 1] states the circulating void fraction in the MSRE was comprised of helium, but no information was found related to how this was known. Presumably, this was inference: the cover gas is comprised of helium therefore it would follow that the

3
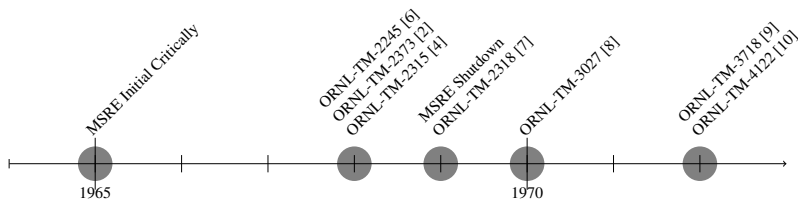
Figure 2: Timeline of ORNL Reports on Circulating Void Behavior

circulating voids would be comprised of helium from gas ingestion. This is, however, not a high resolution view of the circulating void composition and activities such as validation of a MSR xenon model would require measurements of trace amounts of non cover gases in the circulating voids.

5   Foam

Given the churning behavior of the fuel salt, some reports have commented on the existence of a *foam* floating on top of the fuel salt in the MSRE. ORNL-TM-3027 [8, p. 20] reports density of fuel salt near the its surface in the pump bowl is low enough to justify the application of the term *"foam"* to describe the near-surface fuel salt, however, unlike a true foam, the near-surface fuel salt is not persistent. ORNL-TM-3464 [14, p. 71] proposed the existence of a xenon rich foam over the fuel salt to explain the differences in xenon behavior between argon and helium cover-gas.

6   Discovery of Circulating Voids in the MSRE

There were some early indications of entrained gas in the MSRE. The 1962 report ORNL-TM-79 [15] states *"gas bubbles were observed in the pump tank volume* [during a water test of the pump]*"* [ibid., p. 14], the report also states *"baffling was devised to prevent the entry of gas bubbles into the pump inlet"*, and this second statement is indicative engineers did

not expect gas bubbles generated in the pump bowel to circulate.

Regardless, the MSRE was initially expected to operate without circulating voids. ORNL-3872 (1965) [16, p. 30] states *"Although the nuclear experiments* [in the MSRE] *showed that there is no undissolved gas circulating in the fuel loop...behavior of the pump-bowl level on stopping and starting the pump suggests the presence of a small compressible volume of gas somewhere in the loop.* The pressure release tests, which ORNL-TM-3464 [14, p. 10] states *"confirmed that some voids were then present even at normal system condition"*, are reported in the referenced document, ORNL-4037 (1969) [12, p. 22]. Nevertheless, the state of knowledge in 1969 on bubbles circulating in the MSRE was considered to be *"meager"* by the authors of ORNL-4069 [17, p. 43].

7   Bubble Size and the Interfacial Area

ORNL-4069 [17, p. 53] (1967) reported the bubble diameter in the MSRE was *"extremely difficult to estimate"* and the only source of information was a water loop used for MSRE pump testing. The bubbles in this apparatus that migrated from the pump bowl to the pump suction were visible and their diameter, described as a *"pinpoint"* , was interpreted to be 2.54×10^{-1} mm (reported as 0.1").

In addition to these direct observations, there is some additional information that may be used for

4

bubble size estimates. ORNL-TM-2373 [2, p. 11] reports bubbles greater than $3\,\mathrm{mm}$ are inherently unstable in water. Furthermore, ORNL-TM-4122 [10, p. 12] reports the maximum bubble diameter in a turbulent fluid can be predicted by Equation 4,

$$D_{max} = K \left(\frac{\sigma g_c}{\rho} \right)^{3/5} \left(\frac{\rho}{\epsilon_{SP} g_c} \right)^{2/5}, \quad (4)$$

which parameterizes the maximum bubble diameter D_{max}, in terms of the gravitational acceleration constant, g_c, the liquid density, ρ, the surface tension, σ, the specific energy of the flow ϵ_{SP}, and a an experimental constant K.

The report states the preceding equation was obtained from a 1955 paper by Hinze [18], however, an equation of the form of Equation 4 was not found in Hinze's paper. Equation 2 in Hinze's paper states is shown in Equation 5 in this paper,

$$D_{max} \left(\frac{\rho}{\sigma} \right)^{3/5} \epsilon_{SP}^{2/5} = K; \quad (5)$$

the parameterization of Equation 5 is the same as Equation 4, except there is no gravitational acceleration constant, g_c, used in Equation 5.

Jain [19] has presented a review of flow induced breakup of drops and bubbles that includes a table for correlations of critical diameters for particles in various conditions. The mean bubble diameter will nominally be less than the critical diameter for a given flow condition since bubbles are unstable at the critical diameter.

The xenon analyses performed in ORNL-4069 [17] and ORNL-TM-3464 [14, p. 48] have approximated the bubble shape as spherical. The spherical bubble simplification allows for a direct relationship to be established between the bubble diameter and interfacial area Note, although no explicit claim of spherical bubbles was found in ORNL-4069, we believe it reasonable to conclude they were modeled as spheres on account of numerous mentions of a *"bubble diameter"* (e.g. [17, p. 54]) - a *diameter* is a property of a sphere. Quigley [20] has investigated the validity of the spherical bubble simplification in bubble columns, however, no like work was found related to MSRs.

8   Laplace Pressure

The Laplace pressure, as described in the book by Butt, Graf, and Kapl [21, p. 8], along with numerous other sources, is a pressure differential caused by surface tension forces around a curved fluid interface. The magnitude of this pressure difference between the liquid and gas phases is given by Equation 6,

$$\Delta P = \sigma \left(\frac{1}{R_1} + \frac{1}{R_2} \right), \quad (6)$$

where ΔP is the magnitude of the pressure difference between the liquid and gas phases, σ is the surface tension, and R_1 and R_2 are quantities called the *principal radii of curvature*, which are measurements that depend on the geometry of the bubble under consideration.

In the case of spherical bubbles, this equation reduces to $\Delta P = \frac{2\sigma}{R_{Bbbl}}$. Therefore, the pressure inside of a spherical bubble is given by Equation 7,

$$P_{Bbbl.} = P_{Liq.} + \frac{2\sigma}{R_{Bbbl.}}, \quad (7)$$

in which $P_{Bbbl.}$ is the total gas pressure inside of the spherical bubble, $P_{Liq.}$ is the pressure of the surrounding liquid, σ is the surface tension, and $R_{Bbbl.}$ is the radius of the spherical bubble.

Taking a closer look at Equation 7, we see that bubble pressure is broken up into two portions. The first portion is the contribution from the liquid pressure, the second is from the surface tension. In the extreme case $2\sigma/R_{Bbbl} \to \infty$ as $R_{Bbbl} \to 0$, meaning that as the bubbles get smaller the contribution from Laplace pressure becomes more important.

Figure 3 illustrates the variation of theLaplace pressure of a spherical bubble for several molten salts. Atmospheric pressure, $101.3\,\mathrm{kPa}$, is shown by the gray horizontal line. The figure contains two plots: the first is a plot of Laplace pressure vs. bubble diameter; the second, lower, figure shows the an enlargement the boxed region in the above plot. The lower plot's abscissa begins at $1 \times 10^{-6}\,\mathrm{m}$ and extends to $1 \times 10^{-6}\,\mathrm{m} + 1 \times 10^{-8}\,\mathrm{m} = 1.01 \times 10^{-6}\,\mathrm{m}$. The difference in the Laplace pressure between FLiNaK and FliBe salt,

1.8×10^4 Pa at the plot's midpoint is shown with the two arrows that extend from the middle of the plot.

During MSRE operation the range of bubble sizes considered for ^{135}Xe analysis were $0.127\,\mathrm{cm} - 0.508\,\mathrm{cm}$ in diameter [14]. For the specified bubble size range, the expected contribution to bubble pressure from surface tension is $7\,\mathrm{mbar} - 15\,\mathrm{mbar}$.[1]

9   Void Coefficient of Reactivity

ORNL-TM-2315 [4, p. 24] reports the MSRE had a reactivity loss of 180 pcm at 1% circulating void fraction. Elsheikh [24, p. 65], in a paper assessing the safety of MSRs compared to light water reactors, reports MSRs have an inherent negative void coefficient. A negative void coefficient is intuitive since a higher void fraction corresponds to less fuel in the core. However, this may not necessarily be true. Furukawa et al. [25, p. 133] state, in the context of reviewing severe accidents for a Molten Salt Breeder Reactor (MSBR),

> *"If the salt temperature reaches the boiling point, there may be a problem caused by a positive void coefficient, but there are hundreds of channels in the core, and even if 100% void happens at 20 channels simultaneously, void reactivity is only 1\$. In addition there is an effect that the fuel itself disappears, and it is unlikely to become a problem. However, further examination is necessary."*

This passage is prefaced by a citation which could either be interpreted as referring to ORNL-4812 [26] or ORNL/TM-7207 [27]. No mention of a positive void coefficient is found in either of these documents.

In 2006, Suzuki and Shimazu [28] investigated a depressurization accident scenario with the FUJI-12 MSR. In their paper, Suzuki and Shimazu state

---

[1]Calculated using the salt F1 from ORNL-TM-2316 [22] on account of its similarity to MSRE fuel salt composition. In-situ Laplace pressure may be reduced due to the action of a mobile solid particulate phase that acts as a surfactant.
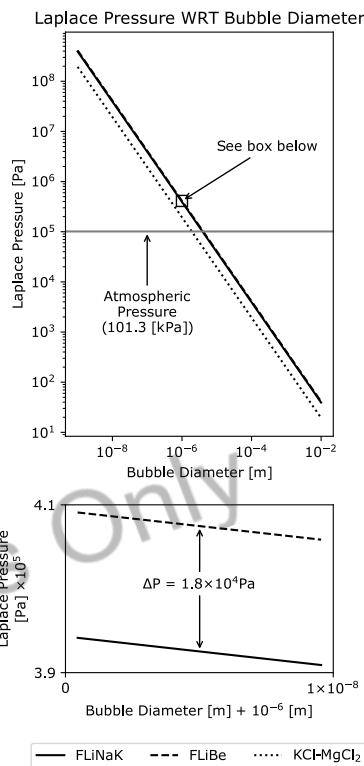
Figure 3: Plot of Laplace pressure with respect to bubble diameter for a spherical bubble for $LiF - NaF - KF$ with a 46.5-11.5-42 mol% composition (colloquially, FLiNaK), $LiF - BeF_2$ with a 67-33 mol% composition (colloquially, FLiBe), and $KCl - MgCl_2$ with a 67-33 mol% composition (no colloquialism known). Surface tensions correlations from equations 2.8, 2.19, and 2.28 in the database compiled by Sohal, Ebner, Sabharwall, and Sharpe [23].

"the void reactivity coefficient of MSRs is positive". They report this coefficient was calculated using *"SRAC95"* with the *"PIJ"* module. The reported void coefficient of reactivity for the FUJI-12 reactor was "0.095 % $\Delta k/k\%void$".

Another paper by Suzuki and Shimazu [29] reported what appears to be a positive void coefficient. More specifically, the *"void"* reactivity coefficient listed in Table 2 of the paper [ibid, p.577] lacks a sign, which typically denotes a positive number, whereas the "fuel temperature" and *"graphite temperature"* reactivity coefficients are explicitly negative and positive respectively. We were unable to determine how these constants were generated. Finally, the change in reactivity due to entrained gas is cited as "$\pm 0.02\% dk/k\%void$, so it's unclear if a positive or negative quantity was used. Given the prior work of Suzuki and Shimazu [28], we are inclined to believe the void reactivity coefficient that they listed was positive.

ORNL-4119 [30, p. 17] (1967) states run 8 of the MSRE (performed in October, 1966) was used to evaluate the reactivity loss due to the steady-state circulating void fraction. This was done by letting the fuel salt settle in the drain tanks for 11 weeks prior to filling the primary loop. When an over-pressure was applied to the system, the fuel salt level in the pump bowel remained stationary – this indicated that there are no circulating voids in the fuel salt since circulating voids would compress and reduce the fuel-salt level as an over-pressure was applied. Comparison of reactivity measurements in run 8 to prior runs, with circulating voids, indicated the MSRE had a reactivity loss of 20 pcm to 40 pcm for a circulating void fraction between 0.1% to 0.2% by volume. These measurements are congruent with the 180 pcm reactivity loss at 1% circulating void fraction reported in ORNL-TM-2315 [4, p. 24] (1968).

It is seen from these reports that there is no consensus on the void coefficient in MSRs. The sign of the circulating void coefficient will depend on the specifics of the design of a reactor. Thermal reactors achieve maximum reactivity at a certain ratio of fuel to moderator. Configurations with less or more moderator density than this optimum are under or over moderated, respectively. Liquid-moderated reactors with solid fuel are designed as under-moderated, such that reducing the moderator density lowers the reactivity. Likewise, solid-moderated reactors with liquid fuel shall be over-moderated to achieve reactivity reduction if the liquid fuel density decreases.

Finally, an account was found that indicates circulating voids can cause power excursions. Engel reports in ORNL-4191 (1967) [31, p. 19] , *"Except for one negative excursion caused by circulating voids immediately after shutdown in run 11, all calculated values of residual reactivity were between..."*. No information was found describing how Engel knew the power excursion was caused by circulating voids.

10 Pressure Coefficient

ORNL-3872 (1965) [16, p. 22] reports three tests were performed with the MSRE to determine the effect of pressure on reactivity in which the system pressure was increased by a factor of two to three then quickly released. A relationship was found between system pressure and reactivity, and this relationship was a function of pressure perturbation frequency. The magnitude of the the pressure coefficient of reactivity varied between 3×10^{-4} to 1.4×10^{-2} $\frac{\delta k}{k\ psi}$ (2.0×10^{-6}/Pa).

In a 1969 paper on MSRE operating experience [32], Haubenreich and Engel report,

> *"The steady-state xenon poisoning in the MSRE varies somewhat with system temperature and pressure..."* [ibid., p. 132]

This claim is expounded in ORNL-TM-3464 [14], which states,

> *"We have already shown that small differences in system temperature and pressure cause significant variations in the circulating helium void fraction and will show subsequently that, with helium cover gas, a higher void fraction leads to higher xenon poisoning."* [ibid., p. 14]

Intuitively, variation in the bubble size, caused by pressure variation, will affect the fuel salt content in core. Furthermore, variation in bubble size will lead

to change in the dynamics of xenon, and other fission product, mass transfer to circulating bubbles.

To this end, Engel states in ORNL-4191 (1967) [31, p. 20], *"The mechanism through which pressure and reactivity are coupled has not yet been established"*, however also posits *"the time constant of the pressure-reactivity is relatively long, suggesting a possible connection through the xenon poisoning"*.

11 Surface Mobility

Bubble mass transfer coefficients are often categorized by the mobility of the bubble surface. According to Wang et al. [33],

> *"a fully mobile bubble surface is a bubble in a pure liquid where there is no hindrance to the surface motion due to the absence of contaminants. A fully immobile surface is conventionally taken to be a surface that acts as a rigid solid surface."*

ORNL-TM-2245[6], which was written in 1968, states,

> *"There does not exist a reliable criterion for specifying the type of bubble interface condition expected for a given condition."*[2]*"*

Conversely, it is also reported [6, p. 17], bubbles smaller than 2 mm behave as rigid interface particles whereas bubbles larger than 2 mm to 3 mm behave as mobile interface particles. If the preceding statement is true, and if the pump loop observations of bubble size mentioned in ORNL-4069 [17, p. 53] are also representative of bubbles in the MSRE, then it follows that the bubbles in the MSRE would behave as rigid interface particles.

12 Gas Production

Gas can enter into the MSR fuel salt either by gas ingress from the cover-gas, which for our purposes

includes active sparging and turbulence frothing in the pump bowl, or through gas produced either from fission or radiolysis. This section explores research that has been conducted on some of the gases produced in an MSR. Note, the gases listed in this section are not exhaustive of all the gases produced in an MSR.

12.1 Tritium

Lyu et al. [34] analyzed the production of tritium in a 2 MW MSR which used a FLiBe (Fluorine, Lithium, Beryllium) based fuel and reported tritium (T) can be produced through the $^6\text{Li}(n, \alpha)\text{T}$, $^7\text{Li}(n, n', \alpha)\text{T}$, or $^{19}\text{F}(n, n', \text{T})^{17}\text{O}$ reactions, through ternary fission, or through ^9Be. To reduce the production of T, the fuel salt in the MSRE used lithium depleted to 99.997% ^7Li. The extra neutron, in comparison to ^6Li, reduces the neutron absorption cross-section since there is already a excess unpaired neutron [35, p. 5]. Tritium is also produced directly from fission. Albenesius [36] reports tritium was observed to form at a rate of $(1-2) \times 10^{-4}$ per fission of natural uranium, enriched uranium, and in a mixture of transuranic isotopes. Finally, ORNL-4119 [30, p. 84] reports hydrogen production in the MSRE was 1.3×10^{-6} g/(MW · d) and tritium production was 4.1×10^{-4} g/(MW · d).

Tritium behavior in molten salts is actively investigated in the context of solid fueled reactors cooled by fluoride salts, see [37, 38].

12.2 Xenon-135

The production of ^{135}Xe in the MSRE has been described in ORNL-4069 [17] and ORNL-TM-3464 [14]. ^{135}Xe is produced either directly through fission or through the decay of the fission product ^{135}I, which is also a decay product of the fission product ^{135}Te. Additionally, as reported by Singh, et al. [39], the A=135 mass chain has numerous other nuclides, such as ^{135}Sb, that may undergo successive β^- decays and transmute into ^{135}Xe. Nevertheless, all text books written on the subject we are aware of, such as Lamarsh's introductory book [40, p. 377], have excluded all isotopes with a proton number less

---

[2]we believe the term *interface condition* is synonymous with the term *surface mobility*, however we were unable to find another source to validate this claim.

than ^{135}Te .

12.3 Free Fluorine

The quantity of free fluorine present in the MSRE while the reactor was operational was reported negligible. ORNL-TM-3708 [41, p. 254] describes a set of experiments in which capsules of a FLiBe based fuel salt were irradiated in the Materials Test Reactor (MTR).[3] ORNL-TM-3144 [43, p. 1] (1970) states, *"These* [capsule experiments] *proved that F_2 was evolved only when the salt was chilled well below the freezing point"*. ORNL-TM-3708 [41, p. 286] reported the results of experiment *"47-6"*, which sampled the off-gas of a capsule during irradiation, states,

> *"A variety of sweep rates, temperatures, and power densities were explored but no CF_4 has been found in the samples that have been analyzed thus far, nor has there been any detectable radioactivity other than that of xenon and krypton. This indicates that neither F_2 nor CF_4 was produced at rates that would be of significance to the MSRE."*

Although free fluorine was thought not to be present in the reactor during operation, the same cannot be said for its shutdown state. ORNL-3529 [11, p. 86] reports on some irradiation experiments an an irradiation capsule denoted *MTR-47-5* and is further described in ORNL-TM-500 [44, p. 28]. The capsules were constructed such that INOR-8 or graphite specimens were contacted with fuel salt that underwent irradiation. Purge gas inlet and outlet lines were installed on each capsule to allow for monitoring of the contents and pressure of the gas space in the top of each capsule. 11.5 days after the irradiation and subsequent cooling of the MTR-47-5 capsule, mass spectrometry revealed a sample of the gas in the *low power* capsule contained 38% He and 5% F_2 as well as *"large amounts"* of Te and I. Analysis of further

---

[3]A $40\,\mathrm{MW}_{th}$ light water cooled and moderated research reactor that operated from 1952 to 1970 at Idaho National Laboratory and had a maximum thermal neutron flux of $4.8 \times 10^{14}/(\mathrm{cm}^2 \cdot \mathrm{s})$. [42]

experimental data from high and low power capsules indicates at $85\,°\mathrm{C}$, the net rate of fluorine evolution was reported to be *zero*.

There is additional information in ORNL-4119 [30, p. 206] related to the production of free fluorine in an MSR. First, in hot cell experiments, it is reported [ibid., p.169] that MSRE fuel salt samples were kept in a hot cell for three months, and this hot cell was kept at a temperature of $300\,°\mathrm{C}$ to prevent fluorine evolution. Therefore, the storage procedures for MSRE fuel salt in a hot cell were written under the assumption that a temperature of $300\,°\mathrm{C}$ was sufficient to prevent the evolution of free fluorine. Second, vaporization experiments on several rare-earth fluorides were reported [ibid., p.206]. We posit vaporization of these rare-earth fluoride compounds is caused by off-gassing of disassociated fluorine.

13 In-core Volume and Reaction Rates

Circulating fuel reactors have fuel in and out of core. Reaction rate calculations, focusing on gas production, are in the form similar to that shown in Equation 8,

$$\dot{N}_i = \gamma_i \Sigma_f \phi V_{IC}, \tag{8}$$

where V_{IC} is the in-core volume, γ_i is the fission yield of a particular isotope, i, Σ_f is the macroscopic fission cross section, and ϕ in the neutron flux.

As the fuel flows about the primary loop, the definition of the in core volume is fuzzy since there are neutrons outside the geometrical core boundaries. Perhaps a better definition would rely on an explicit cutoff value of the neutron flux as a fraction of the peak flux.

14 Bubble Model Requirements

Xenon-135 neutron absorption cross-section of $2.6\,\mathrm{Mb}$ makes description and prediction of its migration in the fuel salt important. Since xenon is a noble gas it can migrate into bubbles in the fuel salt.

For a complete review of MSR Xenon behavior see our 2019 review paper [45]. Our investigations of MSR xenon behavior have lead to the following list of requirements for a complete MSR bubble model. The bubble model shall be capable of: continuous re-circulation of the bubbles; predicting the total quantity of interfacial area in fluid volumes on the order of tens of cubic meters; predicting interfacial area in laminar, turbulent, and transition flow. And it shall account for: the effect of temperature variation; the effect of pressure variation; differences in bubble behavior caused by differences in cover-gas composition; the effects of fuel-pump impeller interaction with the bubbles; the effects of particulate on bubble behavior; changes in volume due to fission or reaction product ingress into the bubbles in circulation; gas ingestion from the fuel-pump; and, foam that floats on top of the fuel-salt.

A model that does not fulfill all of these requirements may still have utility in the prediction and description of MSR xenon behavior. Furthermore, due to the findings of ORNL-TM-3464 [14], we believe that accounting for foam behavior to be a critical part in successful prediction on MSR xenon behavior.

15   Conclusions

Several aspects of circulating void behavior in molten salt reactors have been reviewed. We conclude with the following points:

- Given the common usage of the term *circulating void fraction*, we believe it reasonable that its definition be subject to standardization.

- Although we were unable to find a report that detailed the bubble formation and coalescence tests, this need not imply a report does not exists. If it does exists, it would be highly-valuable in providing evidence for the use of a lumped-parameter bubble model, such as that employed by Shimazu [46].

- The use of a radiation-source based densitometer has been the predominate method by which the circulating void fraction has been measured, although other methods do show promise.

- Although foaming effects have been proposed as an explanation for the differences in observed xenon behavior, no models of precisely how this would work have been found. The body of work related to industrial foam processes may be a promising area for cross-pollination.

- Despite early attempts to mitigate the circulation of voids in the fuel-loop of the MSRE, voids were nevertheless circulated, and their effect on xenon behavior wasn't modeled until the same year in which the reactor was shutdown.

- There has been work done to characterize the maximum size of bubbles in a flow, and there has also been attempts to infer bubble sizes in an MSR from water analogues, however, complete characterization of the size distribution of bubbles in an MSR has been unattempted.

- The Laplace pressure on micro-scale bubbles in an MSR is not negligible.

- The void coefficient of reactivity in an MSR may be positive or negative, and there has been concerned express about the potential for an over-heat accident scenario in an MSR with a positive void coefficient.

- A reliable means for predicting the mass transfer coefficient for bubbles in an MSR is predicated on a reliable criteria for classifying the surface mobility of the bubbles and such a criteria, to the best of our knowledge, has yet to be established.

- There are numerous sources of gas production in an MSR, although our preliminary investigation seems to indicate the magnitude of this gas production to be negligible in many MSRs.

16   Research Questions

The following research questions arose during the development of this paper:

- What kind of in-situ instrumentation can be used to measure bubble size?

- Is it appropriate to use a single bubble reference diameter for analyses such as xenon analysis?

- What is the relationship between bubble size, pressure, reactivity, void coefficient, and xenon behavior?

- Is there a minimum bubble size, below which the the effects of bubbles for analysis are indistinguishable from a homogeneous mixture?

- Is there a bubble size below which the Laplace transfer prevents mass transfer of xenon into the bubble?

- Are circulating void fraction measurements made at the fuel-pump inlet representative of the circulating void fraction of the entire reactor?

- How much does the circulating void fraction vary over the entirety of the reactor and do operational factors influence this variation?

Nomenclature

D_{max}	Maximum bubble diameter	(m)
K	Constant of proportionality	(-)
$\dot{N_i}$	Rate of change of species i	(1/s)
P	Pressure	(Pa)
P_{gas}	Gas Phase Pressure	(Pa)
P_{liq}	Liquid Phase Pressure	(Pa)
R_1/R_2	Principal Radii of Curvature	(m)
$R_{Bbbl.}$	Bubble radius	(m)
V_{FS}	Fuel Salt Volume	(m^3)
V_{IC}	Inc Core Volume	(m^3)
V_{gas}	Gas Volume	(m^3)
f_{CV}^{I}	Definition I of the circulating void fraction	(-)
f_{CV}^{II}	Definition II of the circulating void fraction	(-)
g_c	gravitational constant of acceleration	(m/s^2)
k	Neutron multiplication factor	(-)
Σ_f	Macroscopic fission cross section	(1/m)
δk	Change in neutron multiplication from critically (k - 1)	(-)
ϵ_{SP}	Specific power	(W/kg)
γ_i	Fission yield of species i	(-)
ϕ	Neutron flux	(1/(m$^2 \cdot$ s))
ρ	mass density	(kg/m^3)
σ	Surface tension	(N/m)

Acronyms

ARE Aircraft Reactor Experiment.

MSBR Molten Salt Breeder Reactor.

MSR Molten Salt Reactor.

MSRE Molten Salt Reactor Experiment.

ORNL Oak Ridge National Laboratory.

PWAR-1 Pratt and Whitney Aircraft Reactor 1.

References

[1] Sorensen, K. Energy From Thorium. http://energyfromthorium.com Last Visited 11/5/2019.

[2] Kohn, H., 1968. ORNL-TM-2373: Bubbles, Drops, and Entertainment in Molten Salts. Tech. rep., Oak Ridge National Laboratory, Oak Ridge, TN, USA.

[3] Prince, B., Ball, S., Engel, J., Haubenreich, P., and Kerlin, T., 1968. ORNL-4233: Zero-Power Physics Experiments on the Molten-Salt Reactor Experiment (MSRE). Tech. rep., Oak Ridge National Laboratory, Oak Ridge, TN, USA. pp. 42, 55, 70.

[4] Fry, D., Kryter, R., and Robinson, R., 1968. ORNL-TM-2315: Measurement of Helium Void Fraction in the MSRE Fuel Salt Using Neutron-Noise Analysis. Tech. rep., Oak Ridge National Laboratory, Oak Ridge, TN, USA.

[5] Rosenthal, M., Briggs, R., and Haubenreich, P., 1973. ORNL-4832: Molten-Salt Reactor Program Semiannual Progress Report - Period Ending August 31, 1972. Tech. rep., Oak Ridge National Laboratory, Oak Ridge, TN, USA.

[6] Peebles, F., 1968. ORNL-TM-2245: Removal of Xenon-135 from Circulating Fuel Salt of the MSBR by Mass Transfer to Helium Bubbles. Tech. rep., Oak Ridge National Laboratory, Oak Ridge, TN, USA.

[7] Robinson, J., and Fry, D., 1969. ORNL-TM-2318: Determination of the Void Fraction in the MSRE Using Small Induced Pressure Perturbations. Tech. rep., Oak Ridge National Laboratory, Oak Ridge, TN, USA.

[8] Engel, J., Haubenreich, P., and Houtzeel, A., 1970. ORNL-TM-3027: Spray, Mist, Bubbles, and Foam in the Molten Salt Reactor Experiment. Tech. rep., Oak Ridge National Laboratory, Oak Ridge, TN, USA.

[9] Kress, T., 1972. ORNL-TM-3718: Mass Transfer Between Small Bubbles and Liquids in Cocurrent Turbulent Pipeline Flow. Tech. rep., Oak Ridge National Laboratory, Oak Ridge, TN, USA.

[10] Gabbard, C., 1972. ORNL-TM-4122: Development of a Venturi Type Bubble Generator for use in the Molten Salt Reactor Xenon Removal System. Tech. rep., Oak Ridge National Laboratory, Oak Ridge, TN, USA.

[11] Briggs, R., 1963. ORNL-3529: Molten Salt Reactor Program Semi-Annual Progress Report For Period Ending July 31, 1963. Tech. rep., Oak Ridge National Laboratory, Oak Ridge, TN, USA.

[12] Briggs, R., 1967. ORNL-4037: Molten-Salt Reactor Program Semiannual Progress Report for Period Ending August 31, 1966. Tech. rep., Oak Ridge National Laboratory, Oak Ridge, TN, USA.

[13] Smith, P., 1970. ORNL-TM-2987: Development of Fuel and Coolant Salt Centrifugal Pumps for the Molten Salt Reactor Experiment. Tech. rep., Oak Ridge National Laboratory, Oak Ridge, TN, USA.

[14] Engel, J., and Steffy, R., 1971. ORNL-TM-3464: Xenon Behavior in the Molten Salt Reactor Experiment. Tech. rep., Oak Ridge National Laboratory, Oak Ridge, TN, USA.

[15] Smith, P., 1962. ORNL-TM-79: Water Test Development of the Fuel Pump for the MSRE. Tech. rep., Oak Ridge National Laboratory, Oak Ridge, TN, USA.

[16] Briggs, R., 1965. ORNL-3872: Molten-Salt Reactor Program Semiannual Progress Report for Period Ending August 31, 1965. Tech. rep., Oak Ridge National Laboratory, Oak Ridge, TN, USA.

[17] Kedl, R., and Houtzeel, A., 1967. ORNL-4069: Development of a Model for Computing Xe-135 Migration in the MSRE. Tech. rep., Oak Ridge National Laboratory, Oak Ridge, TN, USA.

[18] Hinze, J., 1955. "Fundamentals of the Hydrodynamic Mechanism of Splitting in Dispersion Processes". *American Institute of Chemical Engineers Journal,* **1**(3), pp. 289–295.

[19] Jain, S., 2017. "Flow-induced breakup of drops and bubbles". *arXiv preprint arXiv:1701.06157*.

[20] Quigley, C., Johnson, A., and Harris, B., 1955. "Size and Mass Transfer Studies of Gas Bubbles". In Chemical Engineering Progress Symposium Series, American Institute of Chemical Engineers, Vol. 1, p. 31.

[21] Butt, H., Graf, K., and Kappl, M., 2006. *Physics and Chemistry of Interfaces*. Wiley. Catalogue entry indicates 495 pages.

[22] Cantor, S., Cooke, W., Dworkin, S., Robbins, D., Thoma, E., and Watson, M., 1968. ORNL-TM-2316: Physical Properties of Molten-Salt Reactor Fuel, Coolant and Flush Salts. Tech. rep., Oak Ridge National Laboratory.

[23] Sohal, M., Ebner, M., Sabharwall, P., and Sharpe, P., 2010. Engineering Database of Liquid Salt Thermophysical and Thermochemical Properties. Tech. rep., Idaho National Laboratory, Idaho Falls, ID, USA.

[24] Elsheikh, B., 2013. "Safety Assessment of Molten Salt Reactors in Comparison with Light Water Reactors". *Journal of Radiation Research and Applied Sciences,* **6**(2), pp. 63–70.

[25] Furukawa, K., Simonenko, V., Mitachi, K., Furuhashi, A., Yoshioka, R., Chigrinov, S., Lecocq, A., and Kato, Y., 2002. "Thorium Cycle Implementation Through Plutonium Incineration by Thorium Molten-Salt nuclear Energy Synergetics". *Thorium fuel utilization: Options and trends*, p. 123.

[26] Rosenthan, M., Haubenreich, P., and Briggs, R., 1972. ORNL-4812: The Development Status of Molten-Salt Breeder Reactors. Tech. rep., Oak Ridge National Laboratory, Oak Ridge, TN, USA.

[27] Engel, J., Baurman, H., Dearing, J., Grimes, W., McCoy, E., and Rhoades, W., 1980. ORNL/TM-7207: Conceptual Design Characteristics of a Denatured Molten-Salt Reactor with Oonce-Through Fueling. Tech. rep., Oak Ridge National Laboratory, Oak Ridge, TN, USA.

[28] Suzuki, N., and Shimazu, Y., 2006. "Preliminary Safety Analysis on Depressurization Accident without Scram of a Molten Salt Reactor". *Journal of Nuclear Science and Technology,* **43**(7), pp. 720–730.

[29] Suzuki, N. Shimazu, Y., 2012. "Reactivity-Initiated-Accident Analysis without Scram of a Molten Salt Reactor". *Journal of Nuclear Science and Technolgy,* **45**(6), pp. 575–581.

[30] Rosenthal, M., Briggs, P., and Kasten, P., 1967. ORNL-4119: Molten-Salt Reactor Program Semiannual Progress Report for Period Ending February 28,1967. Tech. rep., Oak Ridge National Laboratory, Oak Ridge National Laboratory.

[31] Rosenthal, M., Briggs, R., and Kasten, P., 1967. ORNL-4191: Molten-Salt Reactor Program Semiannual Progress Report For Period Ending August 31, 1967. Tech. rep., Oak Ridge National Laboratory, Oak Ridge, TN, USA.

[32] Haubenreich, P., and Engel, J., 1969. "Experience with the Molten-Salt Reactor Experiment". *Nuclear Applications and Technology,* **8**(2), pp. 118–136.

[33] Wang, W., Zhou, Z., Nandakumar, K., Xu, Z., and Masliyah, J., 2003. "Effect of Surface Mobility on The Particle Sliding Along a Bubble or a Solid Sphere". *Journal of Colloid and Interface Science,* **259**(1), pp. 81–88.

[34] Lyu, X., Xia, X., Zhang, Z., Cai, J., and Chen, C., 2016. "Analysis of Tritium Production in a 2 MW Liquid-Fueled Molten Salt Experimental Reactor and its Environmental Impact". *Nuclear Science and Techniques,* **27**(4), p. 78.

[35] Haubenreich, P., Engel, J., Prince, B., and Claiborne, H., 1964. ORNL-TM-730: MSRE Design and Operations Report. Part III. Nuclear Analysis. Tech. rep., Oak Ridge National Laboratory, Oak Ridge, TN, USA.

[36] Albenesius, E., 1959. "Tritium as a Product of Fission". *Physical Review Letters,* **3**(6), p. 274.

[37] Forsberg, C. W., Peterson, P. F., Sridharan, K., Hu, L., Fratoni, M., and Prinja, A. K., 2018. MIT-ANP-TR-180: Integrated FHR Technology Development: Tritium Management, Materials Testing, Salt Chemistry Control, Thermal Hydraulics and Neutronics, Associated Benchmarking and Commercial Basis. Tech. rep., Massachusetts Institute of Technology, Cambridge, MA, USA.

[38] Qin, H., Wang, C., Qiu, S., Zhang, D., Tian, W., and Su, G. H., 2018. "Study of tritium transport characteristics in a transportable fluoride-salt-cooled high-temperature reactor". *International Journal of Energy Research,* **42**(4), pp. 1536–1550.

[39] Singh, B., Rodionov, A., and Khazov, Y., 2008. "Nuclear data sheets for A= 135". *Nuclear Data Sheets,* **109**(3), pp. 517–698.

[40] Lamarsh, J., and Baratta, A., 2001. *Introduction to Nuclear Engineering*, third ed. Prentice Hall, Upper Saddle River, NJ, USA. Library catalogue indicates 626 pages.

[41] Briggs, R., 1964. ORNL-3708: Molten-Salt Reactor Program Semiannual Progress Report For Period Ending July 31, 1964. Tech. rep., Oak Ridge National Laboratory, Oak Ridge, TN, USA.

[42] Research Reactor Database. International Atomic Energy Agency. www.nucleus.iaea.org/RRDB/ Last accessed, 27/3/2019. Entry with IAEA code US0081.

[43] Haubenreich, P., 1970. ORNL-TM-3144: Fluorine Production and Recombination in Frozen MSR Salts After Reactor Operation. Tech. rep., Oak Ridge National Laboratory, Oak Ridge, TN, USA.

[44] Grimes, W., 1963. Radiation Chemistry of MSR System. Tech. rep., Oak Ridge National Laboratory, Oak Ridge, TN, USA.

[45] Price, T., Chvala, O., and Taylor, R., 2019. "Molten salt reactor xenon analysis: Review and decomposition". *Journal of Nuclear Engineering and Radiation Science.*

[46] Shimazu, Y., 1977. "Transient Xenon Analysis in a Molten Salt Breeder Reactor". *Journal of Nuclear Science and Technology,* **14**(11), pp. 805–810.

14

Attachment 7

Xenon in Molten Salt Reactors: The Effects of Solubility, Circulating Particulate,

Ionization, and the Sensitivity of the Circulating Void Fraction

Published in the journal of Nuclear Engineering and Technology

Xenon in Molten Salt Reactors: The Effects of Solubility, Circulating Particulate, Ionization, and the Sensitivity of the Circulating Void Fraction

Terry J. Price[1]
Terry.Price@UOIT.net

Ondrej Chvala[2]
OChvala@UTK.edu

Zack Taylor[2]
RTaylo45@Vols.UTK.edu

[1] University of Ontario Institute of Technology
[2] University of Tennessee, Knoxville

November 2018

Abstract

Xenon behaves differently in molten salt reactors (MSRs) compared to solid fuel reactors. This behavior needs exploring due to the large reactivity effect of the ^{135}Xe isotope, given the current interest in MSR power plant development for commercial deployment. This paper focuses on select topics in xenon transport, reviews relevant past works, and proposes specific research questions to advance the state of the art in each of the focus areas. Specifically, the paper discusses the issue of xenon solubility in MSRs, the behavior of particulates circulating in MSR fuel salt and its influence on the xenon transport, the possibility of ionization of xenon atoms which changes its effective size and thus affects its mass transport, and finally the issue of circulating void fraction and how it is measured. This work presents specific recommendations for MSR designers to research the limits of Henry's law validity, circulating particulate scrubbers, validity of mass transport coefficients in high radiation fields, and the effects of pump speed on circulating void fraction.

1 Introduction

Molten salt reactors (MSRs) use a molten alkali-halide fuel salt as both a working fluid and a fuel matrix.* Actinium fluorides, dissolved in the fuel salt, circulate between a graphite moderating region and a heat exchanger. Whilst the fuel salt is in the moderating region, neutrons become sufficiently thermalized such that an ongoing nuclear chain reaction is sustained, generating heat. Upon leaving the moderating region, the fuel salt flows into the heat exchanger, where the heat is transferred to a secondary side. Finally, the fuel salt travels through a fuel pump which imparts inertia to the fuel salt and maintains salt circulation and a particular mass flow rate. A review of MSRs, including historical reactors and the involvement in Generation-IV, is given by Serp et al. [1].

The fission product, ^{135}Xe ($t_{1/2} = 9.10\,\text{h}$)†, is of considerable interest to reactor physics considerations, given its microscopic thermal neutron absorption cross section, which is often stated as 2.6 Mb. ^{135}Xe is produced in fission, along with the ^{135}Xe progenitors, ^{135}Te ($t_{1/2} = 19$ s), and ^{135}I ($t_{1/2} = 6.57\,\text{h}$), which successively decay, through β^- decay, into ^{135}Xe. Note, early ^{135}Xe models, such as that which is reported in ORNL-TM-1070 [3] (published in 1965), did not include ^{135}Te behavior. This may be because, as reported by Kathawa, Fry, and Thoennessen [4], the half-life of ^{135}Te was not *"observed"* until 1969, although, there were some estimates before then. Furthermore, we note that there is, in fact, a non-trivial yield of ^{135}Sb from fission, which transmutes, eventually, into ^{135}Xe, and this ^{135}Sb has, in prior analyses, been omitted.

There are phenomenological differences in ^{135}Xe behavior in a fluid fueled reactor, such as an MSR, compared to a solid fueled reactor, such as a pressurized water reactor. Whereas in a solid fueled reactor the solid fuel matrix acts to immobilize the ^{135}Xe,

---

*This paper focuses on graphite moderated systems with fluorine as the halide, due to vast past experience and current popularity of this choice.

†Unless otherwise stated, half-life and cross-section data is obtained from the chart of nuclides prepared by Baum, Knox, and Miller. [2]

the ^{135}Xe is free to migrate in an MSR. There exists a porous gas space within the moderator, and there are also bubbles (also called circulating voids in the literature) circulating with the fuel salt, and ^{135}Xe is free to migrate to these gaseous spaces. The existing theory of MSR xenon behavior, as presented in the annex of ORNL-4541 [5], states that xenon behavior, in an MSR at steady state, will obey Equation 1.

$$\{Generation\ Rate\} = \{Burnup\ Rate\ in\ Salt\}$$
$$+ \{Migration\ Rate\ to\ Graphite\}$$
$$+ \{Migration\ Rate\ to\ Bubbles\}, \tag{1a}$$

$$\{Graphite\ Migration\} = \{Decay\ Rate\ in\ Graphite\}$$
$$+ \{Burnup\ in\ Graphite\}, \tag{1b}$$

$$\{Bubble\ Migration\} = \{Decay\ Rate\ in\ Bubbles\}$$
$$+ \{Burnup\ in\ Bubbles\}$$
$$+ \{Stripping\ Rate\ in\ Bubbles\}. \tag{1c}$$

The major numerical work in this field began with the 1961 report ORNL-CF-61-5-62 [6] by Miller, which investigated the effects of the mass diffusion coefficient and xenon stripper efficiency on the xenon poison fraction. Miller's model used a first order rate equation to model the xenon stripper and a slab diffusion equation to model the migration of ^{135}Xe from the fuel salt into the graphite. The next major model was the 1969 report ORNL-4069 [7] by Kedl and Houtzeel. In this model, diffusion into the graphite stringers was changed from a slab diffusion model to a cylindrical diffusion model. Furthermore, Kedl and Houtzeel's model was the first one to include migration into bubbles and subdivide the reactor into regions based on neutron flux. In 1971, a model reported in ORNL-TM-3464 [8] by Engel and Steffy was formulated by lumped volume methods and was the first model to investigate transient behavior. The thread of transient work was later continued by Shimazu [9], who presented a transient model that was substantially simpler than the ORNL-TM-3464 xenon model. Shimazu's 1977 work would be later expanded by Suzuki and Shimazu in 2004 to include a balance of plant model [10].

In regards to experimental investigations, the two major reports on this subject are ORNL-4069 [7] and ORNL-TM-3464 [8]. Both report on experimental and operational data obtained from the Molten Salt Reactor Experiment (MSRE). The data in ORNL-4069 highlight the *Krypton Experiment*, an experiment performed in the pre-operational phase of the MSRE operation that aimed to measure mass transfer coefficients through measurements of radioactive krypton off gas. Actual xenon transient and steady state xenon load data was reported in ORNL-TM-3464.

To the best of our knowledge, no models of MSR xenon behavior that can be reasonably said to be validated exist. Although, the prior major modeling efforts outlined in ORNL-4069 [7] and ORNL-TM-3464 [8] did have some limited success in fitting their model to particular scenarios, we believe it is reasonable to assert the general case is as of yet unresolved. Indeed, because of this lack of success, we believe it reasonable to consider there may be phenomenological blind spots in the current understanding of MSR xenon theory. Therefore, this paper attempts to investigate, review, and explore some of the phenomenology relevant to MSR xenon theory and plot a path forward for future research efforts.

This paper builds on our 2019 review article [11] and attempts to clarify and expand on some of the concepts we laid out in regards ^{135}Xe behavior in an MSR in the context of xenon solubility, circulating particulate, and the size and ionization of ^{135}Xe in an MSR. The paper discusses potential issues and outlines potentially fruitful research questions relevant for MSR design.

2 Solubility of Xenon

Prior xenon analyses have assumed the xenon in the fuel salt is sufficiently dilute so that Henry's law,

$$H = \frac{C_i}{P_i}, \tag{2}$$

is applicable, and, as such, extensive use of this constant is made in the mass transfer relations employed in MSR xenon analyses. Henry's law, however, assumes the solution acts as a *ideal dilute solution*, which technically is only true as the concentration of the xenon solute approaches zero. No experimental evidence was found that indicated any sort of upper bound for xenon concentration, past which Henry's

law would not be applicable, nor were there any measurements of ^{135}Xe concentration in the fuel salt. Westh and Haynes [12], however, did experimentally investigate the extent of the Henry region in some non-molten salt substances and concluded there is a lower limit, in terms of mole-fraction, of Henry-like behavior on the order of 1×10^{-5} for a water solute and hexane solvent and 1×10^{-4} for hexane solutes and solvents[‡]. That being said, these values are likely far too high for ^{135}Xe in molten salts, considering the solubility of xenon in LiF-BeF$_2$ (64-36 mol%)is on the order of 4.2×10^{-8} to 3.0×10^{-7} mol% [13]. Furthermore, molten salts are different chemical systems than water/hexane systems, and, as such, are likely to be considerably different.

Apart from xenon concentration itself, there is the potential for other gases dissolved in the fuel salt to influence the xenon behavior. In nucleation theory if a cluster of atoms, with a phase different than its parent phase, exceeds a *critical radius*,

$$r_c = \frac{2\gamma_{12}}{\Delta G_r},$$

(3)

a discrete phase inclusion will form. [14, p. 8-23] Presumably, this cluster of atoms need not necessarily be limited to one isotopic or chemical species, and, as such, a xenon atom will nucleate if it joins a cluster of existing gas atoms with equal to or greater than the critical radius. Note, the critical radius is a function of the Gibbs energy, ΔG_v, which is a function of temperature, pressure, and fuel salt composition. It therefore follows that the critical radius will change as a function of fuel salt composition, which changes as a function of burn-up.

This brings us into considerations of xenon solubility in the fuel salt. Although there have been several studies of xenon solubility in fuel salt (see [13] for example), the following research questions are, to the best of our knowledge, unanswered:

- How does the solubility limit, as measured in-lab, relate to the solubility limit, in-situ?

- What happens the ^{135}Xe produced after the fuel salt has reached its solubility limit? A priori, we expect it to form discrete gaseous phase inclusions, but no direct observational evidence of this was found.

[‡]C and N hexane

- If discrete gaseous phase inclusions are formed, what are their fate? Do they join the existing circulating void phase? Are there mass transfer processes that apply specifically to these newly formed phase inclusions that do not affect the existing circulating void phase?

- If gaseous phase inclusions are formed, what are they comprised of? Is it only xenon, which has amalgamated, or a collection of other substances that is dependent on the fuel composition? For the purposes of modeling efforts, are these new phase inclusions functionally the same as the existing circulating void phase?

- Does the phenomenology of newly formed phase inclusions effectively reduce to the phenomenology of the circulating void fraction? Can xenon behavior, in a reactor operating past its solubility limit, be predicted by a validated bubble model alone or is a more in-depth modeling effort necessary?

Given that there exists a critical radius, we propose there also exists a corresponding *bubble-out concentration*, C_{BO}, of dissolved gas, beyond which all newly generated ^{135}Xe will form discrete phase inclusions. Thus, we propose, the concentration of dissolved gases can be delineated into three distinct regimes:

1. THE IDEAL DILUTE SOLUTION REGION where the behavior of ^{135}Xe is effectively predicted by Henry's law.

2. THE NON-HENRY-LIKE REGION, in which the behavior of ^{135}Xe deviates, by some predetermined magnitude, from Henry's law.

3. THE BUBBLE-OUT REGION Where all new ^{135}Xe produced in the reactor immediately forms discrete phase inclusions.

The precise concentrations of ^{135}Xe, and other gases, which delineate these regions, have yet to be established for any salt. Ideally, there would be a method to correlate a particular fuel salt's Henry's constant, burn-up, and solubility to the three aforementioned regions.

3 Circulating Particulate

Prior work on MSR xenon modeling has neglected any effects of circulating particulate on ^{135}Xe behavior. That being said, there are some considerations that can be made here.

First, is the effects of a mobile solid phase on ^{135}Te behavior. ORNL-4865 [15], which is a report on fission product behavior in the MSRE, states, in the context of the MSRE, *"Nobel metal fission products [such as Te] do not form fluorides which are stable in salt at the redox potential of the fuel salt"* [ibid., p. 27]. Furthermore, *"recent observations ... suggest that a soluble, reactive form of [the] telluride ion can exist in molten salt at a presently undefined redox potential"* [ibid., p. 29], and *"it is plausible tellurium is largely associated by undissolved solids by chemisorption or reaction"* [ibid., p. 29]. Contrary to this, the ORNL-4069 [7] and ORNL-TM-3464 [8] xenon models both assume ^{135}Te remains in solution as an ion. Note, ORNL-4865 was published in 1975, after both ORNL-4069 and ORNL-TM-3464, which were published in 1969 and 1971 respectively, so the authors of ORNL-4069 and ORNL-TM-3464 would likely not have been aware of the observations from ORNL-4865. With this being said, it is foreseeable that, in terms of ^{135}Xe behavior, the behavior of ^{135}Te, and its interplay with particulate, may be negligible; however, no evidence was found that indicates this is the case.

Additionally, there is the potential for the poison isotopes to interact with circulating corrosion product particulate. ORNL-TM-3464 reported *"Holdup in corrosion-product scale was shown to be significant in an aqueous system due to iodine adsorption."* [8, p. 5] Prior modeling efforts had ignored any sort of behavior related to holdup of poison isotopes onto corrosion products. ORNL-4865 reported 20-90% of tellurium was associated with metal in the MSRE. [15, p. 139] The xenon model [16] for the HRT[§] included phenomenology related to ^{135}I diffusion onto corroded wall surfaces; however, no information was found that indicated that any MSR xenon model had included ^{135}I adsorption phenomenology.

There also exists the potential for surface active particles (surfacants) to affect circulating void behavior,

which*, would, in turn, effect ^{135}Xe behavior, since ^{135}Xe migrates to the circulating voids. In the classical two-film theory, the phase boundary resistance is assumed to be negligible [17]. However, we propose, when surfacants are present they tend to accumulate on the phase boundaries. This will in turn create an added resistance that must be taken into account when developing the mass transport across the surface. In ORNL-TM-3884 [18, p. 27], floating scums, which are likely formed, in-part, by the coagulation and de-entrainment of circulating particulate, were hypothesized to posses many properties of a surfacant. ORNL-TM-4122 [19, p. 12] reported a correlation by Hinze, which is a function of surface tension, that predicts the maximum bubble diameter in turbulent flow,

$$d_{max} = K_1 \left(\frac{\gamma_{12}g}{\rho_c} \right)^{3/5} \left(\frac{\rho_c}{\epsilon_{sp}g} \right)^{2/5} . \qquad (4)$$

Given that surfacants lower the surface tension of a substance, and the maximal bubble size, in turbulent flow, is determined by the surface tension, it follows that the addition of circulating particulate, which is hypothesized to act as a surfacant, to the fuel-salt, would affect the maximal bubble size, and hence, the ^{135}Xe behavior. Presumably, the addition of a surfacant would lead to a lower surface tension, which would lead to a lower maximal bubble diameter, which would lead to more bubbles required to encompass the same void fraction, which would lead to more surface area for mass transfer, which would lead to more hold-up of ^{135}Xe in the circulating voids. Additionally, since the rate of mass transfer induced by bubble stripping is, likely, not the same as the rate of mass transfer induced by fuel salt stripping, it follows that the steady-state xenon poison fraction in the reactor core will likewise change with the addition of surfacants. There is observational evidence for this in MSRE venturi jet tests, where smaller bubbles were generated when a surface active material was present. [18, p. 27] Furthermore, Vazirzadeh, Bouchard, and Chen reported fine particles affected both the interactions of bubbles as well as bubble weight and volume in a flotation column. [20]

Variation in surface tension, induced by the addition of particulate, which acts as a surfacant, we claim, will also affect the bubble pressure. The Laplace pressure

---

[§]The Homogeneous Reactor Test, a 5.0 MW$_{th}$ aqueous homogeneous reactor operated at Oak Ridge National Laboratory 1957-1961,

4

[21, p. 61],

$$p_b = p_l + \frac{2\gamma_{12}}{r_b}, \qquad (5)$$

which describes pressure inside a bubble, is a function of surface tension. Therefore, as surface tension is decreased, by the addition of particulate which acts as a surfacant, the pressure inside the bubble is likewise decreased, and, correspondingly, the quantity of ^{135}Xe potentially stored within a single bubble will likewise decrease. This becomes increasingly important with bubbles with small bubble radii, r_b, such as those, which presumably, would be generated by the amalgamation of gaseous fission products, such as ^{135}Xe.

Finally, we note the possibility for circulating particulate to deposit and *coat* the surface of graphite stringers, and thereby, change the amount of surface area available for mass transfer to the graphite stringers. Migration of noble fission products to the graphite stringers was studied in ORNL-TM-3884 [18]; however, no information was found related to how the accessibility of the graphite pore-space would be affected, or the change in effective mass transfer area due to particulate deposition. Post-irradiation examination of MSRE graphite was reported in ORNL-TM-4174 [22], however, no information was found on the surface evolution of MSRE graphite stringers. We therefore propose the following research questions:

- Can significant quantities of particulate collect on the surface of MSR graphite?

- If so, what effect does this have on ^{135}Xe mass transfer into the graphite?

- What steps can be taken to mitigate the accumulation of particulate on graphite stringer surfaces such that the ^{135}Xe remains constant over the lifetime of the reactor?

- If a surface layer of particulate has formed, are there any active solutions to remove the collected particulate on graphite stringer surfaces?

4   Size of ^{135}Xe and Ionization

The sum of all xenon's ionization energies is $\approx 0.2\,\text{MeV}$. [23] Fission products are *born* with a kinetic energy, split between the products, in excess of $160\,\text{MeV}$. [24]

Additionally, each fission generates $6\,\text{MeV}$ of prompt γ-radiation energy. [25] Since the energy generated in fission is much greater than the ionization energy of xenon, we therefore propose that much of the ^{135}Xe found in an MSR, with a sufficient radiation field, will exist in an ionized state. Furthermore, if we accept an ^{135}Xe atom is *born* ionized, due to the kinetic energy of the fission process, we also propose that, so long as there is a sufficient radiation field, such as the γ-radiation from fission, the ^{135}Xe will remain ionized.

We set up our discussion on the effect of ionization with the following consideration: the atomic radius of ^{135}Xe is related to its mass transfer behavior through the mass diffusion coefficient. Since xenon behavior is predicted, in existing models, by the mass transfer coefficient, k_m, which is given through the Sherwood Number, Sh, and the Sherwood number is a function of the mass diffusion coefficient, D, and the mass diffusion coefficient can be predicted through the Einstein-Stokes equation [26, p. 126],

$$D = \frac{k_b T}{6\pi \mu r_{xe}}, \qquad (6)$$

and the Einstein-Stokes relationship is a function of the atomic radius of xenon, it follows that the xenon behavior is dependent on the size of the xenon atom. With that being said, given that the Einstein-Stokes equation assumes in its derivation that the diffusing particle is in a continuous medium, and the constituent molecules of molten salts have a comparable radius to xenon, it is questionable if the Einstein-Stokes equation is applicable to ions diffusing in molten salts. This, however, was investigated by Brockis and Reddy who investigated a number of tracers in molten salts, and compared experimental data for mass diffusion coefficients with mass diffusion coefficients produced by the Einstein-Stokes equation with crystal radii used for the atomic radius parameter. [27, p. 655] Brockis and Reddy state,

> "The essential applicability of this phenomenological equation is clearly shown by using the numerical comparison of $D\mu/T = k_b/6\pi$. The right-hand side is 0.7×10^9 for $r = 300$ pm, and the mean of the experimental values is 0.6×10^9, which is not bad!"

The question What is the size of the xenon atom? is a question in itself; i.e. what is

5

meant by the size of the xenon atom? This sentiment is reflected in Pau, Berg, and McMillan's 1990 paper [28] on the application of Stoke's law to ions in aqueous solutions,

> *"One of the most difficult questions involved in the transition from a continuum medium to the case of real solvent molecules of size comparable to the atomic dimensions of the mobile ion is unit is the meaning to be attached to the particle radius".*

Some atomic radii for xenon are listed in Table 1. It is unclear to us which would be most appropriate to use for the calculation of the mass diffusion coefficient. Blander, Grimes, Smith, and Watson report the radii of rare gas atoms in a solid would be a *"lower limit"* of a hole created by a gas atom in a molten salt. [29]

Table 1: Atomic radii of xenon

Type	Radius [Å]	Source
Covalent Radius	1.36	[30, p. 9-58]
van der Waal's Radius	2.16	[ibid.]
Lennard-Jones Collision Radius	2.02	[31, p.24]
Grimes, Blander, Watson	2.18	[29]
Kinetic Theory	1.75	[32, p. 249]

Now, in consideration of the effect of the ionization, mentioned at the start of this section, the ionization of ^{135}Xe, Born states, in his book on atomic physics [32, p. 249],

> *"We see¶ that the negative ions, which have an inert gas configuration with a smaller nuclear charge then the corresponding inert gas, are larger than the latter, the reason being of course that the electrons in these ions are more loosely bound so that their orbits have greater radii. A corresponding, mutatis mutandis, hold for positive ions also."*

Given that ionization effects the atomic radius of an atom, and, as previously argued, ^{135}Xe produced in the reactor is in an ionized state, it follows that the

---
¶In an attached tabulation of ionic radii

radius of ^{135}Xe in an active nuclear reactor will be different than the ^{135}Xe in a non-radioactive experiment. Specifically, since

$$Sh \propto^{-1} D, \tag{7}$$

and,

$$D \propto^{-1} r_{Xe}, \tag{8}$$

and r_{xe} is smaller in a radioactive environment than a non-radioactive environment, it follows that

$$Sh \propto r_{Xe} \implies k_m \propto r_{Xe}, \tag{9}$$

and k_m in a non-nuclear mock-up will be greater than that of a operating nuclear system.

5 Circulating Void Fractions

Given that, according to the analysis in ORNL-4069 [7], it is possible the majority of the ^{135}Xe to be found in the circulating voids, it follows that consistent ^{135}Xe behavior will likely depend on a consistent quantity of gas circulating with the fuel salt. Modeling and prediction is complicated by two factors: determining what the circulating void fraction is and keeping the circulating void fraction consistent.

ORNL-TM-2318 [33] reports an attempt was made to determine the void fraction in the MSRE using pressure perturbations. These pressure perturbation experiments produced a *"large spread"* of results between 0.023% and 0.045%. Additionally, ORNL-TM-2315 [34] reports using neutron noise analysis to determine the void fraction in the MSRE. The neutron noise experiments concluded that the void fraction in the MSRE is *"more nearly zero than the previously accepted value of 0.1%"*. According to the ORNL-4069 xenon model, the xenon poison fraction contributed by the bubble ^{135}Xe content would vary by a factor of ≈ 5 between the minimum investigated value of $\approx$ 0.05% and 0.1%.

Furthermore, as reported in ORNL-TM-3464 [8], the void fraction is not only dependent on the type of cover-gas used, but also on the rotational speed of the fuel pump. Indeed, a 100 RPM variation in fuel pump speed, in one case, lead to an increase in circulating void fraction in excess of 6.5 fold.

6

6 Conclusions

This paper has examined some aspects of MSR xenon behavior related to solubility, circulating particulate, the size and ionization of ^{135}Xe, and the circulating void fraction. A brief review of MSR xenon theory has been given. The interplay between solubility and xenon concentration has been discussed, and three regimes of xenon concentration have been proposed along with several research questions related to the solubility of xenon in the fuel salt. Furthermore, the potential effects of circulating particulate on xenon behavior have been described along with several related research questions. Additionally, the size of ^{135}Xe and the potential for ionization of ^{135}Xe to affect that size and diffusion properties has been explored. Finally, this paper has looked at the circulating void fraction and examined some potential barriers to proper modeling of it. There are certainly many uncertainties related to ^{135}Xe in MSRs, and this paper has attempted to examine some of them.

7 Recommended Future Work

The following recommendations are made to guide future work:

1. Efforts should be made to delineate the precise concentration of ^{135}Xe, and other gases, in molten salts which Henry's law is valid for. If reactors are not expected to operate within the Henry region, efforts should be made to formulate mass transfer laws which do not depend on Henry's constant.

2. If we accept that it is reasonable to presume that circulating particulate will affect ^{135}Xe behavior, efforts should be made to mitigate the quantity of circulating particulate in the fuel salt and control its evolution with respect to time. Then, ^{135}Xe behavior can be maintained at a constant, and the ^{135}Xe behavior at the beginning of the fuel cycle life will, more likely, be the same as the ^{135}Xe behavior at the end of the core life.

3. Experimentation should be performed to test the hypothesis that xenon mass transfer coefficients, in a sufficiently strong radiation field, will be less than mass transfer coefficients outside of a radiation field. If this hypothesis is found to be true, then mass transfer coefficients measured in a non-nuclear mock-up should be considered an upper limit to the actual mass transfer coefficients.

4. If there is indeed an operating region where minor variations in pump speed will lead to major variations in circulating void fractions, efforts should be made to avoid this operating region and carefully control pump speed such that the circulating void fraction remains constant.

Nomenclature

ΔG_r	Change in Gibb's energy by the formation of a bubble
ϵ_{sp}	Specific energy dissipation
γ_{12}	Surface tension between phases 1 and 2, in this paper, the fuel-salt and a gaseous phase, such as the contents of a bubble
μ	Dynamic viscosity
ρ_c	Density of the continuous phase (the fuel salt); as opposed to the dispersed phase(s) (the circulating voids)
C_i	Concentration of a species
D	Mass diffusion coefficient
d_{max}	Maximum bubble diameter
g	Acceleration due to gravity
H	Henry's Constant
K_1	An experimentally determined constant
k_b	Boltzman's constant
k_m	Mass transfer coefficient
p_b	Bubble pressure
P_i	Partial pressure of a species
p_l	Liquid pressure
r_b	Bubble radius
r_c	Critical radius
r_{xe}	Radius of a xenon atom
Sh	Sherwood number
T	Temperature
$t_{1/2}$	Half-life

7

References

[1] J. Serp, M. Allibert, O. Beneš, S. Delpech, O. Feynberg, V. Ghetta, D. Heuer, D. Holcomb, V. Ignatiev, J. Kloosterman, L. Luzzi, E. Merle-Lucotte, J. Uhlíř, R. Yoshioka, and D. Zhimin. The Molten Salt Reactor (MSR) in Generation IV: Overview and Perspectives. *Progress in Nuclear Energy*, 77:308–319, 2014.

[2] E. Baum, H. Knox, and T. Miller. *Nuclides and Isotopes: Chart of the Nuclides*. Lockheed Martin, 16 edition, 2010.

[3] S. Ball and T. Kerlin. ORNL-TM-1070: Stability Analysis of the Molten-Salt Reactor Experiment. Technical report, Oak Ridge National Laboratory, 1965.

[4] J. Kathawa, C. Fry, and M. Thoennessen. Discovery of palladium, antimony, tellurium, iodine, and xenon isotopes. *Atomic Data and Nuclear Data Tables*, 99 (1):22–52, 2013. ISSN 0092-640X.

[5] R. Robertson. ORNL-TM-4541: Conceptual Design Study of a Single-Fluid Molten-Salt Breeder Reactor. Technical report, Oak Ridge National Laboratory, 1971.

[6] J. Miller. ORNL-CF-61-5-62: Xenon Poisoning in Molten Salt Reactors. Technical report, Oak Ridge National Laboratory, 1961.

[7] R. Kedl and A. Houtzeel. ORNL-4069: Development of a Model for Computing Xe-135 Migration in the MSRE. Technical report, Oak Ridge National Laboratory, 1967.

[8] J. Engel and R. Steffy. ORNL-TM-3464: Xenon Behavior in the Molten Salt Reactor Experiment. Technical report, Oak Ridge National Laboratory, 1971.

[9] Y. Shimazu. Transient Xenon Analysis in a Molten Salt Breeder Reactor. *Journal of Nuclear Science and Technology*, 14(11):805–810, 1977.

[10] K. Suzuki and Y. Shimazu. Transient Xenon Effect on Plant Control in MSRs-Validation of Simulation Model. In *Proceedings of ICAPP '04*, Pittsburgh, PA, USA, 2004.

[11] T. Price, O. Chvala, and R. Taylor. Molten salt reactor xenon analysis: Review and decomposition. *Journal of Nuclear Engineering and Radiation Science*, 2019. Accepted, awaiting publication.

[12] P. Westh, C. Haynes, and Y. Koga. How Dilute Is the Henry's Law Region? II. *The Journal of Physical Chemistry B*, 102(25):4982–4987, 1998.

[13] G. Watson, R. Evans III, W. Grimes, and N. Smith. Solubility of Noble Gases in Molten Fluorides. In LiF-BeF2. *Journal of Chemical and Engineering Data*, 7 (2):285–287, 1962.

[14] J. Groza and J. Shackelford. *Materials Processing Handbook*. CRC Press, 2007.

[15] E. Compere, S. Kirslis, E. Bohlmann, F. Blankenship, and W. Grimes. ORNL-4865: Fission Product Behavior in the Molten Salt Reactor Experiment. Technical report, Oak Ridge National Laboratory, 1975.

[16] W. Burch. ORNL-TM-228: Measurement of Xenon Poisoning in the HRT. Technical report, Oak Ridge National Laboratory, 1962.

[17] James R. Welty, Charles E. Wicks, and Robert E. Wilson. *Fundamentals of Momentum, Heat and Mass Transfer*. John Wiely and Sons, Inc., New York, 1969.

[18] R. Kedl. ORNL-TM-3884: The Migration of a Class of Fission Products (Noble Metals) in the Molten-Salt Reactor Experiment. Technical report, Oak Ridge National Laboratory, 1972.

[19] C. Gabbard. ORNL-TM-4122: Development of a Venturi Type Bubble Generator for use in the Molten Salt Reactor Xenon Removal System. Technical report, Oak Ridge National Laboratory, 1972.

[20] A. Vazirizadeh, J. Bouchard, and Y. Chen. Effect of particles on bubble size distribution and gas hold-up in column flotation. *International Journal of Mineral Processing*, 157:163–173, 2016.

[21] L. Schramm. *Emulsions, Foams, and Suspensions: Fundamentals and Applications*. Wiley, 2006.

[22] H. McCoy and B. McNabb. ORNL-TM-4174: Postirradiation Examination of Materials From the MSRE. Technical report, Oak Ridge National Laboratory, 1972.

[23] A. Kramida, Yu. Ralchenko, J. Reader, and and NIST ASD Team. NIST Atomic Spectra Database (ver. 5.6.1), [Online]. Available: https://physics.nist.gov/asd [2018, November 13]. National Institute of Standards and Technology, Gaithersburg, MD., 2018.

[24] M. James. Energy Released in Fission. *Journal of Nuclear Energy*, 23:517–536, 1969.

[25] S. Oberstedt, R. Billnert, A. Gatera, W. Geerts, and P. Halipr. Prompt fission γ-Ray Spectra Characteristics - a First Summary. *Physics Procedia*, 64:83–90, 2015.

[26] E. Cussler. *Diffusion: Mass Transfer in Fluid Systems*. Cambridge University Press, third edition, 2007.

[27] J. Bockris and A. Reddy. *Modern Electrochemistry, Volume 1, Ionics*. Kluwer Academic Publishers, 1998.

[28] P. Pau, J. Berg, and W. McMillan. Application of stokes' law to ions in aqueous solution. *Journal of Physical Chemistry*, 94(6):2671–2679, 1990.

[29] M. Blander, W. Grimes, N. Smith, and G. Watson. Solubility of Noble Gases in Molten Fluorides. II. In the Lif-NaF-LF Eutectic Mixtures. *The Journal of Physical Chemistry*, 63(7):1164–1167, 1959.

[30] W. Haynes, editor. *CRC Handbook of Chemistry and Physics, 97th Edition*. CRC Press, 2016.

[31] R. Svehla. R-132: Estimated viscosities and thermal conductivities of gases at high temperatures. Technical report, NASA, 1962.

[32] M. Born. *Atomic Physics: 8th Edition*. Dover Publications, 2013.

[33] D. Robinson, J. Fry. ORNL-TM-2318: Determination of the Void Fraction in the MSRE Using Small Induced Pressure Pertubations. Technical report, Oak Ridge National Laboratory, 1969.

[34] D. Fry, R. Kryter, and R. Robinson. ORNL-TM-2315: Measurement of Helium Void Fraction in the MSRE Fuel Salt Using Neutron-Noise Analysis. Technical report, Oak Ridge National Laboratory, 1968.

Acknowledgements

Attachment 9

The Maneuverability of Molten Salt Reactors

Unpublished

The Maneuverability of Molten Salt Reactors

Terry Price

April 2019

1   Introduction

This report is a response to Dr. Bereznai's instructions to compare the xenon behavior in molten salt reactors (MSRs) and the xenon behavior in CANDU reactors. The following activities have been documented in this report:

- Xenon behavior in solid fuel reactors has been described
- The Reactivity balance of a reactor has been described and how the xenon reactivity load influence the reactivity balance
- Reactivity control devices in solid fuel reactors have been described
- The assumption that reactivity control devices can be modeled as linear devices has been examined
- Reactivity control devices in a CANDU reactor have been described
- The iodine pit in a CANDU reactor has been described.
- Xenon behavior in a molten salt reactor has been described
- The action of a xenon stripper in a molten salt reactor has been described

Furthermore, a model of a 1000 MWe molten salt reactor has been developed. This model includes sub-models for,

- Neutronics
- Thermal behavior
- Xenon behavior

- Control rod behavior

The equations used in the neutronics model have been derived in Appendix Appendix A. With this model, a parametric study was performed which examined the effect of various xenon stripper related parameters on the steady-state xenon poison fraction. Furthermore, the following parametric studies were performed which examined transient xenon behavior with respect to:

- Graphite mass transfer coefficient
- Bubble mass transfer coefficient
- Circulating void fraction
- Fuel salt stripping efficiency
- Bubble stripping efficiency
- Xenon stripper flow-rate

Observations were made related to these parametric studies and a commentary has been developed on the xenon holdup in a MSR with and without a xenon stripper. Finally, the xenon behavior of MSRs and CANDUs have been compared.

2   Xenon Behavior in Solid Fuel Reactors

The evolution xenon in solid fuel reactors, such as CANDUs, can be described by,

$$\frac{dC_{Xe}}{dt} = \gamma_{Xe}\Sigma_f\phi - \sigma_a^{Xe}C_{Xe} - \lambda_{Xe}C_{Xe} + \lambda_I C_I \tag{1a}$$

$$\frac{dC_I}{dt} = \gamma_I\Sigma_f\phi - \lambda_I C_I + \lambda_{Te}C_{Te}, \tag{1b}$$

$$\frac{dC_{Te}}{dt} = \gamma_{Te}\Sigma_f\phi - \lambda_{Te}C_{Te}. \tag{1c}$$

All the source and sink terms in Equation 1 are nuclear properties, material properties, or the magnitude of the neutron flux. Since the nuclear properties are static, the only way to change the evolution of xenon in a solid fuel reactor is

2

to change the material properties of the reactor or the magnitude of the neutron flux.

Since, by definition, the fuel in a solid fuel reactor is unable to move, and for the intents and purposes of xenon behavior, has a macroscopic fission cross section, Σ_f, that is invariant with time, it follows that it is not practicable to vary the Σ_f term in Equation 1, and the only means left to control the evolution of xenon is variation in the neutron flux of a reactor, ϕ.

The neutron flux in a reactor can be described by the neutron transport equation,

$$\frac{1}{v}\frac{\partial \phi}{\partial t} = (\nu\Sigma_f - \Sigma_a)\phi - \nabla^2\phi + S. \tag{2}$$

Assuming that external neutron sources, such as neutron emanation from nuclear reactions induced by background radiation, are much less than the neutron flux in a reactor,

$$S << \phi, \tag{3}$$

Equation 2 can be rewritten,

$$\frac{1}{v}\frac{\partial \phi}{\partial t} = (\nu\Sigma_f - \Sigma_a)\phi - \nabla^2\phi. \tag{4}$$

The neutron absorption cross-section, Σ_a, can be decomposed into four parts:

1. the inherent neutron absorption cross-section, Σ_a^0, which comes from the materials the reactor is constructed from without any reactivity devices inserted;

2. The xenon neutron absorption cross section, Σ_a^{Xe}, which is given by the product $\sigma_a^{Xe}C_{Xe}$ and governed by Equation 1;

3. The fuel neutron absorption cross section, Σ_a^{Fuel}, which can be parameterized in terms of a power history, and excludes any absorption from xenon;

4. the reactivity control device absorption cross-section, $\Sigma_a^{C.D.}$, which represents the neutron absorption in reactivity control devices. This cross-section can be parameterized in terms of the state of the reactivity device (described in Section 4);

and the total neutron absorption cross section can be written,

$$\Sigma_a = \Sigma_a^0 + \Sigma_a^{Xe} + \Sigma_a^{Fuel} + \Sigma_a^{C.D.}. \tag{5}$$

Of these four components, only $\Sigma_a^{C.D.}$ can be intentionally controlled by changing the state of reactivity control devices. Therefore, in order to control xenon evolution in a solid fuel reactor, we must control the neutron flux, and this must be done through reactivity control devices.

3   The Reactivity Balance of A Nuclear Reactor

The action of a nuclear reactor can be conceptualized as a time-varying population of free neutrons. Neutrons are born in fission and loss through absorption or leakage. In the fission process, an incident neutron interacts with a nucleus, splits the nucleus into a number of fission products, and a number of free neutrons (either prompt or delayed - more on this later). We can therefore discretize the time-variation of this process as occurring in a number of *generations*; neutrons from a preceding generation induce fission and produce neutrons of the next generation.

If the generations in a chain reacting system are enumerated, the time-evolution of a nuclear reactor can be described by a quantity called the multiplication factor, which is denoted by a K and is defined as,

$$K = \frac{\text{Neutron Born in Generation N} + 1}{\text{Neutron Lost in Generation N}}. \tag{6}$$

A related quantity, the reactivity, ρ (detailed in Subsection Appendix A.5), defined as

$$\rho = \frac{K - 1}{K}, \tag{7}$$

Is also used to describe the inter-generational change of the reactor. Positive reactivity increases the neutron born to loss ratio whereas negative reactivity decrases it.

There are numerous sources of reactivity in a nuclear reactor. Some sources include

Net Positive Nominal Reactivity The reactivity of the reactor materials, in its nominal state above critical

Thermal Reactivity Effects Variation in reactivity due to variation in temperature beyond the nominal core configuration

Xenon Reactivity Load Reactivity lost due to the presence and evolution of ^{135}Xe in a reactor

Control Device Reactivity Effects Changes in reactivity due to positioning of reactivity control devices (described in Section 4)

In order for a reactor to be controllable the reactivity control devices must be able to out maneuver the other sources of reactivity in the reactor.

4 Reactivity Control Devices in Solid Fuel Reactors

Reactivity control devices (occasionally shortened to just *control devices* change the material configuration of the core and thereby alter the neutron multiplication factor, k_{eff}. The most common type of reactivity control device is the *control rod* - a rod made of a neutron absorbing substance that is inserted or withdrawn from the reactor core. Control rods have been a integral part of nuclear reactor design since the Manhattan Project: three cadmium rods were used to control the reactivity of the Chicago Pile 1 (CP-1) nuclear reactor, the world's first nuclear reactor, in 1942. (C.F. [1, p. 10]

Reactivity control devices can be said to have a *state* which describes the quantity of negative reactivity inserted by the reactivity control devices. The state of the control rod, for example, can be described by its penetration distance.

Reactivity control devices can also be said to possess a certain am mount of reactivity worth, denoted $\underline{\mathcal{RW}}$, which is am measure of how much a reactivity control device changes the reactivate of the system,

$$\rho = \rho_0 + \underline{\mathcal{RW}}. \tag{8}$$

Since control devices occupy a finite amount of space, it follows that only a finite number of reactivity devices can be fit into a reactor. This is an inherit limit in the design of a solid fueled reactors: the xenon load in a solid fueled reactor is inherently more difficult to change than the inclusion of reactivity devices, but the inclusion of reactivity devices is limited by space. Due to the fluid nature of the fuel of a molten salt reactor, however, their xenon load is more amenable to intentional control and permits the reactor designer a greater degree of freedom.

5 The Assumption of A Linear Control Device

If the state of a reactivity control device can be described by a single scalar quantity, such as the position of a control rod, the reactivity control device may be modeled as a linear device with the position and reactivity worth related by a multiplicative factor,

$$\rho_{C.D.} = \underline{\mathcal{RW}} X_{ins.}. \tag{9}$$

This assumption, however, may not necessarily be true. The tips of the control rods that were involved in the 1986 Chernobyl disaster were comprised of graphite whereas the rest of the control rod was comprised of Boron Carbide. This difference in composition caused an initial increase in reactivity in the reactor involved in the Chernobyl disaster when the control rods were inserted. (C.F. [2, ch. 5])[1]

6 Reactivity Control Devices in a CANDU Reactor

According to Groh [4], reactivity in a CANDU reactor can be intentionally manuvered with:

- Refuelling Operations: replacing a spent fuel bundle with a fresh one.

- Liquid Zone Compartments: Compartments of light water embedded in the reactor which have a controllable level of light water.

- Control Absorbers: Devices which provide power power maneuvering capabilities to the CANDU

- Adjuster Rods: Devices which provde flux flattening and can be removed for a xenon override maneuver (C.F. section 7).

Additionally, CANDU reactors implement a two redundant shutdown systems, Shutdown System #1 (SDS 1), a set *shutdown rods* which have a high control rod worth, and Shutdown System #2 (SDS), which either dumps the moderator or injects gadolinium nitrate into the moderator.

---

[1] Whereas Plokhy states the control rods were comprised of Boron, the paper by Smith, Luckhurts, and Maccabee [3] states the control rods in the RMBK reactor were comprised of Boron Carbide.

7 The Iodine Pit in a CANDU Reactor

a xenon transient in a CANDU reactor, following a step reduction in power, have, like most reactors, a distictivee *humped* shape in which the xenon builds up to a maxmimum then falls. As reported by [5], CANDU reactors have a nominal, steady-state xenon load of 28 mk. After a reactor shutdown, a peak xenon load approaching 100 mk appears around 10 hours after the transient. Adjuster rods in a CANDU reactor can accommodate a step reduction in reactor power of 40 %. Once an iodine pit begins to form, there is a brief period of time called the *poison override time* during which a poison out may be prevented. This period of time is typically 35 to 40 minutes after a reactor shutdown. Furthermore, due to the large size of a CANDU reactor, a phenomenon known as *xenon oscillations* during which the xenon concentration is at various levels in the core and *rings* during the xenon transient (for more information C.F. [6]).

8 Xenon Behavior in a Molten Salt Reactor

Unlike a solid fueled reactor, where the xenon is effectively stationary, the xenon in a circulating fuel reactor, such as a molten salt reactor, is free to migrate. Due to this, the behavior of xenon in a molten salt reactor is qualitatively different than that of a liquid fuel reactor. Prior MSR xenon analyses ([7] for example) have applied a *in solution assumption* in which the xenon precursors tellurium and iodine are assumed to remain in solution whereas the xenon is free to migrate. Molten salt reactors which are graphite moderated may have a gaseous graphite pore space in which the xenon may migrate. Essentially, because the graphite is produced through an extrusion process, microscopic pores form in the graphite and the xenon can migrate into these pores. The pore space of the graphite has been assumed to be free of any fuel-salt, and therefore, no fission occurs within the graphite. Additionally, there may be an inventory of entrained circulating gas called the circulating void and measured via a parameter called the circulating void fraction. In addition to the circulation into the graphite, the xenon can also migrate into the circulating voids. Finally, analysis is made possible by assuming the xenon in the fuel salt is sufficiently dilute that the fuel salt acts as a *ideal dilute solution* and Henry's law can be applied to relate the gas-phase xenon concentration to the liquid (fuel salt) phase xenon concentration.

9   The Xenon Stripper

A *xenon stripper* (also called the *xenon removal system* is a device which removes xenon from MSR fuel salt. The development of the xenon removal system for the aircraft reactor test (operated in 1954) was documented in ORNL-2376 [8]. Conceptually, xenon strippers can be reduced down to a two-port device. Incoming fuel salt has some sort of initial xenon concentration, C_1, and outgoing fuel-salt has some sort of concentration of xenon after the striper, C_2. We can therefore define the ratio of these two numbers as the efficiency of the xenon stripper,

$$\eta = \frac{C_2}{C_1}. \tag{10}$$

If we define the bubble density, ρ^B, to bee the the number of bubbles per unit volume, then we can define a bubble stripping efficiency,

$$\eta_B = \frac{\rho_2^B}{\rho_1^B}. \tag{11}$$

In this way, xenon strippers remove xenon from both the fuel salt and the bubbles.

10   Modeling of a 1000 MWe Molten Salt Reactor

10.1   Introduction

A model of a 1000 MWe MSR was developed based on the reactor developed in ORNL-3996 [9]. The modeling was done in Mathworks Simulink. The subsequent sections describe the sub-models used in the model. The simulation was run for a simulation time of 1×10^7 s. The automatic variable-step solver selection of Simulink was used, and this automatic selection chose the ODE15S solver with a 1000 s maximum step-size.

10.2   Neutronic Model

The neutronic model used the decay point kinetics (DPK) model,

$$\frac{dN(t)}{dt} = \frac{\rho - \beta}{\ell}n(t) + \sum_{i=0}^{1}\beta_i\lambda_i, \tag{12a}$$

$$\frac{dC_i(t)}{dt} = \frac{\beta_i}{\ell}n(t) - \lambda_i C_i(t) - \frac{C_i(t)}{\tau_c} + \frac{C_i(t-\tau_l)e^{-\lambda_i\tau_i}}{\tau_c}. \tag{12b}$$

Equation Set 12 was implemented using two `integrator` block. The coupling between Equation 12a and 12b, through the second term of equation 12a, was carried out through a `sum of elements` block. The delay factor, $C_i(t - \tau_l)$, of the last term in Equation 12b,was implemented using a `transport delay` block. Note, the `transport delay` block, in Simulink 9.1 (R2018a), implements its time-delay is a compile-time block parameter rather than a run-time input; therefore, the model is unable to model flow transients, which would require a perturbed circulation time.

Initial efforts used a linearized version of the decay point kinetics equation,

$$\frac{dN(t)}{dt} = \frac{\rho - \beta}{\ell}n(t) + \sum_{i=0}^{1}\beta_i\lambda_i, \tag{13a}$$

$$\frac{dC_i(t)}{dt} = \frac{\beta_i}{\ell b_i}n(t) - \frac{\lambda_i}{a_i b_i}C_i(t), \tag{13b}$$

$$a_i = \frac{\lambda_i\tau_c}{\lambda_i\tau_c - e^{-\lambda_i\tau_c}}, \tag{13c}$$

$$b_i = 1 + \frac{\tau_l}{\tau_c}e^{-\lambda_i\tau_c}, \tag{13d}$$

presented in ORNL-TM-2489 [10, p. 37]; however, convergence issues were experienced upon testing.

The model used two groups of DNPs. The neutron kinetics parameters used are shown in Table 1.

9

Parameter	Magnitude
β_1	1.02×10^{-3}
β_2	1.62×10^{-3}
λ_1	$2.446 \times 10^{-2}\,\mathrm{s}^{-1}$
λ_2	$2.245 \times 10^{-1}\,\mathrm{s}^{-1}$
ℓ	$0.36\,\mathrm{ms}$
τ_c	$1.6\,\mathrm{s}$
τ_l	$6.97\,\mathrm{s}$

Table 1: Model Neutron Kinetics Parameters

10.3   Thermal Model

A lumped parameter approach was used to model the thermal behavior of the reactor. A diagram of the reactor thermal model is shown in Figure 1. each lumped volume in the model has the lump temperature, T, as the dependent variable and the rate of heat flow, $\dot{Q}$, as the flow variable. The arrows in Figure 1 point in the direction of interaction.

With reference to Figure 1, energy enters the system through nuclear fission (1) at a rate of $\gamma_f \Sigma_f \phi$ $[FLt^{-1}]$ per unit volume of in-core fuel-salt. The energy produced is either directly deposited into the in-core volume (5) or is deposited into the graphite moderator (4) through gamma or neutron interactions. The graphite volume (4), the in-core volume (5), and the ex-core voolume (8) each have a corresponding temperature, specific heat, and mass. The specific heat of the in-core volume (5) is the same as the specific heat of the ex-core volume (8) since they are both comprised of fuel-salt.

The change in temperature of a given node is given by they typical

$$\frac{dQ}{dt} = MC\Delta T.$$ (14)

Heat transfer between the graphite volume and the in-core volume (6) is governed by,

$$\frac{dQ}{dt} = K_G^H A_G (T_{IC} - T_G).$$ (15)

Since heat is transport by fuel salt flow between the in-core (5) and ex-core (8) volumes by advection (7), heat transfer is governed by,

$$\frac{dQ}{dt} = \dot{F}_{FS} C_{FS} (T_{IC} - T_{EC}).$$ (16)
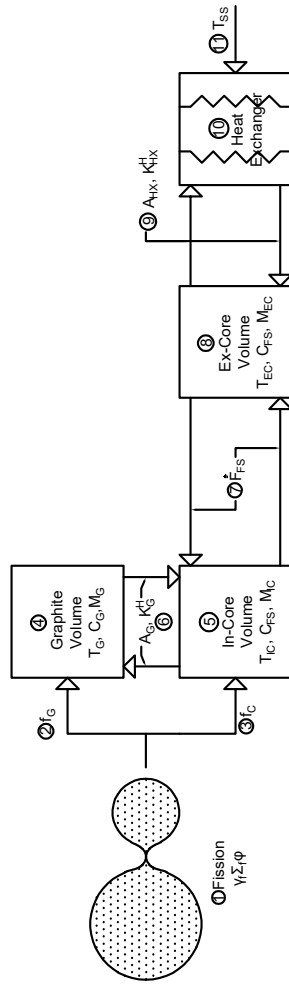
Figure 1: Reactor Thermal Model

Heat is finally exchanged with the secondary side via the heat exchanger (10) and the heat exchange rate is governed by,

$$\frac{dQ}{dt} = A_{HX} K_{HX}^H (T_{EC} - T_{SS}). \tag{17}$$

The values of the thermal model parameters used in this model are shown in Table 2.

The heat transfer coefficients for Equation 15 and Equation 15 was calculated by a Dittus-Botler-Like Correlation,

$$Nu = 0.023 Re^{0.8} Pr^{1/3}; \tag{18}$$

The hydraulic diameter used in the Re term of this correlation was 2.5 cm for the graphite (fuel-channel hydraulic diameter) and 1.16 cm for the heat-exchanger (tube diameter inside the heat-exchanger). Fuel salt properties used to calculate Re and Pr were taken from salt F1 in ORNL-TM-2316 [11].

Quantity	Value	Unit
f_G	10	[%]
f_C	90	[%]
M_G	1.22×10^5	[kg]
M_{IC}	2.71×10^4	[kg]
M_{EC}	2.71×10^4	[kg]
C_G	1.76×10^3	[J kg^{-1} °C^{-1}]
C_{FS}	1.21×10^3	[J kg^{-1} °C^{-1}]
A_G	1.57×10^2	[m]
A_{HX}	6.23×10^2	[m]
K_H^G	9.83×10^3	[W m^{-1} °C^{-2}]
K_{HX}^H	2.11×10^4	[W m^{-1} °C^{-2}]
T_{SS}	800	[°C]
$\dot{F}_{FS}$	1.19×10^4	[kg s^{-1}]

Table 2: Thermal model parameters

The two dependent variables of the thermal model which are used by the neutronics model are the graphite temperature, T_G, and the in-core temperature, T_{IC}. These two variables are used in the thermal reactivity perturbation

12

calculation,

$$\Delta\rho_T = \alpha_G(T_G - T_G^{Nom.}) + \alpha_{FS}(T_{IC} - T_{IC}^{Nom.}). \tag{19}$$

The parameters used in Equation 19 are listed on Table 3.

Quantity	Value	Unit
α_G	6.05×10^{-5}	$[°C^{-1}]$
α_{FS}	5.45×10^{-5}	$[°C^{-1}]$
$T_G^{Nom.}$	1150	$[°C]$
$T_{FS}^{Nom.}$	1000	$[°C]$

Table 3: Thermal reactivity model parameters

10.4 Xenon Model

The xenon sub-model used in this analysis is shown on Figure 2. The xenon production process begins with fission (1), which produces ^{135}Te (5), ^{135}I (9), or ^{135}Xe (6) with yield fractions of γ_{Te} (2), γ_I (4), or γ_{Xe} (3) respectively. The ^{135}Te (5) transmutes into into ^{135}I (9) via the first-order decay law, $\dot{N} = -\lambda N$, with a rate constant of λ_{Te} (4). Likewise, ^{135}I (9) transmutes into ^{135}Xe (6) with a rate constant λ_I (7). This model applies the in-solution assumption and only the ^{135}Xe can migrate to the bubbles or graphite. Regardless of where the ^{135}Xe is in the system, the ^{135}Xe whereas ^{135}Te and ^{135}I remain in solution. The ^{135}Xe is only produced in the fuel-salt (14). Mass transfer can occur either between the graphite (10) and fuel salt (14) or the bubbles (13) and the fuel salt (14). The fuel salt (14) occupies volume V_{FS}. Note, the fission process only occurs inside the in-core volume (not shown), so the volumetric fission rate is calculated using an effective flux,

$$\phi_{eff} = \frac{V_{IC}}{V_{IC} + V_{EC}}\phi. \tag{20}$$

The bubbles (13) are governed by the circulating void fraction f_{cv}, and a reference radius, r_b. The circulating void fraction represents the relative volume of gas entrained in the fuel salt whereas the reference radius represents the mean radius of a bubble entrained and circulating with the fuel salt. The model assumes the bubbles are effectively spherical in shape, and

$$N_B = \frac{Total\ Gas\ Volume}{Volume\ Per\ Bubble} = \frac{f_{cv}V_{FS}}{\frac{4}{3}\pi r_b^3}. \tag{21}$$

Mass transfer to the bubbles is governed by the bubble mass transfer coefficient K_M^B, and the bubble interfacial area, A_B, (both shown at (15)) through,

$$\frac{dN_{Xe}^B}{dt} = K_B^M A_B \left(C_{FS} - HRT\frac{N_{Xe}^B}{f_{CV}V_{FS}}\right). \tag{22}$$

13

Mass transfer to the graphite (10) is governed by the graphite mass transfer coefficient, $_M^G$, and the graphite surface area, A_G (both shown at (11)) through,

$$\frac{dN_{Xe}^G}{dt} = K_G^M A_G \left(C_{FS} - HRT\frac{N_{Xe}^G}{\epsilon V_G} \right). \tag{23}$$

Finally, the xenon stripper (18), which operates at a volumetric flow rate $\dot{Q}$, removes xenon from both the bubbles (13) and the fuel salt (14) with efficiencies η_B (16) and η_{FS} respectively, where

DEFINITION $\Rightarrow$
$$\eta_B \overset{def}{=} \frac{\text{Bubble Density in Stream After Stripper}}{Bubble Density in Stream Before Stripper}, \tag{24}$$

where

DEFINITION $\Rightarrow$
$$\text{Bubble Density} \overset{def}{=} \frac{N_B}{V_{FS}}, \tag{25}$$

and

DEFINITION $\Rightarrow$
$$\eta_{FS} \overset{def}{=} \frac{\text{Xe Concentration in Fuel Salt Stream Before Stripper}}{\text{Xe Concentration in Fuel Salt Stream After Stripper}}. \tag{26}$$

Finally, the xenon in all compartments is subject to decay or burnout (12 for bubbles and fuel-salt and 20 for graphite). The radioactive decay is governed by the first order decay law, which, again, is $\frac{dN}{dt} = -\lambda N$. All xenon in all compartments is subject to radioactive uniformly. The burnout,

$$\text{Burnout Rate} = \sigma_a \phi, \tag{27}$$

which is shown at the first term at (12) and (19), accounts for the transmutation of of ^{135}Xe into ^{1}36Xe via neutron absorption. The effective flux, ϕ_{eff}, is used for the burnout of the bubbles and fuel-salt since the xenon in these two compartments spend only part of their time in-core. The graphite is subject to burnout at all times, so its burnout is calculated with the unweighted neutron flux, ϕ.

The parameters used in the xenon models are shown in Table 4.

The reactivity effect due to ^{135}Xe is found by

$$\rho_{Xe} = \rho_{Xe}^{SS} \frac{N_{Xe}^{Tot}}{^{SS}N_{Xe}^{Tot}}, \tag{28}$$

where ρ_{Xe} is taken as a reference value, and $^{SS}N_{Xe}^{Tot}$ is the model steady-state total xenon content in all compartments. The reference value for ρ_{Xe}^{SS} was taken as 330 mK, a value congruent with measurements in the MSRE [12, p. 29].

Since the behavior of xenon operates on a multi-day timescale, a `rate transition block` with a sample time of 1000 s was used to transition from the rest of the model to the xenon behavior.

14
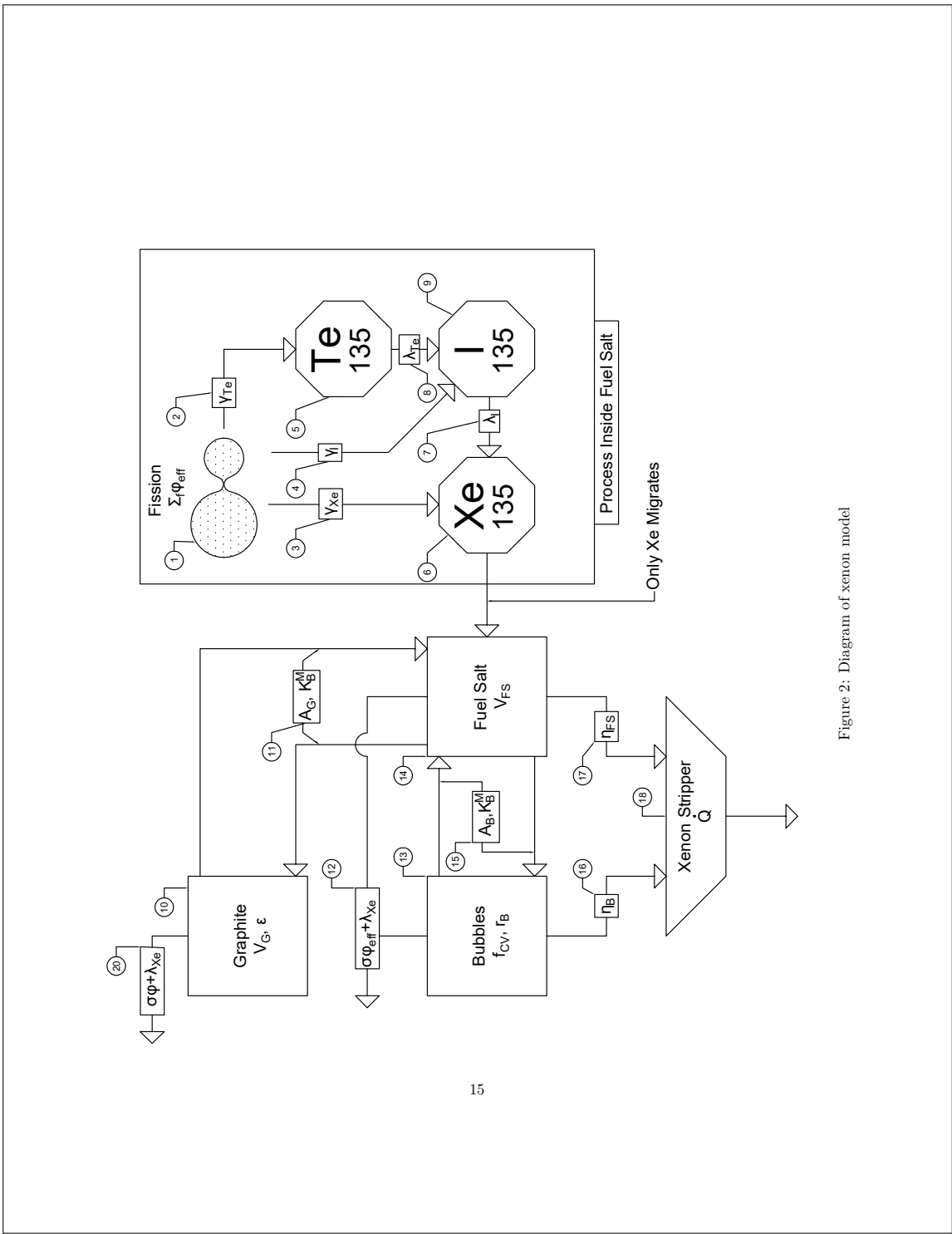
Figure 2: Diagram of xenon model

15

Quantity	Value	Unit
Σ_f	1.5×10^{-1}	$[\mathrm{m}^{-1}]$
V_{IC}	8.1	$[\mathrm{m}^3]$
V_{EC}	8.1	$[\mathrm{m}^3]$
γ_{Te}	3.22×10^{-2}	[-]
γ_I	2.93×10^{-2}	[-]
γ_{Xe}	2.57×10^{-3}	[-]
λ_{Te}	3.65×10^{-2}	$[\mathrm{s}^{-1}]$
λ_I	2.93×10^{-5}	$[\mathrm{s}^{-1}]$
λ_{Xe}	2.11×10^{-5}	$[\mathrm{s}^{-1}]$
σ_a	2.6	[Mb]
K_B^M	1.69×10^{-4}	$[\mathrm{m\,s}^{-1}]$
K_G^M	4.23×10^{-6}	$[\mathrm{m\,s}^{-1}]$
f_{CV}	1	[%]
r_B	2.54	[m]
A_G	157.1	[m]
V_G	66.3	[66 3]
ϵ	10	[%]
η_B	10	[%]
η_{FS}	12	[%]
$\dot{Q}$	3×10^{-2}	$[\mathrm{m}^3\,\mathrm{s}^{-1}]$

Table 4: Xenon model parameters

10.5   Control Rod Model

A linear control rod model (C.F. 5 was used to model a 200 cm control rod. The rod worth was 80 mK. The rod kinetics were modeled as a variable velocity device to approximate the action of a low-backlash stepper motor. A maximum rod velocity of $10\,\mathrm{cm\,s}^{-1}$ was used. A PD (proportional-derivative) controller was used to control the rod position against a set-point. The input to the PD controller was a fractional error. The proportional gain of the controller was 1, the derivative gain was 2 and the filter coefficient was set to 100. The rod position start-up position was at 100 cm of insertion.

10.6   Reactivity Calculation

The reactivity used in Equation 12 was calculated by summing the reactivity contributions of the control rod from the thermal effects, the xenon model, and the control rod contribution, as well as a net positive reactivity worth, ρ_0 of the core of 1.4 mK.

$$\rho = \rho_0 + \rho_T + \rho_{CR} + \rho_{Xe}. \tag{29}$$

11 Parametric Study of Xenon Stripper Behavior

A parametric study was performed which analyzed the response of the MSR model to a requested 75 % step-back in reactor power. THe response of the xenon sub-model is detailed in the following figures:

Figure 3 Shows the response of each of the sub models at 1 minute, 10 minute, and 1 hour time-scales

Figure 4 Shows the response of variation in various xenon stripper parameters on the steady state xenon poisoning. For this plot, steady-state values were generated by running the model at 100 % FP for 1×10^7 s.

Figure ?? Shows the influence of variation in the bubble mass transfer coefficient on transient behavior

Figure 5 Compares the influence of the variation in bubble mass transfer coefficient on transient behavior.

Figure ?? Shows the influence of variation in the graphite mass transfer coefficient on transient behavior

Figure 6 Compares the influence of variation in the graphite mass transfer coefficient on transient behavior

Figure ?? Shows the influence of variation in the circulating void fraction on transient behavior

Figure 7 Compares the influence of variation in the circulating void fraction on transient behavior

Figure ?? Shows the influence of variation in the fuel salt xenon stripping efficiency on transient behavior

Figure 9 Shows the influence of variation in the bubble stripping efficiency on transient behavior

Figure 10 Shows the influence of variation in the xenon stripper flow rate on transient behavior

c
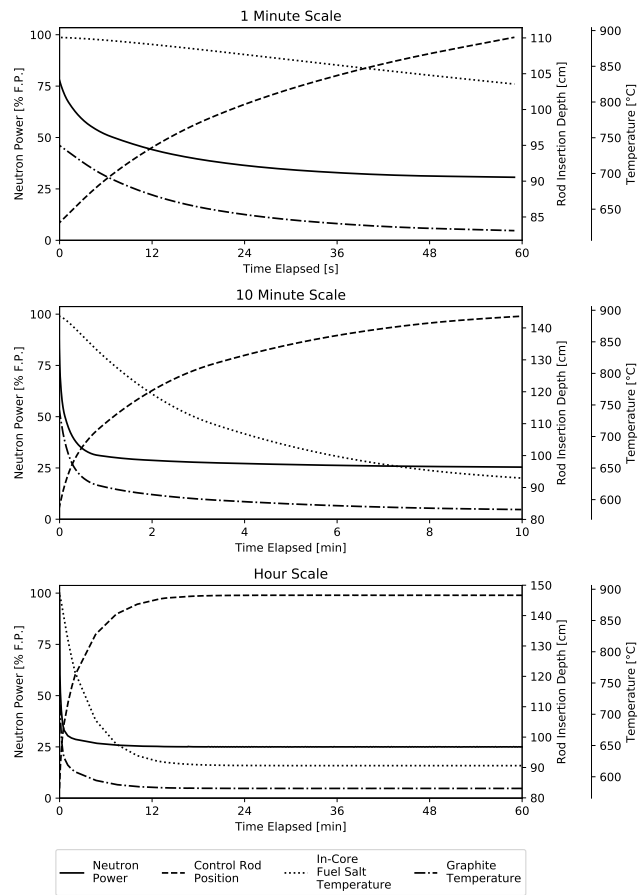
Figure 3: System Response to 75 % step-decrease in reactor power set-point
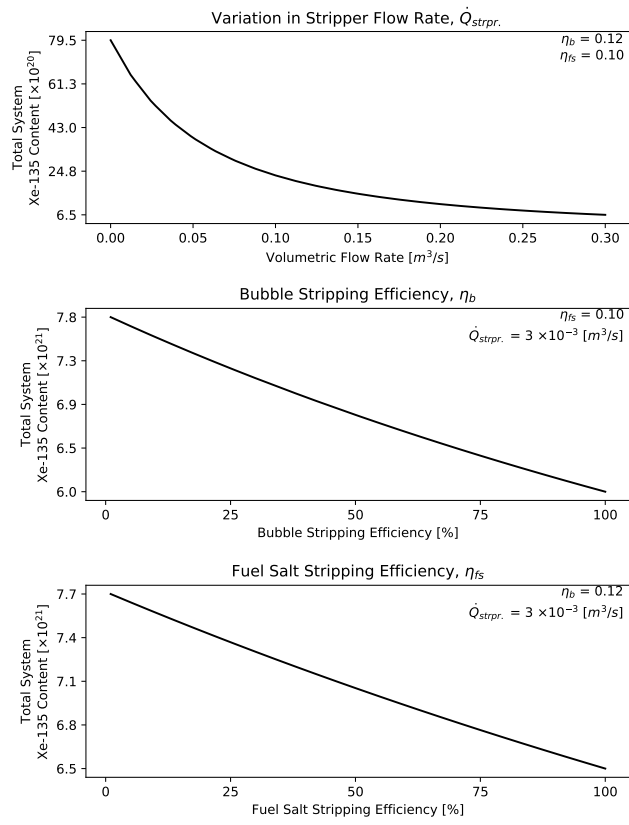
Figure 4: Parametric study of influence of xenon stripper parameters on steady-state xenon poison content
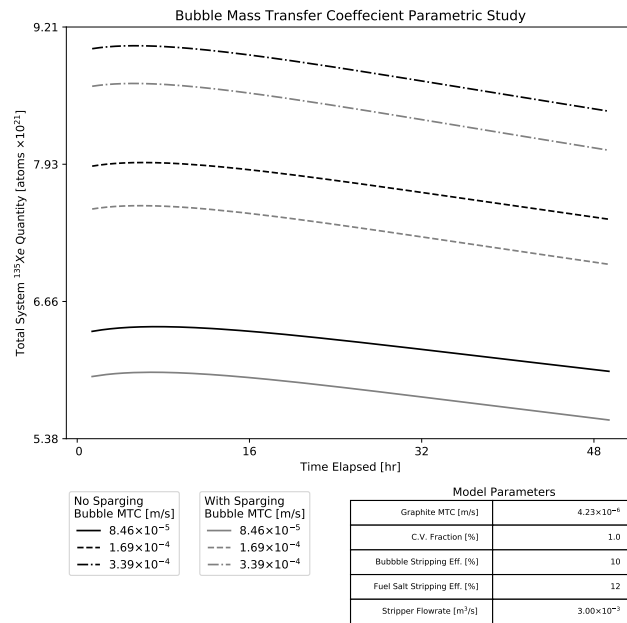
Figure 5: Parametric study on bubble mass transfer coefficient - comparison plot
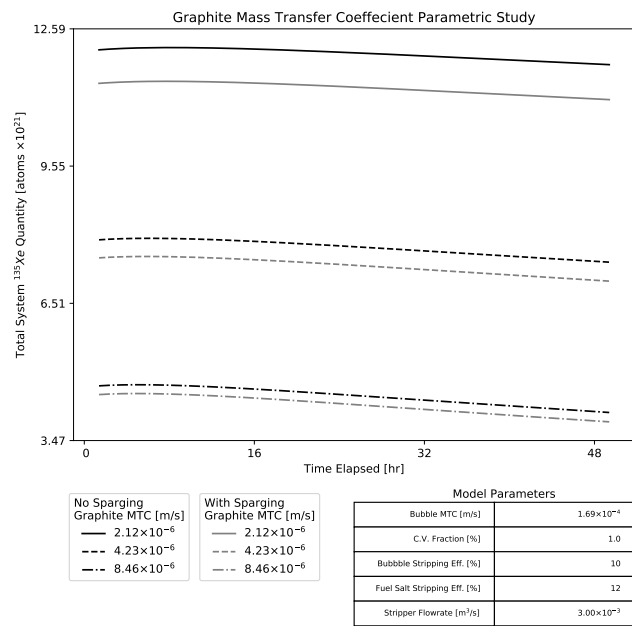
Figure 6: Parametric study on graphite mass transfer coefficient - comparison plot
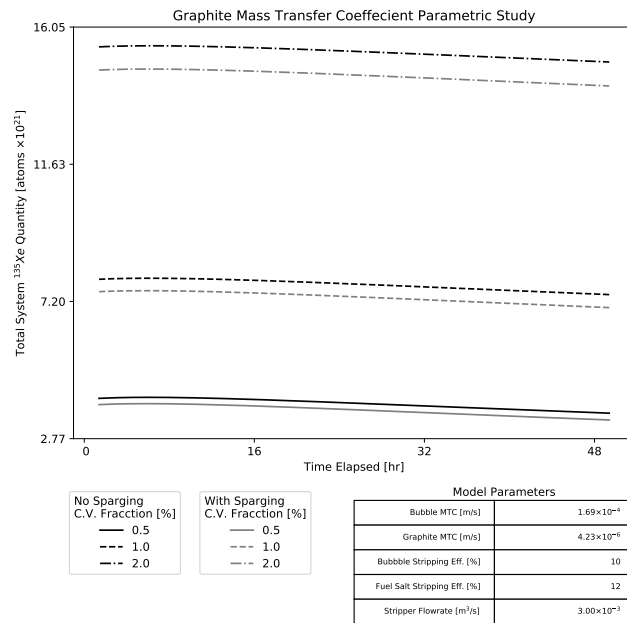
Figure 7: Parametric study on circulating void fraction - comparison plot
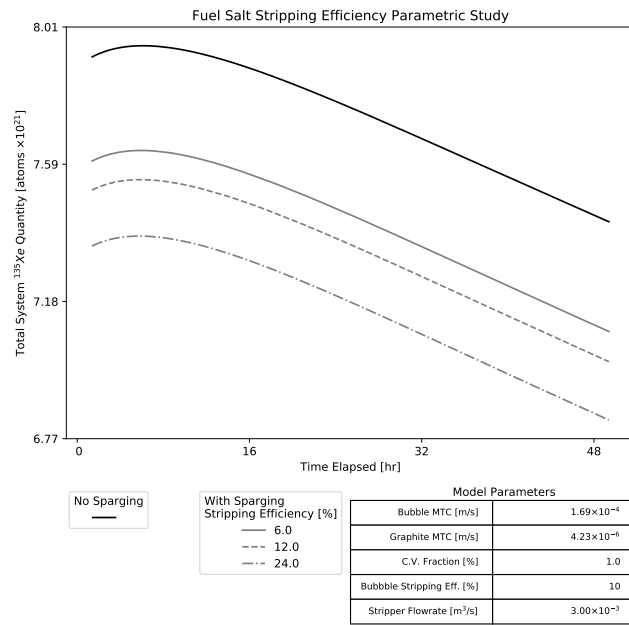
Figure 8: Parametric study of xenon stripper fuel salt stripping efficiency
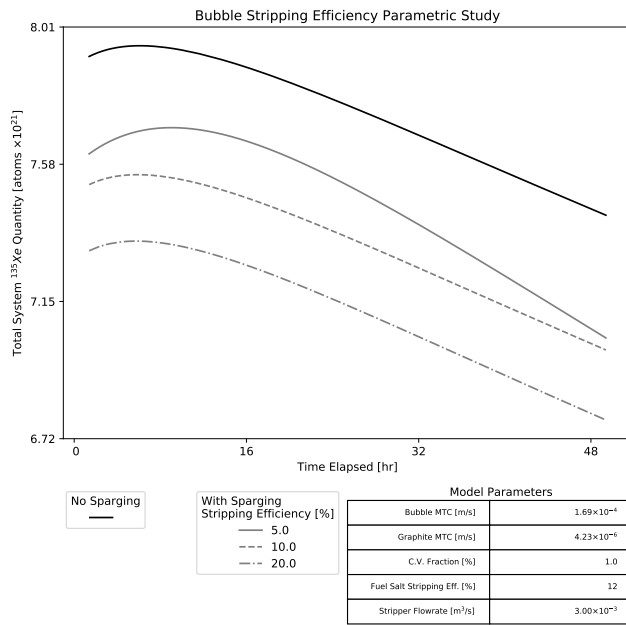
Figure 9: Parametric study of xenon stripper bubble stripping efficiency

Xenon Stripper Flow Rate Parametric Study
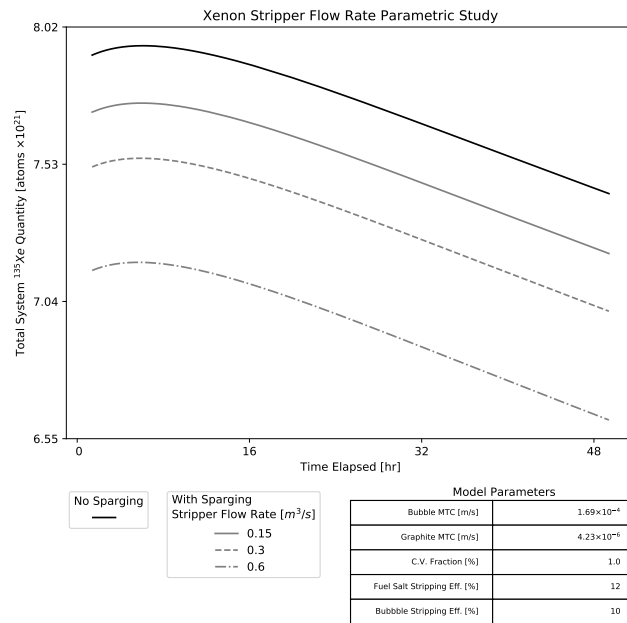
Figure 10: Parametric study of xenon stripper flow rate

12 Xenon Holdup With and Without a Xenon Stripper

As shown in Section 11, the magnitude of the xenon holdup in a MSR with a xenon stripper is lower than the magnitude of xenon holdup in a MSR without a stripper. Furthermore, based on the model shown in Figure 2, there is no lower limit to the fraction of xenon removed through the xenon stripper. Indeed, an upper limit on the xenon stripping rate is an engineering constraint more-so than than a physics constraint. We can therefore identify the *maximal flow rate per volume of apparatus* as the design parameter of interest in selecting xenon stripper equipment. To the best of our knowledge, this has not been investigated anywhere in the literature. A caveat to this is that, as shown in Figure 4, the relationship between xenon stripper flow rate and steady-state xenon hold-up is clearly non-linear, and there is a point beyond which increasing xenon stripper flow rate yields diminishing returns on decreased steady-state xenon hold-up.

Some further control of the xenon hold-up can also be exercised by controlling the graphite or bubble mass-transfer coefficients, as shown in figures 6 and 5. Both of these mass transfer coefficients can be controlled by controlling the flow parameters of the fuel-salt. In general since

$$\mathbf{Sh} \propto \mathbf{Re}, \tag{30}$$

and

$$K_m \propto \mathbf{Sh}, \tag{31}$$

a more turbulent flow (Higher $\mathbf{Re}$) will lead to a higher mass-transfer coefficient. There is, however, a competing dynamic, in the system studied, since, as shown by figures 6 and 5, a higher bubble mass transfer coefficient will lead to a higher system xenon hold-up, whereas a higher graphite mass transfer coefficient will lead to a lower system xenon hold-up.

Perhaps one of the most promising parameters for changing the system xenon hold-up is the circulating void fraction, studied in figures **??** and 7. The studied system demonstrates minimizing the system circulating void fraction will also minimize the xenon hold-up in the system. This approach, however, should be pursued with caution since there is an associated void-fraction coefficient of reactivity. The positive correlation between circulating void fraction and xenon hold-up also indicates that a MSR stands to gain rather than loose xenon hold-up upon rapid ingress of gas into the reactor.

Finally, we note that figures 6 and 5 indicate that control of the graphite and bubble mass-transfer coefficients will lead to some variation in the length of time which an iodine-pit produces has a xenon poison hold-up above the reactor's steady-state value.

Category	Solid Fuel Reactor	Molten Salt Reactor
Theoretical Development	Described in numerous textbooks and reactor physics codes	Documented in several Oak Ridge reports and academic papers
Theoretical Validation	The iodine-xenon model was sufficient to explain xenon behavior in the Hanford-B model	Models able to describe observed behavior with numerous assumptions and unable to do so in all situations
Design-space considerations	A Property of nuclear configuration	A property of both nuclear configuration and mechanical properties
Dynamic Coupling Parameters	None known	Temperature, pressure, and void fraction
Steady-State Xenon Behavior	A function of reactor power history	A Function of reactor power history, sparging activities, and entrained gas
Transient Xenon Behavior	Static	Controllable through sparging

Table 5: Comparison of molten salt reactor and solid fuel reactor xenon behavior

13 Comparison of Molten Salt Reactor and CANDU Reactor Xenon Behavior

An attempt to compare MSR xenon behavior to CANDU reactor xenon behavior would result in a catagorical mis-match. A CANDU is a particular type of solid-fuel reactor whereas a MSR is an abstract category (class) of reactor.

Therefore, instead of comparing MSR xenon behavior to CANDU xenon behavior, we can instead compare MSR xenon behavior to solid fuel reactor xenon behavior. In this way, we are comparing two entities at the same level of abstraction. Table 5 details a comparison between MSR xenon behavior and solid fuel reactor xenon behavior.

Conversely, the other way to analyze this problem is to compare the xenon transient behavior of an instance of the class MSR class of reactors and an instance of the CANDU class of reactors. ORNL-TM-3464 [12, p. 18] provides data that describes the xenon reactivity load with respect to time for a step power decrease, from 100 % full power to 0 % full power transient for the MSRE. The time it took for the MSRE to return to base-line after the transient began was approximately 12 hours. In 1976, J. Kotlarz studied xenon transients in

27

a CANDU reactor as part of his master's thesis [13]. In Kotlarz's thesis, it is reported a CANDU reactor will return to its nominal xenon load after nearly 48 hours after a step decrease in reactivity from 100 % full power to 0 % full power.

Appendix A   Derivations

This section details the derivation of a point-kinetics equation for a circulating fuel reactor. These derivations are based on the content in [14] and [15].

Appendix A.1   The Mean Path, λ_{MFP}

In this subsection, we aim to derive expressions for the probability, $P_r(x)$, a neutron will undergo a reaction when traversing a distance, x, and its compliment, $P'_r(x)$, that a neutron will not under go a reaction while traversing a distance, x.

We begin by asserting, given a sufficiently small distance, δx, the probability of reaction is directly proportional to the distance a neutron travels,

$$P_r(x) \propto x. \tag{32}$$

Therefore, if denote Σ the constant of proportionality which relates the probability of reaction to the distance a neutron travels,

$$P_r(\delta x) = \Sigma \delta x, \tag{33}$$

and,

$$P'_r(\delta x) = 1 - \Sigma \delta x. \tag{34}$$

> **Note**
>
> Note, terminologically, the phrase *"the probability a neutron will travel to distance x"* is synonymous with the notation $P'_r(x)$, and the phrase *"the probability a neutron will react in distance x"* is synonymous with the notation $P_r(x)$.

The probability that a neutron will not interact up to distance $x + \delta x$, where δx is small, is given by the conjunction of the probability a neutron will travel to distance x, $p'_r(x)$, and the probability a neutron will travel distance distance $p'_r(\delta x)$,

$$P'_r(x + \delta x) = P'_r(x)P'_r(\delta x). \tag{35}$$

That is, the neutron must first travel to distance x (and) then travel distance δx. Substituting Equation 34 into Equation 35,

$$P'_r(x + \delta x) = P'_r(x)(1 - \Sigma \delta x), \tag{36}$$

which can be rearranged to,

$$\frac{P'_r(x + \delta x) - P'_r(x)}{\delta x} = -\Sigma. \tag{37}$$

Taking the limit as $x \to 0$ and applying the definition of the limit,

$$\lim_{x \to 0} \frac{P'_r(x + \delta x) - P'_r(x)}{\delta x} = \frac{dP'_r(x)}{dx}, \tag{38}$$

and thus,

$$\frac{dP'_r(x)}{dx} = -\Sigma, \tag{39}$$

which is the differential form of the expression for $P'_r(x)$. To obtain a closed form expression for Equation 39, we observe,

$$P'_r(x) = e^{-\Sigma x} + C, \tag{40}$$

is a solution to Equation 39. The constant of integration, C, can be eliminated by notation that at $x = 0$, there is no chance for the neutron to interact (since it has travel no distance), and

$$P'_r(x = 0) = 1. \tag{41}$$

I.E. there is a 100 % probability the neutron will not interact at $x = 0$. Therefore,

$$P'_r(x) = e^{-\Sigma x}, \tag{42}$$

and its complement,

$$P_r(x) = 1 - e^{-\Sigma x}, \tag{43}$$

by virtue of the principle that the probability of an event and its complement exhausts the probability space,

$$P'_r(x) + P_r(x) = 1. \tag{44}$$

Now, the probability a neutron will interact between distance x and $x + \delta x$ is equal to the conjunction of the probability that a neutron will survive (not react) to distance x and the probability that the neutron will interact within distance dx,

$$P_r(\delta x | x) = P'_r(x) P_r(\delta x). \tag{45}$$

Substituting Equation 42 and Equation 33 into Equation 45,

$$P_r(\delta x | x) = e^{-\Sigma x} \Sigma \delta x. \tag{46}$$

As $\delta x \to 0$, $\delta x \implies dx$ and,

$$P_r(\delta x | x) = e^{-\Sigma x} \Sigma dx. \tag{47}$$

30

If we define the mean free path (MFP), λ_{MFP}, as the mean distance a neutron will travel before interacting, then we can use the definition of the weighted average,

$$\bar{x} = \frac{\int_0^\infty w(x)x\,dx}{\int_0^\infty w(x)\,dx}, \qquad (48)$$

and substitute in Equation 47 as the weighting function,

$$\lambda_{MFP} = \frac{\int_0^\infty e^{-\Sigma x}\Sigma x\,dx}{\int_0^\infty e^{-\Sigma x}\Sigma\,dx}, \qquad (49)$$

which evaluates to,

$$\lambda_{MFP} = \frac{1}{\Sigma}. \qquad (50)$$

Therefore, the mean free path and the macroscopic cross-section are reciprocals of each other.

Appendix A.2 The Leakage Probability, P_L, Non-Leakage Probability, P_{NL} and their Relation to the Leakage Factor, Γ

let us define Γ as the *leakage factor*[2], which is defined as,

DEFINITION ⇒
$$\Gamma \stackrel{def}{=} \frac{Neutrons\ Leakage\ Rate}{Neutron\ Absorption\ Rate}. \qquad (51)$$

We also define the *leakage probability* as,

DEFINITION ⇒
$$P_L \stackrel{def}{=} \frac{Neutrons\ Leakage\ Rate}{Neutrons\ Loss\ Rate}. \qquad (52)$$

> **Note**
>
> The neutron fission cross-section, Σ_f, is included in the neutron absorption cross-section, Σ_a. The ENDF-6 Formats Manual [16, p. 23] lists the neutron absorption cross-section (MT=27) as the sum of the neutron fission cross-section (MT=18) and the *neutron disappearance* cross-section (MT=101).

---

[2]More precisely, this should be called the leakage-to-absorption factor, however the term leakage factor is used here as a short-hand.

> **Note**
>
> There is a distinction in terminology between neutron absorption and neutron loss. Neutron loss is a phenomena that includes both neutron leakage and neutron absorption.

Thus,

$$P_L = \frac{\Gamma \Sigma_a \phi}{\Sigma_a \phi + \Gamma \Sigma_a \phi} = \frac{\Gamma}{1 + \Gamma}. \tag{53}$$

and its complement, the non-leakage probability is defined as,

DEFINITION ⇒
$$P_{NL} \stackrel{def}{=} \frac{Neutron\ Absorption\ Rate}{Neutrons\ Loss\ Rate}, \tag{54}$$

on account of the fact that if a neutron does not leak, it must be absorbed. Thus,

$$P_{NL} = P'_L = 1 - P_L = \frac{\Sigma_a \phi}{\Sigma_a \phi + \Gamma \Sigma_a \phi} = \frac{1}{1 + \Gamma}. \tag{55}$$

Appendix A.3 The Neutron Lifetimes - ℓ_∞ and ℓ

We define the infinite-medium neutron lifetime, ℓ_∞, to be the time t, a neutron takes, traveling at velocity v, to traverse the mean free path (C.F. Appendix A.1) to absorption, λ_a.

DEFINITION ⇒
$$\ell_\infty \stackrel{def}{=} t \quad S.T. \quad tv = \lambda_a. \tag{56}$$

Therefore,

$$\ell_\infty = \frac{1}{v \Sigma_a}. \tag{57}$$

Since ℓ_∞ does not factor in leakage, it is effectively an infinite medium quantity (ergo, the ∞ subscript). In order to transform this quantity to a form usable in finite reactors, we must introduce the notion of a *interaction time*, which is defined to be the total time a population of neutron spends interacting with a medium. For a infinite reactor this is,

$$t_{Interact}^\infty = \ell_\infty N. \tag{58}$$

In a finite reactor, only P_{NL} neutrons remain in the reactor and are able to interact with the reactor medium, so

$$t_{Interact} = t_{Interact}^\infty P_{NL}. \tag{59}$$

We can there define the finite medium neutron lifetime, ℓ as,

DEFINITION ⇒
$$\ell \stackrel{def}{=} t \quad S.T. \quad t = t_{Interact} N, \tag{60}$$

in a finite reactor. Therefore,

$$\text{DEFINITION} \Rightarrow \qquad t_{Interact} \stackrel{def}{=} \ell_\infty N P_{NL} \implies \ell N = \ell_\infty N P_{NL}, \qquad (61)$$

and thus, we can finally write,

$$\ell = \ell_\infty P_{NL}, \qquad (62)$$

or

$$\ell = \frac{P_{NL}}{v\Sigma_a}. \qquad (63)$$

Thus, by inspection of Equation 57

$$\frac{\ell}{\ell_\infty} = P_{NL}. \qquad (64)$$

Which implies larger reactors tend to have longer neutron lifetimes and bolsters the conclusion that large reactors tend to act slower than small reactors.

Appendix A.4 K_∞, K_{eff}, and P_{NL}

The neutron multiplication factor, K, is defined as,

$$k = \frac{\text{Neutron Born in Generation N} + 1}{\text{Neutron Lost in Generation N}}. \qquad (65)$$

Since the concept of a *neutron generation* is essentially an artificial construct (How does one track the neutrons in such a way so as to define when one generation starts and stops? Furthermore, what happens if neutrons in one generation have a wide spread in their position in the time coordinate so as two successive generations overlap?), we can operationalize Equation 65 into measurable quantities with the definition,

$$\text{DEFINITION} \Rightarrow \qquad k \stackrel{def}{=} \frac{Neutron\ Production\ Rate}{Neutron\ Loss\ Rate}. \qquad (66)$$

in an infinite medium, the only way in which neutrons are lost is through absorption. Therefore, the infinite medium neutron multiplication factor, K_∞, is written as

$$\text{DEFINITION} \Rightarrow \qquad k_\infty \stackrel{def}{=} \frac{Neutron\ Production\ Rate}{Neutron\ Absorption\ Rate}. \qquad (67)$$

Conversely, in a finite medium, neutrons are either lost through leakage or absorption. Therefore, we define the finite medium (effective) neutron multiplication factor as, K_∞, is written as

$$\text{DEFINITION} \Rightarrow \qquad k_{eff} \stackrel{def}{=} \frac{Neutron\ Production\ Rate}{Neutron\ Absorption\ Rate + Neutron\ Leakage\ Rate}. \qquad (68)$$

33

Recall from Equation 54,

$$P_{NL} = \frac{Neutron\ Absorption\ Rate}{Neutrons\ Loss\ Rate}, \tag{69}$$

The ratio of the infinite and finite medium neutron multiplication factors can then be written,

$$\frac{K_{eff}}{K_\infty} = \frac{\frac{Neutron\ Production\ Rate}{Neutron\ Absorption\ Rate + Neutron\ Leakage\ Rate}}{\frac{Neutron\ Production\ Rate}{Neutron\ Absorption\ Rate}} \tag{70}$$

$$= \frac{Neutron\ Absorption\ Rate}{Neutron\ Absorption\ Rate + Neutron\ Leakage\ Rate}.$$

Since the only two ways in which neutrons are lost is through absorption or leakage ($loss\ =\ absorption\ +\ leakage$), Equation 70 reduces to,

$$\frac{K_{eff}}{K_\infty} = P_{NL}. \tag{71}$$

Appendix A.5   Reactivity, ρ, And Its Relationship To The Multiplication Factor, K

Briefly, let's introduce the notion of reactivty, ρ. If we define the *multiplication factor defect*, δK, as the deviation of the multiplication factor from critical,

DEFINITION $\Rightarrow$
$$\delta K \stackrel{def}{=} K - 1, \tag{72}$$

Then a commonly used quantity, the *reactivty*, ρ, can be also defined as the multiplication factor defect normalized by the normalization factor itself,

DEFINITION $\Rightarrow$
$$\rho \stackrel{def}{=} \frac{\delta K}{K} = \frac{K - 1}{K}. \tag{73}$$

Figure 11 illustrates the relationship between reactivity, *rho*, and the multiplication factor K. When $\rho > 0$, the reactor is super-critical on prompt neutrons alone. When $\rho = 0$, the reactor is critical on prompt neutrons alone (prompt critical). When $\rho < 0$, the reactor is sub-critical on prompt-neutrons. Note, the inclusion of delayed neutron, as will be seen subsequently may increase or decrease the net neutron population of the reactor.

In this discussion, the reactivity will be defined in terms of a finite medium,

DEFINITION $\Rightarrow$
(NOMENCLATURE
OVERLOADED)
$$\rho \stackrel{def}{=} \frac{\delta K_{eff}}{K_{eff}} = \frac{K_{eff} - 1}{K_{eff}}. \tag{74}$$
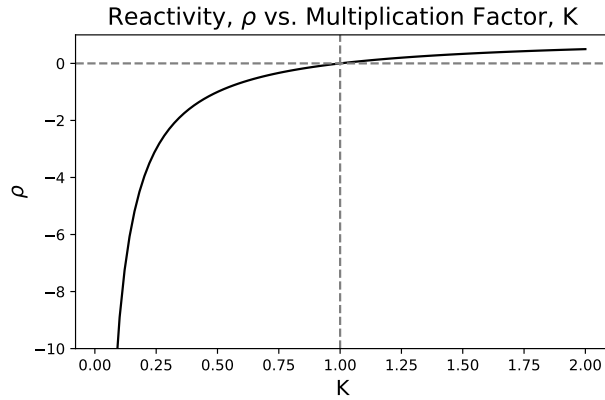
Figure 11: Illustration of the relationship between reactivity, ρ, and the neutron multiplication factor, K

Note, the definition of Equation 74 has overloaded the notation of the definition of Equation 73 for the purposes of this discussion. That being said, there's no reason why an infinite medium reactivity couldn't be defined,

DEFINITION $\Rightarrow$

$$\rho_\infty \stackrel{def}{=} \frac{\delta K_\infty}{K_\infty} = \frac{K_\infty - 1}{K_\infty}, \tag{75}$$

although a use for such a definition is lacking.

Appendix A.6   The Relationship Between K and the measurable quantities Σ_a and Σ_f

The infinite medium neutron multiplication, K_∞ (C.F. the definition of Equation 67) is a quantity that cannot be reasonable measured directly since it would require knowledge of the total number of neutron produced and the total number of neutrons absorbed. If we assume all neutrons produced are done so in nuclear fission, then,

$$Neutron\ Production\ Rate = \nu \Sigma_f \phi. \tag{76}$$

Furthermore, the neutron absorption rate can be found by,

$$Neutron\ Absorption\ Rate = \Sigma_a \phi. \tag{77}$$

35

Therefore,

$$k_\infty = \frac{Neutron\ Production\ Rate}{Neutron\ Absorption\ Rate} = \frac{\nu \Sigma_f \phi}{\Sigma_a \phi}. \tag{78}$$

Therefore,

$$k_\infty = \frac{\nu \Sigma_f}{\Sigma_a}. \tag{79}$$

and by Equation 71,

$$k_{eff} = \frac{\nu \Sigma_f P_{NL}}{\Sigma_a}. \tag{80}$$

Appendix A.7   The Neutron Generation Time, Λ, and its Relationship to K_{Eff} and ℓ

After a single fission event, the neutrons released must each travel, on average, a distance $\frac{\lambda_f}{\nu}$ before another fission event will occur - the quantity λ_f is divided by ν since ν neutrons are released, on average, in fission. Let's call this distance the *neutron production path length* λ_p since it is the distance a neutron must travel, on average, before another fission occurs and further neutrons are produced. We can then define a related quantity, the neutron generation time, Λ, to be the time it takes for a neutron to travel the neutron production path length,

DEFINITION $\Rightarrow$
$$\Lambda \overset{def}{=} t \quad S.T. \quad vt = \lambda_p. \tag{81}$$

Since,

$$\lambda_p = \frac{\lambda_f}{\nu} = \frac{1}{\Sigma_f \nu}, \tag{82}$$

and,

$$\Lambda = \frac{\lambda_p}{v}, \tag{83}$$

it follows,

$$\Lambda = \frac{1}{v \nu \Sigma_f}. \tag{84}$$

Since, according to Equation 80

$$k_{eff} = \frac{\nu \Sigma_f P_{NL}}{\Sigma_a}, \tag{80 Revisited}$$

and according to to Equation 63,

$$\ell = \frac{P_{NL}}{v \Sigma_a}, \tag{63 Revisited}$$

36

it follows,

$$\Lambda = \frac{\ell}{K_{eff}}$$ (85)

$$= \frac{\frac{P_{NL}}{v\Sigma_a}}{\frac{\nu\Sigma_f P_{NL}}{\Sigma_a}},$$

and therefore,

$$\Lambda = \frac{1}{v\nu\Sigma_f}.$$ (86)

Appendix A.8   The Delayed Neutron Fraction, DNF, and the Delayed Neutron Precusor Yield β

Neutrons are either immediately from the fission process or are emitted from a fission product called a delayed neutron precursor (DNP). The fraction of neutrons in a chain reacting system which arise from delayed neutron precursors is called the *delayed neutron fraction*, denoted DNF,

DEFINITION $\Rightarrow$ $$DNF \stackrel{def}{=} \frac{\text{Neutrons from DNP in Population}}{\text{Total Neutron Population}}.$$ (87)

This, however, is not a property of the nucleus undergoing fission. Therefore, we define a related quantity, the delayed neutron precursor yield, denoted β,

DEFINITION $\Rightarrow$ $$\beta \stackrel{def}{=} \frac{\text{Precursor Neutrons Per Fission}}{\text{Prompt Neutrons in Per Fission} + \text{ Precursor Neutrons Per Fission}}.$$ (88)

> **Note**
>
> This discussion was paraphrased from the website "NukeFacts" [17]. Other sources, such as Lewis [15], define β as the fraction of neutron that do not come from delayed sources. The definition made here is justified on the grounds that it explicitly relates β to a property of the fissioning nucleus.

Each delayed neutron precursor emits a neutron through radioactive decay with a characteristic half-life. The half-life of the DNP is dependent its nuclear composition and energy level. Calculations are often simplified by grouping the DNP into groups, each with a characteristic decay constant, λ_i, and delayed

37

neutron fraction, β_i. The total delayed neutron fraction is then the sum of the delayed neutron fractions of the groups,

$$\beta = \sum \beta_i. \tag{89}$$

Appendix A.9   The Point Kinetics Equation

Appendix A.9.1   The Neutron Component

The rate of change of neutrons in a reactor is given by,

$$\frac{dn(t)}{dt} = (Neutron\ Injection\ Rate\ From\ External\ Sources) \tag{90}$$
$$+ (Prompt\ Neutron\ Production\ From\ Fission)$$
$$+ (Neutron\ Production\ From\ DNP)$$
$$- (Neutron\ Absorption\ Rate) - (Neutron\ Leakage\ Rate),$$

First, let us consider the neutron injection from external sources. We us the notation,

DEFINITION $\Rightarrow$ $\qquad S(t) \stackrel{def}{=} (Neutron\ Injection\ Rate\ From\ External\ Sources). \tag{91}$

We assert $S(t)$, in most experimental or power reactors either originates from cosmic radiation or an external, man-made, neutron source, such as a ^{252}Cf start-up source. We assert it a reasonable assumption that the magnitude of cosmic neutron source is negligible with respect to the magnitude of the neutron population in the reactor. Furthermore, we impose the condition all external neutron sources have been removed from the system. Under this assumption and this condition, the entire $S(t)$ term can be removed from the analysis.

We now examine the prompt neutron production from fission. Recall from the definition shown in 88,

$$\beta \stackrel{def}{=} \frac{Precursor\ Neutrons\ Per\ Fission}{Prompt\ Neutrons\ in\ Per\ Fission +\ Precursor\ Neutrons\ Per\ Fission},$$
$$\tag{88 Revisited}$$

38

the quantity,

$$1 - \beta = 1 - \frac{\text{Precursor Neutrons Per Fission}}{\text{Prompt Neutrons in Per Fission} + \text{Precursor Neutrons Per Fission}}$$
$$= 1 \times \frac{\text{Prompt Neutrons in Per Fission} + \text{Precursor Neutrons Per Fission}}{\text{Prompt Neutrons in Per Fission} + \text{Precursor Neutrons Per Fission}}$$
$$- \frac{\text{Precursor Neutrons Per Fission}}{\text{Prompt Neutrons in Per Fission} + \text{Precursor Neutrons Per Fission}}$$
$$= \frac{\text{Prompt Neutrons in Per Fission}}{\text{Prompt Neutrons in Per Fission} + \text{Precursor Neutrons Per Fission}}.$$

$$(92)$$

Therefore, let us define the compliment of the delayed neutron precursor yield, β, the prompt neutron yield, $1 - \beta$.

Since fission generates ν neutrons per fission at a rate of $\Sigma_f v n$, it follows the prompt neutron production rate from fission will be,

$$(Prompt\ Neutron\ Production\ From\ Fission) = (1 - \beta)\nu\Sigma_f V n(t). \quad (93)$$

Since neutrons are generated from DNP via radioactive decay, neutrons will be generated from DNP at the rate at which they decay. Since the DNPs are discretized into groups according to their half-lives, the contributions from each of the DNP groups must be summed. Therefore,

$$Neutron\ Production\ From\ DNP = \sum_i \lambda_i C_i(t). \quad (94)$$

The neutron absorption rate is trivially,

$$(Neutron\ Absorption\ Rate) = \Sigma_a V n(t). \quad (95)$$

Finally, the leakage rate can be found by employing he leakage factor and applying it to the neutron absorption rate

$$(Neutron\ Leakage\ Rate) = \Gamma\Sigma_a V n(t). \quad (96)$$

Inserting equations 93, 95, 94 and 96 into Equation 90 then neglecting the external source term, we get,

$$\frac{dn(t)}{dt} = (1 - \beta)\nu\Sigma_f V n(t) + \sum_i \lambda_i C_i(t) - \Sigma_a V n(t) - \Gamma\Sigma_a V n(t). \quad (97)$$

39

or,

$$\frac{dn(t)}{dt} = (1-\beta)\nu\Sigma_f V n(t) + \sum_i \lambda_i C_i(t) - (1+\Gamma)\Sigma_a V n(t). \qquad (98)$$

Recall,

$$P_{NL} = P_L' = 1 - P_L = \frac{\Sigma_a \phi}{\Sigma_a \phi + \Gamma \Sigma_a \phi} = \frac{1}{1+\Gamma}, \qquad (55 \text{ Revisited})$$

which can be rearranged to

$$(1+\Gamma) = \frac{1}{P_{NL}}. \qquad (99)$$

Therefore, Equation 98 can be rewritten,

$$\frac{dn(t)}{dt} = (1-\beta)\nu\Sigma_f V n(t) + \sum_i \lambda_i C_i(t) - \frac{1}{P_{NL}}\Sigma_a V n(t). \qquad (100)$$

Recall,

$$k_{eff} = \frac{\nu\Sigma_f P_{NL}}{\Sigma_a}, \qquad (80 \text{ Revisted})$$

and,

$$\ell = \frac{P_{NL}}{V\Sigma_a}. \qquad (63 \text{ Revisited})$$

Therefore, Equation 100 becomes,

$$\frac{dn(t)}{dt} = (1-\beta)\frac{K_{eff}}{\ell}n(t) - \frac{1}{\ell}n(t) + \sum_i \lambda_i C_i(t), \qquad (101)$$

that is,

$$\frac{dn(t)}{dt} = \frac{(1-\beta)K_{eff} - 1}{\ell}n(t) + \sum_i \lambda_i C_i(t). \qquad (102)$$

Recall, in the intermediary step of Equation 85,

$$\Lambda = \frac{\ell}{K_{eff}}, \qquad (103)$$

and from Equation 74,

$$\rho = \frac{K_{eff} - 1}{K_{eff}}, \qquad (104)$$

and, applying these equalities in the algebraic manipulations,

$$
\begin{aligned}
\frac{(1-\beta)K_{eff}-1}{\ell} &= \frac{K-\beta K_{eff}-1}{\Lambda K_{eff}} \\
&= \frac{K_{eff}-1-\beta K_{eff}}{\Lambda K} \\
&= \frac{1}{\Lambda}\frac{K_{eff}-1}{K_{eff}} - \frac{\beta K_{eff}}{\Lambda K_{eff}} \\
&= \frac{\rho-\beta}{\Lambda},
\end{aligned}
\tag{105}
$$

we finally derive our statement which describes the neutronic evolution of a reactor from the perspective of point-kinetics,

$$
\frac{dn(t)}{dt} = \frac{\rho-\beta}{\Lambda}n(t) + \sum_i \lambda_i C_i(t);
\tag{106}
$$

the neutronic equation for the point-kinetics set of equations, or, more colloquially, the neutric component of the point kinetics equation.

Appendix A.9.2 The Precursor Component

We now derive the equation which describes the evolution of delayed neutron precursors (DNP) in a circulating fuel reactor. Consider the flow model shown in Figure 12. There are effectively two regions in which fuel salt can flow, the in-core volume and the ex-core volume[3]. The distinction between the in-core and ex-core regions is that fission rate in the ex-core region is sufficiently small that the production of DNP in the ex-core region is, for the intents and purposes of a point-kinetics analysis, negligible.

Recall, the delayed neutron precursor yield,

$$
\beta \overset{def}{=} \frac{\text{Precursor Neutrons Per Fission}}{\text{Prompt Neutrons in Per Fission} + \text{Precursor Neutrons Per Fission}},
\tag{88 Revisited}
$$

can be interpreted,

$$
\beta = \frac{\text{Precursor Neutrons Per Fission}}{Total\ Neutrons\ Per\ Fission},
\tag{107}
$$

---

[3]The heat-exchanger and pump are also elements of the ex-core volume. Although they do not factor into the analysis at all, they have been included for the sake of clarity.
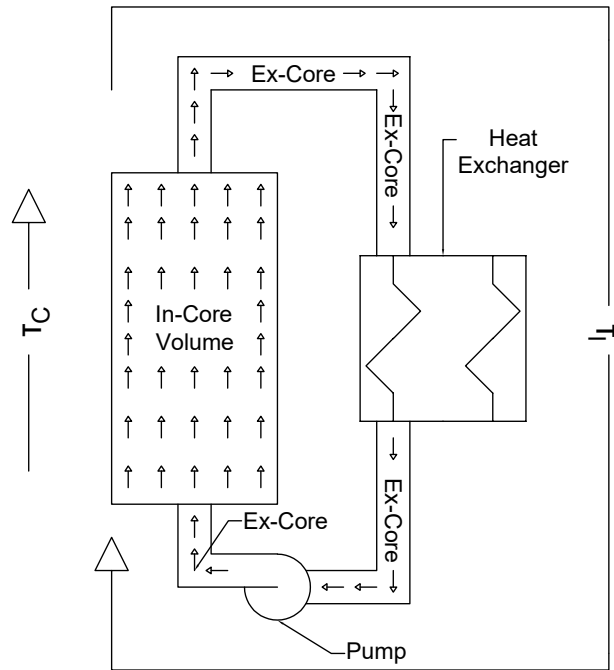
Figure 12: Precursor transport model

42

since neutrons produced are either prompt or precursors (ergo, we add the two to get the total). Therefore, the product,

$$\beta\nu = \frac{Precursor\ Atoms\ Produced}{Fission\ Event}, \tag{108}$$

since,

DEFINITION ⇒

$$\nu \overset{def}{=} \frac{Total\ Mean\ Number\ Of\ Neutrons\ Produced}{Fission\ Event}. \tag{109}$$

Therefore,the DNP production rate is given by,

$$DNP\ Production\ Rate = \beta\nu\Sigma_f v n(t). \tag{110}$$

Recall,

$$\Lambda = \frac{\ell}{K_{eff}}, \tag{103 Revisited}$$

Furthermore,

$$K_{eff} = \frac{\nu\Sigma_f P_{NL}}{\Sigma_a}, \tag{80 Revisited}$$

and,

$$\ell = \frac{P_{NL}}{v\Sigma_a}. \tag{63 Revisited}$$

Therfore, inserting Equation 80 and Equation 63 into Equation 103,

$$\Lambda = \frac{\ell}{K_{eff}} = \frac{\frac{P_{NL}}{v\Sigma_a}}{\frac{\nu\Sigma_f P_{NL}}{\Sigma_a}} = \frac{1}{v\nu\Sigma_f}. \tag{111}$$

Substituting this finding into Equation 110,

$$DNP\ Production\ Rate = \frac{\beta}{\Lambda}n(t). \tag{112}$$

In addition to the production of DNP from fission, DNP also decay at a rate,

$$DNP\ Decay\ Rate = \lambda_i C_i(t), \tag{113}$$

where λ_i is the effective half-life for the precursor group i and C_i is its concentration. There is also advection out of the corer, which is given by,

$$DNP\ Egress\ Rate = -\frac{C_i(t)}{\tau_c}. \tag{114}$$

This statement is derived from the fact species will advect at a rate, $\dot{N} = VC$, and the inverse of the velocity in a circulating system is the period, τ.

Finally, there is the rate at which DNP enter the core,

$$DNP\ Ingress\ Rate = \frac{C_i(t-\tau_l)e^{-\lambda_i\tau_l}}{\tau_c}. \tag{115}$$

43

This term states that the rate it which the DNP re-enter the core is equal to their concentration at time $t - \tau_l$, but reduced by a factor $\frac{A}{A_0} = e^{-\lambda_i \tau_l}$, and a rate equal to $\frac{1}{\tau_C}$.

Therefore, if the evolution of DNP is given by,

$$\frac{dC(t)}{dt} = \text{(DNP Production Rate)} - \text{(DNP Decay Rate)} - \text{(DNP Egress Rate)} + \text{(DNP Ingress Rate)}, \tag{116}$$

then we can write,

$$\frac{dC_i(t)}{dt} = \frac{\beta}{\Lambda} n(t) - \lambda_i C_i - \frac{C_i(t)}{\tau_c} + \frac{C_i(t - \tau_l) e^{-\lambda_i \tau_l}}{\tau_c}. \tag{117}$$

References

[1] J. Wood. *Nuclear Power*. Energy Engineering Series. Institution of Engineering and Technology, 2007 (cit. on p. 5).

[2] S. Plokhy. *Chernobyl: The History of a Nuclear Catastrophe*. Basic Books, 2018 (cit. on p. 6).

[3] D. Smith, D. Luckhurst, and A. Maccabee. "Design and control characteristics of the RBMK reactor". In: *Chernobyl: A Technical Appraisal*. British Nuclear Energy Society. London, 1986, p. 3 (cit. on p. 6).

[4] J. Groh. *Supplement to Accompany Lesson 13 of Reactor Physics Fundamentals: Reactivty Control Devices in the Control Loop (Power Control)*. Tech. rep. Canteach, 1996 (cit. on p. 6).

[5] *The Essential CANDU*. Tech. rep. University Network of Nuclear Engineering Excelence, 2018 (cit. on p. 7).

[6] *Science and Reactor Fundamentals - Reactor Physics*. Tech. rep. Candian Nuclear Safety Comission: Technical Training Group, 2003 (cit. on p. 7).

[7] R. Kedl and A. Houtzeel. *ORNL-4069: Development of a Model for Computing Xe-135 Migration in the MSRE*. Tech. rep. Oak Ridge, TN, USA: Oak Ridge National Laboratory, 1967 (cit. on p. 7).

[8] G Samuels and Lackey. *ORNL-2376: ART Fuel Pump and Xenon Removal System Development, Test Evaluation and Aircraft Application*. Tech. rep. Oak Ridge, TN, USA: Oak Ridge National Laboratory, 1957 (cit. on p. 8).

[9] P. Kasten, E. Bettis, and R. Robertson. *ORNL-3996: Design Studies of 1000-MW(e) Molten-Salt Breeder Reactors*. Tech. rep. Oak Ridge National Laboratory, 1966 (cit. on p. 8).

[10] W. Sides. *ORNL-TM-2489: MSBR Control Studies*. Tech. rep. Oak Ridge National Laboratory, 1969 (cit. on p. 9).

[11] S. Cantor, W. Cooke, S. Dworkin, D. Robbins, E. Thoma, and M. Watson. *ORNL-TM-2316: Physical Properties of Molten-Salt Reactor Fuel, Coolant and Flush Salts*. Tech. rep. Oak Ridge National Laboratory, 1968 (cit. on p. 12).

[12] J. Engel and R. Steffy. *ORNL-TM-3464: Xenon Behavior in the Molten Salt Reactor Experiment*. Tech. rep. Oak Ridge, TN, USA: Oak Ridge National Laboratory, 1971 (cit. on pp. 14, 27).

[13] Joseph Kotlarz. "Xenon Transient Studies for a CANDU reactor". PhD thesis. McMaster University, 1976 (cit. on p. 28).

[14] T. Jevremovic. *Nuclear Principles in Engineering*. New York, NY, USA: Springer, 2009 (cit. on p. 29).

[15] E.E. Lewis. *Fundamentals of Nuclear Reactor Physics*. Elsevier Science, 2008 (cit. on pp. 29, 37).

[16]   A. Trkov, M. Herman, and D. Brown. *ENDF-6 Formats Manual*. Tech. rep. Upton, NY, USA: National Nuclear Data Center, 2012 (cit. on p. 31).

[17]   *NUKEFACTS #1: Beta is Not The Delayed Neutron (Population) Fraction*. 2012. URL: `http://archive.is/st3e` (cit. on p. 37).

Attachment 9

Xenon Behavior in Molten Salt Reactor Graphite

Published in the ASME Journal of Nuclear Engineering

Xenon Behavior in Molten Salt Reactor Graphite

Terry J. Price[1]
Terry.Price@UOIT.net

Ondrej Chvala[2]
OChvala@UTK.edu

Zack Taylor[2]
RTaylo45@Vols.UTK.edu

[1] University of Ontario Institute of Technology
[2] University of Tennessee, Knoxville

January 2019

Abstract

This article discusses aspects of ^{135}Xe behavior in molten salt reactor (MSR) graphite. Models of MSR graphite are described. The related mass transfer and mass diffusion coefficients are described and means by which they can be calculated are detailed. Xenon reactivity effects are explored. A method is presented to model the internal xenon distribution within the graphite stringers.

1 Introduction

Molten salt reactors (MSRs) use an alkali fluoride fuel salt melt as both a working fluid and the fuel matrix. In thermal spectrum MSRs, the fuel salt circulates between a moderating region and a heat exchanger. For reference, MSRs are described, in detail, in the book by Dolan [1]. A review of MSR xenon behavior is given in our 2019 paper [2]. In many MSR designs, the moderator is comprised of porous graphite. The graphite used in the Molten Salt Reactor Experiment (MSRE), an experimental $7.4\,\mathrm{MW}_{th}$ reactor which operated at Oak Ridge National Laboratory (ORNL) 1965-1969, was *"grade CGB"* graphite [3, p. 85], which has been described as *"extruded petroleum coke bounded with coal tar pitch"* [4, p. 1].

Isotope ^{135}Xe is a product of the fission process. ^{135}Xe has an unusually high thermal neutron absorption cross-section, typically cited at $2.6\,\mathrm{Mb}$ [5]. This high cross-section makes its evolution and migration significant for the reactor behavior.

In a solid fueled reactor, the ^{135}Xe remains stationary in the solid fuel matrix; however, in a fluid fueled reactor, such as an MSR, the ^{135}Xe is free to migrate about the reactor. One such potential region for ^{135}Xe migration is a pore space of the graphite moderator. This paper examines the behavior of ^{135}Xe and its modeling in MSR graphite.

2 Models of Xenon Behavior in Graphite

The processes which governs xenon behavior in MSR graphite can broadly be broken into one of two categories, nuclear processes and migrational processes. In regards to nuclear processes, ^{135}Xe is removed through either burn-out[*] or nuclear decay. Burn-out refers to the process in which ^{135}Xe absorbs a neutron and transmutes into ^{136}Xe, i.e. ^{135}Xe (n,γ)^{136}Xe. The volumetric burn-out reaction rate is given by,

$$\dot{R}_{BO}(\vec{x}) = \int_E \phi(E,\vec{x})\sigma_a^{Xe}(E)C_{Xe}(\vec{x})dE. \quad (1)$$

The other nuclear process, which governs ^{135}Xe behavior, is *decay*, through which ^{135}Xe transmutes into ^{135}Cs via β^- decay process. The volumetric decay rate is given by,

$$\dot{R}_D(\vec{x}) = \lambda_{Xe}C_{Xe}(\vec{x}). \quad (2)$$

In addition to these nuclear processes, behavior of ^{135}Xe in graphite is governed by a mass transfer process. When the ^{135}Xe migrates the porous graphite, its behavior within the graphite has been modeled as a porous media reaction-diffusion equation.

$$\frac{\partial C_{Xe}}{\partial t} = \frac{D_g}{\epsilon}\nabla^2 C_{Xe} - (\sigma_a^{Xe}\phi + \lambda_{Xe})C_{Xe}, \quad (3)$$

This reaction diffusion equation approach was used in the ORNL-4069 [6] xenon model as well as the work by

---

[*] Some references, such as ORNL-4069 [6] refer to *burn-out* and *burn-up*. We, however, make the distinction that *burn-up* can also refer to the nuclear transmutation of the fuel, therefore we refer to this specific ^{135}Xe transmutation process as burn-out, since it is *burning* ^{135}Xe *out* of the system.

Shimazu [7] in 1977. Alternatively, a lumped-volume approximation,

$$J = K_m(C_{FS} - HRTC_G), \tag{4}$$

could also be used.

Note, although the graphite mass-diffusion coefficient D_g and porosity ϵ have been written as constants in the past, and invariant with respect to position in the graphite, this is a simplification and, as described Section 4, can vary with position.

The earliest appearance of a graphite model with a form congruent to Equation 3 was in Miller's 1961 [8] analysis of MSR xenon. Miller derived a form of Equation 3 with the graphite stringer simplified into a one-dimensional slab (see Annex A of [8]), and solved it, in steady-state, using a boundary condition that the surface concentration on both sides of the slab were the same. An implicit presupposition of Miller's use of a *symmetric concentration* boundary condition is that the ^{135}Xe in the fuel salt acts as a well-mixed solution — I.E. the ^{135}Xe concentration is the same at all points.

In the ORNL-4069 xenon model, the graphite stringers were modeled as infinite right circular cylinders, and Equation 3 was solved in cylindrical coordinates. Note, there is often a considerable difference in the magnitudes of the D_g/ϵ and $(\sigma_a\phi + \lambda_{Xe})$ terms which, in our experience, makes Equation 3 numerically stiff. In ORNL-4069 [6, p. 45], a steady state solution to the cylindrical form Equation 3 was coupled to a lumped parameter model of the graphite boundary layer in order to derive an expression for the mass flux into the stringer,

$$J = \frac{k_m C_{FS}}{1 + \frac{K_m HRT}{\beta D_g} \frac{I_0(\beta r_g)}{I_1(\beta r_g)}}. \tag{5}$$

The term β, is the graphite β factor and is determined numerically through the expression, $\beta^2 = \epsilon/D_g(\sigma_a^{Xe}\phi + \lambda_{Xe})$.

Typically MSR xenon analyses are formulated as systems of ODEs of the form $\frac{\partial \vec{x}}{\partial t} = \mathbf{A}\vec{x}$; however, Equation 3 is a PDE. This seeming non congruence may be overcome by either the use of Equation 5 to represent mass transfer to graphite, using a lumped

volume approach, or by discretizing the reaction diffusion equation through a technique such as the finite difference method (FDM) into a set of ODEs. In our experience, high values of graphite β require very small mesh sizes. More recently, as shown by van Schijndel [9], the system modeling software Mathworks Simulink [10], which can be used to model a set of ODEs, can be coupled with the PDE modeling software Comsol [11] and this provides another route to overcome this non congruence.

In addition to the porous reaction-diffusion model, shown in Equation 3, Shimazu [7] reports lumped parameter model of the form,

$$J = K_m\left(C_{FS} - \frac{HRT}{\epsilon}C_G\right), \tag{6}$$

by to model xenon mass transfer. ORNL-TM-3464 [12] also uses a lumped parameter model of the form,

$$\frac{dC_{Xe}}{dt} = \frac{K_m A}{V_{GR}}\left(C_{FS} - HRTC_G\right). \tag{7}$$

The applicability of a lumped parameter model to mass transfer to graphite in MSR xenon modeling is questionable given that many texts (such as [13]) state the Biot number, $Bi_m = k_m L/D$, should be less than 0.1 for a lumped parameter analysis.

For both the porous reaction-diffusion and lumped parameter models, there are considerations of stringer geometry. Prior porous reaction-diffusion models of MSR graphite have assumed either slab or cylindrical geometry. In the case of cylindrical geometry, three potential methods by which this geometric reduction can be accomplished are: (1) conservation of surface area, (2) conservation of stringer volume, or (3) conservation of hydraulic diameter. For the lumped parameter model, the surface area and volume can be decoupled, the surface area for mass transfer set equal to the wetted surface area of the original stringer and the volume can be set to that of the original stringer and the concentration of ^{135}Xe inside the stringer determined by $N_{Xe}/\epsilon V_{GS}^1$. We are unaware of any investigations which determine which method of geometric reduction would be most appropriate.

The diffusion of ^{135}Xe in graphite was investigated in 1962 report, ORNL-TM-0262 [14]. The report

2

claims that within certain ranges of D_g and ϵ, a one dimensional cylindrical or semi-infinite slab representation of graphite stringer geometry should *"closely approximate"* the full graphite stringer geometry. [ibid, p. 14] The report concludes that at values of $D_g < 10^{-5}\text{cm}^{-2}\text{s}^{-1}$, the semi-infinite slab is more appropriate whereas higher values of D_g are better represented by the cylindrical case. Intuitively, at low values of the mass diffusion coefficient, the diffusion process sees the geometry as a slab whereas at higher values of the mass diffusion coefficient, the geometric effects become important and a cylinder becomes appropriate. Presumably, by extension of the prior statements, at even higher values of the mass diffusion coefficient, the cylinder representation will become insufficient, and a full two-dimensional model of the stringer will become necessary, on account of its increased geometric complexity.

3 Mass Transfer Coefficients

Using either a lumped parameter model, Equation 6, or the porous reaction diffusion model, Equation 5, to model xenon behavior in MSR graphite requires an overall mass transfer coefficient, K_m, in order to calculate the rate of mass transfer. Note, in some older literature, the mass transfer coefficient is referred to as the *mass velocity*, on account of its units, $[ms^{-1}]$.

ORNL-4037 [15, p. 165] claims that the mass transfer coefficient, for ^{135}Xe mass transfer from the fuel salt to the graphite pore space, can be approximated by $K_m \approx D_{FS}^{Xe}\epsilon/\tau t_{pen.}$.

In prior analyses, mass transfer coefficients were generated through mass transfer correlations, which were derived from heat transfer correlations. In particular, ORNL-4069 [6, p. 71] used the correlation of Dittus and Boetler (introduced by McAdams) as well as the correlation of Sieder and Tate. These heat transfer correlations were transformed into mass transfer correlations by replacing the Nusselt number with the Sherwood number and the Prandtl number with the Schmidt number.

In addition to the method, used in ORNL-4069 [6], of interchanging Sherwood and Nusselt as well as Prandtl and Schmidt numbers, there exists numerous `heat / mass transfer analogies` that can be employed to determine mass transfer coefficients. These

mass transfer analogies provide a relationship between either the heat transfer and mass transfer or the friction factors and mass transfer, and are documented in numerous texts, such as Sherwood's 1975 book. [16, p. 159]

The validity of a mass correlation, similar to the Dittus Bottler correlation, was reported by Sherwood, who states *"The data from a large number of tests were well correlated by the dimensionless equation,*

$$Sh = 0.023Re^{0.88}Sc^{0.44}."\ [17]. \tag{8}$$

The experimental setup that produced the data used in this correlation involved a liquid, that ran along the wall of a column, vaporizing into a turbulent gas stream. The situation in an MSR is different: a gas dissolved in a liquid core is transferred to a gaseous pore space. Furthermore, the tests Sherwood was referring to were not conducted with molten salts.

Heat transfer correlations in molten salts was reviewed by Yoder in 2014 [18]. Yoder reviewed, evaluated, and summarized existing liquid salt heat transfer data, and compared these data to existing heat transfer correlations. Yoder concluded *"The [heat transfer] data in the database [of molten salts] can be reasonably predicted using conventional heat transfer correlations for common fluids"*; although he also warns, *"The accuracy of the heat transfer analysis depends on the accuracy of the properties of the salt being analyzed"*. As previously mentioned heat transfer correlations may be transformed into mass transfer correlations through heat / mass transfer analogies.

There was work done at ORNL to measure heat transfer correlations in molten salts during the MSR program. This work was reported in the 1976 report ORNL-TM-5335 [19]. Note, due to the relatively late publication date of this work, prior modeling efforts in MSR xenon analysis would likely have not been aware of its findings. ORNL-TM-5335 performed heat transfer measurements on two different molten salts in a tubular forced convection loop and concluded that there was *"satisfactory agreement with the empirical Sieder-Tate correlation"*, and *"the experimental data followed a modified Hausen equation"* between Reynolds numbers of 2,100 and 15,000. The report does note that there was *"insufficient data taken in the*

laminar region to allow any conclusions to be drawn". In contrast to this, Yoder [18] drew his conclusions with data which was measured down to a Reynolds number of 400 – a number below the typical Reynolds number which is considered to be the cutoff point for Laminar flow (2,100).

4 Mass Diffusion Coefficient

We are aware of two reports which document the investigation of diffusion in MSR graphite, ORNL-4148 [20] and ORNL-4398 [21]. The first serves a theoretical primer and a description of experiments performed, whereas the second investigates graphite stringer impregnation and provides some theoretical considerations into the transport of gaseous fission products in the MSRE's graphite stringers. ORNL-4389, in its considerations of ^{135}Xe behavior states *"diffusion through the salt primarily controlled the ^{135}Xe characteristics of the reactor"* [21, p. 35], and *"unless D_{Xe} were considerably less than 10^{-4} cm^{2}s^{-1} little or no absorption resistance could be expected on the part of the graphite in the absence of the xenon-salt diffusion"* [21, p. 35]. We propose these claims can be used to justify the use of the lumped parameter model in Equation 6.

Another consideration related to the behavior of ^{135}Xe is the effect of the graphite pore space contents on diffusion. Scott and Eatherly [22] state *"The fuel salt must be excluded from the graphite to prevent local overheating and also to decrease fission-product poisoning"*. In ORNL-TM-2136 [23, p. 35], calculations were performed to determine the magnitude of the pressure differential which would be required to cause fuel salt to intrude into the graphite pore space. The report states *"Calculations indicate that a pressure difference of approximately 300 psia [20.4 atm or 2.06 MPa] would be required to start the intrusion of fuel salt into the larger pore entrances (approximately 0.4 μ of the grade CGB graphite used in the MSRE"*. Additionally, it is claimed that radiation, fission product deposition, nor fission product fluoride contamination change the graphite's non-wetting characteristic. We therefore propose that whatever the substance inside the MSRE graphite pore space was, it was not fuel salt. Furthermore, we note that if there is penetration of fuel salt into the graphite

stringers, Equation 3 and Equation 6 will no longer be justifiable models of ^{135}Xe in the graphite due to the advection of fuel salt into the stringers.

We hypothesize the mass diffusion coefficient for ^{135}Xe in graphite is independent of pore-space contents. The previously mentioned report, ORNL-4389, states that diffusive transport in grade CGB graphite is predominated by Knudsen diffusion, a mode of diffusion where interactions with the pore-wall are dominate. The Knudsen diffusion coefficient, as stated by Cussler [24, p. 26] and numerous other sources, is given by the expression,

$$D_{Kn} = \frac{d}{3} \sqrt{\frac{8RT}{\pi M_{Xe}}}. \tag{9}$$

Given that the dominate mechanism of diffusion is Knudsen in grade CGB graphite, and the Knudsen diffusion coefficient is not a function of the pore-space contents, it follows that, given an MSR with porous graphite, which has its diffusion dominated by the Knudsen mechanism, the ^{135}Xe diffusion behavior in the graphite will be independent of the graphite pore space contents, and, as such, will be unaffected by the chemical and isotopic evolution of the pore-space gas.

Additionally, we note the potential for the build up of solid particulate inside the graphite pore-space to affect the ^{135}Xe diffusion in the graphite stringers. Given that the Knudsen diffusion mechanism (Equation 9) is a function of pore diameter, and the porous media mass diffusion coefficient is a function of constrictivity ($D_{PM} = \frac{D_F \epsilon \delta_c}{\tau}$), it follows that a nontrivial build up of substance on the walls of the graphite pore-space will lead to a change in the mass diffusion coefficient of ^{135}Xe in the graphite. The only study found on this subject was done by Baes in the 1966 report ORNL-4037 [15, p. 158]. Baes investigated the potential for ^{135}Cs-C formation from ^{135}Xe decay. Baes calculated the formation rate of Cs-C, assuming all the ^{135}Cs born in the graphite remained within it. Using parameters representative of an MSBR, the study concluded *"cesium carbide formation can be expected to occur in an MSBR, but in such small amounts as to be of little concern."*. We propose a more complete analysis would account for accumulation of noble metal fission products as well as the formation of fission product carbides.

4

Furthermore, although prior MSR xenon analyses assume spatially invariant D_g and ϵ, this may not be entirely true. Impregnation processes as well as accumulation of particulate and fission products may change the spatial distribution of the graphite parameters. The radial variation in porosity and density in MSRE graphite was examined in ORNL-4389 [21, p. 16]. It was found that, comparing a graphite sample taken from the center of the stringer specimen with a graphite sample taken from the edge of the stringer specimen, the porosity varied from 10.1% to 11.1%; the density varied from $1.874\,\mathrm{g/cm^3}$ to $1.850\,\mathrm{g/cm^3}$; and, the Knudsen mass diffusion coefficient ranged from $0.249 \cdot 10^{-4}\,\mathrm{cm/s^2}$ at the periphery, to $7.97 \cdot 10^{-4}\,\mathrm{cm/s^2}$ at the center. Finally, we note post operational inspection of a MSRE graphite stringer, reported in ORNL-TM-4174 [25, p. 8], revealed the existence of a crack, originating a the installation slug and extending *"halfway around the bar"*. We further propose the development of cracks may introduce new intrusion pathways for ^{135}Xe and change the distribution of ^{135}Xe in the graphite stringers. As such, to ensure consistent ^{135}Xe behavior, graphite bars should be kept crack free.

5 Change in Xenon Distribution with Graphite Beta

According to ORNL-4069 [6, p. 45], the distribution of ^{135}Xe in a graphite stringer can be modeled by an infinite right circular cylinder and its ^{135}Xe concentration, at steady state, is given by,

$$C_{Xe}(r) = C_G^{Surf.} \frac{I_0(\beta r)}{I_0(\beta r_0)}, \tag{10}$$

where

$$\beta = \sqrt{\frac{\epsilon}{D_g}(\sigma_a^{Xe}\phi + \lambda_{Xe})}. \tag{11}$$

This is the solution to Equation 3 at steady state in cylindrical coordinates.

As an qualitative interpretation, the graphite β factor determines the *nearness* of the ^{135}Xe to the surface of the graphite. A small beta factor indicates that the ^{135}Xe tends to be more homogeneously distributed in the graphite whereas a large beta factor indicates that the ^{135}Xe is predominately found near the surface of the stringer.
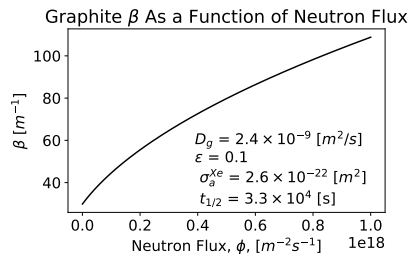
Figure 1: Example of variation of graphite β with respect to flux.

Since graphite β is parameterized by neutron flux, the distribution of ^{135}Xe in a graphite stringer changes with the reactor's the power level changes. An example of how graphite β varies with neutron flux in illustrated in Figure 1.

The ^{135}Xe distribution changes as the graphite β is varied. Several samples of how the graphite stringer ^{135}Xe distribution changes are shown in Figure 2. The plots in Figure 2, show a graphite stringer with a radius of $9\,\mathrm{mm}$, at various magnitude of β. In each plot there are three vertical lines that delineate, from right to left, where 90%, 99%, and 99.9% of the ^{135}Xe is contained. The X-axis is the distance (mm) from the stringer center. The Y-axis is the normalized ^{135}Xe concentration.

The first three plots (starting at the top) in Figure 2 show the variation in xenon concentration as the neutron flux is changed from 1% full power to 10% full power to 100% full power for a graphite stringer with parameter similar to that which were used in the MSRE. As we can clearly see, given this set of parameters, there is negligible variation in xenon distribution as the flux changes, which is fortunate, since if there was substantial changes, different reactivity coefficients would be needed to be formulated for each power level.

The change in the graphite β with respect to flux is given by taking the derivative of Equation 11 with

respect to flux,

$$\frac{\partial \beta}{\partial \phi} = \frac{\sigma_a^{Xe} \epsilon}{2 D_g \sqrt{\frac{\epsilon(\lambda_{Xe} + \sigma_a^{Xe} \phi)}{D_g}}}. \qquad (12)$$

Since the all of the parameters of this equation are positive, the graphite β monotonically decreases with respect to ϕ. This is unfortunate from a safety design perspective since the xenon reactivity load decreases with β. Intuitively, as the flux increases, the xenon distribution in the graphite becomes more sharp and thereby reduces the xenon reactivity effect – albeit, this is not very apparent at values around $\beta = 100/\text{m}$. A more thermal reactor, with a larger σ_a^{Xe}, will have greater sensitivity to graphite β with flux.

Finally, the bottom two plots in Figure 2 show the variation in xenon concentration for graphite β values of $1000/\text{m}$ and $10\,000/\text{m}$ respectively – which may be achievable depending on the type, quality, and impregnation of the graphite used.

Parameter	Value
D_g	$2.4 \cdot 10^{-9}\,\text{m/s}^2$
ϵ	10 %
ϕ	$7.6/(\text{m}\,\text{s}^2)$
σ_a^{Xe}	1.18 Mb

Table 1: Parameters for graphite stringer used in xenon distribution variation illustration

6 Modeling of Xenon in Graphite

The distribution of xenon in graphite stringers presents a problem for computational modeling. The distribution of xenon in these stringers is continuous, whereas all reactor physics codes we are aware of only allow for discrete distributions of isotopes in cells through material cards. Our solution to modeling this was to generate a number of annular rings around each fuel channel and set the concentration of ^{135}Xe in each annular ring equal to the xenon concentration at the midpoint of the ring according the Equation 10. This section describes our modeling efforts in this regards.

Variation of Graphite ^{135}Xe Concentration
With Respect to Graphite β
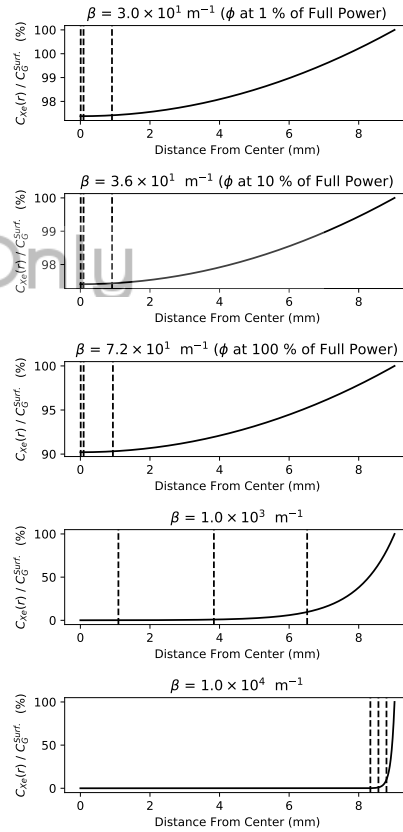
Figure 2: Variation of ^{135}Xe concentration with respect to graphite.

6.1 Methodology

An infinite Cartesian lattice of MSR fuel channels were modeled in the reactor physics code Serpent-2 [26]. The fuel channels were circular and annular rings of graphite were constructed around each fuel channel spaced equidistantly from the diameter of the fuel channel to the edge of the cell. The fuel surface xenon concentration at the edge of the graphite stringer was related to the bulk liquid xenon concentration through Henry's constant,

$$C_G^{Surf.} = HRT\,C_{Xe}^{FS}. \tag{13}$$

Again, the ^{135}Xe concentration in each annular ring equal to the xenon concentration at the midpoint of the ring according the Equation 10. The fuel salt composition used in the model was a replica of the MSRE fuel salt as per the constituents listed in ORNL-TM-0728[†]. The material temperature was set to 900 K and thermal scattering data was used with the graphite moderator. A periodic boundary condition was used to simulate infinite geometry. The other parameters used in the model are shown in Table 2.

Parameter	Quantity
C_{Xe}^{FS}	$1 \cdot 10^{14}/\text{cm}^3$
H_{Xe}	$2.714 \cdot 10^{-8}/(\text{m}^3\,\text{Pa})$
T	900 K
Pitch	7.2 cm
r_{fc}	1.6 cm
# Slices	20
$\rho_{mod.}$	1.86 g/cm
ρ_{FS}	2.2 g/cm

Table 2: Nominal parameters for Serpent 2 model

Each of the scenarios shown in Figure 2 were simulated with 20,000 histories. 120 cycles were preformed; the first 20 cycles were inactive. The JEFF 3.1.1 [27] cross section data were used. The value of k_{eff} was determined from Serpent-2's `implicit` k_{eff} estimator.

Two analyses were performed using the model:

- The first analysis was a *two dimensional* sensitivity analysis. The first dimension of the sensitivity

[†]See Table 2.1 on p. 8 of [3]

analysis was the graphite β factor and it was varied from $1 \cdot 10^1/\text{m}$ to $1 \cdot 10^4/\text{m}$. and the second dimension of the sensitivity analysis was obtained by perturbing each of the parameters listed in Table 2 by $\pm 25\%$. For each of these analyses 30 simulations were performed; 10 equidistantly spaced for each decade of graphite β.

- For the second analysis, two simulations were performed. The first simulation used the aforementioned *slicing* method. The second simulation set the graphite xenon concentration equal to the average of that which was computed by Equation 10. The β factor for these simulations was set to 100, a value that we estimate to be near the MSRE graphite β.

6.2 Results and Discussion

Figure 3 shows the results of the analyses. Plots A to F shows the results of the sensitivity analysis for each of the parameters mentioned in Table 2. Note, since Henry's constant, the ideal gas constant, and the temperature all acted as a multiplicative factor in the behavior of the model, these were perturbed as a group, shown in plot C.

Each analysis shows a sigmoidal characteristic that flattens out around graphite β values below 100 and above 1000 — the region between $1 \cdot 10^2/\text{m}$ to $1 \cdot 10^3/\text{m}$ exhibits high sensitivity to perturbation. The region of low graphite β corresponds to a graphite stringer with a near homogeneous distribution of xenon whereas a graphite stringer with a high β corresponds to a graphite stringer in which all the xenon tends to appear near the surface.

Clearly, the model is most sensitive to perturbation in the cell pitch, shown in plot E. As we can see from plot D, at low values of graphite β, the model appears to be robust against perturbation in the number of annular slices used in the modeling effort, which is fortunate since, it cannot be known how many slices should be used in the modeling effort a priori.

Plot G shows the results of the analysis that compared a model with a uniform *lumped average* xenon concentration to the slicing method. Clearly there is a substantial difference between the lumping method

and the slicing method and this indicates that modeling the internal behavior of xenon within the graphite is a necessary part of studying xenon behavior.

7 Conclusion

This paper has examined the modeling of ^{135}Xe behavior in MSR graphite. Models of ^{135}Xe behavior in graphite were reviewed. Details of the calculation of the mass transfer and mass diffusion coefficients were detailed. The ^{135}Xe reactivity defect and its dependence on the graphite β factor were examined. Given our findings with the stochastic modeling efforts, it seems reasonable to conclude that the beta factor and internal behavior of xenon in the graphite has a non-trivial influence on the xenon reactivity defect and should be accounted for.

8 Research Questions

The following research questions arose during our work:

- In the past MSR xenon poison fraction to xenon concentration correlations have been formulated in terms of xenon concentration alone. The distribution of xenon, in a graphite stringer, however, is a function of neutron flux. Are there certain quantities of graphite β in which is becomes important to parameter the xenon poison fraction correlation in terms of neutron flux as well as xenon concentration.

- How accurately does the radial reaction diffusion equation approximate the actual distribution of xenon in a graphite stringer?

- How does the evolution of the graphite over the course of the reactor life time affect the distribution of xenon within the graphite? Is it necessary to have different reactivity correlations at the beginning of life and end of life of the core?

- What is the impact of stringer defects, such as cracks or manufacturing defects, on the distribution of graphite within a stringer?

Nomenclature

α Constant of proportionality between the *occluded area per unit volume*, $C_{Xe}\sigma_a^{Xe}$, and the xenon reactivity defect

β Graphite beta factor. $\beta^2 = \epsilon/D_g(\sigma_a^{Xe}\phi + \lambda_{Xe})$ [1/m]

δ_c Constrictivity [dimensionless]

$\dot{R}_{BO}$ Volumetric Rate of burn out [mol/(m^3 s)]

$\dot{R}_D$ Volumetric Rate of decay [mol/(m^3 s)]

ϵ Porosity [dimensionless]

λ_{Xe} Xenon radioactive decay constant

$\left(\frac{\delta k}{k}\right)_{Xe}$ Xenon reactivity defect

$\overline{C_{Xe}}$ The *"importance averaged xenon concentration"* mentioned in ORNL-TM-3464 [12] [mol/m^3]

ϕ Neutron flux [1/(m^2 s)]

ρ_{FS} Fuel salt density [kg/m^3]

$\rho_{mod.}$ Graphite moderator density [kg/m^3]

σ_a^{Xe} xenon microscopic absorption cross section [b]

τ Tortuosity [dimensionless]

$\vec{x}$ Position vector

C_G Graphite ^{135}Xe concentration[mol/m^3]

$C_G^{Surf.}$ Concentration of ^{135}Xe at the surface of the graphite, in the gas side mol/m^3]

C_{FS} Fuel salt ^{135}Xe concentration [mol/m^3]

C_{GR} Concentration ^{135}Xe in a homogenized graphite region [mol/m^3]

C_{Xe} Xenon concentration

C_{Xe}^{FS} Xenon concentration in fuel salt [1/m^3]

C_{Xe}^{Gi} Concentration of xenon at the graphite interface [mol/m^3]

d Pore diameter[m]

D_F Mass diffusion coefficient of the diffusing substance in the fluid without a porous matrix [m^2/s]

D_g Graphite mass diffusion coefficient [m^2/s]

D_{FS}^{Xe} Mass diffusion coefficient of xenon in fuel salt [m^2/s]

D_{Kn} Knudsen diffusion coefficient [m^2/s]

D_{PM} Porous media mass diffusion coefficient [m^2/s]

E Energy

H Henry's constant[mol/(m^3 Pa)]

I_0/I_1 Modified Bessel function of the first kind of order 0/1

J Mass flux [mol/(m^2 s)]

K_m Overall mass transfer coefficient [m/s]

M_{Xe} Molar mass of ^{135}Xe [kg/mol]

R Ideal gas constant[J/(mol K)]

r Radial coordinate [m]
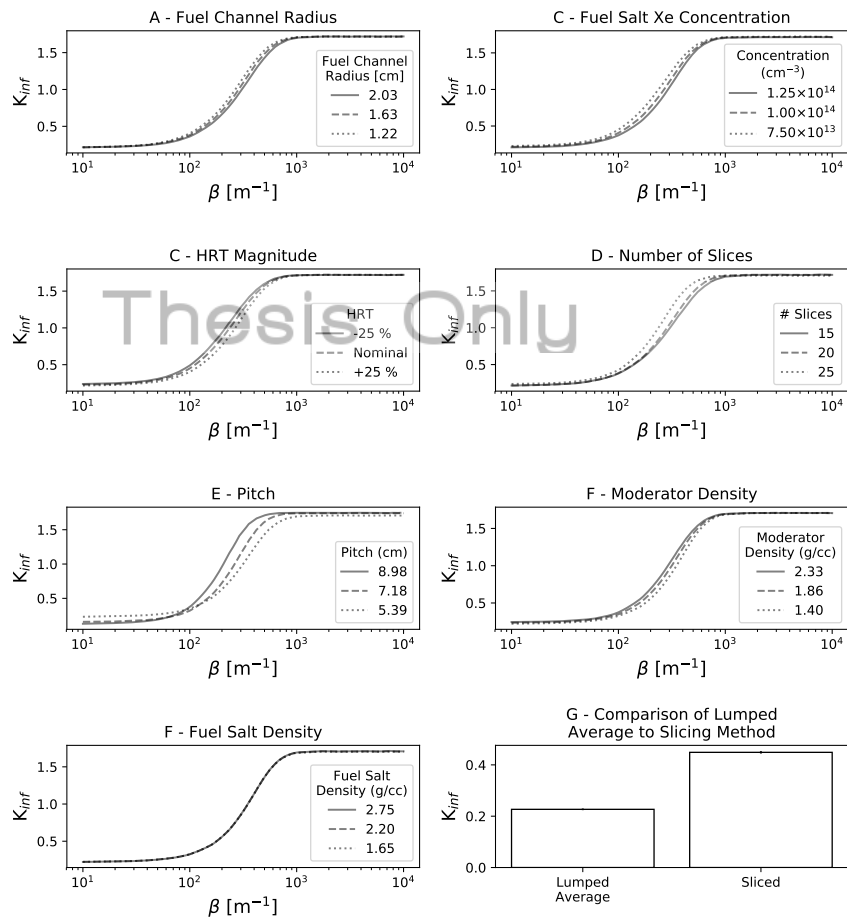
Figure 3: Results of Monte Carlo modeling

r_0	Extent of graphite stringer [m]
r_{fc}	Fuel channel radius [m]
Re	Reynold's number
Sc	Scmidt number
Sh	Sherwood number
T	Temperature [K]
t	Time
$t_{1/2}$	Half life [s]
$t_{pen.}$	Thickness of fuel salt penetration into the graphite stringers [m]
V_{GR}	Volume of a homogenized graphite region [m^3]

References

[1] T. Dolan. *Molten Salt Reactors and Thorium Energy.* Woodhead Publishing, 2017.

[2] T. Price, O. Chvala, and R. Taylor. Molten salt reactor xenon analysis: Review and decomposition. *Journal of Nuclear Engineering and Radiation Science*, 2019. Accepted, awaiting publication.

[3] R. Robertson. ORNL-TM-0728: MSRE Design and Operations Report. Technical report, 1965.

[4] J. Moore, T. Godfrey, and D. McElroy. *Thermal Properties of Grade CGB Graphite.* ORNL-P-150. Oak Ridge National Laboratory, 1964.

[5] E. Baum, H. Knox, and T. Miller. *Nuclides and Isotopes: Chart of the Nuclides.* Lockheed Martin, 16 edition, 2010.

[6] R. Kedl and A. Houtzeel. ORNL-4069: Development of a Model for Computing Xe-135 Migration in the MSRE. Technical report, Oak Ridge National Laboratory, 1967.

[7] Y. Shimazu. Transient Xenon Analysis in a Molten Salt Breeder Reactor. *Journal of Nuclear Science and Technology*, 14(11):805–810, 1977.

[8] J. Miller. ORNL-CF-61-5-62: Xenon Poisoning in Molten Salt Reactors. Technical report, Oak Ridge National Laboratory, 1961.

[9] A. Van Schijndel. Integrated modeling of dynamic heat, air and moisture processes in buildings and systems using SimuLink and COMSOL. In *Building Simulation*, volume 2, pages 143–155. Springer, 2009. ISBN 1996-3599.

[10] Mathworks Simulink. URL www.mathworks.com/products/simulink.html.

[11] COMSOL. URL www.comsol.com.

[12] J. Engel and R. Steffy. ORNL-TM-3464: Xenon Behavior in the Molten Salt Reactor Experiment. Technical report, Oak Ridge National Laboratory, 1971.

[13] W. Janna. *Engineering Heat Transfer, Second Edition.* Heat Transfer. Taylor & Francis, 1999.

[14] G. Watson and R. Evans. ORNL-TM-262: Xenon Diffusion in Graphite: Effects of Xenon Absorption in Molten Salt Reactors Containing Graphite. Technical report, Oak Ridge National Laboratory, 1962.

[15] R. Briggs. ORNL-4037: Molten-Salt Reactor Program Semiannual Progress Report for Period Ending August 31, 1966. Technical report, Oak Ridge National Laboratory, 1967.

[16] T. Sherwood, R. Pigford, and C. Wilke. *Mass Transfer.* McGraw-Hill, 1975.

[17] T. Sherwood. Mass transfer and friction in turbulent flow. *Transactions of the American Institute Chemical. Engineers*, 36:817, 1940.

[18] G. Yoder. Examination of Liquid Fluoride Salt Heat Transfer. In *Proceedings of ICAPP 2014*, Charlotte, 2014.

[19] H. Silverman, M. Huntley, W., Rrobertson. ORNL-TM-5335: Heat Transfer Measurements in a Forced Convection Loop with Two Molten-Fluoride Salts: LiF-BeF2-ThF2-Uf4, and Eutectic NaBF4-NaF. Technical report, Oak Ridge National Laboratory, 1976.

[20] A. Malinauskas, J. Rutherford, and R. Evans. ORNL-4148: Gas Transport in MSRE Moderator Graphite. Part 1: Review of Theory and Counterdiffusion Experiments. Technical report, Oak Ridge National Laboratory, 1967.

[21] R. Evans, J. Rutherford, and M. Malinauskas. ORNL-4389: Gas Transport in the MSRE Moderator Graphite: II. Effects of Impregnation; III. Variation of Flow Properties. Technical report, Oak Ridge National Labs, 1969.

[22] D. Scott and W. Eatherly. Graphite and Xenon behavior and their influence on molten-salt reactor design. *Nuclear Applications and Technology*, 8(2): 179–189, 1970.

[23] P Kaaten. ORNL-TM-2136: Graphite Behavior and Its Effects on MSBR Performance. Technical report, 1969.

[24] E. Cussler. *Diffusion: Mass Transfer in Fluid Systems.* Cambridge University Press, third edition, 2007.

[25] H. McCoy and B. McNabb. ORNL-TM-4174: Postirradiation Examination of Materials From the MSRE. Technical report, Oak Ridge National Laboratory, 1972.

[26] Jaakko Leppanen. *Serpent – a Continuous-energy Monte Carlo Reactor Physics Burnup Calculation Code.* 2012. URL http://montecarlo.vtt.fi/.

[27] A. Santamarina, D. Bernard, P. Blaise, M. Coste, A. Courcelle, T. Huynh, C. Jouanne, P. Leconte, O. Litaize, S. Mengelle, et al. The jeff-3.1. 1 nuclear data library. *JEFF report*, 22(10.2):2, 2009.

Acknowledgements

Attachment 10

A Review of Molten Salt Reactor Xenon Analysis Literature

Published in the ASME Journal of Nuclear Engineering

A Review of Molten Salt Reactor Xenon Analysis Literature

T. J. Price,[1] O. Chvala[2]

[1]University of Ontario Institute of Technology, Oshawa, Ontario, Canada
[2]University of Tennessee, Knoxville, Tennessee, United States

Terry.price@uoit.net, ochvala@utk.edu

Abstract

This paper presents a review of xenon analyses literature related to molten salt reactors. A brief primer of reactor xenon theory is presented for fluid fueled reactors. A review of xenon analysis literature is presented for both the work done by the Oak Ridge National Laboratory, and the later work in academia. A review of experimental work is presented. The paper concludes with describing some of the difficulties in establishing a priori xenon models and includes a commentary on the sensitive dependence of the molten salt reactor xenon behavior on the circulating void fraction.

1.   Introduction

Molten Salt Reactors (MSRs) are a type of Generation IV nuclear reactor concept set forward for development by the Generation IV international forum [1]. Several private companies are currently developing MSRs for deployment in the late 2020s. Unlike traditional reactors, which use a solid fuel matrix, MSRs circulate a molten alkali and actinide fluoride fuel salt between the reactor core region and a heat exchanger. While passing through the active core region, some of the actinides within the salt undergo heat generating nuclear fission. The heat is transferred to the fuel salt which acts as a working fluid. The fuel salt then circulates to a heat exchanger, where the heat stored in the salt is transferred to the secondary side working fluid. The molten salt fuel then recirculates back through the core to undergo fission again. The heat from the secondary side of the heat exchanger is transferred to a third working fluid that powers a turbine generator, thereby producing electricity.

When fission occurs, it creates fission products as well as free neutrons. Since the induction and production of fission both arise from the same source, free neutrons, a sufficient mass of fissionable material will chain react and sustain itself (or increase) without an external source of free neutrons. For the chain reaction process to be self-sustaining, at least the same number of neutrons must be created (through fission) as are absorbed. One of the major absorbers of free neutrons is the isotope Xenon 135 with its 2.6 Mb (Mega barn, 10^{-22} m^2) neutron absorption cross-section in the thermal region (see [2], p. 467). When Xe-135 absorbs a neutron it transmutes into a stable Xe-136, which has a low neutron cross-section. For this reason, Xe-135

is called a parasitic neutron absorber. In addition to Xe-135, is its metastable form, Xe-135m, which can be produced through either beta decay of I-135 of directly from fission. Xe-135m has a half-life of 15.3 m and has a neutron absorption cross-section of 10.17 Mb. A minority of fissions and decays result in Xe-135m [18].

This paper provides a brief primer on Xe-135 theory in thermal spectrum MSRs, assuming graphite is the moderating material, and then delves into the history of research in the field. Summarized details of previous experimental work, including problems related to predicting circulating void fractions are provided here. Details about problems predicting circulating void fractions are exposited. The chronology of this paper is divided into the 'first' and 'second' eras of MSRs. Although it is difficult to bound these eras by precise years, in general, the first era of MSR technology is related to historical work performed at Oak Ridge National Laboratory (ORNL) around MSR development, whereas the second era focuses on MSRs as a Generation IV-type reactor design.

2.   Primer on theory

Xenon analyses for MSRs has some unique aspects that are not present in xenon analyses for solid fueled reactors. In solid fueled reactors, the xenon stays relatively immobilized by the fuel matrix, and the complete behavior of xenon within the fuel can be described by a set of three coupled ordinary differential equations:

$$\frac{dN_{Xe}}{dt} = \gamma_{Xe}\Sigma_f\phi + \lambda_I N_I - \lambda_{Xe}N_{Xe} - \Sigma_a^{Xe}\phi$$
$$\frac{dN_I}{dt} = \gamma_I\Sigma_f\phi + \lambda_{Te}N_{Te} - \lambda_I N_I \tag{1}$$
$$\frac{dN_{Te}}{dt} = \gamma_{Te}\Sigma_f\phi - \lambda_{Te}N_{Te}$$

Where γ is the yield per fission, λ is the decay constant, which has units , N is the quantity of a particular isotope, Σ_a is the macroscopic absorption cross section, Σ_f is the microscopic fission cross section, and ϕ is the flux, for Xe-135, Te-135, and I-135 respectively.

In fluid fueled reactors, however, the xenon is dissolved within the fuel and is transported throughout the primary heat transport system, and additional terms must be included.

Briefly stated, an MSR has three containers in which the xenon can be held: the fuel salt, the graphite void space, and the circulating bubbles (voids). Each of these has its own source and sink terms. Iodine and tellurium are assumed to stay in solution whereas the xenon is free to migrate between the three containers. Xenon adsorption onto reactor surfaces and graphite is assumed to be negligible as per the discussion in ORNL-4069 [3]. There is some evidence for adsorption of radioiodine into corrosion product layers. The steady state analytical model, as

discussed by ORNL-4541 [4] notes steady state, xenon behavior is described by the following set of rate equations:

(generation rate) $=$ (decay rate in salt) $+$ (burnup rate in salt)
$+$ (migration rate to graphite)
$+$ (migration rate to circulating bubbles)

(migration rate to graphite) $=$ (decay rate in graphite) $+$ (burnup rate in graphite) (2)

(migration rate to bubbles) $=$ (decay rate in bubbles) $+$ (burnup rate in bubbles)
$+$ (stripping rate of bubbles)

The void space inside of the graphite is gaseous since the graphite is non-wetting. The mass transfer process to the graphite void space takes place in two parts, from the bulk salt to the boundary layer, and from the boundary layer to the pore space. According to Shimazu [5], the mass transfer to the graphite boundary layer can be modeled with:

$$Flux = k_m A \left(C_L - \frac{HRT}{\epsilon} C_{graphite} \right)$$ (3)

Where k_m is the mass transfer coefficient in , A is the surface area of a fuel-channel, C_L is the salt xenon concentration, H is the Henry's Constant for xenon in the fuel salt, R is the universal gas constant, T is the temperature in Kelvin ,ϵ is the porosity factor of the graphite, and $C_{graphite}$ is the concentration of xenon in the graphite.

The flux[1] of xenon from the boundary layer of the fuel-salt into the bulk graphite is given by:

$$Flux = \frac{D_g}{\epsilon} \left(\frac{dC_{graphite}}{dr} \right)$$ (4)

The term D_g is the *porous-medium mass diffusion coefficient* of the graphite. In the Molten Salt Reactor Experiment (MSRE)[2], the mass transfer rate from the fuel salt to the graphite was rate limited by the mass transfer rate from the bulk salt to the boundary layer [3].

Mass transfer into bubbles, is governed by:

---

[1] Quantity of xenon passing through a unit area per unit time.
[2] The Molten Salt Reactor Experiment (MSRE) was an experimental reactor designed, built, and operated by ORNL in the 1960s. Brief given in [6] and detailed in [7].

$$Flux = k_m A(C_L - HRTC_B) \tag{5}$$

If mass transfer into the plenum space is to be considered, a similar expression can be developed for diffusing off gassing into the plenum space:

$$Flux = k_m A_e(C_L - HRTC_{plenum}) \tag{6}$$

The nomenclature is the same as before, save for A_e which is the effective area term, and C_{plenum}, which is the plenum xenon concentration. The effective area term includes time averaged surface perturbations, scum effects, mist, spray, and foam effects.

3.   The Xenon Stripper
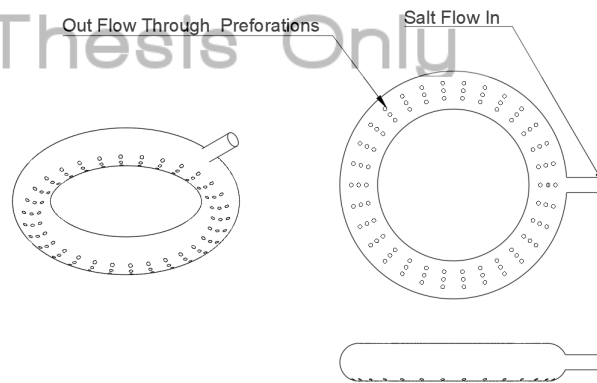
Figure 1 Illustration of a xenon stripper

In the MSRE, the xenon was removed from the system through a device called the *xenon stripper* (see Figure 1). Xenon is *stripped* from the molten salt by increasing the area of the molten salt which is in contact with *purging gas*. The xenon stripper is suspended above a pool of molten salt. xenon laden fuel-salt enters the xenon stripper through the inlet, circulates through the toroidal ring, then exits out small perforations in the bottom, whereupon it rejoins the bulk of the molten salt, with a reduced xenon content.

 There are two important parameters associated with a xenon stripper: the liquid stripping efficiency, and the bubble stripping efficiency. The liquid stripping efficiency, according to ORNL-4069 [3, p.42],

$$\eta_L = \frac{C_{Xe}^{II}}{C_{Xe}^{I}},$$

Where C_{Xe}^{I} is the concentration of dissolved xenon in the liquid salt before the xenon stripper and C_{Xe}^{II} is the concentration of dissolved xenon in the liquid salt after the xenon stripper. A formal definition of the bubble stripping efficiency was not found, therefore, we propose the bubble stripping efficiency can be defined as,

$$\eta_B = \frac{\rho_B^{II}}{\rho_B^{I}},$$

Where ρ_B^{I} is the bubble density (bubbles per unit volume) before entering the xenon stripper and ρ_B^{II} is the bubble density after passing through the xenon stripper. How these two parameters depend on the condition and flow parameters of the fuel salt is an open research question.

Finally, we note that, in our experience, there are three related concepts which would benefit from some disambiguation: *stripping, spraging,* and *off gassing. Stripping*, as in xenon stripping, is the process of removing a gas from a liquid. *Sparging*, specifically refers to bubbling a gas through a liquid to remove a dissolved gas. The xenon stripper is a stripper rather than a sparger since it contacts liquid with a gas through spraying rather than by bubbling. Finally, *off gassing* is a more general term which encompasses all forms of gas removal from a liquid, including diffusive processes from the bulk liquid contacting the purge gas. In this sense, sparging is a type of stripping, stripping is a form of off gassing, and by inference, sparginig is also a type of off gassing.

4.   The first era of MSRs

The earliest research considered in this paper related to Xe behavior in MSRs include three unpublished ORNL reports related to Xe transport in graphite for MSRs. The first document was written in 1960 and titled "*Xenon Transport in MSRE graphite*" [8]. The second document was written in 1961 and titled "*Xenon Diffusion in Graphite: Effects of Xenon Absorption in MSRs Containing Graphite*" [9]. Finally, there was an undated document titled "*Xenon Migration to the MSRE Graphite*" [10]. All of these documents were unpublished, and copies of them could not be found.

Reference to these documents was found in the report ORNL-4069 [3] (discussed later),

> "Xenon-135 poisoning in the MSRE was considered previously (refs. 5-7)[3] but these calculations were generally of an approximate design nature because of the lack of information on the values of rate constants involved." [3, p. 7]

It appears that, based on the ORNL literature reviewed, xenon behavior in the graphite was a performance concern during early MSR development.

MSR xenon poisoning was explored in a 1961 ORNL memo titled *"Xenon Poisoning in Molten Salt Reactors"* [11]. The report discusses the migration of xenon into graphite and presents

---

[3] References 5-7 in ORNL-4069 map to references [8] [9] [10] in this paper.

analytical expression for the diffusion. The number of xenon absorption per neutron produced is calculated, and sensitivity analysis are performed on xenon removal times (through stripping) and graphite mass diffusion coefficients. Although the scope of the report was to calculate the xenon poison fraction for a 1000-MW$_e$ molten salt breeder reactor, no analysis of circulating voids was made.

A brief discussion on Xenon-135 behavior in the MSRE was given in the 1964 progress report, ORNL-3078 [12]. The production and destruction mechanisms were discussed (later called source and sink terms). The xenon stripping efficiency was also briefly discussed, but there was no mention of any of the xenon migration mechanisms.

The first major report about MSRE xenon poisoning analysis was the 1967 report ORNL-4069, *"Development of a Model for Computing Xe-135 Migration in the MSRE"* [3]. This report was effectively pre-operational in that operational experience from the MSRE was not incorporated into the model developed. The report details the conduct and analysis of the "krypton experiment" (described later) as well as the development and results of a xenon model for the MSRE.

The ONRL-4069 xenon model accounted for generation, burnup, decay, xenon stripping[4], and bubble and graphite mass transfer. The core was discretized into 72 annular regions, and the contribution to the poison fraction was calculated with an adjoint flux weighting factor for each region. In the final calculation, the regions were summed, and the steady state xenon poison fraction was determined. The number density of xenon was related to the xenon poison fraction by a constant of proportionality. Sensitivity analyses were performed. These calculations were performed for cases with and without circulating void fractions. In the cases where the poisoning was calculated, the poison fraction was calculated as the void fraction was varied.

In 1968, Peebles investigated mass transfer of Xe-135 to circulating bubbles in the report ORNL-TM-2245 [13]. It was reported that the mass transfer coefficient was highly dependent on whether or not the bubbles had a mobile, or a rigid, salt-gas interface. Mass transfer correlations are given in terms of Sherwood number for both turbulent and laminar flow. Details about experimental validation of the mass transfer correlations are given, and an experiment is proposed to simulate MSBR contact conditions.

A paper, published in 1970 , by Scott and Eatherly, detailed the interplay between graphite and xenon and their influence on MSR design [14]. Although much of the paper is devoted to the description of xenon and its lifetime behavior, details are given pertaining to xenon yields, solubility, bubble mass transfer rates, and the predicted Molten Salt Breeder Reactor (MSBR)

---

[4] The term *'stripping'*, or more specifically, *xenon-stripping* refers to the removal of xenon from the fuel-salt through mechanical agitation.

xenon poison fraction. The paper concludes with some design considerations concerning graphite and xenon for MSRs.

The other major report detailing an MSRE xenon model was the 1971 report ORNL-TM-3464 [15]. This report detailed the predicted and observed xenon behavior in the MSRE. Furthermore, the report presented the development of a second xenon model for the MSRE, and the predictions made thereby.

The xenon poisoning model in ORNL-TM-3464 [15] included bubble and xenon migration sub-models. These models fed into each other to calculate both the steady state and transient xenon behavior in the MSRE. Additional details about the transient model are given in the 1967 report ORNL-4119 [16]. The bubble sub-model could be switched between a soluble or insoluble cover gas model. The soluble cover gas model was used to model xenon behavior with a helium cover gas; whereas the insoluble cover gas model was used to model the argon cover gas behavior. The bubble model used a lumped region approach which included the reactor core, the heat exchanger, the upstream piping, and the pump bowl. For each region in the bubble model, there were constituent liquid and gas sub regions where the mass balance equations were calculated. The xenon model included all the regions of the bubble model, but also included several sub regions that were not included in the bubble model. The reactor core included six sub-regions for moderating graphite. The core graphite was subdivided into one of five regions dependent on the flow conditions about the graphite. The Xe-135m was lumped into a single graphite sub-region. The pump bowl also contained liquid and gas sub-regions, and a sub-model for cover-gas behavior. In the cover-gas sub-model the xenon was transferred from the liquid circulating fuel salt and from the circulating bubbles to the cover gas through the MSRE's xenon spray ring. All the regions and sub-models were connected through a system of first order ordinary differential equations and solved with custom ORNL solver libraries.

A parameter space exploration was undertaken to attempt to match the ORNL-TM-3464 [15] xenon model to observed xenon behavior. Both steady state and transient calculations were performed. One of the more prominent goals in this exploration was fitting the observed difference in xenon poison fraction between the helium and argon cover gasses given a low circulating void fraction. Although this was achieved by switching the cover gas models between the soluble and insoluble sub-models, it could not be done with the measured xenon spray ring stripping efficiency. It was hypothesized that this inability to fit the data was due to the existence of a floating foam covering the pump bowl which reduced the efficiency of the xenon spray ring bubble stripping factor. Another difficulty encountered was the inability to match the transient behavior without adding a mass transfer term from the circulating bubbles directly to the graphite. Nevertheless, agreement was able to be achieved between the xenon model and observed xenon behavior.

One of the last works in the first era of MSRs was a 1977 paper by Shimazu [5]. The paper described a transient xenon analysis in a molten salt breeder reactor. The method reduces the complete MSR system into a set of six first order ordinary differential equations, and a core block sub-model. Startup, shutdown, load increase and decrease, and load following transients were simulated, and the results of both MSR and Pressurized Water Reactor (PWR) xenon behavior compared. In general, the MSR xenon behavior was found to be more attenuated than the PWR xenon behavior.

5.   The second era of MSRs

Suzuki and Shimazu created a lumped parameter model of the Molten Salt Breeder Reactor in 2004 [17]. The model was used to investigate the response of the reactor to various reactivity perturbations. The xenon model developed previously by Suzuki (1977) was implemented in the control model, and xenon effects were investigated. The lumped parameter model included both nuclear and balance of plant regions. The nuclear regions included in-core and out-of-core region with graphite nodes. The balance of plant section included both the heat exchanger and the steam generator. The nuclear kinetics used a point kinetics approximation with two groups of circulating delayed neutron precursors.

In 2016, Eades et al. published a paper analyzing the influence of Xe-135m on steady state xenon poisoning in thermal MSRs [18]. During the first era of MSR development, there were no data available for Xe-135m absorption cross sections; thus its influence on neutronic behavior was ignored in the historical ORNL models. Indeed, it has since been found that Xe-135m has a 10.1 Mb absorption cross section, approximately 5 times larger than the Xe-135 absorption cross section of 2.6 Mb. The analysis synthesized a zero-dimension (point) reactor model and one dimension reactor model with an in-core and out-of-core section. It was found that the influence of Xe-135m increased the steady state xenon worth in both models.

A 2017 paper by Chen et al. was published related to the xenon analysis in a thorium-based MSR [19]. As reported in the abstract (note, the abstract is in English whereas the body of the paper is in Chinese. An English translation of the paper itself was not found), the aim of the study was to implement the MSRE Xe-135 poison model and apply it to the Thorium Molten Salt Reactor Test Reactor (TMSR).

Wu et al. investigated the flow effect on I-135 and Xe-135 behavior in an MSR in 2017 [20]. Their approach discretized the in-core and out-of-core regions of an MSR into a series of nodes that iodine and xenon evolution equations were solved on. To simulate flow, the equations are solved recursively such that the output of each node is fed into the input of its successive node. Cross sectional data was prepared using the DRAGON code and the results were checked against SCALE [21,22].

6.   Development of theory

The early work on MSR xenon poisoning was primarily concerned with the effects of xenon absorption in graphite. Indeed, the xenon analysis in the 1961 xenon poisoning memo made no mention of circulating voids [11]. When ORNL-4069 was written, it was not known if the MSRE would have circulating voids or not, and their existence was only confirmed during pressure release tests [3]. It was found in the modeling of ORNL-4069 that the circulating void fraction would indeed have a significant impact on the xenon behavior within the MSRE. Furthermore, it was found in ORNL-4069 that the mass transfer process of xenon into the MSRE graphite was not rate limited by the graphite mass diffusion coefficient, but rather was rate limited by the mass transfer coefficient from the bulk fuel salt to the graphite boundary layer. Furthermore, concerns about graphite adsorption onto moderating graphite were dismissed by the work of Cannon et al. as well as Salzano [23,24]. Indeed, the shift away from graphite concerns was further bolstered by the work in ORNL-TM-3464 where it was postulated that another mass transfer mechanism, direct transfer from the circulating bubbles to the graphite was in effect, and it was this postulated mass transfer mechanism that allowed the developed xenon model to fit the experimental transient behavior [15].

Bubble models used in MSR xenon models also underwent development. The bubble model in ORNL-4069 used a single mean reference bubble diameter and a mass transfer coefficient. Bubbles were of fixed size and population. Two separate bubble models were employed in ORNL-TM-3464, one for soluble and another for insoluble cover gas. The ORNL-TM-3464 bubble model had separate regions for the pump bowl, reactor core, piping, and heat exchange. Each of these regions had separate sub regions for liquid and gas phase where mass balance equations were solved. The gas ingestion rate was accounted for, and bubble size was allowed to vary from an initial reference size throughout the loop of the reactor. In total, there was an increase in complexity and aspects considered from the ORNL-4069 to the ORNL-TM-3464 bubble model; however, there has been no work on bubble models since then.

7.   Experimental work related to MSR xenon models

Several pre-operational experiments were performed to determine the parameters related to the MSRE xenon models. The stripping efficiency of the pump bowl spray ring was measured at the University of Tennessee as part of a master's thesis using a CO_2-water system as well as an O_2-water system. MSRE fuel pump testing was done using both a water loop and a molten salt loop. This water loop had a Plexiglass window in which bubbles could be observed [25,26]. A full scale water mockup of the water vessel was used to study the core flow patterns and aid in the evaluation of mass transfer constants [27].

ORNL-4069 summarizes the "Krypton Experiment" and its subsequent analysis [3]. Essentially, to characterize xenon behavior in the MSRE, a number of characteristic rate constants, such as the graphite to fuel-salt mass transfer coefficient, needed to be known. These rate constants could
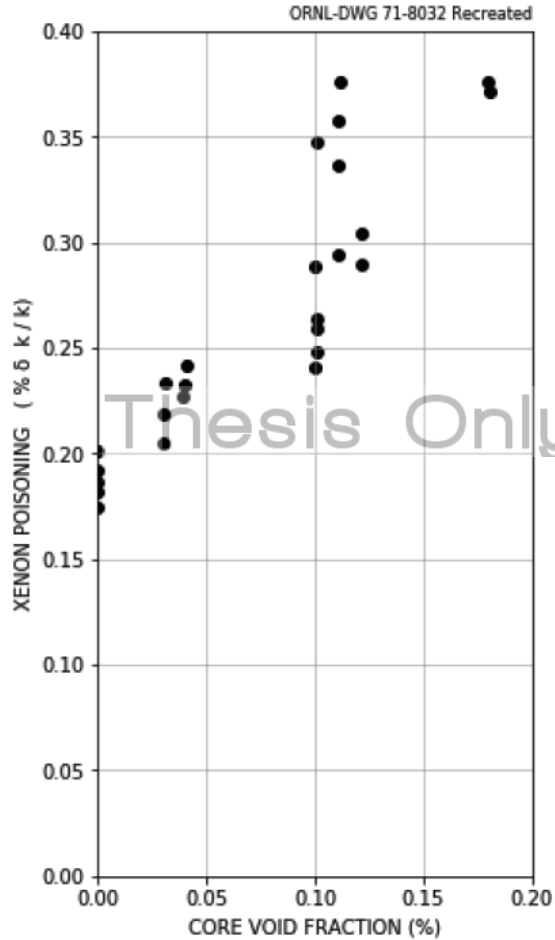
*Figure 2: A recreation of Figure 5 from [15] recreated.
MSRE xenon poisoning vs. core void fraction*

either be determined one by one in laboratory bench experiments, or all at once by an in-situ experiment. For the sake of expediency, it was decided to conduct the in-situ experiment.

In the krypton experiment, the reactor was filled with radioactive krypton, and the krypton was allowed to saturate all the compartments of the reactor primary circuit. Once the krypton level had equilibrated, the krypton supply was cut off and the MSRE off-gas line was monitored for krypton concentration. The observed concentrations were logged as a function of time. This data log created a flux-time curve which could be decomposed into a series of exponential decay processes. Five exponential curves, one for each expected xenon mass transfer process, were recursively subtracted from the flux-time curve, and their characteristic decay constant extracted. These five decay constants were then correlated to each of the five supposed xenon mass transfer processes and the system thereby characterized.

In addition to the exponential peeling analysis, described in the previous paragraph, it was also attempted to fit a system of differential equations to the experimental data, and determine the rate constants therein. This fitting process was not successful, and the results not reported. Another unsuccessful analysis

with the krypton experiment was the determination of graphite void fraction by integrating the area under the flux-time curve. The void fraction determination, depending on the set of assumptions made, either severely under or overestimated the graphite void fraction of the MSRE moderator.

8.   Difficulty with circulating void fractions

In the establishment of an MSR xenon model, one of the most significant influences on xenon behavior is the circulating void fraction. ORNL-TM-3464 reports that for identical void fractions, different xenon poison fractions were measured (C.F. Figure 2)

This spread in measured xenon poisoning was attributed to either the uncertainty in the void fraction measurements or the difference in operation parameters (temperature, pressure, etc.). Furthermore, in the MSRE, it was found that the system void fraction was a function of the pump speed. The operational history and cover gas composition was also found to have an influence on the void fraction. The MSRE operational timeline was subdivided into two periods, one period with a U-233 based fuel salt and another with a U-235 based fuel salt [15]. The circulating void fraction was different depending on which fuel was used – detailed in ORNL-TM-3464 (see p. 12 in [15]).

The circulating void fraction was also found to depend on the cover gas composition in the reactor. There is the possibility that fuel salt isotopic evolution may also influence the circulating void fraction. Attempts were made to account for calculating the circulating void fraction by considering the gas ingestion by the cover gas. All these factors create a situation in which the circulating void fraction is difficult to predict.

In addition to the circulating void fraction is the ratio of interfacial area to volume void fraction, and it is this interfacial area that, with the mass transfer coefficient, determines the rate of mass transfer of xenon from the fuel salt to the circulating voids. Even if the circulating void fraction can be resolved completely, there is also the matter of determining the amount of interfacial area available for mass transfer. In the ORNL MSR xenon models, it was assumed that the bubble was spherical in shape. This is not necessarily true, as the dynamics of bubble behavior would suggest [28, 29]. Nevertheless, the mass transfer of xenon to the circulating voids is directly proportional to the interfacial area, that is given by the bubble shape.

9.   Conclusion

This brief literature review spans about six decades of research into Xe behavior in MSRs, and is considered by the authors to be fairly comprehensive. Our review of MSR xenon analysis literature indicates there has been a considerable evolution in the phenomenology included in in MSR xenon modeling. Furthermore, we have seen no evidence of successful predictive modeling

of xenon behavior for MSRs. All previous operational experience with MSRs has been limited to low power, experimental reactors. [5]

Based on the information found during this literature review, it appears that a more complete description of xenon behavior in a MSR is required, and more accurate models need to be developed. This includes a development of gas bubble-graphite interaction sub-models, only mentioned in ORNL-TM-3464, which would improve the interpretation of the transient Xe behavior. Theories of bubble-graphite interaction are non-existent outside of a scant few sentences in ORNL-TM-3464, even though the transient xenon behavior in the MSRE was not able to be modeled without them.

Nomenclature

Symbols

C	Concentration	m^{-3}
D	Diffusion Coefficient	$m^2 \cdot s^{-1}$
H	Henry's Constant	$m^{-3} \cdot Pa^{-1}$
K	Neutron Multiplication Factor	
N	Quantity	-
R	Ideal Gas Constant	$J \cdot K^{-1} \cdot mol^{-1}$
T	Temperature	T
Σ	Macroscopic Cross Section	m^{-1}
A	Area	m^2
k	Coefficient / Transfer Constant	$m \cdot s^{-1}$
r	Radial coordinate	m
γ	Fission Yield	-
δ	Change in	-
η	Stripping Efficiency	-
λ	Decay Constant	s^{-1}

---

[5] The Aircraft Reactor Experiment (ARE), operated at ORNL in 1954 and the MSRE, operated at ORNL in the 1960s. No information was found on the Pratt and Whitney Aircraft Reactor (PWAR-1) xenon behavior.

ρ	density	$kg \cdot m^{-3}$ or m^{-3}
ϵ	Porosity	-
ϕ	Neutron Flux	$m^{-2}s^{-1}$

Super and Sub Scripts

B	Bubble
I	Iodine 135
L	Liquid phase of fuel salt
Plenum	Upper plenum / head
Te	Tellurium 135
Xe	Xenon 135
a	Absorption
e	effective
f	Fission
g	Graphite

Acronyms

MSR   Molten Salt Reactor

MSRE   Molten Salt Reactor Experiment

ORNL   Oak Ridge National Laboratory

PWR   Pressurized Water Reactor

TMSR   Thorium Molten Salt Reactor Test Reactor

References

[1] U.S. Department of Energy and Generation IV International Forum, *GIF-002-00: U.S. Department of Energy and Generation IV International Forum*. Generation IV International Forum, 2002. 97 pages. Available online at https://www.gen-4.org/gif/ (last accessed August 26, 2019).

[2] J. Lamarsh and A. Baratta, Introduction to Nuclear Engineering, Third. Upper Saddle River, NJ, USA: Prentice Hall, 2001. 783 pages.

[3]   R. Kedl and A. Houtzeel, "ORNL-4069: Development of a Model for Computing Xe-135 Migration in the MSRE," Oak Ridge Natl. Lab , Oak Ridge, TN, USA, 1967. 77 Pages.

[4]   R. Robertson, "ORNL-TM-4541: Conceptual Design Study of a Single-Fluid Molten-Salt Breeder Reactor," Oak Ridge Natl. Lab , Oak Ridge, TN, USA, 1971. 189 Pages.

[5]   Y. Shimazu, "Transient Xenon Analysis in a Molten Salt Breeder Reactor," *J. Nucl. Sci. Technol.*, vol. 14, no. 11, pp. 805–810, 1977.

[6]   H. MacPherson, "The Molten Salt Reactor Adventure," *Nucl. Sci. Eng.*, vol. 90, no. 4, pp. 374–380, 1985.

[7]   R. Robertson, "ORNL-TM-0728: MSRE Design and Operations Report," Oak Ridge Natl. Lab, Oak Ridge, TN, USA, 1965. 536 pages.

[8]   I. Spiewak, "MSR-60-28: Xenon Transport in MSRE Graphite." Oak Ridge National Laboratory, Oak Ridge, TN, USA, 02-Nov-1960. Unpublished.

[9]   G. Watson and R. Evans III, "Xenon Diffusion in Graphite: Effects of Xenon Absorption in Molten Salt Reactors Containing Graphite." Oak Ridge National Laboratory, 15-Feb-1961. Oak Ridge Natl. Lab, Oak Ridge, TN, USA Unpublished.

[10] H. S. Weber, *Xenon Migration in MSRE Graphite*. Oak Ridge National Laboratory. Oak Ridge, TN, USA . Unpublished.

[11] J. Miller, "Xenon Poisoning in Molten Salt Reactors," Oak Ridge National Laboratory, Oak Ridge, TN, USA 1961. 18 Pages.

[12] R. B. Briggs, "ORNL-3078: Molten Salt Reactor Program Semiannual Progress Report for Period Ending July 31, 1964." Oak Ridge National Laboratory, Oak Ridge, TN, USA. Nov-1964. 395 pages.

[13] F. Peebles, "ORNL-TM-2245: Removal of Xenon-135 from Circulating Fuel Salt of the MSBR by Mass Transfer to Helium Bubbles," Oak Ridge Natl. Lab, Oak Ridge, TN, USA., 1968. 33 Pages.

[14] D. Scott and W. Eatherly, "Graphite and Xenon behavior and their influence on molten-salt reactor design," *Nucl. Appl. Technol.*, vol. 8, no. 2, pp. 179–189, 1970.

[15] J. Engel and R. Steffy, *ORNL-TM-3464: Xenon Behavior in the Molten Salt Reactor Experiment*. Oak Ridge National Laboratory, Oak Ridge, TN, USA., 1971. 112 pages.

[16] M. Rosenthal, P. Briggs, and P. Kasten, "ORNL-4119: Molten-Salt Reactor Program Semiannual Progress Report for Period Ending February 28, 1967," Oak Ridge National Laboratory, Oak Ridge, TN, USA., 1967. 219 pages.

[17] S. Katsumi and S. Yoichiro, "Transient Xenon Effect on Plant Control in MSRs-Validation of Simulation Model," American Nuclear Society, 555 North Kensington Avenue, La Grange Park, IL 60526 (United States), 2004.

[18] M. J. Eades, E. S. Chaleff, P. F. Venneri, and T. E. Blue, "The influence of Xe-135m on steady-state xenon worth in thermal molten salt reactors," *Prog. Nucl. Energy*, vol. 93, pp. 397–405, 2016.

[19] G. Chen, J. Ruimin, C. Jingen, and L. Guimin, "Xenon Analysis of Thorium Molten Salt Experiment Reactor-Liquid Fuel," Nucl. Tech., vol. 40, no. 4, 2017.

[20] J. Wu, C. Guo, X. Cai, C. Yu, C. Zou, J. Han, Chen, "Flow effect on 135I and 135Xe evolution behavior in a molten salt reactor," *Nucl. Eng. Des.*, vol. 314, pp. 318–325, 2017.

[21] G. Marleau, A. Hébert, and R. Roy, "A user guide for DRAGON 3.06," *Rep. IGE-174 Rev*, vol. 7, 2008. 166 pages.

[22] S. M. Bowman, "SCALE 6: comprehensive nuclear safety analysis code system," *Nucl. Technol.*, vol. 174, no. 2, pp. 126–148, 2011.

[23] M. C. Cannon, W. R. Grimes, W. T. Ward, and G. M. Watson, "Adsorption of Xenon and Argon on Graphite," *Nucl. Sci. Eng.*, vol. 12, no. 1, pp. 4–9, 1962.

[24] F. J. Salzano, *Absorption and diffusion of xenon in high density graphite at high temperatures*. Brookhaven National Laboratory, Brookhaven, NY. 1960. 13 Pages.

[25] P. Smith, "ORNL-TM-2987: Development of Fuel and Coolant Salt Centrifugal Pumps for the Molten Salt Reactor Experiment," Oak Ridge National Laboratory, 1970. 50 Pages.

[26] P. Smith, "ORNL-TM-79: Water Test Development of the Fuel Pump for the MSRE," Oak Ridge National Laboratory, Oak Ridge, TN, USA, 1962. 47 Pages.

[27] P. Briggs, "ORNL-3419: Molten Salt Reactor Program Semiannual Progress Report for Period Ending January 31, 1963," Oak Ridge National Laboratory, Oak Ridge, TN, USA 1963. 148 pages

[28] C. E. Brennen, *Cavitation and Bubble Dynamics*. Cambridge University Press, New York, NY, USA, 2013. 249 Pages

[29] R. Clift, J. R. Grace, and M. E. Weber, *Bubbles, Drops, and Particles*. Dover Publications, Mineola, NY, USA, 2013. 400 Pages

Attachment 11

Total Bibliography

Bibliography

Below is a list of resources consulted in the development of this thesis.

COMSOL. URL `https://www.comsol.com/`. LAst Accessed: 9/10/2018.

DYMOLA Systems Engineering. URL `https://www.3ds.com/products-services/catia/product` Last Accessed 9/10/2018.

Energy From Thorium. URL `https://energyfromthorium.com/pdf/`. Last Accessed 5/9/2019.

FEniCS. URL `https://fenicsproject.org/`. Last Accessed: 9/10/2018.

FiPy. URL `https://www.ctcms.nist.gov/fipy/`. Last accessed 09/10/2018.

IBM 7090 Data Processing System. URL `https://www-03.ibm.com/ibm/history/exhibits/mainframe/mainframe_PP7090.html`. IBM, Last Accessed 9/10/2018.

Matlab PDE Toolbox. URL `https://www.mathworks.com/products/pde.html`. Last accessed 9/10/2018.

Research Reactor Database. URL `nucleus.iaea.org/RRDB/`. Last Accessed: 27/3/2019.

OpenFOAM. URL `https://openfoam.org/`. Last Accessed: 9/10/2018.

Serpent: a Continious-Energy Monte Carlo Reactor Physics Burnup Calculation Code. VTT, Last Accessed: 9/10/2018.

Mathworks Simulink. URL `https://www.mathworks.com/products/simulink.html`.

Transatomic Github. URL `https://github.com/transatomic/reactor`. Last Accessed 11/2/2018.

Oak Ridge National Laboratory Project: VERA_CS High Fidelity LWR Core Simulator for CSL. URL `https://www.ornl.gov/division/rnsd/projects/vera-cs`. Last Accessed 9/11/2018.

HP-2115A and HP-2116A Brochure. Technical report, Hewlett Packard, 1967. URL `http://www.decadecounter.com/vta/pdf/hp2116a-2115a.pdf`. Last Accessed 11/7/2018.

Science and Reactor Fundamentals - Reactor Physics. Technical report, Candian Nuclear Safety Comission: Technical Training Group, 2003.

NUKEFACTS #1: Beta is Not The Delayed Neutron (Population) Fraction, 2012. URL `http://archive.is/st3e`. Last Accessed: 9/42019.

Gavin Ridley MSRE Repository, jun 2018. URL `https://github.com/arfc/msr-neutronics`.

Japan Atomic Energy Agency - Nuclear Data Center - Fission Product Yields, 2018. URL `https://wwwndc.jaea.go.jp/cgi-bin/FPYfig`.

Modelica, 2018. URL `https://www.modelica.org/`. Last Accessed: 9/10/2018.

Scilab - XCos, 2018. URL `http://scilab.io/products/xcos/`. Last Accessed 9/10/2018.

The Essential CANDU. Technical report, University Network of Nuclear Engineering Excellence, 2018.

Wolfram System Modeler, 2018. URL `http://wolfram.com/system-modeler/`. Last Accessed: 9/10/2018.

J. Ahrens, B. Geveci, and C. Law. Paraview: An end-user tool for large data visualization. 717, 2005.

E. Albenesius. Tritium as a Product of Fission. *Physical Review Letters*, 3(6): 274, 1959.

L. Albright. *Albright's Chemical Engineering Handbook*. Taylor & Francis, 2008.

L. Alexander, W. Carter, C. Craven, D. Janney, T. Kerlin, and R. Van Winkle. ORNL-TM-1060: Molten Salt Converter Reactor. Design Study and Power Cost Estimates for a 1000 MWe Station. Technical report, Oak Ridge National Laboratory, 1965.

W. Ambrosini, N. Forgione, A Manfredini, and F. Oriolo. On Various Forms of the Heat and Mass Transfer Analogy: Discussion and Application to Condensation Experiments. *Nuclear Engineering and Design*, 236(9):1013–1027, 2006.

Ansys. Ansys Fluent. jan 2018. URL `http://www.ansys.com/Products/Fluids/ANSYS-Fluent`.

K. Asano. *Mass Transfer: From Fundamentals to Modern Industrial Applications*. Wiley, 2007.

I. Asimov. *A Short History of Chemistry*. Greenwood Press, 1979.

4

P. Atkins, J. De Paula, and J. Keeler. *Atkins' Physical Chemistry*. Oxford University Press, 2018.

R. Avery, R. Blum, R. Briggs, J. Chernick, W. Cooper, J. Draley, J. Evans, E. Hayes, T. LeClair, MacPherson, J. McKamey, F. Miles, C. Newman, R. Ritzman, and V. Walker. Report of the Fluid Fuel Reactors Task Force. Technical report, Atomic Energy Comission, 1959.

D. Bailer-Jones. *Scientific Models in Philosophy of Science*. University of Pittsburgh Press, 2009.

S. Ball. ORNL-TM-1445: Simulators for Training Molten-Salt Reactor Experiment Operators. Technical report, Oak Ridge National Laboratory, 1966.

S. Ball and R. Adams. ORNL-TM-1933: "MATEXP" A General Purpose Digital Computer Program for Solving Ordinary Differential Equatioons by the Matrix Expoenential Method. Technical report, 1967.

S. Ball and T. Kerlin. ORNL-TM-1070: Stability Analysis of the Molten-Salt Reactor Experiment. Technical report, Oak Ridge National Laboratory, 1965.

G K Batchelor. The stability of a large gas bubble rising through liquid. *Journal of Fluid Mechanics*, 184:399–422, 1987. ISSN 1469-7645.

5

E. Baum, H. Knox, and T. Miller. *Nuclides and Isotopes: Chart of the Nuclides*. Lockheed Martin, 16 edition, 2010.

S. Beall, P. Haubenreich, R. Lindauer, and J. Tallackson. ORNL-TM-732: MSRE Design and Operations Report, Part V. Technical report, Oakridge National Laboratory, United States, 1964.

J Bear and Y. Bachmat. *Introduction to Modeling of Transport Phenomena in Porous Media*. Springer Netherlands, Dordrecht, jun 1990.

J. Bear and Y. Bachmat. *Introduction to Modeling of Transport Phenomena in Porous Media*. Springer Netherlands, 2012.

G. Bell and S. Glasstone. *Nuclear reactor theory*. Van Nostrand Reinhold Co., 1970.

J. Bess and J. Gullifor. International Reactor Physics Experiment Evaluation (IRPhE) Project. IRPhE Handbook-2015 edition. Technical report, 2015.

E. Bettis, R. Schroeder, G. Cristy, H. Savage, R. Affel, and L. Hemphill. The Aircraft Reactor Experiment—Design and Construction. *Nuclear Science and Engineering*, 2(6):804–825, 1957.

E. Bettis, L. Alexander, and H. Watts. ORNL-TM-3832: Design Studies of a

Molten-Salt Reactor Demonstration Plant. Technical report, 1972.

B. Betzler, J. Powers, A. Worrall, S. Robertson, L. Dewan, and M. Massie. ORNL-TM-2016-742: Two-Dimensional Neutronic and Fuel Cycle Analysis of the Transatomic Power Molten Salt Reactor. Technical report, Oak Ridge National Laboratory, 2017.

D. Bhaga and M. Weber. Bubbles in viscous liquids: shapes, wakes and velocities. *Journal of fluid Mechanics*, 105:61–85, 1981.

B. Binks. Particles as surfactants—similarities and differences. *Current Opinion in Colloid & Interface Science*, 7(1):21–41, 2002.

R. Bird, W. Stewart, and E. Lightfoot. *Transport Phenomena*. John Wiley & Sons Inc., 2002.

M. Blander, W. Grimes, N. Smith, and G. Watson. Solubility of Noble Gases in Molten Fluorides. II. In the Lif-NaF-LF Eutectic Mixtures. *The Journal of Physical Chemistry*, 63(7):1164–1167, 1959.

J. Bockris and A. Reddy. *Modern Electrochemistry, Volume 1, Ionics*. Kluwer Academic Publishers, 1998.

M. Born. *Atomic Physics: 8th Edition*. Dover Publications, 2013.

D Brennan and M J Graham. The Adsorption of Krypton and Xenon on Evaporated Metal Films. *Philosophical Transactions of the Royal Society of London. Series A, Mathematical and Physical Sciences*, 258(1089):325–345, 1965.

S. Bretsznajder and P. Danckwerts. *Prediction of Transport and Other Physical Properties of Fluids.* Pergamon Press, 2013.

R.C. Briant. Ornl-1170: Aircraft nuclear propulsion project quarterly progress report for period ending december 10, 1951. Report, Oak Ridge National Laboratory, Oak Ridge, TN, USA, 1952. 172 enumerated pages.

R.C. Briant. Ornl-1556: Aircraft nuclear propulsion project quarterly progress report for period ending june 10, 1953. Report, Oak Ridge National Laboratory, Oak Ridge, TN, USA, 1953. xi + 129 enumerated pages.

R.C. Briant and C.B. Ellis. Ornl-1154: Aircraft nuclear prpulsion project quarterly progress report for period ending september 10, 1951. Report, Oak Ridge National Laboratory, Oak Ridge, TN, USA, 1951. 207 enumerated pages.

R.C. Briant and A.J. Miler. Ornl-1227: Aircraft nuclear propulsion project quarterly progress report for period ending march 10, 1952. Report, Oak Ridge National Laboratory, Oak Ridge, TN, USA, 1952. xxi + 192 enumer-

ated pages.

R.C. Briant, J.H. Buck, and A.J. Miler. Ornl-1294: Aircraft nuclear propulsion project quarterly progress report for period ending june 10, 1952. Report, Oak Ridge National Laboratory, Oak Ridge, TN, USA, 1952a. xv + 185 enumerated pages.

R.C. Briant, J.H. Buck, and A.J. Miler. Ornl-1375: Aircraft nuclear propulsion project quarterly progress report for period ending september 10, 1952. Report, Oak Ridge National Laboratory, Oak Ridge, TN, USA, 1952b. xii + 168 enumerated pages.

R.C. Briant, J.H. Buck, and A.J. Miler. Ornl-1515: Aircraft nuclear propulsion project quarterly progress report for period ending march 10, 1953. Report, Oak Ridge National Laboratory, Oak Ridge, TN, USA, 1953a. xi + 185 enumerated pages.

R.C. Briant, J.H. Buck, and A.J. Miler. Ornl-1439: Aircraft nuclear propulsion project quarterly progress report for period ending december 10, 1952. Report, Oak Ridge National Laboratory, Oak Ridge, TN, USA, 1953b. xiii + 210 enumerated pages.

R.C. Briant, A.J. Miler, and W.B. Cottrell. Ornl-1609: Aircraft nuclear propulsion project quarterly progress report for period ending september

10, 1953. Report, Oak Ridge National Laboratory, Oak Ridge, TN, USA, 1953c. xi + 159 enumerated pages.

R.C. Briant, W.H. Jordan, A.J. Miller, and A.W. Savolainen. Ornl-1692: Aircraft nuclear propulsion project quarterly progress report for period ending march 10, 1954. Report, Oak Ridge National Laboratory, Oak Ridge, TN, USA, 1954a. xii + 142 enumerated pages.

R.C. Briant, A.J. Miller, and W.B. Cottrell. Ornl-1649: Aircraft nuclear propulsion project quarterly progress report for period ending december 10, 1953. Report, Oak Ridge National Laboratory, Oak Ridge, TN, USA, 1954b. xii + 137 enumerated pages.

P. Briggs. ORNL-3419: Molten Salt Reactor Program Semiannual Progress Report for Period Ending January 31, 1963. Technical report, Oak Ridge National Laboratory, 1963a.

R. Briggs. ORNL-3529: Molten Salt Reactor Program Semi-Annual Progress Report For Period Ending July 31, 1963. Technical report, Oak Ridge National Laboratory, Oak Ridge, TN, USA, 1963b.

R. Briggs. ORNL-3708: Molten-Salt Reactor Program Semiannual Progress Report For Period Ending July 31, 1964. Technical report, Oak Ridge National Laboratory, Oak Ridge, TN, USA, 1964.

R. Briggs. ORNL-3872: Molten-Salt Reactor Program Semiannual Progress Report for Period Ending August 31, 1965, 1965.

R. Briggs. ORNL-3913: Molten-Salt Reactor Program Semiannual Progress Report For Period Ending February 28,1966. Technical report, 1966.

R. Briggs. ORNL-4037: Molten-Salt Reactor Program Semiannual Progress Report for Period Ending August 31, 1966. Technical report, Oak Ridge National Laboratory, Oak Ridge, TN, USA, 1967a.

R. Briggs. ORNL-4037: Molten-Salt Reactor Program Semiannual Progress Report for Period Ending August 31, 1966. Technical report, Oak Ridge National Laboratory, 1967b.

R. Briggs and C. Nestor. ORNL-TM-4804: A Method for Calculating the Steady-State Distribution of Tritium in a Molten-Salt Breeder Reactor. Technical report, Oak Ridge National Laboratory, Oak Ridge, TN, USA, 1975.

R. Briggs, C. Winters, S. Beall, R. Lyon, R. Lyon, E. Bohlmann, D. Fergunson, E. Taylor, and M. Kelly. ORNL-2561: Homogeneous Reactor Project Quarterly Progress Report For Period Ending April 30 and July 31, 1958. Technical report, Oak Ridge National Laboratory, 1959.

R S Brodkey and H C Hershey. *Transport Phenomena: A Unified Approach.*
Brodkey Pub., 2003. ISBN 978-0-9726635-8-8.

D. Brown, M. Chadwick, R. Capote, A. Kahler, A. Trkov, M. Herman, A. Son-
zogni, Y. Danon, A. Carlson, M Dunn, D. Smith, G. Hale, G. Arbanas,
R. Arcilla, C. Bates, B. Beck, B. Becker, F. Brown, R. Casperson, J. Con-
lin, D. Cullen, M. Descalle, R. Firestone, T. Gaines, K. Guber, A. Hawari,
J. Holmes, T . Johnson, T. Kawano, B. Kiedrowski, A. Koning, S. Kopecky,
L. Leal, J P Lestone, C. Lubitz, J. Márquez Damián, C. Mattoon, E. Mc-
Cutchan, S. Mughabghab, P. Navratil, D. Neudecker, G. Nobre, G. Noguere,
M. Paris, M. Pigni, A. Plompen, B. Pritychenko, V. Pronyaev, D. Roubtsov,
D. Rochman, P. Romano, P. Schillebeeckx, S. Simakov, M. Sin, I. Sirakov,
B. Sleaford, V. Sobes, E. Soukhovitskii, I. Stetcu, P. Talou, I. Thompson,
S. van der Marck, L. Welser-Sherrill, D. Wiarda, M. White, J. Wormald,
R. Wright, M. Zerkle, G. Žerovnik, and Y. Zhu. ENDF/B-VIII.0: The 8th
Major Release of the Nuclear Reaction Data Library with CIELO-project
Cross Sections, New Standards and Thermal Scattering Data. *Nuclear Data
Sheets*, 148:1–142, 2018.

J. Bulmer, E. Gift, R. Holl, A. Jacobs, S. Jaye, E. Koffman, R. McVean,
R. Oehl, and R. Rossi. CF-56-8-204: Fused Salt Fast Breeder Reactor
Design and Feasibility Study. Technical report, Oak Ridge School of Reactor
Technology, 1956.

W. Burch. ORNL-TM-228: Measurement of Xenon Poisoning in the HRT. Technical report, Oak Ridge National Laboratory, 1962.

W. Burch, M. Watson, and H. Weeren. ORNL-CF-60-2-2-: Xenon Control in Fluid Fuel Reactors. Technical report, Oak Ridge National Laboratory, 1960.

H. Butt, K. Graf, and M. Kappl. *Physics and Chemistry of Interfaces*. Wiley, 2006. ISBN 9783527606405.

M. Cannon, W. Grimes, W. Ward, and G. Watson. Adsorption of Xenon and Argon on Graphite. *Nuclear Science and Engineering*, 12(1):4–9, 1962.

S. Cantor, W. Cooke, S. Dworkin, D. Robbins, E. Thoma, and M. Watson. ORNL-TM-2316: Physical Properties of Molten-Salt Reactor Fuel, Coolant and Flush Salts. Technical report, Oak Ridge National Laboratory, 1968.

E Capelli, O Beneš, and R J M Konings. Thermodynamics of soluble fission products cesium and iodine in the Molten Salt Reactor. *Journal of Nuclear Materials*, 501:238–252, 2018. URL http://www.sciencedirect.com/science/article/pii/S0022311517317373.

J. Carroll. Henry's law: a historical view. *Journal of Chemical Education*, 70 (2):91, 1993. ISSN 0021-9584.

G. Chen, J. Ruimin, C. Jingen, and L. Guimin. Xenon Analysis of Thorium
Molten Salt Experiment Reactor-Liquid Fuel. *Nuclear Techniques*, 40(4):
40602, 2017.

Sungkoo Cho, Sang Hyoun Choi, Chul-Young Yi, and Chan Hyeong Kim.
Atom-mird hybrid voxel model for monte carlo calculations of organ doses:
A complement to a physical phantom. *Journal of Nuclear Science and Tech-
nology*, 45(sup5):306–308, 2008.

S. Chu, L. Ekström, and R. Firestone. The LUND/LBNL nuclear
data search, version 2.0, Entry for Xe-135m, jun 1999. URL
`http://nucleardata.nuclear.lu.se/toi/nuclide.asp?iZA=540435`.

S. Churchill. Friction-factor Equation Spans all Fluid-Flow Regimes. *Chemical
engineering*, 84(24):91–92, 1977.

R. Clift, J. Grace, and M. Weber. *Bubbles, Drops, and Particles*. Dover
Publications, 2013.

FLUKA Collaboration et al. Fluka manual. 2011.

E. Compere, S. Kirslis, E. Bohlmann, F. Blankenship, and W. Grimes. ORNL-
4865: Fission Product Behavior in the Molten Salt Reactor Experiment.
Technical report, Oak Ridge National Laboratory, 1975.

W. Cottrell, H. Hungerford, J. Leslie, and J. Meerv. ORNL-1845: Operation of the Aircraft Reactor Experiment. Technical report, Oak Ridge National Laboratory, 1955.

F. Coutelieris and J. Delgado. *Transport Processes in Porous Media*. Springe, 2012. ISBN 978-3-642-27909-6.

J Crank. *The Mathematics of Diffusion*. Clarendon Press, 1979. ISBN 978-0-19-853411-2.

E. L. Cussler. *Diffusion: Mass Transfer in Fluid Systems*. Cambridge University Press, third edition, 2007.

H. de Regt, S. Leonelli, and K. Eigner. *Scientific Understanding: Philosophical Perspectives*. University of Pittsburgh Press, 2009.

P. Delhaes. *Graphite and Precursors*. CRC Press, 2014.

S. Delpech, C. Cabet, C. Slim, and G. Picard. Molten Fluorides for Nuclear Applications. *Materials Today*, 13(12):34–41, 2010.

H DeVoe. *Thermodynamics and Chemistry*. Prentice Hall, 2001.

L. Dewan and M. Massie. Molten Salt Reactor, 2014.

15

L. Dewan, M. Massie, R. Wilcox, and M. Short. Nuclear reactors and related methods and apparatus, 2013.

PJ Dimbylow. Fdtd calculations of the whole-body averaged sar in an anatomically realistic voxel model of the human body from 1 mhz to 1 ghz. *Physics in Medicine & Biology*, 42(3):479, 1997.

T. Dobre and J. Marcano. *Chemical Engineering: Modeling, Simulation and Similitude*. Wiley, 2007.

T. Dolan. *Molten Salt Reactors and Thorium Energy*. Woodhead Publishing, 2017.

J. Duderstadt and L. Hamilton. *Nuclear Reactor Analysis*. Wiley, 1976.

M. Eades, E. Chaleff, P. Venneri, and T. Blue. The Influence of Xe-135m on Steady-State Xenon Worth in Thermal Molten Salt Reactors. *Progress in Nuclear Energy*, 93:397–405, 2016.

W. Egen. CF-57-2-130: The Physics of the Fused-Salt Reactor Experiment. Technical report, Oak Ridge National Laboratory, 1957.

B. Elsheikh. Safety Assessment of Molten Salt Reactors in Comparison with Light Water Reactors. *Journal of Radiation Research and Applied Sciences*,

6(2):63–70, 2013.

J. Engel. ORNL-CF-62-11-69: Preliminary Equations to Describe Iodine and Xenon Behavior in the MSRE. Technical report, Oak Ridge National Laboratory, 1962.

J. Engel and P. Haubenreich. ORNL-TM-378: Temperature in the MSRE Core During Steady-State Power Operation. Technical report, Oak Ridge National Laboratory, 1962.

J Engel and Haubenreich P. ORNL-TM-378: Temperature in the MSRE Core During Steady-State Power Operation. Technical report.

J. Engel and B. Prince. ORNL-TM-1796: The Reactivity Balance in the MSRE. Technical report, Oak Ridge National Laboratory, 1967.

J. Engel and R. Steffy. ORNL-TM-3464: Xenon Behavior in the Molten Salt Reactor Experiment. Technical report, Oak Ridge National Laboratory, 1971a.

J. Engel and R. Steffy. ORNL-TM-3464: Xenon Behavior in the Molten Salt Reactor Experiment. Technical report, Oak Ridge National Laboratory, Oak Ridge, TN, USA, 1971b.

J. Engel, P. Haubenreich, and A. Houtzeel. ORNL-TM-3027: Spray, Mist, Bubbles, and Foam in the Molten Salt Reactor Experiment. Technical report, Oak Ridge National Laboratory, Oak Ridge, TN, USA, 1970.

J. Engel, H. Baurman, J. Dearing, W. Grimes, E. McCoy, and W. Rhoades. ORNL/TM-7207: Conceptual Design Characteristics of a Denatured Molten-Salt Reactor with Oonce-Through Fueling. Technical report, Oak Ridge National Laboratory, Oak Ridge, TN, USA, 1980.

P. Engel, J., Haubenreich. ORNL-TM-0378: Temperature in the MSRE Core During Steady-State Power Operation. Technical report, Oak Ridge National Laboratory, 1962.

W. Ergen, A. Callihan, C. Mills, and D/ Scott. The Aircraft Reactor Experiment—Physics. *Nuclear Science and Engineering*, 2(6):826–840, 1957. ISSN 0029-5639.

Allen M Eshaya and Richard H Wiswall. The Chemistry Of Fission Products in a Molten Metal Nuclear Fuel. *Transactions of the New York Academy of Sciences*, 21(8 Series II):668–681, 1959. ISSN 2164-0947.

R. Evans, J. Rutherford, and M. Malinauskas. ORNL-4389: Gas Transport in the MSRE Moderator Graphite: II. Effects of Impregnation; III. Variation of Flow Properties. Technical report, Oak Ridge National Labs, 1969.

E Fermi, S Esposito, and O Pisanti. *Neutron Physics for Nuclear Reactors: Unpublished Writings.* World Scientific, 2010. ISBN 978-981-4291-22-4.

P Ferrari and G Gualdrini. An improved mcnp version of the norman voxel phantom for dosimetry studies. *Physics in Medicine & Biology*, 50(18):4299, 2005.

T. Filburn and S. Bullard. *Three Mile Island, Chernobyl and Fukushima: Curse of the Nuclear Genie.* Springer International Publishing, 2016.

Matthias Fippel. Fast monte carlo dose calculation for photon beams based on the vmc electron algorithm. *Medical physics*, 26(8):1466–1475, 1999.

R. Firestone and V. Shirley. *Table of Isotopes, 8th Edition.* Wiley, 1996.

N. Fletcher. Size Effect in Heterogeneous Nucleation. *The Journal of Chemical Physics*, 29(3):572–576, 1958.

C. Forsberg. Molten Salt Reactor Experience Applicable to LS-VHTR Refueling. In *LS-VHTR Meeting.* Oak Ridge National Laboratory, 2006.

A. Fraas and A. Savolainen. ORNL-2095: Design Report on the Aircraft Reactor Test. Technical report, Oak Ridge National Laboratory, 1956.

19

M. J. Frick, S. Gupta, and J. Bechhoefer. When geometry is irrelevant for heat diffusion: The transition from lumped-element to field formulations. *European Journal of Physics*, 39(6):065104, 2018. ISSN 0143-0807.

D. Fry, R. Kryter, and R. Robinson. ORNL-TM-2315: Measurement of Helium Void Fraction in the MSRE Fuel Salt Using Neutron-Noise Analysis. Technical report, Oak Ridge National Laboratory, Oak Ridge, TN, USA, 1968.

K. Furukawa, V. Simonenko, K. Mitachi, A. Furuhashi, R. Yoshioka, S. Chigrinov, A. Lecocq, and Y. Kato. Thorium Cycle Implementation Through Plutonium Incineration by Thorium Molten-Salt nuclear Energy Synergetics. *Thorium fuel utilization: Options and trends*, page 123, 2002.

S. Furusaki. *The Expanding World of Chemical Engineering*. Taylor & Francis, 2001. ISBN 978-1-56032-917-6.

C. Gabbard. ORNL-TM-4122: Development of a Venturi Type Bubble Generator for use in the Molten Salt Reactor Xenon Removal System. Technical report, Oak Ridge National Laboratory, 1972a.

C. Gabbard. ORNL-TM-4122: Development of a Venturi Type Bubble Generator for use in the Molten Salt Reactor Xenon Removal System. Technical report, Oak Ridge National Laboratory, Oak Ridge, TN, USA, 1972b.

M. Gaune-Escard. *Molten Salts: From Fundamentals to Applications*. Springer Netherlands, 2012.

Z. Ge, H. Wu, G. Chen, and R. Xu. CENDL project, the chinese evaluated nuclear data library. In *EPJ Web of Conferences*, volume 146, page 2002. EDP Sciences, 2017. ISBN 2100-014X.

S. Ghabezloo. Effect of porosity on the thermal expansion coefficient: A discussion of the paper 'Effects of mineral admixtures on the thermal expansion properties of hardened cement paste by Z. Shui, R. Zhang, W. Chen, D. Xuan, Constr. Build. Mater. 24 (9)(2010) 1761–1767. *Construction and Building Materials*, 24(9):1796–1798, 2010. ISSN 0950-0618.

A J Ghajar and D Yunus A. Cengel. *Heat and Mass Transfer: Fundamentals and Applications*. McGraw-Hill Education, 2014.

A J Ghajar and D Yunus A. Cengel. *Heat and Mass Transfer: Fundamentals and Applications*. McGraw-Hill Education, 2015.

L. Glicksman and J. Lienhard. *Modeling and Approximation in Heat Transfer*. Cambridge University Press, 2016.

A. Goodwin, K. Marsh, and W. Wakeham. *Measurement of the Thermodynamic Properties of Single Phases*. Experimental Thermodynamics. Elsevier

21

Science, 2003.

J. Grace, T. Wairegi, and T. Nguyen. Shapes and Velocities of Single Drops and Bubbles Moving Freely Through Immiscible Liquids. *Transactions of the Institute for Chemical Engineering*, 54:167–173, 1976.

W. Grimes, N. Smith, and G. Watson. Solubility of Noble Gases in Molten Fluorides. I. In Mixtures of NaF–ZrF4 (53-47 Mole %) and NaF–ZrF4–UF4 (50–46–4 Mole %). *The Journal of Physical Chemistry*, 62(7):862–866, 1958.

J. Groh. Supplement to Accompany Lesson 13 of Reactor Physics Fundamentals: Reactivty Control Devices in the Control Loop (Power Control). Technical report, Canteach, 1996.

Gianfranco Gualdrini and Paolo Ferrari. A review of voxel model development and radiation protection applications at enea. *Radiation protection dosimetry*, 140(4):383–390, 2010.

Jonathan E Guyer, Daniel Wheeler, and James A Warren. FiPy: Partial differential equations with Python. *Computing in Science & Engineering*, 11(3), 2009. URL `https://www.ctcms.nist.gov/fipy/`.

J. Hartwell, D. Scates, J. Walter, and M. Drigert. INL/EXT-07-12455: Determination of the Quantity of I-135 Released from the AGR-1 Test Fuels at

the End of ATR Operating Cycle 138B. Technical report, Idaho National
Laboratory, 2007.

P. Haubenreich. ORNL-TM-611: Inherent Neutron Sources in Clean MSRE
Fuel Salt. Technical report, Oak Ridge National Laboratory, 1963.

P. Haubenreich. ORNL-TM-3144: Fluorine Production and Recombination in
Frozen MSR Salts After Reactor Operation. Technical report, Oak Ridge
National Laboratory, Oak Ridge, TN, USA, 1970.

P. Haubenreich and J. Engel. Experience with the Molten-Salt Reactor Ex-
periment. *Nuclear Applications and Technology*, 8(2):118–136, 1969.

P. Haubenreich and J. Engel. Experience with the Molten-Salt Reactor Ex-
periment. *Nuclear Applications and Technology*, 8(2):118–136, 1970.

P. Haubenreich, J. Engel, B. Prince, and H. Claiborne. ORNL-TM-730: MSRE
Design and Operations Report. Part III. Nuclear Analysis. Technical report,
Oak Ridge National Laboratory, Oak Ridge, TN, USA, 1964.

W. Haynes, editor. *CRC Handbook of Chemistry and Physics, 97th Edition*.
CRC Press, 2016.

G T Hefter and R P T Tomkins. *The Experimental Determination of Solubili-*

ties. Wiley Series in Solutions Chemistry. Wiley, 2003. ISBN 9780470864272.

J. S. Hendricks, G. W. McKinney, L. S. Waters, T. L. Roberts, H. W. Egdorf, J. P. Finch, H. R. Trellue, E. J. Pitcher, D. R. Mayo, and M. T. Swinhoe. Mcnpx extensions version 2.5.0. *Los Alamos National Laboratory*, 2005.

R. Hesketh, A. Etchells, and T. Russell. Experimental Observations of Bubble Breakage in Turbulent Flow. *Industrial & Engineering Chemistry Research*, 30(5):835–841, 1991.

J. Hinze. Fundamentals of the Hydrodynamic Mechanism of Splitting in Dispersion Processes. *American Institute of Chemical Engineers Journal*, 1(3): 289–295, 1955.

Bruce Hoglund. MoltenSalt.org, 2012. URL `http://moltensalt.org/`.

A. Houtzeel and F. Dyer. ORNL-TM-3151: A Study of Fission Products in the Molten-Salt Reactor Experiment by Gamma Spectrometry. Technical report, Oak Ridge National Laboratory, 1972.

Jaakko Leppanen. *Serpent – a Continuous-energy Monte Carlo Reactor Physics Burnup Calculation Code*. 2012. URL `http://montecarlo.vtt.fi/`.

S. Jain S. Flow-induced Breakup of Drops and Bubbles. *arXiv preprint arXiv:1701.06157*, 2017.

M. James. Energy Released in Fission. *Journal of Nuclear Energy*, 23:517–536, 1969.

W. Janna. *Engineering Heat Transfer, Second Edition*. Heat Transfer. Taylor & Francis, 1999.

G. Janz. *Molten Salts Handbook*. Elsevier Science, 2013.

G. Janz, F. Dampier, G. Lakshminrayanan, P. Lorenz, and R. Tomkins. NSRDS-NBS 15 - Molten Salts: Volume 1, Electrical Conductance, Density and Viscosity Data. Technical report, U.S. Department of Commerce National Bureau of Standards, 1968.

G. Jenkins. The Thermal Expansion of Polycrystalline Graphite. *Journal of Nuclear Materials*, 13(1):33–39, 1964. ISSN 0022-3115.

T. Jevremovic. *Nuclear Principles in Engineering*. Springer, New York, NY, USA, 2009.

W.H. Jordan, S.J. Cromer, R.I. Strough, A.J. Miler, and A.W. Savolainen. Ornl-1771: Aircraft nuclear propulsion project quarterly progress report for

period ending september 10, 1954. Report, Oak Ridge National Laboratory, Oak Ridge, TN, USA, 1954a. xii + 184 enumerated pages.

W.H. Jordan, A.J. Miller, and A.W. Savolainen. Ornl-1729: Aircraft nuclear propulsion project quarterly progress report for period ending june 10, 1954. Report, Oak Ridge National Laboratory, Oak Ridge, TN, USA, 1954b. xii + 143 enumerated pages.

P. Kaaten. ORNL-TM-2136: Graphite Behavior and Its Effects on MSBR Performance. Technical report, 1969.

T Kaiho. *Iodine Chemistry and Applications*. Wiley, 2014.

P. Kasten, E. Bettis, and R. Robertson. ORNL-3996: Design Studies of 1000-MW(e) Molten-Salt Breeder Reactors. Technical report, Oak Ridge National Laboratory, 1966a.

P. Kasten, E. Bettis, and R. Robertson. ORNL-3996: Design Studies of 1000-MW(e) Molten-Salt Breeder Reactors. Technical report, Oak Ridge National Laboratory, 1966b.

J. Kathawa, C. Fry, and M. Thoennessen. Discovery of Palladium, Antimony, Tellurium, Iodine, and Xenon Isotopes. *Atomic Data and Nuclear Data Tables*, 99(1):22–52, 2013.

J. Kay and R. Nedderman. *Fluid Mechanics and Transfer Processes*. Cambridge University Press, 1985.

R. Kedl. ORNL-TM-1810: A Model for Computing the Migration of Very Short Lived Nobel Gases into MSRE Graphite. Technical report, Oak Ridge National Laboratory, 1967.

R. Kedl. ORNL-TM-3884: THe Migration of a Class of Fission Products (Noble Metals) in the Molten-Salt Reactor Experiment. Technical report, Oak Ridge National Laboratory, 1972a.

R. Kedl. ORNL-TM-3884: THe Migration of a Class of Fission Products (Noble Metals) in the Molten-Salt Reactor Experiment. Technical report, Oak Ridge National Laboratory, 1972b.

R. Kedl and A. Houtzeel. ORNL-4069: Development of a Model for Computing Xe-135 Migration in the MSRE. Technical report, Oak Ridge National Laboratory, Oak Ridge, TN, USA, 1967.

J. Keiser. ORNL-TM-6002: Status of Tellurium-Hastenlloy N Studies in Molten Fluoride Salts. Technical report, Oak Ridge National Laboratory, 1977a.

J. R. Keiser. ORNL/TM-6002: Status of Tellurium–Hastelloy N Studies in

Molten Fluoride Salts. Technical report, Oak Ridge National Laboratory, 1977b.

Y. Khavkin. *Theory and Practice of Swirl Atomizers*. Combustion: An International Series. Taylor & Francis, 2003.

H. Kohn. ORNL-TM-2373: Bubbles, Drops, and Entertainment in Molten Salts. Technical report, Oak Ridge National Laboratory, Oak Ridge, TN, USA, 1968.

A. Koning and D. Rochman. Modern Nuclear Data Evaluation with the TALYS Code System. *Nuclear data sheets*, 113(12):2841–2934, 2012. ISSN 0090-3752.

A. J. Koning, D. Rochman, S. Van der Marck, J. Kopecky, J .Ch. Sublet, S Pomp, H Sjostrand, R. Forrest, E. Bauge, H. Henriksson, and Others. TENDL-2015: TALYS-Based Evaluated Nuclear Data Library, 2015.

Joseph Kotlarz. *Xenon Transient Studies for a CANDU reactor*. PhD thesis, McMaster University, 1976.

A. Kramida, Y. Ralchenko, and J. Reader. NIST Atomic Spectra Database Ionization Energies Data for Xenon, 2018.

F. Kreith. *The CRC Handbook of Thermal Engineering*. Mechanical Engineering. Springer Berlin Heidelberg, 2000.

T. Kress. ORNL-TM-3718: Mass Transfer Between Small Bubbles and Liquids in Cocurrent Turbulent Pipeline Flow. Technical report, Oak Ridge National Laboratory, 1972a.

T. Kress. ORNL-TM-3718: Mass Transfer Between Small Bubbles and Liquids in Cocurrent Turbulent Pipeline Flow. Technical report, Oak Ridge National Laboratory, Oak Ridge, TN, USA, 1972b.

R. Krishna and J. van Baten. Mass Transfer in Bubble Columns. *Catalysis Today*, 79-80:67–75, 2003. ISSN 0920-5861.

J R Lamarsh and A J Baratta. *Introduction to Nuclear Engineering*. Pearson Education, third edition, 1983.

John Lamarsh. Introduction to Nuclear Reactor Theory, 1966.

J. Lane, H. MacPherson, and F. Maslan. *Fluid fuel reactors*. Addison-Wesley books in nuclear science and metallurgy. Addison-Wesley Pub. Co., 1958.

F. Lantelme and H. Groult. *Molten Salts Chemistry: From Lab to Applications*. Elsevier Science, 2013.

D. LeBlanc. Molten salt reactors: A new beginning for an old idea. *Nuclear Engineering and Design*, 240(6):1644–1656, 2010. ISSN 00295493. doi: 10.1016/j.nucengdes.2009.12.033.

E. Lemmon, M. Huber, and M. McLinden. NIST Reference Fluid Thermodynamic and Transport Properties—REFPROP, 2002. URL `https://www.nist.gov/srd/refprop`.

A Lemosquet, I Clairand, L De Carlan, D Franck, I Aubineau-Laniece, and J-F Bottollier-Depois. A computational tool based on voxel geometry for dose reconstruction of a radiological accident due to external exposure. *Radiation protection dosimetry*, 110(1-4):449–454, 2004.

J. Leppanen. VTT-640: Development of a New Monte Carlo Reactor Physics Code. Technical report, VTT, Helsinki, 2017.

Jaakko Leppanen. VTT-640: Development of a New Monte Carlo Reactor Physics Code. Technical report, VTT, 2007.

Jaakko Leppänen. Serpent–a continuous-energy Monte Carlo reactor physics burnup calculation code. *VTT Technical Research Centre of Finland*, 4, 2013.

Jaakko Leppänen. Serpent–a continuous-energy monte carlo reactor physics

burnup calculation code. *VTT Technical Research Centre of Finland*, 4, 2013.

E. Lew is. *Fundamentals of Nuclear Reactor Physics*. Elsevier Science - Academic Press, Burlington, MA, USA, 2008.

E.E. Lewis. *Fundamentals of Nuclear Reactor Physics*. Elsevier Science, 2008.

V. Linek, M. Kordač, and T. Moucha. Mechanism of mass transfer From Bubbles in Dispersions: Part II: Mass Transfer Coefficients in Stirred Gas–Liquid Reactor and Bubble Column. *Chemical Engineering and Processing: Process Intensification*, 44(1):121–130, 2005.

Q. Liu and K. Fukuda. Transient Heat Transfer for Forced Convection Flow of Helium Gas. *JSME International Journal Series B Fluids and Thermal Engineering*, 45(3):559–564, 2002.

F. Lorenz. Modeling Level: A Question of Semantics. In *IMACS ESIEE CESA '96 Multiconference*, pages 1198–1202, Lille, France, 1996.

J. Lorimer, H. Clever, and C. Young. Solubility Data Series Volume 45/46: Gases in Molten Salt. Technical report, International Union of Pure and Applied Chemistry, 1991.

W. Loveland, D. Morrissey, and G. Seaborg. *Modern Nuclear Chemistry*. Wiley, 2017.

L. Luzzi, V. Di Marcello, and A. Cammi. *Multi-physics approach to the modelling and analysis of molten salt reactors*. Nova Science Publishers, 2016. ISBN 9781614700005.

Xiao-Wen Lyu, Xiao-Bin Xia, Zhi-Hong Zhang, Jun Cai, and Chang-Qi Chen. Analysis of Tritium Production in a 2 MW Liquid-Fueled Molten Salt Experimental Reactor and its Environmental Impact. *Nuclear Science and Techniques*, 27(4):78, 2016. ISSN 1001-8042.

D. R. MacKenzie and R.H. Wiswall Jr. Compound Formation by γ-Irradiation of Xenon-Fluorine Mixtures. *Inorganic Chemistry*, 2(5):1064, 1963.

H. MacPherson. The Molten Salt Reactor Adventure. *Nuclear Science and Engineering*, 90(4):374–380, 1985.

A. Malinauskas, J. Rutherford, and R. Evans. ORNL-4148: Gas Transport in MSRE Moderator Graphite. Part 1: Review of Theory and Counter-Diffusion Experiments. Technical report, Oak Ridge National Laboratory, 1967.

Mark Massie and Leslie C Dewan. Nuclear reactors and related methods and

apparatus, 2013. Transatomic Power Corp, US20130083878A1.

H. McCoy and B. McNabb. ORNL-TM-4174: Postirradiation Examination of Materials From the MSRE. Technical report, Oak Ridge National Laboratory, 1972.

Wes McKinney. Pandas: a foundational python library for data analysis and statistics. *Python for High Performance and Scientific Computing*, pages 1–9, 2011.

J. Meem. ORNL-CF-54-5-1: The Xenon Problem in the ART. Technical report, Oak Ridge National Laboratory, 1954.

H Mehrer. *Diffusion in Solids: Fundamentals, Methods, Materials, Diffusion-Controlled Processes*. Springer Berlin Heidelberg, 2007. ISBN 978-3-540-71488-0.

J. Miller. ORNL-CF-61-5-62: Xenon Poisoning in Molten Salt Reactors. Technical report, Oak Ridge National Laboratory, 1961.

J. Moore, T. Godfrey, and D. McElroy. *Thermal Properties of Grade CGB Graphite*. ORNL-P-150. Oak Ridge National Laboratory, 1964.

S. Mughabghab. *Neutron Cross Sections: Neutron Resonance Parameters and*

Thermal Cross Sections, Part A: Z 1-60. Elsevier Science, 2012.

M. Muruganant, A. Chirazi, and B. Raj. Frontiers in Materials Processing, Applications, Research and Technology: Select Proceedings of FiMPART 2015. Hyderabad, 2017. Springer Singapore.

J. Nicholas and D. Winkler. ORNL-TM-1735/NASA CR-72172: A Program for Calculating Optimum Dimensions of Alphaa Radioisotope Capsules Exposed to Varying Stress and Temperature. Technical report, Oak Ridge National Laboratory, 1967.

J Nielsen, J Villadsen, and G Lidén. *Bioreaction Engineering Principles: Second Edition*. Springer US, 2012. ISBN 978-1-4615-0767-3.

Nobel Media. Nobel Prize Lectures: The Rare Gasses of the Atmosphere, 2018.

Fakir S. Nooruddin and Greg Turk. Simplification and repair of polygonal models using volumetric techniques. *IEEE Transactions on Visualization and Computer Graphics*, 9(2):191–205, 2003.

K. Notz. ORNL-TM-9756: Extended Storage-in-Place of MSRE Fuel Salt and Flush Salt. Technical report, Oak Ridge National Laboratory, 1985.

Oak Ridge National Labs. ORNL-4396: Molten-Salt Reactor Program Semi-annual Progress Report. Technical report, 1969.

S. Oberstedt, R. Billnert, A. Gatera, W. Geerts, and P. Halipr. Prompt fission γ -Ray Spectra Characteristics - a First Summary. *Physics Procedia*, 64: 83–90, 2015.

K. Ogawa. *Chemical Engineering: A New Perspective.* Elsevier Science, 2007.

T. Okawa, N. Shimada, A. Kotani, and I. Kataoka. An experimental study on the mass transfer rate of droplets in annular two-phase flow. *JSME International Journal Series B Fluids and Thermal Engineering*, 49(2):271–278, 2006.

J. Orear, E Fermi, A. Rosenfeld, and R. Schluter. *Nuclear Physics: A Course Given by Enrico Fermi at the University of Chicago.* Midway Reprints. University of Chicago Press, 1950. ISBN 9780226243658.

R. O'Sullivan, J. Tomlinson, and T. Griffiths. Feasibility Study of a Pilot Scale Molten Salt Reactor Demonstration, 2015.

Jacques Padet. Transient convective heat transfer. *Journal of the Brazilian Society of Mechanical Sciences and Engineering*, 27(1):74–95, 2005.

P. Pau, J. Berg, and W. McMillan. Application of Stokes' Law to Ions in Aqueous Solution. *Journal of Physical Chemistry*, 94(6):2671–2679, 1990.

F. Peebles. ORNL-TM-2245: Removal of Xenon-135 from Circulating Fuel Salt of the MSBR by Mass Transfer to Helium Bubbles. Technical report, Oak Ridge National Laboratory, Oak Ridge, TN, USA, 1968a.

F N Peebles. ORNL-TM-2245: Removal of Xenon-135 from Circulating Fuel Salt of the MSBR by Mass Transfer to Helium Bubbles. *ORNL-TM-2245, Oak Ridge National Laboratory*, 1968b.

D.B. Pelowitz. Mcnpx user's manual version 2.6. 0. los alamos national laboratory; 2008.

R. Perry and D. Green. *Perry's Chemical Engineers' Handbook*. McGraw-Hill Education, 2007.

S. Petrucci. *Ionic Interactions: From Dilute Solution to Fused Salts*. Elsevier Science, 2012.

S. Plokhy. *Chernobyl: The History of a Nuclear Catastrophe*. Basic Books, 2018.

B. Prince. ORNL-TM-496: Methods of Computing the Reactivity Effects of

Distributed Xenon, Graphtie Shrinkage, and Fuel Soakup in the MSRE. Technical report, Oak Ridge National Laboratory. No date. Under preparation in 1964.

B. Prince, S. Ball, J. Engel, P. Haubenreich, and T. Kerlin. ORNL-4233: Zero-Power Physics Experiments on the Molten-Salt Reactor Experiment (MSRE). Technical report, Oak Ridge National Laboratory, Oak Ridge, TN, USA, 1968a.

B. Prince, S. Ball, J. Engel, P. Haubenreich, and T. Kerlin. ORNL-4233: Zero-Power Physics Experiments on the Molten-Salt Reactor Experiment (MSRE). page 70, 1968b.

B. Pritychenko and S. Mughabghab. Neutron Thermal Cross Sections, Westcott Factors, Resonance Integrals, Maxwellian Averaged Cross Sections and Astrophysical Reaction Rates Calculated from the ENDF/B-VII.1, JEFF-3.1.2, JENDL-4.0, ROSFOND-2010, CENDL-3.1 and EAF-2010 Evaluated Data Library. *Nuclear Data Sheets*, 113(12):3120–3144, 2012.

R J Pugh. *Bubble and Foam Chemistry*. Cambridge University Press, 2016.

C. Quigley, A. Johnson, and B. Harris. Size and Mass Transfer Studies of Gas Bubbles. In *Chemical Engineering Progress Symposium Series, American Institute of Chemical Engineers*, volume 1, page 31, New York, 1955.

J. Rasmussen. *Defending the Correspondence Theory of Truth*. Cambridge University Press, 2014.

R. Rhodes. *The Making of the Atomic Bomb*. The Making of the Nuclear Age. Simon & Schuster, 1986. ISBN 9780684813783.

L.S. Richardson, D.C. Vreeland, and W.D. Manly. Ornl-1491: Corrosion by molten fluorides. interim report – september 1952. Report, Oak Ridge National Laboratory, Oak Ridge, TN, USA, 1953. URL https://www.osti.gov/servlets/purl/4127448. 19 enumerated pages.

G. Robbins, S. Wang, and J. Stuart. Using The Static Headspace Method to Setermine Henry's Law Constants. *Analytical Chemistry*, 65(21):3113–3118, 1993.

R. Robertson. ORNL-TM-0728: MSRE Design and Operations Report. Technical report, 1965a.

R. Robertson. ORNL-TM-0728: MSRE Design and Operations Report. Technical report, 1965b.

R. Robertson. ORNL-TM-4541: Conceptual Design Study of a Single-Fluid Molten-Salt Breeder Reactor. Technical report, Oak Ridge National Laboratory, 1971.

M. Robinson. ORNL-1924: A Theoretical Study of Xe-135 Poisoning Kinetics in Fluid-Fueled, Gas-Sparged Nuclear Reactors. Technical report, Oakridge National Laboratory, 1956.

D. Robinson, J. Fry. ORNL-TM-2318: Determination of the Void Fraction in the MSRE Using Small Induced Pressure Perturbations. Technical report, Oak Ridge National Laboratory, Oak Ridge, TN, USA, 1969.

W. Rohsenow, J. Hartnett, and Y. Cho. *Handbook of Heat Transfer*. McGraw-Hill, 1998.

P. K. Romano, N. E. Horelik, B. R. Herman, A. G. Nelson, B. Forget, and K. Smith. Openmc: A state-of-the-art monte carlo code for research and development. *Annals of Nuclear Energy*, 82:90–97, 2015.

M. Rosenthal, P Briggs, and P. Kasten. ORNL-4119: Molten-Salt Reactor Program Semiannual Progress Report for Period Ending February 28,1967. Technical report, Oak Ridge National Laboratory, Oak Ridge National Laboratory, 1967a.

M. Rosenthal, R. Briggs, and P. Kasten. ORNL-4191: Molten-Salt Reactor Program Semiannual Progress Report For Period Ending August 31, 1967. Technical report, Oak Ridge National Laboratory, Oak Ridge, TN, USA, 1967b.

M. Rosenthal, P. Kasten, and R. Briggs. Molten-salt reactors—history, status, and potential. *Nuclear Applications and Technology*, 8(2):107–117, 1970. ISSN 0550-3043.

M. Rosenthal, R. Briggs, and P. Haubenreich. ORNL-4832: Molten-Salt Reactor Program Semiannual Progress Report - Period Ending August 31, 1972. Technical report, Oak Ridge National Laboratory, Oak Ridge, TN, USA, 1973.

Murray W Rosenthal. ORNL/TM-2009/181: An account of Oak Ridge National Laboratory's Thirteen Nuclear Reactors. Technical report, Oak Ridge National Laboratory, 2009.

W. Rosenthal, R. Briggs, and P. Haubenreich. ORNL-4728: Semiannual Progress Report - Period Ending August 31, 1971. Technical report, Oak Ridge National Laboratory, 1972.

M. Rosenthan, P. Haubenreich, and R. Briggs. ORNL-4812: The Development Status of Molten-Salt Breeder Reactors. Technical report, Oak Ridge National Laboratory, Oak Ridge, TN, USA, 1972.

R. W. Rousseau. *Handbook of Separation Process Technology*. A Wiley-Interscience publication. Wiley, 1987.

E. Rutherford. *Radioactive Substances and Their Radiations*. CUP Archive, 1913.

T. Salmi, J. Mikkola, and J. Warna. *Chemical Reaction Engineering and Reactor Technology*. Chemical Industries. Taylor & Francis, 2011. ISBN 9781420092691.

Salome. Salome Website, 2017. URL `http://salome-platform.org/`. Last Accessed; 1/1/2017.

F. Salzano and A. Eshaya. Sorption of Xenon in High Density Graphite at High Temperatures. *Nuclear Science and Engineering*, 12(1):1–3, 1962.

G Samuels and Lackey. ORNL-2376: ART Fuel Pump and Xenon Removal System Development, Test Evaluation and Aircraft Application. Technical report, Oak Ridge National Laboratory, Oak Ridge, TN, USA, 1957.

M. F . et al. Sanner. Python: a programming language for software integration and development. *J Mol Graph Model*, 17(1):57–61, 1999.

A. Santamarina, D. Bernard, P. Blaise, M. Coste, A. Courcelle, T. Huynh, C. Jouanne, P. Leconte, O. Litaize, S. Mengelle, et al. The jeff-3.1. 1 nuclear data library. *JEFF report*, 22(10.2):2, 2009.

E. Schneid and B. Rosner. Study of (d, p) and (d, t) Reaction on the Xe 136 Isotope. *Physical Review*, 148(3):1241, 1966.

L. Schramm. *Emulsions, Foams, and Suspensions: Fundamentals and Applications*. Wiley, 2006.

D. Scott and W. Eatherly. Graphite and Xenon behavior and their Influence on Molten-salt reactor design. *Nuclear Applications and Technology*, 8(2): 179–189, 1970.

D. Scott, G. W. Alwang, E. F. Demski, W. J. Fader, E .V. Sandin, and R.E. Malenfant. ORNL-2536: A Zero Power Reflector-Moderated Reactor Experiment at Elevated Temperature. Technical report, Oak Ridge National Laboratory, 1958.

J. Serp, M. Allibert, O. Beneš, S. Delpech, O. Feynberg, V. Ghetta, D. Heuer, D. Holcomb, V. Ignatiev, J. Kloosterman, L. Luzzi, E. Merle-Lucotte, J. Uhlíř, R. Yoshioka, and D. Zhimin. The Molten Salt Reactor (MSR) in Generation IV: Overview and Perspectives. *Progress in Nuclear Energy*, 77:308–319, 2014.

R. Serrano-López, J. Fradera, and S. Cuesta-López. Molten Salts Database for Energy Applications. *Chemical Engineering and Processing: Process Intensification*, 73:87–102, 2013.

S. Shekhar and H. Xiong. *Encyclopedia of GIS*. Encyclopedia of GIS. Springer US, 2007. ISBN 9780387308586.

T. Sherwood, R. Pigford, and C. Wilke. *Mass transfer*. McGraw-Hill, 1975.

T. K. Sherwood. Mass transfer and friction in turbulent flow. *Transactions of the American Institute Chemical. Engineers*, 36:817, 1940.

T. K. Sherwood and B. B. Woertz. Mass Transfer between Phases Role of Eddy Diffusion. *Industrial & Engineering Chemistry*, 31(8):1034–1041, 1939. ISSN 0019-7866.

K. Shibata, O. Iwamoto, T. Nakagawa, N. Iwamoto, A. Ichihara, S. Kunieda, S. Chiba, K. Furutaka, N. Otuka, T. Ohsawa, T. Murata, H. Matsunobu, A. Zukeran, S. Kamada, and J. Katakura. JENDL-4.0: A New Library for Nuclear Science and Engineering. *Journal of Nuclear Science and Technology*, 48(1):1–30, jan 2011.

Y. Shimazu. Transient Xenon Analysis in a Molten Salt Breeder Reactor. *Journal of Nuclear Science and Technology*, 14(11):805–810, 1977.

Y. Shimazu. *A Study on the Nuclear Characteristics of a Molten Salat Breeder Reactor*. PhD thesis, Hokkadio University, 1980.

W. Sides. ORNL-TM-2489: MSBR Control Studies. Technical report, Oak Ridge National Laboratory, 1969.

H. Silverman, M. Huntley, W., Rrobertson. ORNL-TM-5335: Heat Transfer Measurements in a Forced Convection Loop with Two Molten-Fluoride Salts: LiF-BeF2-ThF2-Uf4, and Eutectic NaBF4-NaF. Technical report, Oak Ridge National Laboratory, 1976.

B. Singh, A. Rodionov, and Y. Khazov. Nuclear data sheets for A= 135. *Nuclear Data Sheets*, 109(3):517–698, 2008. ISSN 0090-3752.

V. Singh, A. Wheeler, M. Lish, O. Chvála, and B. Upadhyaya. Nonlinear dynamic model of Molten-Salt Reactor Experiment – Validation and operational analysis. *Annals of Nuclear Energy*, 113:177–193, 2018.

D. Smith, D. Luckhurst, and A. Maccabee. Design and control characteristics of the rbmk reactor. In *Chernobyl: A Technical Appraisal*, page 3, London, 1986. British Nuclear Energy Society.

P. Smith. ORNL-TM-79: Water Test Development of the Fuel Pump for the MSRE. Technical report, Oak Ridge National Laboratory, Oak Ridge, TN, USA, 1962.

P. Smith. ORNL-TM-2987: Development of Fuel and Coolant Salt Centrifugal

Pumps for the Molten Salt Reactor Experiment. Technical report, Oak Ridge National Laboratory, Oak Ridge, TN, USA, 1970.

M. Sohal, M. Ebner, P. Sabharwall, and P. Sharpe. Engineering Database of Liquid Salt Thermophysical and Thermochemical Properties. Technical report, Idaho National Laboratory, Idaho Falls, ID, USA, 2010.

N. Soppera, M. Bossant, and E. Dupont. JANIS 4: An Improved Version of the NEA Java-based Nuclear Data Information System. *Nuclear Data Sheets*, 120:294–296, 2014.

Kirk Sorensen. Energy From Thorium. URL `http://energyfromthorium.com`.

K. Suzuki and Y. Shimazu. Transient Xenon Effect on Plant Control in MSRs-Validation of Simulation Model. In *Proceedings of ICAPP '04*, Pittsburgh, PA, USA, 2004.

Nobuhide Suzuki and Yoichiro Shimazu. Preliminary Safety Analysis on Depressurization Accident without Scram of a Molten Salt Reactor. *Journal of Nuclear Science and Technology*, 43(7):720–730, 2006.

Y. Suzuki, N. Shimazu. Reactivity-Initiated-Accident Analysis without Scram of a Molten Salt Reactor. *Journal of Nuclear Science and Technolgy*, 45(6):

575–581, 2012.

R. Svehla. R-132: Estimated Viscosities and Thermal Conductivities of Gases at high Temperatures. Technical report, NASA, 1962.

J. Talbot. ORNL/TM-5104: A Stidy pf Trotoi, Removal From Fusion Reactor Blankets of Molten Salt and Lithium-Aluminum. Technical report, Oak Ridge National Laboratory, Oak Ridge, TN, USA, 1976.

Z. Taylor, R. Salko, and B. Collins. Implementation of General Species Transport Capability into VERA-CS for Molten Salt Reactor Analysis. In *Transactions of the American Nuclear Society*, volume 118, Philadelphia, Pennsylvania, 2018.

R. Thomas. Bubble Coalescence in Turbulent Flows. *International Journal of Multiphase Flow*, 7(6):709–717, 1981.

M. Tramšek and B. Žemva. Synthesis, Properties and Chemistry of Xenon (II) Fluoride. *Acta Chim. Slov*, 53:105–116, 2006.

A. Trkov, M. Herman, and D. Brown. ENDF-6 Formats Manual. Technical report, National Nuclear Data Center, Upton, NY, USA, 2012.

H . Tyrrell. The Origin and Present status of Fick's Diffusion Law. *Journal*

of chemical education, 41(7):397, 1964. ISSN 0021-9584.

A. Van Schijndel. Integrated modeling of dynamic heat, air and moisture pro-
cesses in buildings and systems using SimuLink and COMSOL. In *Building
Simulation*, volume 2, pages 143–155. Springer, 2009. ISBN 1996-3599.

A. van Schijndel. Integrated modeling of dynamic heat, air and moisture
processes in buildings and systems using simulink and comsol. In *Building
Simulation*, volume 2, pages 143–155. Springer, 2009.

Various Quora Users. Which is the best book for studying Mass Transfer? URL
`https://www.quora.com/Which-is-the-best-book-for-studying-Mass-Transfer`.
Last Acessed: 15/72018.

A. Vazirizadeh, J. Bouchard, and Y. Chen. Effect of Particles on Bubble Size
Distribution and Gas Hold-Up in Column Flotation. *International Journal
of Mineral Processing*, 157:163–173, 2016.

A. Vértes, S. Nagy, Z. Klencsár, and R. Lovas. *Handbook of Nuclear Chemistry*.
Springer Reference, 2003.

James R. W., Charles E. W., and Robert E. W. *Fundamentals of Momentum,
Heat and Mass Transfer*. John Wiely and Sons, Inc., New York, 1969.

D. Wagman, W. Evans, V. Parker, I. Halow, S. Bailey, and R. Schumm. NBS 270-3: Selected Values of Chemical Thermodynamic Data. Technical report, United States Department of Commerce, 1968.

W. Wang, Z. Zhou, K. Nandakumar, Z. Xu, and J. Masliyah. Effect of Surface Mobility on the Particle Sliding Along a Bubble or a Solid Sphere. *Journal of Colloid and Interface Science*, 259(1):81–88, 2003. ISSN 0021-9797.

K. Wardle. Hybrid multiphase CFD simulation for liquid–liquid interfacial area prediction in annular centrifugal contactors. *Proceedings of the Global 2013*, page 7650, 2013.

G. Watson and R. Evans. ORNL-TM-262: Xenon Diffusion in Graphite: Effects of Xenon Absorption in Molten Salt Reactors Containing Graphite. Technical report, Oak Ridge National Laboratory, 1962a.

G. Watson and R. Evans. ORNL-TM-262: Xenon Diffusion in Graphite Effects of Xenon Absorption in Molten Salt Reactors Containing Graphite. Technical report, Oak Ridge National Laboratory, 1962b.

G. Watson, R. Evans III, W. Grimes, and N. Smith. Solubility of Noble Gases in Molten Fluorides. In LiF-BeF2. *Journal of Chemical and Engineering Data*, 7(2):285–287, 1962.

J. Wei. *Product Engineering: Molecular Structure and Properties.* Topics in Chemical Engineering. Oxford University Press, 2007.

A. Weinberg. *The First Nuclear Era: The Life and Times of a Technological Fixer.* American Institute of Physics, 1994. ISBN 9781563963582.

A. Weingberg. Ornl-528: The aircraft nuclear propulsion program and general reactor technology quarterly progress report for period ending november 30, 1949. Report, Oak Ridge National Laboratory, Oak Ridge, TN, USA, 1950. 41 enumerated pages.

P. Westh, C. Haynes, and Y. Koga. How Dilute Is the Henry's Law Region? II. *The Journal of Physical Chemistry B*, 102(25):4982–4987, 1998.

Alexander M Wheeler, Vikram Singh, Laurence F Miller, and Ondřej Chvála. Exploring Molten-Salt Reactor Source Terms. *Transactions of the American Nuclear Society*, 118:829–832, 2018.

R. Wichner and C. Baes. ORNL-CF-72-6-12: Sidestream Processing for Continuous Iodine and Xenon Removal from the MSBR Fuel. Technical report, Oak Ridge National Laboratory, 1972.

J. Wilkes. Molten Salts and Ionic Liquids-Are They Not the Same Thing? *ECS Transactions*, 3(35):3–7, 2007. ISSN 1938-6737.

M.A. Winkler and M Winkler. *Chemical Engineering Problems in Biotechnology*. Critical reports on applied chemistry. Springer Netherlands, 1990. ISBN 9781851664542.

S. Wolfram. Wolfram Alpha. URL `www.wolframalpha.com`. Last Accessed: 9/52018.

J. Wood. *Nuclear Power*. Energy Engineering Series. Institution of Engineering and Technology, 2007.

J. Wu, C. Guo, X. Cai, C. Yu, C. Zou, J. Han, and J. Chen. Flow effect on I-135 and Xe-135 Evolution Behavior in a Molten Salt Reactor. *Nuclear Engineering and Design*, 314:318–325, 2017.

J. Wu, X. Li, J. Hu, J. Chen, C. Yu, C. Zou, and X. Cai. ICONE26-82352: Influence of Xe-135 Dynamic Behavior on Core Operation Safety for a Molten Salt Reactor. In *Proceedings of the 2018 26th International Conference on Nuclear Engineering, ICONE26*, 2018.

Y. Yang and J. Maa. Bubble Coalescence in Dilute Surfactant Solutions. *Journal of Colloid and Interface Science*, 98(1):120–125, 1984. ISSN 0021-9797.

G. Yoder. Examination of Liquid Fluoride Salt Heat Transfer. In *Proceedings*

of ICAPP 2014, Charlotte, 2014.

S. Zhang, Q. Zhou, X. Lu, Y. Song, and X. Wang. *Physicochemical Properties of Ionic Liquid Mixtures*. Springer, New York, NY, 2016.

Attachment 12

Defense Slides

A Dynamic Model of Xenon Behavior in a Molten Salt Reactor

November 28, 2019

PhD Defense Presentation,

Ontario Technical University

Oshawa, Ontario Canada

Terry J. Price

Presentation Outline

Background on Molten Salt Reactors (MSRs)

Xenon 135 and its effects in nuclear reactors

Major contribution (the dynamic model)

Additional efforts and contributions

Conclusions + Q&A

Background

What is a Molten Salt Reactor?

- **Uses Liquid Circulating Fuel**
- **Alkali halide fuel salt as primary working fluid + fuel matrix**

- **In this thesis specifically:**
  - **Graphite Moderated**
  - **Thermal Spectrum**

1. Fuel Inlet
2. Flow Distributor
3. Distribution Channels
4. Downcomer
5. Lower Plenum
6. Fuel Channels
7. Graphite Stringers
8. Upper Plenum
9. Fuel Outlet

4
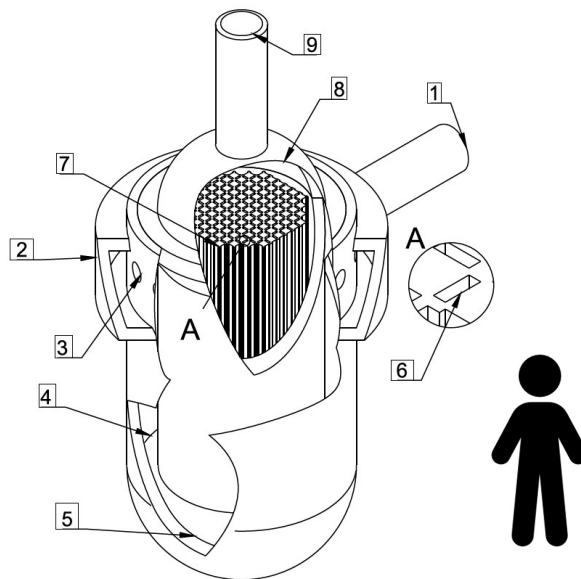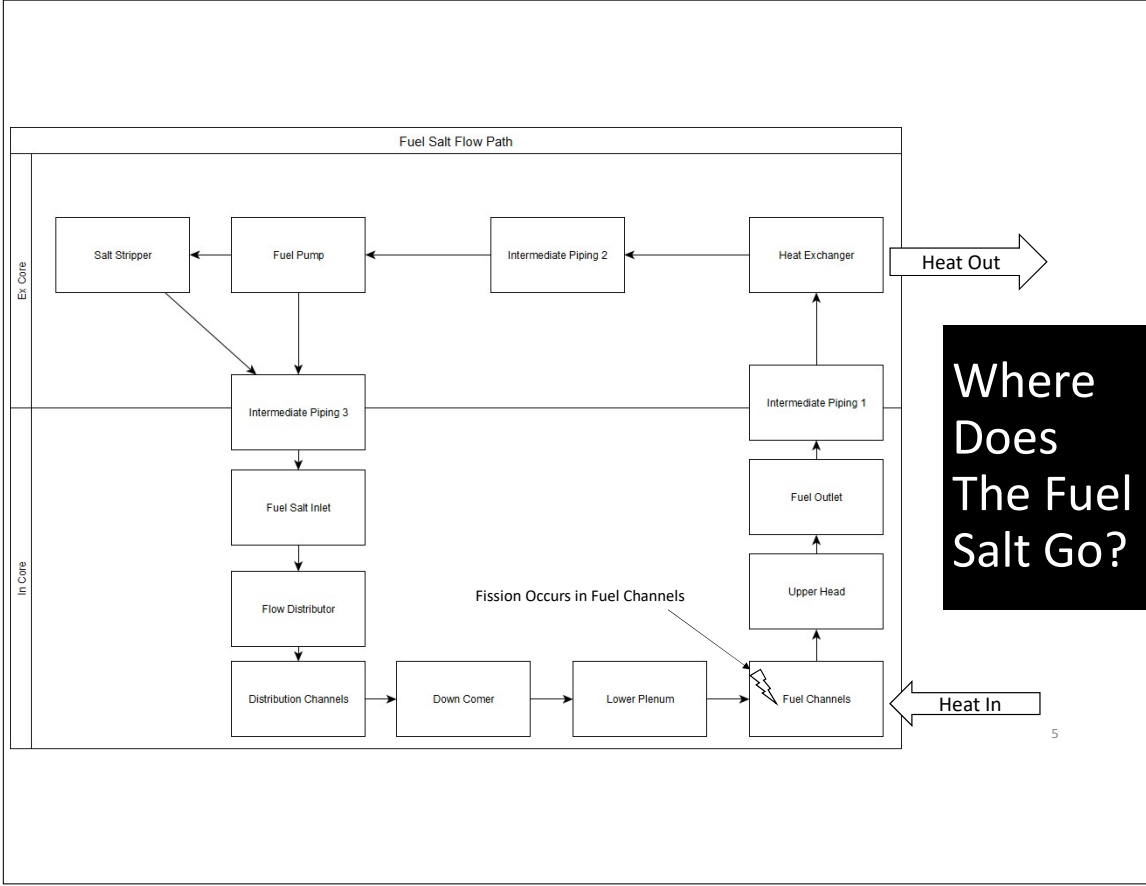
Why Do We Want Molten Salt Reactors?

High Temperature
- Process heat
- High thermal efficiency
- Thermal storage / transfer

Circulating Liquid Salt Fuel
- Drain tank emergency core ejection (geometry changes)
- Continuous online refueling
- Online fuel processing
- Homogeneous fuel, no radiation damage
- Multi decade / century long fuel life cycles
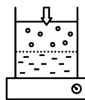
Near Atmospheric Pressure
- No pressure drive to disperse radionuclides, smaller containment
- Thinner walled primary circuit

There are advantages imbued by the engineered attributes of an MSR!

6

Why Do We Not Want Molten Salt Reactors?

Unproven Technology

Proliferation Risk

Materials Challenges

No Support Infrastructure

Physics Technology Challenges

Li-7 Procurement

7
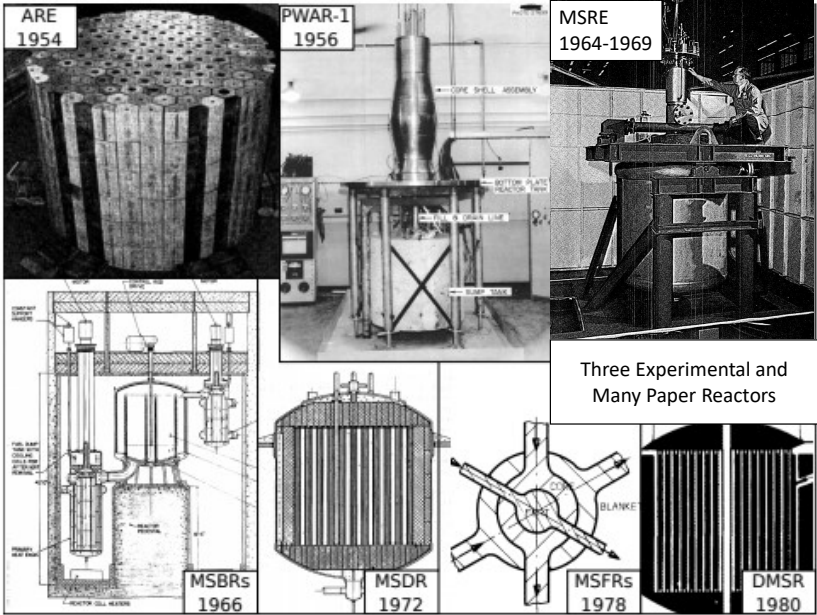
Prior Reactors

Three experimental and numerous paper reactors

ARE 1954
PWAR-1 1956
MSRE 1964-1969
Three Experimental and Many Paper Reactors
MSBRs 1966
MSDR 1972
MSFRs 1978
DMSR 1980

8

Why Was MSR Development Stopped?

The MSR wasn't dropped for technical reasons

"I found myself increasingly at odds with the reactor division of the AEC. [The director of the reactor division at the time was Milton Shaw]….[Shaw] had a very successful career with Admiral Rickover's naval reactor division and had been the program manager of the Shipping Port project,. Milt was cut very much from the Rickover cloth: he had a singleness of purpose and was prepared to bend the rules and regulations in achievement of his goal. At the time he became director of reactors, [of] the AEC, at President's Nixon's direction, [he] had made the liquid metal cooled fast breeder (LMFBR) the primary goal of [the] reactor program. Woe unto anyone who stood in his way. This caused problems for me since I was still espousing the molten salt breeder"

"That something was seriously amiss became apparent to me around 1972. Floyd Culler and I were talking to Chet Holifeld about our work on reactor safety. Chet was clearly exasperated with me and finally bultered out 'Alvin, if you are concerned about the safety of reactors, then I think it may be time for you to leave nuclear energy'."

"I suddenly realized that my tenure as director of the Oak Ridge National Laboratory might be coming to an end. …, late in 1972, John Swartout, my former deputy, who by this time was vice president for research of the Union Carbide Corporation in New York, told me I had to go."

- A. Wienberg in The First Nuclear Era, 1994

Shaw had a different story

A. Wienberg - Director 1955 -1973

M. Shaw – ORNL Director 1973 -

9

The MSR Project In One Graph
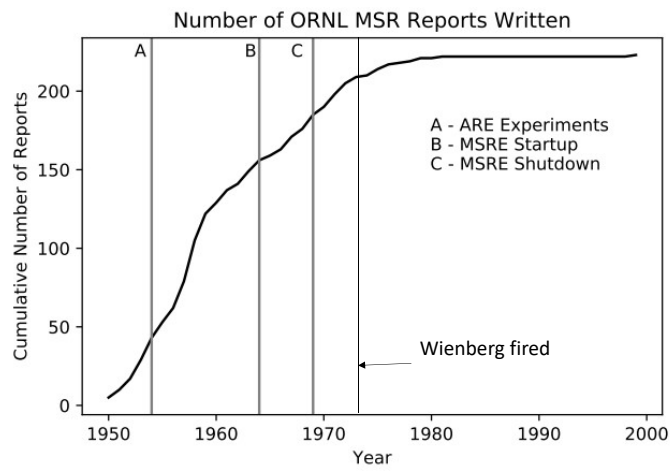
Discover

Nuclear Technology Abandoned Decades Ago Might Give Us Safer, Smaller Reactors

The Crux | By M. Mitchell Waldrop | February 26, 2019 5:38 PM

"Certainly no one expects to have a prototype power plant operating before the mid-2020s, or to field full-scale commercial reactors until the 2030s. Still, says Schönfeldt, "it will be exceedingly hard, but that is significantly better than impossible."

Bloomberg Environment

Advanced Nuclear Reactors Targeted for Late 2020s, Companies Say

BY BOBBY MAGILL
Feb. 13, 2019, 3:01 PM

"Kairos Power's fluoride salt reactor also aiming for operation before 2030"

BUSINESS INSIDER

A Bill Gates-backed energy company is developing what could be a game-changing nuclear reactor

"Terrestrial Energy, a Canadian company, wants to commercialize the design for its Integral Molten Salt Reactor by the late 2020s. And in the UK, Moltex Energy is making a Stable Salt Reactor, which uses molten-salt fuel. Moltex plans on deploying its product at a nuclear-reactor site by 2030"

MSRs Are Coming Soon!

11

The Subject of This Thesis

Xenon-135
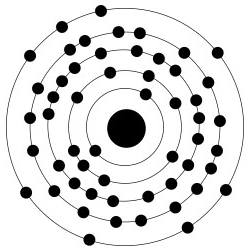
- Noble gas
- $T_{boil} = -108\ °C$
- Found in atmosphere < 100 ppb
- Xe-135 is a neutron poison
  - 81 neutrons, 54 protons
    - 82 is a magic number
  - 2.6 Mb thermal absorption cross section
    - A thermal neutron is 4444 times more likely to be absorbed in Xe-135 than U-235

Nuclear Evolution of Xe-135

Without migration (solid fueled reactor)

[(1)]Te-135 Fission
Production

[(4)] I-135 Fission
Production

[(7)] Xe-135 Fission
Production

[(2)] Te-135 $\xrightarrow{\quad}$ [(3)]$t_{1/2} = 19$ s $\quad$ [(5)] I-135 $\xrightarrow{\quad}$ [(6)] $t_{1/2} = 6.57$ h $\quad$ [(8)] Xe-135 $\xrightarrow{\quad}$ [(11)] $t_{1/2} = 9.1$ h $\quad$ [(12)] Cs-135

[(9)]
n^0 Absorption

[(10)] Xe-136

Illustration of Xenon Poisonout Event

The Xenon Transient

Quantity	Magnitude
$\Sigma_f\ [m^{-1}]$	0.15
$\phi\ [m^{-2}s^{-1}]$	10^{17}
$V\ [m^3]$	2
$\lambda_{Te-135}\ [s^{-1}]$	3.645×10^{-2}
$\lambda_{I-135}\ [s^{-1}]$	2.926×10^{-5}
$\lambda_{Xe-135}\ [s^{-1}]$	2.106×10^{-5}
γ_{Te-135}	3.225×10^{-2}
γ_{I-135}	2.935×10^{-2}
γ_{Xe-135}	7.539×10^{-4}
$\sigma_g^{Xe-135}\ [Mb]$	2.6
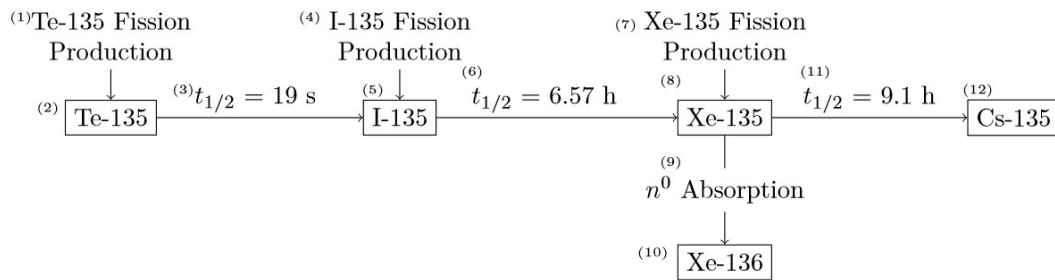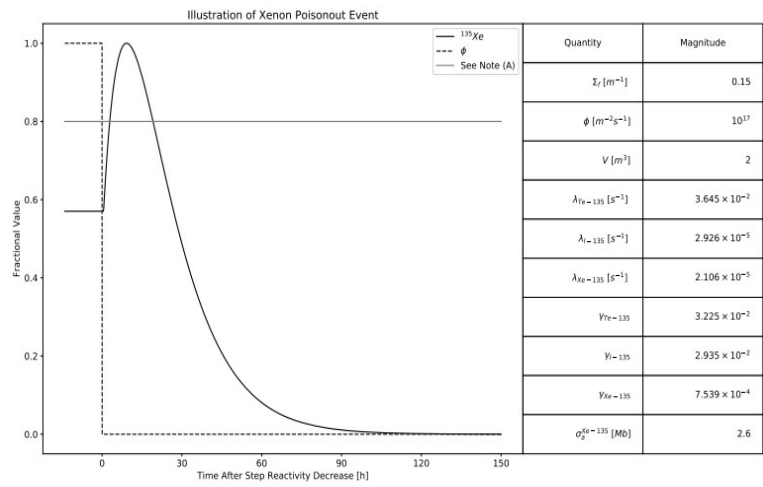
- The dynamics of reactor power influences the evolution of Xe-135 in the reactor
- *Note (A): The grey line represents the maximum xenon reactivity that can be removed with the reactor's reactivity control mechanisms (E.G. control rods)*

15

Inventory of ^{135}Xe, ^{135}I, and, ^{135}Te During A Step Decrease in Reactivity

Legend:
- Xe
- I
- Te

Y-axis: Number of Atoms ($\times 10^{20}$)
X-axis: Time [h]
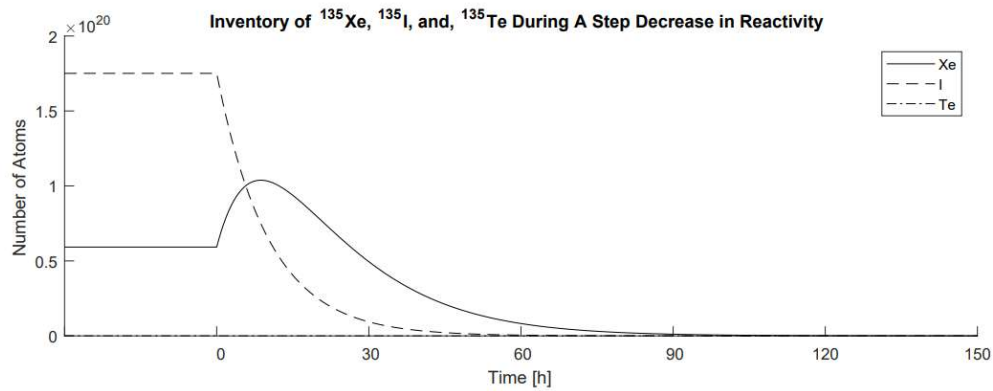
Details of the Xe-135 Transient

- Step decrease in Te-135 content
- Gradual reduction in I-135 content
- Increase then decrease of Xe-135 content

16

The Qualitative Difference in MSR vs Solid Fuel Reactor Xenon Behavior
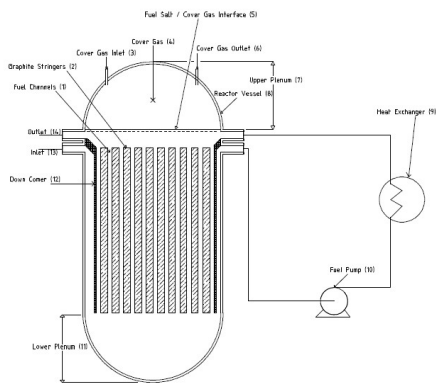
Molten Salt Reactor
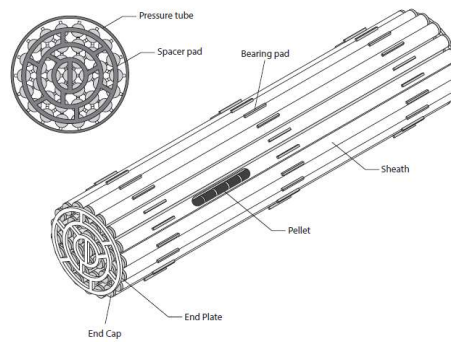
CANDU fuel bundle from Canteach

17

Entrained bubbles
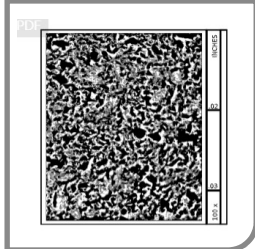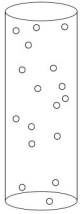
Graphite pore space

Where does the xenon go?

dissolved gas in liquids migrate to gas spaces

18

The Graphite / Salt Interface

1. Bulk liquid
2. Boundary Layer
3. Pure diffusion region
4. Pore Space
5. Solid Graphite Matrix
6. Boundary layer film side
7. Boundary layer interface side1

The Salt / Gas Interface

Modeling Xenon Migration To Gas Spaces

Gasses migrate in liquids
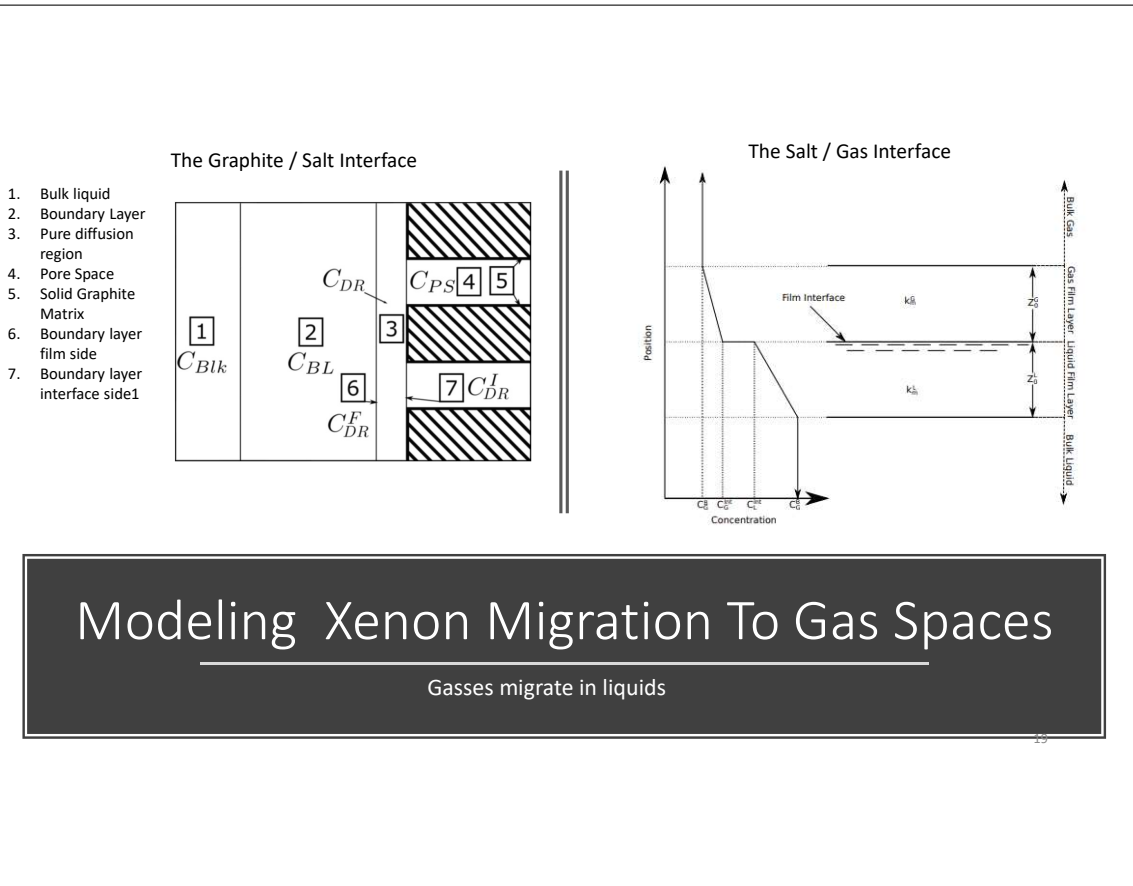
Xenon Within Graphite

Mixture of material and nuclear properties
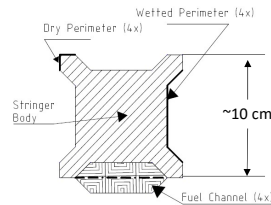
$$\frac{\partial C_{Xe}}{\partial t} = \frac{D_g}{\epsilon}\nabla^2 C_{Xe} - (\sigma_a^{Xe}\phi + \lambda_{Xe})C_{Xe}$$

$$C_{Xe}(r) = C_G^{Surf.}\frac{I_0(\beta r)}{I_0(\beta r_0)}$$

$$\beta = \sqrt{\frac{\epsilon}{D_g}(\sigma_a^{Xe}\phi + \lambda_{Xe})}.$$

Graphite β As a Function of Neutron Flux

$D_g = 2.4 \times 10^{-9}\ [m^2/s]$
$\epsilon = 0.1$
$\sigma_a^{Xe} = 2.6 \times 10^{-22}\ [m^2]$
$t_{1/2} = 3.3 \times 10^4\ [s]$
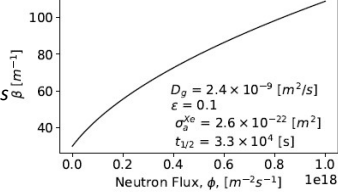
Variation of Graphite ^{135}Xe Concentration With Respect to Graphite β
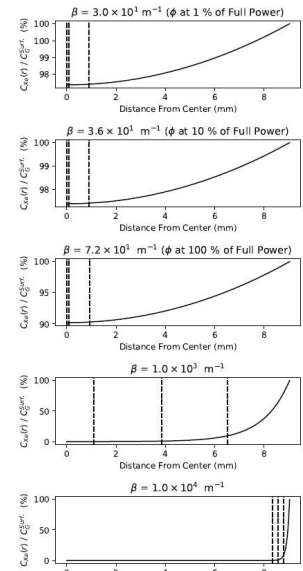
Engineered Control of Xe-135

A xenon stripper removes Xe-135 from BOTH the gas and liquid phases
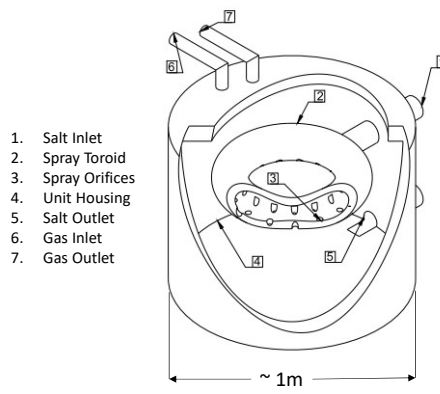
1. Salt Inlet
2. Spray Toroid
3. Spray Orifices
4. Unit Housing
5. Salt Outlet
6. Gas Inlet
7. Gas Outlet

~ 1m

Illustration of a xenon stripper
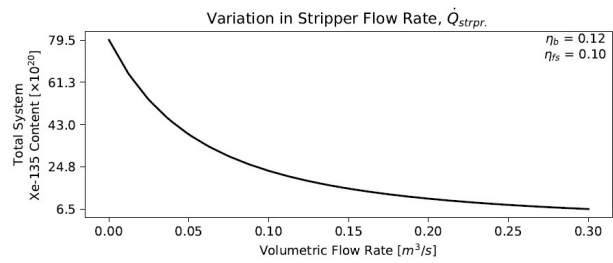
Steady State Xe-135 content as predicted by a first order lumped parameter Xe-135 model

A Model of MSR Xenon Behavior
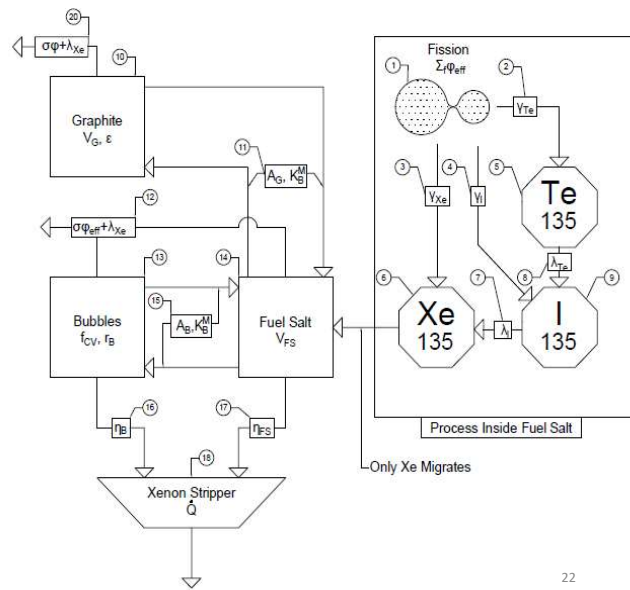
Prior Major Modeling Efforts
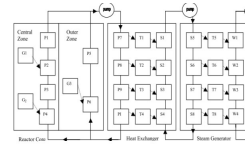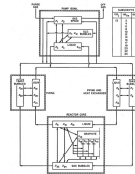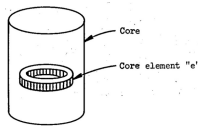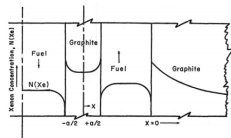
Miller, 1961

Modeled:
- Graphite
- Xenon Stripper

Investigated
- Graphite diffusion coefficient
- Stripper Efficiency

Kedl, Houtzeel, 1968

Modeled:
- Graphite
- Xenon Stripper
- Bubbles
- Discretized Core

Investigated:
- Predicted SS MSRE Xenon Poisoning Fraction
- Effects of Bubbles

Engel & Steffy 1971

Modeled:
- Graphite
- Stripper
- Bubbles
- Lumped Parameter

Investigated:
- Attempted Fitting to Experimental Data
- Transient Analysis

Suzuki & Shiamazu, 1977 / 2004

Modeled:
- Graphite
- Xenon Stripper
- Bubbles
- Set of ODEs / PDEs

Investigated
- Transient Analysis
- Balance of Plant

23

The Gap

The Prior modeling efforts did not

- Investigate or account for thermal effects
- Consistently describe multiple instances of reactor behavor with one set of parameters

My Work

My Main Contribution

Built for the MSRE from ORNL reference data

First model to account for thermal effects

Developed a Xenon Dynamics Model

Benchmarked against operational data

Parametric studies allowed the model to fit experimental data

Overview of The Model

The Model Contains Several Submodels

- Nuclear processes
  - Production, burnup, and decay
- Graphite migration
  - 1140 graphite stringers homogenized into 5 flow regions, modeled using second order method of lines solution to reaction diffusion equation
- Bubble migration
  - 13 node lumped volume approach
- Removal by sparging
  - First order removal process with separate removal efficiencies for bubble and fuel salt

Implemented in Mathworks Simulink

- Thousands of computational blocks
  - details in the thesis and backup slides

Thermal Effects

First model to do this

Variation in circulating void fraction (expansion of gas)

Expansion of fuel salt into the pump bowel

Variation in mass transfer coefficients (graphite + bubble)
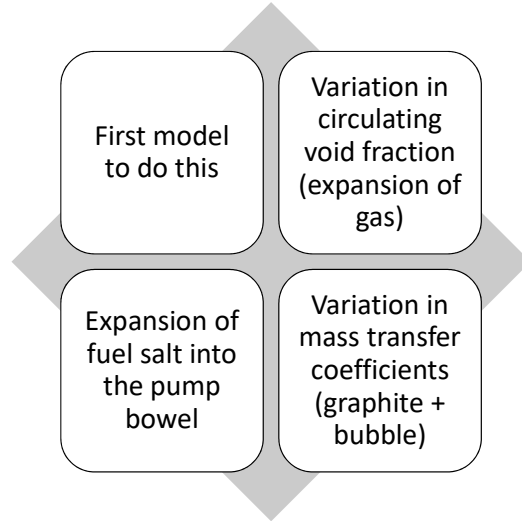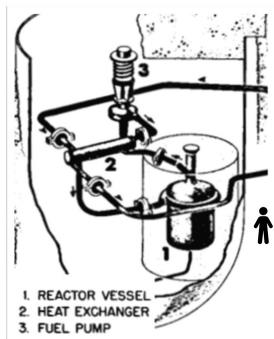
What I Modeled: The Molten Salt Reactor Experiment

- Modeled xenon behavior in the primary side

1. REACTOR VESSEL
2. HEAT EXCHANGER
3. FUEL PUMP

FUEL OUTLET
CONTROL ROD THIMBLES
GRAPHITE-MODERATOR STRINGER
FUEL INLET
REACTOR CORE CAN
REACTOR VESSEL
FLOW DISTRIBUTOR

Images from ORNL-TM-0728

29
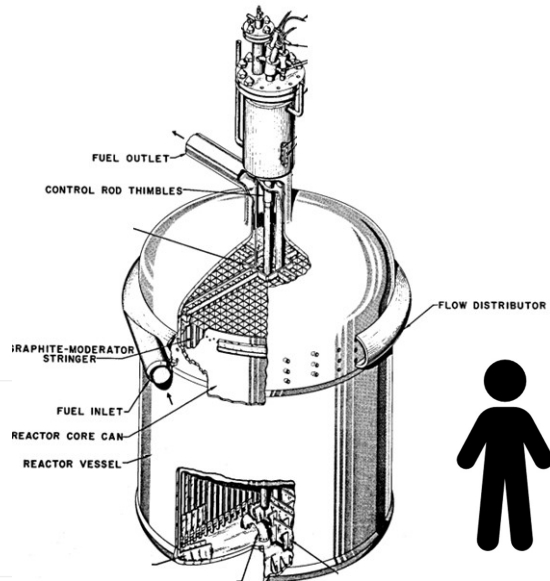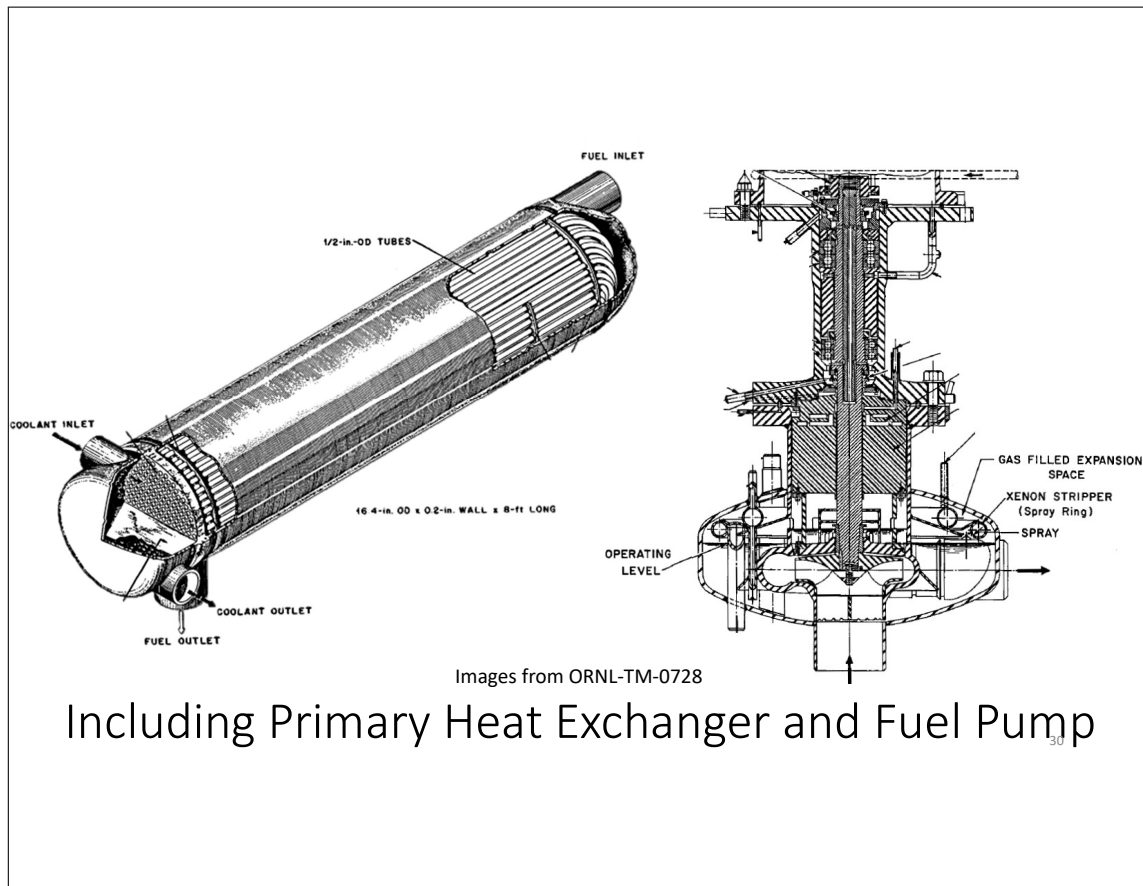
Images from ORNL-TM-0728

Including Primary Heat Exchanger and Fuel Pump

30

Where we want to be

Where we are at

Nuclear Science
November 2018

**International Handbook
of Evaluated Reactor Physics
Benchmark Experiments**
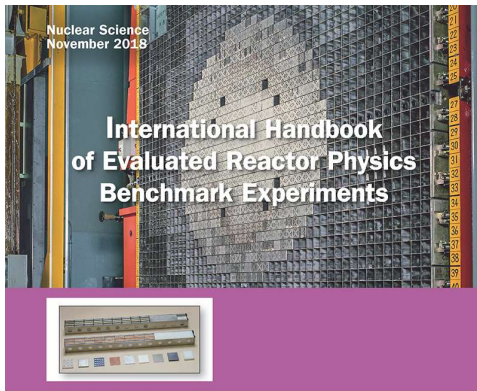
**Phenomena Important in Modeling and
Simulation of Molten Salt Reactors**

Manuscript Completed:

April 23, 2018

Prepared by:

David J. Diamond,[1] Nicholas R. Brown,[2] Richard Denning,[3]
and Stephen Bajorek[4]

[1]Brookhaven National Laboratory
Upton, NY 11973-5000

[2]Pennsylvania State University
University Park, PA 16802

[3]Consultant
Columbus, Ohio 43220

[4]Office of Nuclear Regulatory Research
U.S. Nuclear Regulatory Commission

Prepared for:

George Tartal
Office of New Reactors
U.S. Nuclear Regulatory Commission

NEA
NUCLEAR ENERGY AGENCY

The Problem With Modeling + Benchmarking / 'Validation'   31

The Solution to the Modeling + Validation / Benchmark Problem

- **Data spread between hundreds of reports and papers**
- **Meant for continuous technical development not benchmarking**
- **Focused on development through building**
- **No NRC / Different Environment**

32
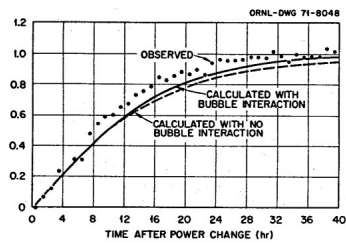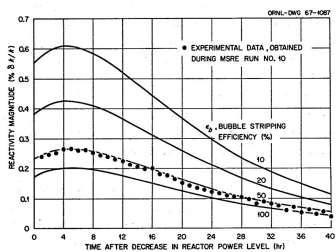
Benchmark Data

- First model to even attempt benchmarking since 1971.
- Standardized MSR benchmark data does not exist.
- Startup and shutdown data digitized from ORNL-TM-3464

33

ORNL Didn't Have Much Luck At Xenon Modeling

1. "The calculations using previously accepted transport mechanisms and parameter values showed again that the steady state results with argon cover gas could be readily duplicated. However, such calculations required the use of bubble stripping efficiencies that were much lower than the bubble removal rates that were observed in the reactor…."

2. "When these steady state results were applied to transient calculations with high argon void fractions, they produced decreases in the xenon poisoning that were much slower than those observed in the reactor after power reductions"

3. "In attempting to describe the reactor results we found it necessary to postulate liquid and bubble stripping efficiencies in the pump bowl that were much higher than predicted and liquid to graphite mass transfer coefficients that were much lower"

Quotes from ORNL-TM-3464 (the last bench marked model)

They did not get one parameter set to describe multiple scenarios --- inconsistent fitting

34

Benchmark Against Startup and Shutdown Transients

- Sensitivity analysis with respect to major model parameters
    - Temperature
    - Density
    - Viscosity
    - Mass transfer coefficient
    - Fission yields (burnup)
    - Neutron fluxes
    - Bubble radii
    - Xenon radii
    - Circulating void fraction
    - Reactivity coefficients
    - Xenon stripper parameters

High Variation, Low variation, Nominal run

<u>Try To Make it Match</u>
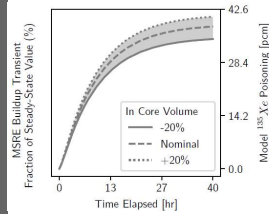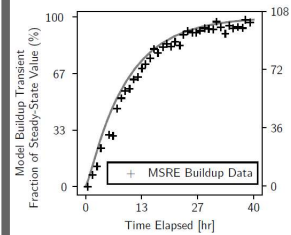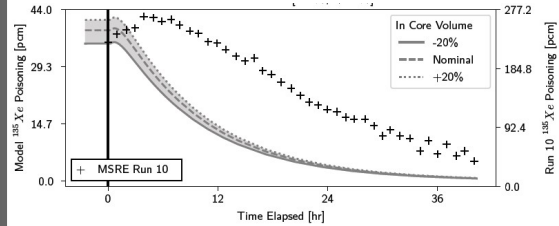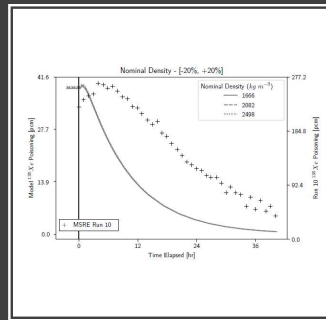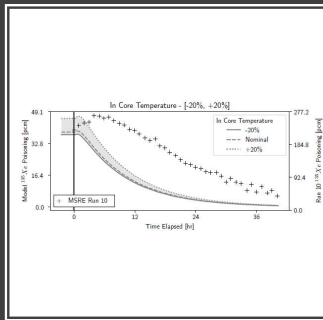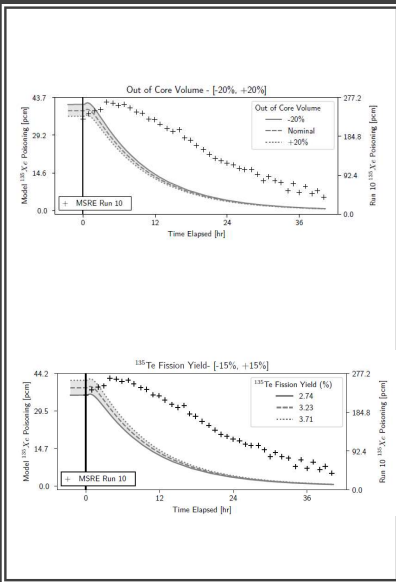
No Match With Extensive Sensitivity Parameter Search

Shutdown transient is categorically underpredicted

The Model Was Highly Sensitive to Variation in Bubble Salt Stripping Efficiency

Xenon Stripper

Liquid Level
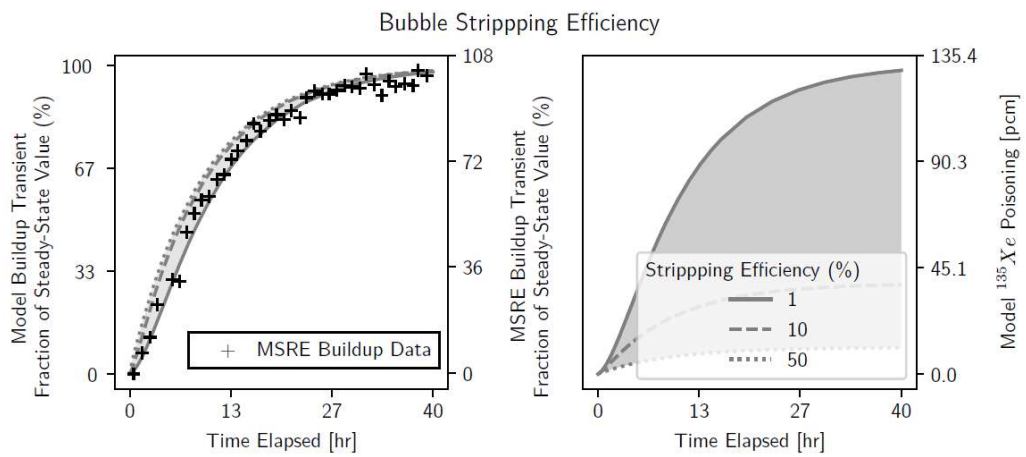
So I Thought…

- How close is the stripper to the fuel salt?
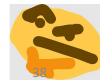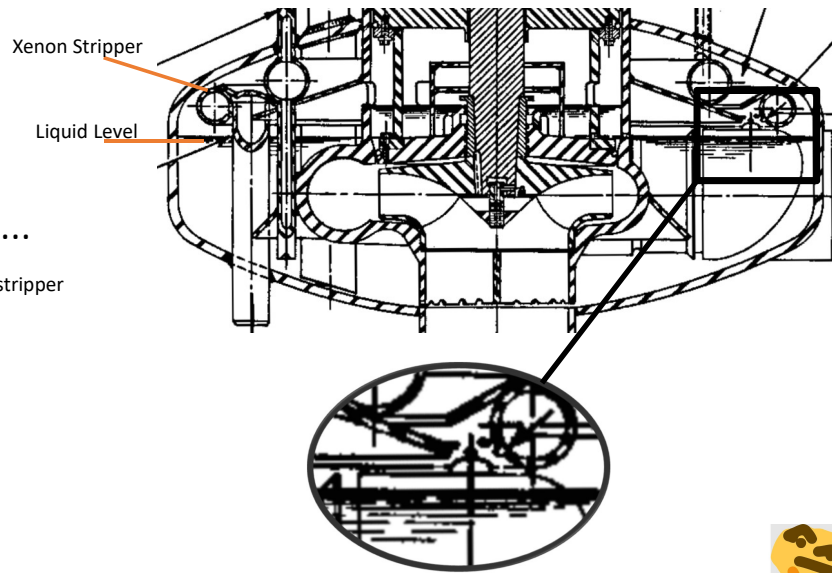
Evidence Points Towards A Suggestion

- ORNL-3872: Bulk fuel salt void fraction between 1.2 % and 3 %
- ORNL-TM-3027:

20% Void Fraction

VOLUTE ℄
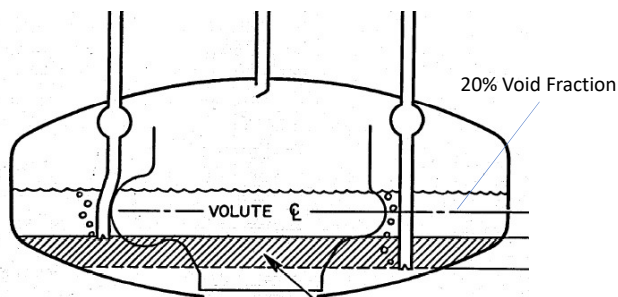
ORNL-TM-3464 hypothesized the existence of a foam to describe discrepancy in some results

"…if the liquid surface in the pump bowl is covered by a "foam" in which the gas phase xenon concentration is much higher than that in the rest of the gas space, the same high rate of bubble exchange would produce a much smaller change in average xenon concentration in the circulating bubbles"

Is the Stripper Covered by Foam?
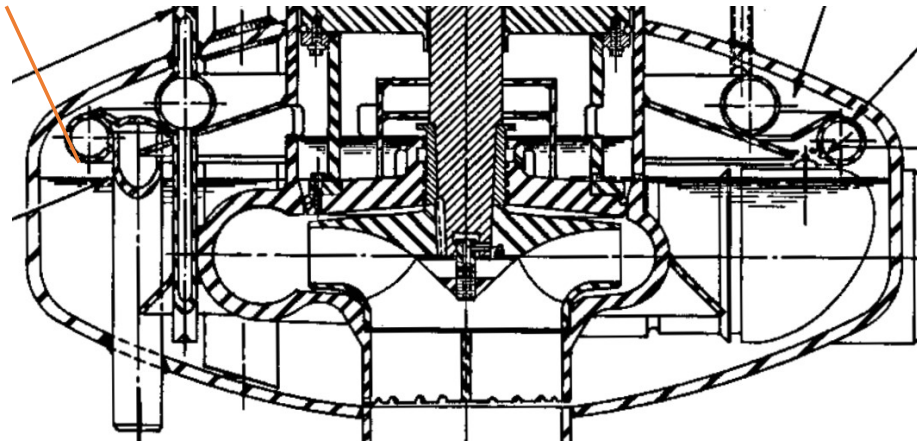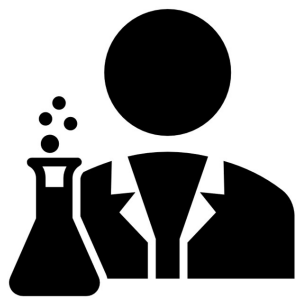
So I Tried It

Xenon stripper fuel salt and bubble stripping efficiency reduced by a factor of 1000

41
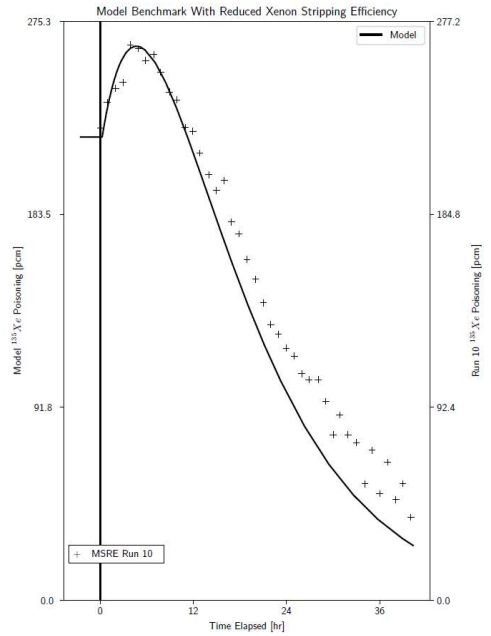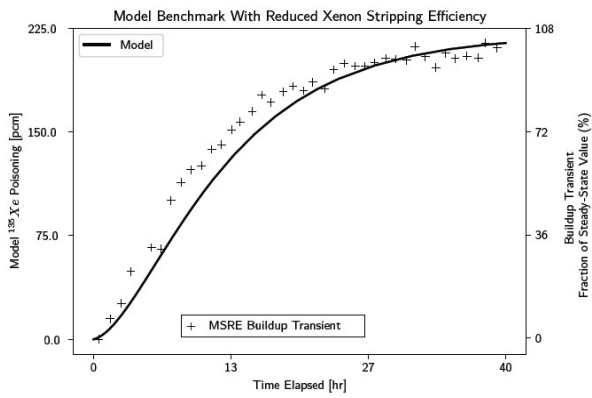
And it Worked!

I have developed the first MSR xenon dynamics model that successfully describes two transients with one parameter set

The Key Difference Between The Models, The Reaction Diffusion Equation

43
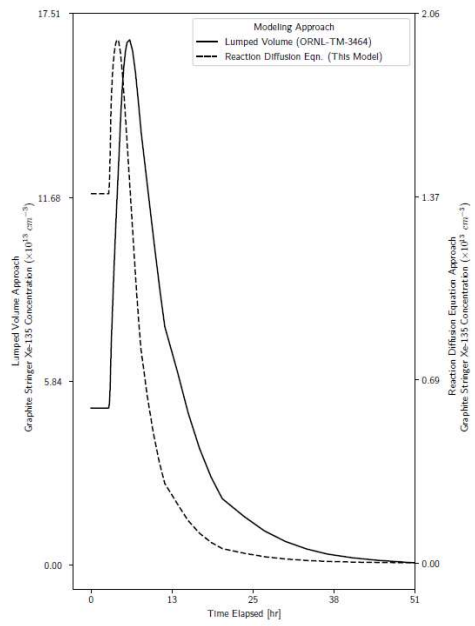
Demonstration of Dynamic Simulation Capabilities

This is the first model that is capable of simulating the effects of temperature perturbation on MSR xenon behavior
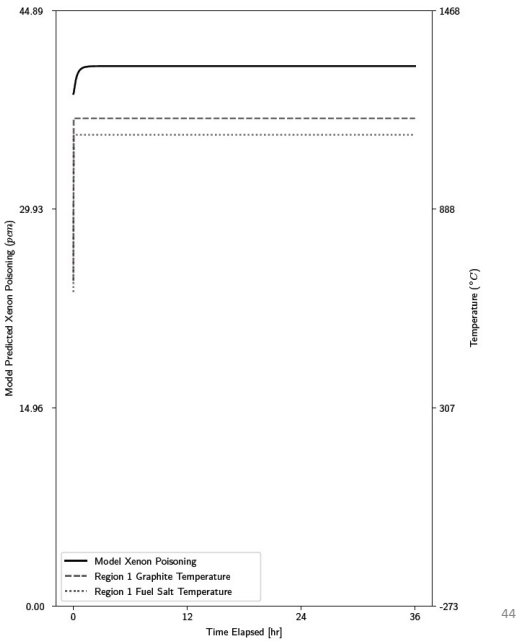
Other Contributions

Additional Accomplishments

Largest database of MSR xenon literature compiled	Investigation of internal distribution of xenon within the graphite on reactivity defect	Developed additional MSR dynamics models	Consulting and Knowledge Transfer for Terrestrial Energy
Collaboration with ORNL Modeling Team	Participation in the development of the UOIT / TEI Agreement	Developed approved research plan for government organization	Development of reactor physics visualization software

Published Papers From My Thesis Work

Journal	Title	Coauthors	Status	
Nuclear Engineering and Technology (NET)	Xenon in Molten Salt Reactors: The Effects of Solubility, Circulating Particulate, Ionization, and the Sensitivity of the Circulating Void Fraction	Ondrej Chvala, Zack Taylor	Accepted	✓
ASME Nuclear Engineering and Radiation Science (NERS)	Xenon Behavior in Molten Salt Reactor Graphite: A Review and A Model of The Reactivity Effect Due To The Xenon Distribution Inside of The Graphite	Ondrej Chvala, Zack Taylor	Accepted	✓
ASME NERS	A Review of Circulating Voids and Gaseous Fission Product Behavior In Molten Salt Reactors	Ondrej Chvala, Zack Taylor	Accepted	✓
ASME NERS	A Review of Molten Salt Reactor Xenon Analysis Literature (Conference Version)	Ondrej Chvala	Accepted	✓
Generation 4 Small Modular Reactor Conference	Molten Salt Reactor Xenon Analysis: Review and Decomposition	Ondrej Chvala, Zack Taylor	Accepted	✓

47

Papers in Development

Journal	Title	Coauthors	Status
ASME Nuclear Engineering and Radiation Science (NERS)	A Theory and Model of Molten Salt Reactor Xenon Behavior After the Solubility Limit	Ondrej Chvala	Accepted Pending Revisions
Undecided	Mass and Heat Transfer to Molten Salt Reactor Graphite	Ondrej Chvala	Under Development
ASME Nuclear Engineering and Radiation Science (NERS)	Galvanic Corrosion in Molten Salt Reactors	To Be Decided	Under Development
Undecided	A Dynamic Model of Molten Salt Reactor Xenon Behavior	Ondrej Chvala	Under Development
Undecided	Research Experience in Molten Salt Reactor Xenon Behavior and Suggestions for Future Work	To Be Decided	Awaiting publication of all other papers (Final paper)

48

Summary

MSR XENON DYNAMICS MODEL DEVELOPED AND BENCHMARKED

NUMEROUS OTHER CONTRIBUTIONS AND MODELING EFFORTS

PAPERS PUBLISHED

THESIS PRESENTED

A "10,000 ft" View of the Model

50
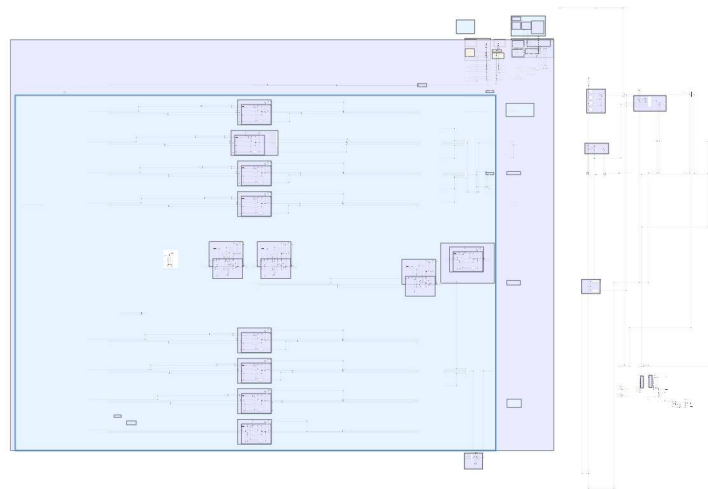
Questions

Backup Slides

NASA Technology Readiness Levels

- **Deploy by the late 2020s**
- **Need to "Prove it is safe before then"**
- **If Xenon is part of that proof, we've got a long way to go in a short period of time.**
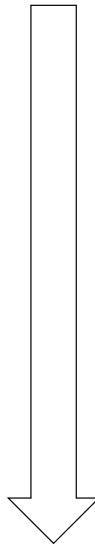
Level	Description
Level 1	Basic principles observed and reported
Level 2	Technology concept formulated
Level 3	Analytical and experimental proof of concept
Level 4	Component validation in lab
Level 5	Component validation relevant environment
Level 6	System Validation relevant environment
Level 7	Prototype demonstration in operation environment
Level 8	Mission qualified through test
Level 9	System proven through multiple successful mission operations

53

How Did They Know What The Density Was Between The Bubblers?

$$\rho = \frac{\Delta P_{gauge} + 2\gamma \left[\frac{1}{r_2(t)} - \frac{1}{r_1(t)} \right]}{gh}$$

Radius of curvature of the bubble

54
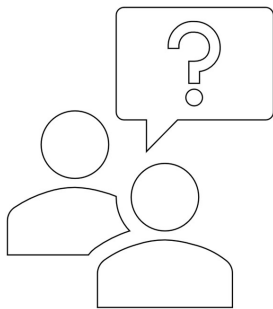
Why Does Parameter X Affect Y?

- Multiple reasons, not one to one
  - Complex computational model. Many interconnected systems
  - There are major and minor reasons
  - Can answer: "Here are some reasons"
  - Can't answer: "Here is THE reason".

Attachment 13

Model Startup Script

```matlab
% --------------------------------------------------------------------
%  Generated by MATLAB on 6-Dec-2018 00:01:02
%  MATLAB version: 9.0.0.341360 (R2016a)
% --------------------------------------------------------------------



D_g = 2.37E-9;

%Thermophysical Properties
T_Mes = 928.15  %Temperature at which the physical properties of the fuel salt was ↙
measured. 1200 deg. F; ORNL-TM-0728, p. 8
%NBL Operation temperature on p. 100 or TM-728.

%Viscosity
FS_Mu_A = 4340;
FS_Mu_K = 0.084;
FS_Mu_MSRE = 0.007027 %17 lb/ft-hr in Pa-s; ORNL-TM-0728 p.8

%Density
FS_rho_A = 3.628;
FS_rho_B = 0.00066;
FS_rho_MSRE = 2082% kg/m^3. from 130 lb/ft^3. ORNL-TM-0728 p. 8



L_GS = 1.6; %ORNL-4069 p. 6 fig 4



N_FC_R1 = 12; %Number of fuel channel, C.F> ORNL-TM-0378
N_FC_R2 = 940;
N_FC_R3 = 108;
N_FC_R4 = 78;
N_FC_tot = 1128; %sum of all the regions



Q_strpr = 0.003155;

Q_tot = 0.07571;

R_gas = 8.314;

Sig_f = 0.15;

T_Salt = 900;
T_Salt_0 = 900;
```

```matlab
U_FC_R1 = 0.607; %ORNL-TM-0378 p.14
U_FC_R2 = 0.183;
U_FC_R3 = 0.454;
U_FC_R4 = 0.250;



epsilon = 0.1;

eta_b = 1E-4%0.1;

eta_fs = 1.2E-4%0.12;

f_cv = 0.004;

gamma_i = 0.0293524;

gamma_te = 0.0322482;

gamma_xe = 0.00257324;

k_b = 1.3806E-23; %Bolzman's Constant


lambda_i = 2.9306070546251702E-5;

lambda_te = 0.036481430555786593;

lambda_xe = 2.0924e-05;

 phi0 = 3.98E+17;

%r_OOC = 0.1;

r_b = 0.000254;

r_fc = 0.79e-2 %EQUIVALENT RADIUS%0.01454;

r_gs = 0.01454;

r_xe = 2.16E-10;

sig_a_xe = 1.18E-22;



h_fc = 1.6; %63" from fig. 4 in ONRL-4069, p. 6
```

```
%Temperature distributions
%From ORNL-TM-0378 p.45 --- graphite
R_gr_m  = [ 0, 7.840134e-02, 7.979743e-02, 1.110706e-01,  ...
            1.725374e-01, 1.969467e-01, 2.502111e-01, 3.137128e-01, ...
            3.643293e-01, 4.295622e-01, 4.933898e-01, 5.427344e-01, ...
            5.979965e-01, 6.285161e-01, 6.302473e-01, 7.042308e-01]

T_gr_K =  [9.479114e+02, 9.471538e+02, 9.628461e+02, 9.660132e+02, ...
            9.685619e+02, 9.684143e+02, 9.666227e+02, 9.627852e+02, ...
            9.586270e+02, 9.516360e+02, 9.443291e+02, 9.384356e+02, ...
            9.306520e+02, 9.265643e+02, 9.234109e+02, 9.149254e+02]

%---fuel salt---
R_fs_m = [ 0, 4.113279e-02, 7.702932e-02, 7.987520e-02, ...
            1.227540e-01, 1.714875e-01, 2.634332e-01, 3.353781e-01, ...
            3.915383e-01, 4.722448e-01, 5.227244e-01, 5.732039e-01, ...
            6.092634e-01, 6.294641e-01, 6.311583e-01, 6.714634e-01, ...
            7.045715e-01,]

T_fs_K = [ 9.156575e+02, 9.155935e+02, 9.153718e+02, 9.309071e+02, ...
            9.327384e+02, 9.333500e+02, 9.322447e+02, 9.301849e+02, ...
            9.281185e+02, 9.244458e+02, 9.217463e+02, 9.190468e+02, ...
            9.170904e+02, 9.159159e+02, 9.131568e+02, 9.118330e+02, ...
            9.107427e+02,]

%effective radii of graphite regions (m). C.F> ORNL-TM-0378 p. 14
r_g_r1 = 3.78*2.54E-2;
r_g_r2 = 24.76*2.54E-2;
r_g_r3 = 26.10*2.54E-2;
r_g_r4 = 27.58*2.54E-2;


T_G_R_1_0 = mean(interp1(R_gr_m,T_gr_K, linspace(0,r_g_r1)))
T_G_R_2_0 = mean(interp1(R_gr_m,T_gr_K, linspace(r_g_r1,r_g_r2)))
T_G_R_3_0 = mean(interp1(R_gr_m,T_gr_K, linspace(r_g_r2,r_g_r3)))
T_G_R_4_0 = mean(interp1(R_gr_m,T_gr_K, linspace(r_g_r3,r_g_r4)))

T_FS_R_1_0 = mean(interp1(R_fs_m,T_fs_K, linspace(0,r_g_r1)))
T_FS_R_2_0 = mean(interp1(R_fs_m,T_fs_K, linspace(r_g_r1,r_g_r2)))
T_FS_R_3_0 = mean(interp1(R_fs_m,T_fs_K, linspace(r_g_r2,r_g_r3)))
T_FS_R_4_0 = mean(interp1(R_fs_m,T_fs_K, linspace(r_g_r3,r_g_r4)))

%INLET AND OUTLET TEMPERATURES. CF. ORNL-TM-0728 P.78
T_OUTLET = (1225 +458.67)*5/9
T_INLET = (1175 +458.67)*5/9
%FROM UH TO HX, T=OUTLET TEMP
T_UH_0 = T_OUTLET
T_P100_0 = T_OUTLET
T_FP_0 = T_OUTLET
T_P101_0 = T_OUTLET
%HX = AVERAGE OF INLET AND OUTLET TEMP
```

```matlab
T_HX_0 = 0.5*(T_OUTLET + T_INLET)
%FROM HX TO LH, T=INLET TEMP
T_P102_0 = T_INLET
T_CA_0 = T_INLET
T_LH_0 = T_INLET


%%%%%%%%%%% GRAPHITE FLUX %%%%%%%%%
%%Digitized form ORNL-TM-0378 p.23
phi_G_R = [ 0.0000,0.0296,0.0635,0.0748,0.0907,0.1180,0.1387,0.1631, ...
            0.1848,0.2130,0.2619,0.3090,0.3966,0.4851,0.5614,0.6264, ...
            0.6867,0.7093,0.7121,0.7281,0.7479]

phi_G_phi = [7.6111E+17,7.4815E+17,7.3889E+17,7.3333E+17, ...
             7.6852E+17,8.0741E+17,8.2407E+17,8.3148E+17, ...
             8.3333E+17,8.2593E+17,8.0000E+17,7.6111E+17, ...
             6.4815E+17,5.0556E+17,3.6852E+17,2.4259E+17, ...
             1.2037E+17,7.4070E+16,4.2590E+16,2.7780E+16,9.2600E+15]


phi_G_R_1 = mean(interp1(phi_G_R,phi_G_phi, linspace(0,r_g_r1)))
phi_G_R_2 = mean(interp1(phi_G_R,phi_G_phi, linspace(r_g_r1,r_g_r2)))
phi_G_R_3 = mean(interp1(phi_G_R,phi_G_phi, linspace(r_g_r2,r_g_r3)))
phi_G_R_4 = mean(interp1(phi_G_R,phi_G_phi, linspace(r_g_r3,r_g_r4)))

%phi_G_R_1 = 5.2053E17;
%phi_G_R_2 = 5.1130E17;
%phi_G_R_3 = 1.5775E17;
%phi_G_R_4 = 9.589E16;

%%%%%%%%
%phi_g_R_1_mult = phi_G_R_1 / phi0;
%phi_g_R_2_mult = phi_G_R_2 / phi0;
%phi_g_R_3_mult = phi_G_R_3 / phi0;
%phi_g_R_4_mult = phi_G_R_4 / phi0;
%%%%%%%%%%



%Surface tension correaltion in formation: A-BT
ST_A = 260
ST_B = 0.12

%Henry's Law coeffecient of temperature
%%From Watson, Evans, Grimes, 1962
%fit data using  f(x) = a*x^2 + b*x + c
%%C.F. Watson.m
%UB 1073 K
%LB 773 K
%Goodness of fit:
%  SSE: 1.218e-18
```

```matlab
%  R-square: 0.9994
%  Adjusted R-square: 0.9983
%  RMSE: 1.103e-09
H_Xe_a = 5.713e-13;
H_Xe_b = -7.937e-10 ;
H_Xe_c =   2.809e-07 ;

%Fuel salt mass at 900K

%t_DC = 0.02 %downcomer thickness
%A_DC = 0.1621 %downcomer cross-sectional area

%upper/lower head/plenum residence times.
t_up = 3.9 % seconds. taken from ORNL-TM-0728 p. 102
t_lp = 3.8
t_ooc = 8.1 %calculated by 25.2 -9.4-3.9-3.8

P_pump = 35420; %47.5 HP;  ORNL-TM-0728 P. 151

cubed_foot_to_cubed_meter = 0.02831685
V_Core_FS_0 = 25*cubed_foot_to_cubed_meter%25 ft^3 ORNL-TM-0728, p.102. 'core volume↙
only'. between the graphite planes
%V_1_FC =  5.03E-4 %Fuel volume in 1 channel

%Volume of fuel salt in the various graphite regions
V_R1_0 = V_Core_FS_0 *N_FC_R1/N_FC_tot
V_R2_0 = V_Core_FS_0 *N_FC_R2/N_FC_tot
V_R3_0 = V_Core_FS_0 *N_FC_R3/N_FC_tot
V_R4_0 = V_Core_FS_0 *N_FC_R4/N_FC_tot

V_FP_0 = (0.9+3.2)*cubed_foot_to_cubed_meter
V_LH_0 = 10.0*cubed_foot_to_cubed_meter
V_UH_0 = 10.5*cubed_foot_to_cubed_meter
V_CA_0 = 9.7*cubed_foot_to_cubed_meter

V_HX_0 = 6.1*cubed_foot_to_cubed_meter
V_P100_0 = 2.1*cubed_foot_to_cubed_meter;
V_P101_0 = 0.8*cubed_foot_to_cubed_meter;
V_P102_0 = 2.2*cubed_foot_to_cubed_meter;
f = 2.2*cubed_foot_to_cubed_meter;
V_Tot_0 = V_FP_0 + V_LH_0 + V_UH_0 + V_CA_0 + V_R1_0 + V_R2_0 + V_R3_0 + V_R4_0 + V_HX_0↙
+ V_P100_0 + V_P101_0 + V_P102_0;
V_IC = V_LH_0+V_UH_0+V_Core_FS_0 %25+10.5+10 cubic feet. C.F. ORNL-TM-0728 p. 102.  Using↙
'core', 'upper head', and 'lower head'

%VF_FP_0 = V_FP_0/ V_Tot_0;
%VF_MP1_0 = V_MP1 / V_Tot_0;
%VF_MP2_0 = V_MP2 / V_Tot_0;
%VF_DC_0 = V_DC / V_Tot_0;
```

```matlab
%VF_R1_0 = V_R1 / V_Tot_0;
%VF_R2_0 = V_R2 / V_Tot_0;
%VF_R3_0 = V_R3 / V_Tot_0;
%VF_R4_0 = V_R4 / V_Tot_0;
%VF_HX_0 = V_HX / V_Tot_0;
%VF_P1_0 = V_P100 / V_Tot_0;
%VF_P2_0 = V_P10001 / V_Tot_0;
%VF_P3_0 = V_P10002 / V_Tot_0;


V_CV_0 = f_cv*V_IC;



%Cooling Annulus
T_CA = 635+273.15 %C.F. ORNL-TM-0728 p. 78
Re_CA = 25800 %C.F. ORNL-TM-0728 p. 93

Re_LH = 1E4 %lower heaed reynolds number
Re_UH = 1E4 %upper heaed reynolds number

r_pipe = (5E-2*2.54)/2;
A_pipe = pi*r_pipe^2;

%heat exchanger
HX_N_Tubes = 159;
HX_r_Tube = ((0.5-0.042)/2)*2.54E-2; %ORNL-TM-2098 p. 9
HX_XS = HX_N_Tubes*(pi*HX_r_Tube^2); %heat exchanger cross-sectional flow area


P_sys = 344738 %50 PSI; from ORNL-TM-0728 p. 78

%REACTIVITY COEFFECIENTS FROM P. 54 of ORNL-TM-3464
%%NB: units in cm^-3 so make sure you multiply the number densities by 1E-6
alpha_FS = 0.517E-16 %
alpha_G_R1 = 0.334E-17
alpha_G_R2 = 0.699E-17
alpha_G_R3 = 0.669E-17
alpha_G_R4 = 0.791E-18

%experimental end time
t_exp_end = 144100;
```

Attachment 14
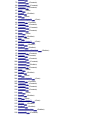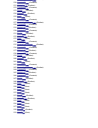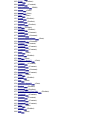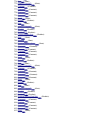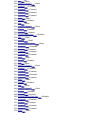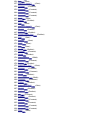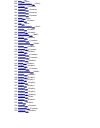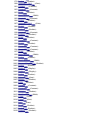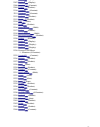
Final Xenon Dynamics Model Design Report
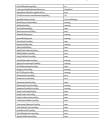
Micro Pages for Xenon Dynamics Model

Terry Price

December 2019

All 2173 of the xenon dynamics model design report can be found below. In PDF format, the pages should be saved with sufficient fidelity for reproduction.

Chapter 3. Subsystems